RECENT ADVANCES IN MARINE SCIENCE AND TECHNOLOGY, 92

NARENDRA K. SAXENA
EDITOR

PACON INTERNATIONAL
P.O. BOX 11568
HONOLULU, HAWAII 96828, U.S.A.

RECENT ADVANCES IN MARINE SCIENCE AND TECHNOLOGY, 92

Edited by

Narendra Saxena
Professor of Civil Engineering
University of Hawaii
Honolulu, Hawaii, U.S.A.

PACON INTERNATIONAL
1993

May 1993

Published by
PACON International
P.O. Box 11568
Honolulu, Hawaii 96828
U.S.A.

ISBN 0-9634343-0-6 (this volume)
ISBN 0-9634343 (series)

Printed in the United States of America

TABLE OF CONTENTS

PREFACE

Recent Advances in Marine Science and Technology, 92 is the first refereed publication of a series based upon papers presented at the fifth Pacific Congress on Marine Science and Technology (PACON 92) held in Kona, Hawaii, 1-5 June 1992. A unique process was adopted to bring about this refereed publication: session chairs selected authors (based on presentations at PACON 92) and recommended their manuscripts for possible inclusion in this publication. Each manuscript was reviewed by the session chairman and an external reviewer. Some revised manuscripts were reviewed a second time by the initial reviewers to see that the modifications were duly made. Out of 205 PACON 92 presentations, 113 papers were recommended by session chairmen, 61 manuscripts were submitted, and finally 47 papers were accepted for this publication. Since this is our first attempt to present a refereed publication, we faced many problems including manuscript format and some late reviews.

Since papers dealt in areas of ocean sciences, technology, management and policy, we have tried to group related papers to facilitate the reader's use of this publication. I hope that readers will find this first volume of 47 papers very useful.

I wish to thank Paula Kuriyama of PACON International, without whose untiring efforts this publication would not have been possible. Acknowledgement is also extended to the Hawaii Natural Energy Institute (HNEI) for providing Mary Kamiya to assist in editing this publication. This work was also made possible due to the generous support of our sponsors: U.S. Geological Survey, National Ocean Survey/National Oceanic and Atmospheric Administration (NOAA), Department of Business, Economic Development and Tourism (DBEDT)/State of Hawaii, Sea Grant College Programs of Hawaii and California, Minerals Management Service/U.S. Department of the Interior, Australian Marine Science Consortium, and Department of Civil Engineering/ University of Hawaii.

Honolulu
April 10, 1993

Narendra K. Saxena

DIGITAL OCEAN MAPPING OF THE PACIFIC EEZ

Rongxing Li and Narendra Saxena
University of Hawaii
Honolulu, Hawaii, U.S.A.

ABSTRACT

This paper describes the recent ocean mapping research conducted at the Pacific Mapping Program (PMP). Three-dimensional bathymetric maps and side-scan sonar image mosaics were generated. Data integration has been a strong point of PMP's research. This includes the generation of integrated maps of bathymetric data and side-scan sonar images, correction of pixel locations of side-scan sonar images by using bathymetric data acquired separately, and the improvement of bathymetric data by shape from shading technique. Research efforts have been made in developing a Marine Geographical Information System.

INTRODUCTION

The Pacific Mapping Program (PMP) was established at the College of Engineering, University of Hawaii, in 1990. It is a joint effort in ocean mapping of the Pacific Islands EEZ supported by the United States Geological Survey (USGS), the National Oceanic and Atmospheric Administration (NOAA), and the University of Hawaii.

The overall goal of the PMP is to facilitate the exploration and development of the resources of the EEZ of the Pacific Islands. The program will serve as a local repository for EEZ information and data in the Pacific Region. In addition, the PMP organizes training programs and workshops on ocean mapping for Hawaii and U.S. territorial islands in the Pacific. The University of Hawaii offers graduate students throughout the Pacific Basin certificate and/or graduate degree programs in ocean mapping.

Since 1990, the PMP has been concentrating its ocean mapping research efforts on data base generation, bathymetric data and side-scan sonar image processing, data integration, seafloor surface modeling, and marine GIS applications. The following sections describe the research work conducted at the PMP.

OCEAN MAPPING DATA PROCESSING

A system for ocean mapping data processing is set up at the PMP and is in full operation. Data sets of the Pacific Islands EEZ are provided by government agencies, institutions, and the private sector. The data processed are mostly bathymetric data, side-scan sonar images, gravity as well as magnetic data. They are processed, displayed, and analyzed for different application purposes.

Hardware and Software Configuration

Figures 1 and 2 depict the hardware and software configuration of the system at the PMP for digital ocean mapping. A SUN SPARC II, a VAX 3200 workstation, and two IBM compatible 386 PCs, running UNIX, VMS, and MS-DOS operating systems, respectively, cover platforms used by most commercial and public domain software packages for ocean mapping. An Ethernet connection between these computers and a link to Internet enable data communication within PMP and with outside hosts.

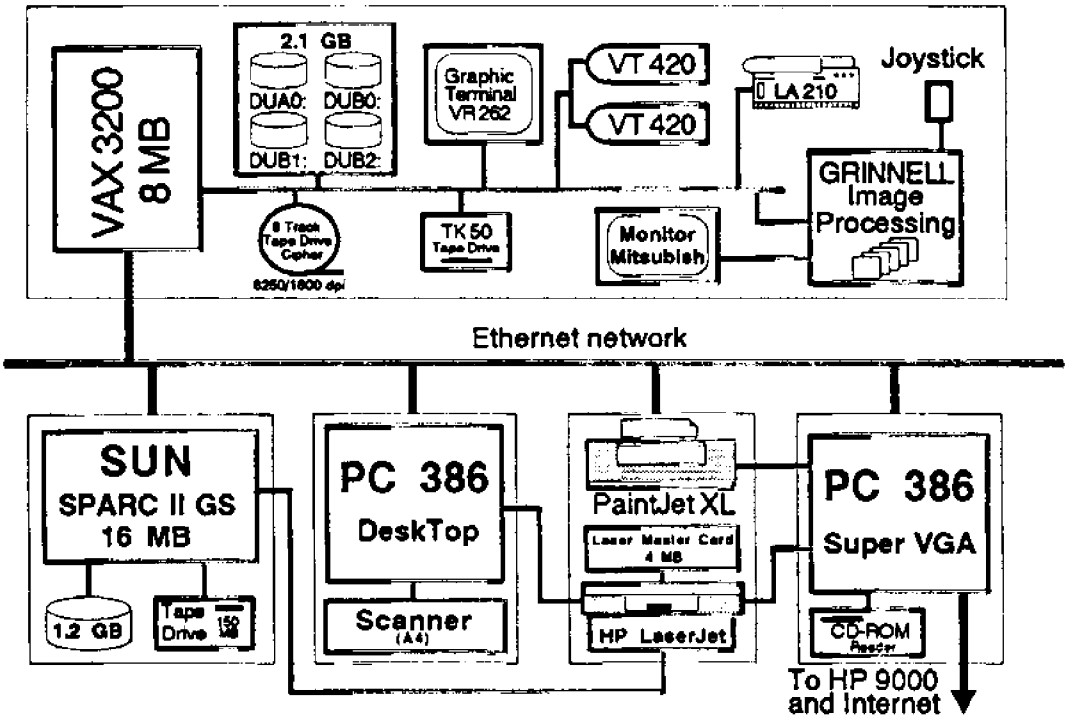

Figure 1. Hardware configuration

Actually, Figure 2 shows an integrated ocean mapping system at the PMP. At the user interface level, data are filtered so that input file formats are compatible with those used by the system. A user interface on the VAX system has been developed. Software applications can be selected from a user friendly task-oriented menu system. Thus, this integrated system approaches system transparency to users. Integrated software packages include commercial and public domain applications for general image processing, GIS, sonar image processing, bathymetric data processing, cartographic processing, modeling, and animation. The PMP has developed software for user interfaces, data integration, shape from shading processing, pixel relocation of sonar images, etc. The integrated system provides a software environment where data sets can be processed and integrated in a unique environment.

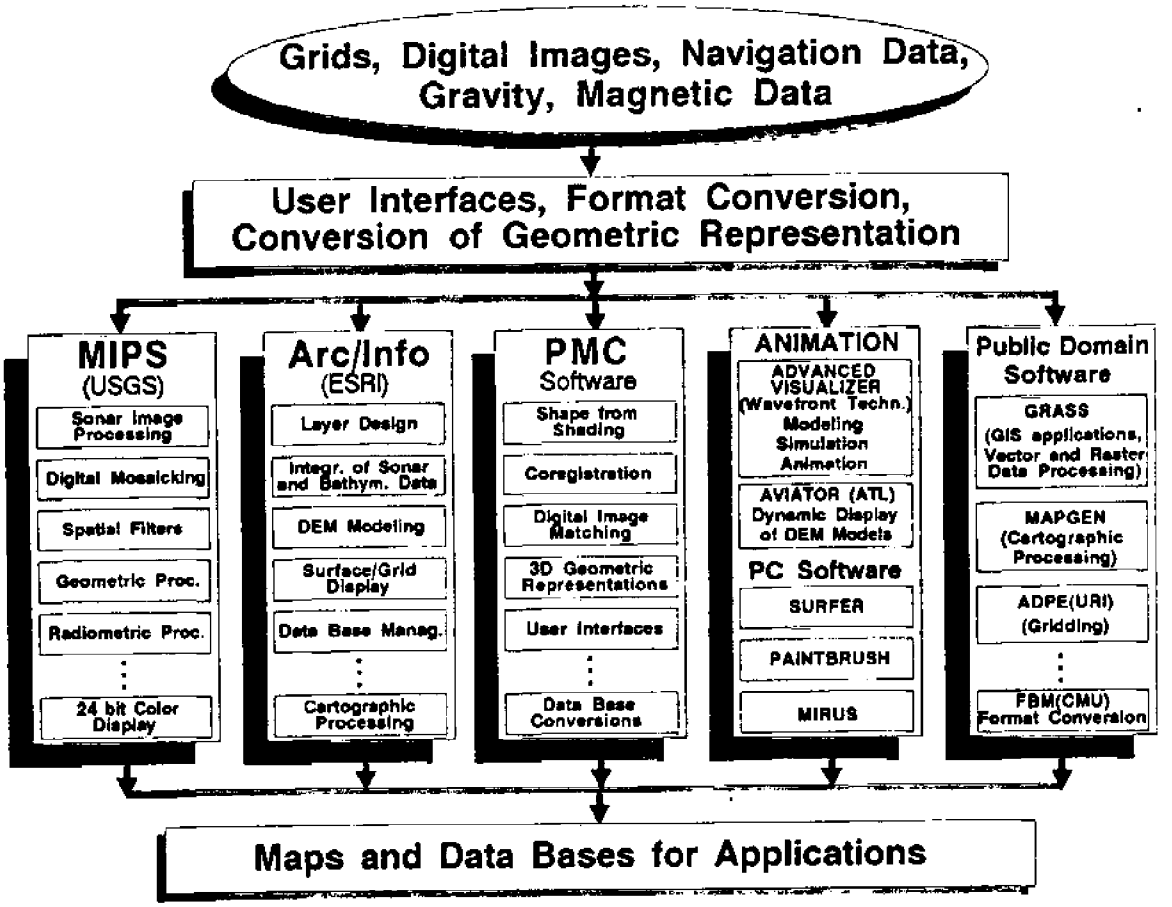

Figure 2. Software configuration

Data Processing

Multi-Beam data are available in the forms of full resolution data ("unthinned" points with coordinates of longitude, latitude, and depth) and grid data (grid points generated from full resolution data or thinned data). These data cover relatively large areas and have been used to generate bathymetric maps, digital seafloor data bases for navigation of under water vehicles, and three-dimensional maps for planning of seafloor explorations.

In many areas there are no Multi-Beam data available. Bathymetric data acquired by single sounding systems from different cruises can be used to generate grids, contour lines, etc. Depth points along track lines are sometimes dense and sometimes sparse depending on the sounding systems used and survey strategies. The overall data distribution of bathymetric points are usually very sparse. Gridded data provide a digital seafloor model with mostly interpolated grid points, while a TIN (Triangulated Irregular Network) preserves the originality of the input data. An improved seafloor model can be achieved by shape from shading using side-scan sonar images (Li and Pai, 1991).

Side-scan sonar images are processed to produce sonar image mosaics and integrated maps of sonar images and bathymetric data. MIPS (Mini Image Processing System), enhanced by the USGS, is used for preprocessing, geometric and radiometric

processing and mosaicking. The USGS standard procedure for digital sonar mosaicking has been adopted in order to produce sonar image mosaics with the same quality of USGS's sonar image mosaic atlas series. Additional correction of pixel locations of sonar images are applied where bathymetric data are available (Li, 1992b).

DATA INTEGRATION

Generation of Integrated Maps

In many applications different data sets presented in one map may be more useful than maps generated from individual data sets. We can create an integrated map of the side-scan sonar images and bathymetric data of an area using a colored mosaic of side-scan sonar images as map background and bathymetric data to generate contour lines. If classes of seafloor bottom material were identified and presented in different colors on the map, it would be very helpful for marine mining applications.

Draping a side-scan sonar image over a digital seafloor model can be accomplished by using many commercial and public domain software systems. This technique certainly helps obtain an intuitive three-dimensional view of the seafloor and interpret image features which could be impossible without viewing the images three-dimensionally. More sophisticated three-dimensional display and modeling of the seafloor surface can be realized by applying appropriate data structures and animation systems.

Shape from Shading

One of the benefits of data integration is to enhance the quality of data sets involved. If bathymetric data are acquired at the same time as sonar images, the technique of corregistration can be used to locate pixel positions of sonar images according to seafloor topography from the bathymetric data. Since pixel positions of sonar images are usually calculated with an assumption that the seafloor surface be flat in profiles across track lines this may cause shifts of pixels in the direction perpendicular to track lines (Chavez, 1986; Reed and Hussong, 1989). Bathymetric data acquired in different cruises may be applied to correct pixel locations of sonar images by data integration (Li, 1992b). Thus, the geometry of the sonar images is strengthened by integrating existing bathymetric information.

Inversely, the geometric information of seafloor surfaces can also be derived from sonar images to enhance bathymetric data. Shape from shading is one of the methods which generates shape models (first derivatives or slopes) of object surfaces by the analysis of gray values (shading) of images. Application of this technique to underwater sonar images enables a conversion of recorded strengths of reflected sonar signals from seafloor surfaces to seafloor slopes which can be transformed to seafloor depths given depths of a boundary in the mapping area (Li and Pai, 1991).

MARINE GEOGRAPHICAL INFORMATION SYSTEM

Geographical Information Systems (GIS) are the primary applications using geographical spatial data. Thematic data can be represented in various layers designed in a unique reference system for efficient data base management, inquiring, analysis, and display. In comparison to a "land based" GIS, a Marine Geographical Information

System (MGIS) is different in a) data and data acquisition systems involved, b) data processing techniques, and c) applications. Efforts have been made at the PMP to develop a MGIS. Since most existing GIS systems are not designed for marine purposes, existing software systems have been integrated to provide the necessary functionalities needed in an MGIS.

Layer Design in GIS vs. MGIS

Bathymetric data are usually used as the basic layer to provide seafloor topography for other thematic layers, such as side-scan sonar images, gravity, magnetic data, and cable routes, etc. There are very few cultural objects on the seafloor. Therefore, features such as address geocoding and building representations are seldom used in an MGIS. Instead, a track line layer of cruises is very important for data analysis and interpretation. For instance, a track line layer may help geologists figure out the geometry between the sonar image acquisition system and the seafloor surface mapped, and thus interpret sonar images easily.

Data Structures

In a MGIS, three-dimensional data structures are often used instead of the two-dimensional line features such as roads, rivers and others in a land-based GIS. TIN data structures can be used to network discrete data points and reserve the originality of the data set. Many processing and analysis functions are available on the TIN structure (ARC/INFO, 1991). However, a grid provides more efficient raster type spatial operations. For spatial modeling and many three-dimensional dynamic engineering applications, octree is a powerful data structure (Samet, 1990; Li, 1992a). It supports compact data storage, efficient Boolean operations, and fast data searching.

Construction of data structures representing regularly shaped objects, which often appear in ocean engineering applications, can be achieved by applying boundary representation (B-rep) and Constructive Solid Geometry (CSG) (Li, 1992a). A successful integration of these data structures will lead to a powerful MGIS.

Dynamic Modeling and Animation

Three-dimensional bathymetric maps provide an efficient way of seafloor visualization. Furthermore, draping sonar images on a digital seafloor model is beneficial for three-dimensional visualization and image interpretation. However, in many cases we need sophisticated three-dimensional dynamic modeling and visualization in order to support applications such as GIS/GPS based real-time navigations, underwater vehicle simulations, and other ocean engineering applications. Successful applications depend on a) a successful selection of three-dimensional data structures to optimize the balance between the data base compactness and operation efficiency, b) corregistration of ocean-related data sets involved, and (c) high performance computers and advanced visualizing systems. Systems fulfilling all three requirements need to be researched.

CONCLUDING REMARKS

In comparison to the land surface of the earth, the seafloor surface has still too much to survey. Ocean mapping will greatly support the increasing extension of human activities from shallow water to deep water areas, and provide first hand data for EEZ exploration, global change monitoring, research in ocean related sciences and others.

Efficient and economic ocean mapping can be achieved by strategic systematic mapping using state-of the-art systems and utilization of available historical data which may be acquired by different institutes using different systems. This requires methods for assessing, processing, and integration of data with different qualities and densities of data distribution. Hardware and software advances in computer graphics provide the possibility of real time ocean related application systems using ocean mapping data. A Marine Geographical Information Systems will be a powerful link between ocean mapping and other disciplines. With a MGIS, the time consuming procedures of conventional ocean mapping would be no longer necessary. Diverse GIS capabilities such data enquiry, spatial modeling, spatial analysis, three-dimensional display, etc. make ocean mapping data more valuable to end users.

ACKNOWLEDGEMENT

Support for the research from USGS, NOAA and the University of Hawaii is gratefully acknowledged.

REFERENCES

ARC/INFO. 1989 and 1991. ARC/INFO User's Guide 5.0 and 6.0. Environmental Systems Research Institute, Inc.

Caswell, D.A. 1992. GIS: The 'big picture' in underwater search operations. *Sea Technology*. February. pp.40-47.

Chavez, P S. 1986. Processing techniques for digital sonar images from GLORIA. Photogrammetric Engineering and Remote Sensing. **52**(8)1133-1145.

Hansen, W.J., V. Goldsmith, and K.C. Clarke. 1992. A marine GIS examines dredging and wetland operations in the New York Bight. Geo Info Systems. April 1992, pp.52-56.

Li, R. 1990. Reconstruction of discontinuous surfaces from digital images by means of area and feature based digital image matching. German Geodetic Commission (DGK), Series C, No.364.

Li, R. 1992a. Generation of object representations of three-dimensional objects in CAD/CAM by digital photogrammetry. *Inter. Archives of Photogrammetry and Remote Sensing*. **XXIX**(714-721).

Li, R. 1992b. Correction of pixel locations of side scan sonar images using bathymetric data acquired separately. *Journal of Marine Geodesy* (in press).

Li, R., and S. Pai. 1991. Improvement of bathymetric data bases by shape from shading technique using side-scan sonar images. In: Proc. IEEE OCEANS'91. pp 320-324.

Reed IV, T.B., and D. Hussong. 1989. Digital image processing techniques for enhancement and classification of SeaMARC II side scan sonar imagery. *Journal of Geophysical Research*. 94(B6):7469-7490.

Samet, H. 1990. The Design and Analysis of Spatial Data Structures. Reading: Addison-Wesley Publishing Company, Inc.

Wavefront. 1991. Advanced Visualizer User's Guide. Wavefront Technologies, Inc. Santa Barbara, CA.

EEZ MAPPING IN CANADA: ADVANCES IN SHALLOW WATER SURVEYING

John E. Hughes Clarke, Larry A. Mayer, and David Wells
University of New Brunswick
Fredericton, New Brunswick, Canada

Gerard Costello
Canadian Hydrographic Service
Dartmouth, Nova Scotia, Canada

Derrick R. Peyton
Geo-Resources Inc.
St. John's, Newfoundland, Canada

ABSTRACT

To meet its needs for coastal and continental shelf surveying, Canada is currently employing a variety of acoustic swath mapping tools capable of working in relatively shallow water. These systems (Navitronics, shipboard and DOLPHIN-mounted EM-100 and EM-1000s) present significantly higher artifact and data volume problems than their corresponding deep-water counterparts.

The operational philosophy behind the deployment of these swath systems reflects the individual system capabilities and the needs of the primary user groups (marine transport and fisheries). Data post-processing and management require that data quality problems (which vary from system to system) be well understood. A "Hydrographic Ground Truthing" experiment is being undertaken, looking at the relative data quality provided by the three acoustic systems currently employed.

INTRODUCTION

Exploration and conservation of EEZ resources have been, and will continue to be, primarily focussed on the continental shelf. Canada, with the longest coastline and one of the largest continental shelves in the world, has critical economic, environmental and strategic interests in more precisely mapping and understanding the vast area of its EEZ.

Although there is a slowly increasing trend towards working in deeper water, the majority of man's interaction with the seabed remains focussed in the waters of the continental shelf and particularily the coastal zone. Only recently have shallow-water acoustic swath systems, capable of providing hydrographic-quality topography and quantitative echo strength data become available. Such systems tend to have a swath width that decreases with water depth and as a result, surveying in shallow water requires a much greater expenditure of ship time. Shallow water systems, nevertheless provide a much greater spatial resolution than their deep-water counterparts resulting in a larger data volume management problem.

Canada, with an unusually large proportion of its EEZ in water depths less than 200 m (the continental shelves, the Artic Island passages and the Great Lakes) has

acquired a number of acoustic swath survey system to address the problem of maximising the efficency of both collection and processing of seabed information.

In order to optimise the existing knowledge-base within Canada, alliances have been formed between government departments, universities and private industries. Two examples of these alliances are the Canadian Ocean Mapping System (COMS) and the NSERC Industrial Chair in Ocean Mapping (Hughes Clarke, et al., 1992). Both these alliances directly address the problems of large-area shallow-water surveying.

In this paper we outline the operational philosophy used for surveying within Canadian waters, the problems associated with this approach and provide examples of the type and quality of data available through implementation of this philosophy.

OPERATIONAL PHILOSOPHY

Multibeam or multitransducer sounders provide the ability to produce high-density narrow-beam sounding without the excessive use of shiptime that would be required with single-beam sounders. Such sounders are usually deployed in such a way that 100+% coverage of the seafloor is obtained. Thus the line spacing will reflect the swath width (usually 80 or 90% of the system coverage).

Because the line spacing required in shallow water is one or more orders of magnitude smaller than that employed in deep water, it is not feasible to undertake a systematic regional coverage program. Priorities, driven by human use and abuse patterns, must first be delineated and those regions of highest priorities given precendence.

The largest users of the Canadian shallow water EEZ are marine transport and the fisheries. As a result safety of navigation (hydrographic quality bathymetry) and surficial seabed lithology (fisheries habitats) are of prime concern.

The choice of acoustic swath system depends upon both the water depth and the operational logistics inherent in the survey location. As a result, shallow water acoustic swath surveying in Canada can be divided into three operational regimes (Figure 1).

Water Depths of 2-15m in Dockside or Estuarine Environments

The system employed for shallowest water is the 200 kHz Navitronics boom sounding system (Burke and Forbes, 1984). As configured on CSS F.G. Smith (Figure 2a), the total swath is 45 m with a total of 36 transducers (there are 14 other Navitronics installations in Canada of which the Smith is the largest). Each beam has a width of 7 degrees (to -3dB points). The Navitronics currently only provides depth information. In water depths greater than 20 m with a beam spacing of 1.4 m the beams overlap. The survey speed of the vessel with booms extended is only about 3 knots and thus the areal extent of coverage is limited. Because the soundings are all based on vertical travel paths, the systems is insensitive to refraction caused by the horizontal stratification in the water column that is so common in coastal and estuarine environmemts. The principal limitiation of the Navitronics system currently is the ambiguity in distinguishing mid water returns (very common at 200kHz) and the true seabed.

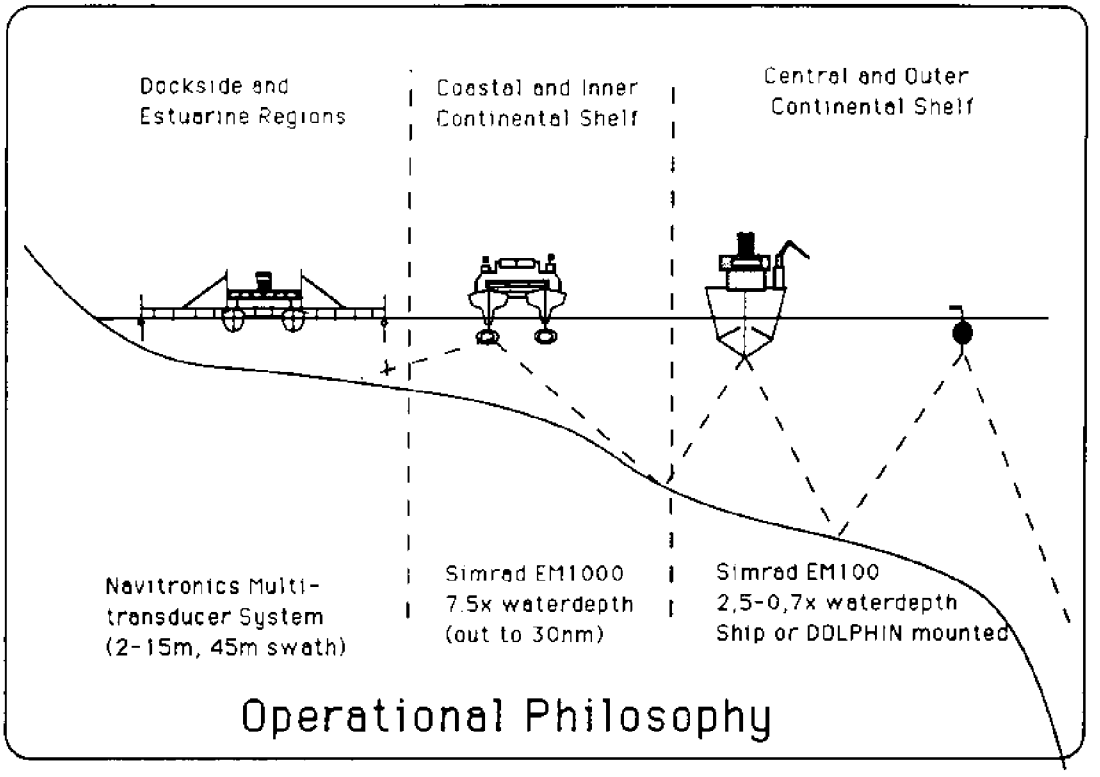

Figure 1. Operational philosophy behind the deployment of acoustic swath systems in Canada

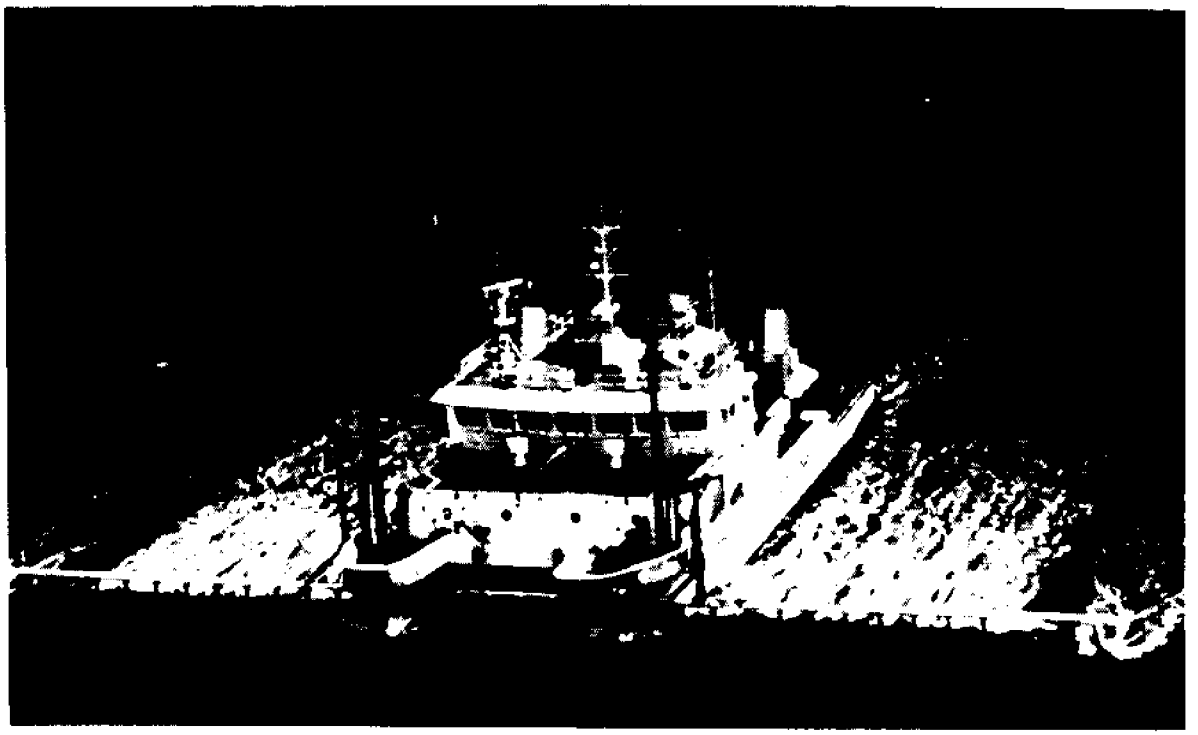

Figure 2a. CSS F.G. Smith with Navitronics boom system deployed

The Middle and Outer Continental Shelf

The middle and outer shelf operations are undertaken using the Simrad EM100 system currently installed on the CSS Matthew (51 m) and until this year, the CSS Lauzier (nm). The EM100 provides 2.4 times water depth up to 150 m, thereafter the swath width reduces to 1.7 times water depth.

Since the beginning of this year the EM100 is also available from the robotic vehicle DOLPHIN. DOLPHIN (Deep-Ocean Logging Platform with Hydrographic Instrumentation and Navigation) is an 7.0 m long diesel powered torpedo-shaped semi-submersible (Figure 2b) which can be controlled through a UHF radio link (Dinn, et al., 1987). As part of the Canadian Ocean Mapping System (COMS, Peyton, 1992b), the DOLPHIN's were fitted with a modified EM100 multibeam sounder and deployed using differential Global Positioning System (DGPS) by Geo-Resources Inc. of Newfoundland (Peyton, 1992a).

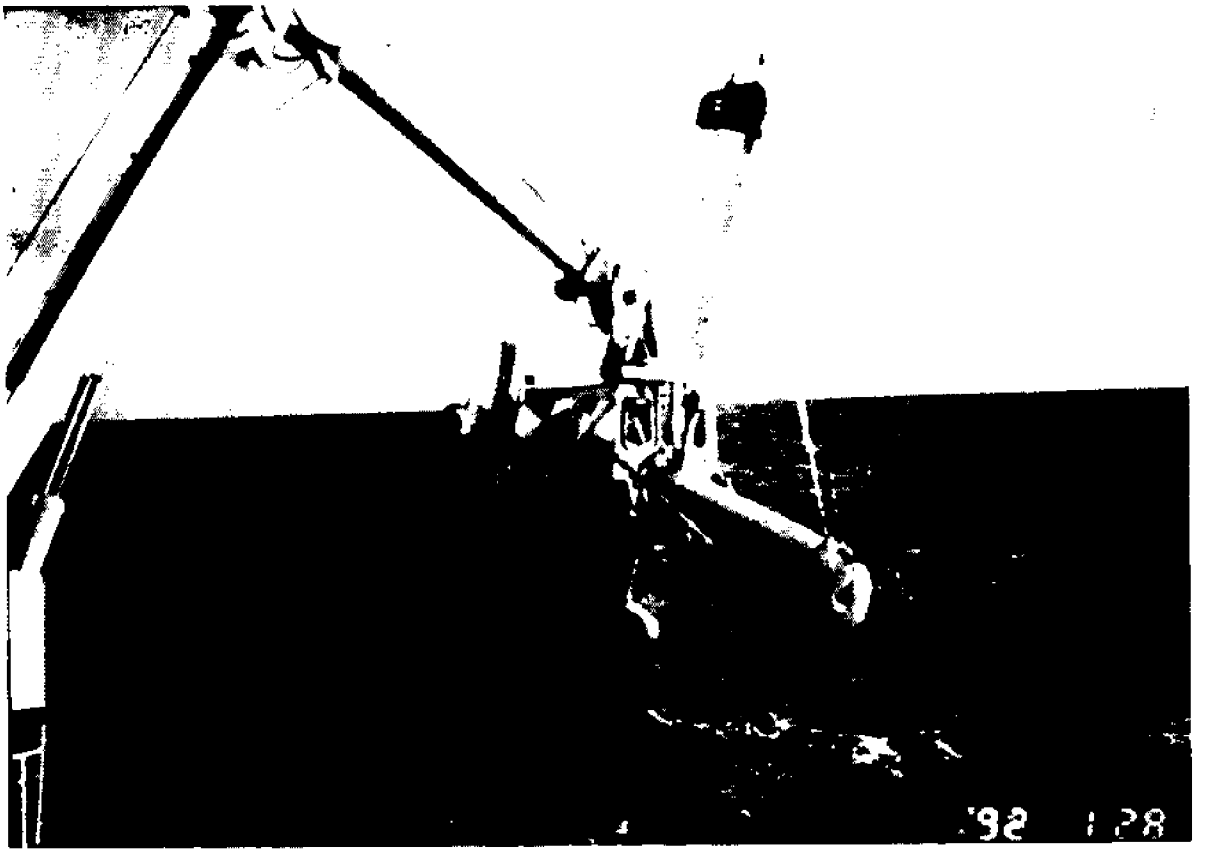

Figure 2b. DOLPHIN and handling system

The DOLPHIN represents an economic method of deploying high resolution multibeam sounders from either a shore station (Figure 3a) or from a mother vessel (Figures 3b,c) in contrast to the cost of purchaseand installation of hull-mounted multibeam sounders which cannot be deployed from ships of opportunity. The maximum economy of using a DOLPHIN occurs when two or more DOLPHINS are deployed at once and either the mother vessel has her own swath system (Figure 3b) or is fully utilised

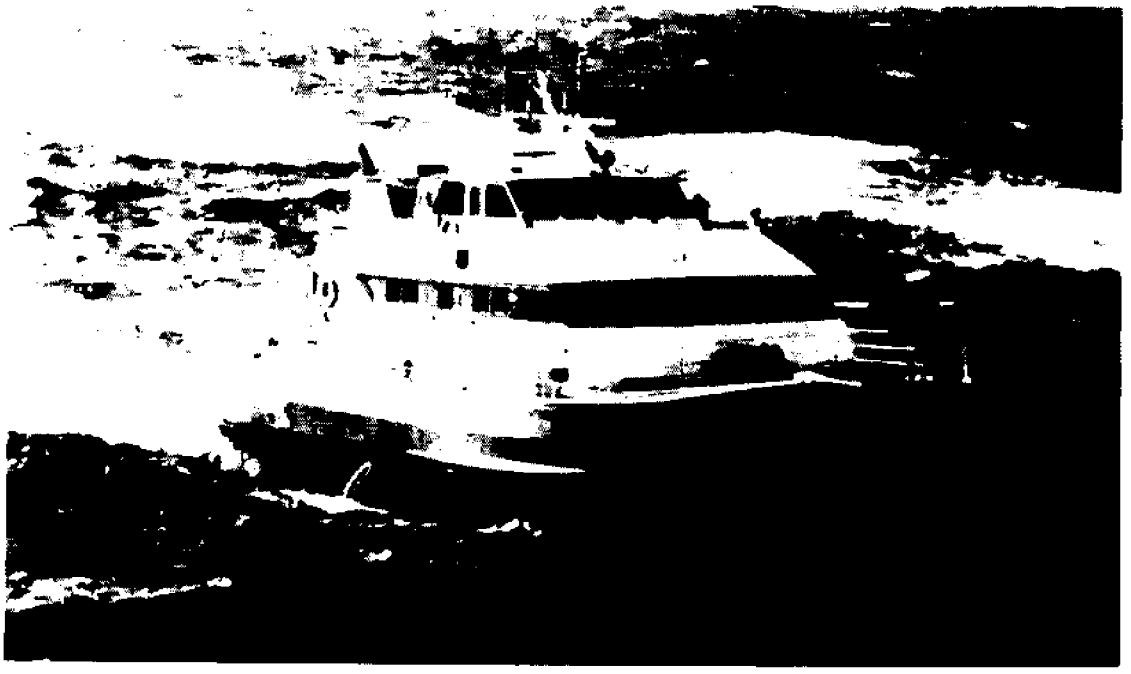

Figure 2c. NSC Frederick G. Creed SWATH vessel underway

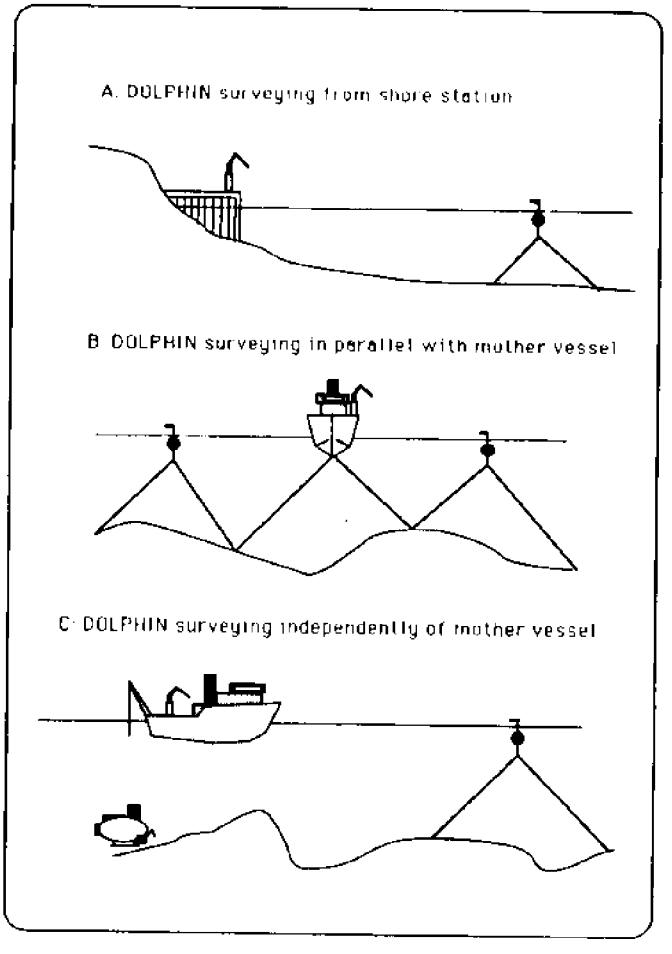

Figure 3. Operational Modes for the COMS DOLPHIN/EM100 System.

a. Shore based deployment (with or without ancillary 10 m survey launch).

b. Deployment in parallel with mother vessel.

c. Deployment independent of mother vessel.

doing other concurrent activities (e.g., bottom sampling or submersible support (Figure 3c)). Using the UHF radio link currently implemented in COMS, the DOLPHINS can work up to a maximum range of 5 km from the shorestation/mother vessel and can run a series of survey lines without direct operator interaction.

The DOLPHINs can operate while collecting hydrographic quality data in higher seastates (up to Seastate 6) than surface vessels configured with the same sounder (Peyton, 1992b). Thus the DOLPHINs are ideally suited for outer continental shelf operations which would otherwise require ocean-going vessels.

Limitations to using the DOLPHIN include operating in areas of high shipping activity and the recovery of the system. To circumvent the first limitation operations can be conducted by installing the DOLPHIN/EM100 data logging gear on a small 10 m long survey launch. A custom shipboard mounted crane (Figure 2b) has been developed to minimise the second limitation and has been field tested in sea states up to 4 with succesful launch and recoverys (Peyton, 1992b). The DOLPHIN has fuel and lubrication for a 24 hour period (at 10 knots) and the recycling time for recovery, fueling, lubrication and redeployment is on the order of 3 hours. Thus a DOLPHIN may be maintained in an operational state for 90 percent of an operation.

Water Depths Greater than 15 m and Within 3 hours Steam of a Port

Until recently, hydrographic surveys carried out in the inner continental shelf (10-50 m) were conducted primarily using single beam echo sounders. The recent development of the EM1000 multibeam sounder by Simrad, has provided an efficent means of collecting very wide swath (7.5 times the water depth) hydrographic quality data.

The EM1000 can be employed with as little as 5 m below the transducer. This system is currently deployed on the SWATH vessel NSC Frederick G. Creed (Figure 2c) and is routinely operated at survey speeds of 16 knots. While the EM1000 is capable of operating to 800 m, the size and berthing of the Creed currently restrict its activities to daily operations. For this reason, the Creed is utilised in coastal and inner shelf environments only.

DATA PROCESSING

In order to handle high volumes of swath bathymetric data, a custom designed commercial software package has been developed for the Canadian Hydrographic Service jointly by the University of New Brunswick and Universal Systems Limited of Fredericton, NB. This system, called HIPS (Hydrographic Information Processing System), relies on the statistical outlier approach developed by Ware, et al. (1991), and incorporates navigational editing and interactive sounding cleaning to produce a tidally-corrected sounding set with a minumum of artifacts. The system then takes the cleaned sounding data into a GIS environment for chart production. The HIPS currently handles Navitronics data, EM100 and EM1000 data and is generic in design so that it can handle any single beam or multibeam data set.

In addition to sounding data both the EM100 and the EM1000 produce information on the strength of the seafloor echo. This data can provide information on seafloor type which in not visible in the bathymetric data. A new processing package has been developed at UNB to provide digital mosaics of the sidescan imagery that is available

from the EM100-1000 series (see Figure 4). For the EM-100, a single amplitude is provided for each of the 32 beams, but for the new EM1000 a calibrated amplitude time series (samples at 0.2 ms intervals) is provided for each of 60 beams totaling up to 4k bytes of data per ping. In order to compile each of the beam amplitude traces into a single sidescan-equivalent (but topographically corrected) image requires a dedicated post-processing toolkit. Recent EM-1000 operations show that is is feasible to both clean the bathymetry and create and digitally mosaic the sidescan data at the same rate as data acquisition, even in the shallowest water depths with ping rates up to 1/4 seconds.

HYDROGRAPHIC GROUND TRUTHING EXPERIMENT

The Hydrographic Ground Truthing Experiment (Wells, et al., 1992) is a three-year strategic grant program, funded by the Canadian National Science and Engineering Research Council (NSERC) which examines the quality and data content of shallow water acoustic swath-map systems. The first phase of this experiment has recently been completed. It involved the acquisition of acoustic swath and subbottom data in both intertidal and subtidal environments in the Bay of Fundy (maximum tidal ranges of 15 m (50 ft)) for comparison to ground truth data collected in the form of aerial photography, CASI imagery, terrestrial topographic surveys, bottom photography and bottom sampling.

While the data has only been recently acquired several new directions appear promising. By independently logging the received echo trace signals for each of the beams within the Navitronics systems, it is apparent that there is the ability to distinguish both in-water echos such as fish or kelp (which show up as a major problem at 200 kHz) and the seabed type from the seabed echo. This would provide a greater degree of confidence in the hydrographic quality of the soundings and a new dimension for seabed classification concurrent with the hydrographic survey.

The Simrad EM1000 swath sounder was deployed for the first time and several capabilities and limitations emerged. The system has a minimum depth capability at approximately 5 m beneath the keel (equivalent to 8 m on the Creed) and this appears to be substrate dependent with improved capability on hard substrates. Offshore in water depths in excess of 25 m the systems performs optimally. Acoustic data was collected from the SWATH vessel at speeds of up to 18 knots. The only apparent degradation in the data was the increased distance alongtrack between soundings.

Because of the remarkably wide swath, the EM1000 system is very sensitive to time lags and/or horizontal accelerations not resolved by the ship motion sensor which produce noticeable roll artifacts in the data. In coastal and especially estuarine waters, the shallow angle of beam forming makes the system extremely sensitive to refraction caused by changes in sound speed in the upper few metres of the water column. Thus the hydrographic quality of the data can be compromised by imperfect knowledge of ship motion and water column structure.

The sidescan imagery from the EM1000 defines sediment boundaries which have no bathymetric expression and thus provides additional useful information. Sediment bedforms with wavelengths as short as 4 m are resolvable in water depths of 80 m. The EM1000 imagery has two advantages over a conventional sidescan: it is corrected for bottom topography; and it is calibrated so that a seafloor type will return the same echo independent of water depth (there is still a grazing angle effect in the data).

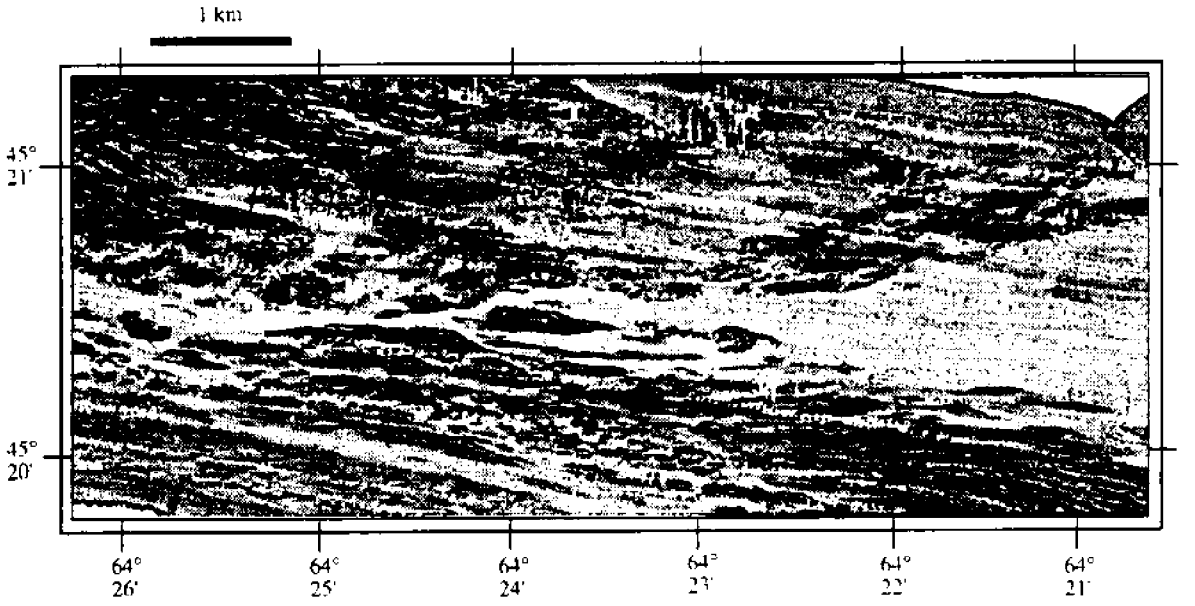

Image A

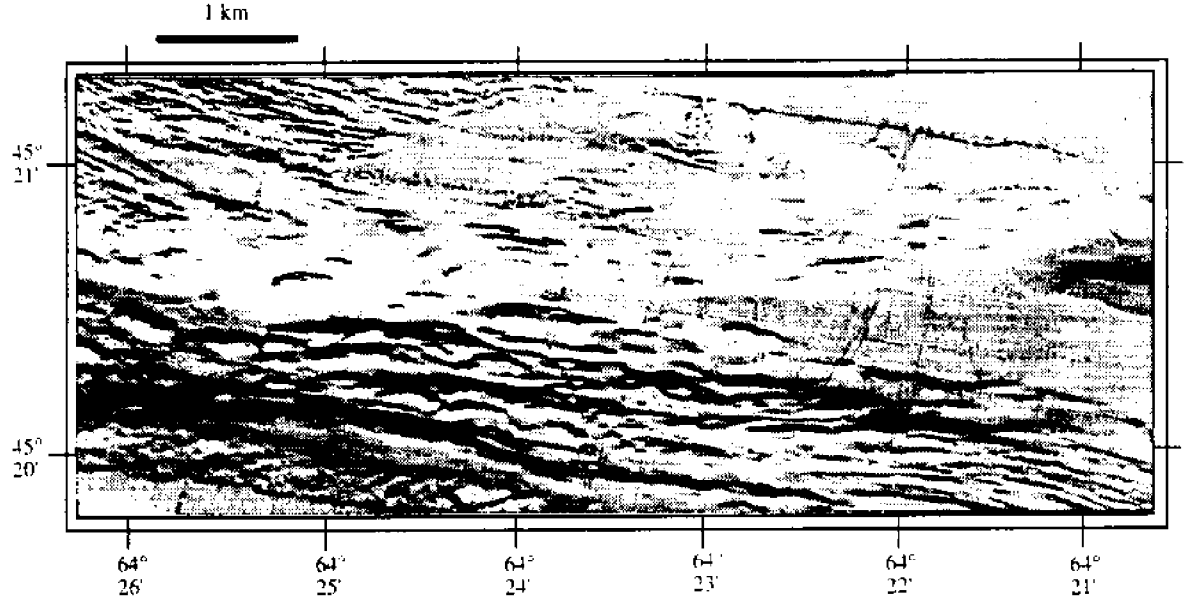

Image B

Figure 4. Example EM1000 data from Minas Channel, Nova Scotia. This data was acquired by the NSC Frederick G. Creed at 16 knots. The image is made up of 12 parallel swaths. The first image (A) shows the sidescan data acquired (loud echos are bright) and the second image (B) shows the sun illuminated topography (illuminated from 190°). Note that the bedrock outcrop is both visible in the sidescan as a change in backscatter, and also resolved by the bathymetry. Water depth varies between 20 and 140m.

CONCLUSIONS

In summary, the choice of acoustic swath system in shallow water depends on the water depth range, the requirements of the survey and the logistics of the operation. Acquisition of high density sounding and echo trace data cannot proceed without adequate data processing. In order to retain the high vertical resolution (decimetres) and detailed horizontal spatial resolution (1-10 m) provided by these new swath systems, the full data content must be maintained. Software, developed in parallel with the acquistion of swath systems in Canada, has attempted to maintain the full integrity of the data.

Continued advances in the capability of shallow water systems will provide end users with the required detailed hydrographic and geologic knowledge of the continental shelf and coastal zone which has previously been unavailable. Such detailed knowledge of the continental shelf and coastal zone is necessary if Canada is to manage effectively its huge Exclusive Economic Zone.

ACKNOWLEDGEMENTS

The recent phase of the Hydrographic Ground Truth project would not have possible without the skill and enthusiasm of the officers and crew of the survey vessels CSS F.G.Smith and NSC Frederick G. Creed and hydrographers Andre Godin and Mike Lamplugh.

REFERENCES

Burke, R.G., and S.R. Forbes. 1984. Vertical acoustic sweep systems - a 'new broom in the closet' for the Canadian Hydrographic Service. In: NOS Hydrographic Service '84, pp. 50-58. Rockville, Maryland.

Dinn, D.F., R.G.Burke, G.D. Steeves, and A.D. Parsons. 1987. Hydrographic instrumentation and software for the remotely controlled survey vehicle DOLPHIN. In: Proceedings of the IEEE/MTS Oceans '87 Conference, v.2, p.601-607.

Hughes Clarke, J.E., G. Costello, L. Mayer, and D. Wells. 1992. Ocean mapping: a Canadian perspective. In: 1991 Exclusive Economic Zone Symposium Proceedings. U.S. Geological Survey Circular 1092, pp. 20-28.

Peyton, D.R. 1992a. Using GPS and ROV's to map the ocean. *GPS World*. January :40-44.

Peyton D.R. 1992b. The DOLPHIN/EM100 ocean mapping system. *The Hydrographic Journal*. **65**:5-9.

Ware, C., W. Knight, and D. Wells. 1991. Memory intensive statistical algorithms for multibeam bathymetric data. *Computers and Geoscience*. **17**:985-993.

Wells, D., L. Mayer, and J.E. Hughes Clarke. 1991. Ocean mapping: from where? to what? *Jour. Canadian Institute of Surveying and Mapping*. **45**:505-518.

BOTTOM CLASSIFICATION USING MULTIBEAM SONAR SYSTEMS

Lawrence J. Fusillo
Computer Sciences Corporation
Huntingdon Valley, Pennsylvania, U.S.A.

John H. Satriano
Naval Command and Control and Ocean Surveillance Center
Warminster, Pennsylvania, U.S.A.

ABSTRACT

Experimental studies in different regions of the oceans have shown that sound backscatter is determined by the paramaters of the sediment only (not relief) at frequencies below 2.5 Khz. At frequencies above 2.5 Khz, both bottom sediment composition and bottom relief play significant roles. A method is presented in this paper to predict backscatter strength from core sample data so that multibeam sonar backscatter data can be used together with synthetic core sample data to both determine sediment boundaries and to determine appropriate weighting functions for interpolation of geological data parameters between core sample locations.

Acoustic Classification

The scattering of sound by the bottom in the "backward" direction has been described theoretically (Brekhovshikikh & Lysanov, 1982). Modern data are expressed in terms of "backscatter strength S", defined as:

$$S = (Iscat/A) / Iinc \qquad \text{in } 1/m2$$

where: Iscat = intensity of sound back-scattered from area A
A = acoustic spot size on the bottom in m2
= c*pulse width/2*cos(thetao)) * 2*depth*sin (beamwidth/2)
Iinc = incident sound intensity at the bottom in uPa//lm

Experimental studies in different regions of the oceans have shown that sound backscatter is determined by the paramaters of the sediment only (not relief) at frequencies below 2.5 Khz. At frequencies above 2.5 Khz, both bottom sediment composition and bottom relief play significant roles.

Backscatter can be considered as a superposition of 3 independent curves. The first curve is dependent on sediment composition only, the second curve is dependent on small scale bottom relief roughness, and the third curve is dependent on large scale bottom roughness.

While sediment sound speed is obtainable from core sample geology, roughness and interface roughness between sub-bottom sediment layers are not.

Thus, core sample data yields a family of backscatter curves dependent on bottom roughness. When the bottom is perfectly flat, then the family of curves reduces to a single "smooth bottom" backscatter curve.

For a totally smooth bottom, backscatter effects are due to sediment composition only. Table 1 shows backscatter strength as a function of sediment composition. The texture, density, and sound speed data in the table are from (Hamilton, 1980) and (Hamilton, 1974). The first curve which models the effects of sediment only is defined by the Mackenzie equation (Mackenzie, 1961). The curve shape is given by:

Mackenzie	= b2 * cos(grazing) ** a	in dB/m2
S3	= 10**(Mackenzie/10.)	in 1/m2

where: a	= log10(b1/b2)/log10(cos(89.99))	
b1	= 10*log10[(Z2-Z1)/(Z2+Z1)] + diffusivity	
b2	= -45. + 1.95*lgs -(lgs-10)*brt1	calcareous
b2	= -46. + 2.00*lgs -(lgs-10)*brt1	slope/shelf/hill
b2	= -47. + 2.05*lgs -(lgs-10)*brt1	diatom
lgs	= log2[grain size um]	
brt1	= grain size sdev / grain size	
grazing	= bottom grazing angle in degrees	
Zi	= ci*di	
ci	= layer i sound speed, di = layer i density	
diffusivity	= -2*sqrt(brt1)	for lgs < 1
	= -2*sqrt(brt1*lgs)	for lgs > 1

Maximum backscatter strength b1 occurs at 90 degrees grazing and is determined from density and sound speed measurements from core sample data.

Between 4 and 0 degrees grazing angle, backscatter strength approaches a minimum b2. Unlike the maximum backscatter strength, this value is frequency dependent. A perfectly flat bottom never actually occurs on the ocean floor. There is always some small amount of roughness associated with a smooth ocean bottom which interacts with the acoustic frequency. Minimum values for backscatter strength are available (Urick, 1983) as a function of sand, silt, clay, and sand-rock mixtures at frequencies ranging from 10 Hz to 300KHz. The frequency dependence was determined to be:

b2(f) = b2(12 KHz) + 2.0*log10[(f+1)/13]*(2+log2[grain size]/2)	f<12 KHz
b2(f) = b2(12 KHz) + 1.5*log10[(f+1)/13]*(13-log2[grain size]/2)	f>12 KHz

where: f = sound frequency in KHz, grain size is in micrometers (um)

The second curve accounts for small scale bottom roughness. In wave-scattering theory (Brekhovskikh,1982), the vertical scale of roughness is usually specified by the "Rayleigh parameter"

$$P=2*k*sigma*\cos(thetao)$$

where: P =	Rayleigh parameter
k =	wave number of sound = 2*Pi*f/c
thetao =	angle of incidence of the sound plane wave
sigma =	root-mean-square displacement of the rough surface from its mean level

At P<<1, the roughness of the surface is acoustically "smooth", and the surface scatters sound slightly, with the main part of the energy specularly reflected as a coherent wave. At P>>1, the surface is acoustically rough and the surface scatters sound

Table 1. Bottom sediment texture backscatter

Texture	Grain Size (um)	Density do g/cm3	Sound Speed co km/sec	Impedance zo=do*co	Backscatter Minimum dB/m2	Backscatter Maximum dB/m2
Rock Quartz	-	2.80	7.500	21.00	-8.00	-0.62
Rock Calcite	-	2.80	7.000	19.60	-	-0.68
Rock Basalt	-	2.80	5.700	15.96	-	-0.82
Rock Shale	-	2.80	5.000	14.00	-	-0.93
Rock Sandstone	-	2.50	5.200	13.00	-	-1.01
Rock Dolomite/Basalt	-	2.50	4.600	11.50	-	-1.14
Rock Shale	-	2.50	3.700	9.25	-	-1.42
Rock Chert	-	2.30	4.300	9.89	-	-1.33
Rock Basalt	-	2.30	4.000	9.20	-	-1.43
Rock Limestone	-	2.30	2.900	6.67	-	-1.99
Rock Shale	-	2.30	2.500	5.75	-	-2.32
Course Sand (shelf/slope)	528.5	2.03	1.836	3.73	-27.91	-3.70
Medium Sand (shelf/slope)	-	1.98	1.742	3.45	-	-4.05
Fine Sand (shelf/slope)	159.3	1.94	1.749	3.39	-31.37	-4.13
Powder Sand (shelf/slope)	-	1.91	1.711	3.27	-	-4.30
Powder Sand (shelf/slope)	96.0	1.86	1.702	3.16	-32.83	-4.48
Silty Sand (shelf/slope)	-	1.83	1.677	3.07	-	-4.37
Silty Sand (shelf/slope)	49.0	1.77	1.646	2.92	-34.77	-4.93
Sandy Silt (shelf/slope)	30.8	1.76	1.652	2.90	-36.11	-4.97
Silt (shelf/slope)	23.7	1.74	1.615	2.81	-36.87	-5.17
Silt (shelf/slope)	-	1.58	1.578	2.49	-	-6.05
Sand-Silt-Clay(shelf/slope)	-	1.56	1.552	2.42	-	-6.30
Sand-Silt-Clay(diatom)	17.9	1.45	1.546	2.24	-38.68	-7.04
Sand-Silt-Clay(shelf/slope)	17.2	1.60	1.579	2.53	-37.74	-5.92
Clayey Silt (shelf/slope)	7.7	1.49	1.549	2.31	-40.11	-6.72
Clayey Silt (hill)	5.6	1.35	1.522	2.05	-41.03	-8.10
Clayey Silt (plain)	5.2	1.45	1.528	2.22	-41.24	-7.13
Clayey Silt (shelf/slope)	-	1.43	1.535	2.20	-	-7.23
Clayey Silt (diatom)	4.9	1.23	1.534	1.89	-42.42	-9.39
Silty Clay (shelf/slope)	2.7	1.42	1.520	2.16	-43.13	-7.44
Silty Clay (plain)	-	1.38	1.535	2.12	-	-7.66
Silty Clay (plain)	2.1	1.35	1.515	2.05	-43.86	-8.10
Silty Clay (diatom)	2.4	1.22	1.525	1.86	-44.47	-9.70
Silty Clay (hill)	-	1.37	1.507	2.06	-	-8.03
Silty Clay (hill)	2.3	1.34	1.508	2.03	-43.60	-8.23
Medium Clay (calcareous)	1.5	1.44	1.556	2.23	-43.83	-7.08
Medium Clay (hill)	1.5	1.41	1.493	2.11	-44.83	-7.72
Medium Clay (plain)	1.4	1.35	1.503	2.03	-45.03	-8.23
Medium Clay (plain)	-	1.26	1.505	1.90	-	-9.24
Ooze (calcareous)	.6	1.40	1.536	2.15	-46.47	-7.49

Maximum Backscatter = $10*\log10[(zo-1.5)/(zo+1.5)]$

Minimum Backscatter = $-46 + 2*\log2[\text{grain size um}]$ shelf/slope/plain
(12 KHz) = $-45 + 1.95*\log2[\text{grain size um}]$ calcareous
= $-47 + 2.05*\log2[\text{grain size um}]$ diatom

in a diffuse manner in a wide angular interval. If sigma is small, then the scattering sound field can be calculated by the Method of Small Perturbation (MSP) (Brekhovskikh & Lysanov, 1982). In this case the problem of wave scattering is reduced to the problem of radiation by a distribution of "virtual" sound sources. For scattering and backscattering where theta = thetao,

S1(theta) = 4 *[k*cos(theta)]**2 *[k*cos(thetao)]**2 *G(x)

where: G(x) = (1/Pi) * (grain size sdev/grain size)**2

To obtain S1 for the backscatter case, we assume the effect of the large-scale underlying changes consists in changing the local angles at which the small-scale roughness is insonified. Setting theta = thetao for backscatter and normalizing the equation for S1 so that it is equal to the maximum backscatter strength when thetao = 0;

S1(thetao) = Vmax * cos(thetao)**4 * G(x)

where: Vmax = maximum backscatter = 10**(b1/10.) in 1/m2

In the above equation the spatial spectrum of small scale isotropic ripple G(x) ranges from 0 to 1. Thus the value for S1 small scale backscatter can never exceed the theoretical Vmax.

The third curve accounts for large scale bottom roughness. The MSP method is only applicable for the case of a small Rayleigh parameter P. However, the roughness amplitude of the ocean bottom is frequently much greater than the sonar sound wavelength and the Rayleigh parameter is large. In these cases, the Method of Tangent Plane (MTP), also known as the Kirchoff approximation, can be used. The tangent plane method yields good results only for those directions of scattering which are close to directions of specular reflection. When both scales of roughness are present we use a method which is the combination of MSP and MTP. It is based on the assumption that the roughness can be divided into two components a small scale component and a large scale one. We obtain the two-scale rough bottom model by superimposing the surface with the small scale displacement upon the surface with a large scale displacement. The scattering coefficent is represented in the form:

S = S1 + S2 + S3

where:
S1 = small scale roughness scattering calculated from MSP
S2 = large scale roughness scattering calculated from MTP
S3 = impedance scattering calculated from MacKenzie

To obtain S2, we assume that the slopes of the large waves are isotropic and normally distributed. In this case;

$$S2 = \frac{V^{**}2 * \exp[-\tan(thetao)^{**}2/(2*slope^{**}2)]}{(8*Pi*slope^{**}2*\cos(thetao)^{**}4)}$$

where: V = reflection coefficient
slope = brt2/2, brt2 = relief height ft / relief period ft

Normalizing the equation for S2 so that large scale backscatter never exceeds the theoretical maximum backscatter strength Vmax:

$$S2 = Vmax^{**}2*\exp[-\tan(thetao)^{**}2/(2*slope^{**}2)] / \cos(thetao)^{**}4$$

Using Core Samples to Predict Backscatter Strength

The scattering strength S1 is considerably less than S2 for small incident angles. At angles > 45 degrees, S1 is greater than S2. Thus, large scale effects dominate at small angles of incidence (large grazing angles) while small scale effects dominate at large angles of incidence (small grazing angles). Figure 1 was generated using the Mackenzie equation for S3 only. Figure 2 was generated using the S1 MSP equation for small scale bottom roughness. Figure 3 was generated using the S2 MTP equation for large scale bottom roughness. Figure 4 shows an example of hybrid set of curves where both small scale and large scale bottom roughness were present.

Most geoacoustic provinces have a sub-bottom basement of solid rock. The sub-bottom basement acts as a reflector, adding a second backscatter curve to the one produced at the water-sediment interface. Even when there is no sub-bottom basement, there are usually 2-5 sediment layers of distinctly different sediment. The interfaces between sediment layers also act as reflectors, multiplying the number of the backscatter curves. In general the additional layer reflectors induce large fluctuations in measured backscatter strength causing ambiguities in classification. In addition, significant changes in sediment composition cause very small changes (0.1 to 0.2 dB) in received backscatter strength.

To eliminate ambiguities in acoustic classification, a vertical profile of the bottom sediment layers must be obtained from core samples from which sound speed can be derived. Even when acoustic sub-bottom profile measurements are available, core samples are needed to identify the correct depth of sediment layers. Acoustic sub-bottom profilers measure impedance which in itself is ambiguous in density and sound speed.

Horizontal and vertical ambiguities in acoustic backscatter province boundaries can best be resolved by statistical models which combine core sample geology and sonar backscatter acoustic measurements into sediment classes such as those proposed in Table 2. In Table 2, the impedance zo is normalized for a water sound speed of 1500 meters/sec. Impedance Z in Table 2 is obtained using thetao = 0.

Table 2 shows that impedances and hence backscatter strengths are ambiguous with respect to texture types. Therefore the geological composition must be known to break the ambiguities. The geological composition is referred to in Table 2 as petrology. Petrologies are based on lattice structure as well as differing amounts of CaCO, CaO3, SiO2, Al2O3, Fe2O3, FeO, MgO and CO2.

The terrigenous/calcareous petrology in Table 2 includes shale, oolites and ostracods. The turbidite/calcareous petrology in Table 2 include petropods and globerina. Monocite quartz has a density of 2.65 and should be grouped under the greywacke petrology which has a density of 2.7. Diocite quartz has a density from 2.8-3.0 gm/cm3. Limestone and chalk are the only petrologies with significant amounts of CO2 (41.5% by weight). Siliceous petrologies contain predominately SiO2 (48.8-89.9% by weight). Calcareous petrologies contain predominately CaCO and CaCO3 (42.6-60.0% by weight). Calcite is 99.9% CaCO3 at a density of 2.6-2.7 gm/cm3.

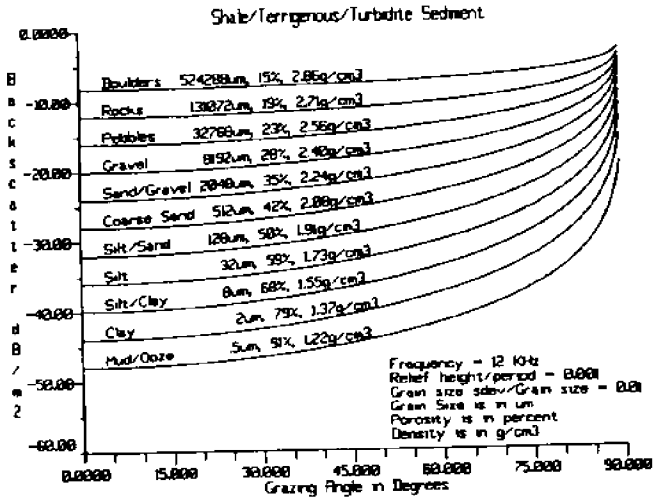

Figure 1. Backscatter strength at 12 KHz due to sediment composition alone

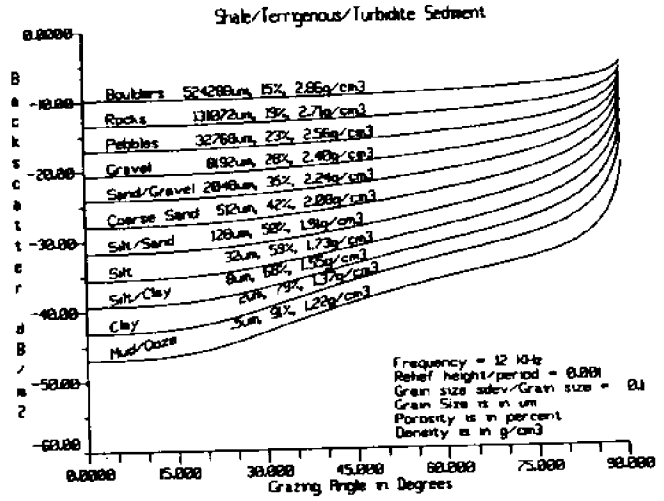

Figure 2. Backscatter strength at 12 KHz due to sediment composition and small scale bottom roughness

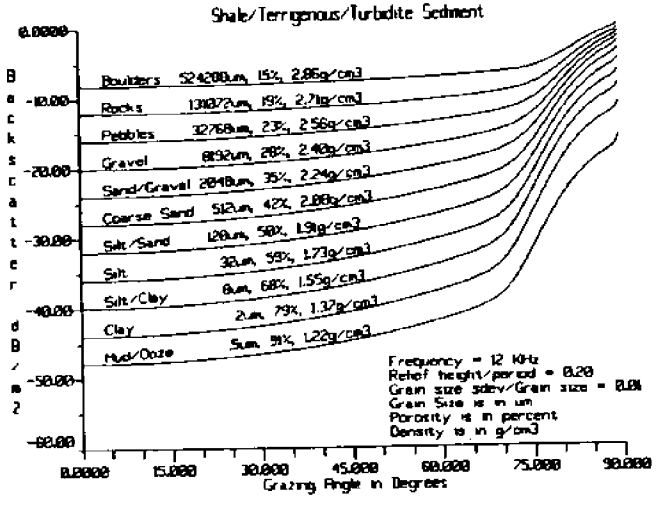

Figure 3. Backscatter strength at 12 KHz due to sediment composition and large scale bottom roughness

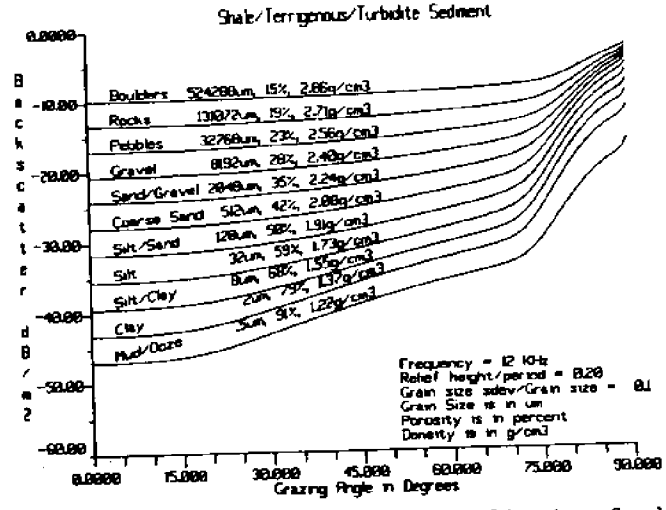

Figure 4. Backscatter strength due to a combination of sediment composition and small and large scale roughness

Backscatter Depth Dependence

The impedances shown in Table 2 are under atmospheric pressure. Sub-bottom sediment impedances are larger than those in Table 2 because of increased pressure which is dependent on the depth below the water-bottom interface and the type of material directly above. Sub-bottom density corrections are given by Hamilton (1980). While backscatter strength will be increased due to increasing pressure in sub-bottom sediments, it will be reduced by bottom sediment attenuation (Hamilton, 1980).

Synthetic core sample backscatter can be made to match sidescan sonar backscatter and sonar sub-bottom profiler backscatter measurements where core sample and sonar measurements are co-located. For sidescan sonar the first 20 meters of sediment must be defined using core samples. For acoustic sub-bottom profilers, the first 200 meters of sediment must be defined using core samples. If possible, it is prudent to define the sediment vertical structure down to the rock basement. The depth dependence of density di in layer i is given by:

$$di = do + depth\_km*1.2*pi \qquad gm/cm3$$

where:	do =	dmin	Quartz/Sandstone/Chert/Diatom/Radiolarite
	do =	dmax	Calcite/Limestone/Chalk/Calcareous
	do =	dmin + .4*(dmax-dmin)	Basalt/Siliceous
	do =	dmin + .6*(dmax-dmin)	Shale/Terrigenous/Turbidite
	dmin =	1.08 + .12*lgs -.0015*lgs**2	for lgs > 0
	dmin =	1.08 + lgs/40	for lgs < 0
	dmax =	1.40 + .078*lgs	

The depth dependence of porosity pi in layer i is given by:

pi = po	for	po < .2
= po + depth_m*(.2-po)/1500	for	.2 < po < .5
= po + depth_m*(-po)/2500	for	po > .5

where:	po =	(pmax - pct*(pmax-pmin) / 100
	pct =	(do-dmin)/(dmax-dmin)
	pmin =	76. -5.00*lgs + .095*lgs**2
	pmax =	98. -7.07*lgs + .144*lgs**2

The depth dependence of sound speed ci in km/sec is given by:

ci = co + (cw-1.5)*po + depth_km*1.4	Calcareous Sediment
ci = co + (cw-1.5)*po + depth_km*0.9	Terrigenous Sediment
ci = co + (cw-1.5)*po + depth_km*0.7	Siliceous Sediment
ci =(co + (cw-1.5)*po)*(depth_m+1)**.015	All Sands

where: co = -.22624253E2 +.97909041E2*do -.16198329E3*do**2
+.13964808E3*do**3 -.66050550E2*do**4 +.16211755E2*do**5
-.16027792E1*do**6
for Shale/Terrigenous/Turbidite Sediment

co = -.15243114E2 +.56831913E3*do -.85824340E3*do**2
+.67838306E3*do**3 -.29583282E3*do**4 +.67405383E3*do**5
-.62509400E1*do**6
for Calcite/Dolomite/Limestone/Chalk/Calcareous Sediment

Table 2. Bottom sediment classifications

Texture	Petrology	Grain Size um	Density do gm/cm3	Sound Speed km/sec	Impedance zo =do*co	Color Assignment
Rock	Lava Flow	4194300-	3.0-2.8	5.8-5.0	17.4-14.0	Grey
Rock	Shale/Basalt	524288		7.0-5.8	21.0-16.2	Midnight
Rock	Calcite			8.0-7.0	24.0-19.6	Slate
Rock	Quartz			8.5-7.5	25.5-21.0	BlueGrey
Cobbles	Shale	370728-	2.8-2.6	5.0-4.0	14.0-10.4	RedOrchid
Cobbles	Basalt	131072		5.7-4.9	16.0-12.7	Thistle
Cobbles	Calcite			7.0-5.5	19.6-14.3	Orchid
Cobbles	Greywacke			7.5-5.8	21.0-15.1	Plum
Pebbles	Shale	65536-23170	2.6-2.4	4.0-2.9	10.4-7.0	Coral
Pebbles	Basalt			4.9-4.3	12.8-10.3	Orange
Pebbles	Dolomite			5.5-3.7	14.3-8.9	IndianRed
Pebbles	Sandstone			5.8-4.7	15.1-6.5	Lavender
Gravel	Shale	16384-6888	2.4-2.3	2.9-2.5	7.0-5.7	Salmon
Gravel	Limestone			3.7-2.9	8.9-6.6	BrickRed
Gravel	Basalt			4.3-4.0	10.3-9.2	SmokeRed
Gravel	Chert			4.7-4.3	11.3-9.9	RedGrey
Granules	Shale	5793-3444	2.3-2.2	2.5-2.2	5.8-4.8	Sienna
Granules	Chalk			2.9-2.4	6.7-5.3	Copper
Granules	Basalt			4.0-3.8	9.2-8.3	Burgundy
Granules	Chert			4.3-3.7	9.9-8.1	IndianBrown
Coarse Sand	Shale	2896-528	2.2-2.1	2.2-2.0	4.9-4.2	Goldenrod
Coarse Sand	Chalk			2.4-2.1	5.3-4.4	Tan
Coarse Sand	Basalt			3.8-3.5	8.4-7.3	Wheat
Coarse Sand	Chert			3.7-3.3	8.2-6.9	Khaki
Sand	Shale	380-96	2.1-2.0	2.0-1.8	4.2-3.6	Gold
Sand	Chalk			2.1-1.9	4.4-3.8	Pea
Sand	Basalt			3.5-3.3	7.4-6.6	Mud
Sand	Chert			3.3-2.8	7.0-5.6	Yellow
Silty Sand	Terrig/Calc	72-40	2.0-1.75	1.9-1.65	3.8-2.9	Brown
Silty Sand	Diatomite			2.8-2.3	5.6-4.0	Bronze
Sandy Silt	Terrig/Calc	39-30	1.75-1.65	1.65-1.57	2.9-2.6	Olive
Sandy Silt	Diatomite			2.3-2.1	4.0-3.4	Green
Silt	Turbid/Calc	29-20	1.65-1.5	1.57-1.55	2.6-2.3	Lime
Silt	Radiolarite			2.1-1.9	3.5-2.8	Marine
Sand-Silt-Clay	Turbid/Calc	19-10	1.5-1.3	1.55-1.53	2.4-2.0	SeaGrey
Sand-Silt-Clay	BioSiliceous			1.9-1.7	2.9-2.2	GreenGrey
Silt-Clay	Turbid/Calc	10- 2	1.3-1.2	1.53-1.52	2.0-1.8	Cornflower
Silt-Clay	Siliceous			1.7-1.6	2.2-1.9	Violet
Mud	Turbid/Calc	2- 1	1.2-1.06	1.52-1.505	1.8-1.6	NavyBlue
Mud	Siliceous			1.6-1.52	1.9-1.7	MotifBlue

co = .12202029E3 -.43917458E3*do +.64898987E3*do**2
-.49815530E3*do**3 +.20966730E3*do**4 -.45860080E2*do**5
+.40838129E1*do**6
for Quartz/Sandstone/Chert/Diatom/Radiolarite Sediment

co = .17753047E2 -.80645998E2*do +.15048633E3*do**2
-.13923871E3*do**3 +.68300461E2*do**4 -.16884488E2*do**5
+.16565830E1*do**6
for Basalt/Siliceous Sediment

cw = water sound speed in km/sec at the water/sediment interface

Calcareous sediments include calcite, dolomite, limestone, chalk, and calcareous silts, clays, and muds. Terrigenous sediments include shale, terrigenous silts and turbidite silts and clays. Siliceous sediments include the remainder of petrologies in Table 2.

Boundary Classification using Sonar Backscatter

Accumulation of large numbers of core samples has made it possible to map geological provinces in the ocean. However, the core samples are still too sparsely positioned to provide precise boundary definitions between ocean bottom provinces. Multibeam Sidescan data (Satriano & Fusillo, 1991) can be used as a means of determining the precise location of surface sediment boundaries in latitude and longitude. Subbottom boundaries may then be inferred through the use of statistical correlation models.

The correlation of Multibeam Sidescan acoustic measurement data with archival core sample geological data can be performed in real time during survey operations. A Grey Level Coherence Matrix (GLCM) Algorithm developed at the Hawaii Institute of Geophysics (Reed, 1989) has the capability of using synthetic core sample backscatter as "low resolution background" data and merging "high resolution sidescan" data from multibeam sonars. Six geophysical texture measures are extracted from high resolution sonar backscatter data using GLCM: (1) Texture Angular Second Moment, (2) Texture Contrast, (3) Texture Entropy, (4) Texture Angular Inverse Difference Moment, (5) Texture Correlation, and (6) Texture Isotropy. These measures have been shown to be insensitive to variations in look direction or gain settings and thus are correlated with sediment type and bottom roughness. The goal for future investigations is to use these sonar backscatter measures together with core sample ground truth to distinguish the 40 different sedimentary bottom types in Table 2 with greater than 95% confidence.

CONCLUSIONS

Peak backscatter strength, backscatter curve shape, and minimum backscatter strength produce ambiguities when attempting to determine sediment granularity, density, and porosity using sidescan sonars. Sidescan can only infer gross differences between high backscatter (rock) and low backscatter (sand-silt-mud sediment).

Accumulation of large numbers of core samples (over 700,000 worldwide) has made it possible to resolve bottom sediment province boundaries in the ocean to within 10-60 nautical miles. Sidescan backscatter measurements could be used to improve province boundary resolution to .1 nautical miles. In addition, sidescan backscatter provides a means to measure fine changes in sediment composition when core samples are

available to break impedance ambiguities. In effect, sidescan backscatter provides a weighting function for sediment texture interpolation between core sample locations.

REFERENCES

Brekhovskikh, L., and Y. Lysanov. 1982. Fundamentals of Ocean Acoustics. New York: Springer-Verlag.

Fusillo, L., and J. Satriano. 1991. Ocean bottom imagery with multibeam sonar systems. In: Proceedings of the Marine Technology Society. October.

Hamilton, E. 1974. Geoacoustic models of the sea floor. In: Physics of Sound in Marine Sediments. New York: Pelnum Press.

Hamilton, E. 1980. Geoacoustic modeling of the sea floor. *J. Acoust. Soc. Am.* **68**:1313-1341.

Mackenzie, K. 1961. Bottom reverberation for 530 & 1030cps sound in deep water. *J. Acoust. Soc. Am.* **33**:1498-1504.

Reed, T., and D. Hussong. 1989. Digital image processing techniques for enhancement and classification of SeaMARC II side scan sonar imagery. *J. Geophys. Res.* **94**:7469-7490.

Urick, R. 1983. Principles of Underwater Sound. New York: McGraw Hill.

AN OVERVIEW OF OCEAN SENSING INFORMATION MODELS

Ai-Nai Ma
Peking University
Beijing, China

ABSTRACT

Recently research in applications of remote sensing from space has been developed using Remote Sensing Information Models (RSIM) and presented at the ISPRS Commission IV Symposium, held in Tsukuba, Japan (Ma, 1990a).

What is the new concept of Remote Sensing Information Models? As well known, remote sensing data which include digital tapes and images are only information of earth objects but not earth objects themselves. Therefore, remote sensing data is a part of the field of the information science. There is a long history since three-dimensional terrain models have appeared. There are physical models which have existed in the laboratory such as a river bed model, a soil erosion model, and a debris flow model, and mathematical models which are information models. However, the RSIM differs from physical models and mathematical models.

The RSIM has analytic geometry similar rules and physical simulated rules. Especially, according to physical simulated rules we could build Ocean Remote Sensing Information Models (ORSIM), such as ORSIM of sea surface temperature, ORSIM of sea surface thermal inertia, ORSIM of sea surface thermal diffusion and ORSIM of sea surface concentration of suspended sediment.

This paper discusses existing and future Ocean Remote Sensing Information Models. Particularly, we discuss the future application of NOAA data in ORSIM, ERS data for three-dimensional ORSIM of sea temperature, ORSIM of wave height with microwave, ORSIM of wind speed with microwave, etc., in China.

GENERAL CONCEPTS

Up to now, modern oceanographical methods differ greatly from classical oceanographical methods. A comparison of these methods are shown in Figure 1.

From Figure 1 we find that Ocean Remote Sensing Information Models (ORSIM) are linked to Image Base (IB) and with Graphics Base (GB), while Ocean-Code Models (OCM) are linked to Attribute Base (AB) and Knowledge Base (KB). This method has been implemented into a P.C. 386 system and developed using C language. It was called the Micro-computer Geographical Expert System (CGES). Since MCGES was used as a tool in oceanography, its name has been changed to Micro-computer Oceanographical Expert System (MCOES).

This paper concentrates on the issue of Ocean Remote Sensing Information Models, an important part of the MCOES. Remote sensing data including digital tapes and images (e.g., NOAA or ERS satellite data) are information of sea surface objects. Processing of these digital tapes or images could be accomplished information science. In general, models are simplified form of natural objects. Since the application of three-

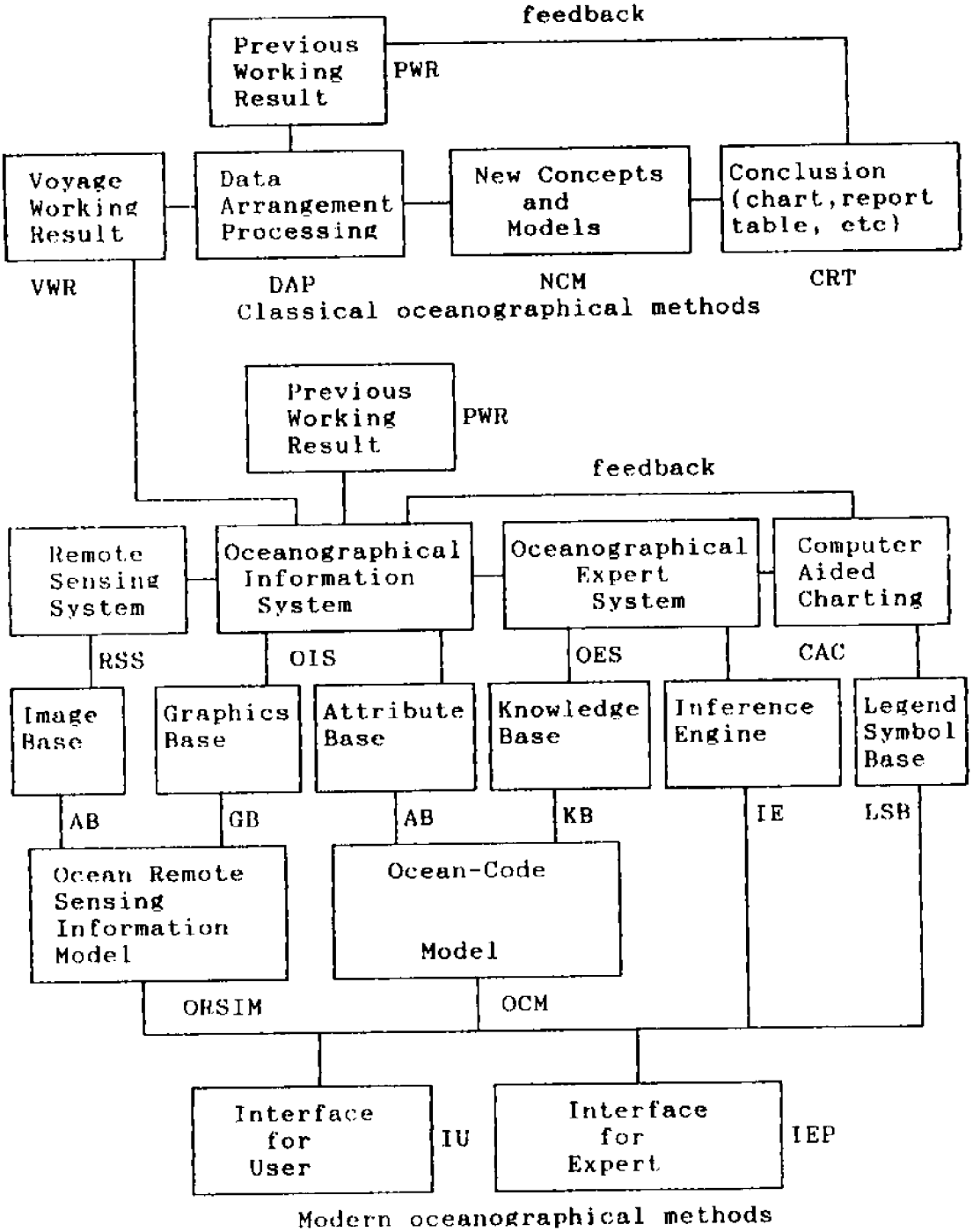

Figure 1. Comparison between classical and modern methods (Ma and Zhou, 1992)

dimensional terrain models, there has been a long history of modeling. There are physical models and mathematic objects, such as river bed models, soil erosion models, estuary models, coast zone models, harbor models, etc. The mathematic models are computer-based information models, such as math models for erosion and sedimentation of coast zone or estuary. ORSIM can be established by applying physical principles and mathematical methods in a remote sensing image processing system.

There are rules of analytic geometric similarity and rules of physical simulations in ORSIM. The analytic geometric similarities include image scale, and projected transformation dimensions of imagery. The physically simulated rules include characteristics of electromagnetic wave bands, e.g., 0.38-0.70 μm is a visible band, 0.8-1.1 μm is a "Greenness band", 8-14 μm is a temperature band. These can be used to identify different objects from different bands and to classify and extract objects from mixed-bands. Although physically simulated rules are very complex and difficult, they are very important for building ORSIMs.

SOME ORSIMS

ORSIMs of Sea Surface Temperature (SST)

Sea Surface Temperature (SST) is a well-known model in ORSIM. When using ch.4 and ch.5 of NOAA AVHRR satellite images:

$$SST = a*ch.4 + b*ch.5 \quad (1)$$

where a and b are coefficients estimated by statistic data measured in the different sea areas. This formula is not really an ORSIM of SST. The actual ORSIM of SST must be inferred from physical principles without too many observation data involved. There is much research to be done in this area.

ORSIM of Sea Surface Heat Diffusion (SSHD) (Ma and Ge, 1991)

Assume a current of hot (or warm) water with diffusion heat flows into cooling sea water. Under specific gravity condition, hot water is lighter than cold water. The hot water will be flattening on the cooling sea surface, with a certain thickness. Therefore, we may be able to approach a slow flow in two dimensions. According to laws of energy conservation, diffusion can be represented as

$$\partial^2T/\partial t^2 = K_0 + K_x(\partial^2T/\partial x^2) + K_y(\partial^2T/\partial y^2) + (\partial K_x/\partial x)(\partial T/\partial x) + (\partial K_y/\partial x) + (\partial K_y/\partial y)(\partial T/\partial y) \quad (2)$$

where T is temperature, $\partial T/\partial t$ is the temperature change with time, K_0 is diffusion constant, K_x and K_y are diffusion coefficients, $\partial T/\partial x$ and $\partial T/\partial y$ are temperature gradients, $\partial K_x/\partial x$ and $\partial K_x/\partial y$ are gradients of diffusion coefficients, $\partial T^2/\partial x^2$ and $\partial^2T/\partial y^2$ are second gradients of temperature. Using NOAA AVHRR, ch.4 + ch.5, we obtain apparent temperatures at digital AT image. The scanning and pathing directions will be constituted a two-dimensional plane in x and y directions. Thus $\partial T/\partial x$, $\partial T/\partial y$, $\partial^2T/\partial x^2$, $\partial^2T/\partial y^2$ will be counted in the images. Using multi AVHRR ch.4 + ch.5 data, we will obtain apparent temperature changes. Certainly, $\partial T/\partial x$, $\partial T/\partial y$, $\partial T/\partial t$, $\partial^2T/\partial x^2$, $\partial^2T/\partial y^2$ are apparent.

By minimizing the sum of squares of deviations of the equation, optional values of K_0, K_x, K_y, $\partial K_x/\partial_x$, and $\partial K_y/\partial_y$ can be calculated. The equation of diffusion (2) is an ORSIM of sea surface heat diffusion. It is very useful for modeling the ocean current movement between warm and cold water. We have applied the method for an electric power station.

ORSIM of Sea Surface Apparent Thermal Inertia (SSATI) (Ma, 1990b)

The thermal inertia

$$P = \sqrt{K_\rho C}$$

where K = thermal conductivity, ρ = density, and C = heat capacity, is a physical property impeding on the extent of temperature changes in objects.

According to the heat transfer equation and the boundary condition of periodicity from Fourier series, this method could infer the following formula:

$$\frac{1-A}{\Delta T} = \frac{1}{2S_0C_2A_i}\sqrt{wp^2 + \sqrt{2w}Bp + B^2} \tag{3}$$

where A is albedo, ΔT is a daily range of temperature, S_0 is solar constant ; C_t is transmissivity of atmosphere, A_i is a function of solar declination and local latitude, ω is the daily angular frequency, and B is a constant of weather and ground states in the same digital tape. In short, S_0, C_t, A_i, ω, and B are constants in the same digital image. The thermal inertia P is a function of the albedo A and the daily range of temperature ΔT, that is

$$P = f\left(\frac{1-A}{\Delta T}\right) \tag{4}$$

$$ATI = \frac{1-A}{\Delta T} \tag{5}$$

where ATI stands for Apparent Thermal Inertia. By using AVHRR, ch.1 + ch.2 can obtain the albedo, AVHRR ch.4 day and night data, and the daily range of temperature. Thus, the temperature difference of day and night can be obtained. This results in a typical ORSIM of SSATI.

ORSIM of Sea Surface Concentration of Suspended Sediment (SSCSS) (Ma and Li, 1986)

Radiation by sedimentary particles transmits into the sea surface water with a diffusible scattering. Assuming there is a thin layer about 20 cm in the water, and using the transmissive equation, the formula for volume concentration of suspended sediment , the water absorption formula, and the formula of backscattering of Mie:

$$R = a + b * [1 - \exp(CS)] \quad (6)$$

where R is the reflectivity of digital density values of NOAA AVHRR ch.1; S is the concentration of suspended sediment; a and b are constants on the same digital imagery; $C=K(h_0/d)$; h_0 is the transmitted depth of water; d is the mean diameter of sediment particles; K is a proportional coefficient; and C is an approximate constant in the same band. The values of a, s and C must be calculated from statistics data of the concentration of suspended sediment of sea surface (20 cm).

ORSIM IN THE FUTURE

Characteristics of imagery spectrum, remote sensing information models and simulations of remote sensing images are important for remote sensing information theories. ORSIMs are based on physical principles, mathematical methods and remote sensing image processing systems. Based on ORSIPs (Ocean Remote Sensing Image Processing System), OIS, OES and CAC, the ORSIM could be developed efficiently.

Using NOAA AVHRR data, we might be able to construct ORSIM of the sea surface temperature and three-dimensional sea temperature with data collected by buoys and satellites. The two-dimensional SST is a limited case of three-dimensional sea temperature. Besides ORSIM of two-dimensional sea surface red tide, petroleum pollution, etc., can also be established.

By using ERS microwave band data, ORSIM of sea surface wave height and wind speed can be developed. Wave heights and wind speed models can be derived by simulations in a computer-aided system. Furthermore, we can simulate the SAR images to the computer with ERS microwave images. This provides an efficient method in ocean remote sensing information science.

In the future, research and development of the ORSIM models for oceanic hydrology and dynamic current could be improved.

REFERENCES

Ma, A.N. 1990a. On remote sensing information model. Presented at ISPRS Commission IV Symp. on Cartographic and Database Applications of Photogrammetry and Remote Sensing. Tsukuba, Japan.

Ma, A.N. 1990b. Automatic mapping for hydrography. XIX Intl. Federation of Surveyors. Helsinki, Finland.

Ma, A.N., and H. Ge. 1991. The remote sensing information model of thermal diffusion. IGARSS, ESPOO. Finland.

Ma, A.N., and J. Li. 1986. A study on concentration of suspended sediment by remote sensing. In: Proc. of the 3rd Intl. Symp. on River Sedimentation. The Union of Mississippi.

Ma, A.N., and Z. Zhou. 1992. The principles of geographical expert system. Presented at 17th ISPRS Symp. Washington, D.C.

MEASUREMENT OF VERTICALLY AVERAGED OCEAN CURRENT VELOCITY USING MULTIPATH INVERTED ECHOSOUNDERS

Tomoyoshi Takeuchi
University of Electro-Communications
Tokyo, Japan

Keisuke Taira
University of Tokyo
Tokyo, Japan

ABSTRACT

A multipath inverted echo sounder (MIES) was developed and tested for measuring vertically averaged currents by accurately measuring time differences between two acoustic signals transmitted in opposite directions along multiple paths in the ocean. The multipath inverted echo sounder has a signal source that is phase-modulated by a maximum length binary sequence and a correlation processing unit that is capable of identifying multipath acoustic signals. The acoustic paths form a "sing around" vertical triangle with a base about 10 km long, and the time differences determine the horizontal component of vertically averaged velocity through a water column. The field tests were conducted by using three multipath inverted echo sounders. Each multipath inverted echo sounder functions as a transponder and records all data. The results of the field tests are presented and discussed.

INTRODUCTION

The "sing around method" of flow measurement is based on the travel time difference of reciprocal acoustic waves between two points. Rossby (1975) discussed the principles and experimented in the laboratory. Reciprocal transmission experiments aimed at the tomographic observation of a midocean vortex was made by Worcester et al. by deploying two moorings 300 km apart in the Northwest Atlantic Ocean west of Bermuda (Worcester, 1985, Howe, 1986). Similar experiments were performed by DeFerrari, et al. (1985) in Florida Straits. Furthermore, Chaplin (1986) has been investigating the measurement of horizontal currents averaged through the whole water column using two inverted echo sounders moored near the bottom.

We have developed a new type of inverted echo sounders called the multipath inverted echo sounder (MIES). Requirements for the system performance are to identify multipath acoustic signals and estimate precise transmission time in underwater channels that are disturbed by noise. The signal processing technique uses a signal whose carrier frequency is phase-modulated by a maximum length binary sequence with correlation processing (Spindle, 1979). We conducted a reciprocal transmission experiment using acoustic waves around a triangle defined by one path directly between two MIES moored with about 10 km horizontal spacing and positioned about 100 m above the ocean bottom and another path reflected off the sea surface halfway between them. The current vectors in the horizontal direction are determined by measuring in two different directions. At the same time, the depth variation of the main thermocline can be measured with multipath inverted echosounders (Watts, 1977). Therefore, the system may be very effective for monitoring transportation phenomena in the ocean.

THE THEORY

The acoustic waves transmitted via the four paths shown in Figure 1.

Sound paths:

1. MIES-A - MIES-B, MIES-B - MIES-A
2. MIES-A - surface - MIES-B, MIES-B - surface - MIES-A
3. MIES-A - surface - MIES-A, MIES-B - surface - MIES-B
4. MIES-A - bottom - MIES-B, MIES-B - bottom - MIES-A

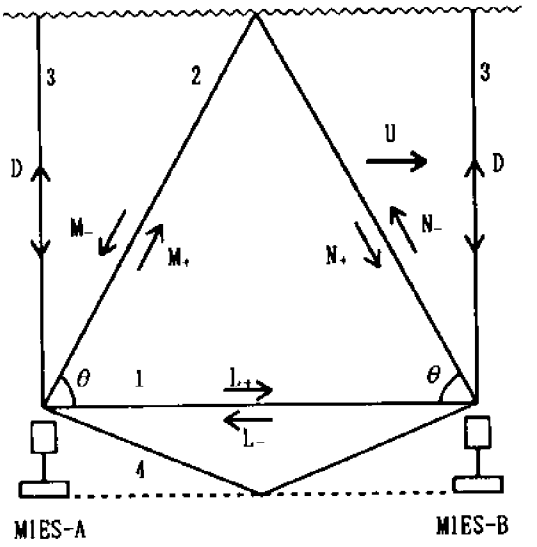

Figure 1. Schematic diagram for vertical mean current velocity

Let the speed of sound be c, then the reciprocal transmission time difference Δt_{12} along a path Γ is given by

$$\Delta t_{12} = t_{12} - t_{21} = \int_{\Gamma} \frac{ds}{c + u_s} - \int_{\Gamma} \frac{ds}{c - u_s} \tag{1}$$

$$\equiv -2 \int_{\Gamma} \frac{u_s}{c} \frac{ds}{c}$$

where u_s is the component of the flow velocity along the path Γ of the sound wave. The approximation involved here is very good, since $u_s/c < 10^{-3}$. Since the acoustic velocity varies in accordance with water temperature, pressure, and salinity, the sound velocity can be written as

$$c = c_o + \delta c \tag{2}$$

where c_o is the mean speed of sound and δ c is its variation. Since in the case of interest to us $\delta c/c_o<0.03$, Eq. (1) can be approximated to

$$\Delta t_{12} \cong -\frac{2}{c_o^2}\int_\Gamma u_s ds \tag{3}$$

Assuming that the vertical component of flow velocity can be ignored, and we consider only the horizontal component u(z).

Referring to Figure 1, we denote travel time along path 2 and path 3 by t_2 and t_3 respectively. These are given by

$$\begin{aligned} t_2 &= M_+ + N_+ \\ t_3 &= M_- + N_- \end{aligned} \tag{4}$$

where M and N are the times for sound to travel along the two sides of the vertical triangle, and + and - denote opposite directions. From Eq. (4), the reciprocal travel time difference Δt is

$$\Delta t = t_2 - t_3 = (M_+ - M_-) + (N_+ - N_-) \tag{5}$$

From Eq. (3), we obtain the following equations.

$$\begin{aligned} M_+ - M_- &= -\frac{2}{c_o^2}\int_{-D}^{0} u(z)\cot\theta dz \\ N_+ - N_- &= -\frac{2}{c_o^2}\int_{-D}^{0} u(z)\cot\theta dz \end{aligned} \tag{6}$$

If the acoustic ray paths are almost straight lines, the following equation applies to Eq. (6).

$$\cot\theta \simeq \frac{\frac{L}{2}}{D} \tag{7}$$

Therefore,

$$\Delta t = -\frac{2L}{c_o^2}\frac{1}{D}\int_{-D}^{0} u(z)dz \tag{8}$$

is obtained. By putting mean current $\bar{U}$,

$$\bar{U} = \frac{1}{D}\int_{-D}^{0} u(z)dz \tag{9}$$

Eq. (10) is obtained from Eq. (8) and Eq. (9).

$$\overline{U} = -\frac{c_o^2}{2L}\Delta t \qquad (10)$$

Thus, the horizontal current averaged from the surface to depth D can be measured from Eq. (10). In this equation, L is obtained from the travel time via the direct path 1.

MOORING DISTANCE BETWEEN MIES-A AND MIES-B

When the vertically averaged velocity as described above is measured, the mooring distance L should be first determined. Equation (10) also represents the relationship between the reciprocal acoustic travel time differences Δt and the mooring distance of the echo sounders taking the current as a parameter. This shows that the transmission time differences Δt are 0.28 - 2.8 ms when L = 3 km and 0.4 - 4 ms when L = 5 km for the assumed range of current velocities. Furthermore, they are 0.78 - 8 ms when L = 10 km, that is to say, the time differences increase with the mooring distance between the individual units and the travel time can be easily measured since higher accuracy is not always needed. However, it should be kept in mind that the curving of acoustic ray paths will influence the measurement. Time measurement accuracy should be better than 0.1 ms. Therefore, the required SNR can be obtained by signal processing which uses the acoustic wave with a carrier frequency of 10 kHz phase-modulated by a maximum length binary sequence with correlation processing. This enables multipath signals to be identified.

ACOUSTIC TRANSCEIVER

The source and receiver are integrated into a mechanical package to form a transceiver as shown in Figure 2 (a). Both are processed and controlled by a single CMOS V40 microprocessor that operates on a 1-MHz time base and is equipped with an RS-232C interface so that the transceiver and personal computer can be interconnected for data communication.

The transmitted signal was chosen to have the following characteristics:

carrier frequency f_o = 10 kHz

digit length = 4 cycles of 10 kHz = 0.4 ms

sequence length = 127 digits = 50.8 ms

transmission length = 1 sequence period = 50.8 ms.

The transmitted signal is generated by reading out from a PROM in which the phase-coded signal is stored. The PROM produces a 10-kHz square wave as shown in Figure 2(b). The two phase states are 0 and π. The phase-coded digital signal is then amplified by a power amplifier, filtered by a combination of a broad band pass filter and an impedance-matching network, and applied to the ring ceramic element. Energy is supplied by lithium batteries.

The receiver consists of two synchronous detectors and a microprocessor-controlled unit that digitizes, correlates, identifies, and records signals on EPROM. The

projector transducer is also used for acoustic signal reception. A single CMOS V40 microprocessor performs both control and signal-processing functions in the receiver. Signal acquisition is initiated by the processor at the source transmit time plus a preset time according to maximum range. The incoming signal is amplified and filtered using a 2-kHz band-pass filter centered at 10 kHz. The filtered signal is then heterodyned to base band before A/D conversion. The resulting in-phase and quadrature components of the signal are passed through 2-kHz low-pass filters, sampled at 50 kHz, and digitized by two A/D converters, one for each component of the signal. Thus the receiver obtains two samples per transmitted signal. Each sample is intercorrelated with the corresponding replica of the transmitted signal.

The processor squares each intercorrelation and sums their results. The arrival time is obtained as the abscissa of the resulting peak value. The transceiver responds after a preset interval from this arrival time. The arrival time in each peak value and the several adjacent amplitudes are stored on a 1-Mbytes EPRON for later analysis.

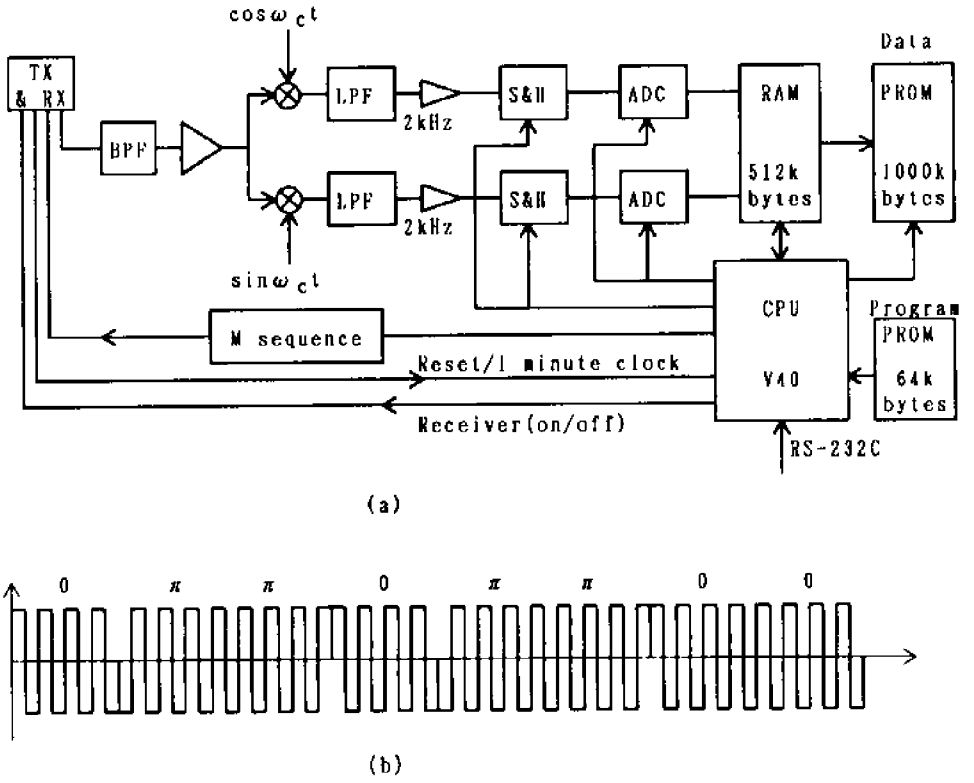

Figure 2. The block diagram of a transmitter and a receiver of multi-path inverted echo sounder (a) and the square wave phase-modulated by a maximum binary sequence (b)

VERTICAL MEAN OCEAN CURRENT VELOCITY

Experiments for measuring vertically averaged currents were designed and conducted in the sea are between Miyake and Mikura islands (Figure 3), where the depth is about 1100 m. Three multipath inverted echo sounders were deployed at the vertices of

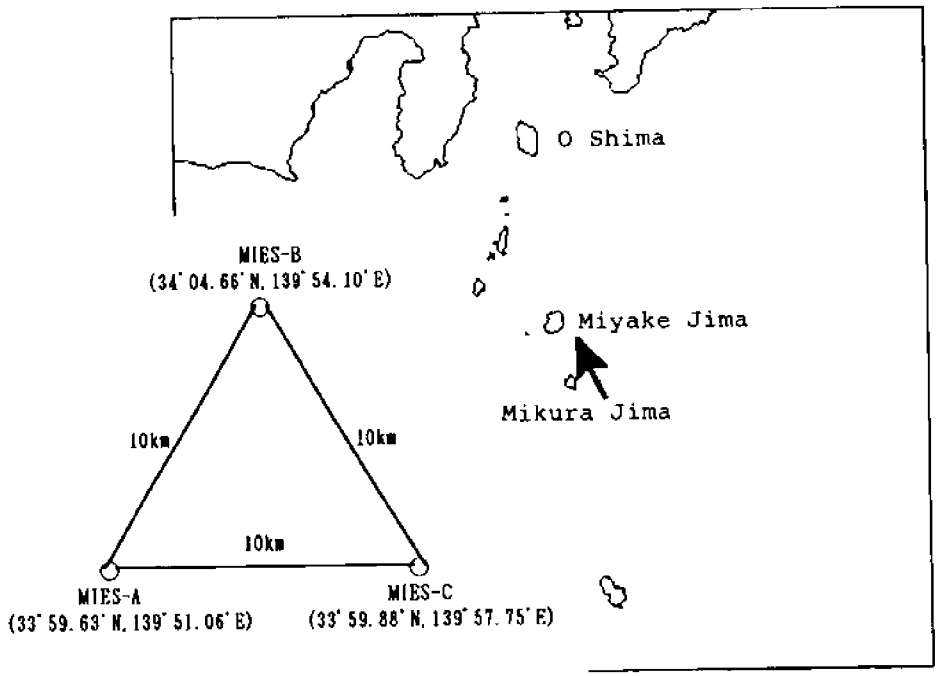

Figure 3. The equilateral triangular network constructed of three multipath inverted echo sounders deployed off Mikura island

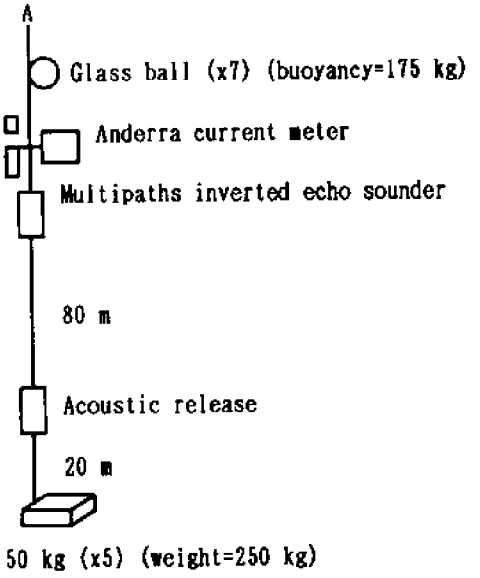

Figure 4. The mooring system consists of multipath inverted echo sounder, Anderra current meter and acoustic release

an equilateral triangle with side of approximately 10 km and at a height of 100 m above the ocean bottom. Figure 4 shows the mooring system which includes an Anderra current meter in order to independently measure bottom current velocity. Figure 5(b) shows the acoustic ray paths calculated from the profile of the water temperature T measured with an XBT (Figure 5(a)). Some bending of the ray paths can be seen near the surface, but this effect can be ignored. Figure 6 shows records of wave shapes processed by the receiver, of which the acoustic waves emitted from MIES-A traveled to MIES-B along paths as shown in Figure 5. We observed three arrival peaks. The first peak consists of direct sound and that reflected from the bottom, which can be seen at the rear edge of this signal. The second peak is the sound reflected by the surface and the third peak is the sound reflected by the surface and the bottom. The travel time differences give the vertically averaged currents in the ocean by using Eq. (10). These signals have sufficient SNR and the multipath acoustic signals are easily identified.

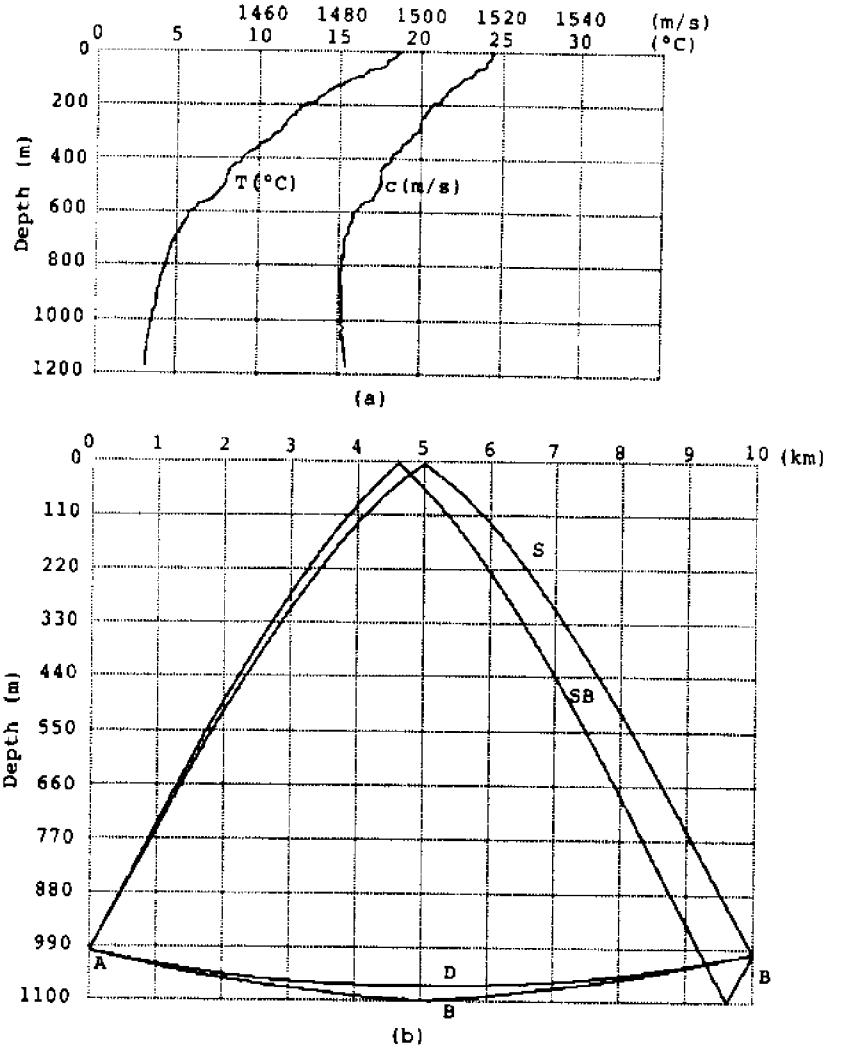

Figure 5. (a) Sound speed profile (c) and (b) four acoustic ray paths D, S, B, and SB calculated from water temperature profile (T) measured with XBT. Multipath inverted echo sounders are moored at points A and B.

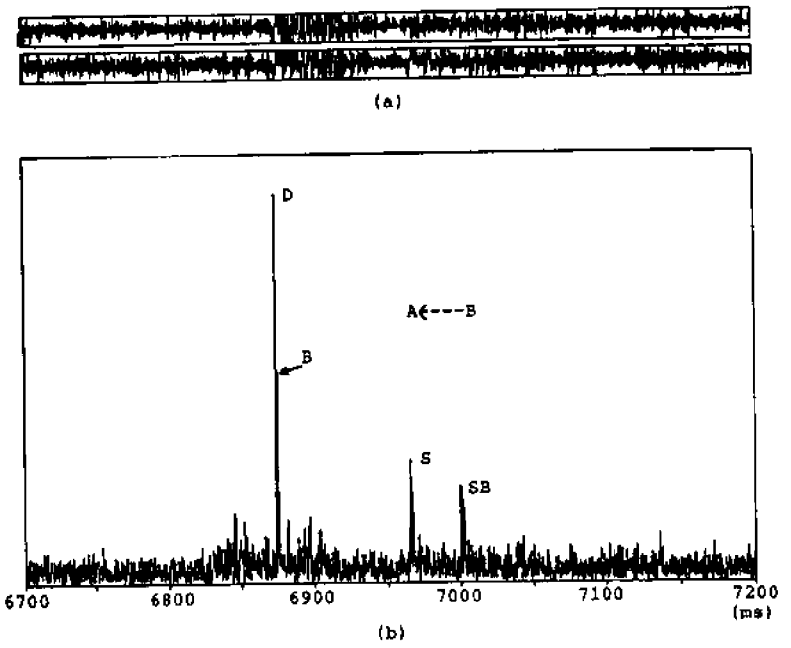

Figure 6. The received signal is heterodyned to base band and then the in-phase and quadrature components (a) are passed through a 2-kHz low-pass filter, and each component is intercorrelated with the replica of the transmitted signal, then they are squared and summed (b).

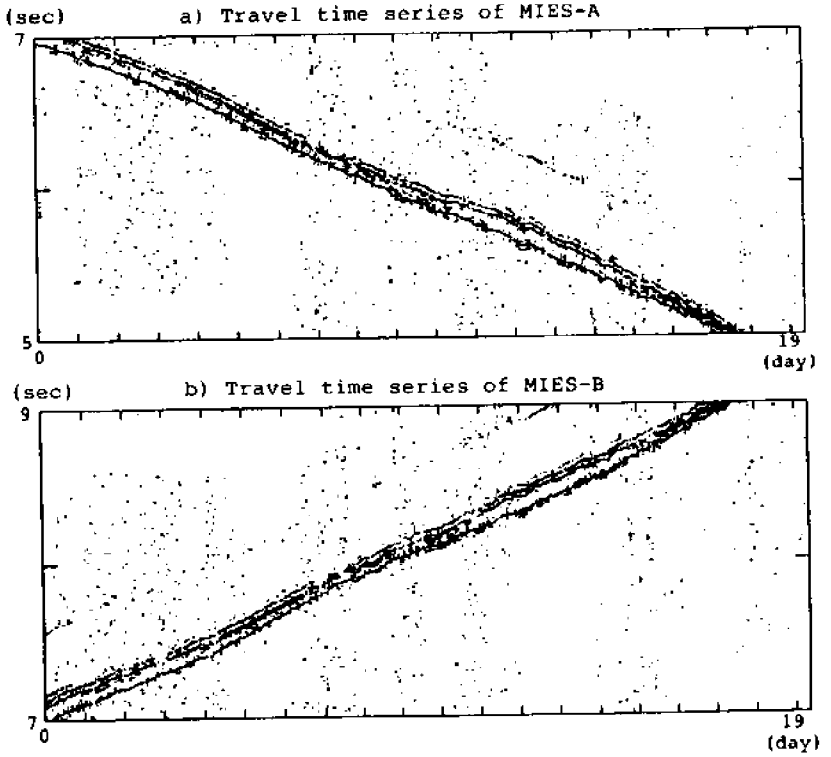

Figure 7. Travel time series for acoustic signals of (a) one way and (b) the opposite way during a 19-day period

Sound travel times along paths 1 and 2 between MIES-A and MIES-B during a 19-day period are shown in Figure 7. The time bases of three multipath inverted echo sounders are synchronized just before deployment by using a quartz oscillator. Figure 7(a) shows the travel time along the direct path and the travel time from MIES-A to MIES-B via the sea surface. Figure 7(b) shows the travel times in the opposite direction. The slopes of these figures are due the drift of the clock circuits. We now discuss effects of clock drift and the motion of the mooring system.

$$\begin{aligned}\Delta t' &= (M_+ + N_+ + \delta_1 + \delta_2 - L_+ - \delta_3) - (M_- + N_- - \delta_1 + \delta_2 - L_- + \delta_1 - \delta_3) \\ &= \Delta t - (L_+ - L_-) \end{aligned} \tag{11}$$

The first part of Eq. (11) expresses the effect of clock drift and the motion of the mooring systems, where δ_1 is the clock drift, and δ_2 and δ_3 are the effects of the motion of the mooring systems reflected M+N ray path and the direct L ray path respectively. If the acoustic travel time along the M+N ray path is measured relative to the acoustic travel time along the L ray path, travel time difference $\Delta t'$ of the acoustic signals transmitted in opposite directions will not be affected by the clock drift and the mooring system motions, since reciprocal transmissions are made within a short interval that is two or three minutes and the clock drift and the motion are frozen as expressed in the second part of Eq. (11). When we use $\Delta t'$, the vertically averaged ocean current velocity relative to the bottom current is obtained from the following expression.

$$\overline{U} - \overline{U}_b = -\frac{c_o}{L_+ + L_- - 2\delta_3}\Delta t' \tag{12}$$

The bottom current velocity can be obtained from reciprocal travel time differences along the direct L ray path. This is, however, affected by clock drift as follows.

$$\overline{U}_b = \frac{\dfrac{L_+ - L_-}{2} - \delta_1}{\dfrac{L_+ + L_-}{2} - \delta_3} c_o \tag{13}$$

Therefore, we use the velocities measured with the Anderra current meters.

Figure 8 shows the bottom current velocity measured by an Anderra current meter. The effects of tidal current can be seen. Figure 9 shows the spectrum of the bottom current. There are three kinds of bottom tidal currents which have periods of a half day, one day and three days. Hence, the vertically averaged velocities were estimated by a moving average over 3 days from the acoustic reciprocal transmission times between the two echo sounders by using Eq. (12). These are shown in Figure 10. Figure 10 (a) shows the vertically averaged velocity flowing in the direction from point A to point B, and (B) is the vertically averaged velocity flowing in direction from point A to point C (Figure 3). The vector of the vertically averaged current can be calculated from these two flows.

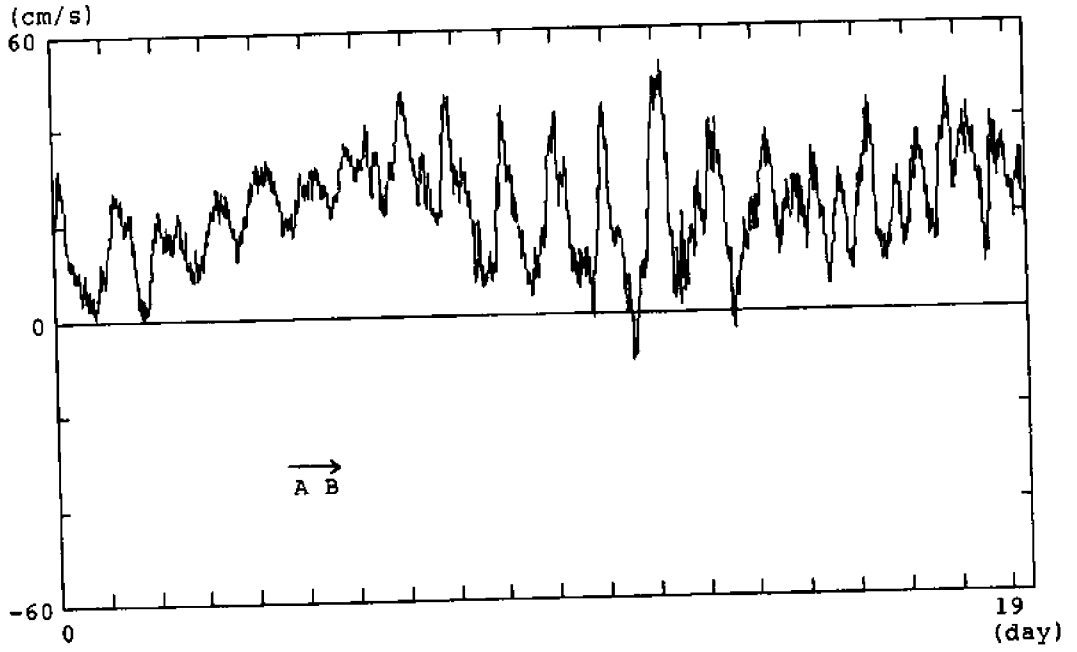

Figure 8. Bottom current velocity measured by an Anderra current meter

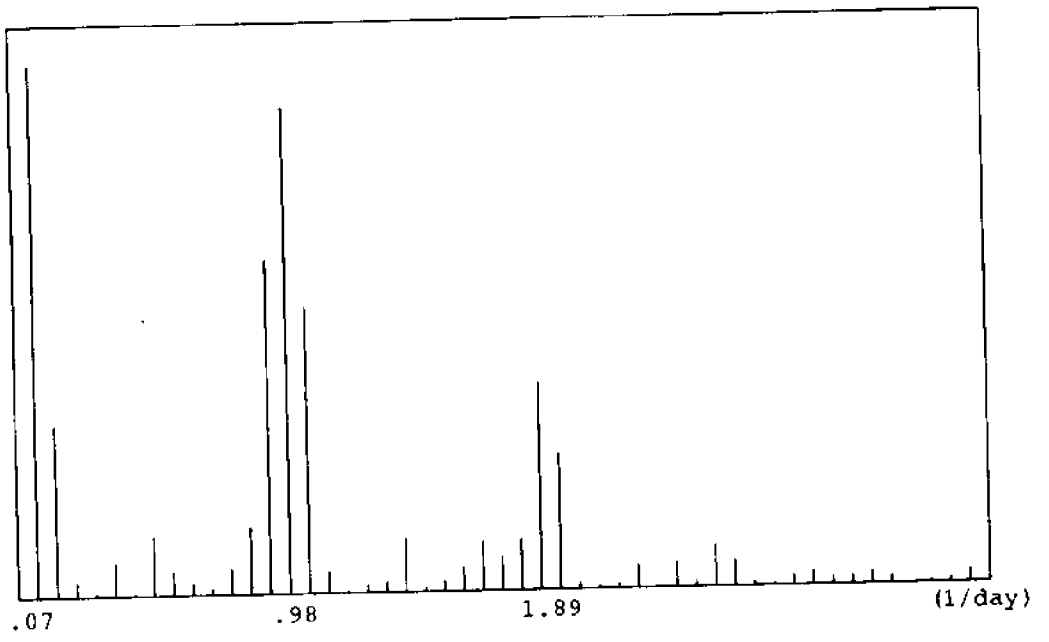

Figure 9. Spectrum of bottom current velocity

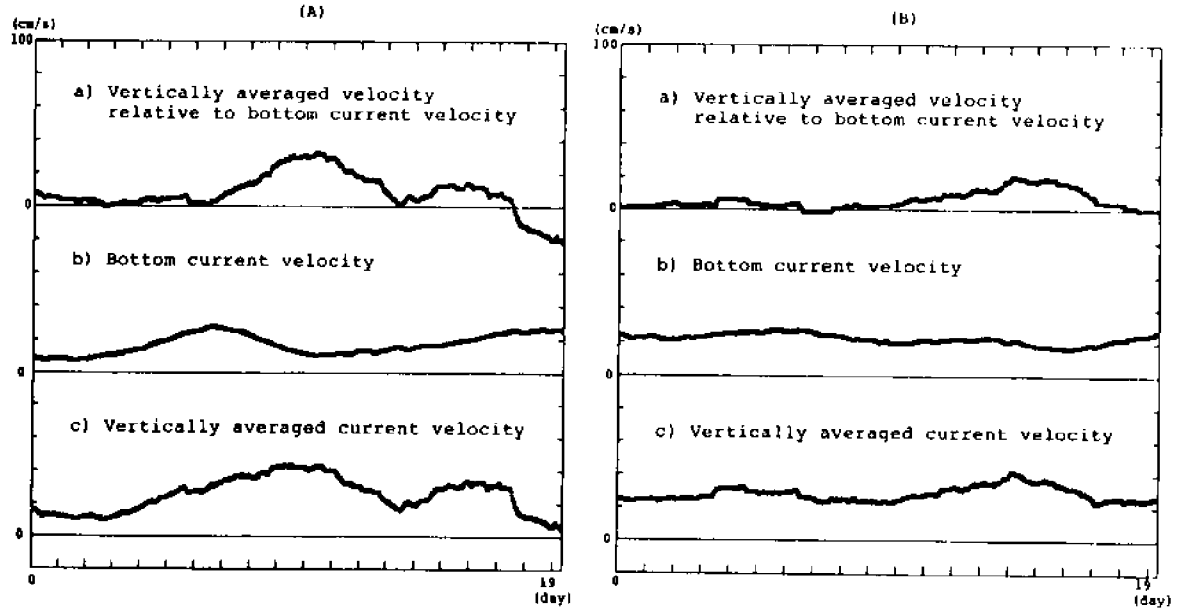

Figure 10. Vertically averaged current velocity flowing (A) from point A to point B and (B) from point A to point C

CONCLUSION

An acoustic method was discussed for measuring vertical average ocean currents by accurately measuring time differences between two acoustic signals traveling in opposite directions along multiple paths in the ocean. Measurement of vertically averaged ocean currents were conducted by using three specially developed multipath inverted echo sounders off Mikura island. It was found that the method is effective for measuring vertically averaged currents in the ocean. Some inaccuracy was caused by drift of the time base clock circuits and motion of the mooring. This motion, however, is due to tidal currents. Therefore, the effect on measurement of current velocity can be reduced by taking a moving average. Drift of time measurement strongly affects the measurement of the bottom current velocity. Therefore, further research is needed to reduce this drift.

ACKNOWLEDGEMENTS

This experiment has been conducted during the KH-92-2nd research voyage of the Hakuho-maru (deployment) and the KT-92-8th research voyage of the Tansei-maru (recovery) belonging to Ocean Research Institute, University of Tokyo, with the cooperation of Professor Asahiko Taira, to whom the authors wish to express their sincere gratitude.

REFERENCES

Chaplin, G. 1986. An acoustic ocean transport meter. In: IEEE Proc. Oceans. pp. 426-429.

DeFerrari, H.A., and H.B Ngue. 1985. Acoustic reciprocal transmission experiments, Florida Straits. *JASA* **79**(**2**):299-315.

Howe, B.M., P.F. Worcester, and R.C. Spindle.1987. Ocean acoustic tomography: mesoscale velocity. *J. Geophys. Res.* **92**(**C4**):3875-3805.

Rossby, T. 1975. An oceanic vorticity meter. *J. Marine Res.* **32**(**2**):212-222.

Spindle, R.C. 1979. An underwater acoustic pulse compression system. *IEEE Trans. on Acoustics, Speech, and Signal Processing*. ASSP-**27**(**6**):723-728.

Watts, D.R. 1977. Measuring dynamic heights with inverted echo sounders: results from MODE. *J. Phys. Oceanograph*. **7**(**5**):345-358.

Worcester, P.F., R.C. Spindle, and B.M. Howe. 1985. Reciprocal acoustic transmissions: instrumentation for mesoscale monitoring of ocean currents, *IEEE J. Oceanic Eng.* OE-**10**(**2**):123-136.

DESIGN OF ACOUSTIC ARRAY OF ELLIPTIC RING TRANSDUCERS

Lixue Wu and Adam Zielinski
University of Victoria
Victoria, British Columbia, Canada

ABSTRACT

A novel array of elliptic ring radiators is proposed which generates a fan-type beam with controllable sidelobe level. Such an array can find several applications in specialized sonars such as sidescan sonars, sonars for fish finding and stock assessment, obstacle avoidance systems and others. A design approach which uses the concept of equivalent linear array is presented. This approach benefits from the existing design techniques developed for linear arrays. It requires only simple matrix operations and does not involve any optimization.

The design examples presented demonstrate that a fan-type beam with sidelobes suppressed to more than 40 dB in all possible directions is achievable.

INTRODUCTION

Fan-type acoustic beams are widely used in specialized sonars such as sidescan sonars, sonars for fish finding and stock assessment, and other systems (Clay, 1977). Such beams are relatively broad (20° ~ 45°) in one direction and narrow (1° ~ 5°) in the direction orthogonal to the broad beam direction. The systems usually consist of linear arrays made from rectangular elements. It is possible to control the radiation pattern in the narrow beamdirection by the application of proper weights to each array element. In the broad beam direction, however, the radiation pattern is determined by the width of the rectangular elements and has large first sidelobes (13.5 dB). Existence of such sidelobes adversely affects sonar performance.

In this paper we propose a novel array consisting of several concentric elliptic ring radiators, which is capable of generating a superior radiation pattern. A design approach which uses the concept of equivalent linear array is presented. This approach benefits from the existing design techniques developed for linear arrays. It requires only simple matrix operations and does not involve any optimization.

The design examples are presented which show that 40 dB or more sidelobe suppression in all possible angular directions in the radiation pattern is achievable. The proposed configuration can be implemented as a receiving array using piezoelectric film and as a transmitting/receiving array using concentric hollow cylinders operating in longitudinal mode.

DIRECTIVITY FUNCTION OF AN ELLIPTIC PISTON

In general the directivity function of an arbitrary piston can be obtained as a suitable integral over its face (Wilson, 1988). The face of an elliptic piston is shown in Figure 1. The directivity function (radiation pattern) of such a planar elliptic radiator of uniform sensitivity, with major and minor axes of $2a$ and $2b$, respectively, placed in an infinite rigid baffle, is given by

$$D_e(\theta,\phi) = \iint_s e^{j\frac{2\pi}{\lambda}(x\sin\theta\cos\phi + y\sin\theta\sin\phi)}dxdy \tag{1}$$

where λ is the wavelength of radiated signal, s the area of integration (surface of the elliptic piston), and θ, ϕ are the angular coordinates shown in Figure 1.

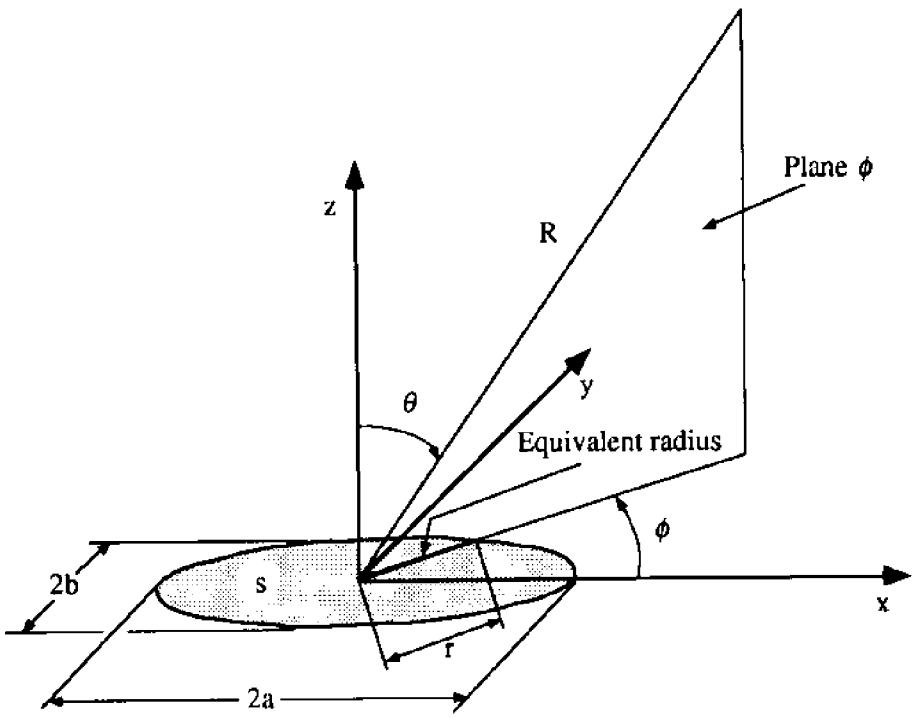

Figure 1. Geometry of an elliptic piston and its equivalent radius

We introduce implicitly the new variables ρ and ψ by the following transformation:

$$x = a\rho\cos\psi, \quad 0 \le \rho \le 1; \qquad y = b\rho\sin\psi, \quad 1 \le \psi \le 2\pi. \tag{2}$$

Now we can rearrange the integral in Eq. (1) to obtain the following form:

$$D_e(\theta,\phi) = \int_0^{2\pi}\int_0^1 e^{j\frac{2\pi}{\lambda}\sin\theta(a\cos\psi\cos\phi + b\sin\psi\sin\phi)} ab\rho d\rho d\psi. \tag{3}$$

Furthermore, if we let

$$\cos\phi' = \frac{a\cos\phi}{\sqrt{a^2\cos^2\phi + b^2\sin^2\phi}}; \qquad \sin\phi' = \frac{b\sin\phi}{\sqrt{a^2\cos^2\phi + b^2\sin^2\phi}} \tag{4}$$

then we can express Eq. (3) as

$$D_e(\theta,\phi) = \int_0^{2\pi}\int_0^1 e^{j\frac{2\pi}{\lambda}\sin\theta\sqrt{a^2\cos^2\phi + b^2\sin^2\phi}\cos(\psi-\phi')}\, ab\rho d\rho d\psi. \tag{5}$$

We note that the integral (5) has the form of the integral expression of the zero-order Bessel function of the first kind. We finally write Eq. (5) as

$$D_e(\theta,\phi) = ab\,\frac{J_1(2\pi\sqrt{a^2\cos^2\phi + b^2\sin^2\phi}\sin\theta/\lambda}{\sqrt{a^2\cos^2\phi + b^2\sin^2\phi}\sin\theta/\lambda} \tag{6}$$

where $J_1(\cdot)$ is the first-order Bessel function of the first kind. For a circular piston transducer for which $a = b$, the above result reduces to that derived in Ristic (1983).

AN ARRAY OF ELLIPTIC RING RADIATORS

The directivity function of an elliptic ring radiator with major axes a_i, a_{i-1}, minor axes b_i, b_{i-1}, uniform sensitivity, and placed in an infinite rigid baffle can be readily obtained by subtracting directivity functions of two elliptic piston radiators given by Eq. (6), that is:

$$D_r(\theta,\phi) = 2\pi a_i b_i\,\frac{J_1(kr_i\sin\theta)}{kr_i\sin\theta} - 2\pi a_{i-1}\,b_{i-1}\,\frac{J_1(kr_{i-1}\sin\theta)}{kr_{i-1}\sin\theta} \tag{7}$$

where

$$r_i = \sqrt{a_i^2\cos^2\phi + b_i^2\sin^2\phi}\,; \qquad r_{i-1} = \sqrt{a_{i-1}^2\cos^2\phi + b_{i-1}^2\sin^2\phi} \tag{8}$$

are defined as the equivalent outer and inner radii, respectively, of an elliptic ring at angle ϕ.

We now consider an array formed by several concentric elliptic ring radiators, each contributing to the overall directivity function with weighting coefficients c_i as illustrated in Figure 2, for the case of three elliptic rings (for the sake of consistency we will also call the central, elliptic portion of the array a ring).

The directivity function of an array with N elliptic ring radiators arranged in such a way can be written as

$$D(\theta,\phi) = 2\pi a_1 b_1 c_1\,\frac{J_1(kr_1\sin)}{kr_1\sin\theta} + \sum_{i=2}^{N} c_i\left\{2\pi a_i b_i\,\frac{J_1(kr_1\sin)}{kr_1\sin\theta} - 2\pi a_{i-1}b_{i-1}\,\frac{J_1(kr_{i-1}\sin)}{kr_{i-1}\sin\theta}\right\} \tag{9}$$

where r_i is the equivalent outer radius of the ith elliptic ring given by Eq. (8).

By varying the weighting coefficients c_i, and the major and minor axes a_i and b_i, one can modify the overall function D to approximate a certain desired function D_d.

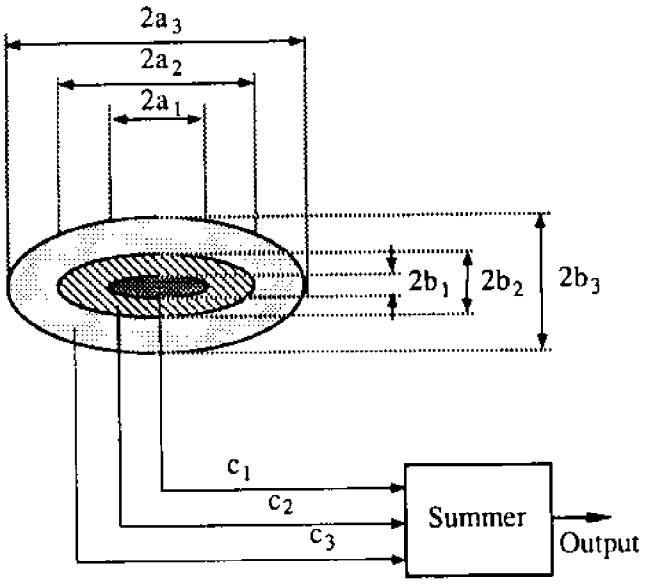

Figure 2. Front face of an array of elliptic ring radiators

DESIGN OF AN ARRAY OF ELLIPTIC RING RADIATORS

An equivalent linear array (ELA) method (Zielinski, 1991) was developed for the design of an array of circular ring radiators. The method benefits from existing design techniques developed for linear arrays. The developed methodology requires only simple matrix operations and does not involve nonlinear optimization. In this section we will extend the ELA method to the array of elliptic ring radiators using the equivalent radius concept described in the previous section. Such an elliptic ring array can generate a radiation pattern which approximates a desired radiation pattern D_d. The directivity function of an elliptic ring array D is given by Eq. (9). The error of approximation e can be defined as

$$e^2 = \|D = D_d\|^2 = < D - D_d, D - D_d > . \tag{10}$$

Here we treat functions as vectors in Hilbert space and use the norm denoted by i ? i to express the error function. The <·> denotes the inner product.

The objective of the design is to determine the array parameters as given in Eq. (9) which minimize the error e. Nonlinear optimization algorithms can be used in array synthesis but are computationally intensive. This presents a practical difficulty for an array of a significant size. Furthermore, the size of the array can not be selected as a variable because of the nature of its effect on the objective function (i.e., approximation error e^2 defined by Eq. (10)).

Equivalent Linear Array of an Elliptic Ring Radiator

A linear array with $2N$ point elements spaced uniformly by d has the directivity function given by Zielinski (1991)

$$D_l(u) = \sum_{j=1}^{N} w_j \cos((2j-1)u) \tag{11}$$

where $\{w_j\}$ are the weighting coefficients and u is defined as $u = (\pi d/\lambda)\sin\theta$.

The directivity function of an elliptic ring radiator with the equivalent outer and inner radii r_i and r_{i-1}, respectively, given by Eq. (8) can be rewritten in the u-domain as

$$D_e(\phi,\theta) = \frac{\pi a_i b_i d}{r_i} \frac{J_1[(2r_i/d)u]}{u} - \frac{\pi a_i b_i d}{r_{i-1}} \frac{J_1[(2r_{i-1}/d)u]}{u} . \tag{12}$$

Assuming an infinite length linear array, it is possible, by proper selection of the weighting coefficients w_j, to obtain a directivity function equal to that of an elliptic ring radiator, that is

$$D_e(u) = \sum_{j=1}^{\infty} w_j \cos((2j-1)u) \tag{13}$$

We call such an array the equivalent linear array to an elliptic ring radiator. As discussed in Zielinski (1991) the functions $\cos((2j-1)u)$ are orthogonal in the u-domain; their inner products are defined as

$$\begin{aligned} <\cos((2i-1)u),\cos((2j-1)u)> &= \frac{4}{\pi}\int_0^{\frac{\pi}{2}} \cos((2i-1)u)\cos((2j-1)u)du \\ &= \begin{cases} 1 & \text{for } i = j \\ 0 & \text{else} \end{cases} . \end{aligned} \tag{14}$$

Applying the inner product defined by Eq. (14) to Eq. (13) we obtain

$$\sum_{j=0}^{\infty} w_j <\cos((2j-1)u),\cos((2i-1)u)> = <D_e(u),\cos((2i-1)u)> \tag{15}$$

which leads to the explicit expression for w_j

$$w_j = \frac{4}{\pi}\int_0^{\frac{\pi}{2}} D_e(u)\cos((2-1)u)du \qquad j = 1,\ldots,\infty \tag{16}$$

To express the radiation pattern of an elliptic ring radiator we need a set of equivalent linear arrays rather than one equivalent linear array as in the case of a circular ring radiator (Zielinski, 1991). Each equivalent linear array produces a radiation pattern which represents the radiation pattern generated by the elliptic ring radiator on a certain plane ϕ. This is illustrated graphically in Figure 3. The weighting coefficient w_j depends on ϕ and therefore depends on the equivalent outer and inner radii r_i and r_{i-1}. It can be shown that under the condition

$$d = \sqrt{\cos^2\phi + \delta^2 \sin^2\phi}\,\lambda/2$$

where $\delta = b_i / a_i$, for $i = 1,2,...,N$, this dependence can be eliminated.

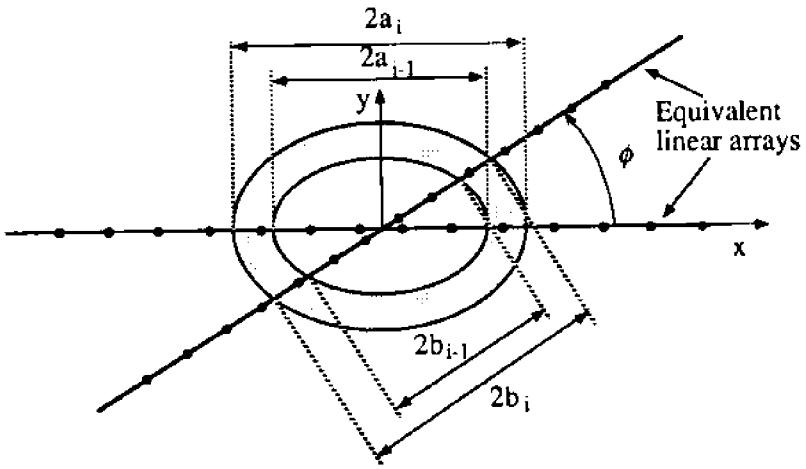

Figure 3. Front face of an elliptic ring radiator and its equivalent linear arrays

Design of an Array of Elliptic Ring Radiators by the Equivalent Linear Array Method

The equivalent linear array method for the design of an array of elliptic ring radiators is a technique in which all elliptic ring radiators are represented by a series of sets of equivalent linear arrays, each for different ϕ. The directivity function of the array of elliptic ring radiators is then the sum of the directivity functions of all equivalent linear arrays. Each equivalent linear array of an elliptic ring radiator has in principle an infinite number of elements and associated weighting coefficients. In general, the magnitude of these coefficients decreases for elements far away from the center of the array. It is therefore possible to truncate the equivalent linear array to a finite number of elements by disregarding elements with small weighting coefficients. This truncating process is studied in Zielinski (1991).

The following are the design steps for obtaining the weighting coefficients for the array of elliptic ring radiators. The procedure presented here is only a summary. The design procedure is similar to that for arrays of circular ring radiators, and is detailed in Zielinski (1991) and Wu (1991).

1. Design a linear array of point radiators with variable spacing d which produces a desired radiation pattern (for example associated with a Dolph-Chebyshev array). As a result, the vector of weighting coefficients w_l, and the size $2N$ (number of elements) of the array are obtained (Elliot, 1966). We call such an array a *prototype*.

2. Consider a series of N elliptic ring radiators, and find their equivalent linear arrays with spacing d and size $2N$ by properly selecting their weighting coefficients. Note that in order to have the same spacing in all equivalent linear

arrays for all elliptic rings we require the major and minor axes of elliptic rings to satisfy the condition $\delta = b_i/a_i$.

3. Arrange the weighting coefficients of the equivalent linear arrays to form a matrix of weighting coefficients as described in Zielinski (1991).

4. Find the weighting coefficients of the elliptic ring array by inverting the matrix formed in step 3 and multiplying it by the vector of weighting coefficients w_l of the prototype formed in step 1. Here the condition $\delta = b_i/a_i$ ensures that the matrix of weighting coefficient is independent of ϕ. Therefore, we obtain a set of weighting coefficients of the array for all ϕ, since they are independent of ϕ.

We performed an array design by applying the above design technique to a Dolph-Chebyshev linear array as a prototype. We assume a prototype of 20 elements with $\delta = 0.2$. Two cases are considered: 30 dB and 40 dB sidelobe suppression. The beamwidths of the prototype were 6.5° (on the plane $\phi = 0°$) ×32° (on the plane $\phi = 90°$) for sidelobe suppression of 30 dB and 7° (on the plane $\phi = 0°$) ×36° (on the plane $\phi = 90°$) for sidelobe suppression of 40 dB. The design of the elliptic ring array with closely matched radiation patterns was performed which resulted in an elliptic ring array of major axis 10λ consisting of 10 elliptic rings. The corresponding normalized weighting coefficients and ring sizes are tabulated in Table 1. The resulting radiation patterns generated by such array are shown in Figure 4 for different angle ϕ and for 30 dB postulated sidelobe suppression. The dotted lines indicate the radiation patterns of the Dolph-Chebyshev prototypes. We see that the resulting radiation patterns are almost identical to those of postulated Dolph-Chebyshev prototypes. Shown in Figure 5 is the 3-D radiation patterns of the resultant elliptic ring array with postulated 30 dB sidelobe suppression. We observe that this is a substantial improvement compared to the radiation pattern of a conventional linear array with rectangular elements.

Table 1. Weighting coefficients and ring sizes of an elliptic ring array for different sidelobe suppression levels

Ring No.	Major Axis (λ)		Minor Axis (λ)		Weighting Coefficient	
i	outer	inner	outer	inner	30 dB	40 dB
1	0.5	0.0	0.1	0.0	0.9423	0.9894
2	1.0	0.6	0.2	0.12	1.0000	1.0000
3	1.5	1.1	0.3	0.22	0.8774	0.8957
4	2.0	1.6	0.4	0.32	0.8727	0.8134
5	2.5	2.1	0.5	0.42	0.7032	0.6691
6	3.0	2.6	0.6	0.52	0.6906	0.5617
7	3.5	3.1	0.7	0.62	0.4679	0.4048
8	4.0	3.6	0.8	0.72	0.5107	0.3224
9	4.5	4.1	0.9	0.82	0.0929	0.1528
10	5.0	4.6	1.0	0.92	0.6900	0.2221

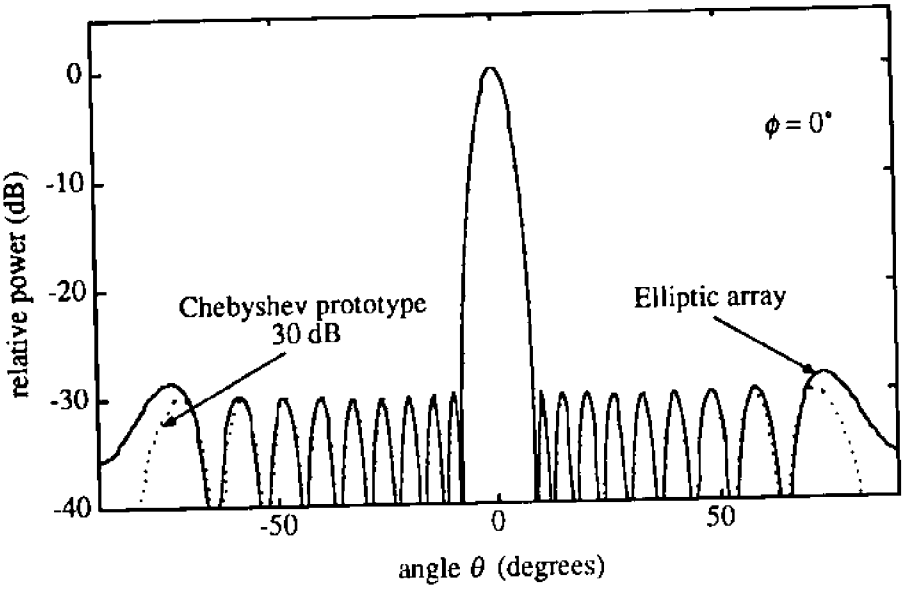

(a)

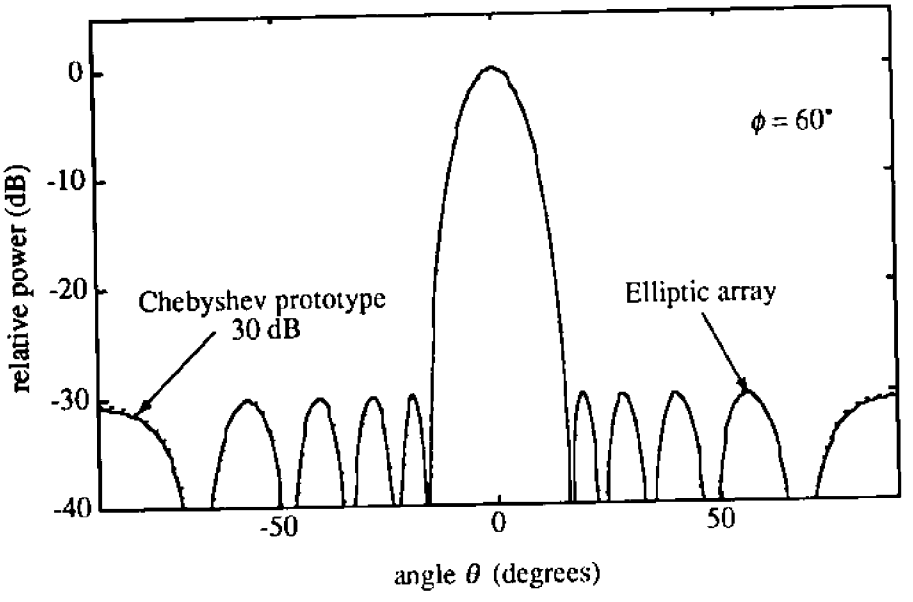

(b)

Figure 4. Radiation patterns of an array of elliptic ring radiators postulated 30 db suppression for different ϕ. (a) $\phi = 0°$, (b) $\phi = 60°$

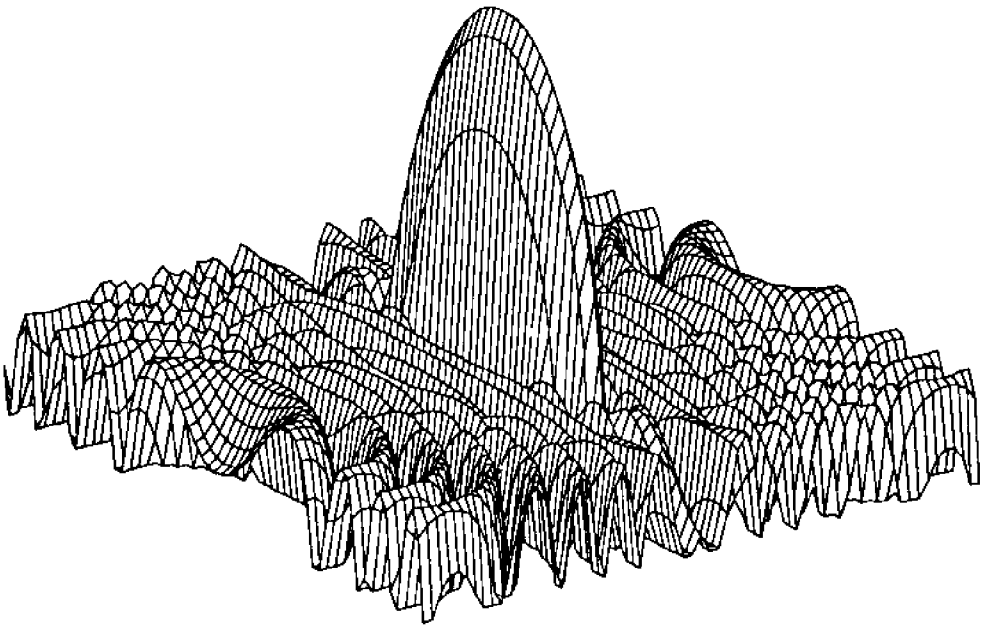

Figure 5. Three-dimensional radiation pattern of an array of elliptic ring radiators postulated 30 dB sidelobe suppression

CONCLUSIONS

Using the novel configuration of an array of elliptic ring radiators it is possible to generate a fan-type beam with greatly suppressed sidelobes. Examples demonstrate that sidelobe suppression of over 40 dB in all possible direction is achievable. This result shows the superior performance of elliptic ring arrays in comparison with rectangular element arrays used in sidescan sonar systems.

ACKNOWLEDGMENT

This work was supported by a Natural Sciences and Engineering Research Council of Canada Operating Grant.

REFERENCES

Clay, C.S., and H. Medwin. 1977. Acoustical Oceanography: Principles and Applications. New York: John Wiley & Sons.

Elliot, R.E. 1966. The Theory of Antenna Arrays. Vol. 2 of Microwave Scanning Antennas, ed. R. C. Hansen. New York: Academic Press.

Ristic, V.M. 1983. Principle of Acoustic Devices. New York: Wiley.

Wilson, O.B. 1988. Introduction to Theory and Design of Sonar Transducers. Los Altos: Peninsula.

Wu, L., and A. Zielinski. 1991. Design considerations for acoustic ring arrays. In: Proc. IEEE Pacific Rim Conf. on Communications, Computers and Signal Processing, pp. 132-137. Victoria.

Zielinski, A., and L. Wu. 1991. A novel array of ring radiators. Special Issue, *IEEE Journal of Oceanic Engineering*. **OE-16**:136-141.

NUMERICAL MODEL OF SOUND PROPAGATION IN THE PACIFIC OCEAN

Renhe Zhang, Yi He, and Hong Liu
Academia Sinica
Beijing, China

ABSTRACT

Although there are many numerical model methods of ocean acoustic fields, each method has certain limitations in application because of the complication of the ocean medium. This paper presents an accurate and fast numerical model method, the WKBZ mode approach, which is a generalization of the well-known WKB method. Numerical simulations show that the approach has not only high accuracy but also fast running speed. The WKBZ mode approach is also extended to gradually range-dependent channels on the basis of the adiabatic mode theory. The approach is applied to the environment in the Philippine Sea, in which gradual horizontal variation of sound velocity is observed. The calculated results are in good agreement with measured data. The presented approach may be further applied to the study of ocean variability using acoustics.

INTRODUCTION

In most regions of the ocean, the vertical gradient of sound velocity is about a thousand times that of the horizontal one, so the ocean is often regarded as a plane-stratified medium in a first approximation (Brekhovskikh, et al., 1982). As the normal mode approach can give an exact solution to the acoustic field in a stratified medium, it is often used to compare with several approximate methods such as ray theory, parabolic equation (PE) method (Tappert, 1977), and Gaussian beam (Porter, et al., 1987) approach, and taken as a criterion to check the accuracy of approximate methods (McDanid, 1975). Although there are many numerical propagation codes based on the mode approach (DiNapoli, et al., 1979), the conventional mode approach is awkward to apply to higher frequency and broadband propagation due to the complication of evaluating a great number of mode eigenvalues and eigenfunctions. The WKBZ approximation (Zhang, 1990; 1981) was proposed, and has been used to evaluate the average and convergence-zone fields in underwater sound channels.

However, in areas of the convergence of cold and warm currents or in regions with meso-scale eddies, the horizontal variation of sound velocity cannot be neglected. The normal-mode method should be extended to range-dependent environment (Pierce, 1965; Milder, 1969) and developed as the coupled mode theory (McDaniel, 1967; Rutherford, et al., 1981; Boyles, 1983). In coupled mode theory, the calculation of eigenvalues, eigenfunctions, and mode coupling coefficients is the most important and difficult problem. When the horizontal variation of an ocean medium is so gradual that the mode coupling may be neglected, an adiabatic mode theory (Nagl, et al., 1987) can be applied and the calculation can be greatly simplified.

In this paper, a new approximate approach to sound propagation in horizontally stratified oceans is first proposed by using the WKBZ approximation, and then the WKBZ mode approach is extended to gradually range-dependent channels on the basis of the

adiabatic mode theory. The first section presents the WKBZ theory. The second section gives numerical simulations of propagation in a North Pacific channel. The third section presents illustrative examples of propagation in the Philippine Sea. The last section summarizes the principal results of this paper.

WKBZ MODE THEORY

In the horizontally stratified ocean, the acoustic field of a harmonic point source in an underwater sound channel is mainly determinated by the waveguide modes, that is,

$$P = \sqrt{\frac{8\pi}{r}} e^{i\frac{\pi}{4}} \sum_{l=0}^{L} \psi_l(z_1)\psi_l(z_2)\sqrt{\upsilon_l}\exp(i\upsilon_l r) \tag{1}$$

where L is the maximum number of waveguide mode, z_1 and z_2 are the source and receiver depths, ν_l and $\psi_l(z)$ are the eigenvalue and eigenfunction of normal mode, respectively.

The WKB approximation is one of the most commonly used approximations to evaluate eigenvalues and eigenfunctions. However, it has singularity at turning depths. In order to overcome the shortcoming of the conventional WKB approximation, the generalized phase-integral approximations were proposed (Zhang, 1981; 1990). Here we call them the WKBZ approximation for short.

Using the WKBZ approximation, the eigenfunction ψ_l with two parameters can be approximately written as

$$\psi_l = \sqrt{\frac{2}{S_l}} \times \begin{cases} \dfrac{\exp\left(-\int_z^{\eta_l} \sqrt{\nu_l^2 - k^2(y,r)}\,dy - \gamma\right)}{\left\{Bb^{4/3} - Db^{2/3}\left[k^2(z,r) - \nu_l^2\right] + 16\left[k^2(z,r) - \nu_l^2\right]^2\right\}^{1/8}} & 0 < z < \eta_l \\ \dfrac{\sin\left(\int_{\eta_l}^{z} \sqrt{k^2(y,r) - \nu_l^2}\,dy + \dfrac{\pi}{2} - \dfrac{\varphi_s}{2}\right)}{\left\{Bb^{4/3} - Db^{2/3}\left[k^2(z,r) - \nu_l^2\right] + \left[k^2(z,r) - \nu_l^2\right]^2\right\}^{1/8}} & \eta_l \le z \le \zeta_l \\ \dfrac{(-1)^l \exp\left(-\int_{\zeta_l}^{z} \sqrt{\nu_l^2 - k^2(y,r)}\right)}{\sqrt{2}\left\{Bb^{4/3} - Db^{2/3}\left[k^2(z,r) - \nu_l^2\right] + 16\left[k^2(z,r) - \nu_l^2\right]^2\right\}^{1/8}} & \zeta_l < z \le H \end{cases} \tag{2}$$

where H is the water depth, $B = 2.152$, $D = 1.619$, $\gamma = -ln(\cos\frac{\varphi_s}{2})$, $b = \left|\frac{\partial k^2(z,r)}{\partial z}\right|$, φ_s the surface phase-shift, S_l the cycle distance of a mode, η_l and ξ_l respectively the turning depths above and below the channel axis.

To illustrate the accuracy of the WKBZ approximation, we discuss the model of a bilinear channel. Figure 1(a) is the sound velocity profile, Figure 1(b) the integrated eigenfunction for l=10, Figure 1(c) the enlarged part of the eigenfunction near the turning depth η_l, in which the solid lines, dashed lines and circular points denote the exact solution, WKB and WKBZ approximations of the eigenfunction, respectively. It can be seen from Figure 1 that the WKB approximation diverges at η_l, while the WKBZ approximation has certain accuracy everywhere.

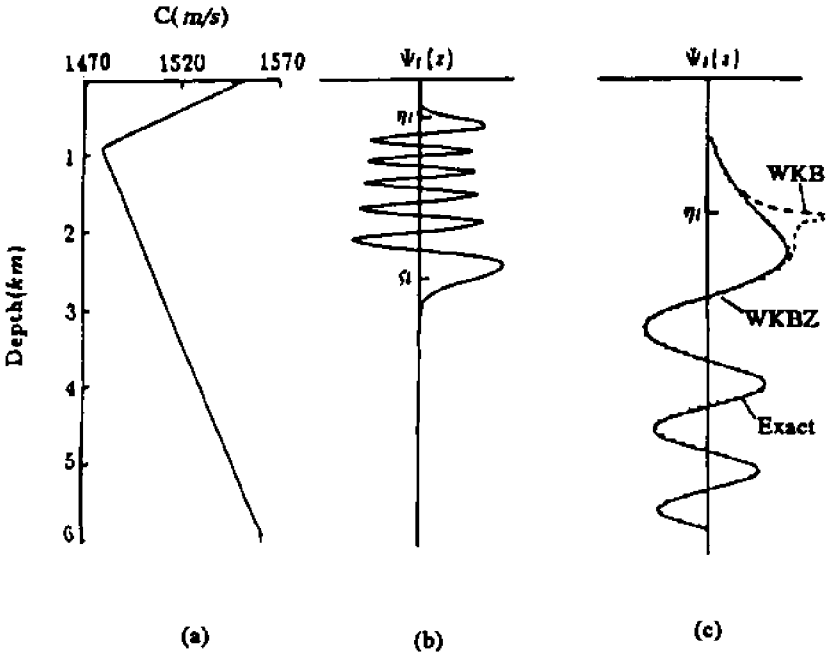

Figure 1. The WKBZ approximation versus the exact solution and WKB approximation

When the upper turning-depth is near surface, it is necessary to take into account the surface phase-shift correction. The eigenvalue equation can be then written as (Haskell, 1951; Tolsoy, 1955; Zhang, 1965)

$$2\int_{\eta_l}^{\xi_l}\sqrt{k^2(y)-\nu_l^2}\,dy-\varphi_s-\varphi_b=2l\pi\ ,\ l=0,1,\ldots,l\ , \tag{3}$$

where φ_s and φ_b are the phase-shifts due to turning (or reflecting) at η_l and ξ_l, respectively. The surface phase-shift φ_s can be expressed as (Zhang, 1965; Murphy, et al., 1974)

$$\varphi_s = \begin{cases} \frac{\pi}{2} + 2\arctan\left(\frac{v(t_0)}{u(t_0)}\right) & t_0 \geq 0 \\ \frac{\pi}{2} + 2\arctan\left(\frac{v(t_0)}{u(t_0)}\right) - 2\omega_0 & t_0 < 0 \end{cases}, \tag{4}$$

where $t_0 = \frac{\left[\nu_l^2 - k^2(0)\right]}{b(0)}$, $b(0) = \left|\frac{dk^2(z)}{dz}\right|_{z=0}$, $\omega_0 = 2/3|t_0|^{3/2}$, $u(t)$ and $v(t)$ are Airy functions (Brekhovskikh, 1980). Incidentally note that the surface phase-shift correction is important for evaluating the eigenvalues (Brown, 1982) and the WKBZ eigenfunctions of the near surface turning modes.

For gradually range-dependent channel, the WKBZ mode approach is easily extended on the basis of the adiabatic mode theory. Assume that the ocean medium varies with horizontal range so gradually that the mode coupling may be neglected, resulting in the "adiabatic approximation". Under the condition of adiabatic approximation, the acoustic field of a harmonic point source may be expressed as (Brekhovskikh, 1982)

$$p(r, z_1, z_2) = \sqrt{\frac{8\pi}{r}} e^{i\frac{\pi}{4}} \sum_l \psi_l(z_1, r)\psi_l(z_2, r)\sqrt{\upsilon_l(0)}\, exp\left(i\int_0^r \upsilon_l(\rho)d\rho\right). \tag{5}$$

where $\nu_l(0)$ and $\nu_l(\rho)$ are the "Local" eigenvalues of modes, $\psi_l(z_1,0)$ and $\psi_l(z_2,r)$ are the "Local" eigenfunctions of modes, respectively at the source and receiver positions.

For definiteness we suppose that the velocity of sea water near the sea-bottom is greater than that near the surface In an ocean channel, there are generally two types of normal modes: the waveguide modes and bottom-reflection modes. For the waveguide modes, the corresponding eigenrays do not touch the sea-bottom, the eigenvalues are real and determined by Eq. (3). For the bottom-reflection modes, the corresponding eigenrays reflect from the sea-bottom, and the eigenvalues are generally complex, i.e., $\nu_l = \mu_l + i\beta_l$. The horizontal wavenumber μ_l and attenuation coefficient β_l are respectively determined by (Zhang, 1974)

$$\int_0^H \sqrt{k^2(y,r) - \mu_l^2(r)}dy = (l + \frac{1}{2})\pi + \frac{1}{2}\varphi_b, \quad l = L+1, L+2, \ldots \tag{6}$$

and

$$\beta_l(r) = \frac{-\ln|V(\mu_l)|}{S_l}, \tag{7}$$

where $V(\mu_l)$ is the bottom-reflection coefficient, $\varphi_b = -\arg V(\mu_l)$.

The contributions of two types of modes to the field are different. The characteristics of long-range propagation, especially the fields in convergence zones are mainly determined by the waveguide modes, while the fields in the deep shadow zones are mainly contributed by the bottom-reflection ones. Since there are a great number of bottom-reflection modes whose spatial interference periods are much shorter, the field of bottom-reflection modes is suitable for smoothly averaging (Zhang, et al., 1990). We then express the whole intensity as $I=I_W+I_B$, where I_W is the intensity of waveguide modes by coherent sum and I_B the smoothly averaged intensity of bottom-reflection modes by incoherent sum.

NUMERICAL SIMULATION OF PROPAGATION IN A NORTH PACIFIC CHANNEL

For illustrative purpose, the WKBZ mode approach is numerically applied to sound propagation in the North Pacific. The sound velocity profile (Boyles, 1984) is showin Figure 2, in which the channel axis is at 686 m and the axis velocity is 1478 m/s.

Figure 3 shows the transmission loss comparison between the WKBZ approximation (WKBZ) and the conventional mode approach (NM), for a frequency of 100 HZ, a source depth of 60 m and a receiver depth of 686 m. In Figure 3, WKBZ-NM denotes the difference of the transmission loss less than 100 dB between WKBZ and NM. It can be seen from the figure that the convergence-zone structures calculated by two codes are coincident very well. As compared to the conventional normal-mode code, the WKBZ mode approach yields reductions of computer time by a factor of 20. So the numerical results show that the WKBZ mode approach is a fast and accurate method to predict the acoustic field of convergence zones in stratified ocean channel, and is suitable for long-range, broadband propagation.

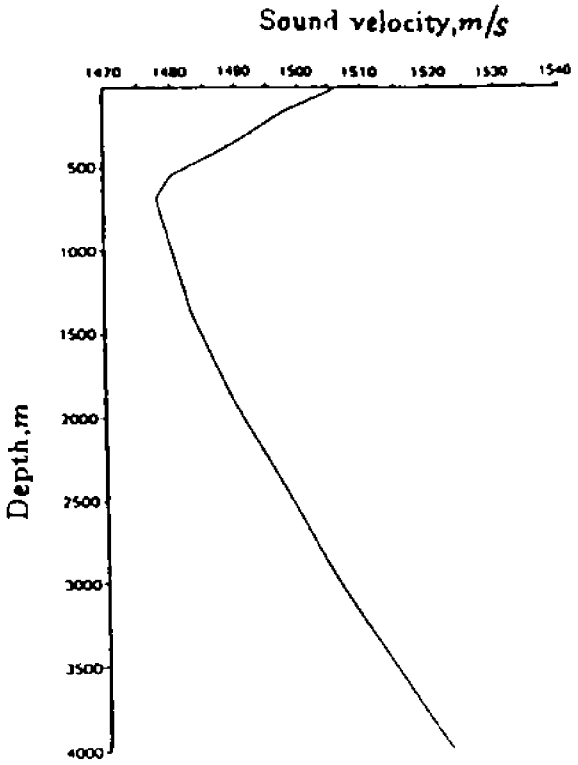

Figure 2. A North Pacific velocity profile

NUMERICAL SIMULATIONS OF PROPAGATION IN THE PHILIPPINE SEA

In this section, we consider sound propagation in the Philippine Sea. Figure 4 shows the velocity profiles measured at 0 and 250 km (Akulichev, 1990), in which the two profiles have obvious difference above the depth of 500 m. So the WKBZ adiabatic mode approach is applied to sound propagation in this region with horizontal variation.

In Figure 5 are shown the transmission-loss curves measured and calculated by using the WKBZ adiabatic mode code for a frequency of 109 Hz, a source depth of 100 m

and a receiver depth of 107 m. Here the sea-water absorption is taken into account in calculated curves. The solid and dashed curves in Figure 5(a) correspond to the intensities of waveguide and bottom-reflection modes; respectively, the curve in Figure 5(b) corresponds to the whole intensities (I_W+I_b), and the curve in Figure 5(c) is the measured one. It can be seen from Figure 5 that the positions and forms of convergence zones calculated and measured are coincident well, and the fields in the deep shadow zones less than 100 km are also consistent with measured data. For the fields in the deep shadow zones beyond 100 km, the measured curve is higher than the calculated one due to the noise background.

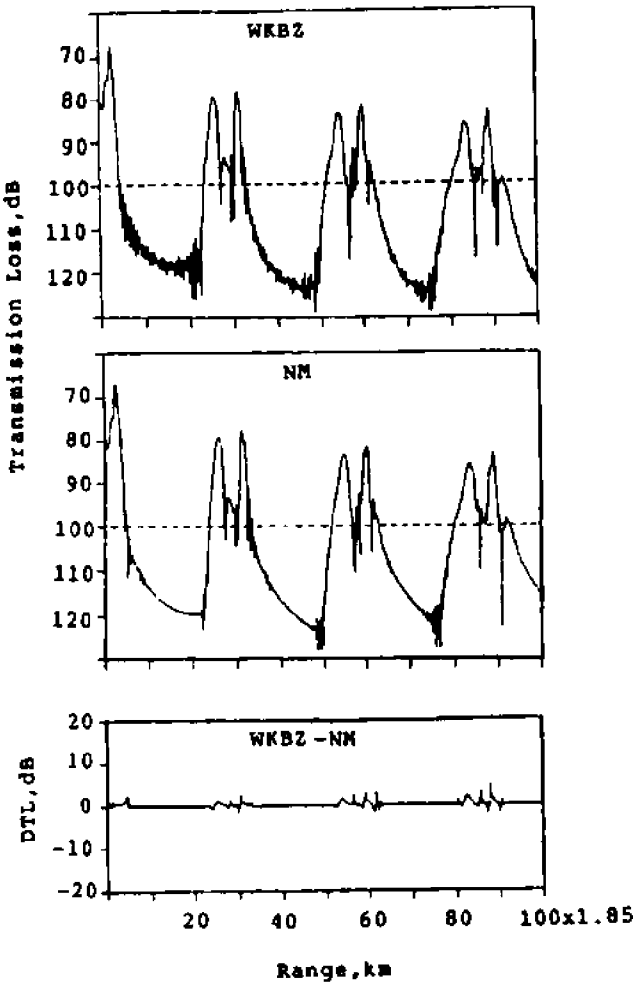

Figure 3. Transmission loss versus range for source depth of 60 m, receiver depth of 686 m, and frequency of 100 Hz

Finally, in Figure 6 is shown a three-dimensional diagram of transmission loss in the Philippine Sea calculated by using the WKBZ adiabatic mode code, in which the spatial structure of acoustic field is demonstrated clearly.

SUMMARY

On the basis of the WKBZ approximation of eigenfunctions and taking account of the surface phase-shift correction, the WKBZ mode approach is proposed in this paper. The WKBZ mode approach has advantages of concise form, easy calculation and high accuracy. The approach is numerically applied to sound propagation in the North Pacific. The comparison of the WKBZ mode approach with the conventional mode approach shows that the WKBZ mode approach is an accurate and fast numerical model method to predict acoustic field of convergence zones in stratified ocean channels.

For gradually range-dependent channels, the WKBZ mode approach is extended on the basis of the abiabatic mode theory. The WKBZ adiabatic mode approach is applied to the environment with gradually horizontal variation of sound speed in the Philippine Sea. The calculated results are in good agreement with measured data. It is noted that the presented approach may be further utilized to study acoustic monitoring of ocean variability.

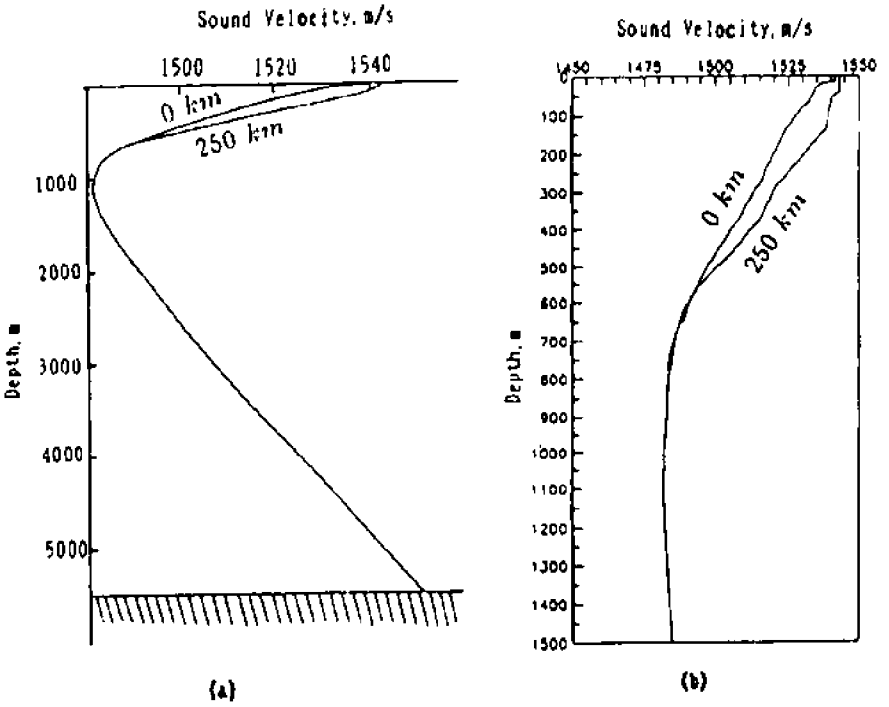

Figure 4. Sound-velocity profiles in the Philippine Sea

REFERENCES

Akulichev, V.A. 1990. Acoustics investigations in Pacific and Indian Oceans. Moscow:Far Eastern Branch of USSR Academy of Sciences.

Boyles, C.A. 1983. Coupled mode solution for a cylindrically symmetric oceanic waveguide with a range and depth dependent refractive index and a time varying rough sea surface. *J. Acoust. Soc. Am.* **73**:800-805.

Boyles, C.A. 1984. Acoustic Waveguide. New York: John Wiley & Sons.

Brown, M.G. 1982. Application of the WKBJ Green's function to acoustic propagation in horizontally stratified ocean. *J. Acoust.S oc. Am.* **71**:1427-1432.

Brekhovskikh, L.M. 1982. Waves in Layered Media. 2nd ed. Academic Press.

Brekhovskikh, L.M., and L. Yu. 1982. Fundamentals of Ocean Acoustics. Berlin: Springer-Verlag.

DiNapoli, F.R., and D.L. Davenport. 1979. Numerical models of underwater acoustic propagation. In: Topics in Current Physics 8: Ocean Acoustics, ed. J.A. DeSanto, Chap. 3, pp. 79-154. New York: Springer-Verlag.

Haskell, N.A. 1951. Asymtotic approximation for the normal modes in sound channel wave propagation. *J. Appl. Phys.* **22**:157-168.

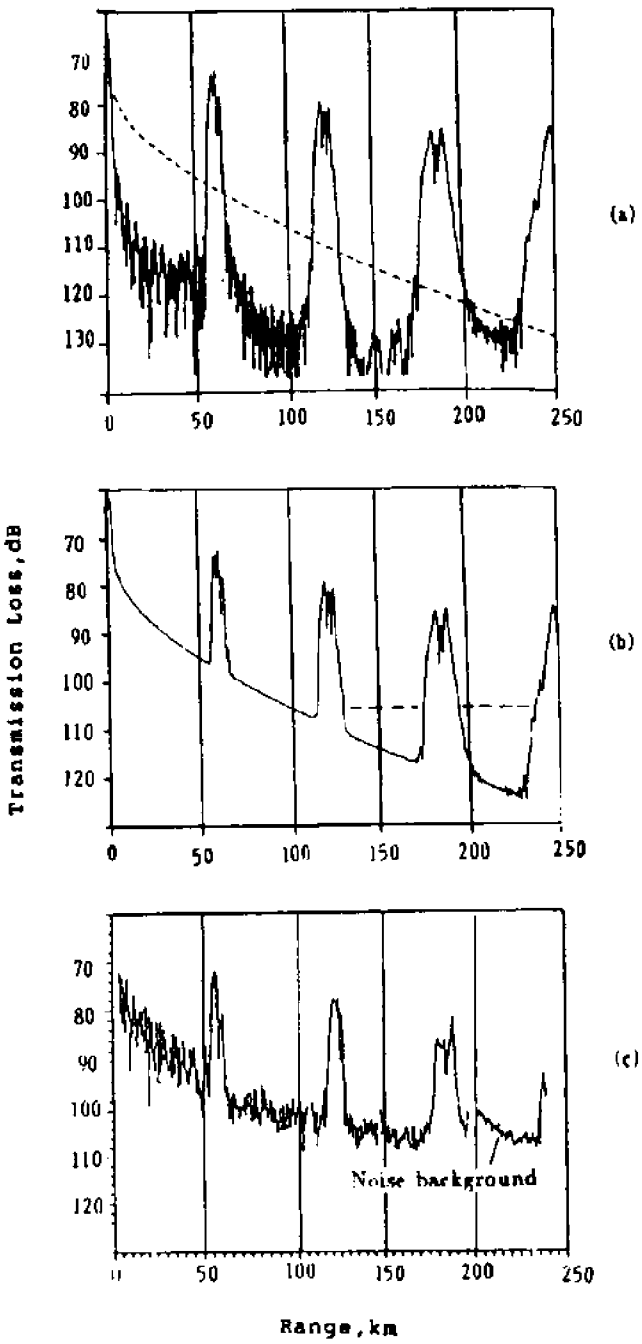

Figure 5. Transmission-loss curves measured and calculated by using the WKBZ adiabatic mode code for frequency of 109 Hz, a source depth of 100 m and a receiver depth of 107 m
(a) Calculated transmission-loss curves corresponding to waveguide (solid curve) and bottom-reflection (dashed curve) modes, respectively
(b) Calculated transmission-loss curves including waveguide and bottom-reflection modes
(c) Measured transmission-loss curve

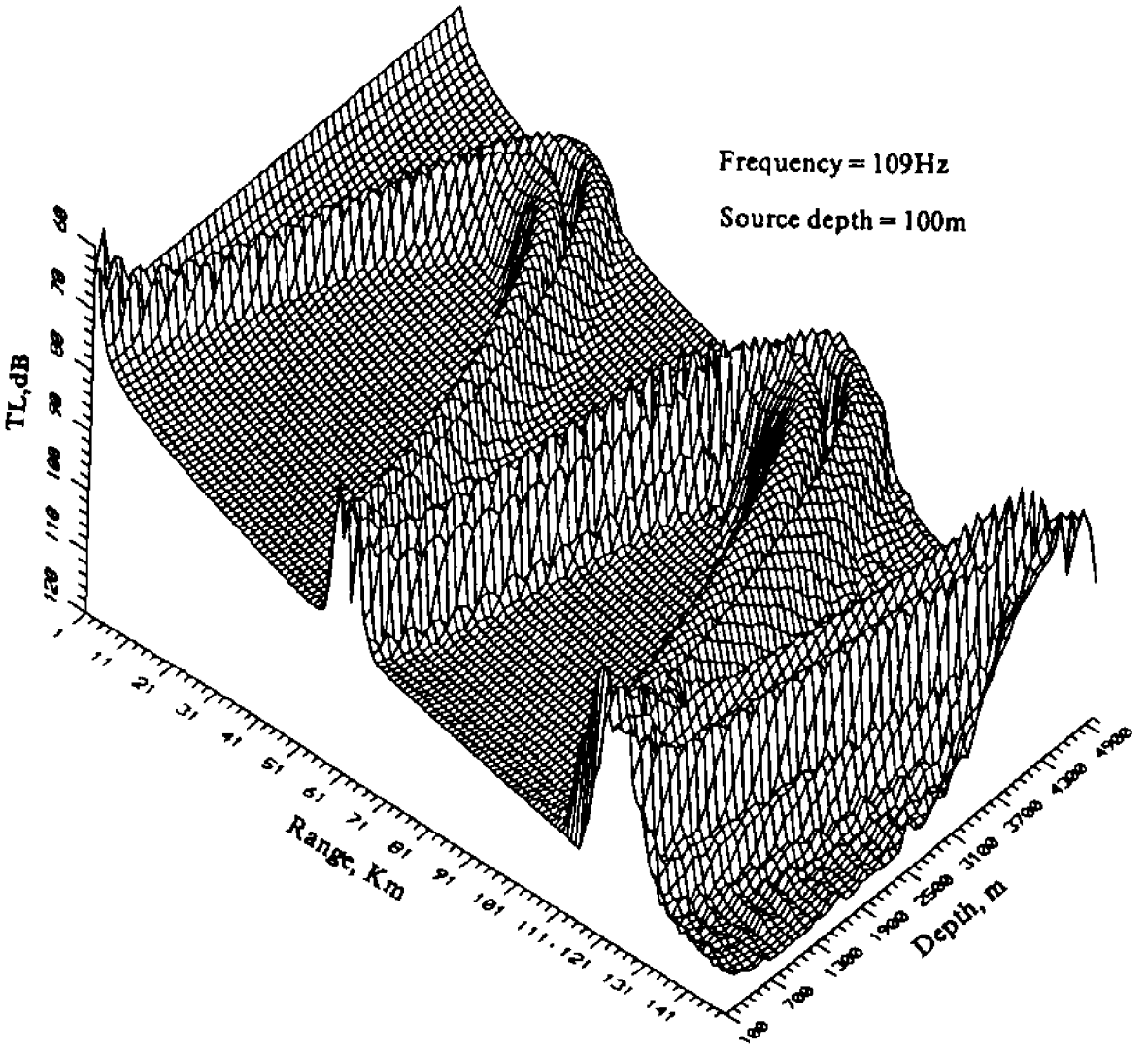

Figure 6. Three-dimensional diagram of acoustic field in the Philippine Sea

McDanid, S.T. 1975. Propagation of normal mode in the parabolic approximation. *J. Acoust. Soc. Am.* **57**:307-311.

McDaniel, S.T. 1967. Coupled power equations for cylindrically spreading waves. *J. Acoust. Soc. Am.* **60**:1285-1289.

Milder, D.M. 1969. Ray and wave invariants of SOFAR channel propagation, *J. Acoust.Soc. Am.* **46**:1259-1263.

Murphy, E.L., and J.A.Davis. 1974. Modified ray theory for bounded media. *J. Acoust. Soc. Am.* **56**:1747-1760.

Nagl.A, H.Uberall, A.Haug, and G.L.Zarur. 1978. Adiabatic mode theory of underwater sound propagation in a range-dependent environment. *J. Acoust. Soc. Am.* **63**:734-749.

Pierce, A.D. 1965. Extension of the method of normal modes to sound propagation in an almost-stratified medium. *J. Acoust. Soc. Am.* **37**:19-27.

Porter, M.B., and H.P. Backer. 1987. Gaussian beam tracing for computing ocean acoustic fields. *J. Acoust. Soc. Am.* **82**:1349-1359.

Rutherford, S.R., and K.E. Hawker. 1981. Consistent coupled theory of sound propagation for a class of nonseparable problem. *J. Acoust. Soc. Am.* **70**:554-564.

Tappert, F.D. 1977. The parabolic approximation method. In: Lecture Notes in Physics, No.70, Wave Propagation and Underwater Acoustics, eds. J.B. Keller and J. Papadakis. Berlin: Springer-Verlag.

Tolsoy, J. 1955. Note on the propagation of normal modes in inhomogeneous media. *J. Acoust. Soc. Am.* **27**:274-278.

Zhang, R. 1965. Normal-mode acoustic field in shallow water with negative speed gradient. *Acta Acoustic.* **2**:24-28.

Zhang, R. 1974. Normal-mode acoustic field in a shallow-water surface channel. *Acta Physical Sinica*. **24**:200-209.

Zhang, R. 1981. Turning-point convergence-zones in underwater sound channel (I). *Chinese Physics*, **1**:1064-1078.

Zhang, R. and Q. Wang, 1990. Range and depth averaged fields in ocean sound channels. *J. Acoust. Soc. Am.* **87**:633-638.

NUMERICAL SIMULATION OF A DISTANT SMALL-SCALE TSUNAMI

Sung B. Yoon and Philip L.F. Liu
Cornell University
Ithaca, New York, U.S.A

ABSTRACT

An efficient numerical model is developed to simulate the propagation of distant small-scale tsunami. The model solves the linear shallow water equations using the finite element leap-frog scheme whose numerical dispersion replaces the physical dispersion of Boussinesq equations. The finite element technique has an advantage over the finite difference scheme in adjusting mesh size according to local water depth and in giving correct dispersion effects. Simulation of the 1983 Japan Sea tsunami reveals many new phenomena such as the role of the Yamato Rise and the submerged ridge as a wave guide.

INTRODUCTION

The seafloor in the Japan Sea contains active earthquake zones which have generated tsunamis causing significant damage along the Japanese coastline. These tsunamis also propagated across the Japan Sea and attacked the southeastern part of the Korean coastline.

An effective way for tsunami hazard mitigation planning is to establish inundation zones along those coastlines vulnerable to tsunami attacks. To produce reliable inundation estimates, it is essential to develop a numerical model which accurately calculates tsunami propagation from a source region to coastal areas (target regions) and the resulting tsunami run-up and flooding.

Because the earthquake zones are located along the east rim of the Japan Sea, tsunamis travel a long distance across the entire Japan Sea before reaching the east coast of Korea. The source dimension, however, is much shorter than the propagation distance. Therefore, the dispersion effects of waves are important for accurate simulation of transoceanic wave propagation.

In this study we develop a finite element model based on the leap-frog scheme to simulate tsunami propagation over a long distance. The finite element model solves the shallow water equations, but the solution given by the model contains the numerical dispersion which plays an equivalent role of physical dispersion of the Boussinesq equations. The numerical model is verified using known analytical solutions and tide gauge records for the 1983 Japan Sea Central Region Earthquake Tsunami.

GOVERNING EQUATION

If the wave length of a tsunami is long in comparison with typical water depth but is much shorter than the tsunami propagation distance, the dispersion effects are important. Since the nonlinearity is negligibly small except for the regions very near the shore, the linear Boussinesq equations can be used for the most part of the open sea. A

conservative form of Boussinesq equations for the case of slowly varying topography can be written as:

$$\eta_t + p_x + q_y = 0 \tag{1}$$

$$p_t + gh\eta_x = -\frac{gh^3}{3}(\eta_{xx} + \eta_{yy})_x \tag{2}$$

$$q_t + gh\eta_y = -\frac{gh^3}{3}(\eta_{xx} + \eta_{yy})_y \tag{3}$$

where p and q are the flux components in the x and y directions, respectively, h denotes water depth and η represents free surface displacement. The subscripts represent partial differentiation. For the unidirectional (1-D) tsunami waves over constant depth, the linear Boussinesq equations can be reduced as:

$$\eta_t + p_x = 0 \tag{4}$$

$$p_t + gh\eta_x = -\frac{gh^3}{3}\eta_{xxx} \tag{5}$$

which gives the following dispersion relationship for a periodic wave train:

$$C \equiv \frac{\omega}{k} = \sqrt{gh}\sqrt{1 - \frac{k^2h^2}{3}} \tag{6}$$

where C is the phase speed and ω and k are the frequency and wave number, respectively. The inclusion of dispersion in Boussinesq equations gives a slower phase speed for $k \neq 0$ than that of infinitely long waves (i.e., $k \approx 0$).

NUMERICAL SCHEME

The leap-frog scheme has been widely employed to simulate short wave propagation over long distances due to its nondissipative nature. However, the leap-frog scheme is subject to numerical dispersion whose effect on propagating short waves is similar to that of physical dispersion. In this study we employ the leap-frog scheme to solve shallow water equations rather than Boussinesq equations and the physical dispersion effect will be represented by numerical dispersion by adjusting the step size according to the time step and local water depth as:

$$\Delta x = \sqrt{4h^2 + gh\Delta t^2} \tag{7}$$

This scheme was first introduced by Imamura (1989) in the framework of a finite difference leap-frog scheme with a staggered mesh.

It is, however, difficult to generate finite difference meshes which satisfy the condition (Eq. (7)) for the cases of a variable depth in two dimensions. To overcome this

shortcoming associated with the finite difference scheme, a finite element scheme is developed to solve the linear shallow water equations:

$$\eta_t + p_x + q_y = 0 \tag{8}$$

$$p_t + gh\eta_x = 0 \tag{9}$$

$$q_t + gh\eta_y = 0 \tag{10}$$

In this study, the Galerkin finite element method is employed to solve the shallow water equation (8)-(10). The flow field is divided into linear triangular elements. The free surface displacement, η, and flux components, p and q, are interpolated as:

$$\eta = \Phi_\alpha \eta_\alpha, \qquad p = \Phi_\alpha p_\alpha, \qquad q = \Phi_\alpha q_\alpha \tag{11}$$

where Φ denotes the linear interpolation function and the variables with subscript α (= 1, 2, 3) represent the value at the αth node of each element. The Galerkin procedure gives the following finite element equations:

$$M_{\alpha\beta}\dot{\eta}_\beta + B_{\alpha\beta}P_\beta + C_{\alpha\beta}q_\beta = 0 \tag{12}$$

$$M_{\alpha\beta}\dot{P}_\beta + R_{\alpha\beta\gamma}h_\beta\eta_\gamma = 0 \tag{13}$$

$$M_{\alpha\beta}\dot{q}_\beta + S_{\alpha\beta\gamma}h_\beta\eta_\gamma = 0 \tag{14}$$

where the dot denotes the time derivative and

$$\begin{aligned} M_{\alpha\beta} &= \int_\Omega (\Phi_\alpha \Phi_\beta) d\Omega \\ B_{\alpha\beta} &= \int_\Omega (\Phi_\alpha \Phi_{\beta,x}) d\Omega \\ C_{\alpha\beta} &= \int_\Omega (\Phi_\alpha \Phi_{\beta,y}) d\Omega \\ R_{\alpha\beta\gamma} &= g\int_\Omega (\Phi_\alpha \Phi_\beta \Phi_{\gamma,x}) d\Omega \\ S_{\alpha\beta\gamma} &= g\int_\Omega (\Phi_\alpha \Phi_\beta \Phi_{\gamma,y}) d\Omega \end{aligned} \tag{15}$$

The time derivatives are approximated by the central difference scheme, for example,

$$\eta_\beta = \frac{\eta_\beta^{n+1} - \eta_\beta^{n-1}}{2\Delta t} \tag{16}$$

where the superscript n denotes time step and all the spatial derivatives are evaluated at the nth time step. Substituting time derivatives into Eqs. (12)-(14) gives:

$$M^{*}_{\alpha\beta} p^{n+1}_{\beta} = M^{*}_{\alpha\beta} p^{n-1}_{\beta} - 2\Delta t R_{\alpha\beta\gamma} h_{\beta} \eta^{n}_{\gamma} \tag{18}$$

$$M^{*}_{\alpha\beta} q^{n+1}_{\beta} = M^{*}_{\alpha\beta} q^{n-1}_{\beta} - 2\Delta t S_{\alpha\beta\gamma} h_{\beta} \eta^{n}_{\gamma} \tag{19}$$

where $M^{*}_{\alpha\beta}$ is the lumped coefficient matrix obtained by row sum of $M_{\alpha\beta}$ to ensure the pure explicit scheme.

The 1-D version of finite element equations (17)-(19) for a constant depth can be represented in the following form:

$$\frac{\eta^{n+1}_{i} - \eta^{n-1}_{i}}{2\Delta t} + \frac{p^{n}_{i+2} - p^{n}_{i-1}}{2\Delta x} = 0 \tag{20}$$

$$\frac{p^{n+1}_{i} - p^{n-1}_{i}}{2\Delta t} + \frac{\eta^{n}_{i+2} - \eta^{n}_{i-1}}{2\Delta x} = 0 \tag{21}$$

where the subscript i represents spatial step and the superscript n denotes time step. Using the Taylor series expansion, Eqs. (20) and (21) can be recast into differential equations:

$$\eta_{t} + p_{x} = 0 \tag{22}$$

$$p_{t} + gh\eta_{x} = -\frac{gh\Delta x^{2}}{3}(1 - \upsilon^{2})\eta_{xxx} + 0(\Delta t^{4}, \Delta x^{4}, \Delta t^{2}, \Delta x^{2}) \tag{23}$$

where υ is the Courant number defined by:

$$\upsilon = \sqrt{gh}\,\frac{\Delta t}{\Delta x} \tag{24}$$

The right-hand side of Eq. (23) represents the numerical dispersion error resulting from the finite element approximation of shallow water equations through the leap-frog scheme. These modified equations give the dispersion relationship for a periodic wave as:

$$C \equiv \frac{\omega}{k} = \sqrt{gh}\sqrt{1 - \frac{k^{2}\Delta x^{2}}{3}(1 - \upsilon^{2})} \tag{25}$$

The above dispersion relationship becomes the same as that given by Boussinesq equations (6) if we define

$$\Delta x = \sqrt{h^{2} + gh\Delta t^{2}} \tag{26}$$

which is slightly different from the condition (7) given by Imamura (1989) due to the different definition of step sizes. For the two-dimensional cases this condition gives slightly less numerical dispersion for the waves propagating obliquely to the mesh alignment than along the main axes (see Imamura & Goto, 1988).

TEST OF NUMERICAL MODEL

To verify the accuracy of the finite element model, tsunami waves propagating radially in two dimension over a horizontal bottom (h = 10 m) are simulated. The initial free surface displacement η is given by Gaussian hump centered at the origin ($x = y = 0$) as:

$$\eta(x,y,t=0) = 2e^{-(x^2+y^2)/a^2} \tag{27}$$

where a, the characteristic width of Gaussian hump, is set to be 50 m.

The exact solution of a linear KdV equation is given by Carrier (1990) as:

$$\eta(r,t) = \int_0^\infty \rho J_o(\rho r)\cos\left(\frac{\rho t}{\sqrt{1+h^2\rho^2/3}}\right)e^{-\rho^2/4}d\rho \tag{28}$$

where $r(=\sqrt{x^2+y^2}/a)$ is the normalized distance from the origin, J_o is the Bessel function of the first kind of order zero. The integration is performed numerically using Gaussian quadratures. As shown in Figure 1, the uniform mesh size $\Delta x(=\Delta y)$ is chosen as 14.142 m which satisfies the condition (26) according to the time step Δt=1 sec.and water depth h= 0 m.

Figure 2 shows the comparison between exact and numerical solution at 300 sec. Numerical solutions are presented along the x-axis ($\overline{OA}$), the y-axis ($\overline{OC}$) and the diagonal line ($\overline{OB}$) (see Figure 1). The numerical result shows stronger dispersion effects than the exact solution in all directions of propagation, and this dispersion effect seems to decrease when the waves propagate obliquely to the main axes as predicted by Imamura & Goto (1988). The finite element leap-frog scheme gives reasonable solutions for leading waves, but slight deviations for the tail of wave group.

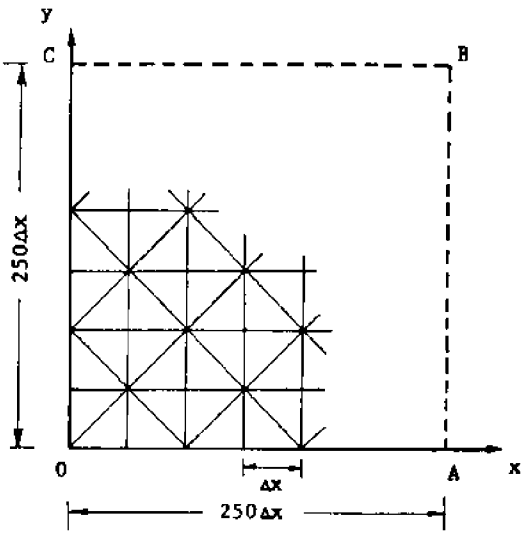

Figure 1. Finite element mesh for model test

SIMULATION OF 1983 JAPAN SEA TSUNAMI

For verification of numerical models developed in this study, the 1983 Japan Sea Central Region Earthquake Tsunami (1983 Tsunami hereafter) is simulated. The Japan Sea is bordered by Russia and Korea on the northwest and by Japan on the southeast as shown in Figure 3. Its dimension is roughly 1200 km x 1200 km. Since the source area of the tsunami is small (30 km x 100 km) in comparison with the entire Japan Sea and the bathymetry is complicated due to the presence of submerged rises and ridges, the finite element model has an advantage over the finite difference model in satisfying Eq. (26) everywhere for the correct dispersion effect.

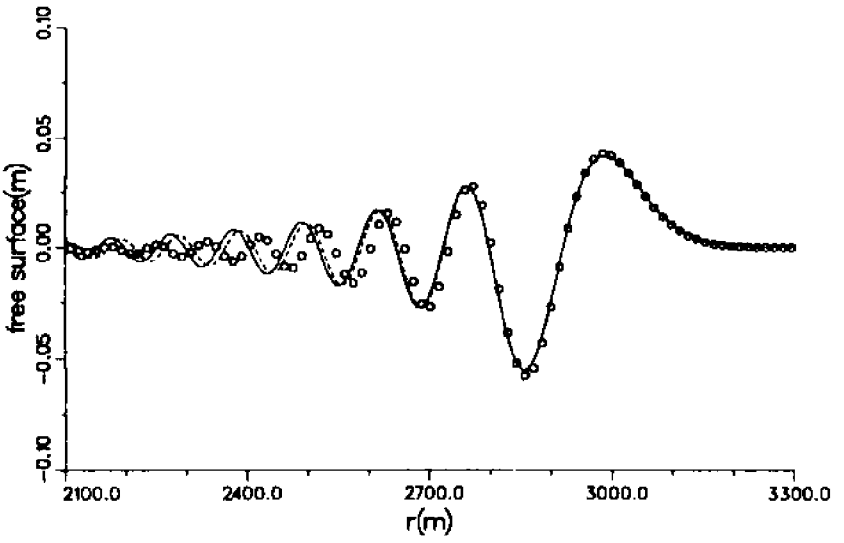

Figure 2. Comparison of free surface displacements at 300 sec.
oooo analytical
--- numerical along x & y axes
------ numerical along y=x

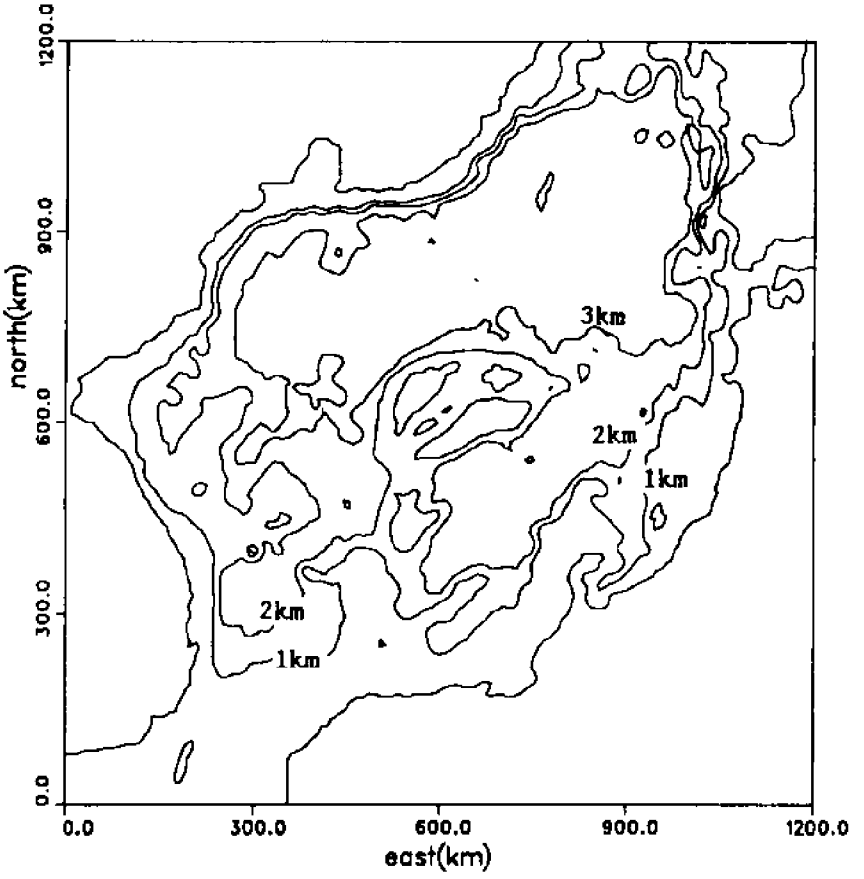

Figure 3. Bathymetry of the Japan Sea

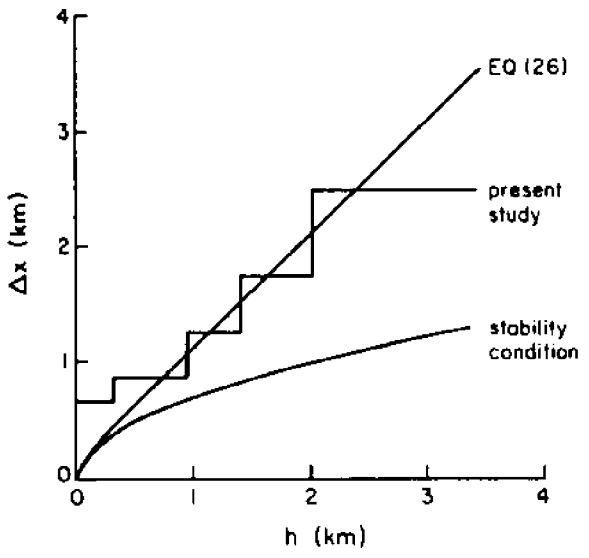

Figure 4. Finite element mesh size based on time step 5 sec.

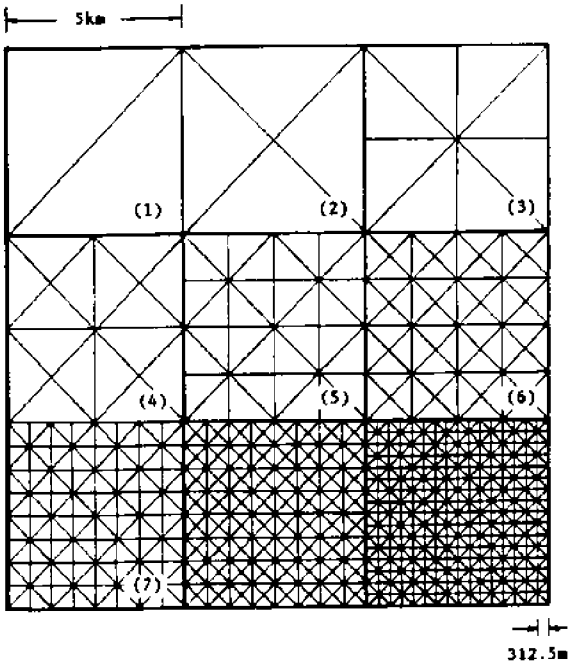

Figure 5. Finite element mesh employed in simulation of 1983 Tsunami

Figure 4 shows the mesh size determined by Eq. (26) for different water depths associated with the given time step of 5 sec. The entire Japan Sea is discretized into 629,147 triangular elements with 317,372 nodes using the first seven types of elements as shown in Figure 5. The distribution of these elements is shown in Figure 6.

To obtain the initial displacement of water surface due to the 1983 Tsunami, the fault parameters of Aida model-10 are employed (Aida, 1984). The vertical displacement of sea bottom at the source area is calculated using the theory of Manshinha and Smylie (1971) and is assumed to be the same as that of the water surface. All the flux components, p and q, are assumed as zero.

The arrival times of the leading wave from simulation are compared with tide gauge record along the southeast coast of Korea and along the northwest coast of Japan in Figures 7 and 8 where the locations are shown in Figure 9. Except for a few locations, the agreement between observed and calculated arrival times are good.

Figure 10 shows the distribution of highest water level obtained from the numerical simulation. The northern Akita coast of Japan (JA) is expected to have the largest wave heights due to the orientation of source and short distance from the source. The main waves propagating over the Yamato Rise (YM) are converged behind the rise and trapped along the submerged ridge joining Yamato Rise and Shimane Peninsula (JF) of Japan. Some portions of the main waves travel toward the east coast of Korea (KA). As a result three main peaks develop near North Akita Coast (JA), Shimane Peninsula (JF), and the east coast of Korea (KA). More local peaks appear at the Yamagata region (JB), the north part of Sado Island (JC), Noto Peninsula (JD), and the Tsuiyama-Maizuru region (JE).

The mesh size used near shore is too coarse to give quantitative agreement with tide gauge records, since the tide gauges are usually located deep inside a harbour

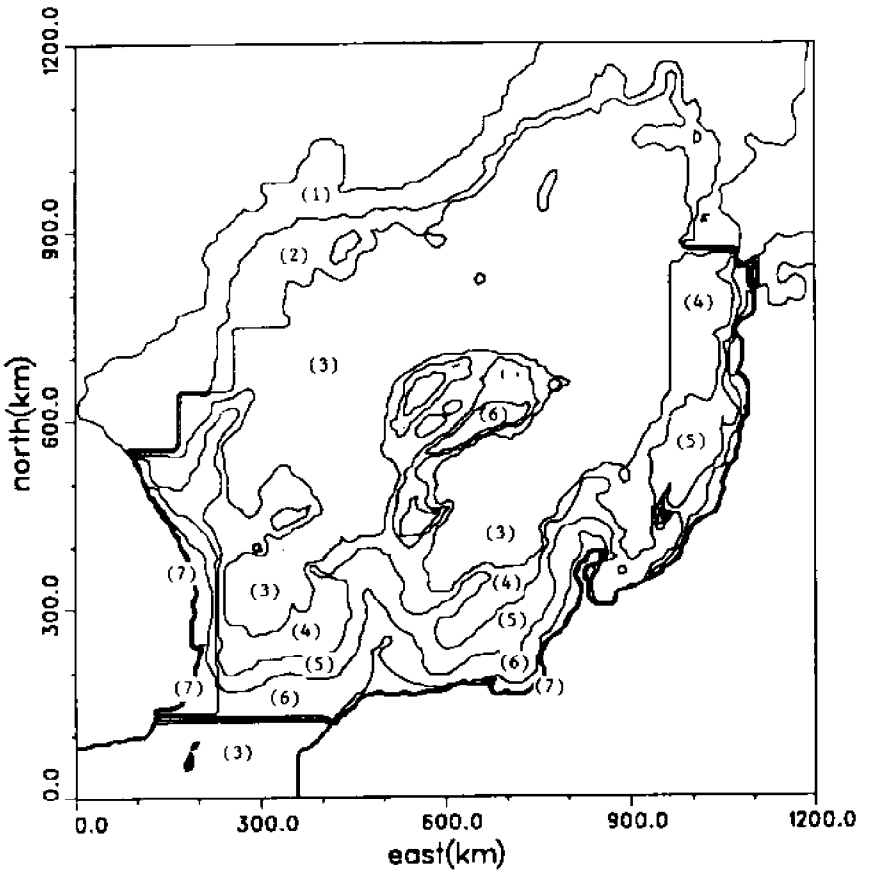

Figure 6. Finite element discretization of Japan Sea for the simulation of the 1983 Tsunami

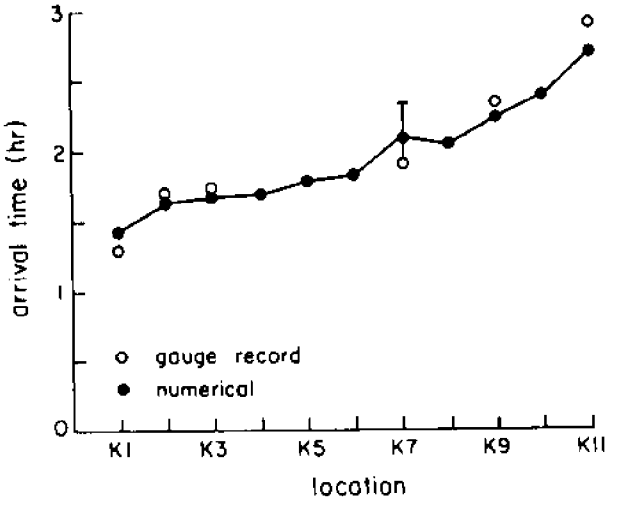

Figure 7. Comparison of arrival time along east coast of Korea (see Figure 9 for locations)

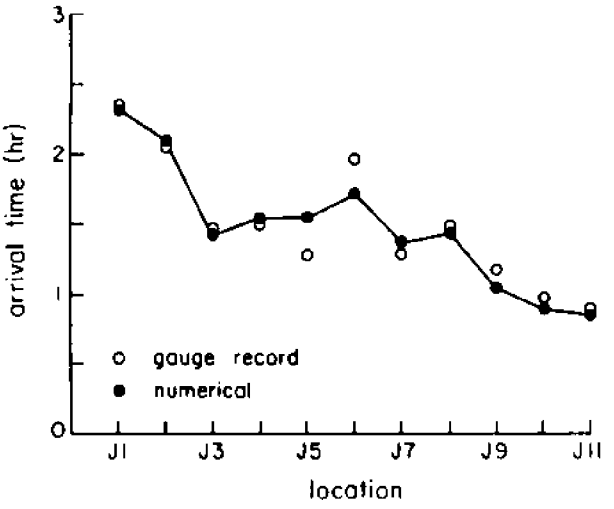

Figure 8. Comparison of arrival time along east coast of Japan (see Figure 9 for locations)

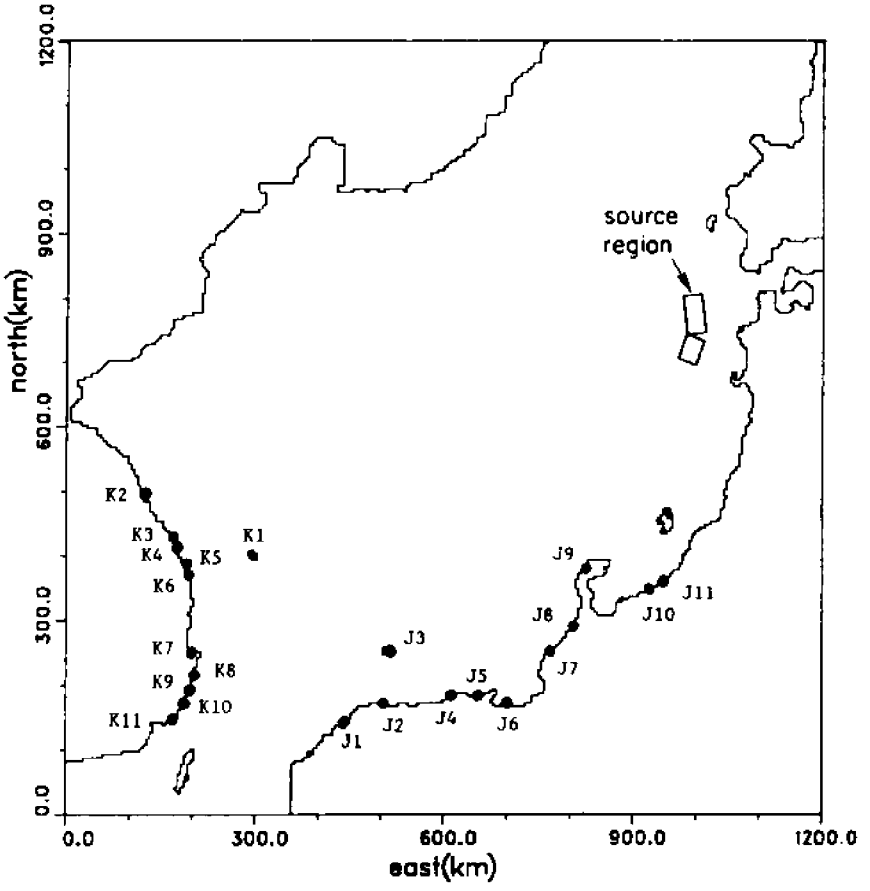

Figure 9. Location of arrival time checking stations

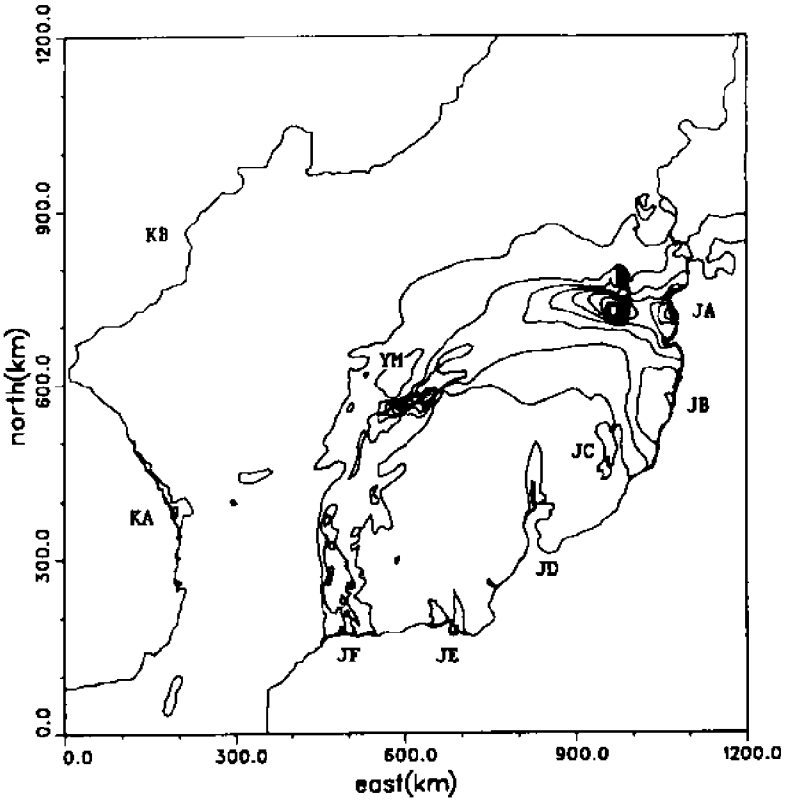

Figure 10. Distribution of computed highest water levels with contour increment of 0.25 m

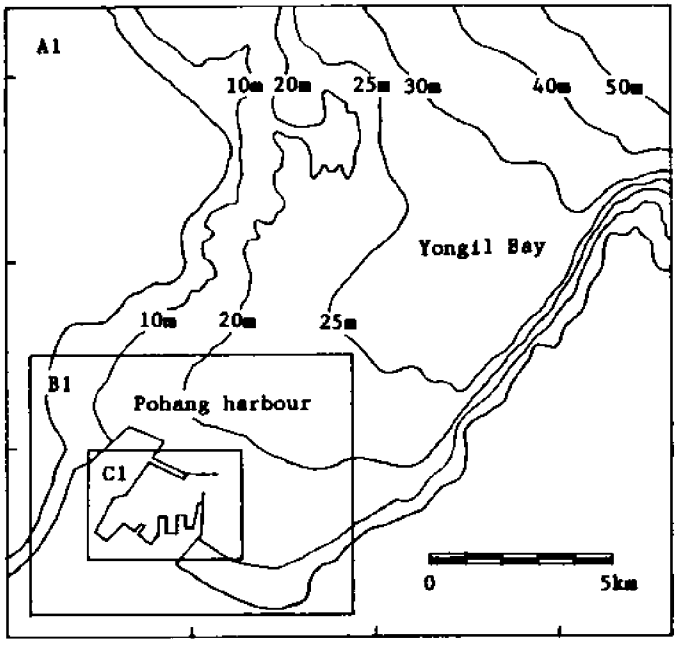

Figure 11. Bathymetry near Pohang Harbour of Korea

protected by coastal structures. For the detailed local computations, the finite difference model developed by Shuto, et al. (1986) is employed. The finite difference model solves the full shadow water equations based on the leap-frog scheme with staggered mesh. Some special features such as wave run-up, overtopping, and nesting etc., are also included in the model to study the interaction of tsunamis with complicated geometry.

The Pohang Harbour located at the southeast coast of Korea is chosen to verify the detailed finite difference model. The bathymetry near Pohang Harbour is presented in Figure 11 which shows three regions, A1, B1 and C1, for the nesting of different mesh size regions. The mesh sizes are 625 m, 208.33 m, and 69.44 m for A1, B1, and C1 regions, respectively. The time step is 1 sec. The time history of fluxes and free surface displacement obtained from the finite element model is prescribed along the open boundaries of the computational domain (A1 region).

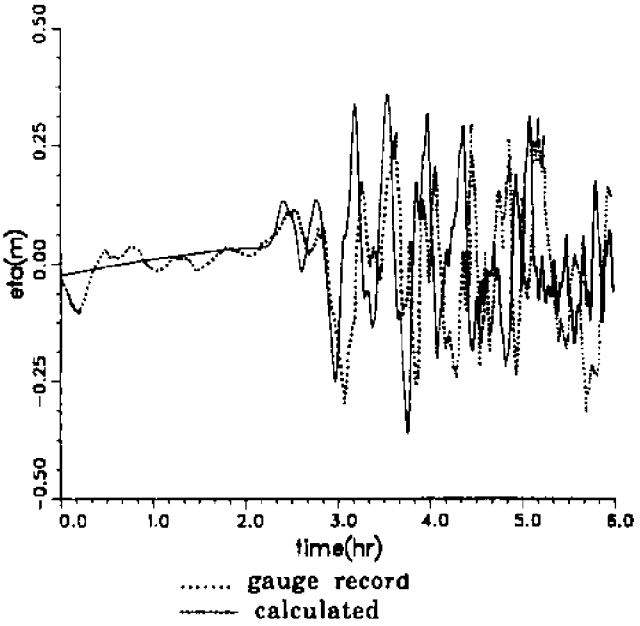

Figure 12. Comparison of water surface elevation time history at gauge station of Pohang Harbour

The calculated time history of water surface at the tide gauge station inside the harbour is compared with the gauge record in Figure 12 for 6 hours after generation of the 1983 Tsunami. The tide gauge record shows some wind waves (wave height of 12.5 cm) and tides before the tsunami wave arrives at the harbour. The first two waves are smaller than the third wave due to the dispersion effect of waves described earlier. This shows clearly that the dispersion effect is important for accurate prediction of a distant tsunami. The predominant period of tsunami waves is approximately 25 min. for both cases of numerical and recorded time histories, while the tide gauge records of other locations along east coast of Korea show much shorter wave periods (10-15 min.). The calculated highest water level gives larger values than the recorded one by 5 cm and the lowest water level from computation is 4 cm lower than observed one. The calculated wave arrives at the gauge point earlier by 5 cm and continuously leads the phase of recorded wave. This discrepancy of wave height and phase could be explained by the characteristics of tide gauge itself (Lander & Lockridge, 1990). The agreement between numerical prediction and tide gauge record is reasonable if the pre-existing wind waves and the tide gauge characteristics are taken into consideration.

CONCLUDING REMARKS

The finite element model developed in this study is shown to be efficient and accurate to simulate the propagation of distant small-scale tsunamis where the dispersion effect is important. The model can be used in conjunction with other detailed run-up models to establish inundation maps for the areas vulnerable to tsunami attacks.

The numerical simulation of the 1983 Tsunami shows that the Yamato Rise acts as a focusing lens and the submerged ridge connecting Yamato Rise to Shimane Peninsula of Japan plays the role of a wave guide. These topographic changes should be taken into account for the accurate estimation of tsunami wave heights for the areas of the east coast of Korea and the west part of Japan.

ACKNOWLEDGMENT

This research was carried out with support from the Korea Power Engineering Company and the National Science Foundation. The finite difference detail model was kindly provided by Dr. N. Shuto and Dr. F. Imamura of Tohoku University, Japan. The 3-D animation of the 1983 Tsunami was made by Miss Catherine Devine of Cornell Theory Center.

REFERENCES

Aida, I. 1984. A source model of the tsunami accompanying the 1983 Nihonkai-Chubu earthquake. *Bull. Earthq. Res. Inst.* **59**:235-265. (in Japanese)

Carrier, G.F. 1991. Tsunami propagation from a finite source. In: Proc. of 2nd UJNR Tsunami Workshop, NGDC, Honolulu, Hawaii. pp. 101-115.

Imamura, F. 1989. Possibility of tsunami numerical forecasting. Ph.D. diss., Tohoku University (in Japanese).

Imamura, F., and C. Goto. 1988. Truncation error in numerical tsunami simulation by the finite difference method. *Coastal Engineering in Japan.* **31**(2):245-263.

Lander, J.F., and P.A. Lockridge. 1990. United States Tsunamis (including United States Possessions) 1690-1988. National Geophysical Data Center, Boulder, Colorado.

Manshinha, L., and D.E. Smylie. 1971. The displacement fields of inclined faults. *Bull. Seism. Soc. Am.***61**:1433-1440.

Shuto, N., T. Suzuki,K. Hasegawa, and K. Inagaki. 1986. A study of numerical technique on the tsunami propagation and run-up. *Science of Tsunami Hazards, the Intl. J. of the Tsunami Society.* **4**(2):111-124.

MODELING TSUNAMI FLOODING OF HILO, HAWAII

Charles L. Mader, George D. Curtis, and George Nabeshima
University of Hawaii
Honolulu, Hawaii, U.S.A.

ABSTRACT

The interaction of tsunami waves with Hilo Bay and harbor is being numerically modeled for specific historical events. The modeling is performed using the *SWAN* code which solves the nonlinear long wave equations.

The 1946, 1960 and 1964 tsunamis are being studied. The tsunami generation and propagation to the Hawaiian Islands were modeled using a 20 minute grid for the North Pacific or for the entire Pacific Ocean. The wave arriving in the region of the Hawaiian Islands was then modeled using a 5 minute grid to follow the wave to the mouth of Hilo Bay. The wave arriving at the mouth of Hilo Bay was then modeled using a 100 meter grid of Hilo Bay, harbor and town. Each grid had a friction coefficient to describe the local roughness (trees, grass, buildings, coral, etc.). The models gave approximately the observed maximum areas of flooding.

The observed levels of flooding at individual locations was not well described by the 100 meter grid, so a 10 meter grid of Hilo was developed to resolve the flooding at individual locations and around large buildings.

The high resolution 10 meter grid of Hilo was used to model the flooding around Hilo Theater by the 1960 tsunami wave. The Hilo Theater was located near the shore, in flat and unobstructed terrain 2.7 meters above sea level. The tsunami flooded level reached 8.5 meters at the seaward side and 6.7 meters at the rear of the Hilo Theater. The third bore-like wave arriving at the harbor entrance in the 100 meter grid model was used as the tsunami source for the high resolution study of flooding around Hilo Theater. The maximum level of flooding observed at Hilo Theater was reproduced by the high resolution numerical model.

THE NUMERICAL MODEL

The tsunami waves and their interaction with the study site topography were numerically modeled using the *SWAN* code which solves the shallow water long wave equations. It is described in detail in the monograph *Numerical Modeling of Water Waves* by Mader (1988).

The long wave equations solved by the *SWAN* code are

$$\frac{\partial U_x}{\partial t} + U_x \frac{\partial U_x}{\partial x} + U_y \frac{\partial U_x}{\partial y} + g \frac{\partial H}{\partial x} = FU_y + F^{(x)} - g \frac{U_x (U_x^2 + U_y^2)^{1/2}}{C^2 (D + H - R)} ,$$

$$\frac{\partial U_y}{\partial t} + U_x \frac{\partial U_y}{\partial x} + U_y \frac{\partial U_y}{\partial y} + g \frac{\partial H}{\partial y} = FU_x + F^{(y)} - g \frac{U_y (U_x^2 + U_y^2)^{1/2}}{C^2 (D + H - R)} ,$$

and

$$\frac{\partial H}{\partial t} + \frac{\partial (D+H-R)U_x}{\partial x} + \frac{\partial (D+H-R)U_y}{\partial y} - \frac{\partial R}{\partial t} = 0 ,$$

where

U_x	=	velocity in x direction (i index)
U_y	=	velocity in y direction (j index)
g	=	gravitational acceleration
t	=	time
H	=	wave height above mean water level
R	=	bottom motion
F	=	Coriolis parameter
C	=	coefficient of DeChezy for bottom stress
$F(x), F(y)$	=	forcing functions of wind stress and barometric pressure in x and y direction
D	=	depth.

As described in the monograph, the *SWAN* code has been used to study the interaction of tsunami waves with continental slopes, shelves, bays and harbors such as Hilo harbor.

The *SWAN* code has been used to study the interaction of tsunami waves with continental slopes and shelves, as described in Mader (1974). Comparison with two-dimensional Navier-Stokes calculations of the same problems showed similar results, except for short wavelength tsunamis.

The SWAN code was used to model the effects of tides on the Musi-Upang estuaries, South Sumatra, Indonesia, by Hadi (1985). The computed tide and water discharge were in good agreement with experimental data.

The *SWAN* code was used to model the large waves that were observed to occur inside Waianae harbor under high surf conditions in Mader and Lukas, (1985). These waves have broken moorings of boats and moved boats up the boat-loading ramps into the parking lot. The numerical model was able to reproduce actual wave measurements. The *SWAN* code was used to evaluate various proposals for decreasing the amplitude of the waves inside the harbor. From the calculated results, it was determined that a significant decrease of the waves inside the harbor could be achieved by decreasing the harbor entrance depth. Engineering companies used these results to support their recommendations for improving the design of the harbor.

The effect of the shape of a harbor cut through a reef on mitigating waves from the deep ocean was studied using the *SWAN* code in Mader, et al. (1986). A significant amount of the wave energy was dissipated over the reef regardless of the design of the harbor. The reef decreased the wave height by a factor of 3. The wave height at the shore can be further decreased by another factor of 2 by a 'V'-shaped or parabolic bottom shape.

Other examples of applications of the *SWAN* code are presented in Mader and Lukas (1984). They include the wave motion resulting from tsunami waves interacting with a circular and triangular island surrounded by a 1/15 continental slope and from surface deformations near the island. The effects of a surface deformation in the Sea of Japan similar to that of the May 1983 tsunami was modeled. The interaction of a tsunami wave with Hilo Bay was described.

The *SWAN* code was used to model the effect of wind and tsunami waves on Maunalua Bay, Oahu as described in the State Department of Transportation draft (1988). The calculated wave behavior at any location in the bay was a function of complicated and time varying wave reflections and interactions.

The *SWAN* code was used to model the interaction of waves with a site near the Mauna Lani Resort on the South Kohala Coast on the Island of Hawaii in Mader (1990a). The calculated results agreed with the results obtained using the procedures developed and applied for flood insurance purposes by the U. S. Army Corps of Engineers and the recent JIMAR study at the University of Hawaii of tsunami evacuation zones for the site.

The 1987-88 Alaskan Bight tsunamis were modeled in Gonzalez, et al. (1990) using the *SWAN* code. The deep sea pressure gauge measurements for those tsunamis could be described using realistic source models for the tsunamis.

A numerical study of effect of the shallow water approximation on tsunami flooding was performed in Mader (1990b). Calculations using the full Navier-Stokes model were compared to *SWAN* code calculations.

The 1946 and 1964 tsunamis were caused by Alaskan earthquakes and the 1960 tsunami by an earthquake in Chile. The 1946 and 1960 tsunamis resulted in extensive flooding of Hilo while the 1964 tsunami caused limited flooding.

The tsunami generation and propagation to the Hawaiian Islands were modeled using a 20 minute grid for the North Pacific or for the entire Pacific Ocean (Mader and Curtis, 1991). The wave arriving in the region of the Hawaiian Islands was then modeled using a 5 minute grid to follow the wave to the mouth of Hilo Bay. The wave arriving at the mouth of Hilo Bay was then modeled using a 100 meter grid of Hilo Bay, harbor and town. Each grid had a friction coefficient to describe the local roughness (trees, grass, buildings, coral, etc.). The use of computational grids of different grid sizes over different geographical domains to model tsunamis is similar to that reported by Kowalik and Whitmore (1991).

The models gave approximately the observed maximum areas of flooding. The large amount of flooding from the 7.6 magnitude 1946 Alaskan earthquake and small amount of flooding from the 8.5 magnitude 1964 Alaskan earthquake were reproduced by the numerical models. This demonstrated the large effect of wave directionality and the necessity of modeling the entire process of tsunami generation, propagation and flooding for each event.

The observed levels of flooding at individual locations was not well described by the 100 meter grid, so a 10 meter grid of Hilo was developed to resolve the flooding at individual locations and around large buildings.

APPLICATION OF THE NUMERICAL MODEL TO INUNDATION OF HILO THEATER

The high resolution 10 meter grid of Hilo was used to model the flooding around Hilo Theater by the 1960 tsunami wave. The Hilo Theater was located near the shore, in flat and unobstructed terrain 2.7 meters above sea level. The tsunami flooded level reached 8.5 meters at the seaward side and 6.7 meters at the rear of the Hilo Theater. A photograph of the Hilo Theater after the May 1960 tsunami is shown in Figure 1.

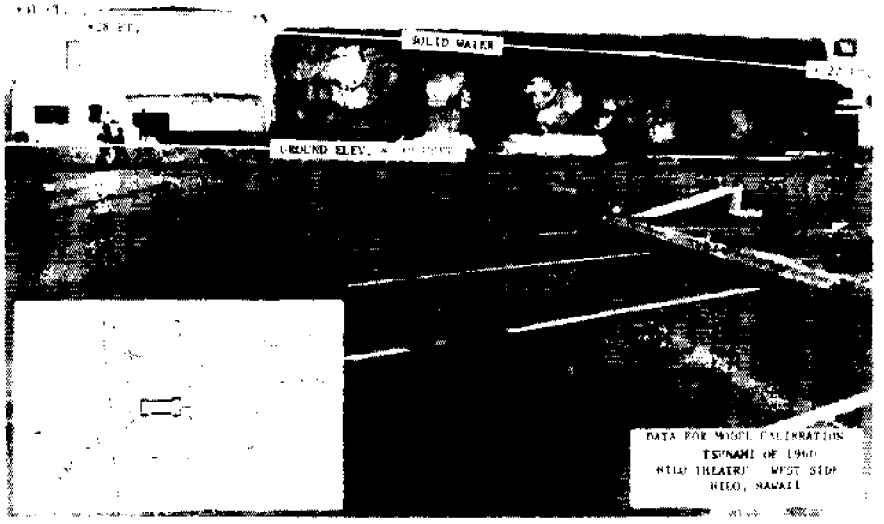

Figure 1. The Hilo Theater after the 1960 tsunami. The solid water water line is 28 to 22 feet above sea level. The building is located 9 feet above sea level. The inset shows the location of the theater relative to the shore line. The photograph is taken from the parking lot on the west side of the building. Note the four men standing on the right side of the photograph.

The grid was 240 by 240 cells of 10 meters on a side. The time step was 0.2 second. The theater building was described by 3 by 6 cells with a height of 11.9 meters. The third wave was a bore-like wave inside the harbor entrance 3 meter high from the North-West. The initial water level was 1 meter lower than the normal sea level to approximate the second wave recession that occurred before the third wave arrived. The wave had a period of 1500 seconds with the first rise occuring in 60 seconds to approximate the bore-like wave.

The surface level of the water, land and theater building is shown at various times in Figure 2. The contour interval is one meter. The building is 11.9 meters high.

The height of the water at locations near the harbor entrance and near the building as a function of time are shown in Figure 3. The front of the theater building (Location 5) was flooded to the 8.5 meter level and the rear of the building (Location 6) to the 8.0 meter level. The rear of the building was calculated to flood to a higher level than observed.

The inundation of the town of Hilo is shown in Figure 4. The inundation continues after the maximum flooding of the theater occurs. The maximum level of inundation calculated is similar to that observed from the 1960 tsunami.

The maximum levels of flooding observed at Hilo Theater was reproduced by the high resolution numerical model using a realistic description for the 1960 tsunami wave.

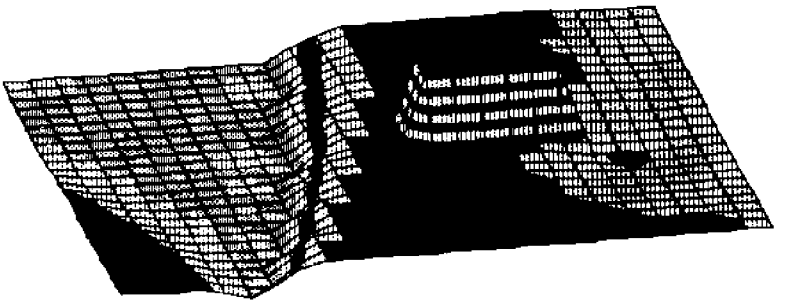

HEIGHT .25E+02sec, INC= .10E+01

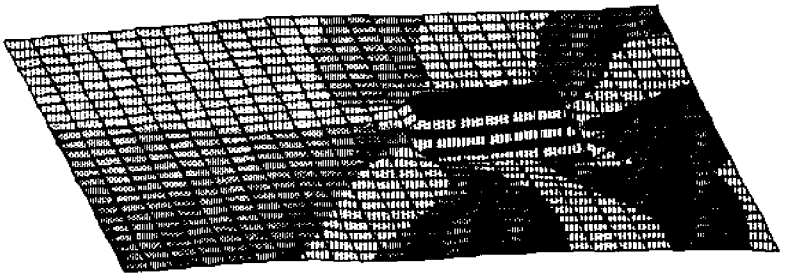

HEIGHT .12E+03sec, INC= .10E+01

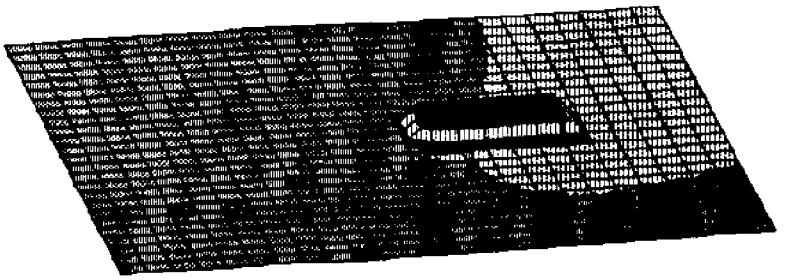

HEIGHT .30E+03sec, INC= .10E+01

Figure 2. The surface level of the water, land and theater building is shown at various times. The contour interval is one meter. The building is 11.9 meters high. The initial water surface is 1 meter below normal sea level to approximate the second wave withdrawal.

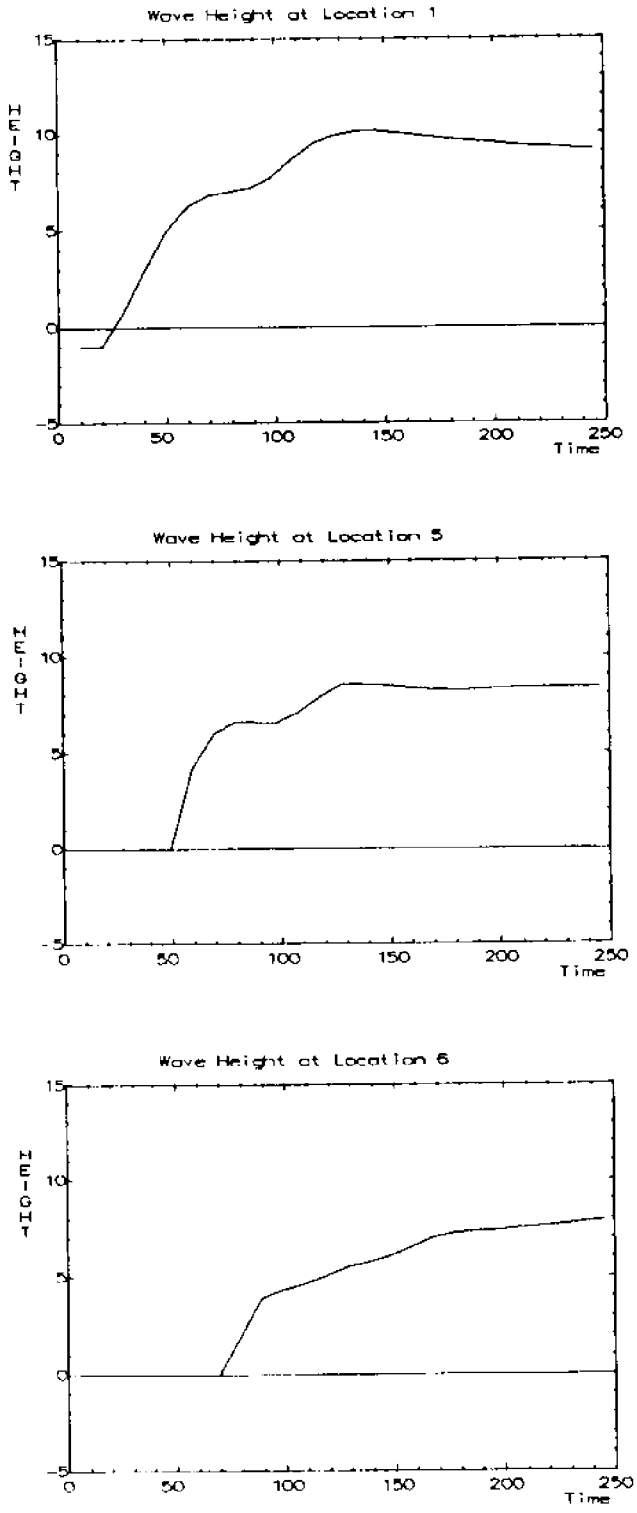

Figure 3. The height of the water at locations near the harbor entrance and near the building as a function of time are shown. Location 1 is in the ocean near the harbor entrance, Locations 5 and 6 are on the front and back of the side of the theater as shown in Figure 1.

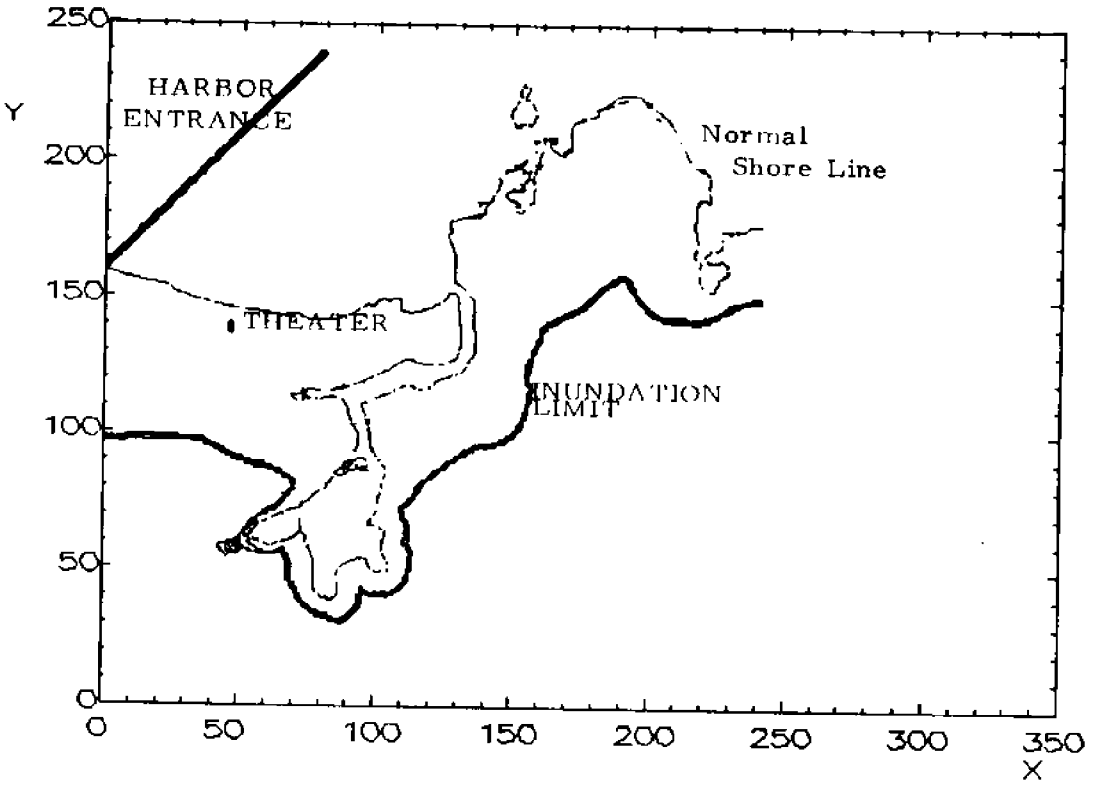

Figure 4. The inundation of the town of Hilo is shown. The inundation continues after the maximum flooding of the theater occurs. The location of the normal shore line and the theater building is also shown.

REFERENCES

Gonzalez, F.I., C.L. Mader, M.C. Eble, and E.N. Bernard. 1990. The 1987-88 Alaskan Bight tsunamis: deep ocean data and model comparisons. *Intl. J. Natural Hazards.* 4:119-140.

Hadi, S. 1985. A numerical tidal model of Musi-Upang estuaries. Ph.D. diss., University of Hawaii, Honolulu.

Kowalik, Z.K., and P.M. Whitmore. 1991. An investigation of two tsunamis recorded at Adak, Alaska. *Science of Tsunami Hazards.* 9:67-84.

Mader, C.L. 1988. Numerical Modeling of Water Waves. Berkeley: Univ. of California Press.

Mader, C.L. 1974. Numerical simulation of tsunamis. *J. Phys. Oceanography.* 4:74-82.

Mader, C.L. 1990a. Modeling tsunami flooding. In: Proc. Pacific Congress on Marine Science and Technology, PACON90. Honolulu: PACON Intl.

Mader, C.L. 1990b. Numerical tsunami flooding study - I. *Science of Tsunami Hazards.* 8:67-77.

Mader, C.L., and G. Curtis. 1991. Modeling Hilo, Hawaii tsunami inundation. *Science of Tsunami Hazards.* 9:85-94.

Mader, C.L. and S. Lukas. 1984. SWAN - a shallow water, long wave code: applications to tsunami models. Univ. Hawaii, Joint Institute for Marine and Atmospheric Research, Report JIMAR 84-077.

Mader, C.L., and S. Lukas. 1985. Numerical modeling of Waianae Harbor. In: Aha Hulikoa Hawaiian Winter Workshop Proc.

Mader, C.L., M. Vitousek, and S. Lukas. 1986. Numerical modeling of atoll reef harbors. In: Proc. of the Intl. Symp. on Natural and Man-Made Hazards, Rimouski .

State Department of Transportation, Harbors Division. 1988. Oahu Intraisland Ferry System - draft environmental impact statement.

TSUNAMI RESPONSE SIMULATION AT GUADALUPE ISLAND (MEXICO)

Salvador Farreras and Jorge Reyes
Centro de Investigación Científica y Educación Superior de Ensenada (CICESE)
Ensenada, Baja California, México

ABSTRACT

Guadalupe Island, located off the coast of Baja California (México), is one of the wave reporting stations equipped with a data collecting platform presently in operation for the Pacific Tsunami Warning System. The knowledge of the tsunami response at the island can give an estimation in advance of the severity of the attack to be expected at neighbouring mainland communities.

The scattering of tsunami waves by the island is examined by solving the linear long wave equation through a time and space centered finite difference approach. The model involves a conformal mapping of a polar coordinate grid onto an image plane where the orthogonal contours reproduce the real island shape at the unit circle, but approach to a circular shape as the radius in the polar system is increased.

Relative amplitude and wave phase lag at several points along the island contour, for the most probable tsunami periods and incident directions to occur according to historical records, are computed.

Maximum amplifications (400%) happen with short tsunami periods (10 minutes) and close to energy convergence zones, where refraction is important. For large tsunami periods (30 minutes), reflection and diffraction become the dominant processes, with amplifications of less than 25%.

The present location of the wave reporting station is confirmed to have adequate amplification characteristics for the tsunami warning system.

Results of the model may be used to obtain tsunami inundation estimates.

INTRODUCTION

Several remote source tsunamis have affected the coastal communities of the Baja California peninsula in northwest México, as it is historically documented (Farreras and Sánchez, 1991). Guadalupe Island, lying outside the continental shelf, 250 km off the coast of Baja California (Figure 1) is one of the wave and sea level reporting stations for the Pacific Tsunami Warning System (Intergovernmental Oceanographic Commission, 1987), the Pacific Satellite Sea Level Network, and the Baja California Regional Tsunami Warning System. It is presently equipped with a sea level pressure gauge connected to a satellite data collecting platform.

Islands, far out from the continental shelves, provide a good option to obtain tsunami records in conditions near to those in the open ocean.

The objective of this study is to determine the tsunami amplitude and phase response along Guadalupe Island contour for several wave periods and incident directions; and obtain through this an estimation of the incoming tsunami wave

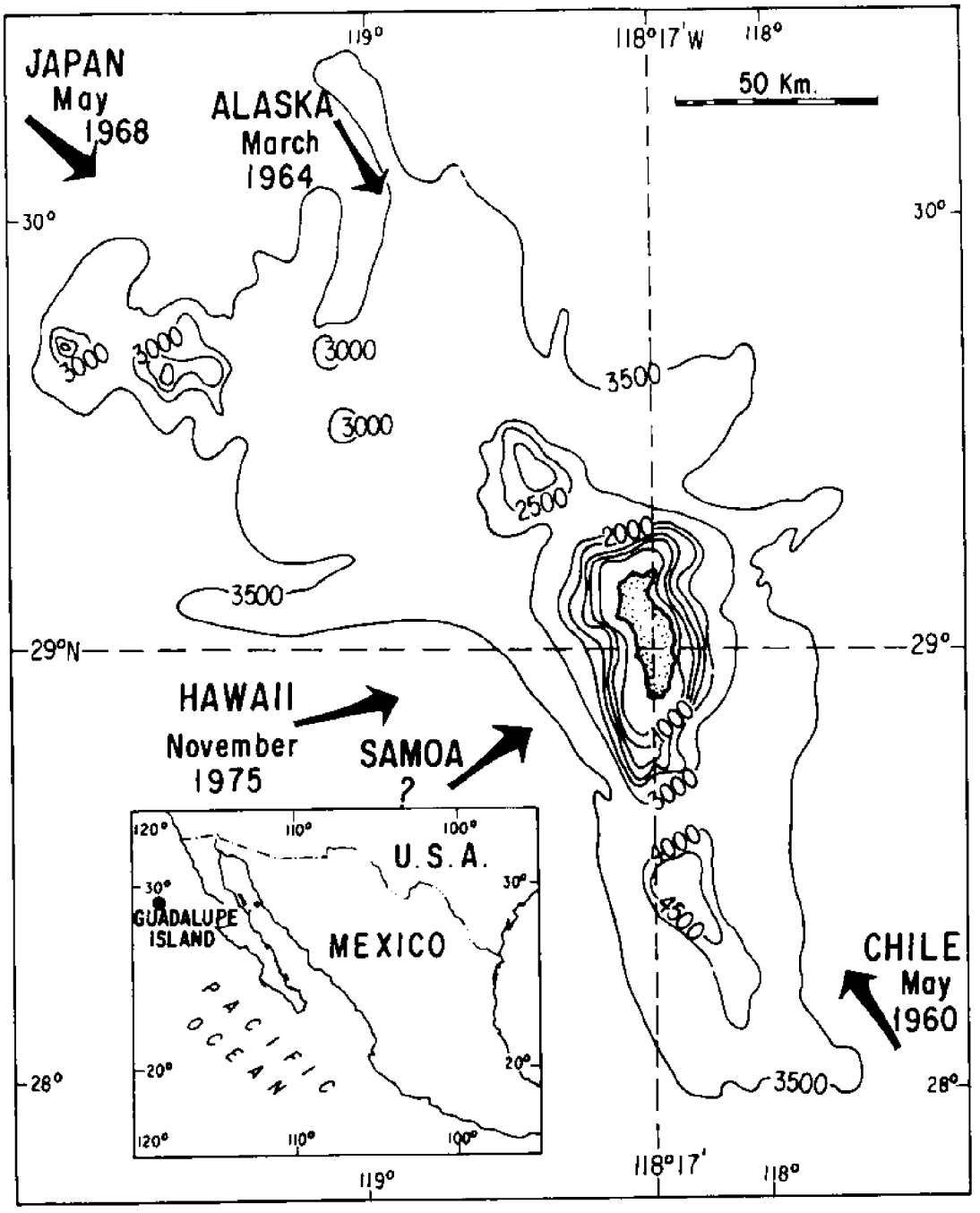

Figure 1. Guadalupe Island location, surrounding bathymetry, and approach direction of the 5 tsunami cases modeled in this study. Depths are in fathoms (1 fathom = 6 feet).

parameters in the open ocean. This estimation can give an information to neighbouring mainland coastal communities on the arrival time and severity of the attack to be expected, before tsunami waves reach them.

METHODOLOGY

Reflection, refraction, shoaling, and diffraction in the local bathymetry and coastal configuration are the main physical processes occurring in the interaction of water waves with an island. About 25% of the tsunami energy is reflected at the continental shelf, while 100% do so at the arrival to the coast (Soloviev and Go, 1974). Miyoshi(1983) states that refraction is the most important interaction process for a tsunami converging onto an island.

Diffraction cause more harm to the coast when the size of the obstacle is comparable with the incident wave length (Dean and Dalrymple, 1984). Although the suitability of linear wave theory application to tsunami wave interaction with a continental shelf is still a matter of discussion (Voit, 1987), it has been succesfully applied to the modeling of tsunami-island (Bernard and Vastano, 1977; Houston, 1978) and tsunami-coast (Tsuji, 1985) interactions.

The linearized long wave equation in polar coordinate(r,θ) and time t is:

$$\frac{\partial^2 \zeta}{\partial t^2} = g\left[\frac{1}{r}\frac{\partial}{\partial r}\left(rD\frac{\partial \zeta}{\partial r}\right) + \frac{D}{r^2}\frac{\partial^2 \zeta}{\partial \theta^2}\right] \tag{1}$$

where ζ is the free surface elevation, D is the mean water depth, and g is the gravitational acceleration.

Bottom friction, surface wind stress, and Coriolis effect are neglected.

Zero component of radial flow $\frac{\partial \zeta}{\partial t} = 0$ and Sommerfeld (1949) radiation condition for the waves scattered outward to infinity $\frac{\partial \zeta_s}{\partial r} + \sqrt{gD}\frac{\partial \zeta_s}{\partial r} \to 0$, are considered as inner and outer boundary conditions respectively.

To solve the equation, a Riemann's conformal mapping of the polar coordinate grid (r,θ) onto an image plane (ρ,ß) where the orthogonal contours reproduce the real island shape at the unit circle, but approach a circular shape as the polar system radius is increased, is performed. The conformal mapping preserves the angles, modifies the radial scale, and adjusts the inner boundary to the real contour to help solve the equation. The transformed grid with 50 × 120 nodes (shown abridged in Figure 2) has a maximum radial increment of 5 km in the outer boundary, decreasing in value towards the coast, where the wave interaction requires more resolution, and a maximum arc length of 13 km. This spacing is consider as adequate for linear tsunami modeling by Tuck (1979). The grid extends 250 km outward and the maximum cell size and its overall dimension are selected so as to obtain a desirable resolution. In the most sharp corners of the island contour resolution is also increased by the high density of rays. The deep open ocean is simulated by a far field of 3.5 km constant depth extending 80 km outwards. The

origin of the coordinate system (Figures 1 and 2) is located such as to avoid or minimize multivaluations of the radius as a function of the directional angle.

After the conformal mapping, the wave equation takes the form:

$$\frac{\partial^2 \zeta}{\partial t^2} = gs^2 \left[\rho \frac{\partial}{\partial \rho} \left(\rho D \frac{\partial \zeta}{\partial \beta} \right) + \frac{\partial}{\partial \beta} \left(D \frac{\partial \zeta}{\partial \beta} \right) \right] \tag{2}$$

where s is a scale factor.

This equation is solved numerically for monochromatic plane incident waves

$$\zeta_I = e^{i(\chi r \cos\theta - \omega t)}$$

where χ is the wave number and ω is the angular frequency, by means of Vastano and Reid (1966) space-time centered finite difference algorithm. An integration time step of one second is used, considering Richtmeyer (1957) stability criteria.

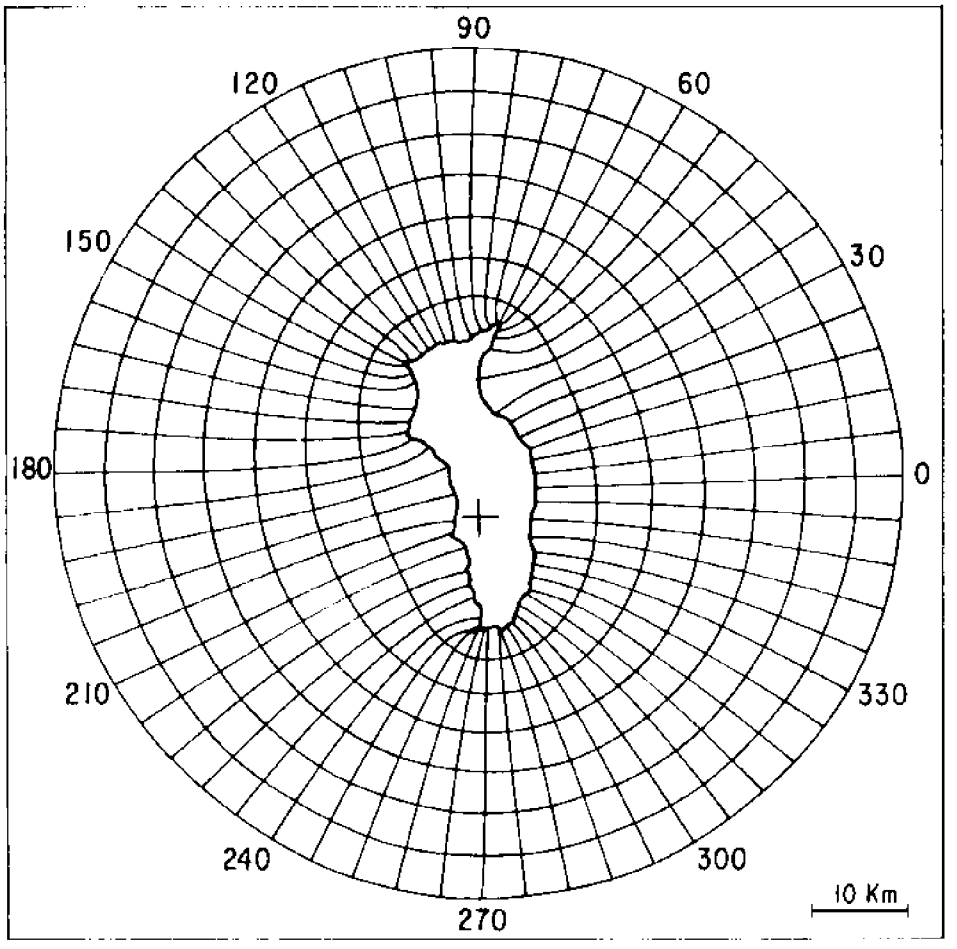

Figure 2. Abridged version of the coordinate grid used for the integration, after conformal mapping

APPLICATION AND RESULTS

Five remote source tsunami arrival cases are modeled. Four of them correspond to real past events with the highest wave heights recorded in the Baja California coastal region according to Sánchez and Farreras (1992): 22 May 1960 from Chile, 28 March 1964 from Alaska, 16 May 1968 from Japan, and 29 November 1975 from Hawaii. The tsunami arriving from Hawaii was the only one recorded at Guadalupe Island, after the sea level gauge installation. The fifth case corresponds to a hypothetical arrival proceeding from Samoa. Location of the source, date if occurred, maximum wave height recorded somewhere in the coast of México, and azimuth of incidence in Guadalupe Island for this five cases are given in Table 1; directions of incidence are shown in Figure 1.

Table 1. Tsunami arrival cases modeled

Location	Tsunami Source Latitude	Longitude	Date (if occurred)			Azimuth of Incidence (°)	Maximum Wave Height (m)
Chile	39.5° S	74.5° W	22	May	1960	300	2.5
Alaska	61.1° N	147.6° W	28	March	1964	114	2.4
Japan	41.5° N	142.7° E	16	May	1968	138	0.4
Hawaii	19.4° N	155.1° W	29	November	1975	189	0.5
Samoa	15.0° S	172.0° W	--	-----	--	213	--

For each approach direction, tsunami wave arrivals of 10, 15, 20, 25, 30, 35, and 40 minute periods were simulated. Amplitudes relative to the incident wave train and phase lags referred to the far field wave timing at an azimuth 90° from the direction of the incident wave train, were obtained as results.

Relative amplitude distribution along contour azimuth positions for a 10 minute period tsunami arriving from Hawaii (Figure 3) shows:

a) for the variable depth real bathimetry, an amplification maximum in the sharp SW corner where wave energy converges due to refraction; and

b) for a constant depth flat bottom, a typical symmetric reflection-diffraction response curve with one main maximum in the wave incidence direction and a secondary one 180 antipodal to the first.

The smoothness of the constant depth response curve, typical of an analytic solution for a simple geometry contour, indicates that Guadalupe Island is in the lower limit of object sizes that may significantly interact through diffraction with tsunami waves of such a period.

Relative amplitude distributions for the other arrival cases are similar.

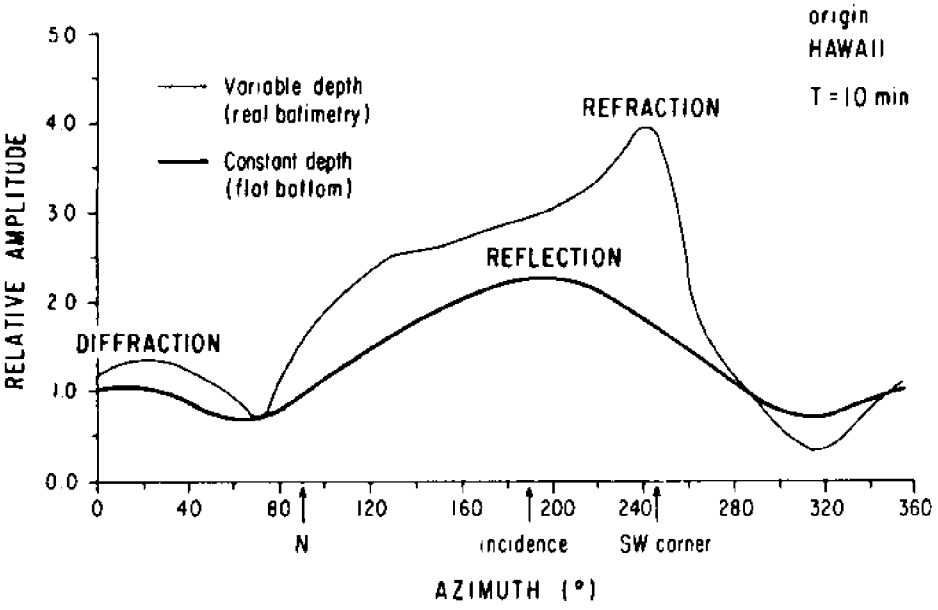

Figure 3. Relative amplitude distribution along contour azimuth positions for a 10 minute period tsunami arriving from Hawaii

Isolines of relative amplitude and phase in a period-azimuth space, for tsunamis arriving from Japan (Figure 4), but similar to the other cases modeled, show:

a) an amplification maximum, due to reflection, for all periods at the azimuth of incidence;

b) another amplification maximum at the sharp SW corner, where refraction is important, but only for less than 15 minute periods;

c) amplification decrease with period increase for all contour azimuthal locations; becoming almost 1.0 or less for periods higher than 35 minutes.

d) almost vertical phase isolines; an indication that this linear model is very little phase-dispersive: waves of different periods travel at about the same speed, without phase lags;

e) near-zero phase at the sharp SW and NE corners for periods higher than 15 minutes;

f) small azimuthal phase gradient in the incidence zone as a result of the wave front arrival almost parallel to the coastal contour; and

g) an increase of the above zone width, until the gradient almost dissapears (horizontal isolines), with decreasing periods. This indicates that the wave front alignes in a larger lateral extension to the coastal contour (simultaneous arrival at all points) as refraction becomes more important.

The response at the SW corner shows significant amplification for most of the periods considered (particularly the short ones) independently of the direction of incidence (Figure 5). This characteristic ensures enough sensitivity for tsunamis of the order

of centimeter open ocean waveheights to be detected and recorded by instruments in this site. This location is also reasonably protected from storm wave action and is easely accesible as to become a permanent sea level and wave reporting station.

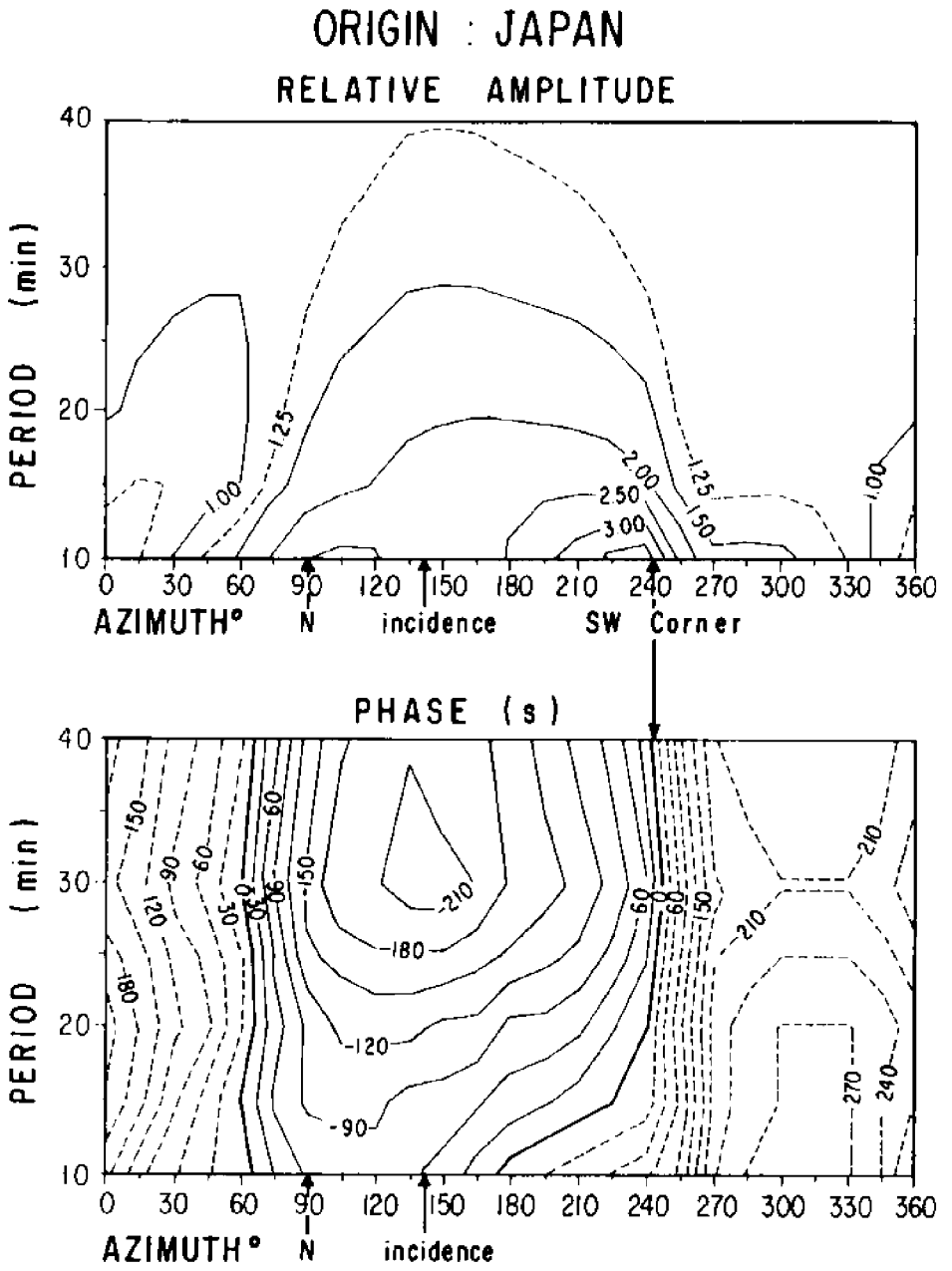

Figure 4. Amplitude and phase response along Guadalupe Island contour for tsunamis of several periods arriving from Japan (azimuth of incidence = 138°)

SUMMARY, CONCLUSIONS, AND RECOMMENDATIONS

The linear model gives a reasonable first approximation of the tsunami response at Guadalupe Island. The results may be used as an input for a near-shore propagation and inland run-up non-linear simulation.

The model needs to be tested with data from future tsunami arrivals.

Guadalupe Island size does not significantly affect the propagation of tsunami waves with periods greater than 35 minutes.

Maximum amplifications (400 %), due to refraction, occur for short periods (less than 10 minutes) near energy convergence zones.

Amplifications are smaller (less than 25%), and mainly due to diffraction and reflection, for periods larger than 30 minutes.

The SW corner is recommended as the permanent site for the sea level and wave reporting station of the tsunami warning systems because of its sensitivity to tsunami arrivals, its accesibility, and its reasonable storm wave protection. An alternate site could be the less accesible NE corner.

The tsunami response of those mainland communities to be protected with the alert information coming from Guadalupe Island, needs to be modeled.

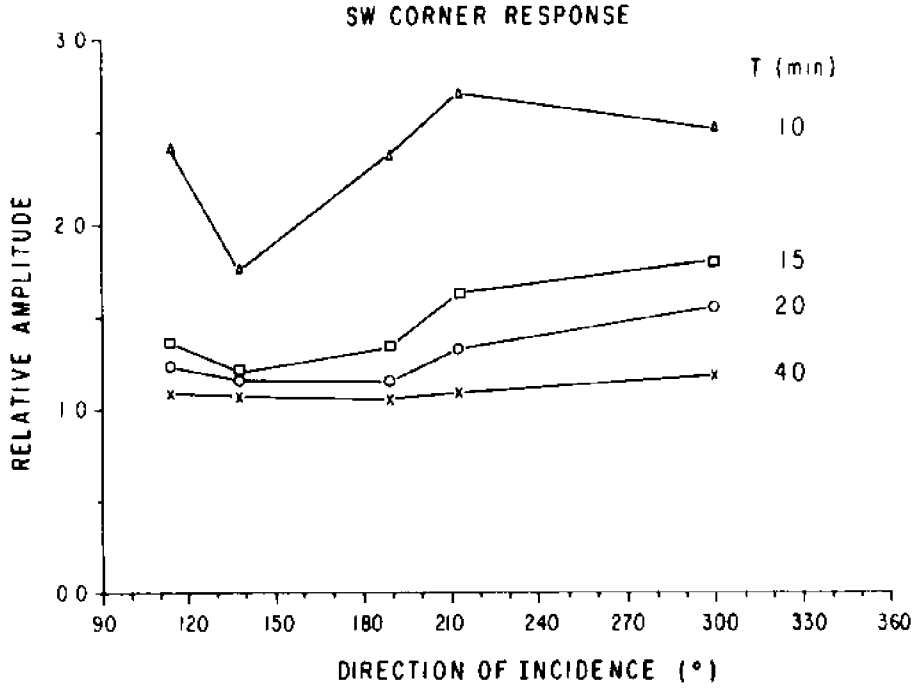

Figure 5. Amplitude response of Guadalupe Island SW corner for tsunami arrivals of several periods and directions of incidence

REFERENCES

Bernard, E.N., and A.C. Vastano. 1977. Numerical computation of the tsunami response for islands systems. *Jour. Phys. Ocean.* **7(3)**:389-395.

Dean, R.A, and R. Dalrymple. 1984. Water Wave Mechanics for Engineers and Scientists. New Jersey: Prentice Hall Inc.

Farreras, S.F., and A.J. Sánchez. 1991. The tsunami threat on the Mexican west coast: a historical analysis and recommendations for hazard mitigation. *Natural Hazards*. **4(2,3)**:301-316.

Houston, J.R. 1978. Interaction of tsunamis with the Hawaiian islands calculated by a finite element numerical model. *Jour. Phys. Ocean.* **8**:93-102.

Intergovernmental Oceanographic Commision. 1987. Master plan for the tsunami warning system of the Pacific. UNESCO, IOC/INF-730 Paris.

Miyoshi, H. 1983. Energy of the tsunami converging into an island. In: Proceedings of the 1983 Tsunami Symposium, ed. E. Bernard. Seattle:PMEL\NOAA U.S. Department of Commerce.

Richtmeyer, R.D. 1957. Difference Methods for Initial Value Problems. New York: Interscience Publishers Inc.

Sánchez, A.J., and S.F. Farreras. 1992. Catalog of tsunamis on the western coast of México. Ensenada: Centro de Investigación Científica CICESE and Secretaría de Marina de México.

Soloviev, S.L., and Go. 1974. A Catalogue of Tsunamis on the Western Shore of the Pacific Ocean. Moscow: Nauka Publishing House.

Sommerfeld, A. 1949. Partial Differential Equations. New York: Academic Press Inc.

Tsuji, Y. 1985. Comparison of observed and numerically calculated heights of the 1983 Japan Sea tsunami. In: Proceedings of the International Tsunami Symposium, eds. T.S. Murty and W.J. Rapatz. Sidney: Institute of Ocean Sciences, Dept. of Fisheries and Oceans.

Tuck, E.O. 1979. Models for predicting tsunami propagation. In: Tsunamis: Proceedings of the National Science Foundation Workshop, eds. L.S. Hwang and Y.K. Lee. Pasadena:Tetra Tech Inc.

Vastano, A.C., and R.O. Reid. 1966. A numerical study on the tsunami response at an island. A & M Project 471, Reference 66-26T. College Station: Dept. of Oceanography, Texas A & M University.

Voit, S.S. 1987. Tsunamis. *Annual Review of Fluid Mechanics.* **19**:217-236.

TELEOPERATOR/TELEPRESENCE SYSTEM (TOPS) CONCEPT VERIFICATION MODEL (CVM) DEVELOPMENT

Mike S. Shimamoto
Naval Command, Control and Ocean Surveillance Center
Kailua, Hawaii, U.S.A.

ABSTRACT

The development of an anthropomorphic, undersea manipulator system, the TeleOperator/telePresence System (TOPS) Concept Verification Model (CVM) is described. The TOPS system design philosophy resulting from NRaD's experience in undersea vehicles and manipulator systems development and operations is presented. The TOPS design approach, task teams, manipulator and vision system development and results, conclusions, and recommendations are presented.

INTRODUCTION

A major step has been taken toward the development of an advanced, telerobotic, undersea work system with the TeleOperator/telePresence System (TOPS) Concept Verification Model (CVM) (Figure 1). The long term objective of the TOPS program is to develop the technologies required to build remote work systems that are functionally equivalent to a diver in performing unstructured undersea tasks. Such a remotely controlled manipulator system would not be constrained by the diver's operational limitations in hazardous areas, great ocean depths, cold temperatures, and submerged operating time. The emphasis of the project is on developing the capability for performing tasks that require the dextrous, adaptive, and judgmental capabilities of man rather than on performing precise, well-defined tasks that can be addressed by purely robotic systems or specialized tools.

Figure 1. TOPS CVM

BACKGROUND

Organizations contributing to the development of the TOPS CVM and their areas of expertise are as follows: NRaD (US Navy remotely operated vehicle and manipulator development); Sarcos, Inc. (SI) and the Center for Engineering Design (CED) at the University of Utah (dextrous hand/arm, entertainment robots, and robotic component development); and Armstrong Aerospace Medical Research Laboratory (AAMRL) at Wright-Patterson Air Force Base and Technology Innovations Group (TIG) (helmet mounted display vision systems development).

Teleoperator Systems Development at NRaD

Over a span of two and a half decades, the Advanced Systems Division of NRaD's Hawaii Detachment has developed manned undersea vehicles; unmanned, remotely operated undersea vehicles (ROVs); unmanned remotely operated ground vehicles (UGVs); and teleoperated manipulator systems (Hightower and Smith, 1983; Hightower, Smith, and Wiker, 1986; Murphy, 1991).

During the development of the Remote Unmanned Work System (RUWS) (Figure 2) and several other ROVs, test operations were conducted in recovery, inspection, and emplacement tasks (Figure 3). The "lessons learned" from those operations provided impetus to the TOPS program.

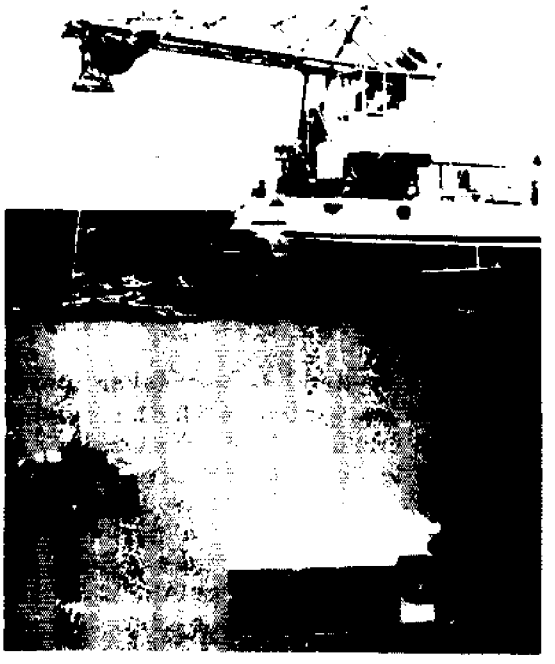

Figure 2. RUWS

Although a set of hydraulic tools had been designed and fabricated for use by the RUWS manipulator, additional special tools were often required for new tasks (Figure 4). During several operations, the tools had to be modified or new tools fabricated, because the task was not quite as it was "supposed to be." Although, lots of pre-operations planning were done and special configurations for the vehicle were implemented, few missions were completed without difficulty. Navy salvage operations, by nature, usually have many "unstructured" tasks when recovering wreckage and items from wreckage.

Simple diver tasks, such as putting a snap hook onto a shackle, proved to be difficult because of the limitations in dexterity of the manipulator and mobility of the vehicle. If currents were present, the object to be worked on was approached with the vehicle heading into the current; this frequently resulted in anorientation to the task that was less than ideal for the manipulator. Maneuvering the vehicle for proper positioning usually resulted in agitation of the bottom sediment, which obscured the remote operator's visibility. Conditions such as those for each mission seemed to provide unique challenges to the operators even when the missions consisted of fairly simple tasks. The operators were often more frustrated than fatigued in attempting to

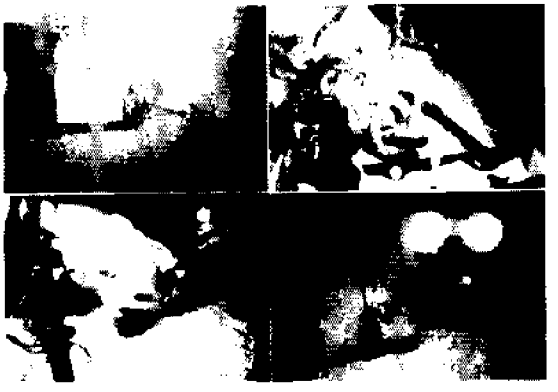

Figure 3. Manipulator work

complete the tasks for a successful mission. Tasks that could easily be performed by divers were not at all trivial for an ROV work system. These lessons indicated that a diver-equivalent work system might provide the work capability needed for many undersea missions where present ROV and manipulator systems are inadequate. The capabilities of such a system could also be applied to other hazardous missions on land and in space.

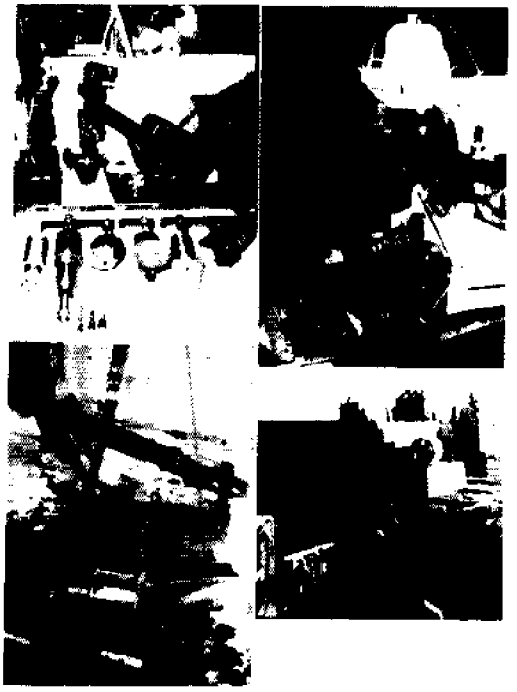

Figure 4. Vehicle configuration

Diver Tasks

An assessment of tasks performed by Navy and civilian divers determined: (1) the importance of various tasks within dive missions, (2) the manipulative and sensing capabilities used by the divers to perform the missions, and (3) the key design parameters for the development of a diver-equivalent manipulator system.

In determining the importance of various tasks within dive missions, it became clear that the major differences between what divers could do and what could be done with manipulators were that divers could perform a series of complex tasks and adapt to the differing tasks to successfully complete a mission. The divers used their own manipulative and sensing capabilities that were required to complete the tasks. Maneuverability, dexterity, and full sensory capability were key to the adaptability and versatility required to successfully complete the variety of tasks within the missions.

In determining the key design parameters for a diver-equivalent manipulator system, it became evident that the best configuration that would allow an operator to perform like a diver was a system configured the same way as the human operator (i.e., an anthropomorphic configuration). A manipulator system with joints and links that matches the operator's (kinematic equivalent) and with all manipulative appendages and sensory systems in the same relative positioning (spatial correspondence) as the operator's appendages and sensory systems would allow the operator to perform the tasks as if he/she were present at the work site.

A system that maintains spatial correspondence between the slave and the operator allows the operator to use his/her experiences from infancy to the present. If spatial correspondence is lost, people can adjust, but only by sacrificing performance. The loss in performance shows up in objective measures such as additional training required to attain proficiency, higher error rates, longer times to complete the tasks, as well as increased mental and muscular fatigue by the operators (Pepper, 1986).

Anthropomorphic Manipulator Development

The first anthropomorphic (human configured) manipulator developed at NRaD was the Remote Presence Demonstration System (Hightower and Smith, 1983; Hightower, Smith, and Wiker, 1986) (nicknamed "Greenman"), shown in Figure 5. It was assembled in 1983 using MB Associates arms and an NRaD-developed torso and head. It had an exoskeletal master controller with kinematic equivalency and spatial correspondence in the torso, arms, and head. Its vision system consisted of two 525-line video cameras each having a 35° field of view and video camera eyepiece monitors mounted in an aviator's helmet.

Figure 5. Remote Presence Demonstration System

Greenman provided NRaD with valuable experience in teleoperation and telepresence issues and designs. Even with its simple claw hands and no force or tactile feedback, novice operators could readily perform manipulative tasks without training. However, it clearly showed that dextrous hands, force feedback, and a high-resolution vision system were necessary for diver-equivalent work capability. Also, the Greenman was not designed for in-water use, and demonstrations of in-water work was deemed necessary to fully demonstrate the diver-equivalent concept.

TOPS PROGRAM DEVELOPMENT

TOPS Long-Term Concept

The long-term concept for a diver-equivalent manipulator system is shown in Figure 6. The master controller "fits" the operator like a business suit and senses his/her hand, body, and head motions. The slave manipulator mimics the operator's motions, senses its interaction with the environment, and provides sensory feedback to the operator via the master controller in a manner natural to him/her.

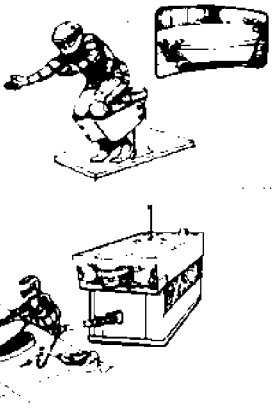

Figure 6. TOPS concept

An assessment was conducted of available, near-term, and long-term technologies in planning for the development of thefirst TOPS model to verify the concept. Because the first model would be a 3-year project only, long-term technologies were not included in the project scope.

Long-term technologies identified for future TOPS systems were: (1) tactile telepresence systems, (2) high-definition TV (HDTV), (3) human equivalent dextrous

hands, (4) the integration of virtual reality with the vision system, (5) advanced manipulator controllers, and (6) passive sonar for underwater directional hearing.

TOPS CVM

The first model of TOPS was called the Concept Verification Model (CVM). This model incorporated available and near-term teleoperation and telepresence technologies including (1) dextrous hands, (2) high-fidelity force feedback, (3) high-resolution head-coupled vision, and (4) an integrated, natural master controller with spatial correspondence. The major thrust of the technologies was in the development of the two major subsystems: (1) the manipulator and (2) the vision system.

TOPS CVM Manipulator Development

The development of the TOPS CVM manipulator was contracted to Sarcos, Inc. and the Center for Engineering Design at the University of Utah. The hand was developed in the first phase; the arm was developed and then integrated to a revised hand in the second phase; and the torso and head were developed and integrated in the third phase. The supporting control system was developed throughout all phases.

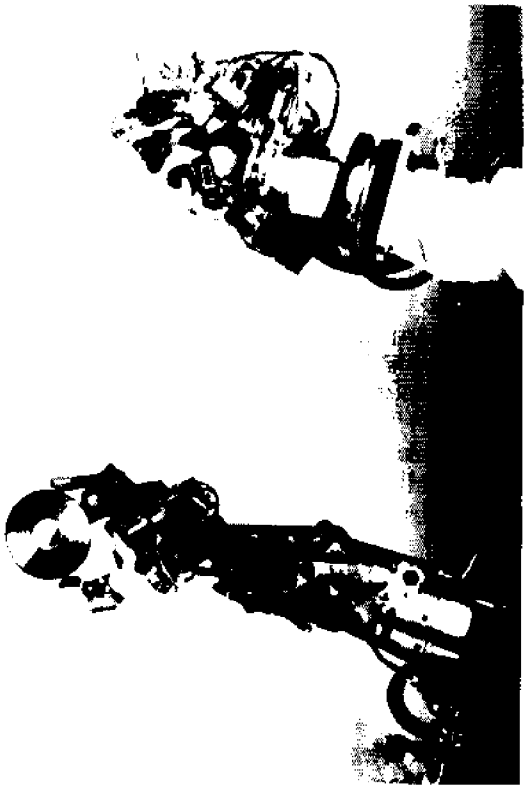

Figure 7. TOPS CVM brassboard hand

In the first phase, the hand development consisted of finger, hand, and wrist design concepts; tendon, actuator, and valve evaluation and development; sensor and supporting structure development; and antagonistic (pull-pull) servo control system development. A brassboard, 9-degree-of-freedom (DOF) hand was developed incorporating a 4-DOF thumb, a 3-DOF index finger, and a 2-DOF middle finger (Figure 7). The hand was attached to a 3-DOF wrist incorporating coincidental axes. The exoskeletal hand master represented a major design breakthrough where the structure fit on the backside of the hand but had virtual joints that matched the operator's finger joints. The brassboard hand was demonstrated at the end of the first phase (1 year). Demonstrations showed that the hand had the capability to perform standard hand grasps and manipulate various objects (such as threading a #10 nut onto a stud, and grasping and using standard hand tools), and showed high-sensitivity force feedback with high inter-system stiffness.

In the second phase, the hand was revised while the arm was developed, then the arm and hand were integrated; low-friction rotary actuators were developed; and development of high-performance servo system components and controllers was continued. The arm was designed with a 3-DOF shoulder and 1-DOF elbow. The 3-DOF

shoulder was designed to allow forearm/elbow orientations for various work task requirements. The exoskeletal arm master allowed full, natural operator control of the slave manipulator.

In the third phase, the torso and head were developed; subsystem and component development of valves, actuators, tendons, sensors, and hand designs were continued; all subsystems were integrated; then the system was tested in water. The 3-DOF torso was developed to provide a natural, short-range mobility and repositioning platform for the arm and vision. The 3-DOF head was developed to provide natural, spatially correspondent visual positioning capability. Force feedback was not incorporated in the torso and head.

TOPS CVM Vision

The development of the vision system capitalized on the efforts by AAMRL on helmet mounted display (HMD) systems for the US Army's Light Helicopter, Experimental (LHX) program. After evaluating HMD prototypes for the LHX, a "pancake window" HMD configuration was selected for TOPS and a contract was awarded for an HMD to Technology Innovations Group (TIG) of New York. The HMD included a pair of 1023-line, monochrome CRTs with 68o field of view optics (approximately the view from a diver's mask); air cooling for comfort; and a "clamshell" rear-hinged section to make it easy to put the helmet on and take it off (Figure 8).

Figure 8. TOPS CVM helmet mounted display

The remote portion of the vision system consisted of a pair of 1023-line monochrome cameras with fixed-focus lens mounted in an underwater housing.

A sophisticated display electronics package was acquired from AAMRL. The display electronics (developed for the LHX program) allows precise distortion correction for each channel, video signal, and CRT display. The correction parameters for each item can be stored on disk to allow rapid component changeout and reconfiguration.

TOPS CVM Overall Objectives Met

The overall TOPS CVM technical objectives were met in the development of an advanced manipulator system that begins to approach diver work capability. A high dexterity (22 DOF) manipulator with high-fidelity force feedback and a high-resolution, head coupled, stereo vision system was achieved. The combination of high dexterity that is kinematically equivalent to the operator, good force reflection, and a spatially correspondent 3-D vision system contributes to a high level of telepresence, i.e., the perception that the system is transparent to the operator. The operator feels that he/she is at the work site performing the task, and can concentrate on the task and not on operating the system.

Lessons Learned

Very valuable lessons were learned during the development and testing of the TOPS CVM (Smith and Shimamoto, 1991). The manipulator demonstrated great potential for performing a variety of manipulative tasks. The force reflecting exoskeletal system was natural and easy to use. However, subtle differences in kinematics and materials had major impacts on system performance. When link lengths and joint axes of the master controller did not properly match the operator's links and joints, and when grasping and positioning were not replicated exactly, the operator usually worked with significantly more caution and at a reduced speed. The fingertip configuration and materials of the slave hand also impacted the ability to securely grasp objects and, hence, the operator's confidence and speed of task performance. The compensation for gravity in the hand and arm for all areas of the workspace is very important to overall system performance and in the minimization of operator fatigue. Also, the capability to freeze operator selected joints would be very valuable for fine positioning tasks.

The tendon system proved too delicate, bulky, and complex for underwater operational systems. Tendon technologies that more closely replicate the human tendon system need to be developed.

The torso proved very useful in extending the manipulator's work volume and capability, in changing the viewing perspective, and in providing a "natural zoom" capability (the ability to position the cameras closer to the work task simply by leaning toward the object).

CONCLUSIONS/RECOMMENDATIONS

Telerobotic systems will continue to be important for environments and tasks that are hostile to humans, but where man's cognitive and manipulative capabilities are needed. This case is particularly true for accidents where explosives, chemicals, nuclear materials, extreme heat or cold, etc., would expose humans to great danger. Accidents also present the high probability of occurrence of unstructured tasks that need to be performed to accomplish the mission.

Unstructured tasks usually require that full manipulative, sensory, and cognitive capabilities be employed. Any manipulative or sensory capability that a manipulator system does not provide is a "handicap" to the operator. The TOPS CVM represents a giant step taken towards minimizing the "handicaps" an operator inherits with a typical manipulator system.

However, as discussed in the section on Lessons Learned, continued refinements are needed in the TOPS CVM design to improved operator machine interfaces and produce a ruggedized, smaller hand for an operational system.

The next development phase requires continued developments in component technologies for increasing hand dexterity, providing underwater directional hearing capability, enhancing vision, and providing tactile telepresence.

Component development required for increased hand dexterity include reliable, low-stiction tendons, biological-like lubricants, and compact tendon routing technologies; small, responsive, lightweight, muscle-like actuators; finger- and palm-padding type material; and tough skin-type material.

The development of small, high-definition TV cameras and monitors are needed for 20/20 color vision systems.

REFERENCES

Hightower, J.D., and D.C. Smith. 1983. Teleoperator technology development. In: Proc. of the 12th Meeting of the United States-Japan Cooperative Program in Natural Resource. San Francisco.

Hightower, J.D., D.C. Smith, and S.F. Wiker. 1986. Development of remote presence technology for teleoperator systems. 14th Meeting of the United States-Japan Natural Resources Committee. September.

Murphy, D.W. 1991. Advances and experience with teleoperated systems incorporating remote presence. 17th Meeting of the United States-Japan Cooperative Program in Natural Resources. May.

Pepper, R.L. Human factors in remote vehicle control. 1986. Annual Meeting of the Human Factors Society.

Smith, D.C., and M.S. Shimamoto. 1991. TeleOperator/telePresence system (TOPS) Concept Verification Model (CVM) testing and demonstration, final report. Unpublished. July.

HISTORICAL TSUNAMI HEIGHTS ALONG THE COAST OF SHIKOKU ISLAND IN JAPAN

Hitoshi Murakami, Tomio Shimada,* Yoshihiko Hosoi,** and Yohko Hiraiwa

University of Tokushima
Tokushima, Japan

*Anan College of Technology
Tokushima, Japan

**Tottori University
Tottori, Japan

ABSTRACT

The coasts facing the Pacific Ocean around Shikoku island in Japan have been attacked by huge tsunamis at intervals of 100-150 years. These tsunamis have inflicted severe damage on human lives and houses in towns and villages along the coast. In order to clarify tsunami characteristics, old data on the heights of four big historical tsunamis along the Shikoku coast have been re-examined. New data, including the inundation heights of three of the historical tsunamis, have been compared with those of the fourth, the 1946 tsunami.

Then, the inundation heights of these historical tsunamis were compared with the values calculated by numerical simulations and the tsunami heights of the 1854 tsunami reproduced using the data of the 1946 tsunami.

INTRODUCTION

The oldest tsunami recorded in a historical document in Japan occurred in 684 and since then many tsunamis have been recorded in historical documents. Figure 1 shows a tsunami map in Japan. The circles show the historical epicenters of earthquakes generated in the sea region near the Japanese coast which caused tsunamis. The size of each circle expresses the tsunami scale or tsunami magnitude m. The coasts facing the Pacific Ocean around Shikoku island in Japan have been attacked by huge tsunamis at intervals of 100-150 years. These tsunamis have inflicted severe damage on human lives and houses in towns and villages along the coast.

First, data on four big historical tsunamis along the Shikoku coast were re-examined in detail in addition to informations of old documents discovered in the recent several years. The tsunamis chosen as the subject of this study are as follows; the Keicyo tsunami on February 3, 1605 (tsunami magnitude m=3, death toll about 2,500 on Shikoku island), the Hoei tsunami on October 28, 1707 (m=4, death toll about 2,800 in Kochi Prefecture), the Ansei Nankai tsunami of December 24, 1854 (m=4, death tolls about 380 in Kochi, and 90 in Tokushima Prefectures) and the Showa Nankai tsunami on December 21, 1946 (m=3, death toll about 1,300 in Japan).

Second, the inundation heights of three historical tsunamis were compared with those of the 1946 tsunami at a location where the tsunami data had been recorded along

the Shikoku coast. Although the tsunamis attacked the same stretch of coast, there are some locations where the tsunami heights are extremely different in size. Numerical simulations for three of these tsunamis except the 1605 event were carried out in order to consider the reason why the tsunami heights at a certain limited location had been amplified.

Furthermore, the inundation heights of the 1854 tsunami were estimated by using the calculated and observed values of the 1946 tsunami.

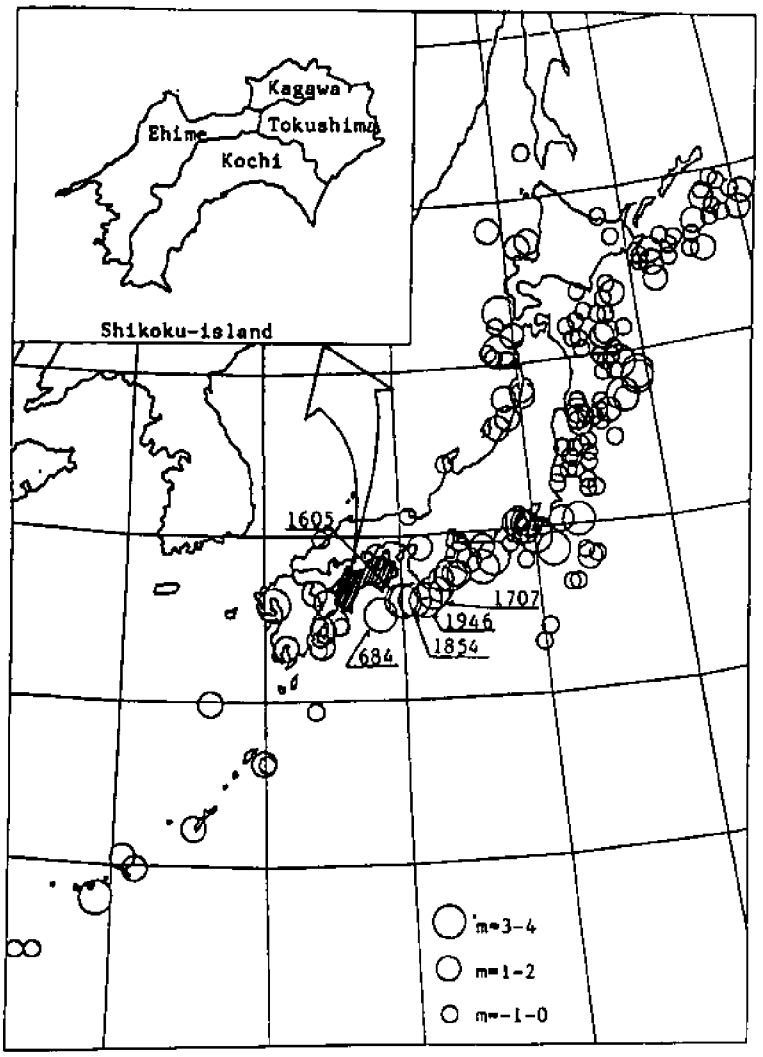

Figure 1. Epicenters of earthquake and tsunami magnitude

THE FOUR HISTORICAL TSUNAMIS ALONG THE SHIKOKU COAST

Details of these tsunamis recorded in historical documents are available for the analysis of tsunamis occurring along the Shikoku coast. We made field surveys along the coast in order to check inundation height which some researchers had surveyed but not in sufficient accuracy. At first, the data of these four tsunamis were checked by surveying obscure inundation heights that had been obtained from historical documents by several researchers and the newly discovered tsunami data from the historical documents were added to the existing data.

Damages along the Shikoku Coast Caused by the Four Historical Tsunamis

Many records of these tsunamis along the Kochi and Tokushima coasts, which lie near tsunami sources have been well recorded in historical documents but there are few records of tsunamis occurring along the Ehime and Kagawa coasts which are located in the Seto Inland Sea.

Figure 2 shows the towns and villages where severe damage was inflicted by the four historical tsunamis.

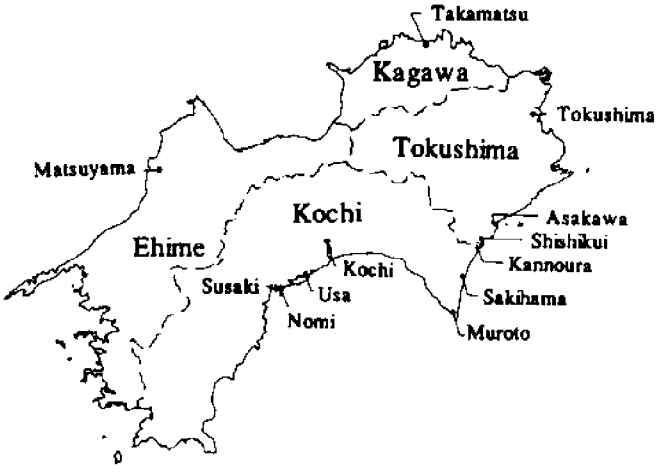

Figure 2. Towns and villages inflicted by severe damage

There were only few data in historical documents about the 1605 tsunami along the Shikoku coast. However, it is estimated from historical documents that this tsunami was very big. The inundation heights at Sakihama fishery harbor and Kannoura in Kochi reached 9.5m and 5.5m and the numbers of deaths were 50 and 350, respectively. At Shisikui in Tokushima, the inundation height reached 5.5m and 1500 people were killed.

In the case of the 1707 tsunami, the tsunami height at Usa bay in Kochi reached 8m and 400 people were killed. At Asakawa in Tokushima, the inundation height was 6.5m and 170 people were killed.

The inundation height of the 1854 tsunami was 7.5m at Usa, 7.5m at Kamikawaguchi in Kochi and 6.5m at Yuki bay and at Asakawa in Tokushima.

Figure 3 shows the inundation heights of the 1946 tsunami around Shikoku island. The vertical axis in this figure indicates the inundation height above the mean sea level. The data of the 1946 tsunami are large in number and would be the most reliable for inundation heights. The tsunami heights in the western part of the Kochi coast were relatively higher than those in the eastern part. The tsunami height in Nomi bay reached 5.2m. Along the Tokushima coast, the maximum tsunami height reached 4.88m in Asakawa bay and 85 lives were lost there. The tsunami heights depend largely on the location and the heights have been comparatively high along the Kochi coast and the southern part of the Tokushima coast. On the other hand, the Ehime and Kagawa coasts located in the Seto Inland Sea have suffered less damage.

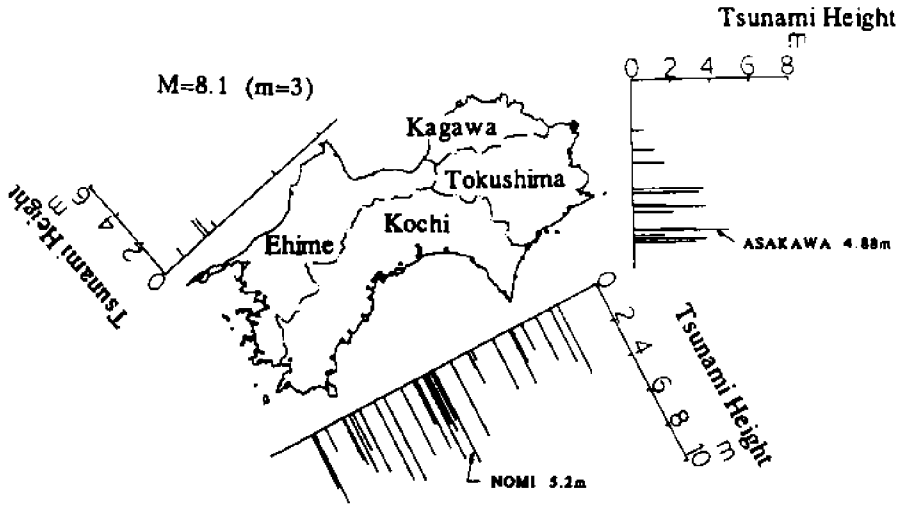

Figure 3. Inundation heights of the 1946 tsunami around Shikoku island

The Comparison of the Four Historical Tsunami Heights

The inundation heights of three historical tsunamis were compared with those of the 1946 tsunami at a location where tsunami data had been recorded along the Shikoku coast (Figure 4). The vertical axis in Figure 4 indicates the ratio R of the tsunami heights of three historical tsunamis to the 1946 tsunami heights. The inundation heights of the 1854 tsunami, the 1707 tsunami and the 1605 tsunami are 1.2-3, 1.2-3.6 and 1-4.6 times as large as those of the 1946 tsunami, respectively. We can see there are some locations where the tsunami heights are extremely huge in comparison to the neighboring villages.

THE NUMERICAL SIMULATIONS FOR THE HISTORICAL TSUNAMIS

The numerical simulation for the general standard of the Nankai Region tsunami is based on an assumption that the sea water surface is still at the beginning and that a tsunami is generated as a given sea surface elevation equal to the vertical displacement of the sea bed by the earthquake. At first the parameters of a fault model were given. Then the final displacement of the sea bed was calculated by the formulation of Mansinha and Smylie (1971). It is supposed that the vertical displacement of the sea bed is linearly increased and completed within a previously appointed time. The fault models used in this numerical simulation are Aida's models (1981) as shown in Table 1.

Table 1. Fault models proposed by Aida (1981)

Tsunami (Model)		L (km)	w (km)	δ (°)	ϕ (°)	z (km)	us (m)	ud (m)	τ (min)	Mo (dyne-cm)
1946 NANKAI (Model 19')	E part	150	70	10	N20W	10	2.4	3.2	0.5	6×10^{28}
	W part	120	120	20	N20W	1	1.2	4.8	3~10	
1854 ANSEI (Model 20')	E part	150	70	10	N20W	10	2.8	3.7	0.5	8×10^{28}
	W part	150	120	20	N20W	1	2.8	5.6	0.5	
1707 HOEI (Model 29')	E part	150	70	10	N20W	10	3.1	4.6	0.5	10.2×10^{28}
	W part I	140	80	20	N50W	1	0	7.0	0.5	
	W part II	60	80	20	N30W	1	0	13.9	0.5	

L : fault length , w : fault width

δ : dip angle , ϕ : dip direction

z : depth of the upper rim of the fault plane

us : dislocation of strike slip component (right lateral)

ud :dislocation of dip slip component (reverse)

τ : duration time of the bottom movement

Mo : seismic moment (rigidity 5 $\times10^{11}$dyne·cm)

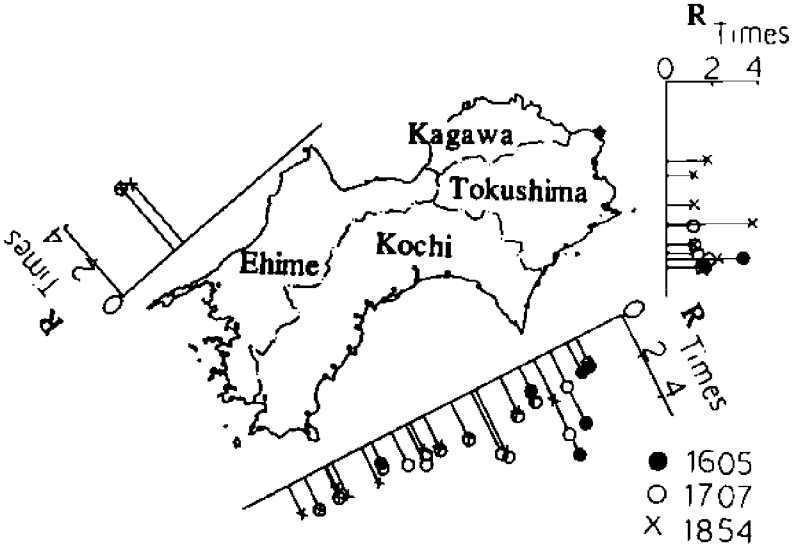

Figure 4. Comparison of historical tsunami heights

Basic Equations

The basic equations in the numerical simulation are the depth-averaged shallow water wave Eqs. (1)-(3) with a friction term and a convection term. It is supposed that the vertical displacement ξ of the sea bed is included.

$$\frac{\partial Q_x}{\partial t}+\frac{\partial}{\partial x}\left(\frac{Q_x^2}{D}\right)+\frac{\partial}{\partial y}\left(\frac{Q_xQ_y}{D}\right)+gD\frac{\partial \eta}{dx}+f_c\frac{Q_x\sqrt{Q_x^2+Q_y^2}}{D^2}=0 \tag{1}$$

$$\frac{\partial Q_y}{\partial t}+\frac{\partial}{\partial y}\left(\frac{Q_y^2}{D}\right)+\frac{\partial}{\partial x}\left(\frac{Q_xQ_y}{D}\right)+gD\frac{\partial \eta}{dy}+f_c\frac{Q_x\sqrt{Q_x^2+Q_y^2}}{D^2}=0 \tag{2}$$

$$\frac{\partial \eta}{\partial t}+\frac{\partial Q_x}{\partial x}+\frac{\partial Q_y}{\partial y}+\frac{\partial \xi}{\partial t}=o \tag{3}$$

Here x and y are the horizontal orthogonal coordinates fixed on the still water surface, Q_x and Q_y are the corresponding components of volume transport velocity integrated from the water surface to the bottom, g is acceleration due to gravity, f_c is the quadratic friction coefficient of the sea bottom, h is still water depth, η is the water surface elevation from still water level, ξ is the vertical displacement of the sea bed and $D=h+\eta-\xi$. These equations are transformed to difference equations.

Computation Region and Boundary Conditions

Figure 5 shows the computation region and the fault model of the 1946 Nankaido earthquake. As shown in Figure 5, the computation region includes the Seto Inland sea and the Pacific Ocean around Shikoku island. The grid size of the computation region is 5km×5km and the time step in the numerical simulations is 5 sec.

As for the boundary conditions, it is assumed that tsunami waves reflect perfectly at the land boundaries and the volume transport velocity perpendicular to the face of solid boundary is zero. Moreover, the volume transport velocity at the offshore boundary is decided by using the relation of $Q_x^2+Q_y^2=gD\eta^2$.

Simulation of the Historical Tsunami

Numerical simulations were carried out for the 1707, the 1854 and the 1946 tsunamis by using the above-mentioned method. Figures 6.1-6.3 show the comparison of the calculated values with the observed values for these three historical tsunamis. The vertical axis shows the ratio R' of the observed value to the calculated value of a tsunami height.

These figures show the calculated values are generally smaller than the observed values. It is natural that the calculated results cannot accurately reproduce the tsunami heights at each location. Because the grid size used in our calculation is 5km in length,

the computation region could not precisely represent the geographical features of the coast.

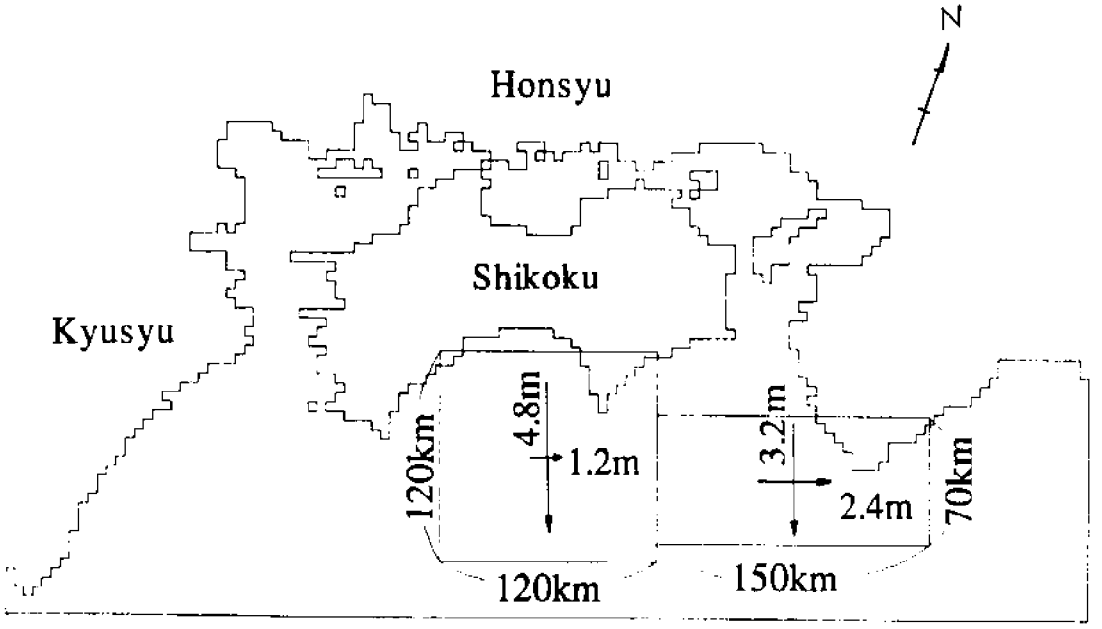

Figure 5. Computation region and the fault model of the 1946 Nankai earthquake

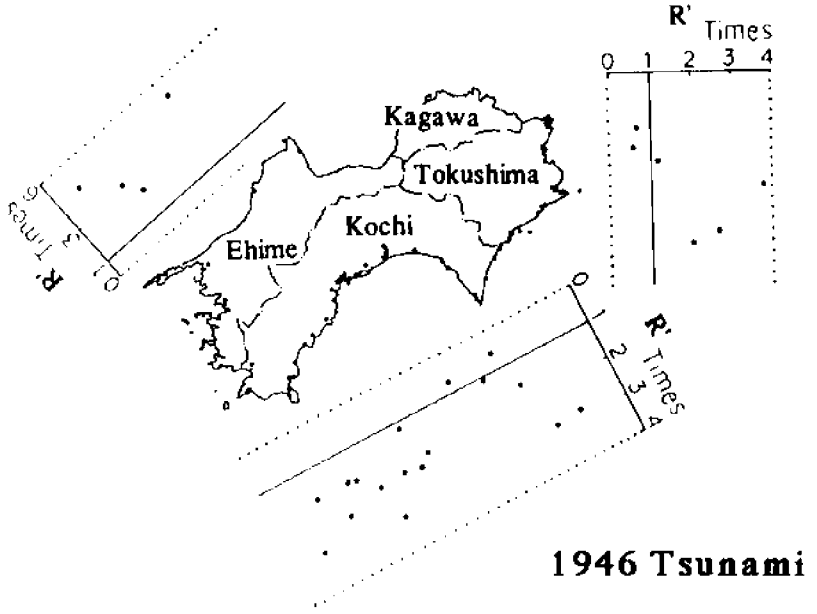

Figure 6.1. Comparison of calculated values with observed values

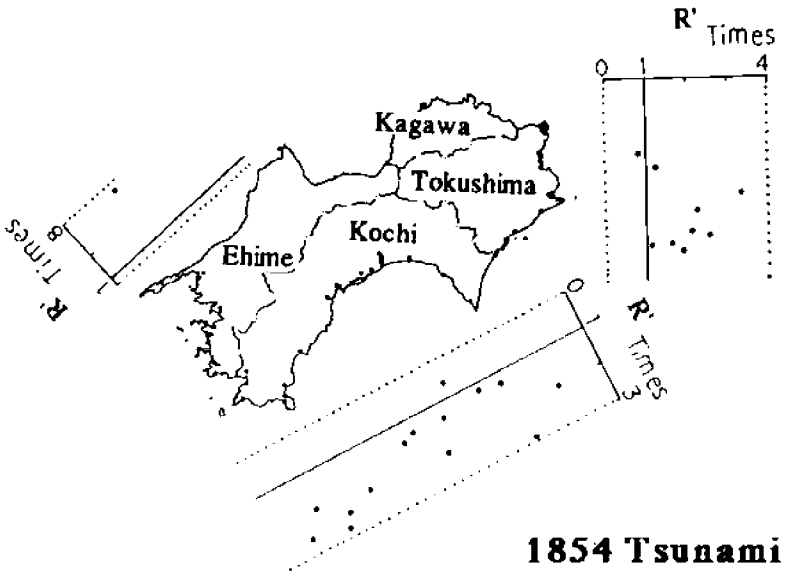

Figure 6.2. Comparison of calculated values with observed values

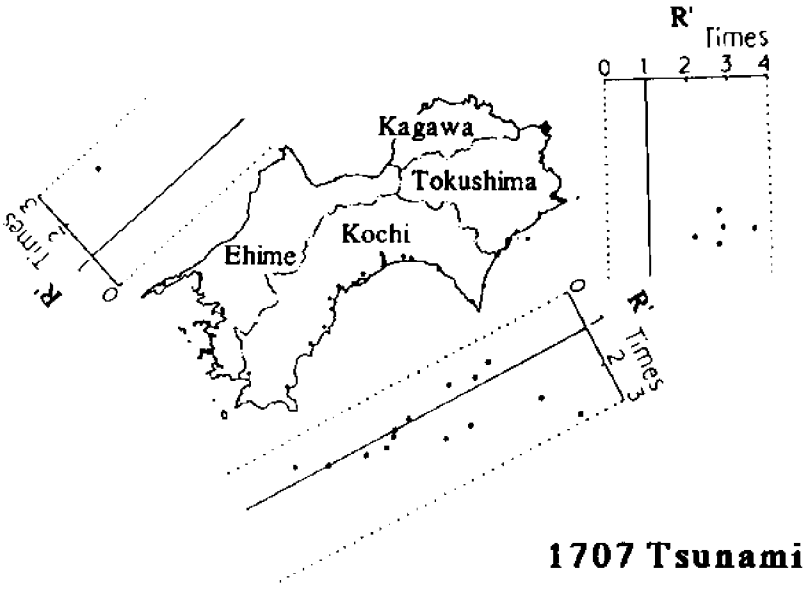

Figure 6.3. Comparison of calculated values with observed values

Figure 6.1 shows R' for the 1946 tsunami. The actual values of tsunami heights obtained by observation are 1-3 times as large as the calculated values along the Kochi coast. Along the Tokushima and Ehime coasts, the ratios maximize 4 times or more. However, the absolute values of the observed tsunami heights along the Ehime coast are not so high. For the 1854 tsunami in Figure 6.2, most values of R' are larger than 1.0 for the same reason mentioned above and the characteristics of R' between the 1946 and 1854 tsunamis show a similar tendency.

Figure 6.3 shows R' for the 1707 tsunami. For a long stretch along the Kochi coast, the values of R' are close to 1.0 and the tsunami heights by survey on the basis of old document are roughly equal to the numerically calculated ones. In the other regions (Tokushima, the eastern part of Kochi and Ehime), the observed values are larger than the calculated values. It is expected that in case of the calculation by 5km grid size, the calculated values are smaller than the observed ones, but most of the calculated values are almost equal to the observed ones for a long stretch along the Kochi coast. With considering these facts, it is necessary to re-estimate the fault parameters for the 1707 tsunami given in Table 1.

The Reproduction of the 1854 Tsunami Using the 1946 Tsunami Data

The characteristics of the 1854 tsunami are similar to those of the 1946 tsunami (See Table 1). So, we considered if the observed tsunami height at each bay end could be estimated by multiplying the calculated value of the 1854 tsunami by the value of R' for the 1946 tsunami.

Figure 7 shows the ratio R" of this estimated value to the observed value for the 1854 tsunami. As shown in Figure 7, these values of R" are plotted around one. As a result, the reproducibility of the 1854 tsunami heights was improved. Where we have data for the 1946 tsunami, we can obtain the corresponding tsunami heights for the 1854 tsunami by assuming that the source earthquakes were similar.

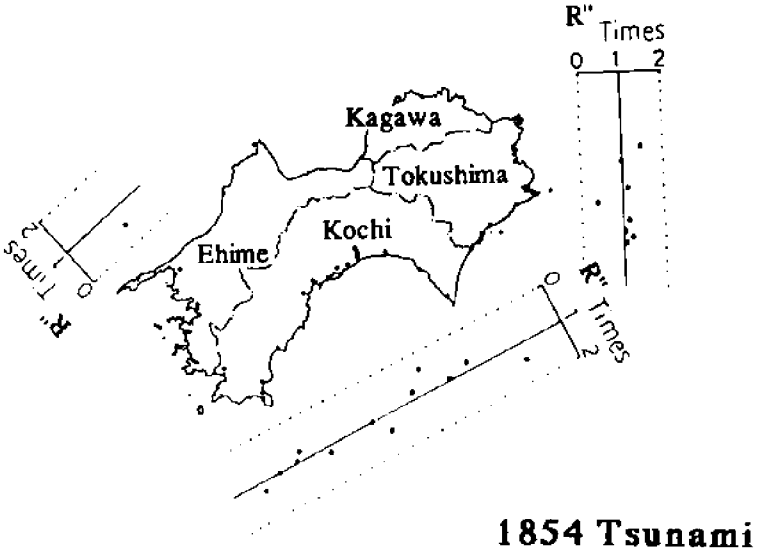

Figure 7. Reproduction of the 1854 tsunami

CONCLUSION

In this study, four big historical tsunamis were investigated in order to clarify tsunamis along the coast of Shikoku island in Japan.

First, data on the heights of these historical tsunamis occurring along the shikoku coast were re-examined. In addition, new data and the inundation heights of three of the historical tsunamis were compared with those of the 1946 tsunami.

Second, the inundation heights of these historical tsunamis were compared with the values calculated by numerical simulations. The following conclusions were obtained:

1) Generally, the values of tsunami heights of the three older tsunamis are 2-4 times as large as those of the 1946 tsunami.

2) It is necessary to re-estimate the fault parameters for the 1707 tsunami given in Table 1, because the observed values of tsunami heights are nearly equal to the calculated values for a long stretch of the Kochi coast in spite of the calculation by the 5km grid size.

3) The tsunami heights of the 1854 tsunami can be reproduced by using the observed data of the 1946 tsunami.

REFERENCES

Aida, I. 1981. Numerical experiments for the tsunami generated off the coast of the Nankaido district. *Bull. of Earthq. Res. Inst.* **56**:713-730. The University of Tokyo. (in Japanese)

Mansinha, L., and D.E. Smylie. 1971. The displacement fields of inclined faults. *Bull. Seismol. Soc. Amer.* **61(5)**:1433-1440.

MULTIPLE RESONANT MODES OF WATERS IN A WIDE-OPEN BAY

Shigehisa Nakamura
Shirahama Oceanographic Observatory
Shirahama, Japan

ABSTRACT

Coastal zones have been highly utilized by humans. Narrow-mouthed bays have been used for their living areas and for their activities. In comparison to these narrow-mouthed bays, few studies have been made on wide-open bays. In this work, a numerical modeling technique is applied for studying the properties of a wide-open bay. For convenience, the author uses a special case study of a bay in the northwestern Pacific. The numerical results are presented with reference to the tsunami threat and of the possible impact on the waters at a forced resonance of local multiple modes. Runup is not considered in this work.

INTRODUCTION

A numerical model is applied for studying multiple resonant modes of waters in a wide-open bay. This model was originally developed by Loomis (1972) and improved in order to study tsunami problems and other related problems (for example, Nakamura, 1980, 1983, 1984, 1985, 1986, 1987). With these improvements and applications, the model used in this work can be assumed to be appropriate for this study. Nakamura (1987) showed that this model could be useful in identifying the mechanism of the observed oscillation as a resonant mode. The resonant mode must surely be one of the important factors in considering tsunami warning and protection works, even though no runup is considered.

In the northwestern Pacific, as in other seismic zones, there are tsunami hazards on the coast facing the ocean. A historical review shows that such tsunami hazards have occurred repeatedly in the past as can be easily found in the published tsunami catalogs (e.g., Iida, et al., 1967; Soloviev and Gao, 1974, 1976; and Watanabe, 1985).

The author once studied the response of a wide-open bay using a numerical model (Nakamura, 1987). He reported that a nodal line is formed off the bay mouth and amplification depends on the configuration of the coastline and bathymetric condition.

In the present study, a specific reference is a coastal zone in the northwestern Pacific. An incident oscillation is given as an input function offshore to propagate into the coastal zone with a wide-open bay. Homogeneous and uniform fluid is assumed in a single layer for convenience.

A real map of the resonant modes is presented for the area around Hii district. Other possible impacts are also presented to exiting oscillations under the influence of the meteorological effects.

OSCILLATIONS IN A BAY

There have been many solutions for a simplified bay model. These solutions are found in the basic texts of, for example, oceanography or coastal engineering.

The simplest example is a semi-infinite ocean without a bay as found in (A) of Figure 1, although the actual coastline is not necessarily rectilinear and the water depth is not uniform. A geometrical simplification of the coast line makes it easy to solve equations by using various mathematical techniques. Problems on an almost-closed bay have also been solved by many scientists, too many to mention here. In this case, the shape of a bay is assumed as found in (B) although the coast of the existing bay is not in a rectangular shape with a slit. A basic study of a bay must be a simple rectangular bay facing an ocean as seen in (C). This is a typical case for applied mathematics. One of the similar cases must be a v-shaped bay as in (D), which shows that the oscillations of the waters can be well-amplified at the head of the bay and a nodal line is formed near the bay mouth. Another interesting case is a coupled bay as shown in (E). An energetic solution was obtained by Nakano (1932) as a solution for the secondary undulations in bays forming a coupled system. Generally speaking, the actual coastline facing the ocean is not so simple so that it is essential to consider the coastal configuration and bathymetric profile. Murty (1977), for example, has noted the relationship between the tsunami threat and oscillations in a bay.

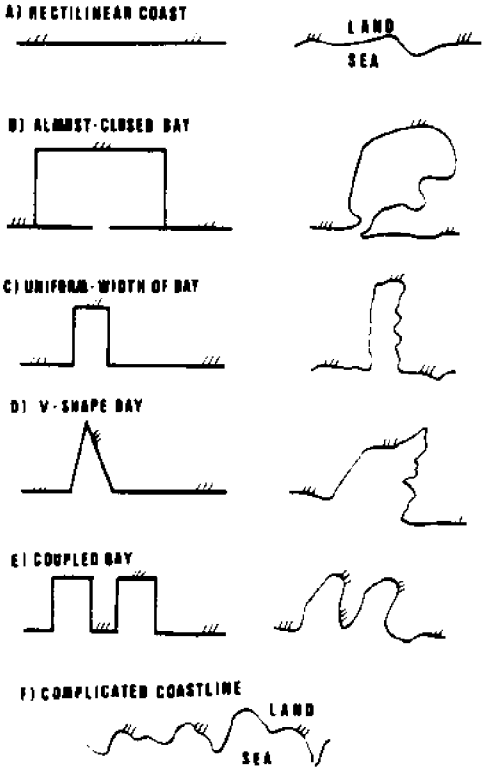

Figure 1. Typical shape of bay (schematic models and realistic configurations)

However, a more practical solution could be obtained by utilizing an appropriate numerical model for a hazardous region.

STUDY SITE OF TSUNAMI THREAT

In this work, the study site is a bay in the northwestern Pacific. It is well-known that the circum-Pacific seismic zone is located almost along the coast lines facing the Pacific (Figure 2). The islands of Japan are also a part of the circum-Pacific seismic zone. The author concentrates this work on the area of a part of the south coast facing the northwestern Pacific. This area is located around the dot in Figure 2 noted as 'KII' district.

In the area around 'KII,' tsunamis have inflicted damage in the past as shown in Table 1. This table was prepared after referring to the citation out of the original documents or historical description with evaluation of what is correct in the terms included in the existing tsunami catalogues. The remarks in the table simply note at-a-glance the damages in Japan.

The study site in this work (Figure 3), the repeated severe damages has been documented. Hence, the tsunami threat in the area is high, so that it is necessary to know when the next hazardous tsunami or tsunamigenic earthquake occurs. In order to establish an effective warning system and to complete a more effective protection works, a prediction of the next hazardous tsunami is in urgently needed.

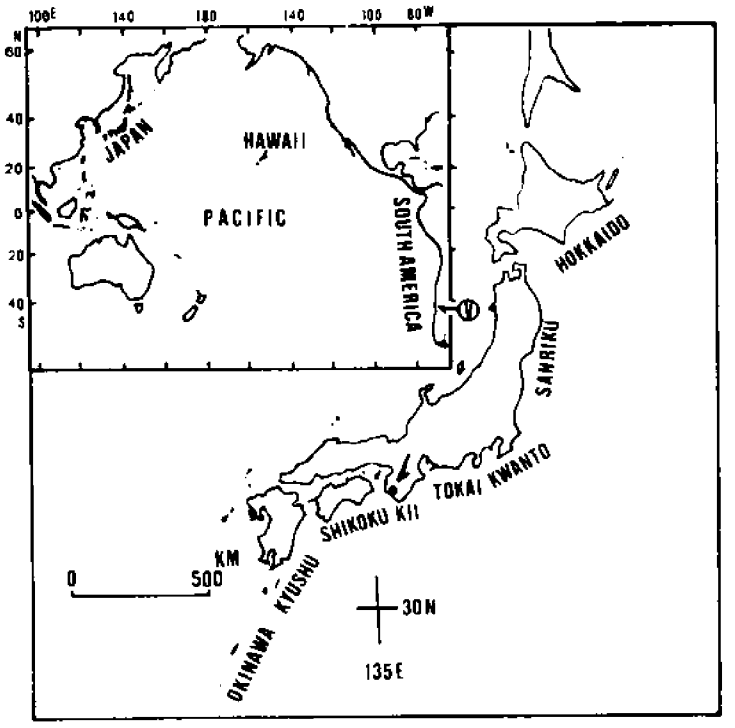

Figure 2. The circum-Pacific coastal zone and zonation of the Japanese coasts

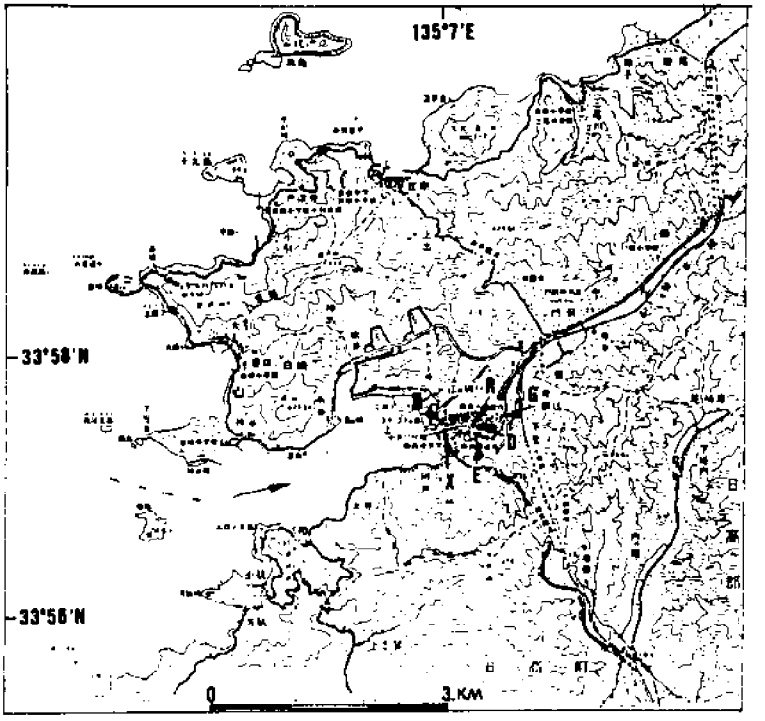

Figure 3. The geographical topography around the modelling area
(The marks X, N, R, D, E and G are the reference points.)

Table 1. Local tsunamis found in historical documents and records

Date	Location			Remarks
1707 Oct 28	M8.4	135.0E	33.2N	49000 persons dead 29000 houses broken Mr. Sakaguchi's document (only 5 houses without any damage in 139 houses; washed out)
1854 Dec 23*	M8.4	137.8E	34.1N	8300 houses broken and drawn 1000 persons dead 300 houses burned Sea booms just after strong shock and then tsunami arrived At Yura, max. ca 4-5 m above the land A hazard map of Yokohama area
1944 Dec 07	M8.3	136.2E	33.7N	Tsunami height 6 m at Owase 998 persons dead 2135 persons harmed 26130 houses completely broken 46950 houses partly broken 3059 houses washed out 11 houses burned
1946 Dec 12	M8.1	135.7E	33.0N	1330 persons dead 9070 houses broken 4283 houses partly broken 1451 houses washed out 2597 houses burned Ground level variations Tsunami hazard map#

Note: The mark of * is cited out of "Yura-Cho-Shi (Shiryo-Hen), 1985
The last two are cited out of "Zoku-Hidaka-Gun-Shi", 1975
The mark # is in "Kii-Yura-Chihou-Shi", 1966

A local hazard map of the event on 21 December 1946 is duplicated in Figure 4 which shows the hatched area as the tsunami-flooded area. In Figure 5, a tsunami hazard map of 23 December 1854 is duplicated to show the maximum water levels above the ground level. These maps suggest that tsunami runup was recorded and shows that a resonant amplification must have appeared for the incident variations of the water level as the tsunamis. This means that the problem of tsunami runup is replaced as the problems related to resonant modes in a bay in order to obtain the essential solution for the warning and protection work.

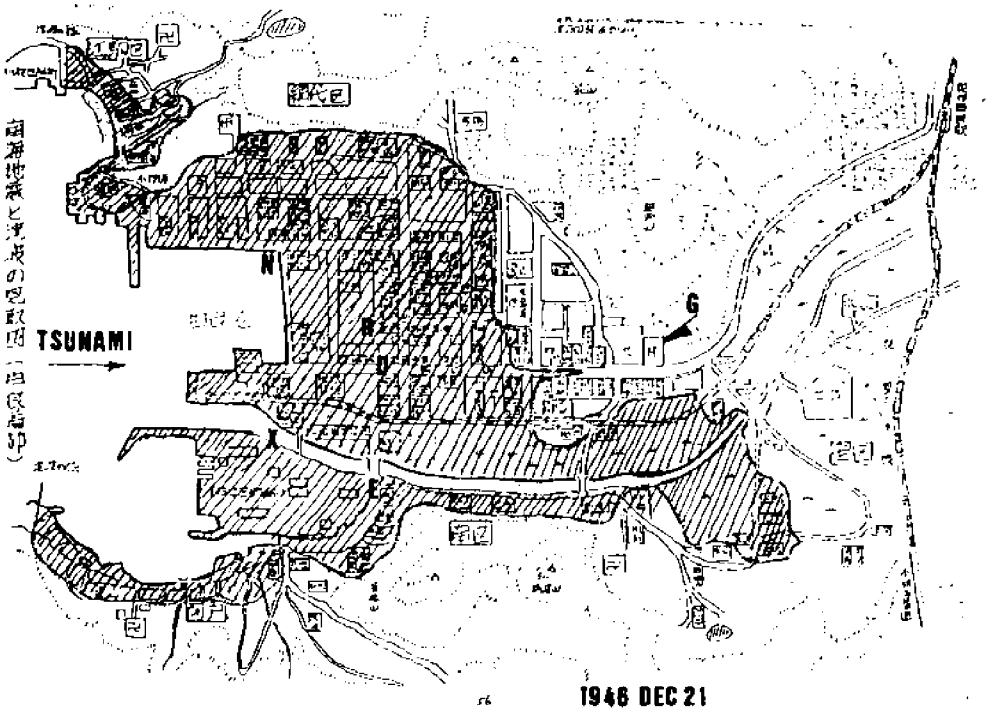

Figure 4. The tsunami hazard map for the 1946 event
(The marks X, N, R, D, E and G are the reference points.)

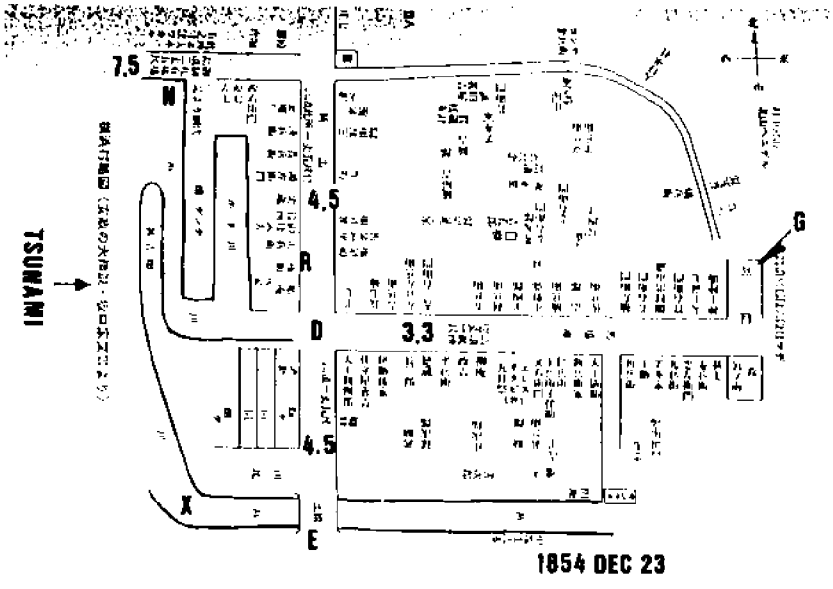

Figure 5. The tsunami hazard map for the 1854 event
(The marks X, N, R, D, E and G are the reference points.)

A SIMPLE NUMERICAL MODELLING

In order to find a solution for the threat of tsunami around the coast facing an ocean, it is preferable to utilize an improved numerical model. For this reason, the author applies his improved numerical model for problems on multiple resonant modes of waters in a wide-open bay. For convenience, an upwind scheme is modified and applied in the numerical computation for the model of interest in this work.

The equation of motion is rewritten in the form of a difference equation, and the equation of continuity is expressed also in the form of a difference equation. The grid size of the numerical computation is considered in order to obtain a stable solution.

A rectangular area covering the interested bay is taken as the model. In this work, the area is a part of the south coast of Japan facing the northwestern Pacific. This area is shown in Figure 6 schematically with the coastline and bathymetric contours of 20 mand 40 m deep around Hii Bay and Yura Bay. The model area is covered by a 400 m grid mesh. The maximum water depth is 66 m in the model area. In order to obtain a sable and reasonable solution numerically, the minimum water depth near coast is taken as 5 m which must be reasonable in this model because the most of the coastal control is directed to keep its water depth at the coastal structures which form the part of the coastline in the model area.

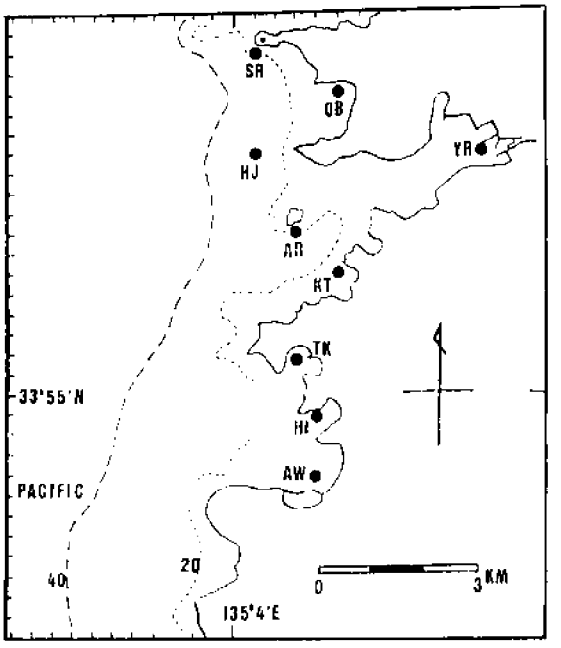

Figure 6. Modelling area for numerical computation and selected points (dots). Depth contours of 20 m and 40 m are shown.

Single-layered homogeneous water is considered and a forcing function as a variation offshore is given by a sinusoidal incident water wave on the western boundary of the model limit.

In Figure 6, several grid points are marked to show the locations, i.e., Shirasaki (SR), Ohbiki (OB), Yura (YR), Hijikijima (HJ), Ari-shima (AR), Katakui (KT), Tsukuno (TK), Hii (HI), and Awo (AW). These points are used for reference in this numerical model.

AMPLITUDE AND FREQUENCY

As a result of numerical computation, a resonant pattern at each point in the model is obtained as a function of an incident sinusoidal wave. The resonant patterns at these points are shown in Figure 7.

In Figure 7, the period of the incident wave is in the range between 12 to 28 minutes, and computation has been undertaken at a step of 1 minutes. So that, a more detailed property is hard to find out of this numerical result. Nevertheless, it is obvious that at YR a peak of resonance is around at the period of 27 or 28 min. of the incident wave. This resonant pattern suggests that a wave with one centimeter offshore may be observed as an about fifteen centimeters' wave at YR.

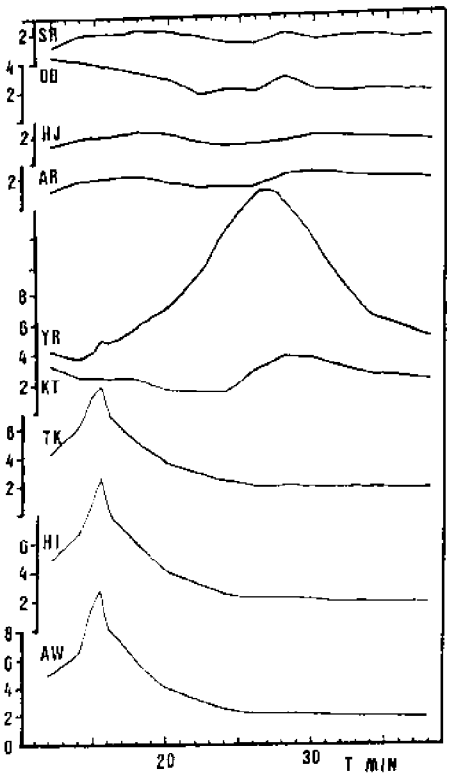

Figure 7. Amplification as local response at each point (same points in Fig. 6)

As for the resonant patterns at TK, HI and AW, a peak is found at the period of 15.5 minutes of the incident wave even though the area is formed by the coast line as a wide-open bay. In 1946 event of the tsunami, the local residents reported that the waters were violent and to-and-fro between HI and AW to form a lateral oscillation.

RESONANT MODES

In this numerical model used by the author, the first mode of the forced oscillation is for the period of 27 minutes of the incident wave and the amplitude pattern can be shown as in Figure 8. This pattern suggests that a nodal line is formed offshore, and the maximum of the amplitude is found at YR. This is understandable considering the resonant pattern shown in Figure 7. This could have been one of the factors of the 1854 tsunami (Figure 5) and the 1946 tsunami (Figure 4). The second mode is shown in Figure 9 to as a resonant amplification around HI and AW, respectively. A time stepping computation clearly illustrates the lateral oscillation between HI and AW.

OBSERVED OSCILLATIONS

In this section, a recent record of oscillations in the model area is introduced and discussed.

A Part of the Tide Record

At station YR (33°57.26'N, 135°7'E), some records were obtained using a pressure sensor settled on the sea floor. A part of the record is shown to demonstrate oscillations induced at the head of the wide-open bay in Figure 10. The sensor has a cut-off function for high frequency so that no wind waves are included in the record.

Possible External Impact

At the station settled offshore tower (SHIRAHAMA) about 40 km southeast of station YR, wind speed (W), wind direction (W_D), air temperature (T_A), water temperature (T_W) and tides (Z) were observed (Figure 11). It is easy to see that the wind speed and direction varied in the early morning on 2 October 1986. Air temperature also rose suddenly about 2°C. No significant variations of water temperature and tides were noticed. This indicates the passage of a atmospheric warm front at the tower. This can be an impact on the sea surface. If this is the case, the variations in the afternoon as found in Figure 10 may possibly be a result of the meteorological impact on the sea surface.

Amplitude Spectra

A result of amplitude spectral analysis is shown n Figure 12. This diagram shows variations of the spectral pattern with time lapse. The marks P-P and R-R indicate the resonant modes appeared in Figure 7 or Figures 8 and 9. With this diagram, the two modes may be taken to be possibly amplified by the meteorological impact on the sea surface. Eliminating the tides from Figure 12, the spectral pattern can be shown as in Figure 13. In this diagram, it becomes clear that the two modes had developed after the impact in the early morning so that the cross marks are the peaks of the spectral pattern.

Inducing the Multiple Modes

In the above examples, the atmospheric impact is also to induce the multiple modes in the coastal area considered in this work as in the case of the hazardous tsunami.

CONCLUSIONS

A numerical model is applied for studying multiple resonant modes of the waters in a wide-open bay. First, various patterns of bays facing an ocean are introduced. Next, this work is considered in relation to the tsunami threat on the coasts facing the circum-Pacific seismic zone. The author's interest concentrated on problems in a wide-open bay located in the northwestern Pacific. A simple numerical modelling was undertaken to find the local resonant mode; especially the first and second modes in the model area in order to discuss their relationship to the tsunami threat. The other possible impact was considered in order to understand variations as induced resonant modes.

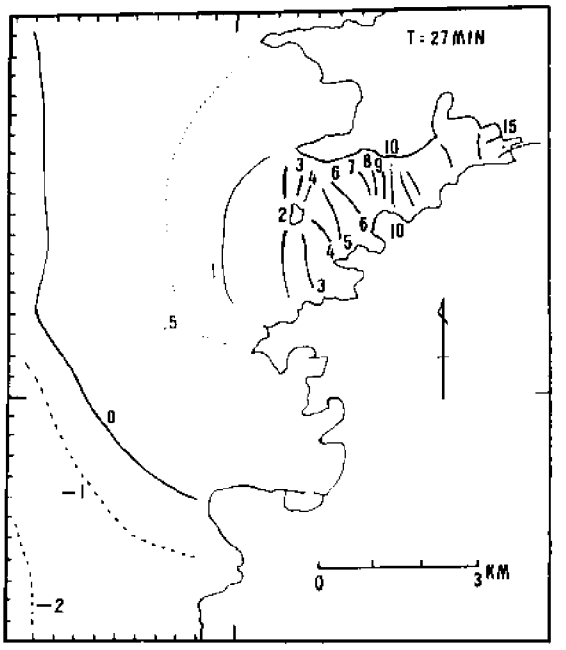

Figure 8. The first mode of the forced response in the model

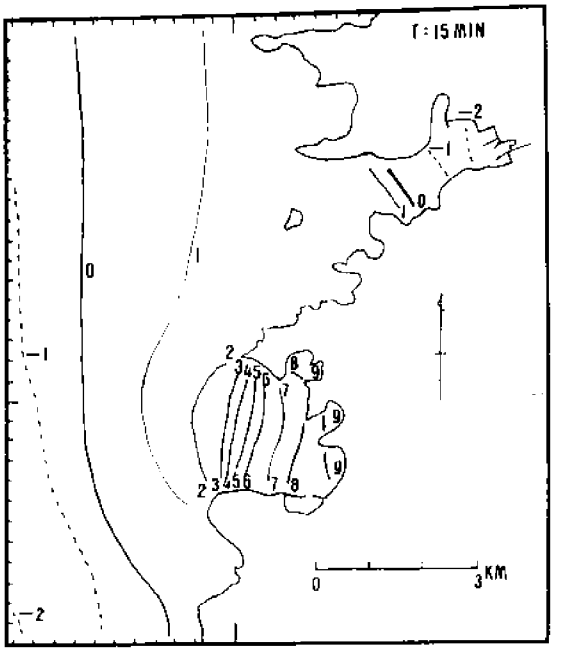

Figure 9. The second mode of the forced response in the model

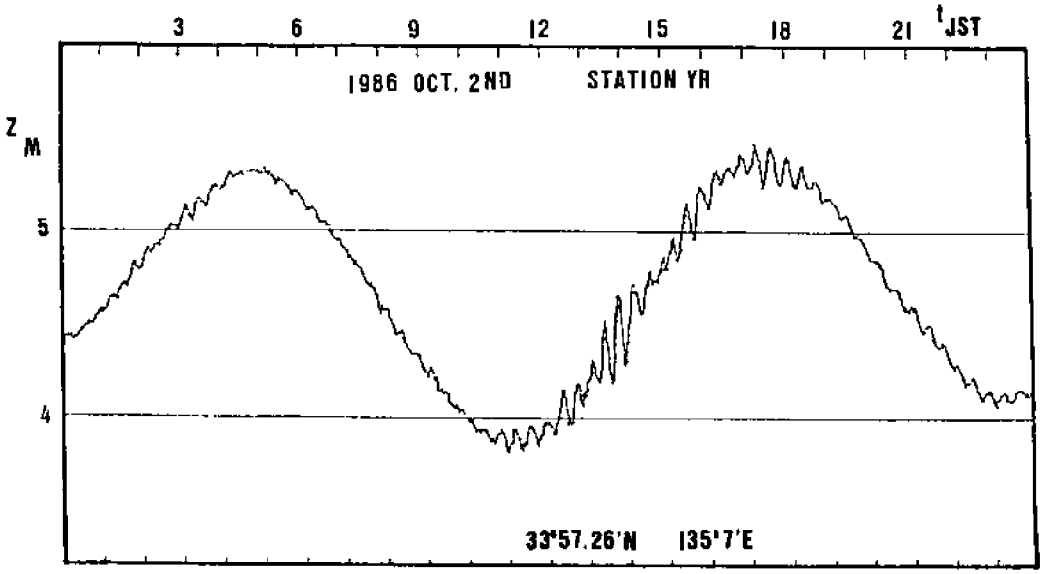

Figure 10. Local tides and variations

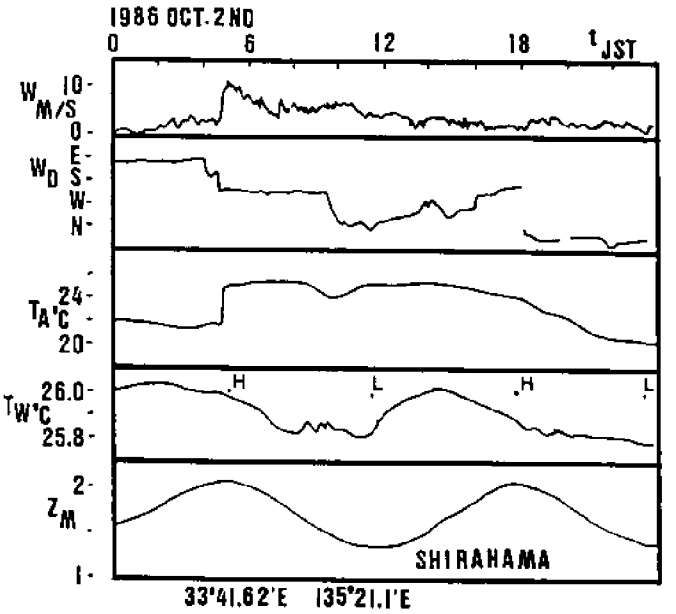

Figure 11. Observed results at the offshore tower station to demonstrate the atmospheric impact on the sea surface

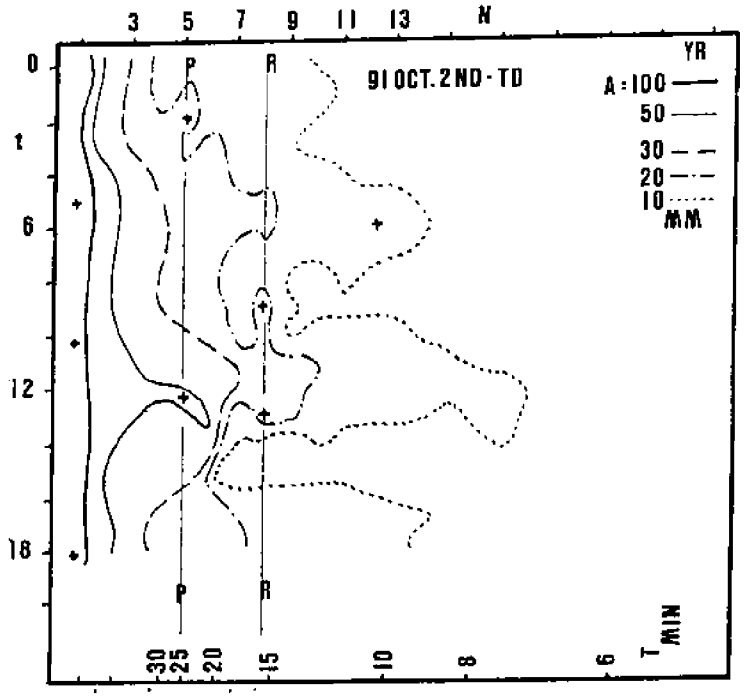

Figure 12. Time evolution of amplitude spectrum (TD) obtained from the data shown in Figure 10

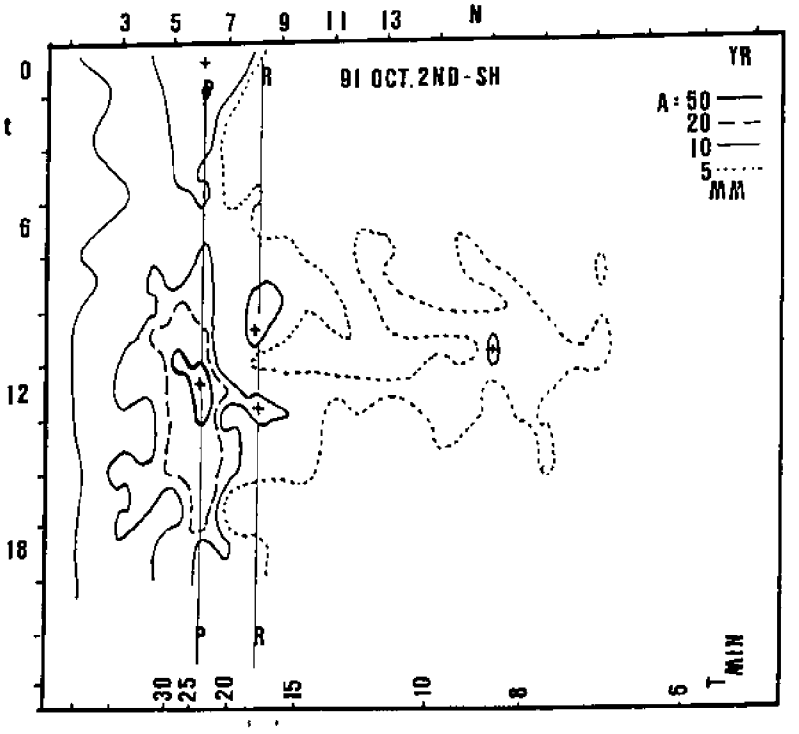

Figure 13. Time evolution of amplitude spectrum (SH) obtained from the data shown in Figure 10

ACKNOWLEDGEMENTS

Professor N.K. Saxena, University of Hawaii, encouraged the author to complete this article. Appreciation is also extended to Dr. Eddie Bernard for presenting this work. Many colleagues and friends are also acknowledged for their support.

REFERENCES

Iida, K., C. Cox, and G. Pararas-Carayannis. 1967. Preliminary catalog of tsunamis in the Pacific. University of Hawaii, HIG-67, Data Report No. 5.

Loomis, H.G. 1972. A package program for time stepping long waves into coastal regions with application to Haleiwa Harbor, Oahu. NOAA-JTRE-79, University of Hawaii, HIG-72-21.

Murty, T.S. 1977. Seismic sea waves (Tsunami). Bull. Fisheries Res. Board of Canada, No. 198.

Nakamura, S. 1980. Sumbawa tsunami in a scope of numerical experiment. *La mer.* **19**:30-37.

Nakamura, S. 1983. Numerical tsunami model in Osaka Bay. Bull. Disas. Prev. Res. Inst., 33:1-14. Kyoto University.

Nakamura, S. 1984. A numerical tracking of the 1883 Krakatoa tsunami. *Sci. Tsunami Hazards.* **2**:41-54.

Nakamura, S. 1985. On response of coastal waters to offshore disturbance. *La mer.* **23**:111-117.

Nakamura, S. 1986. Tsunami threat evaluation by historical documents, numerical model and stochastic model. In: Proc. 20th Conf. Coastal Eng., pp. 2620-2630. ASCE.

Nakamura, S. 1987a. A response of wide-open bay in a numerical model. *Marine Geodesy.* 11:241-250.

Nakamura, S. 1987b. A numerical prediction of semidiurnal current patterns in Tanabe Bay. Bull. Disas. Prev. Res. Inst., 37:91-105. Kyoto University.

Nakano, M. 1932. The secondary undulations in bays forcing a coupled system. In: Proc. Phys. Math. Soc. Japan, Ser. 3, pp. 372-380.
Soloviev, S.L., and C.N. Gao. 1974. Katalog tsunami na zapadnom poberezie Tixogo Okeana, Akad. Nauk (USSR), Izdat. Nauk.

Soloviev, S.L., and C.N. Gao. 1976 atalog tsunami no vostochnom poberezie Tixogo Okeana, Akad. Nauk (USSR), Izdat. Nauk.

Watanabe, H. 1985. Japanese catalog of the hazardous tsunamis. University of Tokyo Press.

STRUCTURE OF SPACE-TIME VARIABILITY OF GEOSTROPHIC CURRENTS IN THE SOUTHERN OCEAN

Robert H. Stewart, Thomas J. Johnson*, Link Ji,
C.K. Shum*, and Byron D. Tapley*

Texas A&M University
College Station, Texas, U.S.A.

*University of Texas
Austin, Texas, U.S.A.

ABSTRACT

Data collected by the U.S. Navy's Geosat Exact Repeat Mission were used to obtain detailed, statistical descriptions of the variability of the surface geostrophic flow field in a portion of the Antarctic Circumpolar Current in the Southeast Pacific. The descriptions provide, for the first time, the information about the flow long available in other branches of fluid dynamics such as aerodynamics; and are useful for guiding the development of numerical models of the circulation. In particular, we have used Geosat altimetric observations of the variability of the two components of sea-surface slope at crossing points of the Geosat ground track. From the slopes we have calculated time series of two components (u', v') of the surface geostrophic current for a 2.5 yr period at a dense grid of points in the current. We then used the time series at each point to map the spatial distribution of the components of the Reynolds stress $\langle u'u' \rangle$, $\langle v'v' \rangle$, and $\langle u'v' \rangle$ and their relationship to the mean flow and to bathymetry. The maps show that bathymetry strongly influence the flow, that flow has statistically significant regions of negative viscosity suggesting baroclinic instability, and that the flow has regions of positive viscosity which slows the mean flow. We have calculated the eddy viscosity in the portion of the flow upstream of the Drake Passage. In this region the flow appears to be a free jet; and the eddy viscosity was 8×10^4 m^2/s. We have also calculated the statistical relations among the components of the current, including probability distribution functions and the correlations among the components of the flow lagged in time and space. The correlations show the structure similar to the variability mapped in the North Atlantic by other groups.

INTRODUCTION

Studies of ocean dynamics have been constrained by a lack of a statistical description of the flow that has been available, for example, in such fields as aerodynamics for more than 60 years. Yet such a description of the oceanic mesoscale variability is necessary for understanding the role of eddy variability in ocean dynamics and for developing more accurate numerical models of the oceanic circulation. Among the various statistical functions describing the flow, the turbulent stress and the time and space lagged correlation functions are perhaps the most useful. They are also the most difficult to measure using conventional oceanographic techniques.

Satellite altimeters measure sea level along the subsatellite track; and the level is the sum of the influence of gravity, geoid, tides, and the influence of ocean dynamics, the oceanic topography. The geoid is fixed in time, but the topography has a permanent and a time-variable component. Because the geoid is not well known for wavelengths shorter than 2000 km, the permanent topography cannot be separated from the geoid. The

temporal variability of the oceanic topography can, however, be observed using repeated profiles of the surface. This allows satellite altimeters to measure the time-varying components of the oceanic circulation with wavelengths of 200–2000 km, including the mesoscale variability. We refer to mesoscale variability as eddy variability for simplicity, although it is due to both turbulence and planetary waves.

The study uses data from the U.S. Navy's GEOSAT which carried a precise altimeter that observed the ocean between ±72° latitude for 3 years. Data from the satellite were previously used primarily for describing the geographical distribution of eddies (Fu and Zlotnicki, 1989), their relationship to bathymetry (Sandwell & Zhang, 1989; Chelton, et al., 1990), and the annual and interannual variability of currents (Cheney & Miller, 1988; Shum, et al., 1990). More recent studies have looked at the contribution of eddies to the dynamics of currents (Stammer & Böning, 1991; Le Traon, 1991).

The importance of eddies is well known. The mean-square variability of the horizontal components of the current and the correlations between the components produce stress, the Reynolds stress, which mediate the transfer of momentum in the ocean. Despite the importance of the Reynolds stress for ocean dynamics, it is difficult to measure; and only a few sporadic measurements have been reported (Webster, 1961; Luyten, 1977; and Lukas, 1987). The use of satellite altimeter data for the study of Reynolds stress is even more limited. Tai and White (1990) used Geosat data to map Reynolds stress in the Kuroshio Extension. They found evidence that eddy kinetic energy accelerates the mean flow; but they noted that only ascending tracks of altimeter data were available, and this led to large uncertainty in the accuracy of the calculated stress. Johnson, et al., (1992), investigating the role of the stress in the Antarctic Circumpolar Current, developed an accurate technique for calculating Reynolds stress directly from altimeter data. At the same time, Morrow, et al. (1992) were calculating the distribution of stress in the Antarctic Circumpolar Current using very similar techniques.

The previous work, while limited, is encouraging. Records as short as one year produced useful values of stress having a smooth spatial distribution. This is in marked contrast with laboratory measurements of turbulence which required averages over several hundred to a thousand eddies to obtain statistically stable results. For the ocean, this would require 20–100 year long records for comparable results.

We report here observations of Reynolds stress made using data from the Geosat exact repeat mission. We have mapped the distribution of the stress, and we have used calculated values of stress to study the dynamics of the Antarctic Circumpolar Current upstream of the Drake Passage.

DATA, FILTERING , AND COMPUTATION OF STRESSES

Geophysical Data Records from the first 54 cycles of the Geosat Exact Repeat Mission were processed using the techniques described by Zhang (1988), and Sandwell and Zhang (1989) to obtain along-track slopes of the sea surface. The data are from November 7, 1986 to November 17, 1989. No data from the last 14 cycles of the mission nor any data from cycle 51 were used because many observations were missing or anomalous. The processing yielded smoothed values of sea level slope every 32.5 km along the subsatellite track. The use of slopes produced a high-pass filter which removed almost all ephemeris errors, which are predominantly at wavelengths of once per orbital revolution, and long-wavelength errors in the corrections applied to the height data. The smoothing reduces short wavelength noise without reducing the signal due to oceanic mesoscale variability.

The along-track value of slope at cross over points was obtained from a linear interpolation between values closest to the cross-over. The sea-level gradient was calculated from the two slopes at each crossover for each cycle. The geostrophic velocity at the sea surface v is directly related to the sea-level gradient relative to the geoid ζ (Wunsch and Gaposchkin, 1980). Because the local geoid, is not accurately known, only the temporal variability of v could be determined. Writing the velocity as the sum of a mean V and a time-varying component v', we computed v' from the temporal variability of the slope after subtracting the temporal mean slope at each cross over point from the slope value for each cycle.

The three components of the stress at each cross-over are:

$$R_{ij} = \rho \langle u'_i u'_j \rangle \tag{1}$$

where $(u'_i, u'_j) = (u', v') = v'$ are the two components of the time-varying surface velocity, $\langle\ \rangle$ denotes the temporal average over all 53 cycles of data, and ρ is the water density. Note R_{11} and R_{22} are the normal stresses, and R_{12} is the shear stress. The two orthogonal components of velocity and the three stresses were calculated at a 32 × 120 grid of points in a large area from 51°S to 66°S and 80°E to 170°E.

ERROR ANALYSIS OF REYNOLDS STRESS COMPUTATION

The errors in computer values of stress were studied by Johnson, et al. (1992), who considered the two largest sources of error, finding that neither substantially influences the results reported here. The two sources of error are: 1) variability in the flow between observations at a cross over point, and 2) statistical uncertainty in the mean product $\langle u'_i u'_j \rangle$.

The first error is proportional to the interval between ascending and ascending passes of the satellite past a cross-over point, which varies between 0.6 and 8.5 days depending on the latitude, and to the decorrelation time of the flow field. We found that the decorrelation time was sufficiently long compared with the time between cross overs that this error is not important.

The second error depends on the statistical significance of the correlation between u' and v'. We found that u' and v' were normally distributed, but that stress was significant at only 20% of the crossover points based on Student's t-test. This implies that stress is carried by a relatively few eddies, a result consistent with laboratory and field observations of turbulence on a much smaller scale.

LAGGED CORRELATIONS IN TIME AND SPACE

We calculated the averaged, weighted, sample correlations γ lagged in time and space using all observations in the 32 × 120 grid of points. The averages were calculated using values of the correlation weighted by the variance of the variable used for calculating the correlation. This gives the most weight to those values with the largest signal-to-noise ratio. The correlations of u' lagged in time and in the x direction were averaged over 2500 pairs of cross-over points in time or space.

We found that the correlation function γ is nearly exponential in time and space (Figure 1). For the u' component of velocity, $\gamma = 1.0 \exp(-b_x x)$ or $\gamma = 1.0 \exp(-b_t t)$, where $b_x = -0.0144$ km^{-1} and $b_t = 0.0648$ d^{-1}. We tested the sensitivity of the result to the time interval between cross overs and obtained the same results for intervals of less than one day and less than three days. The results are also consistent with values for the North Atlantic (Le Traonn, 1991) and with the integral time scales observed in the Drake Passage (Inoue, 1985).

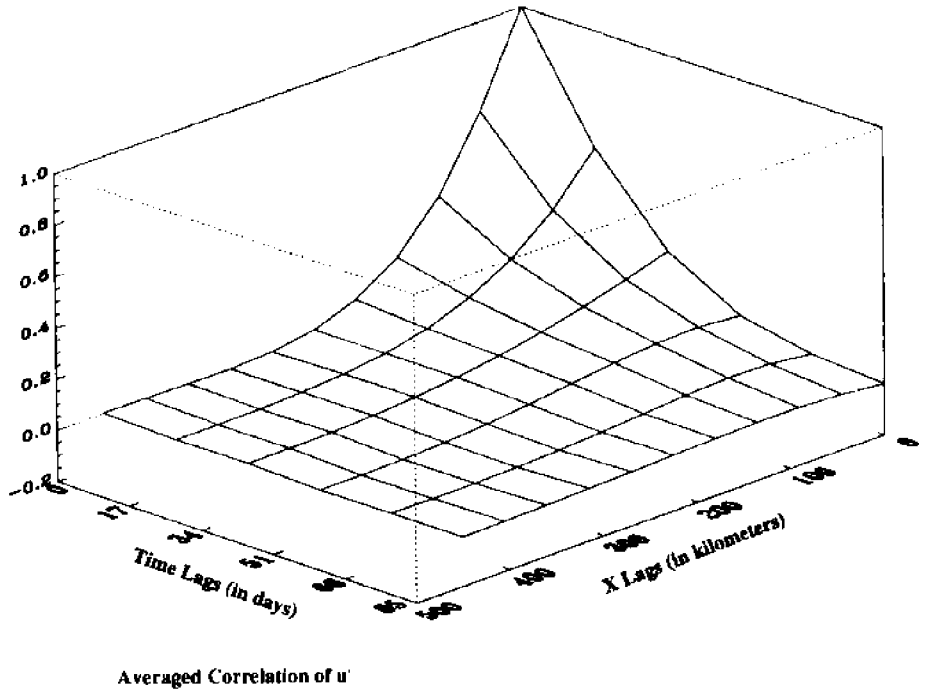

Figure 1. Space-time correlation function for eastward velocity u' for all data for which the interval between ascending and descending passes was less than three days. The correlation is nearly exponential near the origin for lags in time and in the x (east-west) direction.

Because the spectrum of sea-surface slope is the Fourier transform of the slope-correlation function, the exponential shape of the correlation implies that the temporal and spatial spectra $S(\omega)$ or $S(k_x)$ must be of the form:

$$S(\omega) = \left[1.0/(b_t^2 + \omega^2)\right]^2 \quad \text{or} \quad S(k_x) = \left[1.0/(b_x^2 + k_x^2)\right]^2 \tag{1}$$

where ω is frequency and k_x is wave number. The result is generally consistent with the spectra of variability calculated by Fu and Zlotnicki (1989) in regions of high variability,

and it provides further support for the idea that the spectrum of eddy variability is well approximated by a power law only for the high frequency or short wave number part of the spectrum. The use of the correlation for calculating spectra has a practical advantage, it allows calculation of variability of each component of velocity using data from a relatively small region. Previous calculations of the spectra required relative long segments of data confined to the satellite's ground track; and the calculations yielded the spectra of only that component of current that is perpendicular to the track.

GEOGRAPHICAL DISTRIBUTION OF STRESS

We mapped the distribution of stress in a broad sector of the southeast Pacific which included the Antarctic Circumpolar Current (Figure 2). All three components of the stress have a spatial distribution similar to that of $\langle u'u' \rangle$ shown in the figure. The distribution of the normal components agrees qualitatively with plots of the variance of surface elevation published by Sandwell & Zhang (1989) and Chelton, et al. (1990), and with plots of eddy kinetic energy (Shum, et al., 1990).

The plot shows that the distribution of stress is strongly associated with bathymetry. Between 200°E and 260°E the stress is tightly confined to the area between the Eltanin and Udintsev Fracture Zones. East of 230°E, the large stress was almost entirely confined to the region between the subantarctic and polar fronts (Nowlin & Klinck, 1986); and by 260°E the axis of high variability centers on 60°S as the current approaches the Drake Passage. West of 230°E the flow is more complex as the current flows between the Eltanin and Udintsev fracture zones and over the Pacific Antarctic Ridge. An area of high variability extends over 4° north of the subantarctic front, and the highest stress occurs between 210°E and 240°E where the flow skirts the Udintsev fracture zone upstream and downstream of the ridge crest, presumably due to turbulence produced as the stream meanders to avoid the shoalest regions immediately above the ridge crest.

In the zone between 238°E and 280°E just upstream of the Drake Passage both the area of high stress and the subantarctic and polar fronts are nearly zonal. Furthermore, the stress becomes weaker in the downstream direction. The flow, therefore, resembles very much a free jet. Such a flow is dynamically interesting, and it can be used for testing theories of the role of eddies in the dynamic. Hence, we chose this region for further study. We are particularly interested in the influence of the stress on the dynamics of the mean currents.

Within this region, we note first that the ratio of $\langle u'u' \rangle$ to $\langle v'v' \rangle$. was 1.65±0.10, indicating that the along-stream fluctuations are larger than the cross-stream fluctuation. This compares well with the value of 1.45±0.25 calculated from moored current meter observations in the Drake Passage (Inoue, 1985).

MEAN DYNAMIC TOPOGRAPHY

Calculations of energy transfer between the mean current and eddies and calculations of the work done by stress require knowledge of the distribution of the mean current U. Because the geoid is not well known in the South Pacific, the mean current cannot be determined from the altimeter data. We therefore calculated the mean current using observations of density made at deep hydrographic stations. The most useful data were from the *R/V Eltanin* surveys between 1963 and 1968, and the *R/V Discovery* survey in 1934 (Figure 3).

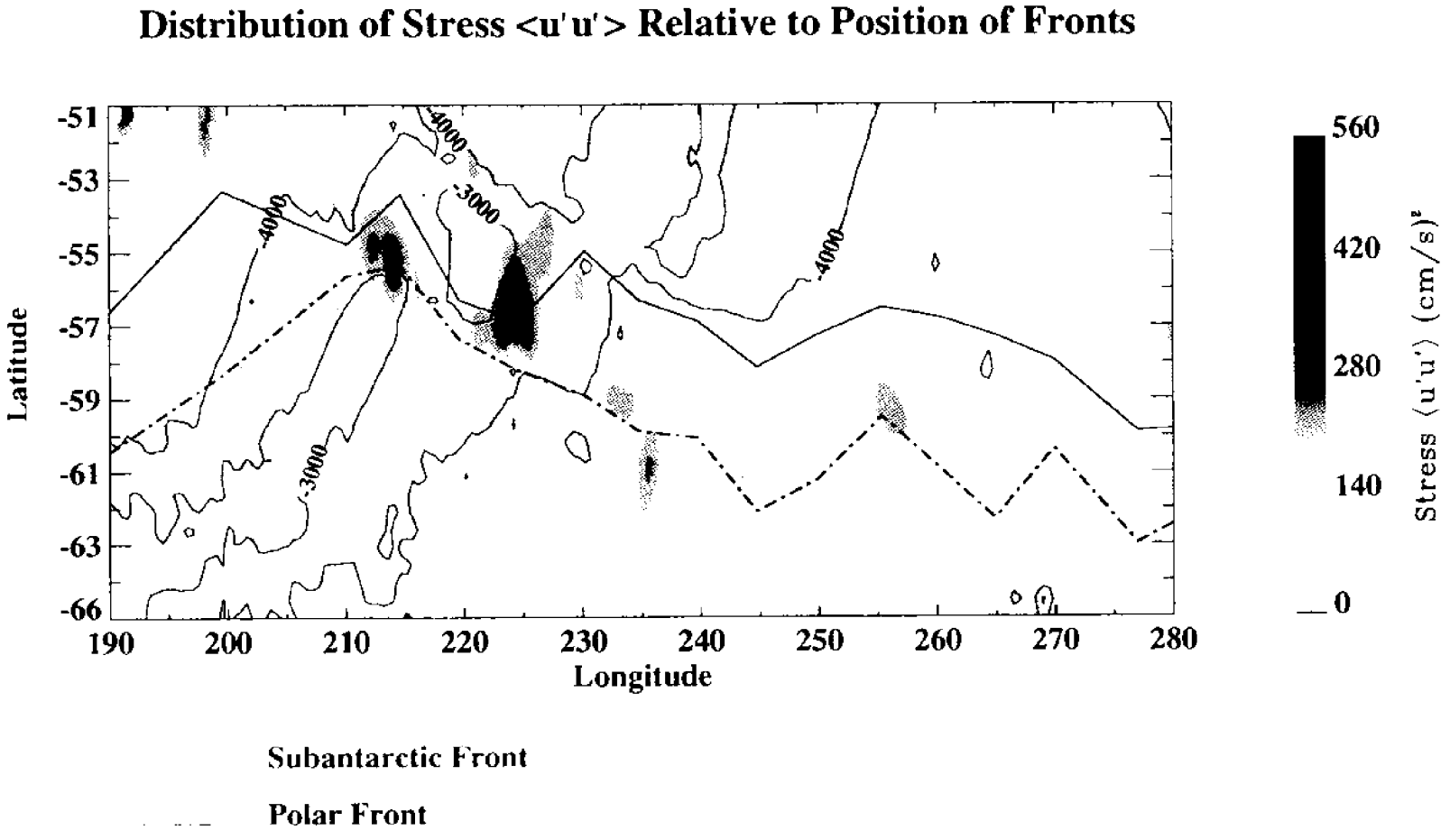

Figure 2. Geographical distribution of stress in the Antarctic Circumpolar Current in the Southeast Pacific. The plot includes contours of bathymetry at intervals of 1000 m, the position of the subantarctic and polar fronts, and the distribution of $\langle u'u' \rangle$ component of stress.

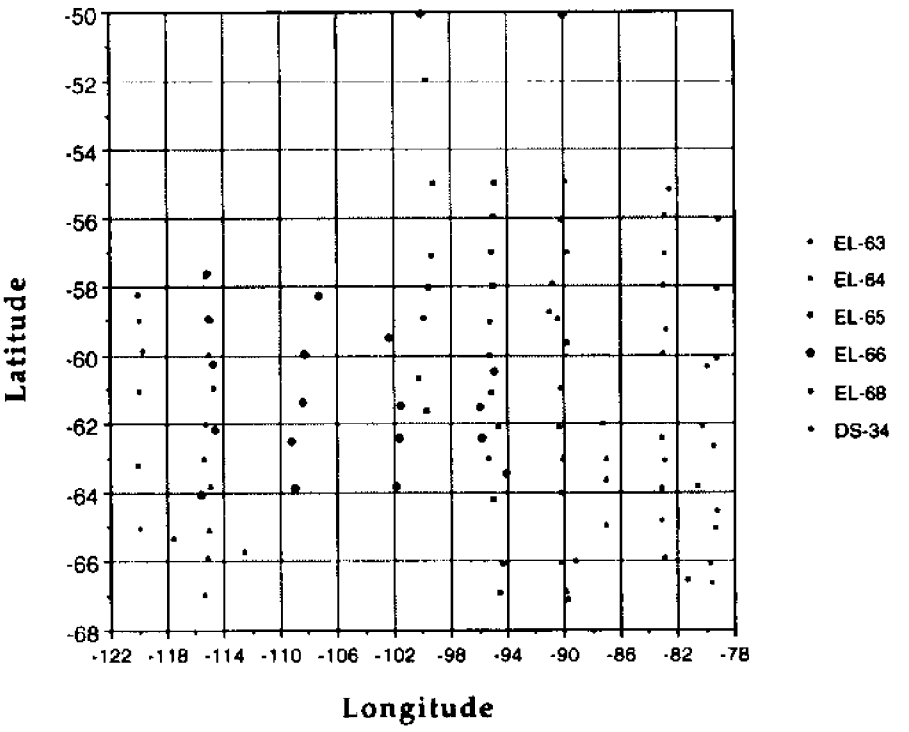

Figure 3. Location of hydrographic stations used for calculating the mean dynamic topography in the region shown in Figure 2. EL-63 denotes data collected by the R/V *Eltanin* in 1963 etc., DS are data from the RSS *Discovery*.

To calculate the mean zonal current in the region upstream of the Drake Passage, we calculated the surface dynamic topography relative to 3000 m, then averaged the topography in the zonal direction between 122°W to 78°W using 0.5° bins (Figure 4). We then fitted a smooth curve through the data, from which we calculated the first and second derivatives of the north-south slope. After trying various polynomial and other approximations to the topography ζ, we used a hyperbolic tangent of the form

$$\zeta = a \tanh(by - c) - d \tag{2}$$

where $a = 0.5944$ m, $b = 0.1636/\text{degree} = 1.458 \times 10^{-6}/\text{m}$, $c = 59°$, and $d = 1.6466$ m are parameters determined by a least-squares fit and y is distance northward measured in degrees of latitude. The curve has the advantage that it defines a zonal jet that closely resembles the observed current. The plot of the normal stress $\langle u'u' \rangle$ (Figure 5a) corresponds closely with the distribution of mean velocity.

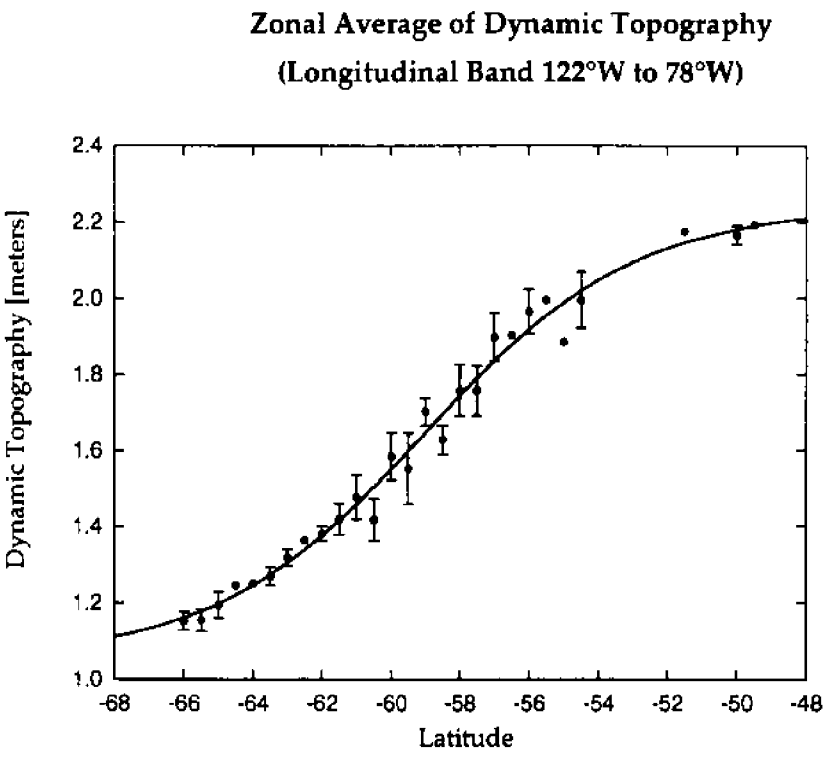

Figure 4. Zonal mean dynamic topography calculated from hydrographic data collected at stations shown in Figure 3. The mean was calculated for data within 0.5° bands of latitude between 122°W and 78°W longitude. The vertical bars give the statistical uncertainty of the mean values.

Using Eq. (2), the mean zonal current is:

$$U = \frac{g}{f}\frac{\partial \zeta}{\partial y} = \frac{abg}{f}\cosh^{-2}(by - c) \tag{3}$$

From this, we can calculate the zonal derivative $\partial U / \partial y$ needed in the next section.

ENERGY TRANSFER

Eddies can either dissipate or accelerate the mean circulation. The latter is an example of negative viscosity which can result from baroclinic instabilities. Because both processes can occur in the Circumpolar Current, we have investigated the influence of the eddies on the mean flow.

The rate at which the kinetic energy of the mean flow U in a zonal jet is changed by eddy stress is given by (Starr, 1968; see also Webster, 1961):

$$\int_{y1}^{y2} \rho\langle u'v'\rangle \frac{\partial U}{\partial y} dy \tag{4}$$

assuming the flow is bounded so that $U(y_1) = U(y_2) = 0$ at latitudes y_1, y_2 on either side of the axis of the flow, and p is water density.

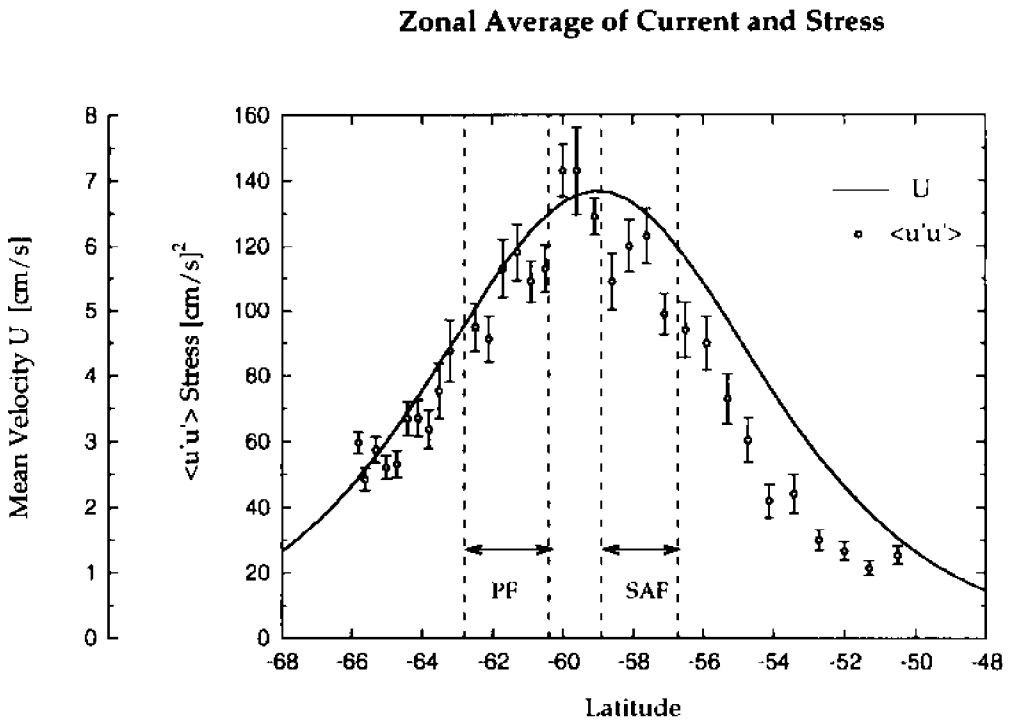

Figure 5a. Zonal average of the <u'u'> component of stress relative to zonal mean current. The stress was calculated from altimetric data; and the mean current was calculated from hydrography using Eqs. (2) and (3). The vertical lines mark the position ± the standard deviation of the zonal mean location of the polar front PF and the subsntarctic front SAF. The means were calculated using data between 122°W and 78°W longitude. The error bars give the statistical uncertainty of the mean value of each point.

We calculated the integrand in Eq. (4) using U computed from Eq/ (3) and $\langle u'v' \rangle$ from the Geosat data. The plot of the zonal averages of $\langle u'v' \rangle$ and U shows that the Reynolds stress and, hence the eddies, tends to decelerate the flow (Figure 5b). We therefore calculated an eddy viscosity A_y (Pond & Pickard, 1983) using:

$$-\langle u'v' \rangle = A_y \, \partial U / \partial y. \tag{5}$$

This yielded $A_y = 8 \times 10^3 \, m^2/s$ with small uncertainty, a value that is consistent with values reported for other oceanic flows.

We also note that the distribution of shear stress (Figure 5b) is not quite symmetric about the maximum value of the mean current. The values between –66° and –63° are positive and statistically different from zero, hence the plot indicates that the stress decelerates the flow near –58° and accelerates the flow near –63°. This implies the eddies transfer momentum from the mean flow at the subantarctic front to the mean flow at the polar front. The measured shear stress is sufficiently large that it can transfer most of the momentum from one front to the other in a few thousand kilometers.

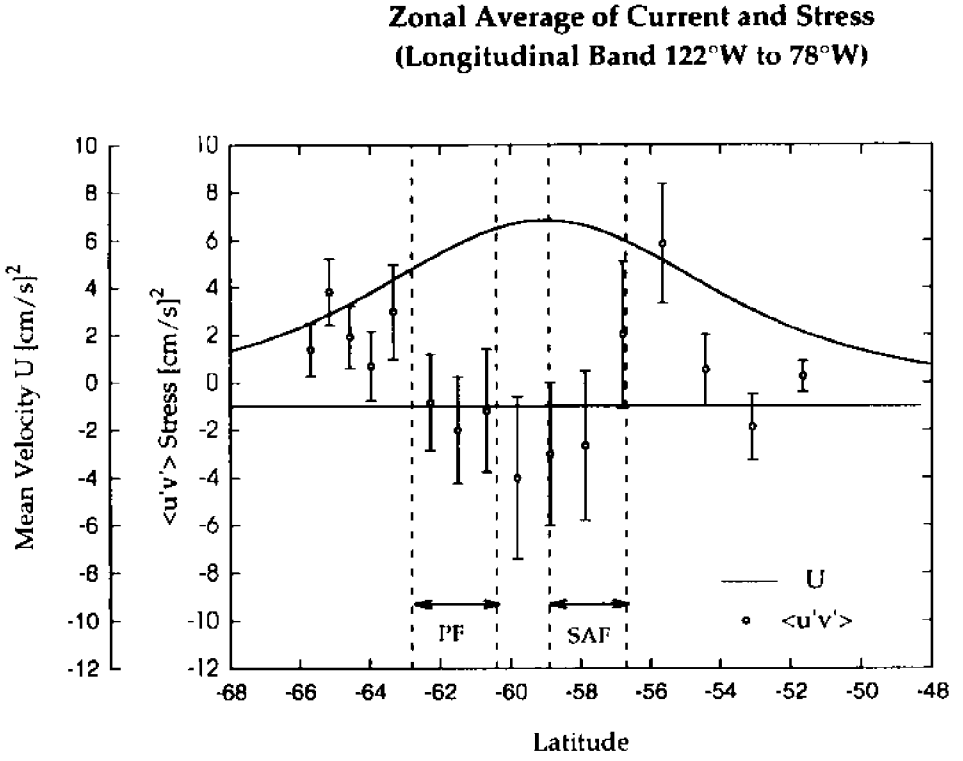

Figure 5b. Same as Figure 5a but for the <u'v'> component of the stress. The data were used for computing an eddy viscosity for the flow.

DISCUSSION

We have used Geosat data to map the distribution of the variability of two orthogonal components of current in the southeast Pacific and to study the relationship of the variability to mean currents calculated from hydrography.

Maps of variability show that regions of high variability are correlated with bathymetry. The variability is greatest in the region where the flow crosses the Pacific Antarctic Ridge, becoming weaker downstream of the ridge crest. The maps also show that the maximum in the variability corresponds closely with the maximum of the mean current calculated from hydrography, and that it does not have maxima at the the positions of the Polar and Subantarctic Fronts. This is surprising. The conventional view of the dynamics of the Antarctic Circumpolar Current is that it consists of bands of current associated with the two fronts. The latitudinal positions of the fronts are thought to vary in time leading to the smooth slope in dynamic topography in the region. The

Geosat data indicate instead that the variability is greatest in the region between the fronts downstream of the ridge crest.

The observed normal components of the stress are large, that is $\langle u'u' \rangle / U^2 \approx \langle v'v' \rangle / U^2 = O(1)$. In fact, the ratio is slightly greater than unity. The large ratio is consistent with variability measured with current meters in various nearby regions of the current (Inoue, 1982; Bryden & Heath, 1985). The shear stress $\langle u'v' \rangle$ is considerable smaller, indicating that eddies are not efficient mechanisms for the transport of momentum into or out of the mean flow.

The distribution of shear stress $\langle u'v' \rangle$ upstream of the Drake Passage shows that the stress acts as an eddy viscosity. Using the shear of the mean current calculated from hydrography together with the spatial distribution of the zonally averaged shear stress, we calculated an eddy viscosity with small uncertainty. The north-south component of the viscosity A_y was found to be $A_y = 8 \times 10^3$ m^2/s. This is somewhat small, but still in the range of values calculated from other data sets. The low value implies that eddy viscosity is not able to balance the wind stress acting on the current, but it is large enough to influence the dynamics of the observed mean current. There is some indication that eddies transport momentum between fronts in the circumpolar flow.

The maps of the distribution of stress also show that the position of strong variability deviates from the position of the fronts in the region of the ridge crest. This implies the current may have two preferred paths for crossing the ridge crest, the position seen in the Geosat data collected in 1986-1988, and the position observed in the hydrography collected by ships more than twenty years earlier.

ACKNOWLEDGMENTS

This work was supported by NASA Grant NAGW-1979 to the Texas A&M University and by NASA/JPL Contract 958122 to the University of Texas.

REFERENCES

Bryden, H.L., and R.A. Heath. 1985. Energetic eddies at the northern edge of the Antarctic Circumpolar Current in the Southwest Pacific. *Prog. Oceanog.* **14**:65–87.

Chelton, D.B., M.G. Schlax, D.L. Witter, and J.G. Richman. 1990. Geosat altimeter observations of the surface circulation of the southern ocean. *J. Geophys. Res.* **95(C10)**: 17,877–17,903.

Cheney, R.E., and L. Miller. 1988. Mapping the 1986–1987 El Nino with Geosat altimeter data. *EOS Trans. Amer. Geophys. Union* **69(31)**:754–755.

Fu, L.L., and V. Zlotnicki. 1989. Observing oceanic mesoscale eddies from Geosat altimetry: preliminary results. *Geophys. Res. Lett.* **16(5)**:457–460.

Inoue, M. 1982. *Vertical structure of the low-frequency currents at Drake Passage*. Ph.D. Thesis, Texas A&M University.

Inoue, M. 1985. Modal decomposition of the low frequency currents and baroclinic instability at Drake Passage. *J. Phys. Oceanog.* **15(9)**:1157–1181.

Johnson, T.J., R.H. Stewart, C.K. Shum, and B.D. Tapley. 1992. Distribution of Reynolds stress carried by mesoscale variability in the Antarctic Circumpolar Current. *Geophys. Res. Lett.* **19(12)**:1201–1204.

Le Traon, P.Y. 1991. Time scales of mesoscale variability and their relationship with space scales in the North Atlantic. *J.Mar. Res.* **49**:1–26.

Lukas, R. 1987. Horizontal Reynolds stresses in the Central Equatorial Pacific. *J. Geophys. Res.* **92(C9)**:9453–9463.

Luyten, J. 1977. Scales of motion in the deep Gulf Stream and across the continental rise. *J. Mar. Res.* **35(1)**:49–74.

Morrow, R., J. Church, R. Coleman, D. Chelton, and N. White. 1992. Eddy momentum flux and its contribution to the southern ocean momentum balance. *Nature.* **357(6378)**: 482–484.

Nowlin, W.D., and J.M. Klinck. 1986. The physics of the Antarctic Circumpolar Current. *Rev. Geophys. Space Phys.* **24(3)**:469–491.

Pond, S., and G.L. Pickard. 1983. *Introductory Dynamical Oceanography.* 2nd ed. Pergamon Press.

Sandwell, D.T., and B. Zhang. 1989. Global mesoscale variability from the Geosat Exact Repeat Mission: correlation with ocean depth. *J. Geophys. Res.* **94**:17,971–17,984.

Shum, C.K., R.A. Werner, D.T. Sandwell, B.H. Zhang, R. S. Nerem, and B.D. Tapley. 1990. Variations of global mesoscale eddy energy observed from Geosat. *J. Geophys. Res.* **95 (C 10)**:17,865–17,876.

Starr, V.P. 1968. *Physics of Negative Viscosity Phenomena*, McGraw-Hill.

Stammer, D., and C.W. Böning. 1991. Mesoscale variability in the Atlantic Ocean from Geosat altimetry and WOCE high resolution numerical modelling. *J. Physical Oceanography* **2(7)**:733–752.

Tai, C.K., and W.B. White. 1990. Eddy variability in the Kuroshio extension as revealed by Geosat altimetry: Energy propagation away from the jet, Reynolds stress, and seasonal cycle. *J. Phys. Oceanog.* **20(11)**:1761–1777.

Webster, F. 1961. The effect of meanders on the kinetic energy balance of the Gulf Stream. *Tellus* **13(3)**:392–401.

Wunsch, C., and E.M. Gaposchkin. 1980. On using satellite altimetry to determine the general circulation of the oceans with application to geoid improvement. *Rev. Geophys. Space Phys.* **18(4)**:725–745.

Zhang, B. 1988. Geosat/ERM altimeter data analysis for the determination of global oceanic mesoscale variability. Ph.D. Thesis, 155pp., The University of Texas at Austin.

THE HAWAII OCEAN TIME-SERIES PROGRAM: RESOLVING VARIABILITY IN THE NORTH PACIFIC

C.D. Winn, R. Lukas, D. Hebel, C. Carrillo, R. Letelier, and D.M. Karl
University of Hawaii
Honolulu, Hawaii, U.S.A.

ABSTRACT

Time-series measurements of biological, chemical and physical parameters in the North Pacific Subtropical Gyre have been made on a regular basis since Octover 1988. These observations now comprise one of the longest sets of time-series measurements in the central Pacific Ocean, and are the only time-series observations available for a variety of parameters in this ocean basin. The time-series observation program has provided a unique view of the extent of variability in the central Pacific, and has begun to improve our knowledge of the dynamics which take place there. The understanding which is emerging from the time-series dataset will be useful for interpreting the historical oceanographic database within the context of future environmental change.

INTRODUCTION

Time-series datasets are rare in the oceanographic literature. This is unfortunate, since it is well-recognized that time series measurements, particularly those made for a decade or more, are powerful tools for understanding and observing the slow process and irregular events that take place in nature (Franklin, 1988). This is now particularly important because of the need to understand the environmental changes that are taking place as a result of anthropogenic influences on the chemistry of the earth's atmosphere and oceans (Magnuson, 1990). Consequently, time-series measurements in a variety of environments are now especially useful. Time-series datasets are not abundant because long-term observation programs are expensive and are usually difficult to maintain. This is especially true of the ocean sciences where data collection requires costly research vessels and sophisticated sea-going equipment.

The usefulness of time-series observations of the natural world has been amply demonstrated. One of the most prominent examples is the over three decade long record of atmospheric carbon dioxide concentrations compiled by Charles Keeling at Scripps Institution of Oceanography (Keeling, et al., 1982; Moore and Bolin, 1987). This dataset has been invaluable for documenting the anthropogenic increase in atmospheric carbon dioxide concentrations and for developing models of the global carbon budget. Other time-series programs have documented changes in the pH of rainwater in the northern hemisphere (Likens, 1983) and documented other long-term changes in the physical and biological conditions in terrestrial environments (Brock, 1985; Peterson, 1984). Time-series observations in the oceans are more rare. For the most part, time-series datasets in the marine environment have involved measurements at higher trophic levels such as commercial fish and zooplankton (McGowan, 1990). A notable exception includes the long time-series of observations made by the California Cooperative Oceanic Fisheries Investigation (Chelton, et al., 1982). This long-term oceanographic study has included chemical and physical measurements as well as estimates of plankton biomass.

The world's oceans act to modulate global climate and are believed to be the predominant sink for anthropogenic carbon dioxide. However, the magnitude of the oceanic sink in various parts of the world's oceans is uncertain (Tans, et al., 1990; Broecker and Peng, 1992; Sarmiento and Sundquist, 1992). In addition, a detailed understanding of the rates and mechanisms of the cycling of carbon within the interior of the ocean is lacking (Longhurst and Harrison, 1989). In large part, this lack of understanding is due a to paucity of data in both space and time. For this reason time-series measurements of the oceanic carbon system are particularly important for understanding and eventually predicting the magnitude and rates of future climate change.

The need for time-series studies was clearly recognized when in 1987 the International Council of Scientific Unions (ICSU) established the Joint Global Ocean Flux Study (JGOFS) as part of its International Geosphere-Biosphere Program (IGPB) for the study of global change. As a consequence, the JGOFS program called specifically for establishment of oceanic time-series studies at strategic ocean sites which were envisioned as being maintained for at least a decade. As a part of the United States JGOFS study, two time-series were begun in 1988. One of these time-series programs was established at the Bermuda Biological Station where the 35 year time-series established at hydrostation "S" would be continued. A second time-series program was established at a new location in the Central Pacific Ocean near the Hawaiian archipelago (Karl and Winn, 1991).

THE HAWAII OCEAN TIME-SERIES PROGRAM

In November 1988, a long time-series program was begun in the Central Pacific Ocean. This research effort was initiated in an effort to produce a time-series dataset for the central Pacific Ocean. The Pacific time-series was named the Hawaii Ocean Time-Series (HOT) program. The primary purpose of this research effort is to identify annual and interannual variability in the physics, chemistry and biology at a single location in the North Pacific Subtropical Gyre. The Hawaii program is a joint effort between the National Science Foundation's Joint Global Ocean Flux Program (JGOFS) and the World Ocean Circulation Experiment (WOCE). This research effort is coordinated by scientists at the University of Hawaii and was funded initially for a 5 year period beginning in May of 1988. Although the program is presently funded for only a five year period, it is anticipated that the program will continue for at least 10 years.

The time-series permanent station is located 100 km due north of the island of Oahu, Hawaii at 22°45'W and 158°00'N (Figure 1). The location of the time-series station was chosen to minimize the influence of the Hawaiian archipelago (island mass effects) on the biogeochemistry of the water column at the time-series station. The permanent time-series station was therefore located upwind (northeast of the Hawaii Archipelago). Station ALOHA (A Long-Term Oligotrophic Habitat Assessment) is located in 4750 m of water and approximately 50 km (one Rossby wave radius) away from the steep topography associated with the Hawaiian Archipelago. A near-shore equipment test site at Kahe Point is also visited each month.

An extensive suite of measurements are made on each HOT cruise. These measurements include standard hydrographic, and optical measurements using continuous sensors mounted on lowered profiling devices, chemical measurements made at discrete depths collected with standard oceanographic sampling bottles, measurements of the rate of primary production as well as the rate of particle flux, and the measurement of upper ocean currents using an acoustic doppler current profiler (Table 1). The results of these routine measurements are available in tabular form in the

Table 1. Time-series parameters measured at station ALOHA

Parameter	Depth Range(m)	Analytical Procedure
I. CTD Measurements		
temperature	0–4750	Thermistor on Sea-Bird CTD package with frequent calibration
salinity	0–4750	Conductivity Sensor on Sea-Bird CTD package, standardization with AGE Inductive Salinometer against Wormly Water
oxygen	0–4750	Polarographic Sensor on Sea-Bird CTD package with Winkler standardization
fluorescence	0–1000	Sea-Tech Flash Fluorometer on Sea-Bird CTD package
II. Optical Measurements		
solar radiance (PAR)	Surface	Licor Cosine Collector and Biospherical 2 pi Collector
underwater irradiance (PAR)	0–150	Biospherical Profiling Natural Fluorometer 4 pi Collector
III. Water Column Chemical Measurements		
oxygen	0–4750	Winkler Titration
total carbon dioxide	0–4750	Coulometry
dissolved inorganic nitrate plus nitrite	0–4750	Autoanalyzer
dissolved ammonium	0–4750	Autoanalyzer
dissolved inorganic phosphorus	0–4750	Autoanalyzer
dissolved inorganic silica	0–4750	Autoanalyzer
dissolved organic carbon	0–1000	persulfate wet oxidation
dissolved organic nitrogen	0–1000	U.V. oxidation
dissolved organic phosphorus	0–1000	U.V. oxidation
particulate carbon	0–1000	high temperature combustion
particulate nitrogen	0–1000	high temperature combustion
particulate phosphorus	0–1000	high temperature combustion
IV. Water Column Biomass Measurements		
chlorophyll *a* and phaeopigments	0–200	Fluorometric Analysis / High Liquid Chromatography
adenosine 5'-triphosphate	0–1000	Firefly Bioluminescence
picoplankton / nanoplankton number	0–1000	Epifluorescence Microscopy
V. Carbon Assimilation and Particle Flux		
primary production	0–200	"clean" ^{14}C incubations
carbon, nitrogen, phosphorus, and mass flux	150, 300, 500	Free-Floating Particle Interceptor Traps
VI. Currents		
Acoustic Doppler Current Profiler	0–300	hull mounted
Acoustic Doppler Current Profiler	0–1000	lowered

annual data reports published by the HOT program (Chiswell, et al., 1990, Winn, et al., 1991). The entire suite of HOT program measurements are also available via the international internet system as described in the annual program data reports. Detailed information about methodology is available in a manual of methods prepared by JGOFS program scientists (Karl, et al., 1990).

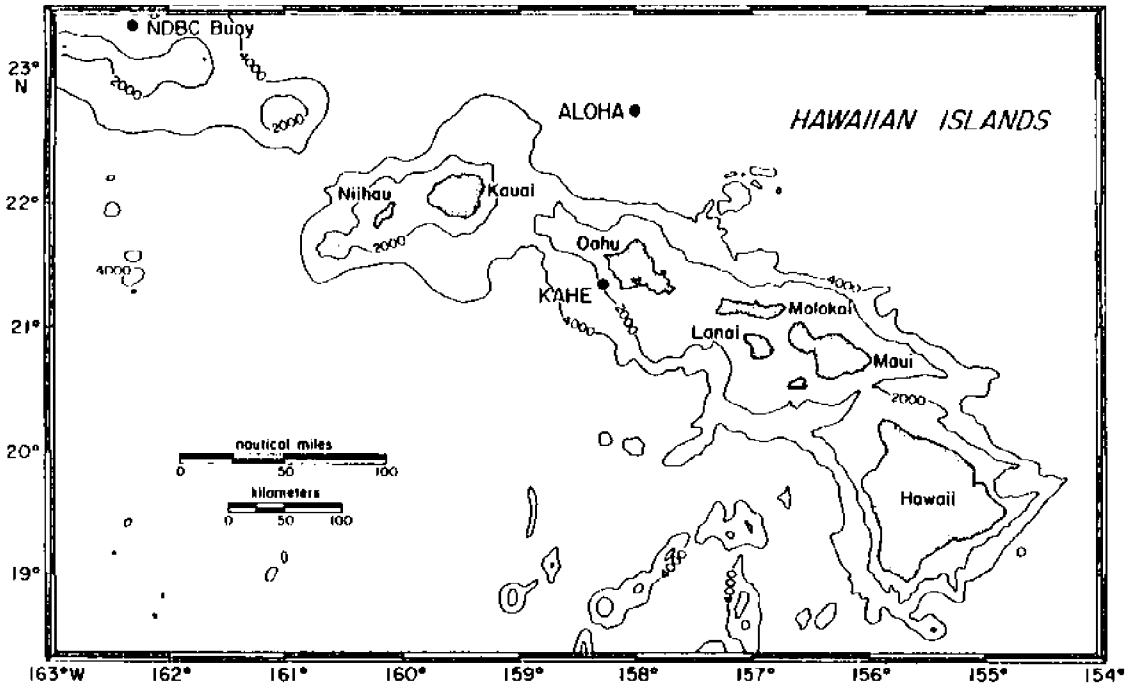

Figure 1. Location of the Hawaiian Ocean Time-series permanent station and the location of the near-shore equipment test site at Kahe Point

SELECTED RESULTS FROM THE HAWAII OCEAN TIME-SERIES PROGRAM

Hydrography

Figures 2 and 3 show contour plots of representative results of hydrographic measurements made over a three-year period at Station ALOHA. Figure 2 shows a contour plot of potential temperature to 1000 decibars. A contour plot of nitrate plus nitrite to 1000 decibars is shown in Figure 3. As one would expect, surface water temperature has varied seasonally from approximately 23 to 26 degrees Celsius at the time-series permanent station. The isotherms below the mixed layer have remained relatively constant with only minor variations. Nitrate plus nitrite has remained low in the surface waters, and there is no evidence of substantial injection of nutrients into the upper ocean as a result of seasonal mixing.

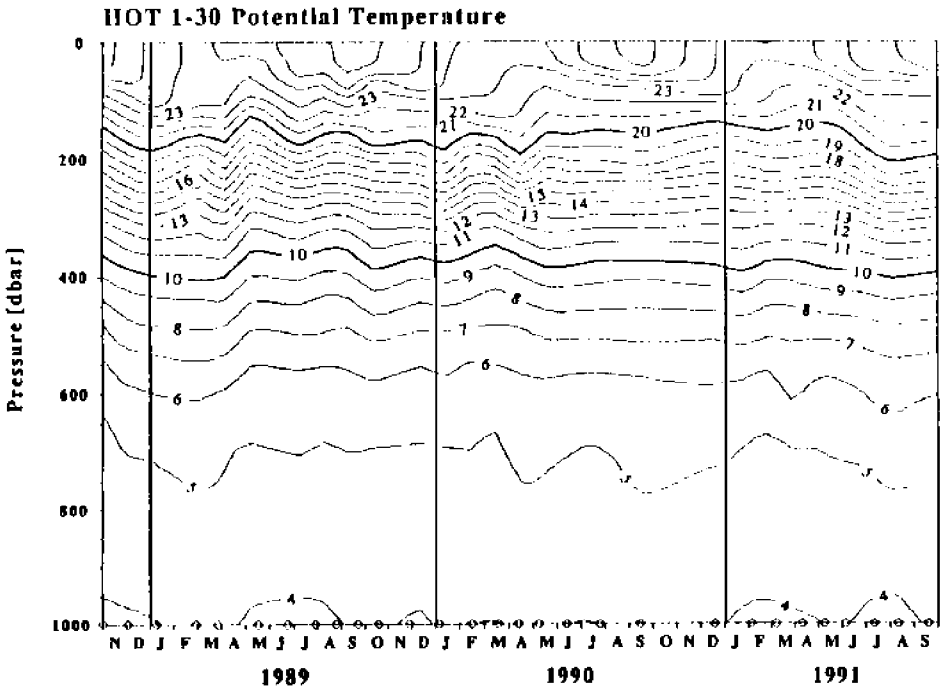

Figure 2. Contour plot of potential temperature (°C) to 1000 decibar versus time at Station ALOHA

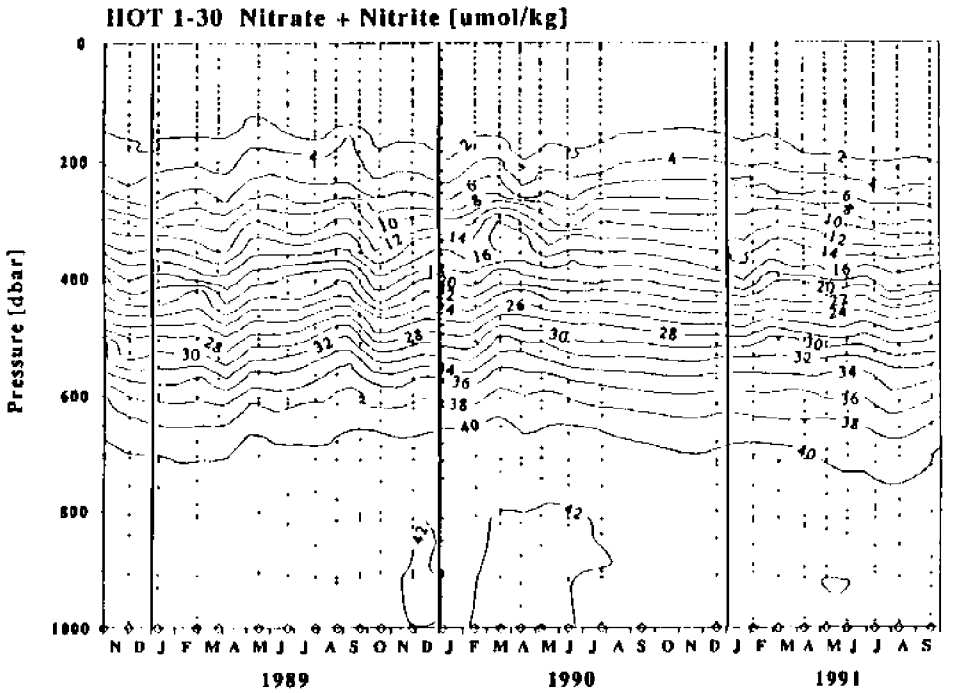

Figure 3. Contour plot of nitrate plus nitrate to 1000 decibar versus time at Station ALOHA

Primary Production and Particle Flux

The results of our time-series measurements of integrated primary production and carbon flux at 150 m are shown in Figure 4. These measurements have been made with carbon-14 using "clean" techniques (Fitzwater, et al., 1982) and 12 hour on-deck and in situ incubations (Karl, et al., 1990; Winn, et al., 1991). These data comprise the longest time-series of primary production and particle flux in the North Pacific Subtropical Gyre. The rate of primary production measured over a three year period ranges from a high of approximately 1100 and low of approximately 250 mg C $m^{-2}d^{-1}$. The highest rate of production was measured on a cruise during August of 1989. A surface accumulation of *Trichodesimum sp.* was observed near Station ALOHA on this cruise (Karl, et al. 1992), and may have been responsible for this anomalously high value. Excluding this value, the rate of primary production measured at the HOT permanent station varies by approximately a factor of 3. The temporal variability observed in the rate of primary production at Station ALOHA appears to be stochastic with little evidence of a seasonal cycle.

The mean rate of primary production is approximately 450 mg C m^{-2} d^{-1}. This rate of production is higher than historical data would suggest (Ryther, 1969), but is remarkably consistent with more recent measurements in the North Pacific Subtropical Gyre using newer "clean" C-14 primary production techniques (Martin, et al., 1987).

The rate of carbon flux at 150 m shows substantial annual variability and ranges over a factor of approximately 3 (Figure 4b). In both 1988 and 1989 there is a peak in carbon flux at 150 m in the spring and a second peak in summer. Although a peak in carbon flux in both 1989 and 1990 is observed in both the spring and the summer, only a single peak is observed in early summer in 1991.

In general, the rate of particle flux in marine environments is believed to be controlled primarily by the rate of primary production in the overlying euphotic zone. Although temporal variability in the flux of particulate material has been measured in several marine environments, most of the direct evidence for a link between primary production and particle flux at depth comes from observations in the Sargasso Sea at or near the Bermuda time-series site. Temporal variability in particle flux at 3200 m in the Sargasso Sea has been shown to vary in a pattern consistent with expected changes in surface water primary production (Deuser and Ross, 1980; Deuser, et al., 1981; Deuser, 1986). More recently, Deuser, et al. (1990) have shown a direct relationship between carbon flux at this depth and satellite derived estimates of surface ocean pigment concentration near the Bermuda time-series site. In addition, Asper, et al. (1992) have recently demonstrated a relationship between primary production measured with carbon-14 incubations and the flux of total particulate material throughout much of the water column at this same location. These results are not surprising, since one would expect the flux of particulate material in the central ocean basins away from the direct influence on terrigenous runoff to be dependent upon the production of biogenic particulate material in the euphotic zone.

It is surprising that the first three years of data collected by the HOT program show little evidence of a relationship between carbon flux at 150 m and euphotic zone primary production. Whereas a clear oscillation in the rate of particle flux is easily resolved by our monthly sampling, a similar trend in the rate of primary production is not evident (Figure 3). Although the poor correlation between these measurements has not yet been explained, several hypotheses can be advanced to account for this observation. These explanations fall into two broad categories. First, it is possible that the

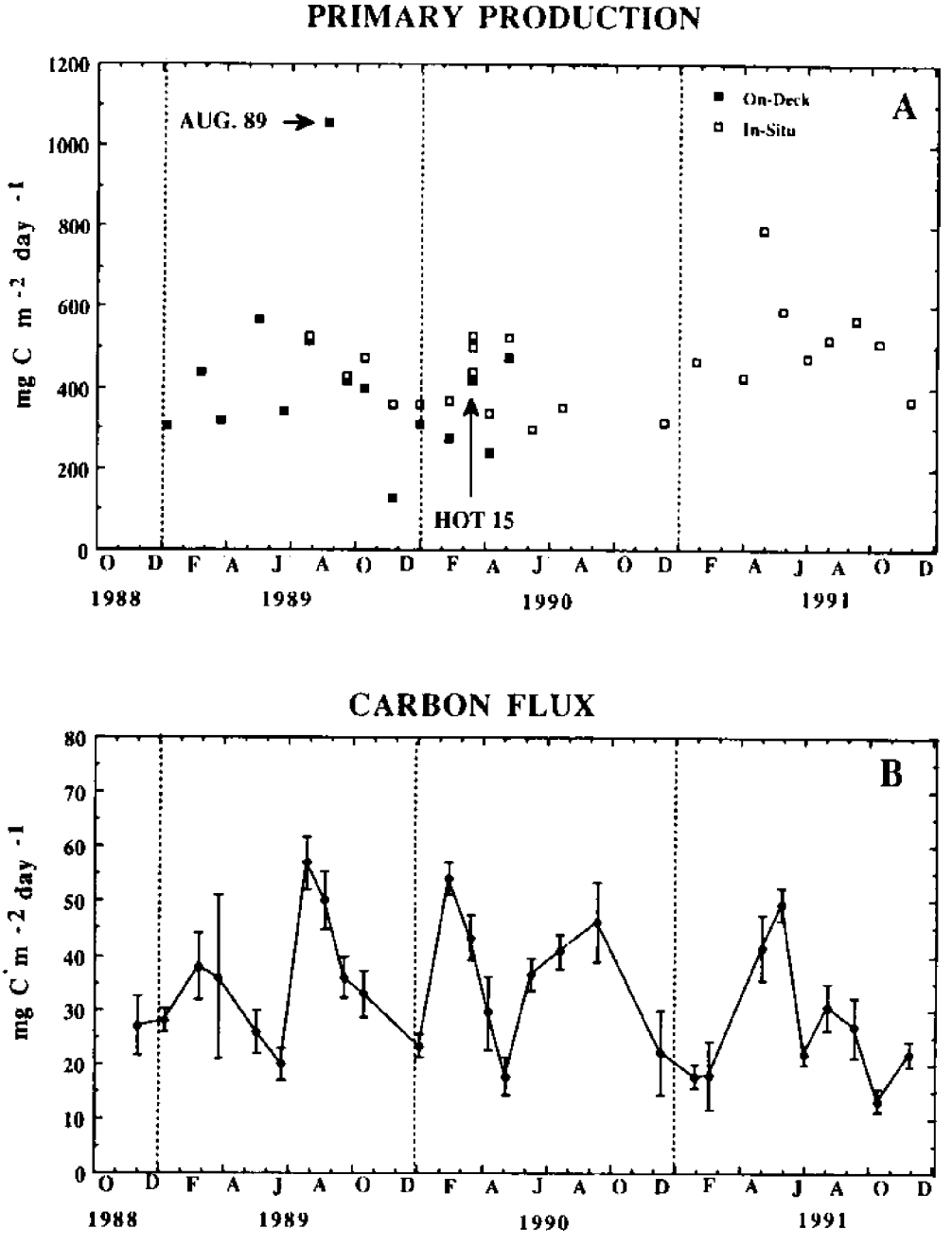

Figure 4. Primary production and particle flux measured over a three-year period at Station ALOHA. Panel A shows primary productivity integrated over the upper 200 m of the water column from eight incubation depths. Panel B shows carbon flux measured at 150 m over a 72-hour period with free-floating sediment traps.

expected relationship between particle flux and primary production exists at Station ALOHA, but our primary production measurements are unable to resolve the annual cycle in primary production that the flux data suggest exists in this process. Second, it is also possible that a tight relationship between primary production and particle flux does not exist at this location, and that the some other process or combination of processes are controlling the measured rate of particle flux.

A correlation between particle flux and primary production may exist at Station ALOHA but, especially in the central Pacific Ocean where temporal variability in the physical and biological conditions are known to be small, our C-14 measurements may not be able to resolve the annual signal in primary production. Support for this scenario can be found in an experiment conducted in March of 1990. On this cruise, primary production was measured in situ on three consecutive days (Figure 3b). The production rates measured over this three day period varied by more than 100 mg C $m^{-2}day^{-1}$. Excluding the one high value measured in August of 1989, this is equivalent to approximately 25% of the range of values measured over the duration of the program. The high degree of variability observed over this 72 hour period could be due to a highly variable rate of production which varies widely from day-to-day. The average rate experienced over the 72 hour trap deployment may therefore not be representative of that measured on a single day. Imprecision in the measurement of primary production may also play a role in this. Since we are calculating the integrated rate of production from a total of only eight incubation depths in the upper 200 m, and since primary production rates measured in incubation bottle maintained at fixed depths are known to be aliased by internal waves, it is possible that a large portion of the variability observed over this 3-day period is also due to "noise" in our primary production measurements.

As an alternative, it is also possible that factors other than primary production may greatly influence particle flux at the time-series site. Variability in the number of grazers and/or vertical migrators, for example, could be responsible for changes in the rate of particle flux independent of a change in the rate of primary production. In addition, atmospheric inputs of dust (Ditullio and Laws, 1991) could also influence the rate of particle flux on time and space scales which are not reflected in rates of primary production.

Whatever the underlying cause in the annual variation in the rate of particle flux at Station ALOHA, it is interesting that the sediment trap particle flux measurements are capable of resolving an annual cycle in an environment that is known for its temporal stability. This observation is especially noteworthy in light of the recent claims that particle traps do not provide accurate measurements of particle flux (Buesseler, 1991). Contrary to Buesseler's finding the results of the time-series program indicate that particle traps do, in fact, provide a excellent record of annual variability in an environment known for its low seasonal variability. Although we cannot yet definitively identify the mechanism which produces the observed annual variability in particle flux it is almost impossible that the regular pattern of variability observed over this three year period is due to random errors in the measured rate of particle flux, and therefore must be indicative of an annual cycle in the physical, chemical or biological conditions in the central Pacific Ocean.

Dissolved Inorganic Carbon

The first time-series measurements of dissolved inorganic carbon and titration alkalinity obtained in the surface waters of the central Pacific Ocean are shown in Figure 5. Specific alkalinity averages approximately 2315 ueq/kg and is very consistent with

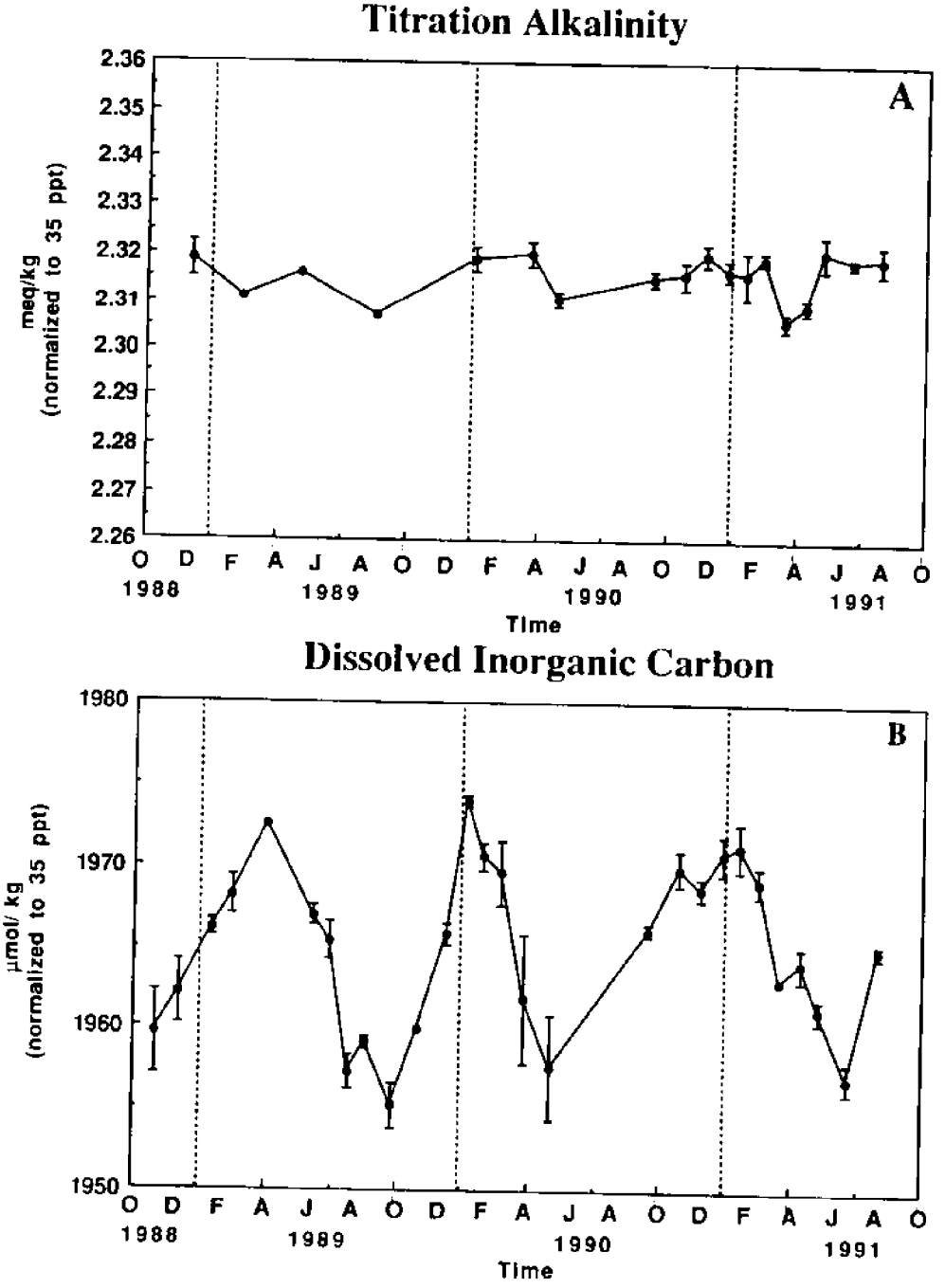

Figure 5. Titration alkalinity and dissolved inorganic carbon measured over a three-year period at station ALOHA. Panel A shows titration alkalinity normalized to 35 ppt salinity. Error bars show the standard deviation of replicate measurements in the upper 50 m. Panel B shows dissolved inorganic carbon normalized to 35 ppt salinity. Error bars represent the standard deviation of replicates in the upper 50 m.

other measurements made in the North Pacific Subtropical Gyre (eg., GEOSECS Program). Although some real variability in the specific alkalinity is evident, variability in titration alkalinity normalized to 35 parts per thousand salinity appears to be stochastic and shows no evidence of a regular annual cycle. In contrast, dissolved inorganic carbon (DIC) averaged over the upper 50 decibars and normalized to 35 parts per thousand salinity, displays a very regular annual cycle with a maximum in surface water in winter and a minimum in summer. Because the partial pressure of carbon dioxide changes by approximately 4% per degree Celcius, this pattern is consistent with a flux of carbon dioxide across the air-sea interface driven by changes in surface water temperature. In winter, when surface water temperature falls, pCO2 also decreases and the net flux of carbon dioxide is from the atmosphere to the ocean. In summer, when surface water temperature rises, the net flux of carbon dioxide is from the ocean to the atmosphere. Using the time-series dataset and assuming that the mixed layer averages 60 m, the seasonal exchange of carbon dioxide between the ocean and the atmosphere at Station ALOHA is approximately 1 mole of carbon per m-2. Therefore approximately 1 mole of carbon is transported across the air-sea interface from the atmosphere to the ocean during fall and approximately this same quantity of carbon dioxide is transported in the opposite direction during spring. This flux is approximately 20 times the projected rate of anthropogenic carbon dioxide accumulation rate (Tans, et al., 1990, and references therein).

CONCLUSIONS

In contrast to the classical view of the central Pacific as a extremely stable environment, the time-series dateset has shown that considerable variability does exist in this region. Particle flux measurements in the upper ocean show an annual cycle in the rate of carbon flux at the time-series site. In both 1989 and 1990, two peaks in particle flux, one in spring and one in summer are observed. In 1991, only a single statistically significant peak in mid-summer is apparent. A similar pattern in primary production is not obvious in any of the three years of time-series observations. Although the cause of the annual and interannual variability in carbon flux has not yet been identified, one interpretation of these data is that carbon flux, measured by free-floating sediment traps, provides a more accurate estimate of biological activity in the overlying euphotic zone than primary production measured with carbon-14.

The time-series observations of upper ocean dissolved inorganic carbon and alkalinity indicate a substantial flux of carbon dioxide across the air-sea interface at Station ALOHA. These data suggest that approximately one mole of carbon dioxide moves in and out of the surface ocean each year. This flux appears to be driven by the annual oscillation in upper ocean temperature. The magnitude of this annual exchange is approximately 15 to 20 times the projected rate of carbon dioxide increase in the surface ocean due to the rise in the increase in atmospheric carbon dioxide, and indicates that several years of regular measurements will be needed to accurately quantify the upper ocean anthropogenic carbon dioxide accumulation rate.

The data collected by the HOT program, comprise the longest and most extensive set of time-series measurements available for the central Pacific Ocean. These data are the first and only time-series available for a variety of parameters in the North Pacific Subtropical Gyre. These time-series data have already provided a unique view of the extent of variability in this ocean basin, and have begun to improve our understanding of the dynamics which take place there. The understanding which is emerging from the time-series dataset will be useful for interpreting the results of the spatial scale studies planned for the central Pacific, and for interpreting the historical database within the context of future environmental and climate change.

REFERENCES

Asper, V.L., W.G. Deuser, G.A. Knauer, and S.E. Lorenz. 1992. Rapid biogeochemical coupling between surface and deep ocean waters via particles. *Nature*. In press.

Broecker, W.S., and T. Peng. 1992. Interhemispheric transport of carbon dioxide by ocean circulation. *Nature*. **356**:587-589.

Brock, T.D. 1985. A Eutrophic Lake: Lake Mendota, Wisconsin. New York: Springer-Verlag.

Buesseler, K.O. 1991. Do upper ocean sediment traps provide an accurate record on particle flux? *Nature*. **353**:420-423.

Chiswell, S.E., E. Firing, D. Karl, R. Lukas, and C.D. Winn. 1990. Hawaii ocean time-series data report #1: 1988-1989. SOEST Technical Report #1. University of Hawaii: Honolulu, Hawaii.

Chelton, D.B., P.A. Bernal, and J.A. McGowan. 1982. Large-scale interannual physical and biological interaction in the California Current. *Journal of Marine Research*. 40:1095-1125.

Deuser, W.G., and E.H. Ross. 1980. Seasonal change in the flux of organic carbon to the deep Sargasso Sea. *Nature*. **283**:364-365.

Deuser, W.G., E.H. Ross, and R.F. Anderson. 1981. Seasonality in the supply of sediment to the deep Sargasso Sea and implications of the rapid transfer of matter to the deep ocean. *Deep-Sea Research*. **28**:495-505.

Deuser, W.G. 1986. Seasonal and interannual variations in deep-sea particle fluxes in the Sargasso Sea and their relation to surface hydrography. *Deep-Sea Research*. **33**:225-246.

Deuser, W.G., F.E. Muller-Karger, R.H. Evans, O.B. Brown, W.E. Esaias, and G.C. Feldman. 1990. Surface-ocean color and deep-ocean carbon flux: how close a connection? *Deep-Sea Research*. 37:1331-1343.

Ditullio, G.A., and E.A. Laws. 1991. Impact of an atmospheric-oceanic disturbance on phytoplankton community dynamics in the north pacific central gyre. *Deep-Sea Research*. **38**:1305-1329.

Fitzwater, S.E., G.A. Knauer, and J.H. Martin. 1982. Metal contamination and its effect on primary production. *Limnology and Oceanography*. **27**:544-551.

Franklin, J.F. 1988. Importance and justification of long-term studies in ecology. In: Long-term Studies in Ecology: Alternatives and Approaches, ed. G.E. Likens, pp. 3-19. Springer-Verlag.

Karl D.M., C.D. Winn, D. Hebel, and R. Letelier. 1990. Hawaii ocean time-series program: field and laboratory protocols. University of Hawaii, Honolulu Hawaii.

Karl, D.M., and C.D. Winn. 1991. A sea of change: monitoring the oceans' carbon cycle. *Environmental Science and Technology*. **25**:1976-1981.

Karl, D.M., R. Letelier, D.V. Hebel, D.F. Bird, and C.D. Winn. 1992. Trichodesmium blooms and new nitrogen in the North Pacific Gyre. In: Marine Pelagic Cyanobacteria: Trichodesmium and other Diazotrophs, eds. E.J. Carpenter, et al., pp. 219-237. Kluwer Academic Publishers.

Keeling, C.D., R.B. Bacastow, and T.P. Whorf. 1982. Measurements of the concentration of carbon dioxide at Mauna Loa Observatory, Hawaii. In: Carbon Dioxide Review, ed. C. Clark, pp. 377-385. New York: Oxford University Press.

Likens, G.E. 1983. A priority for ecological research. *Bulletin of the Ecological Society of America*. **64**:234-243.

Longhurst, A.R., and W.G. Harrison. 1989. The biological pump: profiles of plankton production and consumption in the upper ocean. *Progress in Oceanography*. **22**:47-123.

Martin, J.H., G.A. Knauer, D.M. Karl, and W.W. Broenkow. 1987. VERTEX: carbon cycling in the northeast Pacific. *Deep-Sea Research*. 34:267-285.

Magnuson, J.J. 1990. Long-term ecological research and the invisible present. *Bioscience*. **40**:495-501.

McGowan, J.A. 1990. Climate and change in oceanic ecosystems: the value of time-series data. *Trends in Ecology and Evolution*. 5:293-299.

Moore, B., and B. Bolin. 1987. The oceans, carbon dioxide and global climate change. *Oceanus*. **29**:9-15.

Peterson, R.O. 1984. Wolves, moose and the allometry of population cycles. *Science*. **224**:1350-1352.

Ryther, J.H. 1969. Photosynthesis and fish production in the sea. *Science*. **166**:72-76.

Sarmiento, J.L., and E.T. Sundquist. 1992. Revised budget for the oceanic uptake of anthropogenic carbon dioxide. *Nature*. **356**:589-593.

Tans, P.P., I.Y. Fung, and T. Takahashi. 1990. Observational contraints on the global atmospheric CO2 budget. *Science*. **247**:1431-1438.

Winn, C.D., R. Lukas, D. Karl, E. Firing, and S.E. Chiswell. 1991. Hawaii ocean time-series data report #2: 1989-1990. SOEST Technical Report #, pp. 175. University of Hawaii: Honolulu, Hawaii.

SELF-GENERATION OF CONTROLLER OF UNDERWATER VEHICLE FOR CONSTANT ALTITUDE OVER COMPLICATED TOPOGRAPHY

Taku Suto and Tamaki Ura
University of Tokyo
Tokyo, Japan

ABSTRACT

A guidance system to keep an autonomous underwater vehicle at a sufficiently low altitude is constructed with the "Self-Organizing Neural-net-Controller System," which has been developed at the Institute of Industrial Science of the University of Tokyo. This system includes an adaptive controller made of an artificial neural network. The forward model network which estimates the dynamics of a vehicle and topography around it is also made of an artificial neural network. In order to construct a precise forward model network, its structure is modularized and the difference type network is introduced. The system is demonstrated in computer simulations by generating a controller which operates the PTEROA150 vehicle over a complicated topography of the seabed.

INTRODUCTION

When an autonomous underwater vehicle (AUV) swims to get scientific data in the vicinity of the seabed, a guidance system to keep a sufficiently low altitude from the seabed is necessary to accomplish the mission. This kind of guidance system may be made based on if-then algorithms. But it seems considerably difficult to cover all the cases that might happen, because the underwater environment is substantially hostile. Therefore, the guidance system for AUVs is required to have high autonomy including adaptability. Here, the "Self organizing neural-net-controller system" (SONCS) developed by Fujii (1990, 1991) and Ura (1989) is introduced to generate an adaptive controller for constant altitude swimming on the basis of range data obtained from echo sounders.

SONCS

Figure 1 shows the overall structure of the SONCS. The major parts of the SONCS are a controller network (CN) and a forward model network (FWDN). Each network is a connectionist model. The CN generates a control signal from the values related to the control, such as state variables and environmental data. The FWDN generates the values which are used to evaluate the result of the control, and transmits back-propagation signals for adjustment of the synaptic weights of the CN.

The adjustment of the CN is carried out so as to reduce the evaluation function which is calculated with the outputs of the FWDN. It should be noted that the synaptic weights of the FWDN should not be changed through this modification because the FWDN represents the real world.

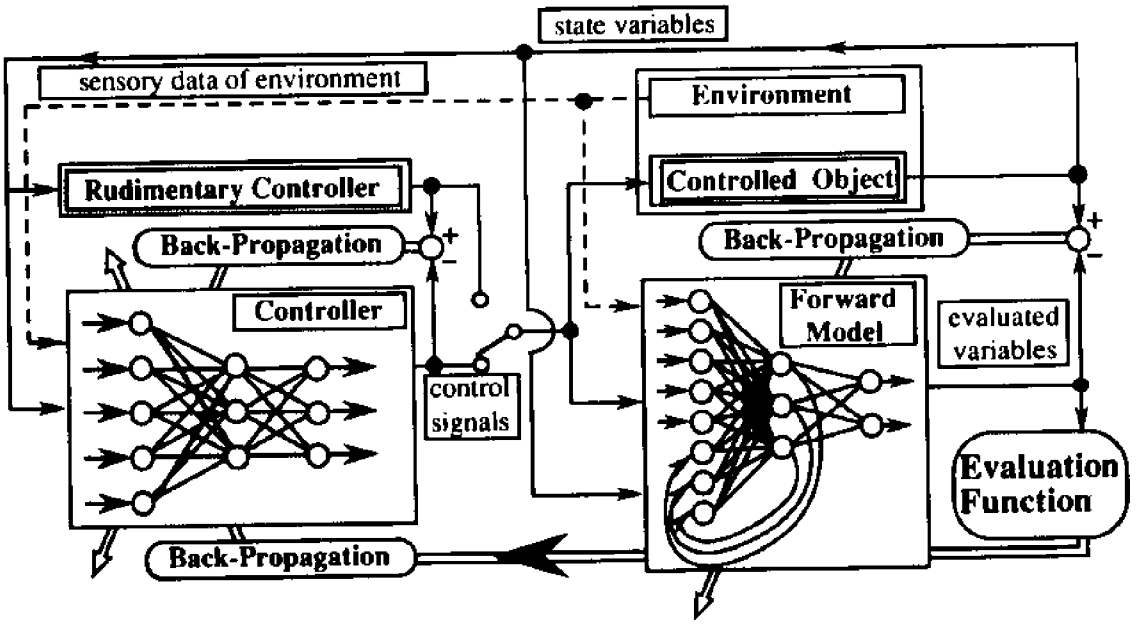

Figure 1. Overall structure of the SONCS

The procedure of the SONCS is divided into 5 stages.

(1) The CN is initialized using the back-propagation method on the basis of navigation data. These data are obtained controlled by an appropriate controller, which is called a "rudimentary controller" because it is not necessary to be highly tuned up. After initialization, the CN controls the vehicle as the same way as the rudimentary controller did.

(2) The FWDN is constructed on the basis of the previous navigation data. Then, the FWDN makes correspondence between the control signals of this time step and the values to be evaluated of the next time step.

(3) The vehicle is navigated by the CN for a certain range.

(4) The CN is modified so as to reduce the evaluation function on the basis of the navigation data obtained in stage (3).

(5) Stages (3) and (4) are repeated till the value of the evaluation function becomes sufficiently small. This repetition corresponds to training of swimming. If the FWDN doesn't make accurate outputs comparing to the corresponding value of the actual vehicle, it should be modified independently on the basis of the vehicle's data through training.

VEHICLE

The equations of motion used in the following simulation (Ura and Otsubo, 1988) is derived from the PTEROA150 in Figure 2 which was developed at the Institute of Industrial Science of the University of Tokyo. The PTEROA150 is 150 cm in length and 220 kg in dry weight. It is equipped with 4 channels of active echo sounders to detect the

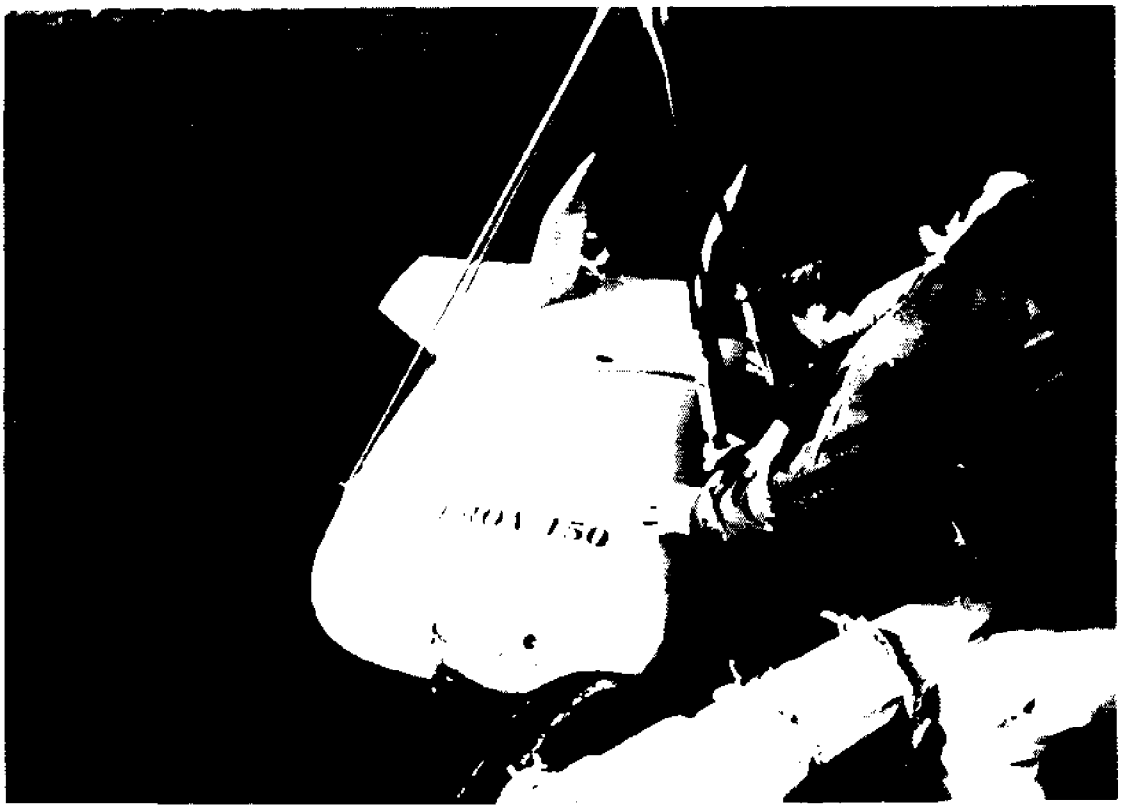

Figure 2. PTEROA150

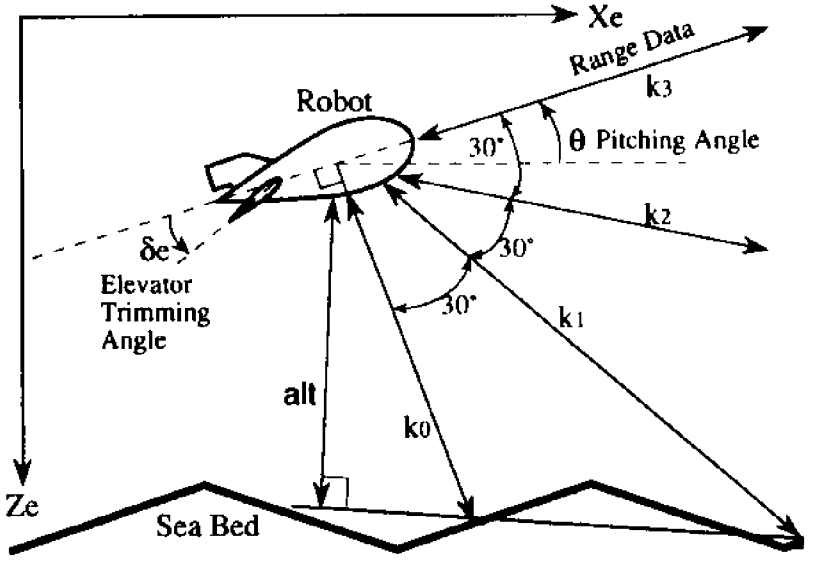

Figure 3. Configuration of robot and direction of echo sounders

topography of the seabed. Logitudinal motion is controlled only by changing the trimming angle of a pair of elevators. The SONCS is adopted to the longitudinal guidance system for the PTEROA150 over a triangular mountains.

Sounders are arranged in the longitudinal plane as illustrated in Figure 3. They are directed from directly downward to straight ahead at angle of 0, 30, 60, and 90 degrees. $k_0 \sim k_3$ are distances to the bed which are measured by the corresponding sonic beam. alt represents an altitude defined by the distance from the vehicle to the line that is determined by the reflecting points of sonic beams for k_0 and k_1. The inertial coordinate system is denoted by Xe and Ze. θ is the pitching angle and δ_e is the elevator trimming angle which is a controllable variable. In the following simulations the thrusting force is fixed at 50 N so that the average speed of the vehicle is approximately 5 knots.

The objective of the control is to swim keeping a constant altitude alt_0 from a seabed which consists of series of triangles as shown in Figure 3.

ENHANCEMENT OF THE FORWARD MODEL

Considering the scheme of the back-propagation method for modification of the CN, the differentiations of the outputs of the FWDN by the control signals should be also accurate in order to adjust the CN quickly and appropriately. For the guidance system, however, it is not easy to construct a simple FWDN with sufficient precision in both the outputs and their differentiations, because the I/O relation is extremely complex to represent. Here, two methods are introduced to realize higher precision of the FWDN.

1) Modularization of structure of the FWDN

For constant altitude swimming, the evaluation function E is defined as:

$$\Sigma E = (alt - alt_0)^2 \tag{1}$$

where alt_0 is the target altitude. So that the output of the FWDN is altitude, and its inputs are the values that are related to the calculation of the altitude of the next time step. Thus, let **S**, **R**, **u** and **O** be a state vector, a range vector,a control vector and an output vector, respectively. Here,

$$\mathbf{S}(t) = \begin{pmatrix} \Delta Xe(t) \\ \Delta Ze(t) \\ \Delta\theta(t) \end{pmatrix}, \ \mathbf{R}(t) = \begin{pmatrix} k_0(t) \\ k_1(t) \\ k_2(t) \\ k_3(t) \end{pmatrix}, \ \mathbf{u}(t) = (\delta_e(t)), \ \mathbf{O}(t) = (alt(t)). \tag{2}$$

The mapping f by the FWDN is given by:

$$\begin{aligned} \mathbf{O}(t+\Delta t) = f(&\mathbf{S}(t), \mathbf{S}(t-\Delta t), \mathbf{S}(t-2\Delta t), \ldots, \\ &\mathbf{R}(t), \mathbf{R}(t-\Delta t), \mathbf{R}(t-2\Delta t), \ldots, \\ &\mathbf{u}(t), \mathbf{u}(t-\Delta t), \mathbf{u}(t-2\Delta t), \ldots) \\ = f(&\mathbf{S}^*(t), \mathbf{R}^*(t), \mathbf{u}^*(t)), \end{aligned} \tag{3}$$

where t represents the present time step and Δt is interval time of control. An assembly of present and past vectors is denoted by *.

Equation (3) can be divided into three mappings as:

$$\mathbf{S}(t+\Delta t) = f_1(\mathbf{S}^*(t), \mathbf{u}^*(t)), \tag{4}$$

$$\mathbf{R}(t+\Delta t) = f_2(\mathbf{S}(t+\Delta t), \mathbf{R}^*(t)), \tag{5}$$

$$\mathbf{O}(t+\Delta t) = f_3(\mathbf{R}(t+\Delta t)). \tag{6}$$

Here, f_1 represents the dynamics of the vehicle and provides the state vector at the next time step $t+\Delta t$. The range data at $t+\Delta t$ are estimated by f_2. Then, the altitude at $t+\Delta t$ is calculated on $\mathbf{R}(t+\Delta t)$. In the same way, the FWDN can be divided into three sub-networks which correspond to Eq. (4) to (6), respectively. Since each network represents a simple mapping, it is expected that high precision is accomplished using a general learning scheme. As a result the FWDN yields high accuracy.

In order to involve past data of input vectors, the sub-networks for f_1 and f_2 include recurrent loops, where the signals from the hidden layer are propagated to the input layer one time step delayed. The past values of input vectors are, therefore, not necessary to be treated explicitly in inputs. To represent the inclusion of the recurrent loops, Eq. (4) and (5) are written as:

$$\mathbf{S}(t+\Delta t) = f_1^*(\mathbf{S}(t), \mathbf{u}(t)), \tag{7}$$

$$\mathbf{R}(t+\Delta t) = f_2^*(\mathbf{S}(t+\Delta t), \mathbf{R}(t)). \tag{8}$$

2) Taking differences between I/O data

Equation (7) can be expressed as:

$$\begin{aligned}\mathbf{S}(t+\Delta t) &= \mathbf{S}(t) + \Delta\mathbf{S}(t) \\ &= \mathbf{S}(t) + \Delta f_1^*(\mathbf{S}(t), \mathbf{u}(t)).\end{aligned} \tag{9}$$

When each component of $\Delta\mathbf{S}(t)$ is small comparing to that of $\mathbf{S}(t)$, it is not easy to construct an accurate network for f_1^*. Because learning by the back-propagation method makes the outputs of a network imitate the teaching data. Since $\Delta\mathbf{S}$ in Eq. (9) can be calculated as precise as $\mathbf{S}$ in Eq. (7), the network should be constructed to express Δf_1^*. Hereafter the network with this structure is called the "difference type network." Eq. (8) could be also expressed by a difference type network.

The overall network for the constant altitude swimming for the PTEROA150 is illustrated in Figure 4. A small circle represents a distributor of which output value is same as its input value. A large circle represents a neuron. At the neuron marked off by black, the corresponding input value is added to the output because the sub-network is a difference type. The leftmost network is the CN, inputs of which are the state vector, the range data and the differences of range data. The output of the CN is the elevator trimming angle. t can be seen that the FWDN consists of three sub-networks, which represent Δf_1^*, Δf_2^*, and f_3, and are called the dynamics, the geometric and the altitude networks, respectively.

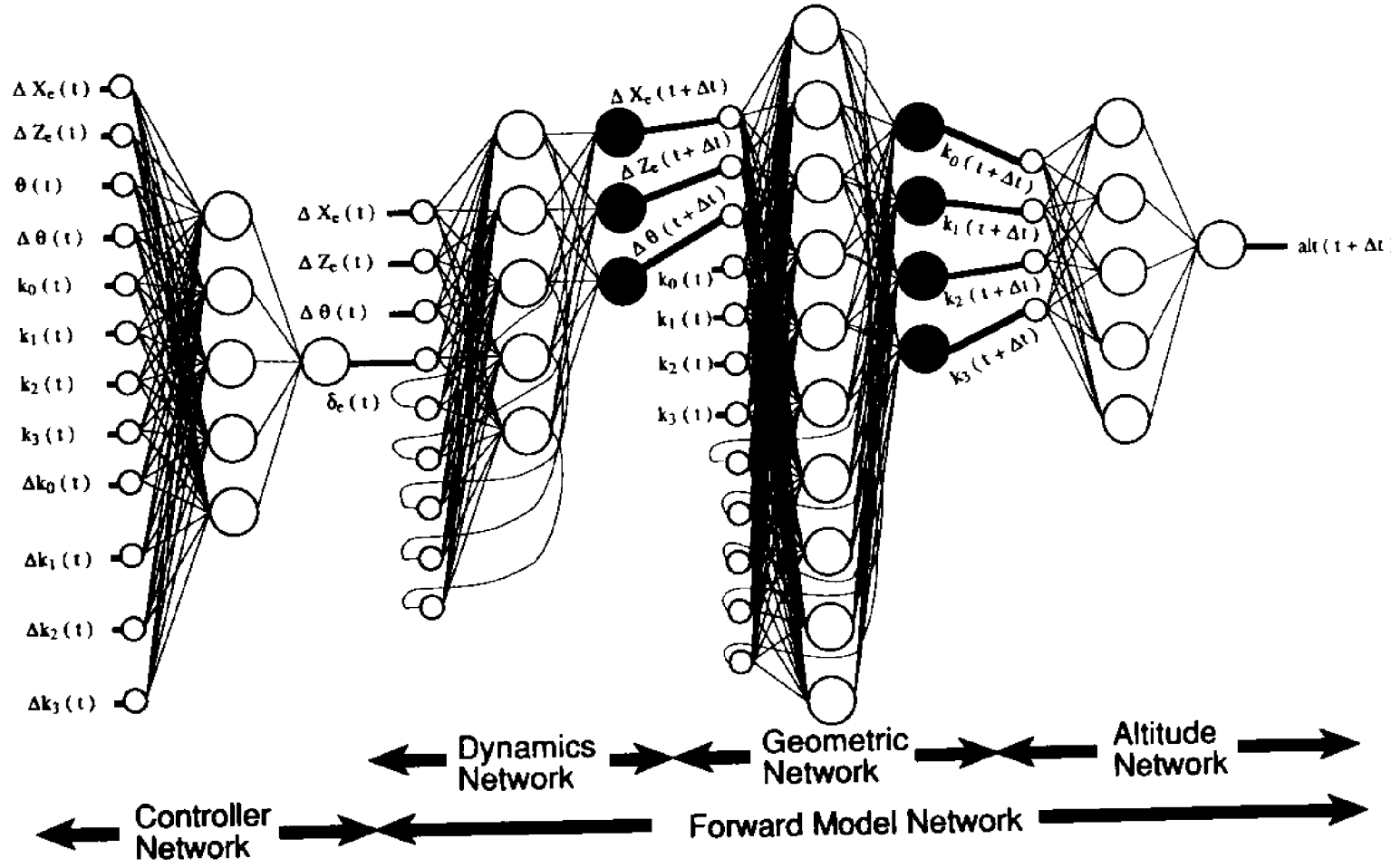

Figure 4. Overall network for constant altitude swimming

INITIALIZATION

The data for the initialization of the CN and the construction of the FWDN are shown in Figure 5. The topography of the seabed consists of a series of triangles 50 m in span and 10 m in height. Since the FWDN is valid inside domain of the teaching data, it is desirable that these data are widely scattered. Therefore the data in Figure 5 contain the frequency from 0.01 Hz to 1.0 Hz in elevator trimming angle. The total sample points are approximately 1,000 in sampling rate of 10 Hz. When range data exceed 200 m, they are regarded as 200 m. The target altitude is 10 m in the following simulations.

Figures 6, 7 and 8 show the outputs of the dynamics, the geometric and the altitude networks, respectively. Here, the outputs of the network denoted by broken lines show good fitting to those of teaching data denoted by solid lines. Despite the range data are not continuous, the learning of the network progresses very well as shown in Figure 7. The altitude network deals with only static relation between the range data and the altitude so that its learning converges quickly.

TRAINING

Figure 9 shows a training process applied to the seabed which is the same topography used in the initialization. The vehicle collides onto the seabed at 45 m in the horizontal range without training. Once trained the vehicle gets the ability to swim avoiding collision. It can be seen that a guidance system to lead the vehicle approximately at the target altitude is constructed after 2 times of training. Thus, the vehicle succeeds in pursuing its mission within ± 6 m discrepancy.

Figure 10 is an example applied to the seabed which consists of triangles 100 m in span and 10 m in height. The top figure shows the trajectory controlled by the resulted controller in Figure 9. Although the maximum discrepancy in trajectory is 6 m at the first trial, it decreases to 3.5 m after 5 times of training.

Figure 11 is another example applied to the seabed of high triangles. Similarly the top figure is the trajectory controlled by the resulted controller in Figure 9. At first, the vehicle comes close to upward slopes. After 9 times of training, the vehicle gets the ability to swim in a good manner over long and steep slopes. In this case, the maximum discrepancy is reduced from 6.5 m to 4.5 m.

In cases of Figures 10 and 11, the geometric network is not exact because the FWDN is generated in the initialization stage and used disregarding difference of topography. But it is interesting that the results are fairly satisfactory. Speed of acquiring the ability of swimming which depends on the accuracy of the FWDN becomes higher than the example in Ura and Suto (1991).

DISCUSSION

The vehicle swims up and down in a short period in every case. This vibration does not decrease mainly because the evaluation function does not include terms related to the pitching angle.

The trajectories in general seem to be lower before the top and higher before the bottom of trough. This tendency mainly depends on the definition of the altitude in Figure 3.

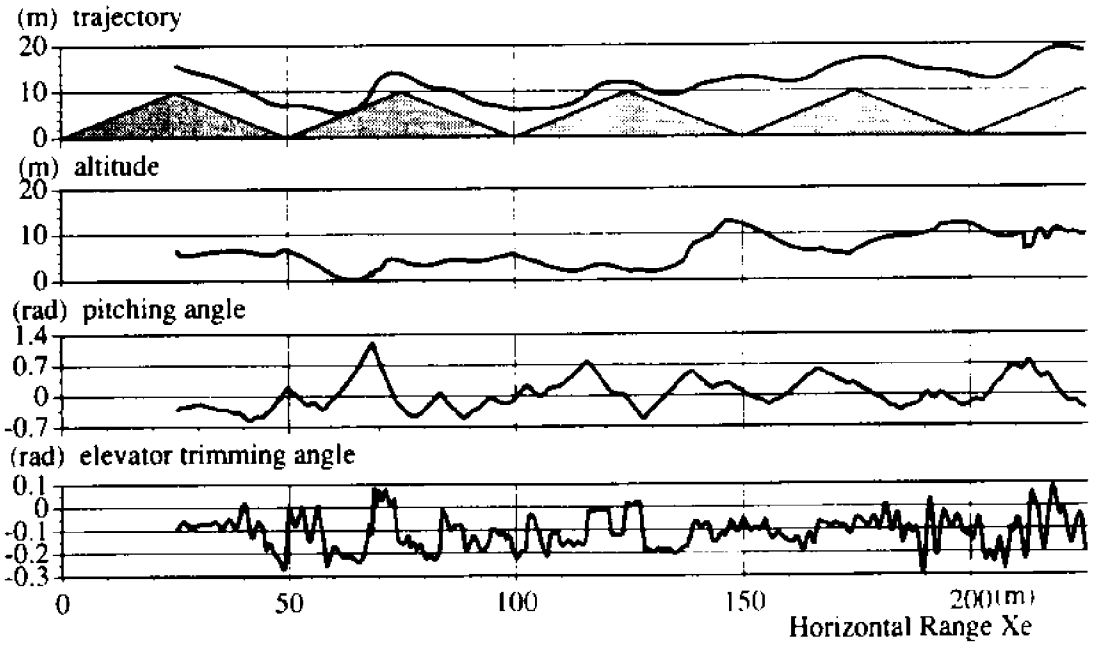

Figure 5. Data for network initialization

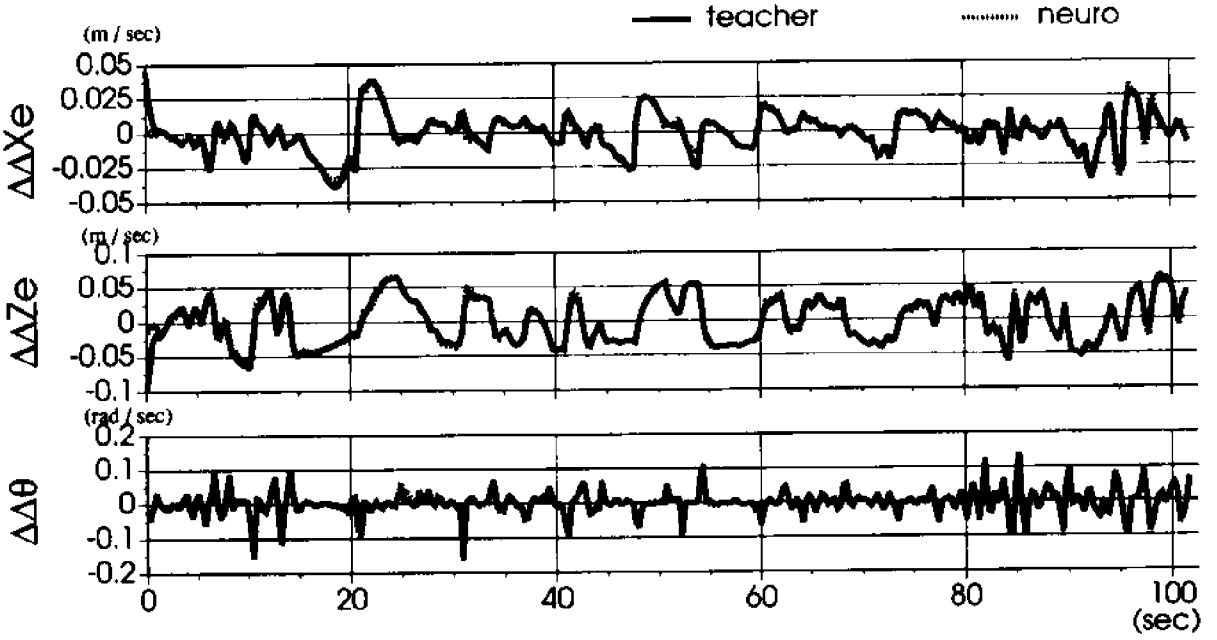

Figure 6. Outputs of the dynamics network after learning

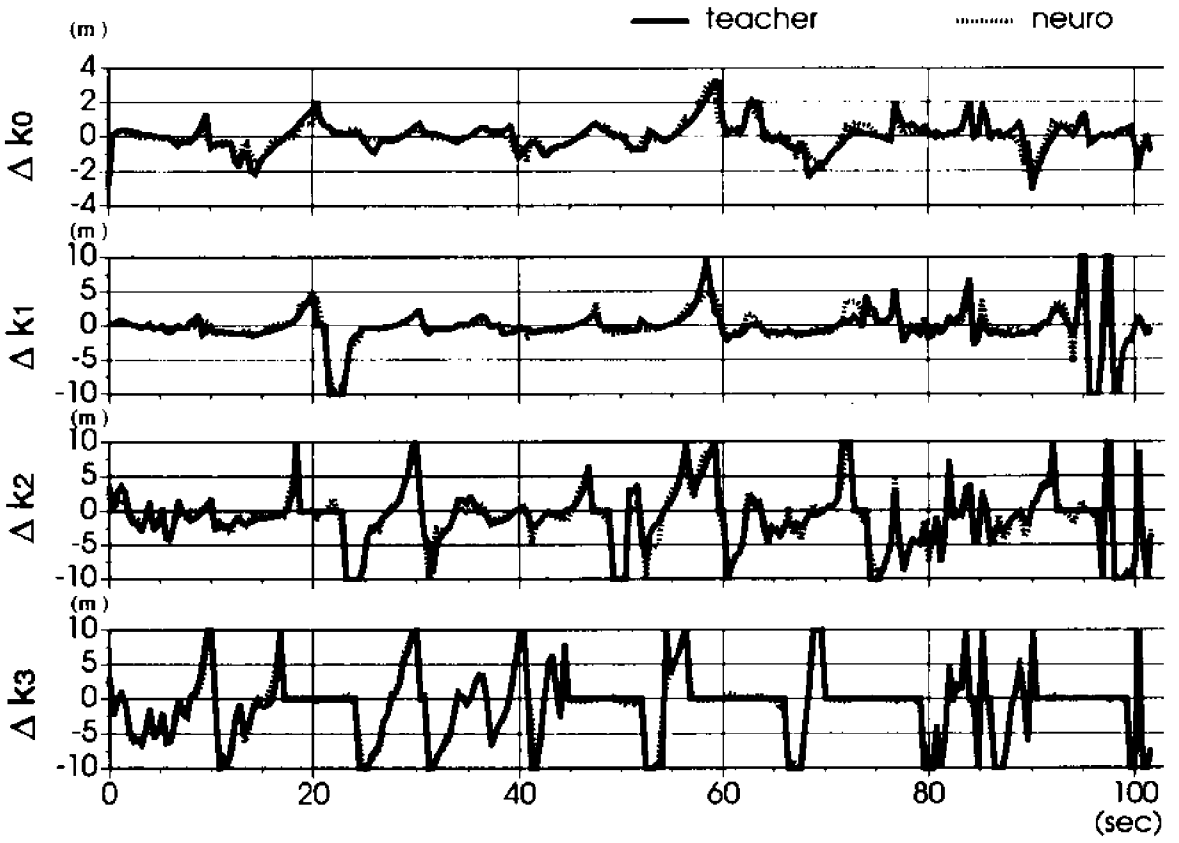

Figure 7. Outputs of the geometric network after learning

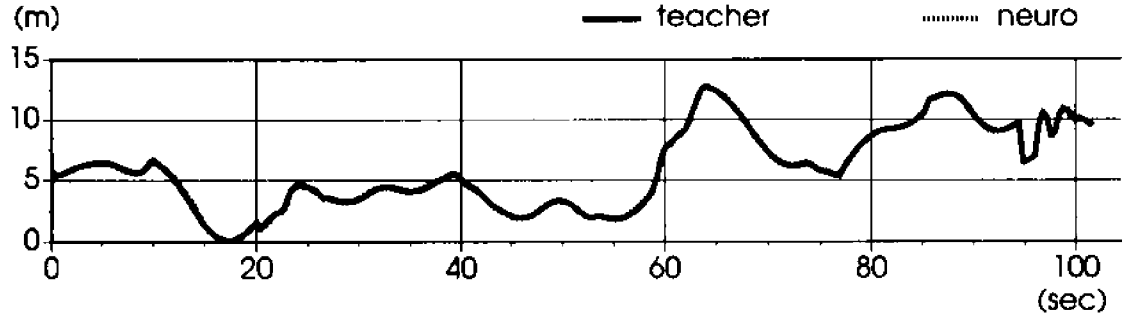

Figure 8. Output of the altitude network after learning

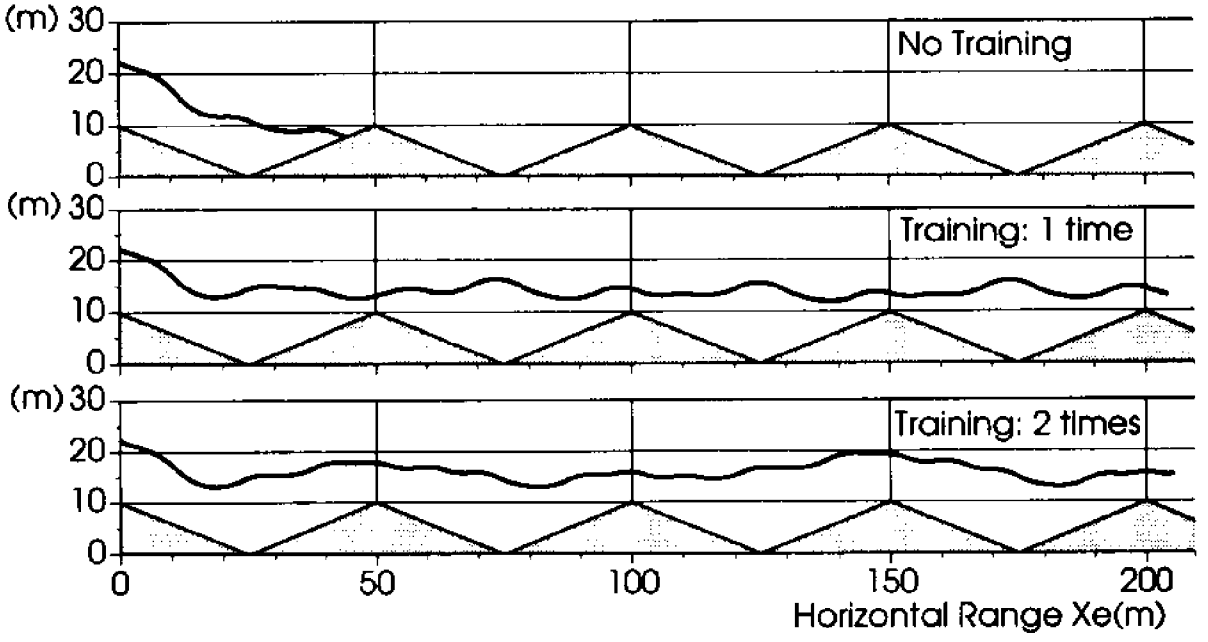

Figure 9. Training process over triangular ridges 50 m in span and 10 m in height

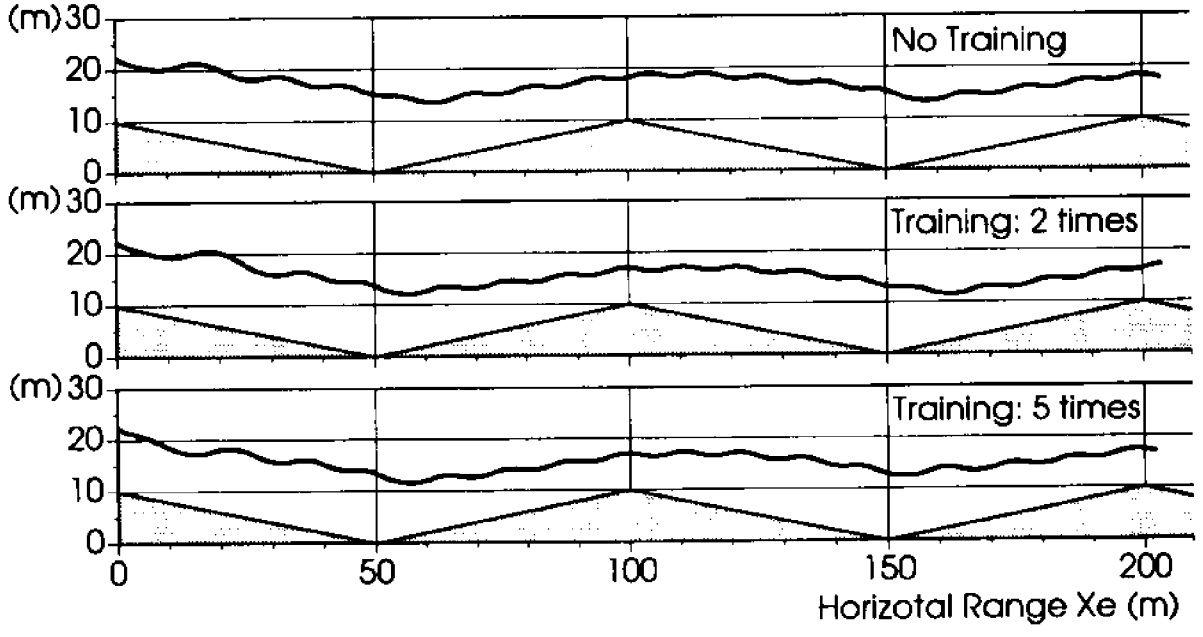

Figure 10. Training process over high triangular ridges 100 m in span and 10 m in height

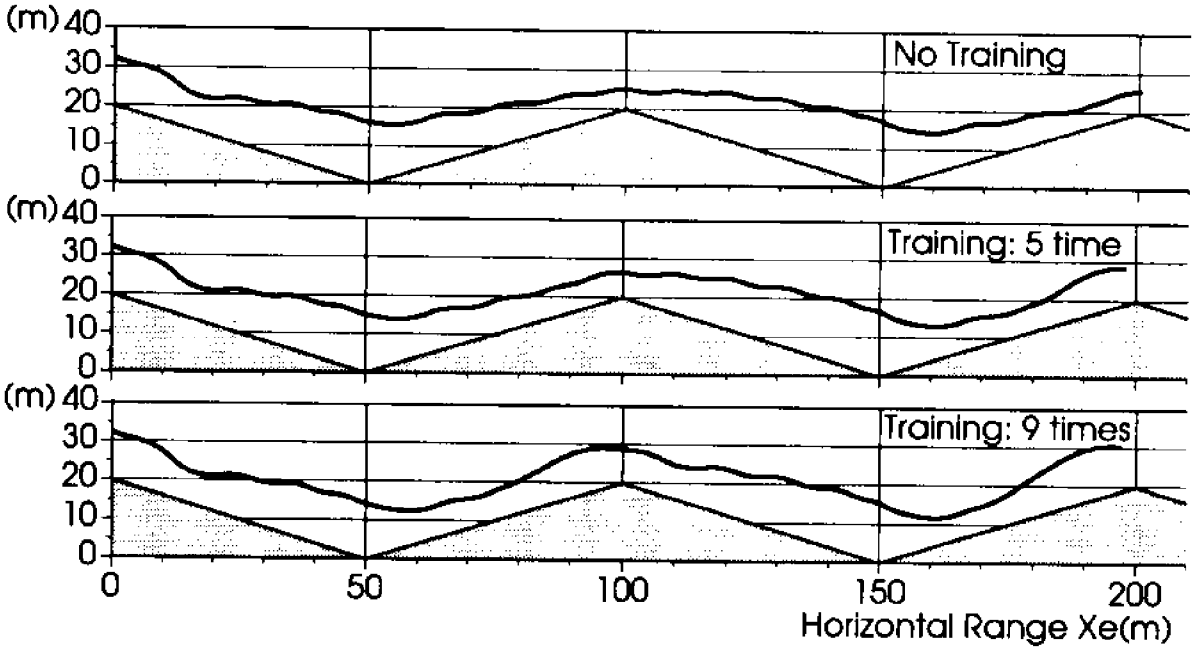

Figure 11. Training process over triangular ridges 100 m in span and 20 m in height

Although no system for collision avoidance is implemented explicitly, the resulted controller operates the vehicle avoiding collision, because slopes are moderate. However, when there is an extremely steep wall in front of the vehicle, pull-up manoeuvre should be done far before the wall. Since the evaluation function Eq. (1) made of k_0 and k_1, cannot distinguish this case, it is necessary that the evaluation function includes terms related to k_2 and k_3.

CONCLUSIONS

It is demonstrated that the Self-Organizing Neural-net-Controller System (SONCS) is applicable to the guidance system for an autonomous underwater vehicle, which is able to take into account of not only the dynamics of the vehicle but also the environmental information. The generation of the controller is accomplished only by giving an evaluation function and repeating training.

Modularization of the FWDN and introduction of the difference type network proposed here to construct a precise FWDN yield high speed acquirement of the ability of swimming.

REFERENCES

Fujii, T., and T. Ura. 1990. Development of motion control system for AUV using neural nets. In: Proc. of AUV90, pp. 81-86. Washington, D.C .

Fujii, T., and T. Ura. 1991. Neural network based adaptive control systems for AUVs. IJEAAI, Special Issue, *Intelligent Autonomous Vehicle Research.*

Ura, T., and S. Otsubo. 1988. Gliding performance and longitudinal stability of free swimming vehicle. In: Proc. of PACON88, OST1/10-18. Honolulu, Hawaii.

Ura, T. 1989. Free swimming vehicle PTEROA for deep sea survey. In: Proc. of ROV '89, pp.263-268 . San Diego, California.

Ura, T., and T. Suto. 1991. Unsupervised learning system for vehicle guidance constructed with neural network. In: Proc. of 7th Intl. Symp. on Unmanned Untethered Submersible Technology, pp. 203-212. Durham, New Hampshire.

DEVELOPMENT OF A 10,000 m CLASS DEEP SEA RESEARCH ROV KAIKO SYSTEM

Shinichi Takagawa, Taro Aoki, Kazuo Watanabe, Akira Takaobushi,
Yoshihei Abe, and Katsuyuki Suzuki
Japan Marine Science and Technology Center (JAMSTEC)
Yokosuka, Japan

ABSTRACT

The Japan Marine Science and Technology Center (JAMSTEC) is now constructing a 10,000 m class deep sea research ROV KAIKO system which consists of a vehicle, a launcher, cables and a cable handling system. This system is installed on the YOKOSUKA, a support vessel for the manned submersible SHINKAI 6500, and the YOKOSUKA carries both the SHINKAI 6500 and the KAIKO system.

Construction began in January 1991 and will be completed in August 1993.

The detailed features and key technologies for the KAIKO system will be discussed in this paper.

INTRODUCTION

The Japan Marine Science and Technology Center (JAMSTEC) is now constructing a 10,000 m class deep sea research ROV KAIKO system which consists of a vehicle, a launcher, cables and a cable handling system (Iwai, 1992; Okada, 1991). This system is installed on the YOKOSUKA, a support vessel for the manned submersible SHINKAI 6500, and the YOKOSUKA carries both the SHINKAI 6500 and the KAIKO system (Figure 1).

With the KAIKO system, the total deep sea research system is complete consisting of the YOKOSUKA with a multi-narrow beam echo sounder for wide area surveys, the KAIKO system for medium range surveys, and the SHINKAI 6500 for precise surveys.

The KAIKO system has three mission modes. The first is to survey the ocean floor to the 6,500 m depth by towing this system. In this mission, the sea floor topography and the stratum beneath the sea floor are surveyed by a side scan sonar and by a sub-bottom profiler fitted on the launcher, respectively, and precise observation by TV camera is done by the freely swimming vehicle. This towing survey is the advanced survey for the precise survey by the manned submersible SHINKAI 6500.

The second mission is to survey the ocean floor for the full ocean depth. In this mission, the launcher is not towed but suspended to nearly 100 m above the sea floor and becomes a platform for the vehicle. The vehicle carries out precise surveys by freely swimming around the launcher within a 200 m radius.

The third mission is to rescue the SHINKAI 6500 if it becomes unable to ascend by itself. This mission is just an application of the second mission.

The construction began in January 1991 and will be completed in August 1993. The fabrication and test of all equipment are now vigorously under way.

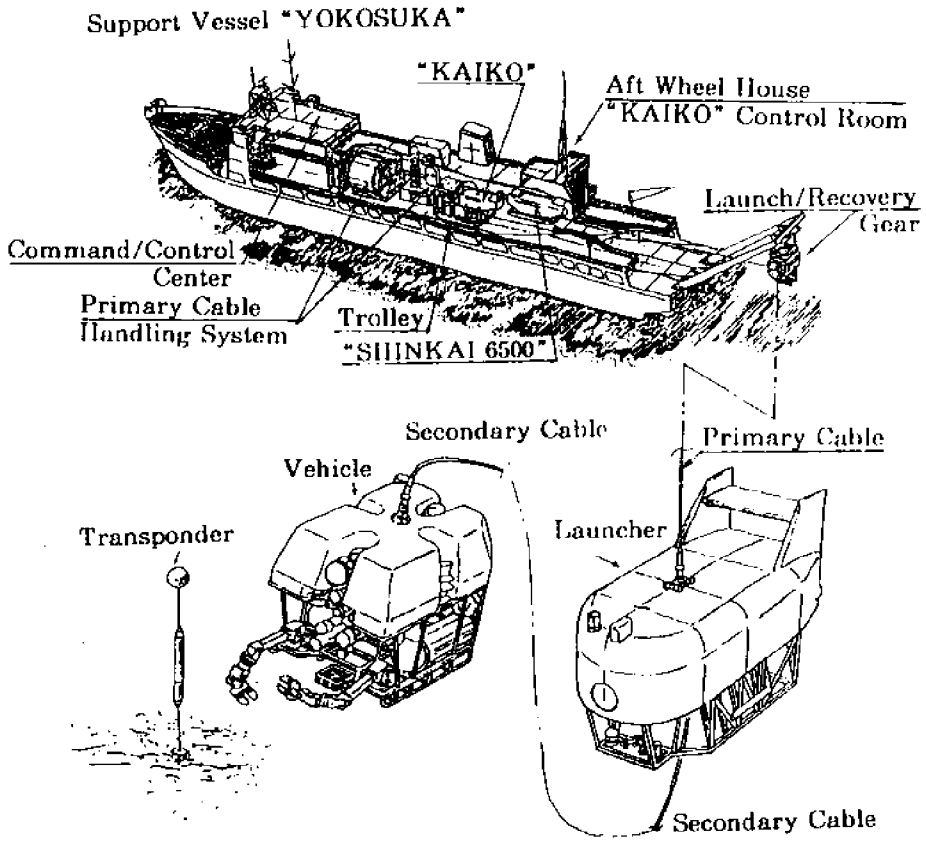

Figure 1. KAIKO system

The features of the KAIKO system are:

(1) It has a broadcasting class color TV camera for precise survey of the ocean floor. It has other four TV cameras for observations on the vehicle and a TV camera for connection monitoring on the launcher.

(2) Very high speed data communication via optical fiber (about 1.2 Gbps) is available which enables video image transmission of these six TV cameras and other data/control signals at the same time.

(3) It has a pair of bilateral manipulators with seven degrees-of-freedom on the vehicle.

(4) The vehicle has a hydraulic screw pump of constant delivery in order to make the acoustic noise emission as low as possible. The launcher has a hydraulic piston pump of variable delivery with noise reduction countermeasures.

(5) The launcher has a side scan sonar and a parametric array sub-bottom profiler for topographic and stratum surveys.

(6) The secondary cable between the launcher and the vehicle is a neutrally buoyant and pressure compensated cable, and the primary cable between the

support vessel and the launcher is a torque-balanced pressure compensated cable.

(7) The cable handling system consists of a launch/recovery gear, a heave compensator, a traction winch and a cable store winch. The heave compensator is a passive ram tensioner. Both the heave compensator and the traction winch have countermeasures against cable twisting problems.

(8) Automatic control of the vehicle and the launcher is extensively introduced for the operation and this relieves the pilots of their complicated loads.

(9) The operation support and recommendation system is developed and installed onboard the support vessel and this helps the captain and the operators to bring and keep the KAIKO into the target zone.

TOTAL DEEP SEA RESEARCH SYSTEM

The total system of the deep sea research consists of the YOKOSUKA, the KAIKO system and the SHINKAI 6500. The concept of this system is as follows.

The YOKOSUKA cruises the survey area activating a multi narrow beam echo sounder. This sounder can measure the sea floor topography with 45° to both sides. Thus the sea floor of 6,500 m depth can be measured by 13 km width. But this width is too wide to spot interesting points for dives of the SHINKAI 6500. So the KAIKO is mobilized for the medium range survey of the potentially interesting area using side scan sonar of the launcher towing at about 100 m above the sea floor and with TV cameras of the freely swimming vehicle. After spotting the interesting point, the SHINKAI 6500 dives to the point for precise survey. This type of survey is down to 6,500 m deep at the maximum.

For survey of the deeper area, the mission mode becomes the second one, where the launcher is not towed but suspended to become a stable platform and the vehicle swims freely to the sea floor for the detailed observations by TV cameras and samplings or instrumentation setting by manipulators.

THE VEHICLE

The main function of the vehicle is to execute surveys of the sea floor by freely swimming. Vehicle survey involves the observation by TV camera and sampling or instrumentation setting by manipulators.

The Feet

It has four lateral thrusters and three vertical thrusters, and proper thrust force allocation of these seven thrusters gives the vehicle motion in any direction. This allocation is automatically done and the operator is required only to order the direction and velocity by joysticks.

The Eyes

It has a broadcasting class color TV camera with focusing and zooming functions on a panning and tilting base. A still camera is mounted on the same base and the same

image can be photographed as the TV. It has also three normal color TV cameras at front. These cameras give a panoramic view of the frontal area to the operators. These cameras can tilt up and down. The other monochrome TV camera is fixed on the rear side to look backwards.

The electric TV signals are sent to a pressure vessel, where the signals are converted to serial optical signals with 1.3 micro-meter wavelength and goes upward via the optical fiber.

The Arms

It has two electro-hydraulic bilateral manipulators each with seven degrees-of-freedom. They have force feed-back functions and even very fragile objects like a raw egg can be handled. Parallax perception of the object can be done using both the high quality TV camera and the panoramic TV cameras.

The Ears and Voice

It has an obstacle avoidance sonar with a maximum range of 200 m and an altitude sonar with a maximum 100 m to minimum 0.5 m. It has also a responder for relative positioning to the launcher.

The Heart

The thrusters, manipulators, and panning and tilting apparatus are actuated by hydraulics. The hydraulics is delivered by a hydraulic pump. In order to keep the acoustic environment quiet, a low-noise screw pump is selected. As this pump is of the constant delivery type, a pressure regulating valve and a forced oil cooler are fitted to keep the pressure and the oil temperature in the proper region. The noise level becomes approximately 30 dB lower than the conventional piston pump of the same capacity. Other items such as the electric motor and the hydraulic thruster motors, etc., are carefully selected and modified minimum noise.

Electronics and Pressure Vessels

In order to make the weight of the vehicle as light as possible, tremendous efforts to reduce the size and the weight of the electronics have been made. These efforts produced very small-size electronics capable of very high-speed data transmission, and are contained in a titanium alloy cylindrical pressure vessel of 28 cm diameter by 140 cm long with hemispherical caps at both ends. There is another pressure vessel containing a voltage regulator, a gyrocompass, and others. This vessel is the same size as that for the electronics.

The Body and Others

The bare weight in water is about 1.8 tons, and this weight is compensated by buoyancy material of about 0.63 gr/cm^3. The pressure tolerance of this buoyancy material is more than 1,600 kgf/cm^2 in order to correspond to the full ocean depth. This material is composed of thick wall glass micro balloons and high strength matrix resin.

The vehicle can bring payloads of 150 kg at the maximum in a sample basket at the front. The 10 kg positive buoyancy at the target depth is achieved by putting payloads and/or proper ballasts in the sample basket.

For electricity distribution, cables for trunk lines are the oil-filled type, but cables for peripheral lines are the rubber molded-type with plastic connectors.

THE LAUNCHER

The main function of the launcher (Figure 2) is to become a stable platform for the vehicle. Also it becomes a towed fish with a side scan sonar and a sub-bottom profiler in order to measure the topography of and the stratum beneath the sea floor.

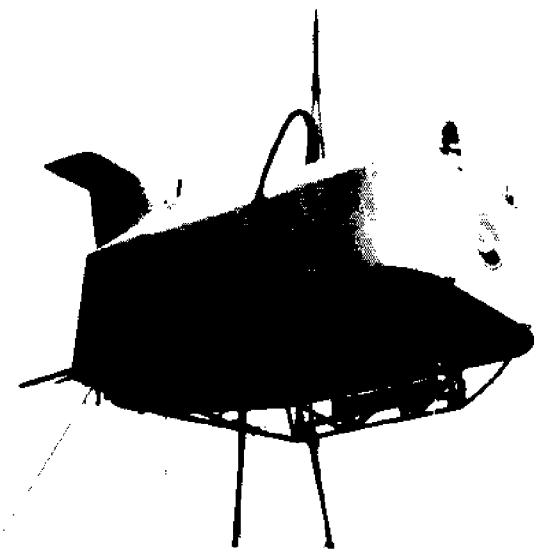

Figure 2. Launcher at dock test

The Platform

During descending and ascending between the surface and the depth adjacent to the sea floor, the launcher holds the vehicle under its body. At the target altitude (usually about 100m above the sea floor), the vehicle leaves the launcher for the survey. After the work is done, the vehicle returns to the launcher. As the heave motion of the launcher is fairly reduced due to the elasticity of the cable and a heave compensator installed on the support vessel, it becomes a stable platform, and smooth control of the vehicle for leaving from and returning to the launcher is achieved. The mating is monitored by a monochrome TV camera and an electric sensor. After confirming that both are mated properly, the mating gear is locked.

The launcher and the vehicle are connected by the secondary cable, and this cable is wound up in a cable reel on the launcher. The distance between the vehicle and the launcher is measured by a SSBL acoustic receiver on the launcher and the secondary cable is automatically paid off/on neither not too tight nor over-slacking to give free swimming capability to the vehicle.

Topographic and Stratum Measurement

In the towed mode, the launcher is also a stable platform for a side scan sonar and a sub-bottom profiler.

The side scan sonar can measure the sea floor topography with 1 km width at each side at an altitude of approximately 100 m from the sea floor.

The sub-bottom profiler is the parametric array type, and a pair of slightly different high frequency acoustic signals give a low frequency signal with narrow beam width of about 9°, which deeply penetrates the earth. The echoes from beneath the sea bottom give a very precise structure of the stratum because this measurement is carried out very close to the sea floor.

Acoustic System

The acoustic system contains an acoustic LBL receiver. A responder installed on the launcher triggs the transponders on the sea floor, and the LBL measurement gives its location precisely. The system also includes an acoustic SSBL system which can measure the location of the vehicle and transponders. Combination of this LBL and SSBL also gives the precise location of the vehicle. The signal from the responder is also heard on the support vessel and its relative location to the support vessel can also be measured.

The system also contains an obstacle avoidance sonar. During the towed mode, the multi narrow beam echo sounder of the support vessel gives the change of the sea floor depth on the routes, and using this data and the obstacle avoidance sonar data, the launcher is elevated or lowered to avoid the collision with seamounts or other obstacles. Thus the safe towing operation is carried out.

Acoustic Noise Countermeasure

As the launcher has many ears, the acoustic noise countermeasure is very important as well as the vehicle. The hydraulic systems are fairly smaller than those of the vehicle because they are for the secondary cable handling system, panning and tilting devices for several equipment and others which require fairly less delivery. Therefore a variable delivery hydraulic pump of smaller capacity with the lower noise level is selected. Moreover the pump is surrounded by a noise isolation wall.

Electronics and Pressure Vessels

The launcher contains three cylindrical pressure vessels with hemispherical caps at both ends made of titanium alloy. The first contains electronics for data transmission and control capable of about 1.2 Gbps communication, the second contains electronics for acoustic devices such as these for the side scan sonar and the sub-bottom profiler, etc. and the third is for voltage regulation, the gyrocompass, and others. The inside diameter of these three vessels is 28 cm and the cylindrical length is 150 cm for the acoustic system and 160 cm for the first and the third vessels.

CABLES

The KAIKO system has two cables. One is the primary cable between the support vessel and the launcher, and the other is the secondary cable between the launcher and the vehicle (Figure 3).

Primary Cable

The primary cable suspends the launcher. For elevationg or lowering the launcher, the cable is paid on/off.

The vehicle in water is neutrally buoyant and the launcher in water weighs about 3 tons. The primary cable is required to be strong, and it is not neutrally buoyant but heavier than sea water. Thus the total load working on the cable becomes about 8 tons at full ocean depth operation. The breaking strength of the cable is more than 40 tons considering the safety factor of more than 5.

The tension member of the cable consists of doubly layered Kevlar rods. The twisting directions of these layers are opposite each other to obtain torque balance. The

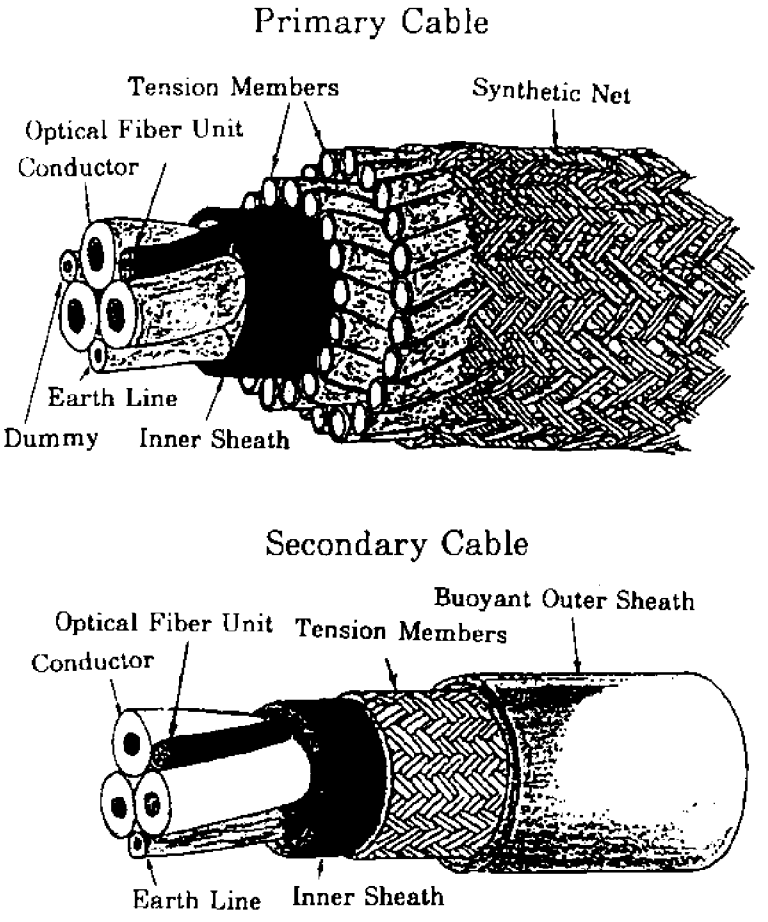

Figure 3. Structure of cables

surface of the cable is covered by synthetic tubular braid and sea water can go into the void space between the rods, which forms the pressure balance for the tension members.

Inside the cable, there are three copper conductors for electricity delivery, a copper conductor for earth and four optical SM fibers for data transmission. Two of the four fibers are for actual use and the other two are spares. One actual use is for data transmission from the vehicle to the support vessel via the launcher by 1.3 micro-meter wave length. The other is for data transmission from the launcher by 1.3 micro-meter wave length and also control signal transmission from the support vessel to the launcher and to the vehicle by 1.55 micro-meter wavelength.

These four optical fibers are loosely inserted in grooves on a nylon rod and the grooves are filled with viscous resin to form pressure balance.

The four conductors and the nylon rod containing the optical fibers are twisted together and are molded by rubber eliminating any void space.

The cable load is sustained by Kevlar tension members but no load on conductors or optical fibers.

The termination at the cable end has a conical shape and this part mates with the launch/recovery gear of the cable handling system at the A-frame crane of the support vessel. This termination is connected to the launcher by gimbal mechanics.

Secondary Cable

The secondary cable transmits data between the vehicle and the launcher, and is is 250m in length. This cable should not restrict the vehicle's motion; it must be flexible enough and also neutrally buoyant.

To make this cable neutrally buoyant, the surface is covered with thick tubular EP rubber with a density of 0.90 gr/cm3.

Beneath the EP rubber are tension members. They are tubular braid of nylon jacketed Kevlar strips. As the estimated maximum load to the cable is very small, the breaking strength is 3 tons. In order to make this tension member pressure balanced, liquid is filled in the void space of the strips.

Inside the cable, there are three conductors for electricity delivery, a conductor for earth and three optical GI fibers for data transmission. As the cable length is only 250 m long, the material of the conductors is aluminum in order to reduce the weight. One of the three fibers is for actual use and the other two are spares. This fiber is for data transmission from the vehicle to the launcher by 1.3 micro-meter wave length and also control signal transmission from the support vessel to the vehicle via the launcher by 1.55 micro-meter wavelength.

The structure of the cable inside the tension member is the same as the primary cable. The termination of the cable is also the same as the primary cable.

CABLE HANDLING SYSTEM

The cable handling system consists of a gimbal sheave hanged down at the A-frame crane of the support vessel, a heave compensator, a traction winch and a cable store winch (Figure 4). The last three are installed in the hangar of the support vessel.

The most important role of this system is to lower and elevate the launcher isolating the pitching and heaving motion of the support vessel so as to make the launcher a stable platform in the water. In order to realize this function, ram tensioners are adopted for the heave compensator which uses an air spring. The spring constant of the ram tensioner can be adjusted by automatically changing the air pressure and the volume of accumulator.

The cable twisting problem by sheaves is usually passed over, but it is a serious problem and sometimes creates cable troubles. There are many sheaves on heave compensator and traction winches and a countermeasure to the cable twisting problem is vigorously introduced. The principle is to make the fleet angle of the cable zero. For this purpose each sheave of the heave compensator is inclined independently. This countermeasure makes the minimum length of the heave compensator very short and it can be theoretically twice the sheave diameter.

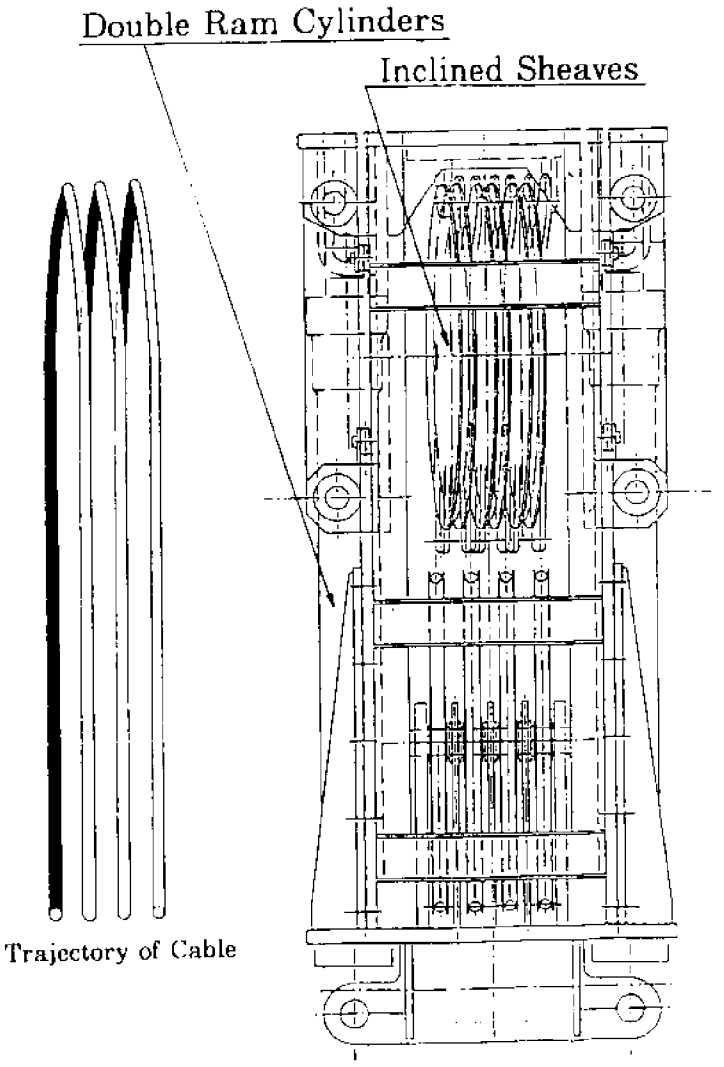

Figure 4. Tension-free sheaves for ram tensioner

It is very difficult to adopt independently inclined sheaves for the traction winch because this winch should drive the cable. So the drive shafts are inclined to each other by a pitch of groove. This method is not perfect to give a zero fleet angle mathematically but is effective in actual use.

The cable tension is calculated by measuring the angles of the cable, inclined angle, and the load of the gimbal sheave.

The cable store winch stores 12,000 m cable at the maximum, pulling with approximately 100 kg constant tension. A sea water sprinkler is adapted to cool down the cable temperature due to the electric current.

CONTROL OF THE KAIKO SYSTEM

The control room is located at the aft wheel house of the support vessel YOKOSUKA. There are three persons in front of the control console: a vehicle operator, a launcher/manipulators operator, and a chief operator manipulating acoustic systems and others. The chief operator may also serve as the KAIKO conductor or another fourth person may be the conductor.

The panoramic view and a broadcasting class TV image in front of the vehicle are shown on the console monitors. The rear view of the vehicle and/or the mating status can be viewed in one of these monitors by changing channel. Obstacle avoidance sonar images of the vehicle and the launcher, positions data of the vehicle, the launcher, the support vessel and the transponders on the sea floor, and control management data can be shown on other CRTs. By looking at these monitors and CRTs data, operators control the KAIKO, handling the joysticks and manipulator master arms.

The conditions at the vessel's stern are taken by ITVs and monitored in the control room.

The sea floor images and other views are monitored at the command and control center just after the wheel house, and the commander and the captain can grasp the whole situation of the KAIKO so the captain can operate the vessel in accordance with the KAIKO operation.

OPERATION OF THE KAIKO

In normal case, the KAIKO and the SHINKAI 6500 are housed in the hangar on the same rail. For the operation of the KAIKO, the SHINKAI 6500 is sled to sideways. Then the KAIKO, that means the launcher, the vehicle and launch/recovery gear with gimbal sheave each on a trolley, is drawn aftward to the stern, dragging the primary cable.

The launch/recovery gear is at first connected with the A-frame crane and a mating device hanging by wires down to the launcher and mates with each other. The launcher, holding the vehicle, is pulled up and the A-frame crane swings aftward. The hanging wires with heave compensators are wound off until the launcher and the vehicle comes to approximately 10m deep. At this stage electricity is supplied and the KAIKO system is activated. After pre-dive check, the wires are wound off to become slack and entire weight of the KAIKO is sustained by the primary cable. The mating device is hydraulically disconnected at this point.

After this stage the whole KAIKO system is controlled at the control room. The primary cable is automatically paid off and the KAIKO descends to the target depth. The captain operates the support vessel following the data shown by the operation support and recommendation system so that the KAIKO can precisely arrive at the target area.

After the survey is completed, the launcher holding the vehicle ascends to the surface by winding up the primary cable.

Beneath the surface at about 10m deep, the winding up is stopped and the mating device of the launch/recovery gear comes down to the launcher and mates automatically. After confirming that they mate precisely, the electricity delivery is stopped and the KAIKO is recovered by the wires. The A-frame crane swings forward and places the

KAIKO onto the trolley. The launch/recovery gear is also placed on the trolley. After fresh water cleaning and post-dive check, the KAIKO and launch/recovery gear on the trolley is drawn forward to the proper position in the hangar.

Thus the KAIKO operation comes to end.

PRESENT SITUATION AND PROSPECTS

At this time, fabrication of every part and examination are vigorously under way. Construction will be completed in August 1993. The final sea trial is scheduled to be carried out at Mariana Trench to confirm the full ocean depth capability.

We expect the KAIKO to contribute greatly to the earth science.

REFERENCES

Iwai, Y., et al. 1992. Key technologies of 10,000m class ROV system under construction, In: ROV '92.

Okada, H., et al. 1991. Outline of 10,000m class remotely operated vehicle under development. In: ROV '91.

RECENT DEVELOPMENT OF THE SUPERCONDUCTING MAGNETOHYDRODYNAMIC SHIP PROPULSION IN JAPAN

Yohei Sasakawa
Sasakawa Foundation
Tokyo, Japan

Seizo Motora
University of Tokyo
Tokyo, Japan

Setsuo Takezawa
Ship & Ocean Foundation
Tokyo, Japan

ABSTRACT

The Ship & Ocean Foundation of Japan has been conducting an extensive research and development project on superconducting magnetohydrodynamic ship propulsion funded by the Sasakawa Foundation since 1985. The purpose of this project is to develop fundamental technologies which are necessary to develop a superconducting MHD thruster, and finally to construct a prototype experimental ship to demonstrate that a ship can really be propelled by MHD thruster with all the necessary equipment on board.

It was also expected that through such actual design and construction of the experimental ship, problems to be solved in developing higher performance MHD ships for practical use in the future can be extracted.

The development of fundamental technologies was successfully achieved by 1988, and the experimental ship was designed and constructed. The ship named YAMATO-1 was completed in the fall of 1991 at the Kobe Shipyard of Mitsubishi Heavy Industries (Figure 1). The ship was launched on March 1992, and a series of sea trials has been started. In this paper the authors intend to describe an outline of the project and of the experimental ship YAMATO-1 and to report some of the results of the sea trials which had been conducted and completed at the time of the presentation of this paper.

INTRODUCTION

The basic principle of MHD propulsion is based on the Flemming left hand rule. If a magnetic flux is generated in seawater by a magnet placed onboard a ship, and electric current is generated through seawater to be perpendicular to the magnetic field, then an electromagnetic force (Lorentz force) will be generated in the seawater and will push the seawater away. Therefore, if the direction of the magnetic flux and the direction of the electric current in seawater are so arranged that the direction of the Lorentz force is rearward, the ship will be pushed forward by the reaction of the Lorentz force which acts directly on the magnet. This idea of propulsion was introduced by Rice (1961).Way of Westinghouse tested MHD propulsion using model ship (EMS-1) in California in 1966 (Way and Devlin, 1967). In 1980, Iwata, Saiji, and Sato (1980) began to adopt superconducting magnets for MHD ship propulsion, and tested a 3.6 m ship model

equipped with an external field-type MHD thruster (ST-500) in a model basin of Kobe University of Mercantile Marine. In the meantime extensive investigations into the feasibility of superconducting MHD ship propulsion was being undertaken in the United States (Mitchel and Gubser, 1988; Brown, et al., 1990).

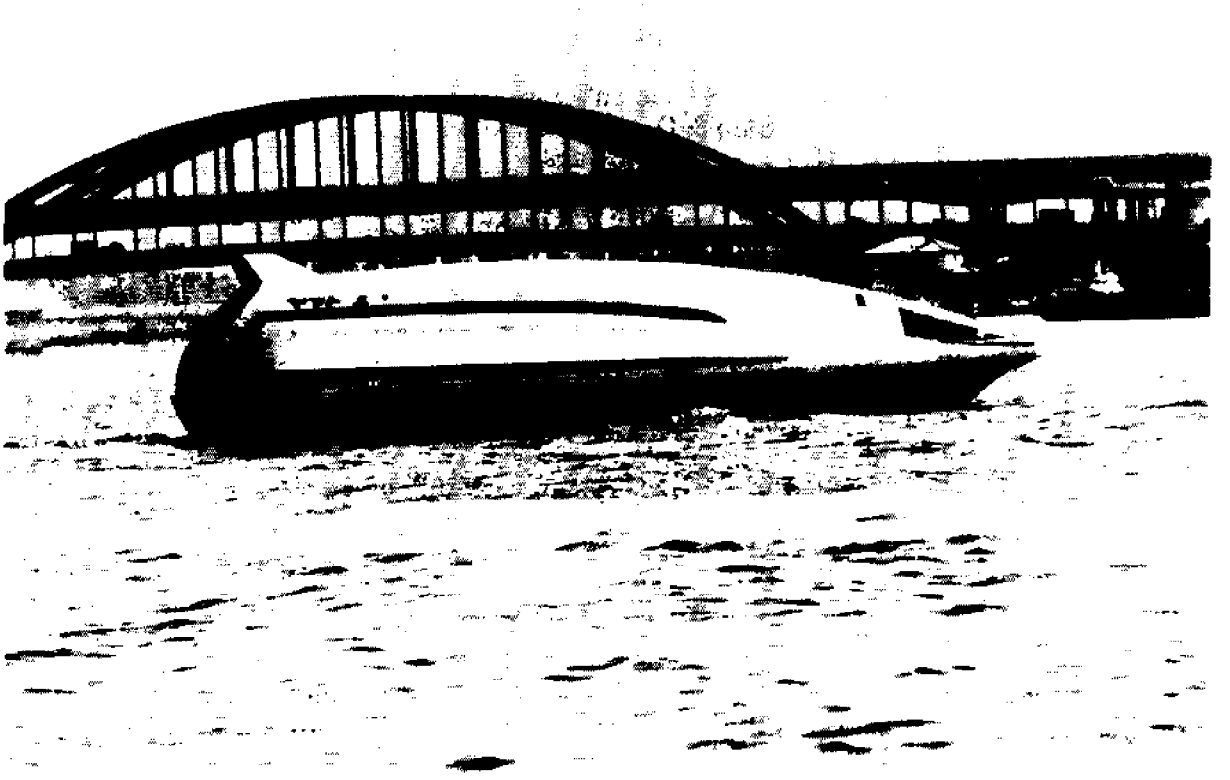

Figure 1. YAMATO-1 at her debut in Kobe Harbor

In view of recent progress in superconducting magnet technology, the Ship & Ocean Foundation set up a committee to conduct an extensive research and development project on superconducting ship propulsion in 1986 aiming to construct a prototype experimental ship equipped with superconducting MHD thrusters. The details of this project were presented at the MHDS 91 Symposium in Kobe, Japan in 1991 (Motora, et al., 1991). In this paper an outline of the project and the experimental ship will be described.

THE MHD THRUSTER

Basic Construction of an MHD Thruster

The basic configuration of a MHD thruster is shown in Figure 2. A water duct is surrounded by a set of dipole superconducting coils which generate a magnetic field perpendicular to the center line of the duct. A pair of electrodes is also provided in the

duct so as to generate an electric current through the seawater to be perpendicular to the magnetic field. As a result, Lorentz force (electro-magnetic force) will be generated in the seawater in the duct and push the seawater rearward. The reaction of the Lorentz force acts directly on the magnet coils and pushes the ship forward. The entire set-up is contained in a cryostat to maintain the temperature of the coils at 4°K.

As the thrust generated by the MHD thruster is proportional to the magnetic flux density, and the efficiency of a MHD thruster is approximately proportional to the square of the magnetic flux density, it is critical to use strong and lightweight, but less energy consuming, magnet coils. Therefore, it is essential to develop strong superconducting magnet coils to make MHD ship propulsion feasible.

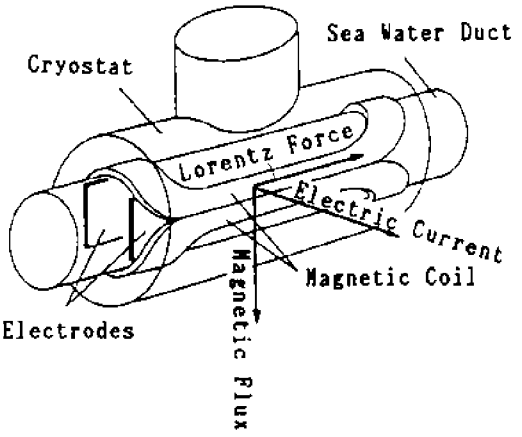

Figure 2. Basic construction of a MHD thruster

Actual Construction of the MHD Thruster Used for the Experimental Ship

Based on the experience of several steps of test manufacture of superconducting MHD thrusters, the thruster to be mounted on the experimental ship was designed and constructed. As the thrust necessary to propel the ship at 8 kt was estimated to be 8,000 N, the necessary Lorentz force to be generated by the thruster(s) was estimated to be 16,000 N where the efficiency in converting Lorentz force into thrust is assumed to be 50%.

As was anticipated, the Lorentz force of 16,000 N was too large to be generated by a thruster. A decision was made to install two MHD thrusters, each of which can generate a Lorentz force of 8,000 N. A fringe-type arrangement of the thrusters in which six unit coils were arranged to form a lotus-like ring was adopted (Figure 3). The reason for

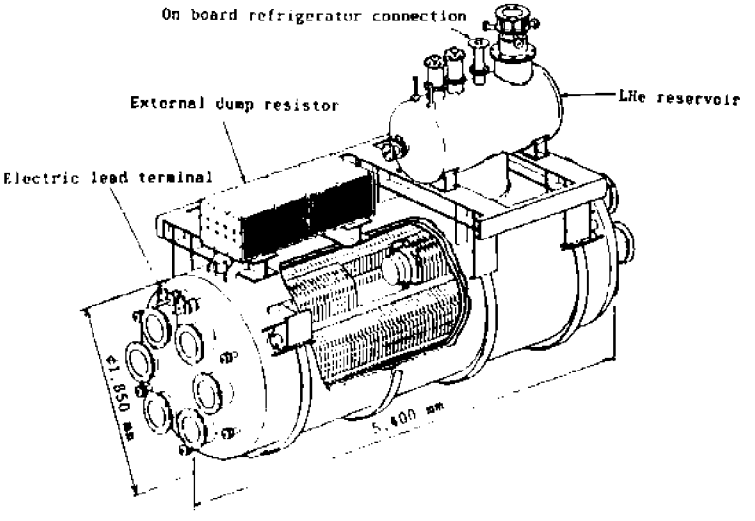

Figure 3. Open view of the MHD thruster

adopting such an arrangement was to minimize the leak of magnetic flux outside the thruster so that magnetic shielding can be eliminated. The particulars of the unit coil is shown in Table 1, and the particulars of the integrated MHD thruster is shown in Table 2. It should be noted that the weight of a thruster is only 18 t instead of 35 t as initially estimated at an early stage of the project.

Figure 3 shows the construction of the MHD thruster and Figure 4 shows an outside view of the completed MHD thruster. The right thruster was constructed by Toshiba Corporation and the left thruster by Mitsubishi Heavy Industries, Ltd. A compact and lightweight helium refrigerator to be mounted on each MHD thruster was also developed for which an expansion turbine of 60,000 rpm was used.

Table 1. Particulars of the unit coil of the MHD thruster

Inner diameter of the coils	0.360m
Inner diameter of the duct	0.240m
Length of the coil (total)	3.70m
Length of the coil (parallel part)	3.00m
Number of turns 220× 2 layers ×2 poles	
Normal electric current	4,600A
Magnetic flux density at center (per single unit)	3.5T

Table 2. Particulars of the MHD thruster

Compound magnetic flux density at center	4T
Electrode current (normal)	2,000A
Lorentz force	8,000N/set
Thrust	4,000N/set
Weight	18t/set

DESIGN AND CONSTRUCTION OF THE EXPERIMENTAL SHIP YAMATO-1

As the weight and size of the MHD thruster became clear, the size, hull form, and basic arrangement of the experimental ship were decided. To contain two bulky MHD thrusters which should be placed under the water line, a peculiar ship form as shown in Figure 5 was adopted. As seen in the figure, the hull form is a shallow monohull with two bulges hanging from the rear part of the main hull. The principle particulars of the ship are shown in Table 3 and the general arrangement is shown in Figure 6.

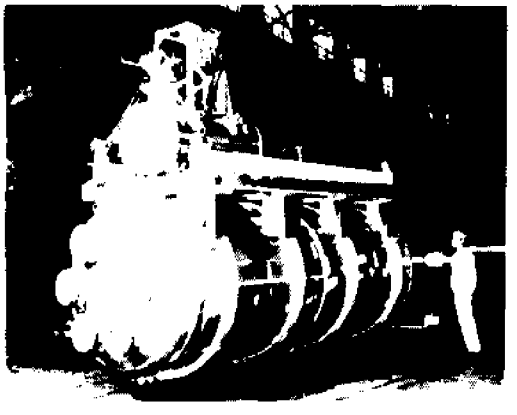

Figure 4. Outside view of the MHD thruster

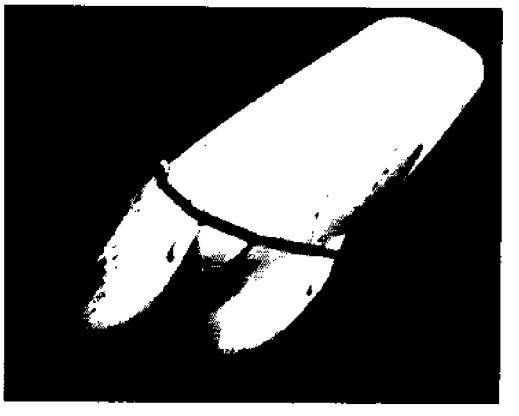

Figure 5. The hull form of YAMATO-1

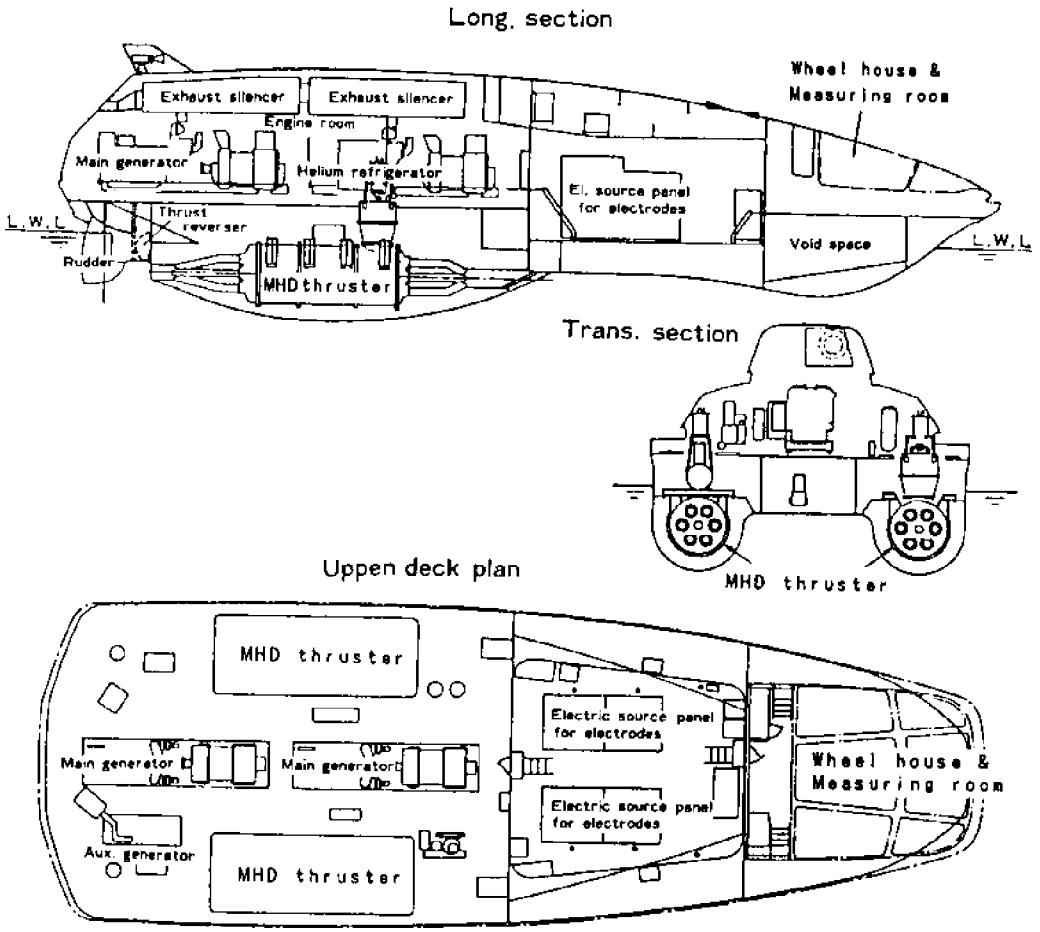

Figure 6. General arrangement of YAMATO-1

Table 3. Principal particulars of YAMATO-1

Length overall	30m
Length between perpendiculars	26.4m
Breadth (moulded)	10.39m
Depth (max)	3.69m
Draft (max)	2.69m
Displacement (including water in the ducts)	185t
Speed (at Lorentz force 16,000N)	about 8kts
Material of the hull	Aluminium
Number of person	10 including 3 crew

The resistance of the hull was measured at a towing tank using a 2 m ship model, and a self-propulsion test at which impellers were used instead of the MHD thrusters, was also performed. Results showed that the ship might run at 8 kt at a thrust of 8,000 N. Maneuvering tests were also conducted by the same model and satisfactory maneuverability was predicted.

As seen in Figure 6, the MHD thrusters are mounted on both sides and in the underwater part of the hull, and the main generators which will produce electric current through seawater are placed at the center of the ship. The controlling systems and the persistent current switches were also incorporated.

The ship was completed at the end of 1991 at the Kobe Shipyard of Mitsubishi Heavy Industries, and named YAMATO-1. After several prudent tests on land, the ship was launched in March 1992 at Kobe Harbor and a series of sea trials was started. At the time of the presentation of this paper at PACON 92, only a bollard pull test to measure the thrust of the ship had been performed. Therefore, the result of the thrust measurement test will be described in the following section.

RESULTS OF THE SEA TRIALS

Trial Condition

The ship

Displacement:	182 tons
Trim:	0.42 m aft

Weather and sea condition

Wind:	WNW 5 m/sec
Temperature:	22.5°C
Wave height:	0.5 m choppy waves
Specific gravity of seawater:	1.022
Water temperature:	20.2°C
Conductivity of seawater:	σ = 3.64 s/m

Mooring Test and Bollard Pull Test

Preceding speed trials, a mooring test and a bollard test were conducted. At the mooring test, the ship was moored at a pier and electric current through seawater was applied to examine whether or not the electric current induced any trouble in the magnets or not.

As it was confirmed that electric current up to 2,000 amp did not give any adverse effect to the magnets, a bollard pull test was conducted to measure the total thrust.

At the bollard pull test, the ship was moored at a bollard on a pier, and a tensiometer was inserted in the towing rope. The towing force which was equal to the total thrust generated by the ship was measured by the tensiometer.

The test was performed with two kinds of magnetic flux density, namely: B=1 T and B=2 T and

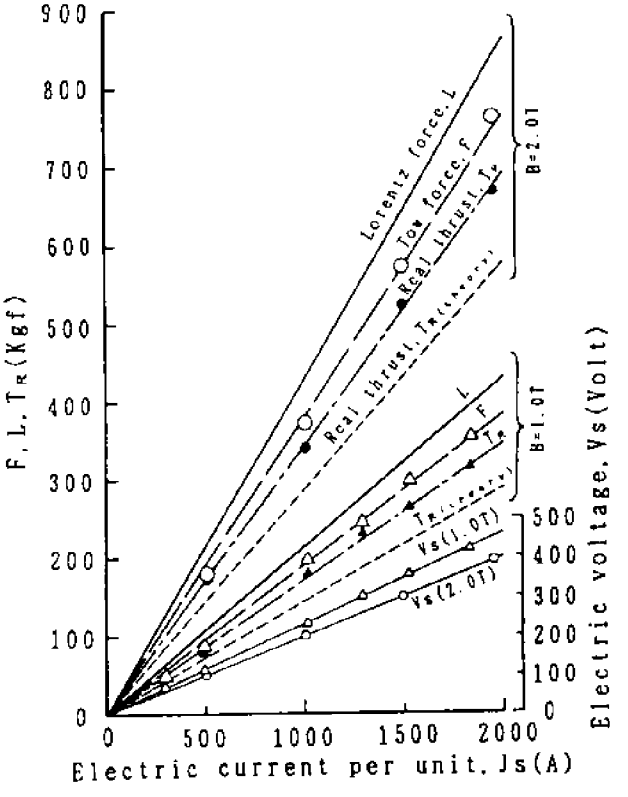

Figure 7. Result of the bollard pull test

electric current through seawater Js being varied from 500-2,000 amp. Hydrodynamic pressure at the inlet and outlet of the thruster duct was also measured. The result is shown in Figure 7.

In Figure 7, F shows the measured value of towing force, in other words, the total thrust of the ship, T_R shows the thrust generated by MHD thrusters including the effect of the duct system which was calculated from measured flow speed and hydrodynamic pressure in the duct, and L shows the Lorentz force which was calculated using actual magnetic flux density B and the electric current Js through seawater. The relation among F, L, and T_R is as follows:

L – loss in the duct = T_R
T_R – pressure induced force around the hull = F
(negative in the present case)

Although the Lorentz force was not measured directly, assuming from the measured value of towing force F and real thrust T_R, it can be derived that the thrusters must generate almost the same order of the Lorentz force as predicted by theory. During the mooring test as well as the bollard pull test, it was observed that a powerful milky jet stream came out of the nozzles of the thrusters. In Figure 8 a picture of a jet stream generated at B = 3T, Js = 1,800 amp is shown. Although the sea surface was covered with sparkling micro bubbles, there was no trace of chlorine gas odor.

Figure 8. A jet stream generated by MHD thruster

Speed Trials

As speed trials were performed in June and July 1992 after the presentation of this paper at PACON 92, the results are not included in this paper. Instead, it will just be mentioned that the YAMATO-1 runs at about 5.5 kt with the magnetic flux density B = 2T and the electric current through seawater Js = 2,000 amp.

REFERENCES

Brown, S.H., J.S. Walker, N.A. Sondergaard, P.L. Reilly, and D.E. Bagley. 1990. Propulsive efficiency of magnetohydrodynamic submerged vehicularpropulsion. DTRC Report 90/009, April.

Iwata, A., Y. Saji, and S. Sato. 1980. Construction of model ship ST-500 with electromagnetic thrust system. In: Proceedings ICEC, pp. 775-781.

Mitchel, D.L., and D.U. Gubser. 1988. Magnetohydrodynamic ship propulsion with superconducting magnet. *J. Superconducting Science and Technology*. 1.

Motora, S., K. Imaichi, M. Nakato, and S. Takezawa. 1991. An outline of the R&D project on superconducting MHD ship propulsion in Japan. Presented at Intl. Symp. on Magnetohydrodynamic Ship Propulsion, MHDS 9. Kobe, Japan.

Rice, W.A. 1961. U.S. patent 2,997,013.

Way, S., and C. Devlin. 1967. Prospects for the electromagnetic submarine. Paper 67-432. AIAA. July 17-21.

CAUSEWAY CONSTRUCTION, ONOTOA, KIRIBATI

Gerry Byrne
Kinhill Riedel & Byrne
Melbourne, Victoria, Australia

ABSTRACT

A causeway is being built between two islands on the atoll of Onotoa in Kiribati. The causeway is mainly a strengthening of an old rock causeway that suffered periodic damage from storms. The new design and construction uses wide beaches in place of vertical rock walls. The paper describes the system of environmental monitoring to assess the effects of the causeway construction and the removal of sand from borrow pits on the sand flats on the lagoon side of the causeway.

INTRODUCTION

Onotoa is the southern-most atoll in the Gilbert chain of islands in Kiribati. The atoll is approximately 20 km long and 5 km wide. On the eastern side of the atoll there are two main islands of Temao and Otowae, with a smaller group of islands at the southern end.

Between the two main islands is a typical coral reef flat with three small islands. On this coral reef flat the people of Onotoa have built a causeway to provide transport between the two main islands. This causeway is presently being upgraded.

For many years the construction of this causeway has been a high priority on the atoll because of the difficulty of access from one island to the other by either walking or canoe (Government of Kiribati and Australian International Development Assistance Bureau, 1988). At high tide it is possible to use a canoe between the north and south but at low tide the exposed reef flat is so wide as to make it extremely inconvenient to travel by canoe. Most people in Kiribati have land holdings on a number of islands but the difficulty of access and transport inhibits the development of agriculture (mainly coconuts, taro, etc.).

HISTORY

Traditional Methods

The I Kiribati have a long history of coastal construction either to provide protection against coastal erosion or to provide land reclamation. In addition, the I Kiribati are very skilled at making elaborate rock fish traps on the ocean fringing reefs (Government of Kiribati and Australian International Development Assistance Bureau, 1988). The techniques of rock placing and securing have been extended to seawalls and also to small causeways connecting adjacent islands.

The traditional method of construction (Figure 1) is to collect either broken reef rock from the ocean side or part of the algal capping near the outer edge of the reef and to build vertical walls with the larger rocks wedged securely together. This method has

worked well for the traditional fish traps because they relatively quickly become cemented with the coralline algae and then become a permanent feature only to be damaged in major storms. The method also works well with some causeways between adjacent islands because the longshore movement of sand provides a buffer on one or both sides of the causeway.

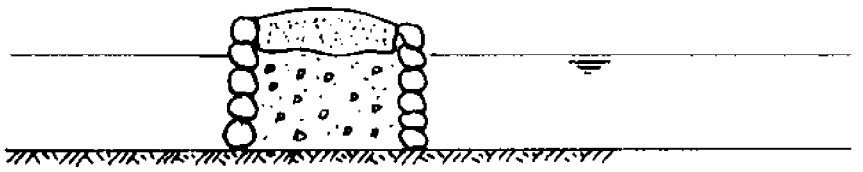

Figure 1. Original construction method

On Onotoa atoll, the method of construction was used for a much more ambitious project to provide a causeway linking the two main islands of Temao and Otowae. The distance between these two islands is approximately 2.2 km and a causeway was built by local labour from each of the villages using the traditional methods. This consisted of two outer vertical walls of large reef rock with a core between of smaller rocks gathered from the reef flat.

Initially the causeway was built just with local labour using hand-placed rocks. However because of the magnitude of the task involved, eventually the local Public Works Department assisted with trucks and excavators.

Problems

A number of problems have occurred with the causeway using these traditional methods.

The most immediate problem was that the height of the causeway was only about 2.2 m above low water mark with a tidal range of about 1.8 to 1.9 m. This meant there was frequent overtopping and the surface behind the large rocks scoured out and eventually caused the rock face to collapse. Because the opening was so long there was not enough longshore sediment transport to bring sand against the causeway and therefore provide some protection.

In the more traditional reclamation projects the scale of the reclamation is small, normally consisting of protection of one to two houses or one family group of houses. In that situation whenever there is storm damage, it is usually very localised and the family has a vital interest in immediately rebuilding the small section of wall that has collapsed.

On a large project such as this causeway, when damage occurred it was on a much larger scale than could be fixed quickly by a team from the local villages. In addition, as it was seen as a public work, there was much more reluctance on the part of individual villagers to take immediate action to fix the damage.

Because of the frequent collapses of the causeway walls and the inevitability of it eventually breaching and remaining breached, the Australian Government, through the Australian International Development Assistance Bureau, provided funds to rehabilitate the causeway to an acceptable level of engineering design.

Initially the work under the Australian contract was done by the local Public Works Department with technical assistance from Australia but for a number of reasons it eventually became the responsibility of the Australian consulting firm of Kinhill Riedel & Byrne (a division of Kinhill Engineers Pty Ltd). Our company is providing the technical designs and also the construction supervision. However all of the construction work is being done by I Kiribati, either seconded from the local Public Works Department or from the villages on Onotoa. The machinery being used for the construction was provided by Australia to the Public Works Department as part of the project.

OPTIONS

There were a number of options for the strengthening and rehabilitation of the causeway. These were studied in detail using a physical model built at the Department of Harbours and Marine Models Laboratory in Brisbane, Australia. The main options studied were a sloping rock wall using larger reef rock and a beach made from a variety of sands and gravels dug from nearby.

The model studies showed that if a rock armour solution (Figure 2) was to be feasible, the height of the rock wall had to be raised by approximately 1 m and the rocks had to be continuous at 1.5:1 slope on both sides with a rock covering over the top. It was not possible at any reasonable cost to design a causeway using a rock solution that prevented overtopping and therefore scour. This necessitated large rocks at the top of the sloping walls and under the road surface.

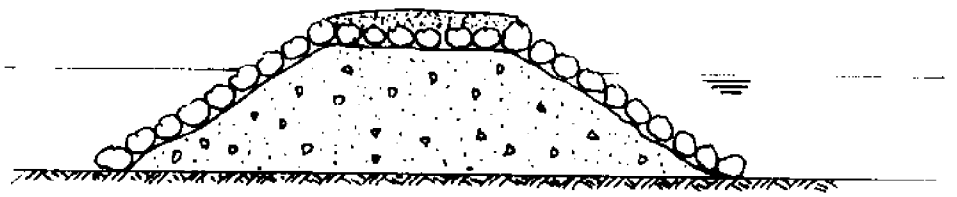

Figure 2. Rock armour alternative

The other alternative was to build a berm on both sides of the existing causeway of sand taken from the lagoonal reef flats (Figure 3). The aim with this alternative was to try to duplicate the coastal regime that existed on much of the nearby islands. Model studies were done of the shape of beach and particularly the height that would be required to limit runup. Conservative assumptions were made on the volume of sand required at any point to allow for immediate storm scour. Calculations were made of the wave refraction/friction across the reef and allowance was made for groynes and offshore breakwaters (on the reef flat) that would limit longshore transport.

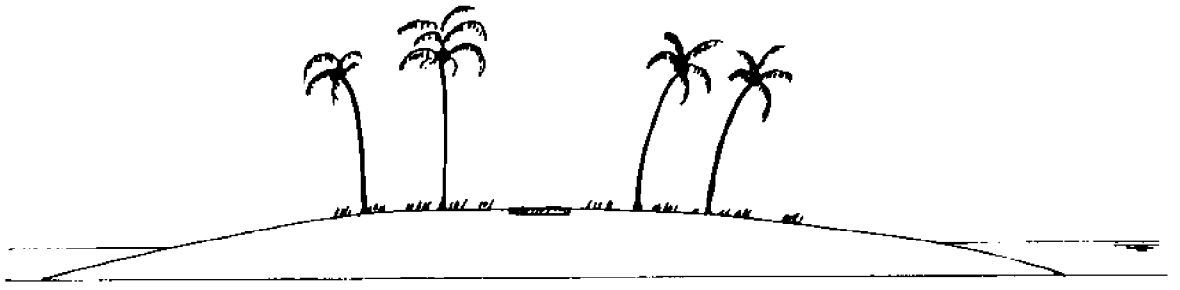

Figure 3. Beach alternative

Studies were also done into the feasibility of using artificial concrete armour units. In particular, an Australian design called Seabee units which could be manufactured easily locally using the cement and the reef muds was examined.

There was some discussion earlier in the project in Kiribati about the relative economics of using a rock wall solution or a sand bund solution. Both were tried initially and it soon became apparent that the sand bund solution was much more efficient in terms of the use of machinery and therefore was more economical.

This solution, which was preferred by the consultant, had two other advantages:

- there was a limited supply of reef rock available for the construction of the conventional causeway and it was considered that the use of this rock on the scale required for the rehabilitation of the causeway would cause considerable damage to the reef flat on the ocean side (there was almost no reef rock available on the lagoon side of the causeway);

- the sand bund solution could be planted up with a variety of trees and eventually would blend into the existing land environment. The material for the sand fill was mainly taken from a number of borrow pits dug from the fan of sand on the lagoon side of the original openings.

The option that is being constructed now is the sand bund solution. Some concrete armour units are being produced and these are being tried on an experimental basis on one of the small islets along the route where the existing road runs close to the shore.

CONSTRUCTION NEEDS

Equipment Maintenance

The equipment being used for the project consist of two excavators of about 15 tonne weight, four trucks, a front end loader and grader. These have been working on the project now for nearly two years in relatively harsh conditions and in salt water. They require constant maintenance because of the salt water environment and a workshop is set up at one end of the causeway.

One of the problems associated with this maintenance is the difficulties of getting spare parts to this remote location. A satellite receiver has been set up at the camp and equipment can be ordered by fax immediately from Australia.

Borrow Pits

The borrow pits for the excavation of the material are all on the lagoon side of the causeway as far away from the causeway as is practical, consistent with a reasonable amount of working time between tides. The material that has been excavated is mainly a mixture of sands which are predominantly foraminiferous and appear to have been derived predominantly from lagoonal sediments.

The sands are about 1 m thick and overlay a thick deposit of coral detritus that appears to have washed through from the ocean side at some stage. This consists of a wide range of materials from fine muds to sands to gravel sized pieces of heliopera with some occasional large boulders of porites. Whenever the porites boulders are found they are segregated and used later for making small offshore breakwaters.

Beach Formation

The method of construction is to place a 14 m wide berm on either side of the existing causeway and to let normal wave action create a beach. Normally a beach begins to form within a couple of days and a relatively stable alignment forms in about one month (Kinhill Riedel & Byrne, 1992d). Once the beach has formed, it tends to have an armouring of coral pieces of 25 to 100 mm grain size. A consequence of this method of construction is that there is quite often a plume of milky fines generated during the beach formation phase which is swept out to sea across the ocean reef flat (Kinhill Riedel & Byrne, 1992a).

Given the limited amount of data on offshore wave directions available before the project started, it was difficult to be confident about the accuracy of forecasts of sediment movement. During the project construction this is being monitored on daily to weekly basis at a number of locations along the causeway. As sediment moves, small offshore breakwaters are being constructed to limit the drift of the sediment movement. These consist of a line of rocks approximately 1 m high. They are on the reef flat about 50 to 100 m offshore of the causeway itself (the ocean reef flat in the area being considered is about 400 m wide).

The longterm response of the beach is being inferred from the position and shape of the very fine muds that are being segregated out from the main part of the fill. Obviously these very fine materials are much more mobile than the larger pieces and give a very quick indication of where there is sediment erosion and sediment build up.

Except for the initial plume that is generated as the beach forms in the first week, very little of the sediment gets washed out across the reef flat. Most of it, even the very fine material, stays as quite a distinct toe at the bottom of the beach slope (Kinhill Riedel & Byrne, 1992d).

ENVIRONMENTAL ISSUES

A comprehensive series of environmental monitoring activities is being undertaken throughout the project. These are described in outline form below.

Transects

At a very local level, transects are being taken at approximately 50 m intervals along the causeways on both sides. These are being monitored on a weekly basis and also immediately after any storm activity. With these transects it is possible to get a very quick picture of a rate of formation of the beaches and the rate of any sediment movement along the beach. It is also possible, particularly using the very fine materials, to gain an understanding of the effectiveness of any groynes and offshore breakwaters that are being installed.

Effects on Corals

There was some concern that the plume generated as the beach forms might affect the corals on the ocean reef flat (Kinhill Riedel & Byrne, 1992a). These corals are very sparse as most of the reef flat is the coralline algae. However control sections have been set up where there are stands of acropora, porites and easily identifiable algal corals both in areas where the plumes are likely to go and in other areas where the plume has no effect. These are being visually monitored on a regular basis to see if there is any observable stress placed on the corals.

Except in the immediate construction zone to date, there has been no observable deleterious effect of the plume.

Current Movements

Current movements in the lagoon are being measured to examine in detail the exchange of water into the lagoon immediately adjacent to the causeway. As the initial causeway was built before this project commenced, the current movements are not measuring the current patterns that would have occurred without a causeway. However it should be possible at the end of the investigations to determine the rate of exchange of water on the lagoon side at various parts of the atoll.

At this stage there are plans for the construction of an opening in the causeway to allow some water from the ocean side into the lagoon. There is an a priori assumption that some exchange is better than what is occurring now.

In previous studies of the more northern atoll of Tarawa, investigations were undertaken of the planktonic distribution across the lagoon. While in many ways these studies were inconclusive, it was quite possible to identify that the plankton in the waters on the windward side of the atoll and in the lagoon on the windward and leeward side of the atoll and in the ocean on the leeward side of the lagoon are all different. It was not possible to say with these plankton what effect the various types had on the ecology of the lagoon. However it was assumed that because they were different, it was important that some at least of the plankton from the ocean on both sides were able to enter the lagoon.

Satellite Imagery

Transects done across the lagoon and particularly on the leeward side of the lagoon have shown large areas of dead coral and coral under stress. There is evidence of

Crown of Thorns infestation in certain areas but the reason for the loss of coral is not clear.

SPOT satellite imagery has been ordered for this atoll and for the next nearest atoll and this imagery will be used to try to examine the differences between this atoll and a nearby atoll that does not have the same level of causeway construction. In this way it may be possible to determine the cause of the problem, whether it is localised or whether it affects the next nearest atoll as well.

There is no existing SPOT image of either atoll however there is a very early Landsat image of the atoll with some cloud cover.

Historical aerial photography is also being purchased and the photography and imagery will be used to map the overall picture of the lagoons.

Borrow Pits

The options for the provision of material for the construction of the causeway are very limited. There is virtually no material available on land as all the available space on the islands is used either for villages or for coconut plantations. The only other options are the reef flats on the lagoon or the ocean side. Earlier activity had taken material from borrow pits on both sides of the causeway. However, it was considered it was less desirable to take material from the ocean side of the causeway than from the lagoon side, specifically because there is some evidence of algal and other growth on the ocean side and virtually none on the lagoon side. In addition, it was much easier to dig the material on the lagoon side.

On the lagoon side the two options were to scrape a very large area of the foraminiferal sands down to about 1 m, or to dig deep ponds and limit the extent of the excavation. To minimise the environmental effects most of the activity has been concentrated on digging deep borrow pits. These borrow pits are being monitored on a regular basis to determine the recolonisation of the borrow pits and whether there are any longterm detrimental effects.

In fact, the borrow pits are extremely popular with fishermen because they seem to be a breeding ground for moray eels which are considered a local delicacy. Even when excavation activity is being undertaken in a particular borrow pit and when that borrow pit is continually milky white from the effects of the excavation, there are large numbers of fish recolonising the pits. Initial monitoring activities were inconclusive because using Western methods and nets, we were unable to catch many fish and we began to draw the conclusion that fish were not recolonising in the pits. However, a local fisherman was engaged to catch fish on a regular basis in the borrow pits using traditional methods and the change in the results was dramatic.

Ciguatera

Ciguatera poisoning is common throughout the Gilbert Group and a number of outbreaks have occurred over the years on Onotoa. Some surveys are being carried out during the project to see whether there is any increase in Ciguatera during this project.

While previous construction activity or damage to coral reefs has been cited in very many papers as an initial cause of the development of Ciguatera, the exact relationship between the destruction of coral reef and the incidence of Ciguatera is not clear.

Certain guidelines had been developed previously on the method of construction of holes or channels in a coral reef environment to try to minimise the extent of the exposed substrate which is known to be the trigger of the series of biological events that eventually can cause an outbreak of Ciguatera.

With the monitoring that is taking place, to date there has been no evidence of any abnormal outbreak of Ciguatera on the islands.

PLANTING

The causeway as constructed consists of a bund 3 m high and about 35 m wide. As the bund is affected by waves, a beach forms with a slope of about 1:6. The eventual width of the construction is about 50 m. Initially the total surface was compacted because of the truck activities but a concerted planting effort is underway where holes are dug at regular intervals and trees are being planted on both sides of a narrow roadway.

The purpose of this is:

- to try to re-establish an acceptable visual outlook along the causeways;
- to develop a root system in the near surface to act as a buffer to delay the erosion of sand during storms;
- to limit the effect of any wind action on the surface and the occasional overtopping that might occur during storms.

Initially on both sides of the roadway, two lines of coconut trees are being planted at approximately 5 m spacings and to the seaward of that is a line of pandanus. In addition, other local coastal vegetation is being encouraged to grow. The planting of the coconut and pandanus is being assisted enthusiastically by people from the local villages because the economic benefits of these can be seen.

Other vegetation which might be important from a coastal stability point of view is growing naturally but with no encouragement from the villagers because the economic benefits are not immediately apparent.

After approximately four months the survival rate of the coconuts is very close to 100% and the survival rate of the pandanus is between 60-80%.

OPENING

There is one existing small opening in the old causeway and water levels and flows on both sides of the old causeway are being monitored both during spring and neap tides and through all stages of the tide. There is virtually a continuous flow of water from the ocean into the lagoon through the existing opening. This appears to be mainly because of wind and wave setup on the ocean side and the moating effect caused by the build up of coralline algae on the ocean side (even though this moating effect is not nearly as pronounced as it is on more southern island groups such as in Tonga and the Cook Islands).

A large opening is being designed at present (approximately 10 m wide) and the effects on this opening will be monitored. At this stage, even though the existing very

small opening of the causeway has been there for some years, it is not possible to easily identify any change in the biota near the opening compared to other places along the causeway.

CONCLUSIONS

There is the general perception within the scientific community that any man-made changes to fragile coral ecosystems is undesirable. There is also a reasonable amount of literature on the detrimental effects of causeways and other excavation activities on coral atolls in the Pacific (Weber & Woodhead, 1972; Maragos & Jokiel, 1978; Goreau, et al., 1991). Because of this, there is some reluctance to embark on projects of this nature. However in the present circumstance at Onotoa, the causeway was constructed and there was an overriding economic and social reason for strengthening the causeway to make it into a functional structure.

In the circumstances, the present construction activity is able to be treated as a full scale experiment of the effects of such construction on a reef and lagoon environment. A number of model studies have been undertaken of the physical effects of the causeway and opening and a comprehensive set of environmental measurements are being undertaken throughout the construction to measure the effects.

It will be some time before the ultimate effects can be known with any certainty. However at this stage approximately nine months after the commencement of large scale activity and several years after the closure of the initial opening by the causeway, there are very few detrimental effects on the nearby biota than can be measured.

Environmental monitoring will continue for the duration of this project and for some time into the future after the project has been completed.

REFERENCES

Banner, A.H., and J.E. Randall. 1952. Preliminary report on marine biology study of Onotoa Atoll, Gilbert Islands. *Atoll Research. Bull.* **13**:1-62.

Cloud, P.E. 1952. Preliminary report on geology and marine environments, Onotoa Atoll, Gilbert Islands.

Goreau, T.J., R.M. Fujita and M.H. Verne. 1991. Global coral reef alliance. Coral Reef Newsletter **23**:23-25.

Government of Kiribati and Australian International Development Assistance Bureau. 1988. Republic of Kiribati North Tarawa & outer islands causeways study.

Kinhill Riedel & Byrne. 1992a. Environmental assessment, Kiribati Outer Island Development Programme, Onotoa Causeway Project. Prepared for Australian Intl. Development Assistance Bureau.

Kinhill Riedel & Byrne. 1992b. Onotoa Causeway Project. Environmental audit of construction camp, 7 June 1992. Prepared for Australian Intl. Development Assistance Bureau.

Kinhill Riedel & Byrne. 1992c. Onotoa Causeway Project. Environmental programme field visit, June 1992. Prepared for Australian Intl. Development Assistance Bureau.
Kinhill Riedel & Byrne. 1992d. Onotoa Causeway Project. Construction Progress Report, August 1992.

Maragos, J., and P.L. Jokiel. 1978. Reef corals of Canton Atoll II. Local distribution. *Atoll Research Bull.* **221**:71-98.

Weber, J.N., and P.J. Woodhead 1972. Carbonate lagoon and beach sediments of Tarawa Atoll, Gilbert Islands. *Atoll Research Bull.* **157**:1-29.

INTRODUCTION OF MARINE ARCHITECTURAL BUILDINGS BUILT INSIDE THE HARBOR OF JAPAN

Osamu Saijo
Nihon University
Chiba, Japan

ABSTRACT

Marine architectural buildings constructed in the last five years in Japan are introduced. The notable features of such marine architectural buildings follow:

a) buildings are built inside the harbor and near the seashore,
b) almost all of them have been constructed by floating-type structural systems, and
c) they have been built in accordance with the Building Standard Law.

The subjects to be discussed are related to the introduction of existing buildings, the reason of application with the Building Standard Law, and remarkable points on the structural design and mooring system.

INTRODUCTION

At this time, construction locations of almost all standing marine architectural buildings are inside the harbor and near the seashore. Half of the structures are floating-type moored by cables or dolphins; and, in many cases, there is a high percentage of reuse of retired ships.

Existing marine architectural buildings are standing not only on the boundary zone in the field of engineering which is mainly covered by naval architectural engineering, civil engineering and architectural engineering but also on the boundary zone under the jurisdiction of supervising government offices which issue building permits. Before these types of marine architectural buildings (particularly those referred to as moored floating structures) had been constructed, government offices could retain the span of work. However, after these types of marine architectural buildings were built and defined, conflict arose in terms of supervision or issuance of building permits.

The general categories of engineering structures are shown in Figure 1. The difference between architectural buildings and other types of buildings can be defined by usage.

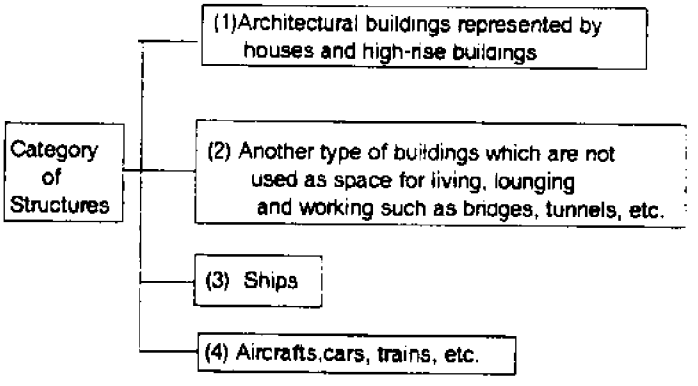

Figure 1. Categories of buildings and structures

In general, building permission for construction of category (1) is under the jurisdiction of the Ministry of Construction. Another type of building in category (2) is controlled by the Ministry of Construction and the Ministry of Transportation. Besides, there is a steady border line between architectural field and civil engineering field in connection with above categories ((1) & (2)). The span of work is clearly and independently maintained as reflected in the Japanese system. For instance, such cases can be seen in university educational system, administration, etc.

Coastal and harbor engineering belong to the civil engineering field. At the present, there are many construction achievements of harbor facilities.

Ship building, aircraft and car industry with relation to vehicles for transportation are under Ministry of Transportation control. Naval architectural engineering has a long history and a lot of experiences. It has continued to offer comfortable living space in ships for crew and passengers.

Figure 2 illustratess the concept of moored floating structures existing on the boundary zone and applicable laws. There are floating structures called "marine architectural buildings" used in the language of architectural engineering, while on the other hand they are called "long-term moored ships" in naval architectural engineering. The figure denotes independent and common portions for construction of marine structures. Each supervising government office insists on its interests with relation to building code interpretation, administrative matters and historical background as to where this building should belong. Therefore, it is a fact that inconsistencies continue to exist and constructors have to submit their design documents to all of the concerned government offices when obtaining building permits.

LAW SYSTEM

A floating type structure moored by cable or dolphin has a particular feature as to where it belongs, under a law system (Floating Structures Association of Japan, 1992). The different applicable laws and supervising government offices are as follows:

a) the Building Standard Law (Housing Bureau, Ministry of Construction)
b) the Port and Harbor Law (Ports and Harbors Bureau, Ministry of Transportation)
c) the Ship Safety Law (Maritime Technology and Safety Bureau, Ministry of Transportation)

The main purpose for writing this paper is to introduce marine structures that have been applied under the Building Standard Law, especially in the field of architectural engineering, and elaborations for such applications will be described.

The reason that the Building Standard Law is applied to these buildings, referred to as retired ships which were used formerly as passenger ships, still depends on its present usage. Public facilities such as aquariums, museums, restaurants, etc. are a few examples.

If forms and structures are similar to ships, and if they are constructed on or under the sea, this is a basis for applicable law to consider the purpose as to what type of service is being offered by the building. Specifically, the 38th article of the Building Standard Law is applicable. This article describes newly-developed material or particular building materials and inventive structural methods with no previous

experience, often called the brand new ones. As they are brand new, requirements are necessary to verify validity or authenticity by the Ministry of Construction so those with greater or equal strength and effects can be compared with former ones.

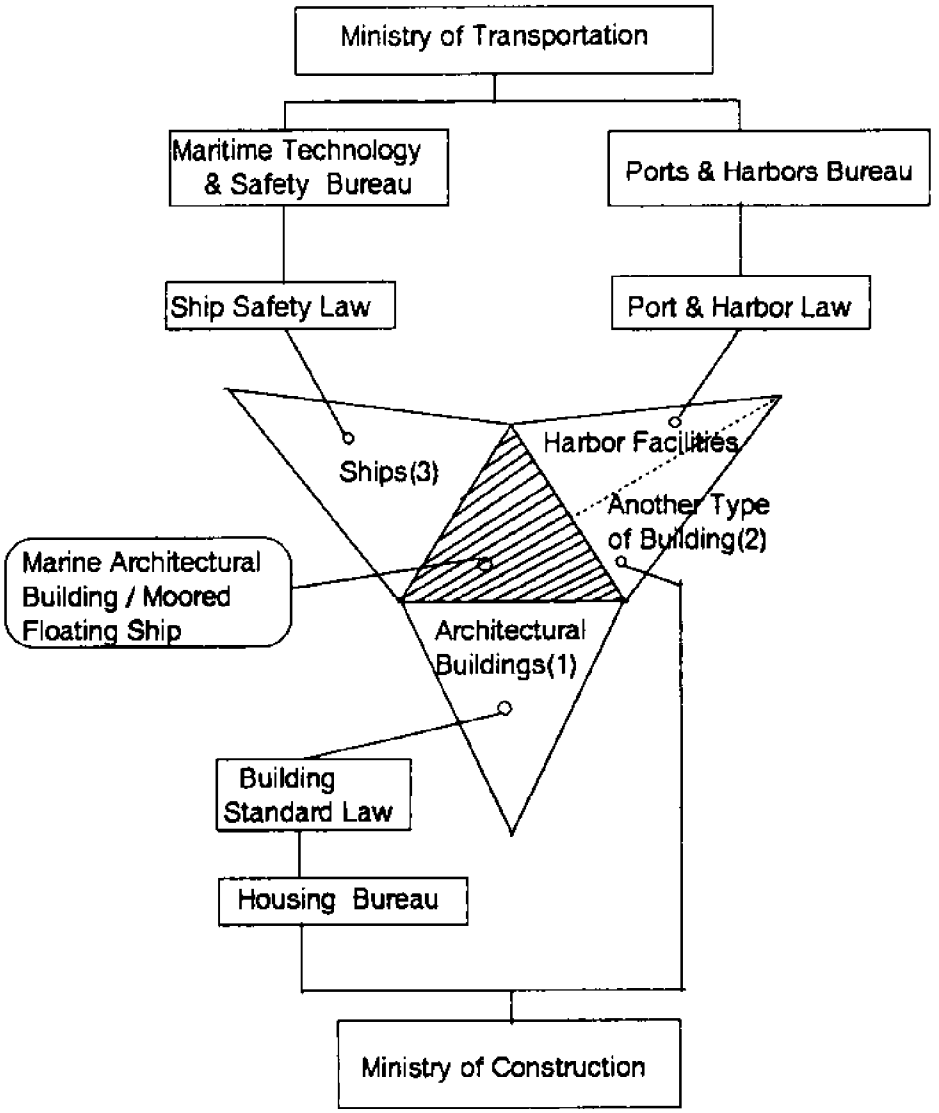

Figure 2. Concept of applicable laws and supervising government offices

MARINE ARCHITECTURAL BUILDINGS EXISTING IN JAPAN

The marine architectural building map (Figure 3) shows that most of the buildings are located in the western part of Japan. One building in Hakodate City on Hokkaido Island and another in Aomori City on Honshuu Island are both used as maritime museums. These are two typical cases of retired ships being used as museums for its secondary purpose in the present time.

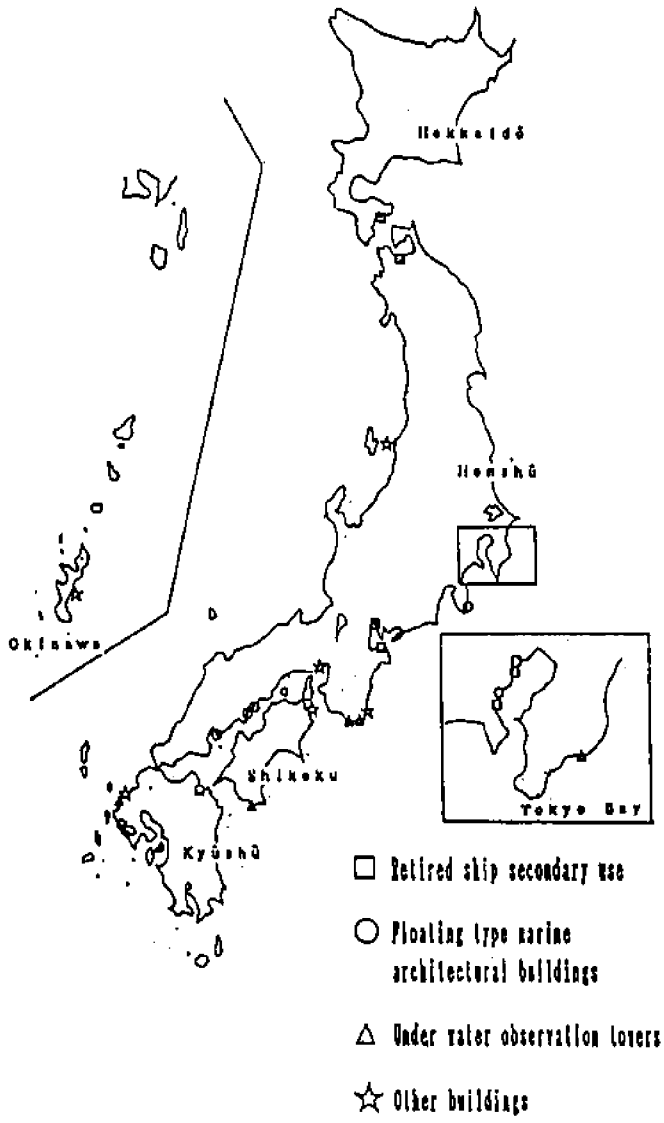

Figure 3. Distribution of marine architectural buildings

Previously these ships served as passenger ferry boats crossing between Aomori City and Hakodate City. They paved the way towards employment and business opportunities to many. Somehow those days were now a part of the past and presently worth reminiscing to a lot of citizens who were once passengers, especially Japanese people. The sweet memories of the good old days using ferry boats remain in their hearts. Because of progress, these ships had become inactive since an undersea bed tunnel was constructed connecting Aomori City and Hakodate City. Both cities and Tokyo have decided to preserve them as commemorative ships.

Table 1 gives a list of retired ships secondary use. *Brazil-maru* was formerly a passenger ship which served in Japanese immigration to South America; at this time it

Table 1. Retired ships secondary use

Name	Location City (Prefecture)	Former service	Present service	Date of permission	Displacement tonnage
Brazil-maru	Toba (Mie)	Passenger ship	Food mall	March 1973	11,000 ton
Souya	Tokyo	Observation ship for the Antarctic Ocean	Museum	July 1978	2,734 ton
Fuji	Nagoya	The same as above	Museum	March 1984	5,250 ton
Oriana	Beppu (Ooita)	Passenger ship	Restaurant Movie theater Conference room	November 1985	41,902 ton
Hakkou-maru	Aomori	Passenger ship	Museum	March 1990	5,382.85 ton
Mashuu-maru	Hakodate (Hokkaido)	Passenger ship	Museum	July 1990	5,374.85 ton
Youtei-maru	Genova Tokyo	Passenger ship	Exhibitio hall (Genova) Museum (Tokyo)	April 1991	5,375.9 ton
FCAP	Yokohama	Cargo ship of cars (1447 cars)	Parking lot (283 cars)	October 1990	5, 225 ton

Table 2. Underwater observation towers

	Location City (Prefecture)	Date of permission	Size Waterdepth (Distance From shore line)
(1)	Shirahama (Wakayama)	March 1966	4m 16m (100m)
(2)	Kushimoto (Wakayama)	February 1969	7m 14m (-)
(3)	Saikai Town (Ehime)	June 1971	- 13m (-)
(4)	Hato Peninsula (Saga)	October 1972	4.3m 20.4m (-)
(5)	Katsuura (Chiba)	March 1977	5.7m 12.7m (-)
(6)	Shirahama (Wakayama)	May 1986	3.9m 17.7m (95m)

is used as a food mall. The ships *Souya* and *Fuji* were used for observing the Antarctic; presently they are being used as museums. The *Oriana* is now in service as a restaurant, catering wedding ceremonies, as well as partly providing rooms for conferences and theater. Three more retired ships namely: *Hakkouda-maru* (Aomori Water Front Co., Ltd., 1990), *Mashuu-maru* (Hakodate Sea Port Plaza Co., Ltd., 1990), and *Youtei-maru* (Museum of Maritime Science, Japanese Foundation for Promotion of Maritime Science, 1991) were also used as ferry boats between Aomori and Hakodate. The first two ships served as museums during this period and the latter sailed to Genova, Italy. After an international exhibition closes in Genova, the *Youtei-maru* will cruise back to Tokyo where it will remain as a commemorative ship. A ship named *FCAP* (Floating Car Park Yokohama Co., Ltd., 1990) which was formerly a cargo ship for exporting cars serves as a parking lot in Yokohama City.

Table 2 shows six underwater observation towers (Japan Kenchiku Center Foundation, 1987). They include corridors enabling viewers to watch amazing underwater scenes.

Floating-type structures are listed in Table 3 and classified by structural type and secondary use or as newly constructed buildings. One floating structure called "floating island" situated at Sakaiga Beach was constructed as an aquarium (Setonaikai Central

Table 3. Classification by structural type and secondary use or newly-constructed buildings

Name	Structural type	New / Secondary use	Date of permission
Tokokushima fishing park	Fixed	(Cancelled)	October 1987
Sakaiga Beach Floating Island	Floating	New	Octooer 1988
Tallship simulation theater	Floating	New	January 1990
Hakkouda-maru (Museum)	Floating	Secondary use	March 1990
Mashuu-maru (Museum)	Floating	Secondary use	Julty 1990
Amusement ship called Royal Phoenix	Floating	New	February 1990
Parking lot ship called FCAP	Floating	Secondary use	October 1990
Sewage facility installed to Sakaiga Beach floating island	Floating	New	October 1990
Floating platform: Waiting hall landing & access bridge restaurant at Yokohama redevelop(ment area for 21 Century	Floating	New	November 1990
Youtei-maru (Museum)	Floating	Secondary use	April 1991
Removal of simulation theater	Floating	Removal	July 1991
Shimoda aquarium	Floating	New	1992

Development Co., Ltd., 1989). A provision for sewage disposal facility is also attached to "the floating island." Another floating-type structure called "simulation theater" allows one to imagine being inside a tall ship at Nagasaki during the 16th century (Nagasaki Holland Village Co., Ltd., 1989). The "Royal Phoenix" at Kure, Hiroshima, provides part of an amusement park (Kure city 1990). The "Shimoda floating aquarium" would be a good example examined by the latest appraisal work (Fujita Kankoo Co., Ltd., 1991). In Yokohama, a floating platform has been installed and is used as a waiting hall, landing and access bridge, and restaurant (Yokohama City, 1990).

The list of architectural buildings which do not belong to categories or Tables 1, 2 and 3 are shown in Table 4. These buildings include the fishing park platform in Kobe City, another which is supposedly used as a fishing park in Tokushima, and others that are used as am office on sea berth and platform, an underwater observation corridor (Japan Shield Engineering Co., Ltd,. 1988), and a base and frame used to display a retired whale ship.

Table 4. Other types of buildings

Name/ Purpose	Location City (Prefecture)	Service / Facilities	Date of permission	Building height (Distance from shoreline)
Fishing park	Kobe	Management office Fishing platform	November 1973	27.5m (400m)
Fishing & Amusement park	Tokushima (Tokushima) (cancelled)	Restaurant Diving spot Fishing platform Underwater corridor Heliport Visitor's platform	October 1987	(-) 4000m
Management of sea-berth	(Okinawa)	Office Sea-berth platform	November 1975	8.3m (1000m)
Living space on Agaoki Kita oil platform	Aga (Nigata)	Management of oil & gas production	December 1982	15.9m
Underwater observation corridor	Chinzei Town (Saga)	Observation	October 1971	5.4m (-)
Construction of base & frame to display a whale ship	Taji Town (Wkayama)	Preservation as a commemorative ship	December 1977	(-)

CLASSIFICATION BY STRUCTURAL TYPE

Table 3 shows a list in relation with structural system of buildings constructed in the past five years. Except for Tokushima fishing park which was later canceled, others were constructed under the floating type structures. There are six newly-constructed floating type structures and four floating-type structures for secondary use.

ENVIRONMENTAL LOAD CALCULATION

Figure 4 is a flow chart of environmental load estimation for structural design. For seismic load effect, floating structures moored by dolphin and fender are also subjects to be examined.

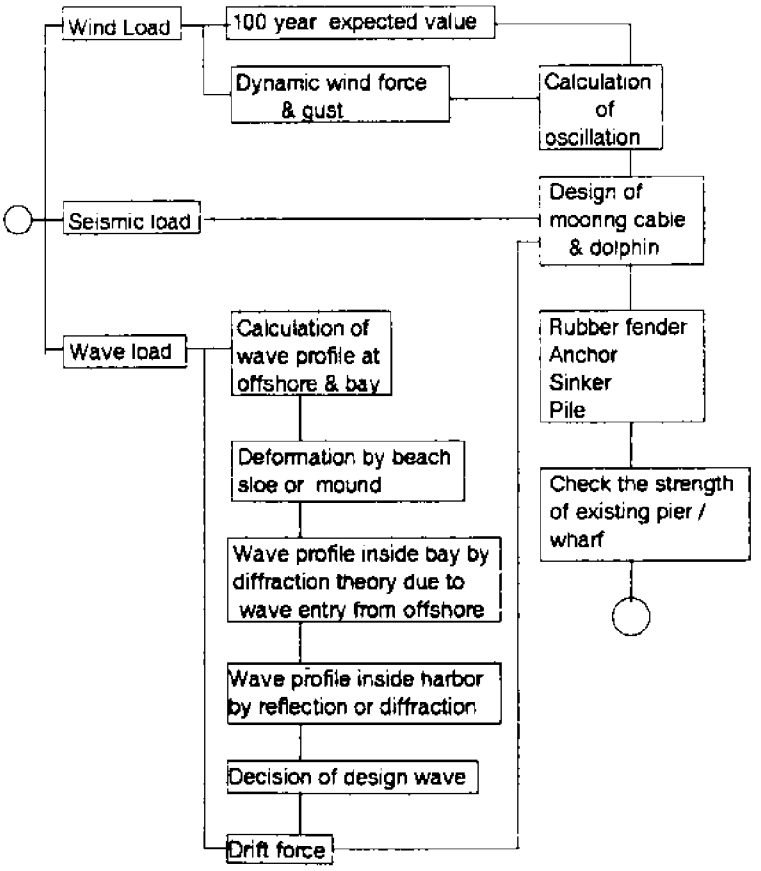

Figure 4. Flow chart of environmental load estimation

MOORING SYSTEM

Table 5 shows illustrations of typical mooring systems. Mooring system No. 1 is illustrates the case of the "floating island" at Sakaiga Beach. This system is composed of chains and sinkers. Horizontal forces transferred to four chains are resisted by passive earth pressure. Soft seabed mud around the sinker was replaced with sand and riprap to keep enough passive earth pressure. Mooring system No. 2 shows the case of Hakkoda-maru. Its mooring system is composed of nylon ropes, dolphins and pillow-type rubber fenders. In particular, the sliding possibility of this existing wharf was checked against forces from the rubber fender caused by wind forces calculated by 100-year return period. System No. 3 to 6 are dolphin-type mooring systems. Each system differs from the other. The basic difference among them is the number of supporting points in horizontal displacements given by a single dolphin. In system No. 3, each single dolphin having one fender controls only one direction either front or rear displacement in surging motion.

Table 5. Mooring system

1	Cable	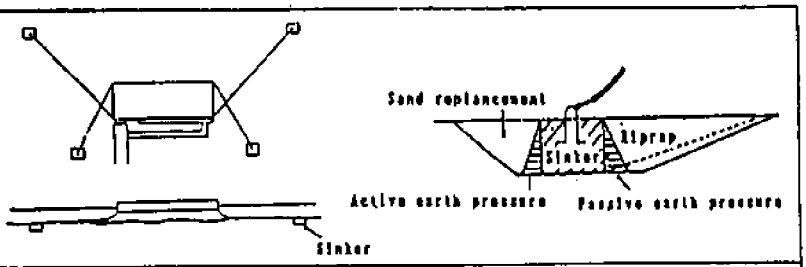
2	Cable & Fender	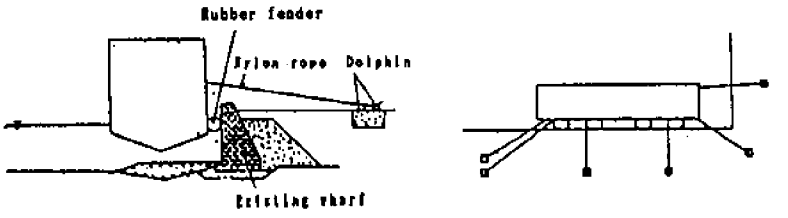
3	Dolphin & Fender	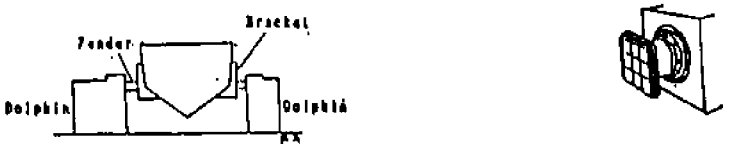
4	Dolphin & Fender	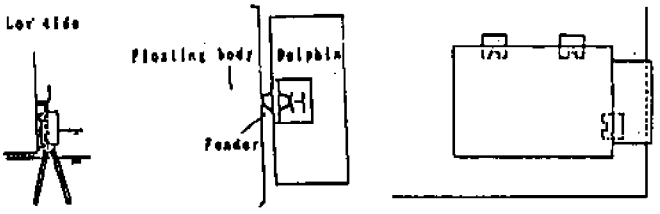
5	Dolphin & Fender	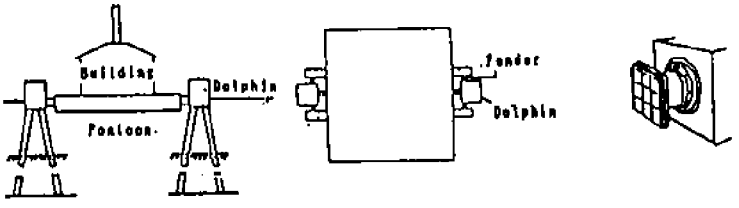
6	Dolphin & Fender	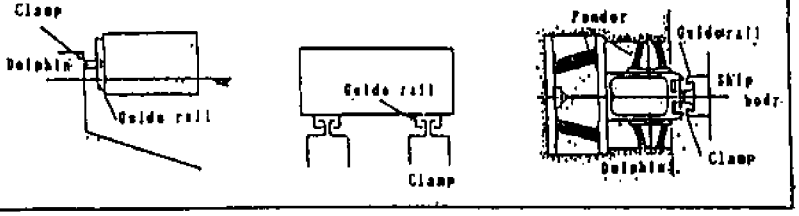

Each single dolphin installed with two fenders in system No. 4 controls two directions in surging motion. For system No. 5, each single dolphin with three fenders controls one direction in swaying motion and both directions in surging motion. In system No. 6 each single dolphin installed with three fenders and one clamp controls four horizontal directions. This system has the most complicated function wherein swaying and surging motions can be controlled by a single dolphin. With respect to vertical displacement, all systems are adjustable to the height of tide.

CHECK POINTS FOR APPRAISAL WORKS

Figure 5 gives a flow chart of general guidelines for prevention against disaster and structural design on the appraisal works.

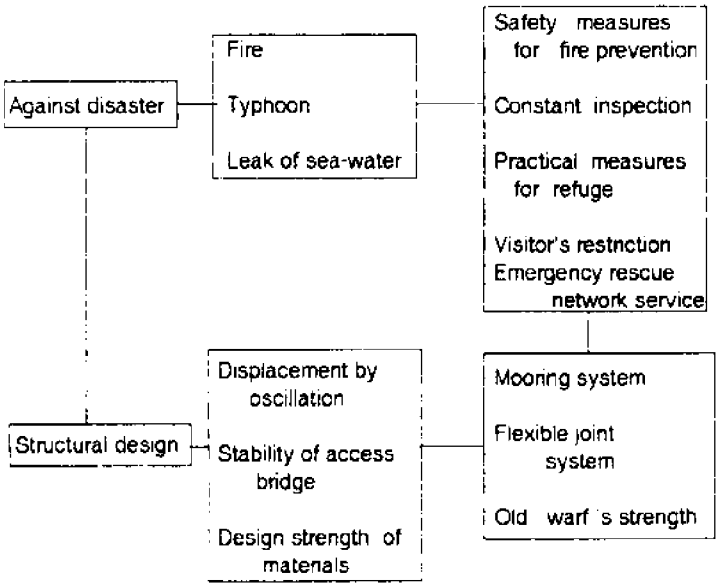

Figure 5. Check points on marine architectural buildings

CLOSURE

Marine architectural buildings appraised by the Building Standard Law have been introduced and discussedd. It is believed that the number of this type of building will surely increase in the near future and a call for a specific law is in demand.

ACKNOWLEDGEMENTS

Sincere thanks are expresse to the Kenchiku (Architectural) Center and to all persons who participated in the design and construction projects, as well as those who have given other forms of assistance.

References for this report have been provided by unpublished data from the Japan Kenchiku Center and also marine architectural building specifications.

REFERENCES

Building Code or Design Recommendation

Architectural Institute of Japan. 1985. Recommendation for Structural Design of the Oceanic Architecture (Fixed-Type Structure) (in Japanese).

Architectural Institute of Japan. 1980. Recommendation for Structural Design of the Oceanic Architecture (Floating-Type Structure) (in Japanese).

Japanese Government. 1950. Building Standard Law of Japan (in Japanese).

Design Specifications

Aomori Water Front Co., Ltd. 1990. Rebuilding of Seikan Ferry Boat; Hakkouda-Mamaru to a commemorative ship (in Japanese).

Floating Car Park Yokohama Co., Ltd. 1990. Construction of Floating Car Park (in Japanese).

Fujita Kankoo Co., Ltd. 1991. Construction of Shimoda Floating Aquarium (in Japanese).

Hakodate Sea Port Plaza Co., Ltd. 1990. Rebuilding of Seikan Ferry Boat; Mashuu-maru to a commemorative ship (in Japanese).

Japan Kenchiku Center Foundation. 1987. List of Appraised Marine Architectural Building (in Japanese).

Japan Shield Engineering Co., Ltd. 1988. Construction of Tokushima City Fishing Park (in Japanese).

Kure City. 1990. Construction of Moored Floating Structure; Royal Phoenix (in Japanese).

Museum of Maritime Science, Japanese Foundation for Promotion of Maritime Science. 1991. Rebuilding of Seikan Ferry Boat; Youtei-maru to a commemorative ship (in Japanese).

Nagasaki Holland Village Co., Ltd. 1989. Construction of Simulation Theater of Tallship (in Japanese).

Setonaikai Central Development Co., Ltd. 1989. Construction of Sakaigahama Floating Island (in Japanese).

The Floating Structures Association of Japan. 1992. Report of Applicable Law for Floating Structures (in Japanese).

Yokohama City. 1990. Construction of Wharf at MM21 Water Front Area in Yokohama (in Japanese).

STORM SURGES AND TIDES AROUND SRI LANKA

R.F. Henry and T.S. Murty
Institute of Ocean Sciences
Sidney, British Columbia, Canada

ABSTRACT

On average, there has been about one damaging surge per decade in the waters around Sri Lanka, with more frequent smaller surges. Although the tidal range is not large, in surge forecasting it is important to have a detailed understanding of the tides, since damage is greater when peak surge coincides with high tide.

Study of storm surges and tides around Sri Lanka is made difficult by the shortage of meteorological and tide gauge records. There are a few relatively short coastal gauge records, but no deep sea tide gauges have been installed within several hundred kilometres of the Sri Lanka coast.

On the west coast of the island, there have been sudden increases in water levels forced by atmospheric gravity waves from mesoscale weather systems. Tropical cyclones from the south Andaman Sea normally pass north of Sri Lanka, but occasionally make landfall on the east coast, causing significant damage. The meteorological and surge information available from past events fall far short of requirements for full hindcasting studies.

Typical wind fields for cyclones, derived from observations in other tropical seas, were used to drive surge models for the east coast, and, similarly, typical wind fields for rissaga were assumed in studies of the west coast. Suitable conditions for forcing tidal models along their outer sea boundaries were deduced from cotidal charts computed with global tidal models, with some modification based on coastal gauge data.

INTRODUCTION

Storm surges are water level oscillations due to tangential surface wind stresses and sea level atmospheric pressure gradients associated with travelling weather systems. Tropical cyclone generated storm surges have had significant effects on the lands surrounding the Bay of Bengal and the Gulf of Mexico. Of the countries around the Bay of Bengal, Bangladesh experiences the most damaging surges, with India and Burma being somewhat less affected. It is not generally realized that Sri Lanka also has a storm surge problem, although the severity and frequency of storm surges there is much less than in Bangladesh.

In Sri Lanka, storm surges associated with tropical cyclones occur mostly on the northeast coast. Tropical cyclones are almost unknown on the west coast of Sri Lanka; however, flooding occurs on occasion, and the causes have never been satisfactorily accounted for. We suggest the so-called "Rissaga phenomenon" as one plausible explanation for the occasional high water levels on the west coast of Sri Lanka. Study of these meteorological effects on water levels is preceded by a discussion of tidal elevations, which, although rather small around Sri Lanka, cannot be ignored.

TIDES AROUND SRI LANKA

To our knowledge, there has been no publication to date in the open literature devoted to tides in the waters around Sri Lanka, although, some information is available from publications on tides in the Indian Ocean. Several studies on global ocean tides show co-tidal charts for the Indian Ocean (e.g., Schwiderski, 1980; Marchuk, et al., 1984). The resolution of the waters around Sri Lanka is so coarse in these models that it is almost impossible to obtain any detailed information on the tidal regime near the coasts.

The numerical model of Bogdanov and Kharkov (1976) for the Indian Ocean made use of a grid of 5°x5° in latitude and longitude; hence the co-tidal charts given for the two main semi-diurnal tidal constituents M_2 and S_2 and the two principal diurnal tidal constituents K_1 and O_1 do not contain much detail. By far the most detailed co-tidal charts produced for the north Indian Ocean are those of McCammon and Wunsch (1977). They constructed these charts by empirical methods from existing data and some deep ocean pressure gauge measurements. Even though these charts provided more detailed results than other studies, they are not detailed enough for the waters around Sri Lanka, except possibly near its southeast coast.

Henry and Murty (1983) and Elahi (1983) used numerical models to construct co-tidal charts for the Bay of Bengal and the Arabian Sea respectively. The modeled areas in these studies are essentially north of the study area and the results do not give any reliable information on tides around Sri Lanka. Thus it is fair to say that, until now, no detailed study of the tidal regime in the waters around Sri Lanka has been published. This paper is an initial effort to coordinate the limited information available.

THE NUMERICAL MODEL

The numerical model used here for simulating tides and storm surges covers a rectangular region from 7°N to 12°N and 77°E to 84°E (Figure 1). Figure 1 also shows the locations of the tide gauges from which data is used in this study. Contours of water depth are shown in Figure 2 and the grid for the numerical model is shown in Figure 3. The grid interval is 9 km in both horizontal directions.

In addition to the numerical simulation of selected storm surge events, our aim is to produce co-tidal charts for the largest constituents. For this purpose we start with the quasi-linear version of the shallow water equations.

$$\begin{aligned} \eta_t &= -(du)_x - (dv)_y \\ u_t &= -g\eta_x + fv - F^{(x)} + G^{(x)} \\ v_t &= -g\eta_x - fu - F^{(y)} + G^{(y)} \end{aligned} \tag{1}$$

where

$\eta(x,y,t)$	=	elevation of water surface above mean level
$u(x,y,t)$	=	depth-averaged velocity in x-direction
$v(x,y,t)$	=	depth-averaged velocity in y-direction
$d(x,y)$	=	mean water depth
x,y	=	Cartesian coordinates in horizontal plane
f	=	Coriolis coefficient (assumed constant)
g	=	acceleration due to gravity
t	=	time

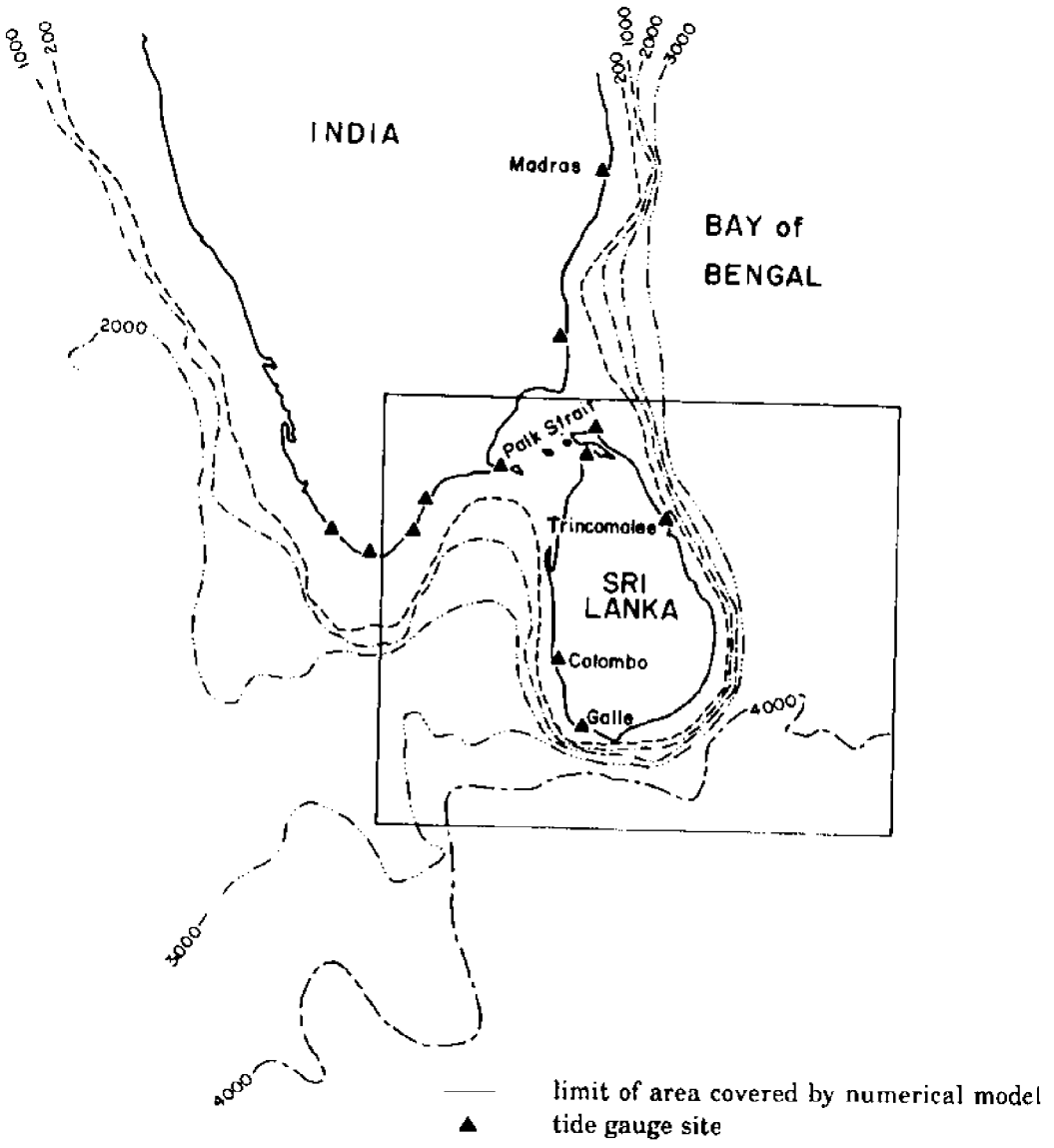

Figure 1. Study area (depths in metres)

$F^{(x)}$ and $F^{(y)}$ are the friction terms in the x and y directions respectively and are represented in the following way:

$$F^{(x)} = \frac{ku(u^2+v^2)^{1/2}}{d},$$

$$F^{(y)} = \frac{kv(u^2+v^2)^{1/2}}{d}$$

where k is the coefficient of friction. A value of 2.5×10^{-3} was used for k. $G^{(x)}$ and $G^{(y)}$ are the forcing terms in the x and y directions respectively. In the tidal model the forcing

terms are put equal to zero, while in the storm surge model they represent the wind stress that drives the model.

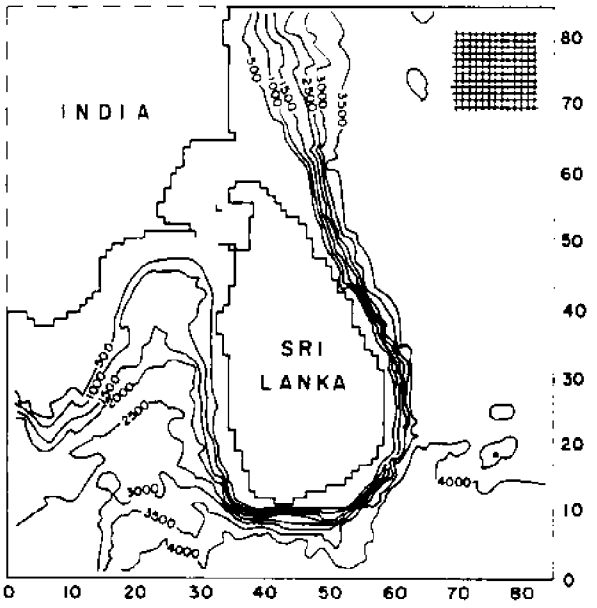

Figure 2. Schematization of coastlines and contour plot of bathymetry used in model (depths in metres); portion of grid shown up upper right

The following finite difference scheme is used as an approximation of the partial derivatives in the above equations (Figure 4):

$$\frac{\eta'_{ij}-\eta_{ij}}{\Delta t} = -\frac{(d_{ij}+d_{i+1,j})u_{i+1,j}-(d_{i-1,j}+d_{ij})u_{ij}}{2.\Delta x} - \frac{(d_{ij}+d_{i,j+1})v_{i,j+1}-(d_{i,j-1}+d_{ij})v_{ij}}{2.\Delta y}$$

$$\frac{u'_{ij}-u_{ij}}{\Delta t} = -g\frac{\eta'_{ij}-\eta'_{i-1,j}}{\Delta x} + f\bar{v}_{ij} - F_{ij}^{(x)} + G_{ij}^{(x)}$$

$$\frac{v'_{ij}-v_{ij}}{\Delta t} = -g\frac{\eta'_{ij}-\eta'_{i-1,j}}{\Delta y} + f\bar{u}_{ij} - F_{ij}^{(y)} + G_{ij}^{(y)} \qquad (2)$$

where

Δt = time step
Δx, Δy = grid interval sizes in x,y directions respectively
d_{ij} = mean water depth at elevation point n_{ij}
$\bar{u}_{ij}$ = $1/4[u_{i,j-1} + u_{i+1,j-1} + u_{ij} + u_{i+1,j}]$
$\bar{v}_{ij}$ = $1/4[v_{i-1,j} + v_{ij} + v_{i-1,j+1} + v_{i,j+1}]$

The primed values refer to terms updated during the current time step, while unprimed variables are the terms evaluated in the previous time step. The minimum time step permissible in order to maintain numerical stability is given by the following:

$$\Delta t \leq \frac{\Delta x.\Delta y}{\left[g d_{max}(\Delta x^2 + \Delta y^2)\right]^{1/2}} \qquad (3)$$

where Δt is the time step, Δx and Δy are the grid mesh sizes in the corresponding directions, d_{max} is the maximum depth of the model.

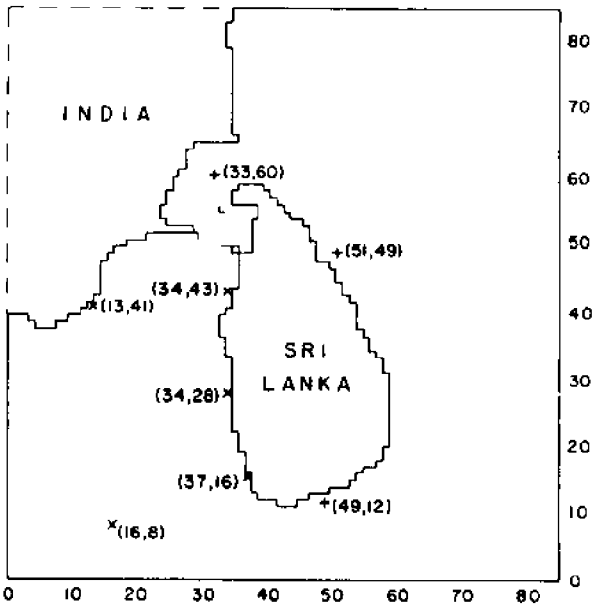

\+ locations referred to in Figures 5 and 6
x locations referred to in Figure 9

Figure 3(a). Model area showing specific elevation points

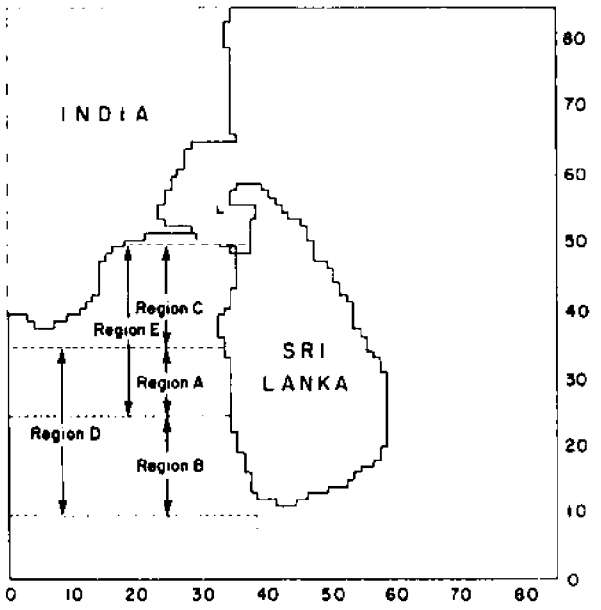

Figure 3(b). Model area showing wind forcing areas for simulated west coast surges

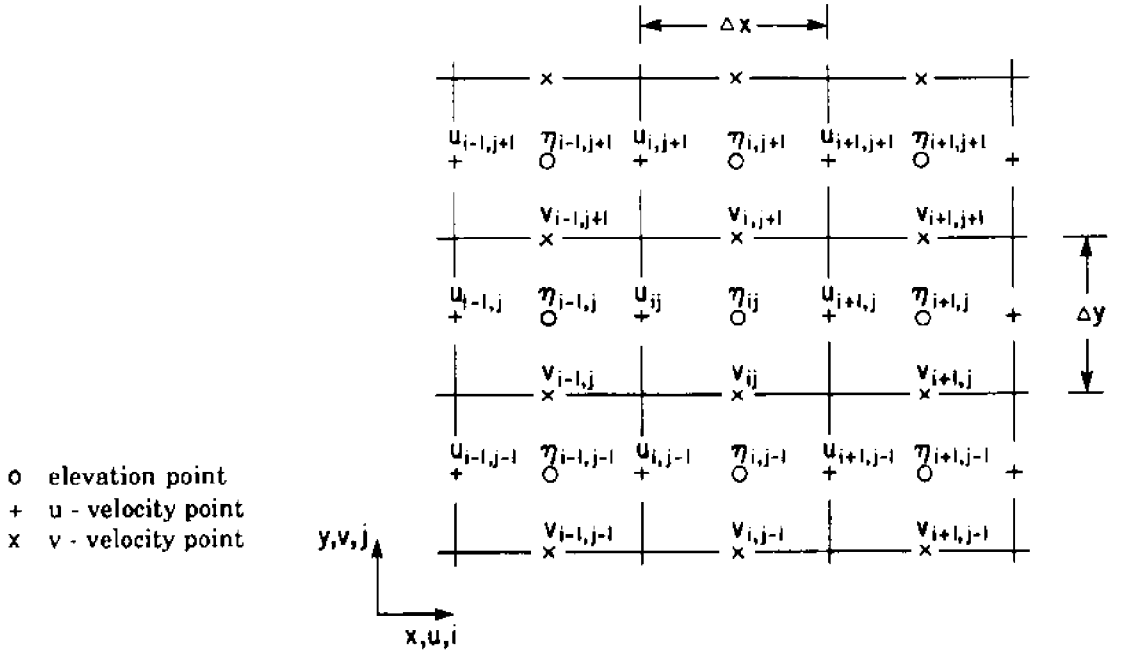

Figure 4. Richardson grid used in numerical model

The calculations carried out by the model depends on the location of the gridpoint. A land boundary, an open sea boundary and a point at the interior of the model all require different calculations. The model therefore allocates an integer code which describes the condition to be dealt with and which controls the corresponding calculation. If the boundary is closed (i.e., a coastline), it is assumed that there is no volume transport across the boundary. In other words, for a land boundary parallel to the y direction u=0; similarly if the land boundary is parallel to the x axis, then v=0. If the boundary is a sea boundary with a specified elevation, boundary conditions must be supplied. This situation is considered in the tidal model where boundary conditions are supplied by tide gauge harmonic analyses found from the Admiralty tide tables. A sea boundary with a radiating condition is considered in the storm surge model. This allows waves reaching the boundary of the model from within to radiate outwards.

For each boundary point an amplitude and a phase is prescribed as:

$$h(t) = A\cos(\omega t - \phi) \tag{4}$$

where h(t) is the height of the wave at time t, A is the amplitude, ϕ is the phase at a given boundary point, ω is the frequency of the harmonic constituent being considered and t is the time. Values of A and ϕ at each open boundary point were obtained by judicious interpolation from existing large-scale cotidal charts, with some corrections from tide gauges on the Sri Lankan and Indian coasts.

The forcing terms for the storm surge model are supplied through the terms $G^{(x)}$ and $G^{(y)}$, given as:

$$G^{(x)} = -\frac{1}{\rho_a}\frac{\partial P_a}{\partial_x} + \frac{\tau_{sx}}{\rho D} \qquad \text{and} \qquad G^{(y)} = -\frac{1}{\rho_a}\frac{\partial P_a}{\partial_x} + \frac{\tau_{sy}}{\rho D} \tag{5}$$

where ρ is the density of water, ρ_a is the density of air, τ_{sx}, τ_{sy} are the components of wind stress in the x and y directions; $\frac{\partial P_a}{\partial x}$ and $\frac{\partial P_a}{\partial x}$ are the sea level atmospheric pressure gradients in the x and y directions (Murty, 1984).

Results from trial runs suggested that the contributions from the pressure gradient terms and the bottom stress terms were not significant, and hence these terms were omitted in certain runs. Then (5) becomes

$$G^{(x)} = \frac{\tau_{sx}}{\rho D} \quad \text{and} \quad G^{(y)} = \frac{\tau_{sy}}{\rho D} \tag{6}$$

The wind stress is given by

$$\tau_s = \rho_a K|V|V \tag{7}$$

where V is wind velocity and K is a drag coefficient. A value of 2.6×10^{-3} was used for K.

It can be seen from Figure 2 that the depth gradient is quite steep off the south-easterly coast of Sri Lanka. On the other hand, the gradient is quite small off the south coast of India. It is also to be noted that there are some shallow areas in Palk Strait. These features will have some effect on the results of the model runs.

To minimize model spin-up time, the amplitude of the tidal forcing was increased linearly over 15 hours of simulated time to the required magnitude, and the coefficient of friction k was set high initially and allowed to decrease exponentially to the required value.

Difference meteorological forcing is required for model studies of east and west coasts of Sri Lanka. Cyclones have been known to hit the East Coast of Sri Lanka. From Ali and Johns (1980), the wind velocity needed to determine $G^{(x)}$ and $G^{(y)}$ is given by:

$$V = V_{max}\left(\frac{r}{R}\right)^{3/2}, \qquad 0 \le r \le R$$

$$V = V_{max}\left(\frac{R}{r}\right)^{1/2}, \qquad r \le R \tag{8}$$

where r=radial distance from the centre of the cyclone and maximum wind speed V_{max} occurs at radius R. A cyclone track and maximum wind speed were specified for each model run. On the west coast, surges were simulated by applying uniform wind fields over certain ocean areas. The wind was increased from zero to full strength over a period of two hours, held steady for two hours, and then gradually removed. Time series of surface elevation were recorded for prescribed points in the model domain during each run.

TIDAL MODEL RESULTS

Each tidal model run was monitored until steady oscillation was reached (eg., Figure 5(a),(b)) and harmonic analysis was then carried out. Avoiding abrupt application of the driving boundary conditions and artificially high initial damping, as described earlier, ensured that steady oscillation was reached within one or two cycles (see Figure 5(c),(d)). While tidal elevations always reached a steady oscillatory condition, velocities sometimes contained a low-frequency component (eg., Figure 6(g),(h)). This usually indicates the presence of topographically trapped waves created accidentally during the spin-up phase and not contributing to the elevation field. Since they are slow to dissipate and are well separated in frequency from the tidal constituent being studied, waves of this type can be ignored during the harmonic analysis.

Comparison of Figures 5(a) and (b) shows the marked effect of shallow waters on tidal behaviour. The tidal elevation record from point (33,60) in the shallows of Palk Strait shows attenuation of amplitude and presence of higher frequency harmonics.

An overall view of each tidal constituent can be shown most conveniently in the form of a cotidal chart. Figure 7(a) shows the computed amplitude for the largest tidal constituent, M_2. Also shown are observed M_2 amplitudes at coastal tide gauges and the M_2 cotidal amplitudes as estimated by Vassie (personal communication, 1985). It can be seen that there is good agreement among all three. In general, the computed M_2 phase, shown in Figure 7(b), agrees well with the observed phase and also with Vassie's estimated co-phase pattern. Since most tide gauges are sited within harbours or estuaries, some differences between harbour readings and computed open coast

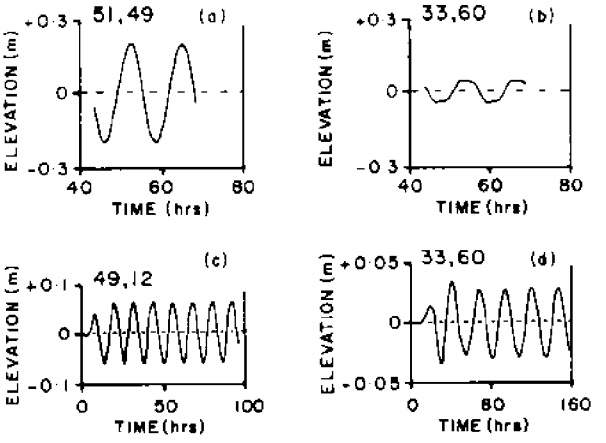

Figure 5. Computed tidal elevations
(a), (b) steady-state stage of M_2 simulation
(c) transient and steady-state stage of S_2 simulation
(d) transient and steady-state stage of O_1 simulation

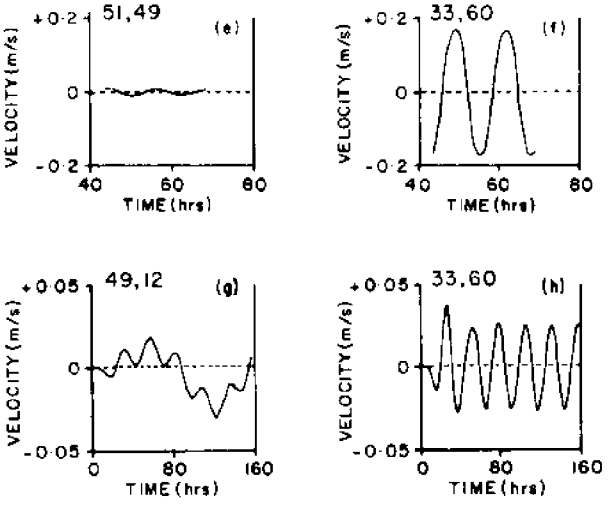

Figure 6. Computed tidal velocities (x-direction only)
(e), (f) steady-state stage of M_2 simulation
(g), (h) transient and study-state stage of O_1 simulation

values are to be expected: the discrepancy is greater the further up the waterway the gauge is sited. Figures 8(a) and 8(b) show the cotidal amplitudes and phases for the S_2 which is the second-largest tidal constituent. Agreement with observed values is good on the east coast of Sri Lanka and somewhat less satisfactory on the west coast.

The largest discrepancies between observed and computed values are on the south-west coast of Sri Lanka, for both M_2 and S_2. The probable explanation in both cases is the uncertainty concerning correct boundary values to supply along the nearby southern boundary of the model. Unlike the case of a passive, radiating boundary, little is to be gained by placing this boundary further south. Only better estimates of the boundary conditions alleviate this problem. Only M_2 and S_2 exceed 10cm in amplitude in the modelled region. Other constituents are substantially smaller and essentially unimportant so far as contributing to surge levels are concerned. For instance, O_1, the largest diurnal constituent, does not exceed 3 cm in amplitude anywhere on the coast of Sri Lanka, according to both observations and simulation.

EAST COAST STORM SURGE MODEL RESULTS

On average, the east coast of Sri Lanka experiences a major surge due to a tropical cyclone every 10 to 15 years. In December 1964, the Rameswaram Cyclone passed over the northern tip of Sri Lanka and then hit the coast of India. It was one of the most severe storms known to have occurred in the North Indian Ocean, and caused several hundred deaths and great property damage in Sri Lanka. Approximate maximum wind speed was 175 knots (324 kph).

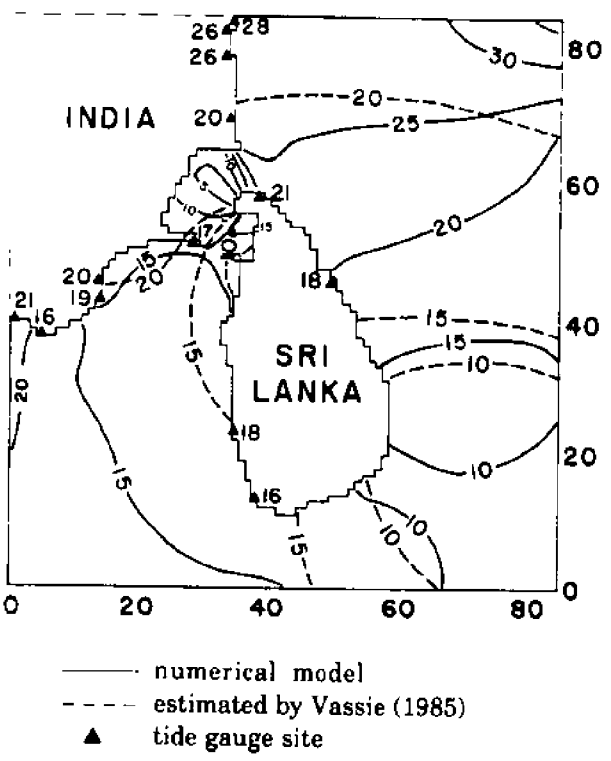

Figure 7(a). Co-amplitudes for M_2 constituent (cm)

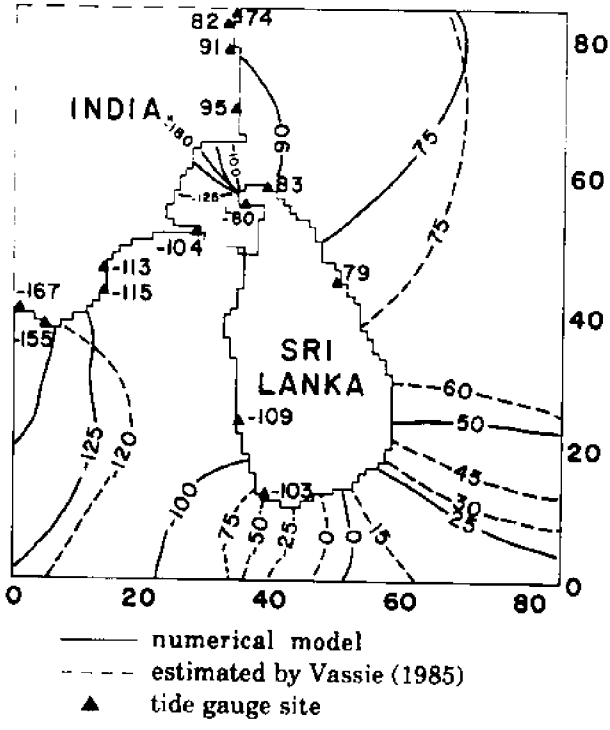

Figure 7(b). Co-phases for M_2 constituent (deg)

Better observations are available (Dharnaratha, 1985) for the next major surge in 1978, which is the one simulated here. The path of the cyclone as it crossed the east coast of Sri Lanka is shown in Figure 10(a). Also shown are three locations in the model grid where computer elevation was monitored. The wind distribution of Eq. (8) was used to represent the cyclone; this wind pattern was assumed to move along the cyclone track at 8 knots (14.8 kph). A maximum wind speed of 100 knots (185 kph) was adopted, in accordance with observed values. Though it is popularly assumed that the surge elevation is a maximum where a storm track crosses the coast, observations and the simulated surge shown in Figure 11 demonstrate that maximum elevations are experienced at coastal points, grid locations (3,57) and (16,16), somewhat beyond the region of maximum winds. The large surges at these two locations can be attributed partly to the shallow bathymetry in their neighbourhoods (Figures 10(b) and (c)). Where the cyclone path crosses the coast, point (20,33) in the model, the shelf is too narrow to amplify the surge, and in addition, the cyclone winds are parallel rather than normal to the coast.

WEST COAST STORM SURGE MODEL RESULTS

Even though there is no record of tropical cyclones ever impinging on the west coast of Sri Lanka, water level oscillations of significant amplitudes, up to 2-3 metres, have been observed on the coasts north and south of Colombo. The associated wave periods are of the order of 5-10 minutes, but unlike cyclone-generated surges, the whole event typically lasts 15-30 minutes. In fact, the meteorological events generating these water level oscillations are of even shorter duration. These episodes occur once or twice per year on average.

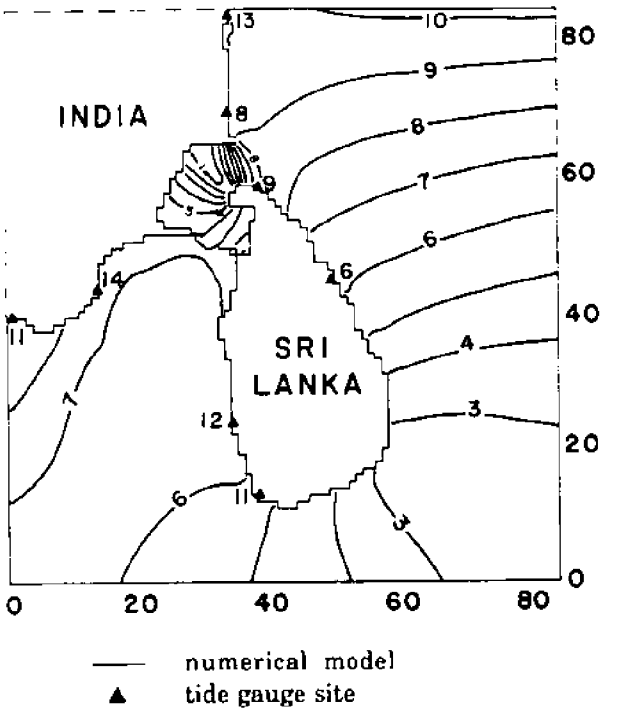

Figure 8(a). Co-amplitudes for S_2 constituent (cm)

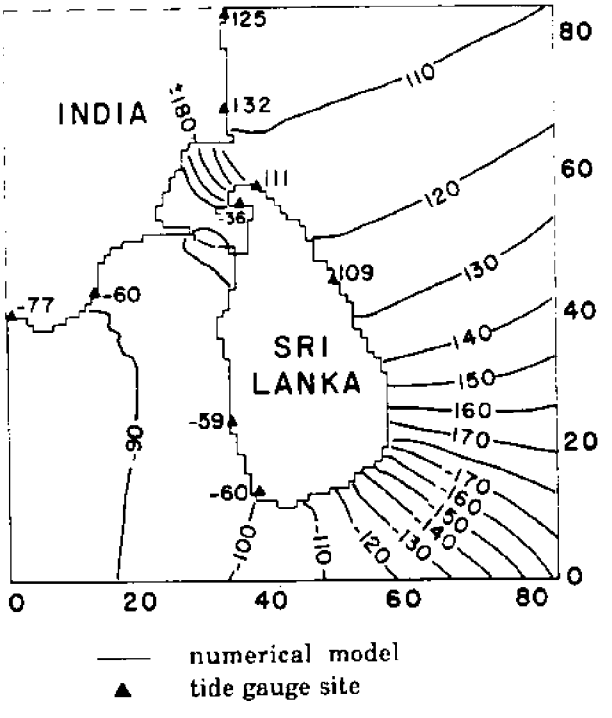

Figure 8(b). Co-phases for S_2 constituent (deg)

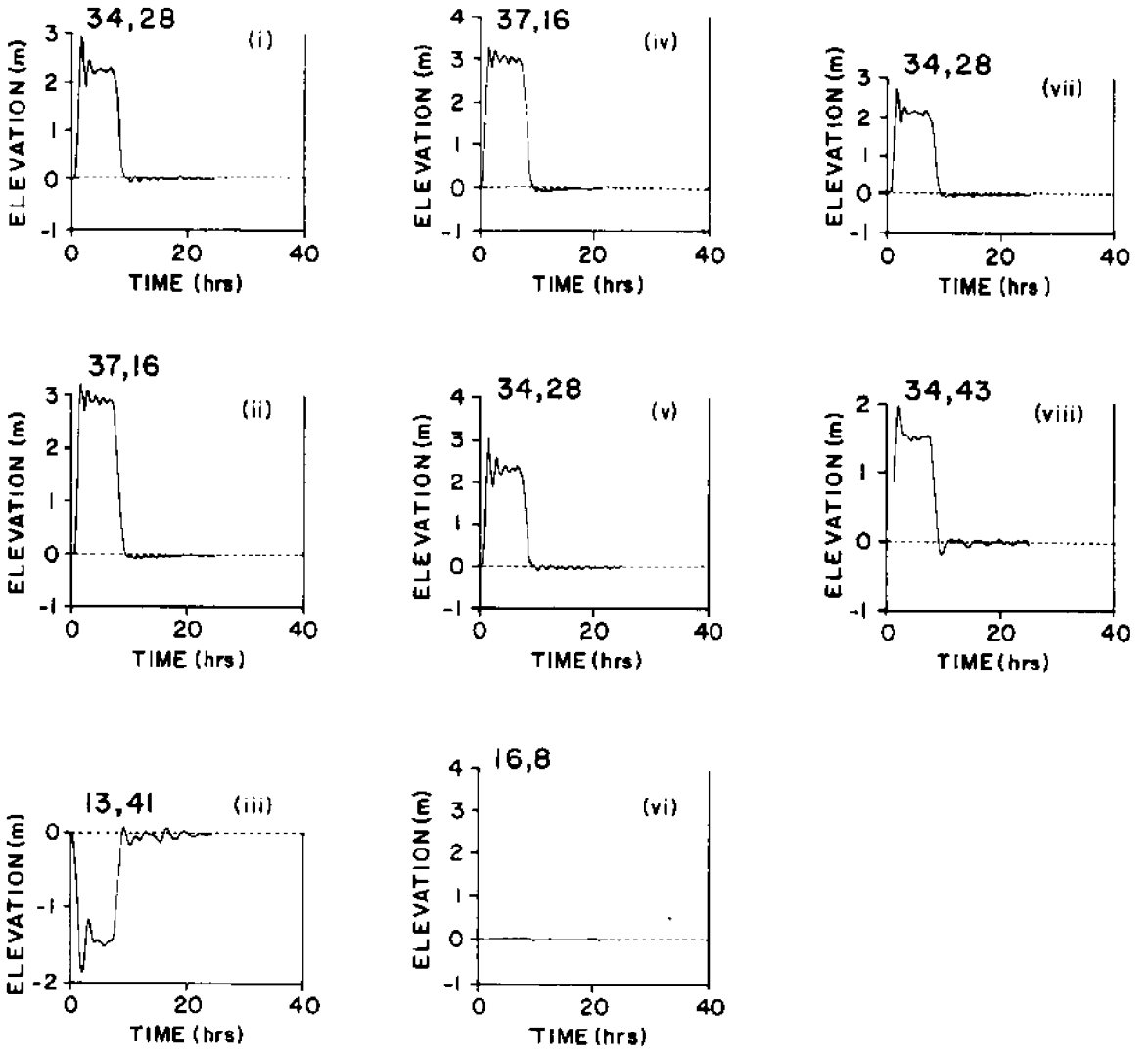

Figure 9. Simulated west coast storm surge elevations

(i), (ii), (iii) Response to wind of 280 kph applied to regions A,B,C (Figure 3(b)) respectively
(iv), (v), (vi) Response to wind of 280 kph applied to region D
(vii) Response to wind of 280 kph applied to region E
(viii) Response to wind of 150 kph applied to region E

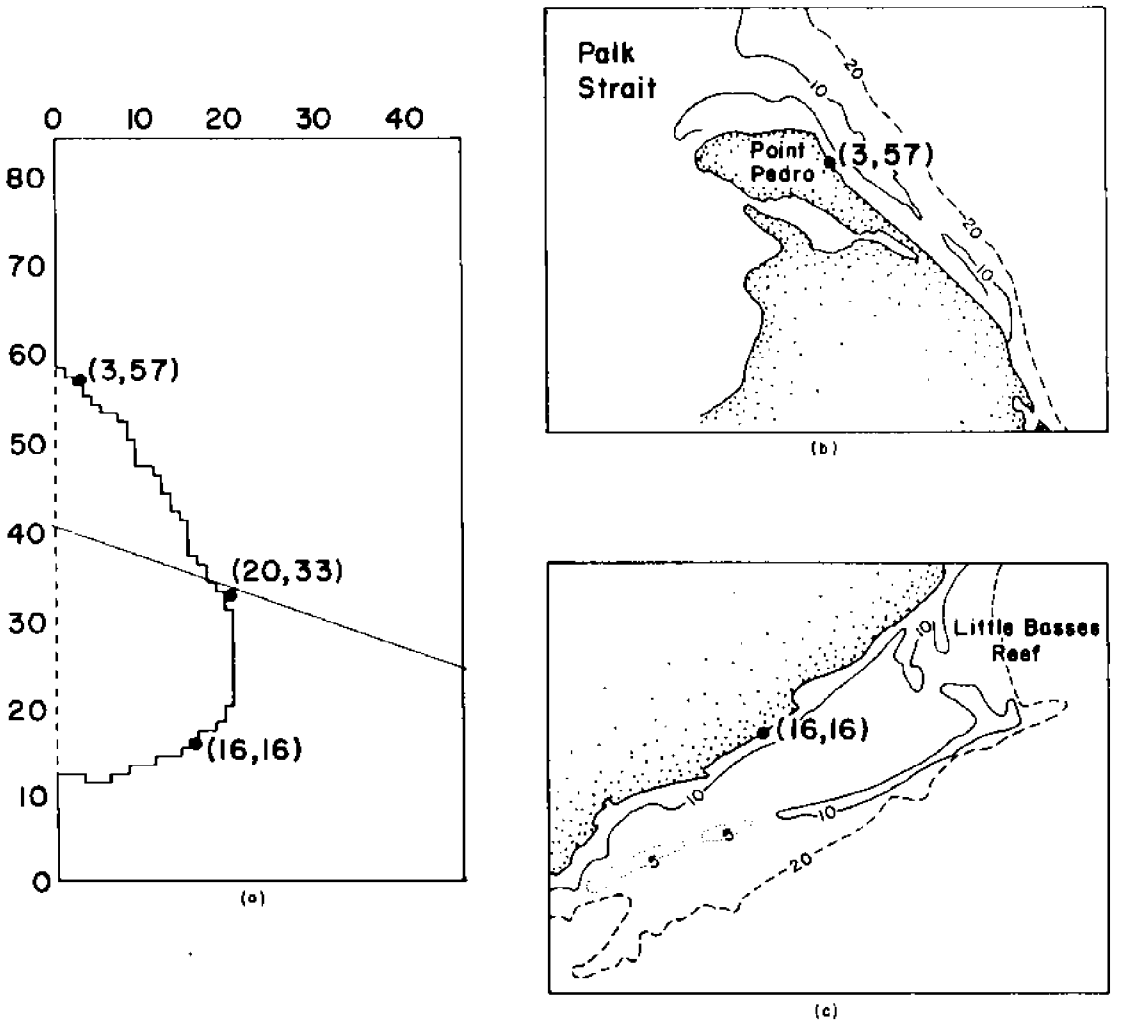

Figure 10. (a) Model grid details and track of simulated east coast cyclone
(b), (c) Detail of bathymetry (depths in metres)

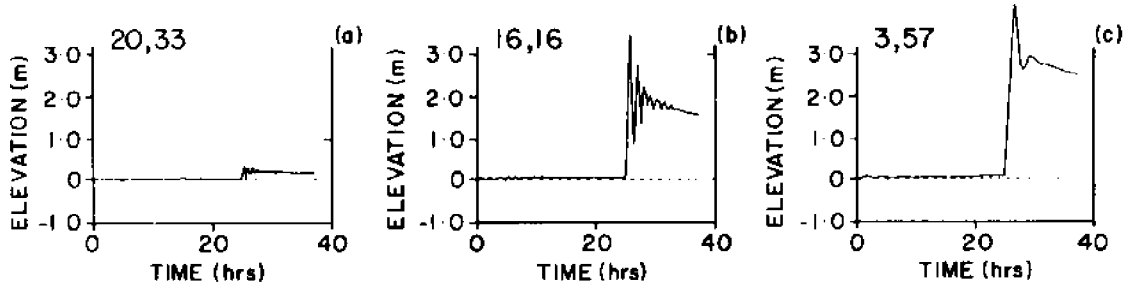

Figure 11. Computed elevations at 3 sites in Figure 10(a) during simulated east coast cyclone

Meteorological observations over the sea west of Sri Lanka are very sparse, but it seems likely that these brief surges are essentially similar to the "Rissaga phenomena" in the Mediterranean, discussed by Monserrat, et al. (1991). There, large short-term fluctuations in atmospheric pressure appear to cause corresponding fluctuations in water level, which are particularly noticeable wherever there is a resonant coupling between the atmospheric gravity wave and a normal mode of basin. In the Sri Lanka weather office records, there is evidence that strong wind gusts occur, extending some tens of kilometres along the coast and for an unknown distance seawards, while corresponding data on the pressure field is lacking. Consequently, in this study it was decided to examine the response in sea-level of the model to wind-fields corresponding in strength to reported cases and extending over different ocean regions west of Sri Lanka. The fact that similar effects were observed at the same time in Coochin, on the south-west coast of India, and north of Colombo suggests that the wind fields involved in these phenomena are quite extensive. The existence of normal shelf modes raises the possibility of some resonant amplification of water level at the coast, similar to that occurring in the Mediterranean.

Based on the sketchy data available, it was judged approporiate to use a wind directed at 10° south of east. Most cases were run at a wind speed of 280 kph, based on estimates of actual events. Significant water level oscillations are known to occur with wind-speeds down to 150 kph.

Model runs carried out with winds of the magnitude described above, applied to various regions, are shown in Figure 9. Whereas the computed maximum elevations are in the range of the reported amplitudes, the model needs over one hour to build up to these levels, which is slower than in nature. (The initial maximum water level is not affected by applying the wind field for longer than the initial phase, as was done in the model runs). There could be several reasons for this discrepancy. The actual phenomenon may have a lower, more quickly attained amplitude, but be subject to dynamic amplification to the observed levels. Physical factors which could cause such amplification are resonance with normal modes of vibration of the shelf and movement of the weather system.

The response is essentially similar in nature at difference places on the Sri Lankan coast, though there is some variation with location and wind forcing region (Figure 9), whereas on the Indian coast (Figure 9(iii)), where the applied wind is offshore, the effect is inverted, as is to be expected. Far from the coasts, there is very little effect on sea-level (Figure 9(vi)).

CONCLUSIONS

To our knowledge, no publication has yet appeared on tides or storm surges in Sri Lankan waters. Although, in principle, much more sophisticated models could be developed, only a simplified model, without non-linear advection terms, has been used in this study. The sparcity of input data makes it pointless to use a more complicated model at this time. In future studies, including advection, all the tidal constituents would then be simulated together, to allow non-linear interaction be taken into account. In that case also, the surge modelling should be done simultaneously with the tidal simulation, as there can be interaction between the two.

ACKNOWLEDGMENT

We wish to thank Sylvia Harrison who did the computer programming for this study.

REFERENCES

Johns, B., and A. Ali. 1981. Reply to J. Holland comment on paper by B. Johns and M.A. Ali, The numerical modelling of storm surges in the Bay of Bengal. *Quarterly Journal of the Royal Meteorological Society*. **107**(271-272).

Anon. 1987. Admiralty Tide Tables. Hydrographer of the Navy, U.K.

Bogdanov, K.T,. and B.V. Kharkov, V. 1976. Calculation of Indian Ocean tides. *Oceanology*. **15**:156-150.

Dharnaratha, C.H.P. 1985. Storm surge forecasting. Dept. Meteorology, Colombo 7.

Elahi, K.Z. 1983. Tidal charts of the Arabian Sea north of 20°N. In: Proceedings of the U.N.E.S.C.O./R.O.P.M.E. Conference, ed. M.I. El-Sabh. Dhahran, Saudi Arabia. October.

Gross, M.G. 1982. Oceanography: A View of the Earth. Third edition. New Jersey. pp 246.

Henry, R.F. 1982. Automated programming of explicit shallow-water models with linearized models with linear or quadratic friction. *Canadian Technical Report of Hydrography and Ocean Sciences*. **3**.

Marchuk, G.I., B.A. Kagan, and D.E. Cartwright (translation editor). 1984. Ocean Tides: Mathematical models and numerical experiments. Oxford: Pergamon Press. 176 pp.

McCammon, C., and C. Wunsch. 1977. Tidal charts of the Indian Ocean north of 15°S. *Journal of Geophysical Research*. **82(2037)**:5993-5998.

Monserrat, S., A. Ibbetson, and A.J. Thorpe. 1991. Atmospheric gravity waves and the `Rissaga´ phenomenon. *Quarterly Journal of the Royal Meteorological Society*. **117**:553-570.

Murty, T.S. 1984. Storm surges - meteorological ocean tides. Ottawa, Bulletin 212, *Canadian Journal of Fisheries and Aquatic Sciences*. pp 1-6, pp 41-44.

Murty, T.S., and R.F. Henry. 1983. Tides in the Bay of Bengal. *Journal of Geophysical Research*. **88(C10)**:6069-6076.

Schwiderski, E.W. 1980. On charting global ocean tides. *Rev. Geophys. Space Phys.* **18(1)**:243-268.

PASSIVE MICROWAVE OBSERVATIONS FOR STORM SURGE MODELLING IN THE BEAUFORT SEA

Venkata R. Neralla, Tad S. Murty* and René O. Ramseier

Ice Center Environment Canada
Ottawa, Ontario, Canada

*Institute of Ocean Sciences
Sidney, British Columbia, Canada

ABSTRACT

Storm surges and the resulting coastal flooding are manifestations of significant increase in water levels caused by the passage of atmospheric disturbances. The study of storm surges in the Beaufort Sea is extremely useful for successful operation of offshore activities, such as navigation, transportation and oil drilling. Presence of sea ice cover helps in damping the amplitude of surges. Hence, a knowledge of sea ice cover is beneficial in the surge modelling. An available storm surge model in presence of ice cover, is described briefly here.

Since June 1987, the Special Sensor Microwave/Imager has been a part of the U.S. Defense Meteorological Satellite Program. The Microwave Group, Ice Services of the Atmospheric Environment Service, with collaboration from the Institute for Space and Terrestrial Science, North York, has been actively involved in the interpretation and analysis of passive microwave sensor data. The availability and applicability of this data in deriving wind stress and sea ice cover for use in the analysis and prediction of storm surges in the Beaufort Sea is presented.

INTRODUCTION

It is well known that wind stress and pressure gradient force contribute about 90% and 10%, respectively, towards the generation of surges. Unavailability of accurate and detailed observations of winds over the Arctic area in general, and the Beaufort Sea in particular, is a major deterrent in conducting detailed investigations of surges. Also, during storms, it is difficult to obtain information on winds. However, with the advent of satellites carrying all-weather passive microwave sensors, one could obtain data on sea ice cover and winds (over open ocean areas) from multifrequency observations. The objective here is to show how the wind and ice cover data are derived from the all-weather passive microwave observations and to demonstrate its potential for the study of storm surges in presence of ice cover.

The Special Sensor Microwave Imager (SSM/I), an all-weather sensor, is a part of the United States Defense Meteorological Satellite Program (DMSP). The SSM/I, operating at four frequencies, 19.35, 22.2, 37.0, and 85.5 GHz with orthogonal polarizations (except at 22.2 GHz) measures atmospheric/oceanic surface brightness temperatures. The spatial resolution is frequency dependent and range from about 50 km at 19.35 GHz to about 15 km at 85.0 GHz. The swath width of SSM/I is 1400 km. Any area of the midlatitudes is observed twice a day. At higher latitudes (e.g., 60°N to about 85°N), due to greater overlapping of successive swaths, the frequency of observations is even greater

than at midlatitudes. The Microwave Group, Ice Services of the Atmospheric Environment Service, Canada with collaboration from the Institute for Space and Terrestrial Science (ISTS), North York, Ontario, Canada has been actively involved in the interpretation and analysis of SSM/I data.

The remaining part of the paper deals with the following material arranged into four more sections. The second section deals with storm surge modelling. The third and fourth sections, respectively, describe the ice conditions in the Beaufort Sea, and ice and wind information derived from the satellite passive microwave observations. The last section provides **concluding remarks**.

BEAUFORT SEA STORM SURGE MODEL

Storm surges belong to the same class of waves as tides and tsunamis (Figure 1). The dynamical theory of tides and surges, in general, is based on depth-averaged hydrodynamical equations. Since the main concern is with fluctuations in water level, not influenced by water currents below the water surface, the elimination of dependence on the vertical co-ordinate resulting from depth-averaging, gives a useful simplification of the problem. For a detailed discussion the reader is referred to Murty (1984) and Neralla and Murty (1991). In the Cartesian co-ordinate system, with x,y in the horizontal plane of the mean sea surface, the depth-averaged equations of motion are used. However, for the application of this model over the polar areas, Kowalik (1984) and Danard, et al. (1989) modified the model to take into account the presence of ice cover. The model is briefly described below.

$$\frac{\partial \eta}{\partial t} = -\frac{\partial}{\partial x} Du - \frac{\partial}{\partial y} Dv \tag{1}$$

$$\frac{\partial u}{\partial t} = fu - g\frac{\partial \eta}{\partial y} + \frac{(1+C)\tau_{ax}}{\rho D} + \frac{C\tau_{ix}}{\rho D} - \frac{\tau_{bx}}{\rho D} + Fx - \frac{1}{\rho}\frac{\partial p_s}{\partial x} \tag{2}$$

$$\frac{\partial v}{\partial t} = fu - g\frac{\partial n}{\partial y} + \frac{(1-C)\tau_{ay}}{\rho D} + \frac{C\tau_{iy}}{\rho D} - \frac{\tau_{by}}{\rho D} + Fy - \frac{1}{\rho}\frac{\partial p_s}{\partial y} \tag{3}$$

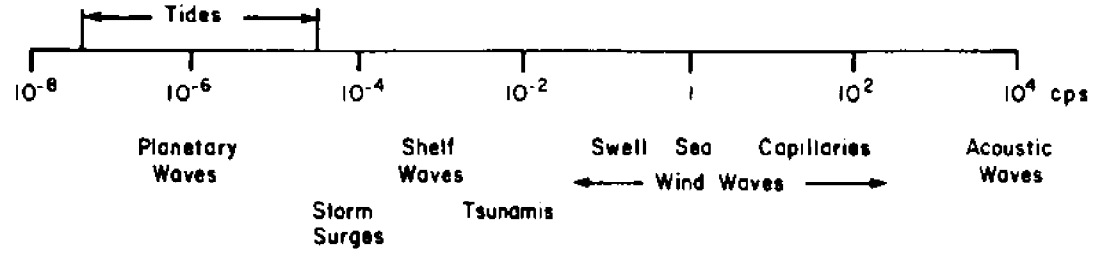

Figure 1. Frequencies of oceanic wave motion in cycles per second (cps)

$$\frac{\partial C}{\partial t} + -\frac{\partial}{\partial x} C u_i - \frac{\partial}{\partial y} C v_i \tag{4}$$

$$\frac{\partial u_i}{\partial t} = f v_i - g \frac{\partial \eta}{\partial x} + \frac{\tau_{aix} - \tau_{ix}}{\rho_i h} + R_{ix} - \frac{1}{\rho} \frac{\partial p_s}{\partial y} \tag{5}$$

$$\frac{\partial v_i}{\partial t} = -f u_i - g \frac{\partial \eta}{\partial y} + \frac{\tau_{aiy} - \tau_{iy}}{\rho_i h} + R_{iy} - \frac{1}{\rho} \frac{\partial p_s}{\partial y} \tag{6}$$

where t is the time, η is the departure of water surface elevation from undisturbed depth, u and v are the components of depth-mean current, D is the undisturbed water depth, f is the Coriolis parameter (= 2 Ω Sin φ, where Ω is the angular velocity of the Earth, and φ is the latitude), g is the acceleration due to gravity, C is the ice concentration, τ_{ax} and τ_{ay} are the components of air stress exerts on water surface, τ_{bx} and τ_{by} are the components of water stress exerts on ocean bottom, τ_{ix} and τ_{iy} are the components of underside ice stress exerts on water, F_x and F_y are the components of water viscous forces, R_{ix} and R_{iy} are the components of internal ice resistance, τ_{aix} and τ_{aiy} are the components of air stress exerts on ice surface, p_s is the air pressure, h is the ice thickness and u_i and v_i are the components of ice velocity.

One can see from Eqs. (2) and (3) that the meteorological forcing which generate storm surges are the wind stress and the horizontal gradient of surface atmospheric pressure. The atmospheric pressure gradients can be prescribed either from observations or from the output of numerical weather prediction models. However, the wind stress is not routinely observed and hence must be derived from wind observations. Over large and inaccessible areas such as the Arctic, satellite observations are extremely useful. Also, since the depth, D, is in the denominator of wind stress terms (see Eqs. (2) and (3)), it could be noticed that the stress is less effective in generating surges in deep water than in the shallow water. In deep water, surges are mainly produced by changes in atmospheric pressure, but in shallow water and in particular on continental shelves and nearer to coasts, wind stress forcing dominates. The continuity Eq. (1) expresses the conservation of water.

As suggested by Wu (1980), the drag coefficient can be specified as a function of wind (Figure 2). As stated earlier, accurate knowledge of wind is essential for the prediction of storm surges especially in shallow water. Given the time and space dependent values of wind and pressure, the dynamical problem of the prediction of storm surges in ice covered waters, is involved in solving Eqs. (1) to (6) in a given region of interest.

Equations (4) to (6) describe a simple viscous approach to obtain ice drift and concentration (Rothrock, 1980). Based on viscous-plastic approach of Hibler (1979), the Atmospheric Environment Service (AES) developed a regional scale sea ice motion model for operational applications (Neralla, et al., 1988). This model uses reasonable physics in the sense of inclusion of all relevant parameters and is well suited for inclusion in the storm surge modelling over the polar areas. At ICEC, a dynamical sea ice model

(Neralla, et al., 1988), known as the Regional Ice Model (RIM) is run daily. The model-generated output of ice coditions is mainly used as numerical guidance in preparing ice analysis and forecasts.

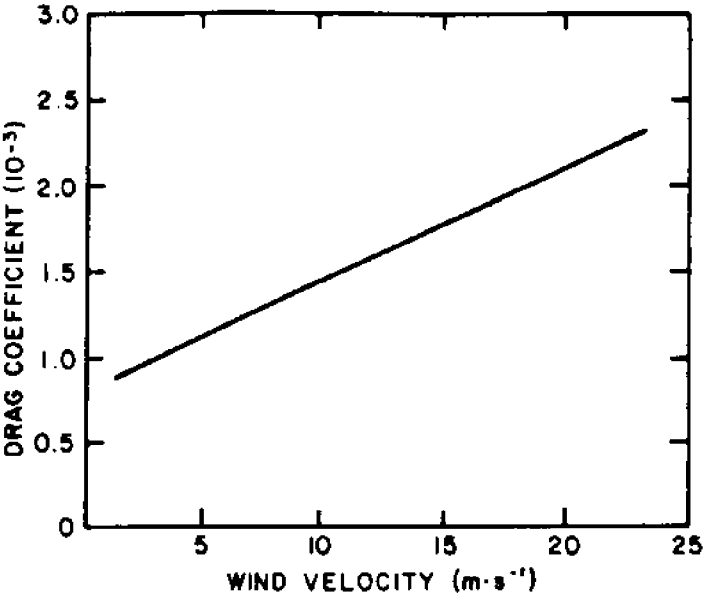

Figure 2. Variation of drag coefficient with wind (Wu, 1980)

The ice conditions as obtained from passive microwave observations will be extremely useful for initializing ice motion equations. A brief discussion on gathering the SSM/I sea ice cover data will be provided in the fourth section.

ICE COVER IN THE BEAUFORT SEA

With mandate from the Federal Government, the Ice Centre Environment Canada (ICEC) of Ice Services has the responsibility to produce daily ice charts valid at 1800 Z. These charts are generated by collating the data gathered during the day, from all the available remotely sensed observations such as satellites (NOAA AVHRR, LANDSAT MSS), aircrafts (STAR-2, DASH-7) and from direct observations from ships, helicopters and land stations. Figure 3 shows an example of conventional composite ice analysis chart produced over the Southern Beaufort Sea. The codes called 'egg' codes depict the detailed ice conditions over a given area. The inset in the diagram gives the explanation of the codes, which are designed by the World Meteorological Organization. For more details on the 'egg' code, the reader is referred to a manual called MANICE (1989).

With the advent of satellite passive microwave observations, such as SSM/I observations, the spatial and temporal coverage over the Canadian Arctic areas is extremely reasonable. Figure 4 shows the ice cover and its coverage over the Southern Beaufort Sea from the SSM/I data. It is interesting to note that the coverage for a day (4 September 1992) is quite abundant. Sea ice concentrations are in percentages. One could, from these charts, easily discern the ice edge. The data coverage of this nature is beneficial for the study of storm surges in ice encumbered waters.

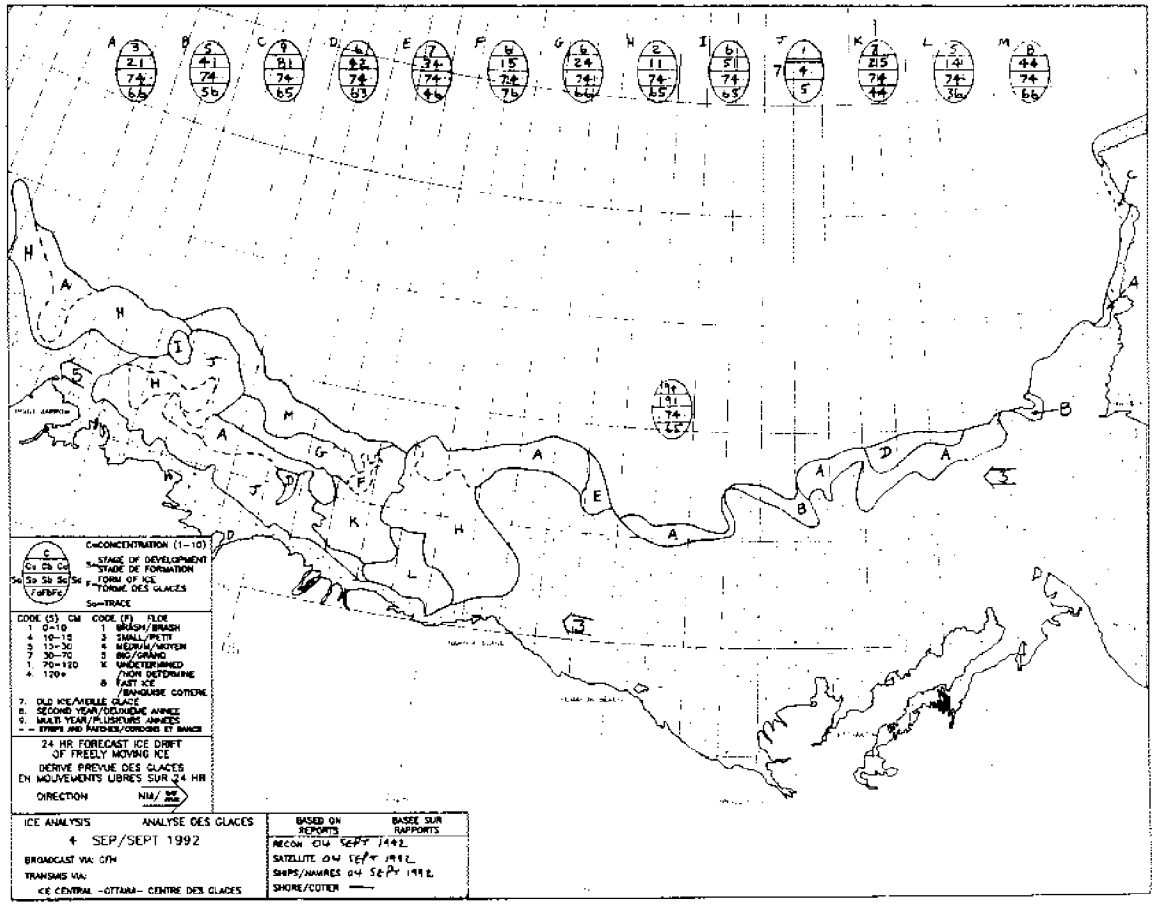

Figure 3. Conventional composite ice chart for the Beaufort Sea, prepared at the Ice Centre Environment Canada, valid at 1800 Z for 4 September 1992

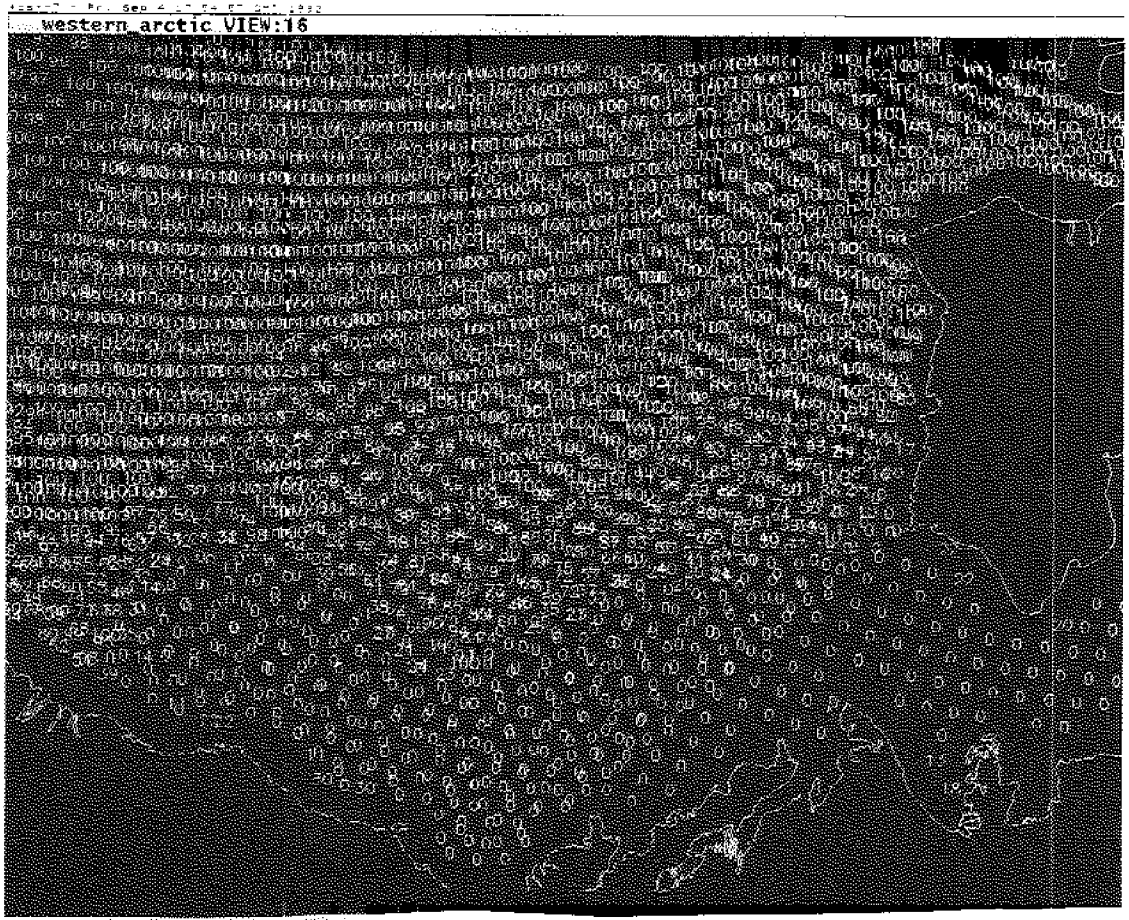

Figure 4. Ice concentration chart as derived from SSM/I observations over the Beaufort Sea valid at 1800 Z for 4 September 1992

PASSIVE MICROWAVE OBSERVATIONS

The Beaufort Sea experiences storm surges set up by northwest winds associated with high latitude storms. As stated earlier, accurate knowledge of winds over the inaccessible regions during a storm situation is essential for obtaining good prediction of surges. With the availability of all-weather passive microwave sensing capability, one could derive winds from the multi-frequency data.

The microwave region of the electromagnetic spectrum is useful for sensing the environmental parameters such as winds, ice, oil spills, etc. The SSM/I was launched as part of the Defense Meteorological Satellite Program (DMSP). The primary environmental parameters to be retrieved from SSM/I are shown in Table 1 (Hollinger, et al., 1987).

The SSM/I is a seven-channel, four-frequency, linearly polarized microwave radiometer receiving both vertically and horizontally linearly polarized radiation at 19.4, 37.0 and 85.5 GHz and vertically at 22.2 GHz. The spacecraft is in a circular sun-synchronous near-polar orbit at an altitude of 833 km with an inclination of 98.8 degrees and an orbit period of 102.0 min. With a swath width of 1400 km, the satellite provides 14.1 full orbits per day (Figure 5).

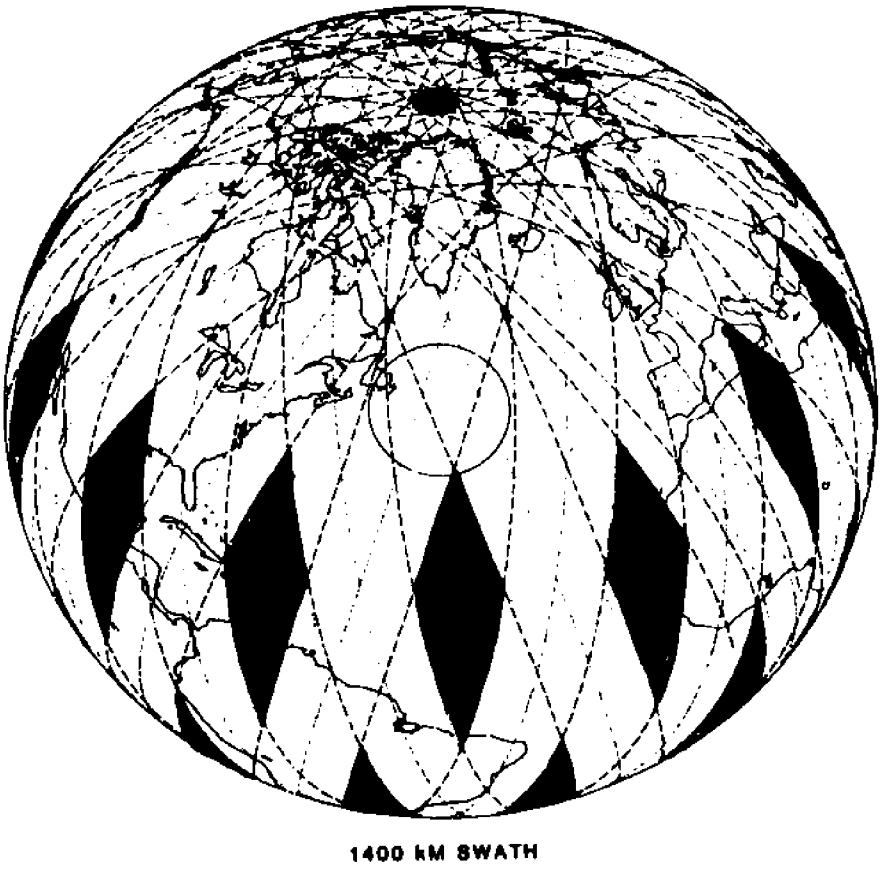

Figure 5. Earth coverage of the SSM/I in one day (Hollinger, et al., 1987)

Table 1. SSM/I environmental products (Hollinger, et al., 1987)

Parameter	Geometric Resolution	Range of Values	Quantization Levels	Absolute Accuracy
Ocean Surface Wind Speed	25	3 to 25	1	+ 2 m/s
Ice				
* Area covered	25	0 to 100	5	+ 12%
* Age	50	1st Year, Multiyear	1yr,>2yr	none
* Edge Location	25	N/A	N/A	+ 12.5km
Precipitation over Land Areas	25	0 to 25	0, 5, 10, 15, 20, > 25	+ 5 mm/hr
Cloud Water (<100μm Diameter)	25	0 to 1	0.05	+ 1.0kg/m^2
Liquid Water (>100μm Diameter)	25	0 to 60	0.10	+ 2.0kg/m^2
Integrated Water Vapor	25	0 to 80	0.5	+ 3.0kg/m^2
Precip. over Water	25	0 to 25	0,5,10,15,20, 25, >25	+ 5 mm/hr
Soil Moisture	50	0 to 60%	1	None
Land Surface Temperature	25	180-340K	1	None
Snow Water Content	25	0 - 50cm	1	+ 3cm
Surface Type	25	12 Types	N/A	N/A
Cloud Amount	25	0 to 100%	1	+ 20%

Theory

Swift (1977) and Munn (1978) demonstrated that wind speeds near the ocean surface can be remotely sensed by both active and passive radiometers. The active sensors (e.g., scatterometers) measure the component of transmitted power that is backscattered from the ocean surface whereas the passive sensors (e.g., SSM/I) measure radiation naturally emitted from the ocean surface. In both cases, the scattered and emitted radiation are affected by ocean surface roughness which in turn is a function of surface wind speed. Gloersen and Barath (1977) state that passive microwave radiometry involved the detection of naturally generated emissions from the earth and atmosphere at microwave frequencies ranging from 1 to 240 GHz (or equivalent wavelengths of 30 to 0.125 cm). The microwave radiation incident on the spacecraft antenna and detected by the microwave radiometer is composed of radiance contribution from the earth and atmosphere (Swift and Cavalieri, 1985) as shown in Figure 6. These radiances can then be expressed as equivalent brightness temperatures (°K).

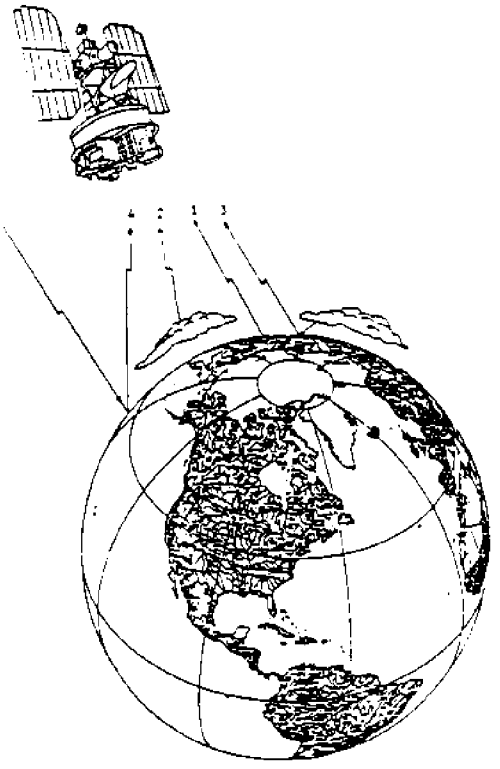

1 2 3 4

Brightness Temperature = Surface Emissivity x Surface Phys. Temp. x Atmos. Absorption + Upwelling Atmospheric Radiation + Reflected Downwelling Atmos. Rad. x Atmos. Abs. + Reflected Space Rad. x Double Atmos. Absorption

$$T_b = \varepsilon T_s \exp(-\tau) + T_{up} + (1-\varepsilon) T_{down} \exp(-\tau) + (1-\varepsilon) T_{sp} \exp(-2\tau)$$

Figure 6. Satellite viewing of the Earth and the radiation transfer equation (Swift and Cavalieri, 1985)

Following Swift and Cavalieri (1985), the brightness temperature (T_B) is expressed as

$$T_{B_{ij}} = \varepsilon_{ij} T_s \exp(-\tau_i) + T_{up_i} + (1-\varepsilon_{ij}) T_{down_i} \exp(-\tau_i) + (1-\varepsilon_{ij}) T_{sp} \exp(-2\tau_i) \qquad (7)$$

where ε is the surface emissivity, T_s is the physical surface temperature, τ is the total atmospheric opacity, T_{up} is the upward emitted radiance contribution to the atmosphere, T_{down} is the total (downward emitted or reflected) atmospheric brightness temperature, T_{sp} is the average brightness temperature of free space, i is the frequency of the received radiation and j is the polarization of the received radiation. A more detailed discussion is given in Swift, et al. (1984).

The frequencies used here for extraction of winds are not hindered by the atmospheric absorption (Figure 7). The surface brightness temperatures as obtained from the sensor at four frequencies (19.4, 22.0, 37.0 and 85.5 GHz) are used in the wind speed retrieval algorithms developed by Environmental Research and Technology Inc. (ERT) under contract to Hughes Aircraft is called the D-Matrix algorithm (Hollinger, et al., 1987).

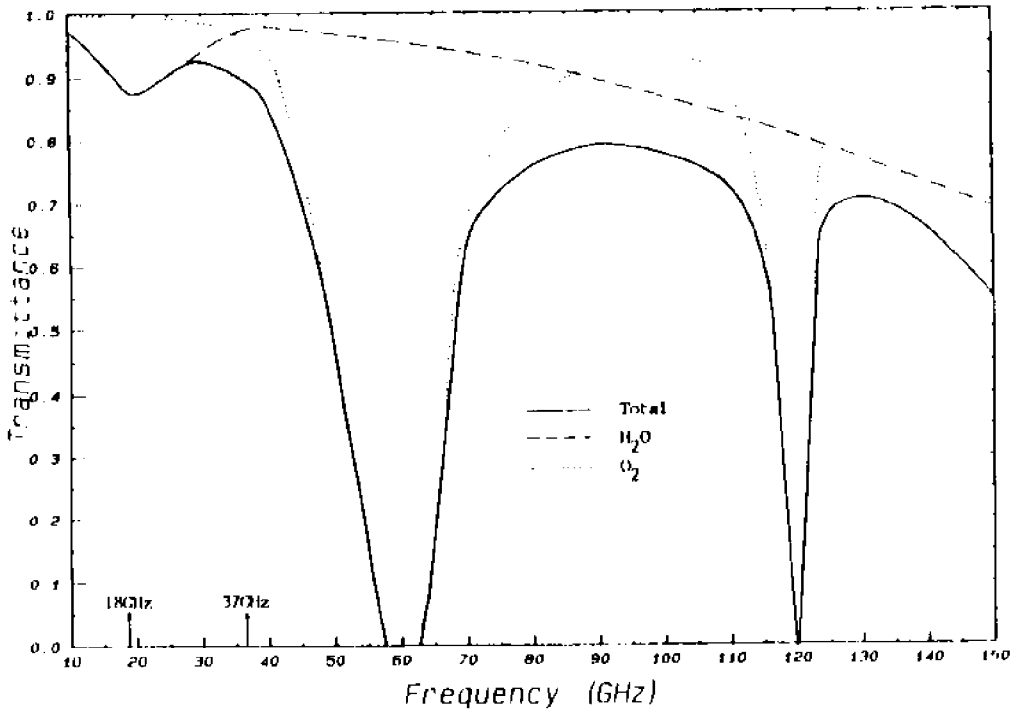

Figure 7. Variation of atmospheric transmittance with frequency

Extraction of Surface Wind

Figure 8 shows the variation of brightness temperature at 19.4 H and V, 22 V and 37 H and V frequencies with ocean surface wind. It can be clearly seen from this figure

that the information from the horizontal channels are more sensitive to wind speed than the vertical channels. Although the variations at vertical polarizations are small, they are by no means negligible. The algorithm (see Goodberlet, et al., 1989; and Lo, 1983) for retrieval of surface wind is given by

$$V_a = C0(j) + C1(j)T_B(19H) + C2(j)T_B(22V) + C3(j)T_B(37V) + C4(j)T_B(37H) \quad (8)$$

where V_a is the surface wind speed in m/s and referenced to height of 19.5 m above the surface. The anemometer level winds can then be obtained by using some form of logarithmic wind profile. The terms $T_B(x)$ represent the SSM/I measured brightness temperature of frequency/polarization combinations. Based on similar procedure and with some modifications to (8) in terms of weather and sea state corrections, AES/YORK (Davies, et al., 1990) obtained surface winds. This algorithm was tested and evaluated thoroughly for several synoptic events. The AES/York was also validated with SSM/I algorithm as developed by Lo (1983).

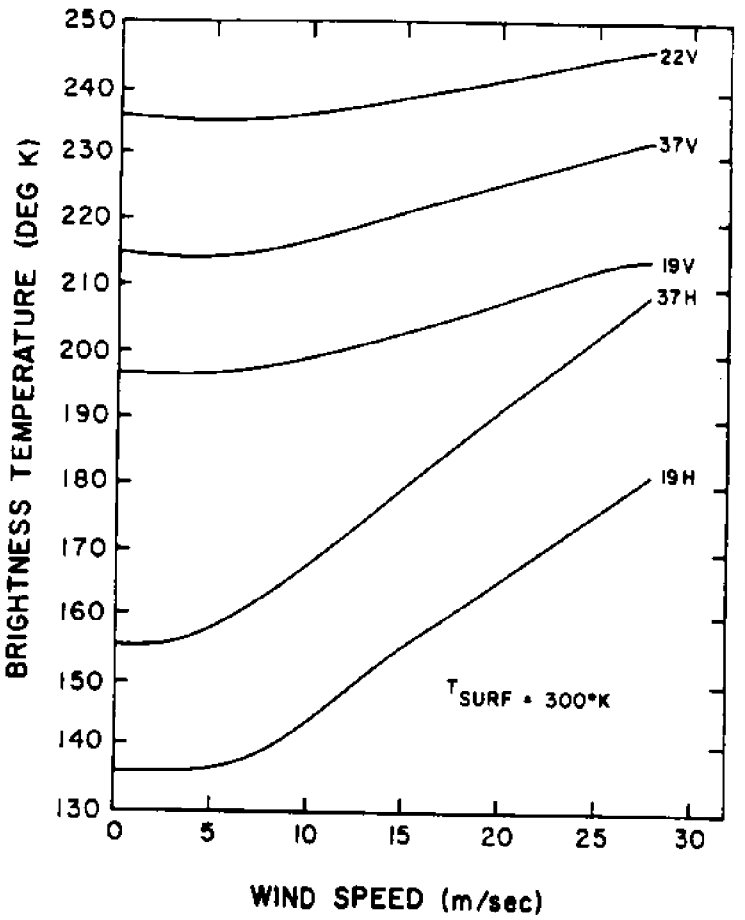

Figure 8. Brightness temperature as function of frequency and wind speed (Hollinger, et al., 1987)

With suitably modified coefficients, Petty and Katsaros (1990) used Eq. (8) by incorporating V19 brightness temperature instead of H19 brightness temperature. More recently, Schluessel and Luthardt (1991) suggested that by using the brightness temperature differences between vertically and horizontally polarized temperatures at the same frequency, in Eq. (8), the main atmospheric contribution is greatly minimized. The algorithm, according to Schluessel and Luthardt (1991), is given by

$$V_a = C0(j) + C1(j)T_B(19V) + C2(j)(T_B(19V) - T_B(19H)) + C3(j)T_B(22V) + \\ + C4(j)T_B(37V) + C5(j)(T_B(37V) - T_B(37H)) \quad (9)$$

This algorithm was tested thoroughly over the North Sea area and found to be in good agreement with observations.

Extraction of Sea Ice Concentration

For a single channel, dually polarized observations, the algorithm for deriving sea ice concentration was developed by Lo (1983) and can be written as

$$C = A_0 + A_1 \{ T_{BV}(37) - T_{BH}(37) \} \quad (10)$$

where A_0 and A_1 are seasonal constants (see Table 2), and $T_{BV}(37)$ and $T_{BH}(37)$ are respectively, the vertical and horizontal polarized brightness temperatures at 37 GHz frequency. The seasonal constants A_0 and A_1 are derived from known average values of ice temperature, atmospheric liquid water content and ice type emissivities which vary with the season. These procedures were thoroughly validated recently (Ramseier et al., 1989). More recent algorithms (e.g., Rubinstein and Ramseier, 1991) incorporate dual frequency observations with same polarization and could generate ice concentrations for different categories such as first year a multiyear ice. However, by acquiring a good knowledge of the total atmospheric water vapor content, the existing algorithms could be modified.

Table 2. Seasonal constants (Lo, 1983)

SEASON	A_0	A_1
SPRING	1.164	- 0.0176
SUMMER	1.163	- 0.0276
FALL	1.164	- 0.0176
WINTER	1.165	- 0.0276

Figure 9 shows an example of derived SSM/I information on sea ice and winds over the East Greenland Sea for 24 July 1990. This was obtained in near-real time on board FS Polarstern during a recent polar expedition (Garrity, et al., 1990). Contours represent the isolines of sea ice concentration. Winds are derived and plotted over the open water areas.

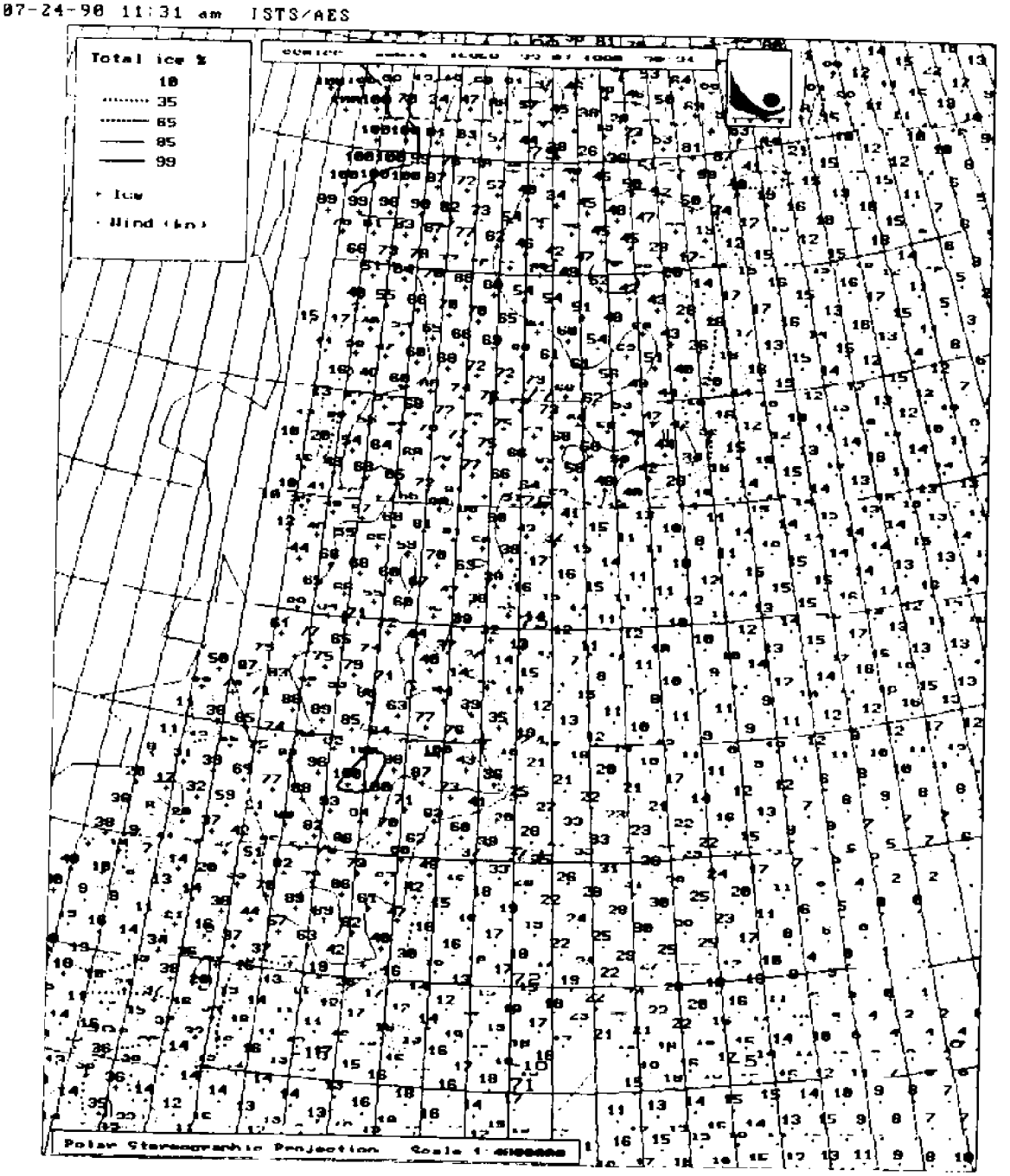

Figure 9. SSM/I ice and wind observations over the East Greenland Sea for 2 July 1990

CONCLUDING REMARKS

A brief description of storm surge modelling iss presented in the second section. It is shown that the wind stress and pressure gradient are the main inputs to study and simulate this phenomenon. If surges occur over the ice covered waters, a good knowledge of ice cover the areas of interest is essential. Information on conventional ice cover data is discussed along with a brief outline of other sources of data for ice concentration. Details of deriving wind and concentration of sea ice from the remotely sensed satellite passive microwave observations is also discussed. The information on wind and ice, thus derived from the SSM/I data is useful in the storm surge studies over the inaccessible areas of the Arctic such as the Beaufort Sea. It would be interesting to compare simulated surges using ice cover data from conventional and from SSM/I observations.

REFERENCES

Danard, M.B., M.C. Rasmussen, T.S. Murty, R.F. Henry, and Z. Kowalik. 1989. Inclusion of ice cover in a storm surge model for the Beaufort Sea. *Natural Hazards*. **2**:153-171.

Davies, A F., I.G. Rubinstein, and R.O. Ramseier. 1990. Meteorological applications of parameters derived from Special Sensor Microwave/Imager (SSM/I) brightness temperatures. ISTS Microwave Laboratory Report. MWG 90-2.

Garrity, C., S. El Naggar, A. Bochert, K.W. Asmus, V.R. Neralla, and R.O. Ramseier. 1990. Remote sensing of the sea in solid and liquid form. Cruise Report. FS Polarstern Expedition, ARKTIS VII/2 - 1990.

Gloersen, P., and F.T. Barath. 1977. The Seasat-A scanning multichannel microwave radiometer. *IEEE J. Oceanic Eng.* **OE-2**:172-178.

Goodberlet, M.A., C.T. Swift, and J.C. Wilkerson. 1989. Remote sensing of ocean surface winds with the Special Sensor Microwave/Imager. *J. Geophy. Res.* **94**:14,547-14,555.

Hibler, W.D. III. 1979. A dynamic thermodynamic sea ice model. *J. Phys. Oceanogr.* **9**:815-846.

Hollinger, J., R. Lo, G. Poe, R. Savage, and J. Pierce. 1987. Special sensor microwave/imager user's guide. Naval Research Laboratory Report.

Kowalik, Z. 1984. Storm surges in the Beaufort and Chukchi seas. *J. Geophys. Res.* **89**:10,570-10,578.

Lo, R.C. 1983. A comprehensive description of the Mission Sensor Microwave Imager (SSM/I) environmental parameter extraction algorithm. U.S. Navy Research Laboratory Memorandum Report 5159, pp. 1-48.

MANICE. 1989. Manual of standard procedures for observing and reporting ice conditions. Ice Centre Environment Canada Report.

Munn, R.E., ed. 1978. IUCRM Colloquium on radio oceanography. *Boundary Layer Meteorl.* **13**:1-429.

Murty, T.S. 1984. Storm surges - Meteorological ocean tides. Canadian Bull. of Fisheries and Aquatic Sciences. No. 12.

Neralla, V.R., R.G. Jessup, and S. Venkatesh. 1988. The Atmospheric Environment Service Regional Ice Model (RIM) for operational applications. *Marine Geodesy*. **12**:135-153.

Neralla, V.R,. and T.S. Murty. 1991. Determination of wind stress for use in real-time storm surge prediction in Bangladesh. In: Proc. Canada Bangladesh Forum Seminar - Bangladesh and Natural Disasters Ottawa, pp. 1-15.

Petty, G.W., and K.B. Katsaros. 1990. New geophysical algorithms for the Special Sensor Microwave Imager. In: Preprints 5th Conf. Satellite Meteorol. and Oceanogr. London, England, pp. 247-251.

Ramseier, R.O., D. Lapp, I.G. Rubinstein, and K. Asmus. 1989. Canadian validation of the SSM/I and AES/York algorithms for sea ice parameters. ISTS/Microwave Group Report.

Rothrock, D.A. 1980. The mechanical behavior of pack ice. *Ann. Rev. Earth Planet.* 3:317-342.

Rubinstein, I.G., and R.O. Ramseier. 1991. Retrieval of sea ice parameters from space-borne multifrequency passive microwave observations. ISTS/Microwave Group Report.

Schluessel, P., and H. Luthardt. 1991. Surface wind speeds over the North Sea from Special Sensor Microwave/Imager observations. *J. Geophy. Res.* **96**:4845-4852.

Swift, C T., ed. 1977. Special joint session on radio oceanography. *IEEE J. of Ocean Engg.* **OE2**:1-159.

Swift, C.T., and D.J. Cavalieri. 1985. Passive microwave remote sensing for sea ice research. *EOS Trans. American Geophy. Union*. pp. 1210-1212.

Wu, J. 1980. Wind stress coefficients over sea surface in neutral conditions- a revisit. *J. Phys. Oceanogr.* **10**:727-740.

EFFECTS OF SEAQUAKES ON FLOATING STRUCTURES

Kyoichi Okamoto and Masaaki Sakuta
Nihon University
Chiba, Japan

ABSTRACT

Seaquakes are caused by propagation of the vibration of the seabed through seawater. From the viewpoint of structural design, the effects of seaquake must be taken into account in considerations of the safety of structures in the earthquake zone.

In this paper, hydrodynamic forces caused by a seaquake are analyzed and their effects on the floating structures are investigated. A numerical method is proposed, and employed to make clear the effects of seaquakes on floating structures.

Effects of seaquakes depend on the width of the seismic seabed and water depth.

INTRODUCTION

There is not much research on response analysis on floating structures by earthquakes, but due to waves. This is the reason why it was generally considered that floating structures do not suffer the effects of an earthquake.

Earthquake waves, however, propagate from seabed through seawater to floating structures or streaming ships near the field where the vertical components of earthquake becomes more vibrated. Its waves generate some damage to these structures. This is called the "seaquake" phenomena, and its existence is evident fromship damage reports.

From the above viewpoint, the structure design must be required in the consideration of seaquakes. The object of this study is to propose a numerical method in order to make clear the effects of seaquakes on floating structures.

In this paper, the Helmholtz equation is applied so that this mechanism, that is, the pressure waves due to vertical vibration which are propagated from seabed through seawater to floating structures, can be grasped. This problem is also formulated using the Hybrid Boundary Element Method which has some merit in application of a fluid problem and also in complex-shaped ocean structures. Thus, consideration on the effects of this propagation by seaquakes is made.

SEAQUAKES AND THEIR STUDIES

The impact due to seaquakes have been actually reported by ship crews, who have described these encountered seaquakes as: "The ship stroke on unknown shoal or rocks," "A sunken vessel refloated and collided against our ship," "We saw an underwater eruption," and so on. Ambraseys (1985) also reported a tanker which encountered a seaquake during a cruise in the Atlantic Ocean and suffered serious damage to its structures and functions.

Recent records in Japan are left concerning ships which suffered damages by seaquakes during the Niigata earthquake of 1964 and the Central Japan Sea earthquake of 1983, as shown by Miyoshi (1983).

As a study on the effects of seaquakes to marine structures, one has been performed by Baba (1987) and Matsuoka (1988) to analyze the behavior of a floating structure due to a seaquake using the potential theory of incompressible fluid. The study reports that a floating structure makes exactly the same movements as that of the seabed when a flat seabed of an open sea area makes vertical movements over a wide range.

As a method of analyzing wave motion by seaquakes, Watanabe (1988) proposed a nonlinear analytical method in one dimension based on his understanding that the effects of seaquakes are mainly caused by acoustic shock wave pressure. Okamoto and Kato (1989) proposed an analytical method in frequency domain using the Laplace equation.

Furthermore, Kiyokawa and Inada (1989), taking seaquakes as a propagation phenomenon of acoustic waves in compressible fluid, have introduced a two-dimensional Green function and formulated the velocity potential.

In experimental studies on seaquakes, vertical shaking tests were performed by Baba (1988) and Hagiwara, et al. (1987). According to Baba, the response magnification of a floating body is nearly unity, irrespective of the distance between the floating body and the tank floor.

NUMERICAL STUDY

Helmholtz equation

In an elastic seabed, a seismic wave propagates with a compressional wave (P wave) and a shear wave (S wave). However, shear waves do not exist in sea water and ground motion propagated with compressional and shear waves of earthquaks up to the surface of the seabed is introduced into seawater with compressional waves.

Therefore, we have the wave equation with reference to Brebbia and Connor (1976),

$$\frac{\partial^2 \Phi}{\partial t^2} = c^2 \nabla^2 \Phi \tag{1}$$

where c is underwater acoustic velocity, and Φ is the velocity potential.

In order to analyze underwater propagation of compressional wave, the Helmholtz equation is introduced as a governing equation in the flow field.

Boundary value problem

Seawater is assumed to be a nonviscous, compressible and irrotational fluid. The time dependence of the fluid motion to be considered is restricted to harmonic motion. The coordinate system is shown in Figure 1, where Γ_B is the boundary at the wetted floating body, Γ_F the boundary at the sea surface, Γ_H is one at the seabed, Γ_E is one of the wave source, and Γ_{SR} denotes the virtual boundaries which divide the flow field into near field inside the boundaries including the floating body and the far field outside the boundaries.

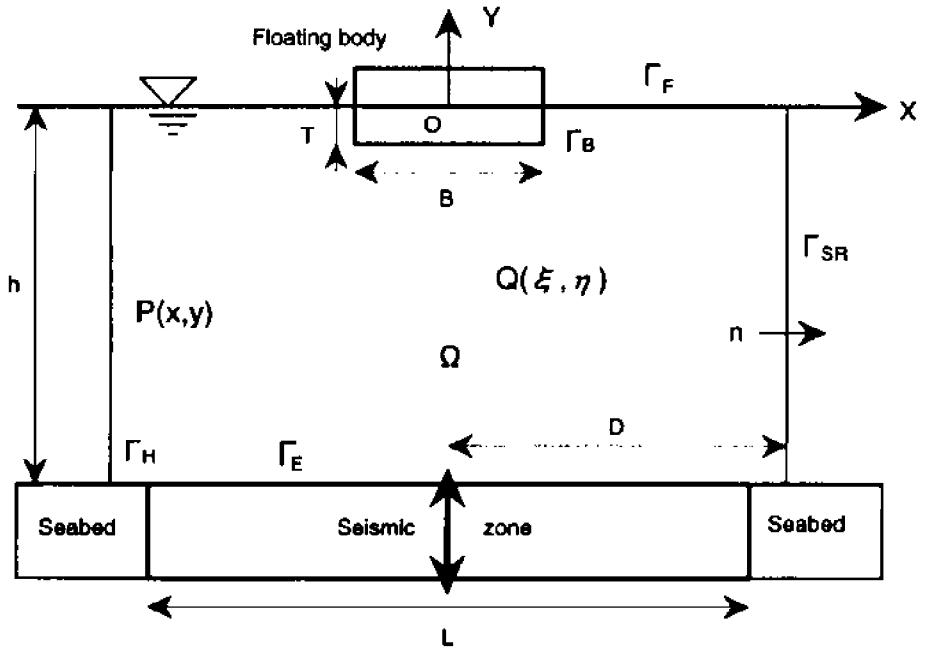

Figure 1. Coordinate system and analytical model
B=body width, T=draft of body, h=depth, L=width of seismic seabed,
D=distance to imaginary boundary, P(x,y)=observation point,
Q(ξ,η)=wave source point

Substituting the velocity potential of Eq. (2) into Eq. (1), the governing equation can be written as

$$\Phi = \phi e^{i\omega t} \tag{2}$$

where $\phi = \phi(x,y)$ and it is assumed that the real part of Φ is required. Then

$$\nabla^2\phi + K^2\phi = 0 \qquad \text{in } \Omega \tag{3}$$

where $K = \omega/c$.

Boundary conditions are shown as follow,

$$\frac{\partial\phi}{\partial n} = 0 \qquad \text{on } \Gamma_B \tag{4a}$$

$$\phi = 0 \qquad \text{on } \Gamma_F \tag{4b}$$

$$\frac{\partial\phi}{\partial n} = 0 \qquad \text{on } \Gamma_H \tag{4c}$$

$$\frac{\partial\phi}{\partial n} = v \qquad \text{on } \Gamma_E \tag{4d}$$

where v is the velocity amplitude of vibration at the sea floor.

The velocity potential in the near field is ϕ and that of the far field is $\bar{\phi}$. Boundary condition of the imaginary boundary are expressed by Eqs. (5a) and (5b).

$$\phi = \bar{\phi} \qquad \text{on } \Gamma_{SR} \tag{5a}$$

$$\frac{\partial \phi}{\partial n} = \frac{\partial \bar{\phi}}{\partial n} \qquad \text{on } \Gamma_{SR} \tag{5b}$$

Formulation of velocity potential

The velocity potential $\bar{\phi}$ of the far field is expressed by Eq. (6) using Eigenfunctions, referred by Morse and Feshbach (1953),

$$\bar{\phi} = \sum_{n=1}^{s} A_n \sin k_n y e^{i\lambda_n x} + \sum_{n=s+1}^{\infty} A_n \sin k_n y e^{i\lambda_n' x} \tag{6}$$

where k_n (n=1,2,...), λ_n (n=1,2,...), λ_n' (n=s+1,s+2,...); constants defined by Eqs. (7a), (7b) and (7c), respectively. Incidentally, s is the maximum integer which makes the right side of the equation (7b) positive.

$$k_n = (2n-1)\frac{\pi}{2h} \tag{7a}$$

$$\lambda_n^2 = \frac{\omega^2}{c^2} - \{(2n-1)\frac{\pi}{2h}\}^2 \tag{7b}$$

$$\lambda_n'^2 = \{(2n-1)\frac{\pi}{2h}\}^2 - \frac{\omega^2}{c^2} \tag{7c}$$

The velocity potential ϕ of the near field is analyzed using the Green's theorem. Here, the fundamental solution ϕ^* is defined in terms of the zeroth-order Hankel function of the second kind.

Direct wave to floating body and reflected wave from the sea surface are considered. Namely,

$$\phi^* = \frac{1}{4\pi}\{H_0^{(2)}(KR) - H_0^{(2)}(KR')\} \tag{8}$$

The first term of the right side of the equation represents directly reaching wave and the second term, reflected wave from the sea surface. Here, R and R' are as follows,

$$R = \sqrt{(x-\xi)^2 + (y-\eta)^2} \tag{9a}$$

$$R' = \sqrt{(x-\xi)^2 + (y+\eta)^2} \tag{9b}$$

where x,y are the coordinates of the observation point P and ξ,η are the coordinates of wave source point Q, respectively. R and R' refer to the distance from the observation point to the source point and the image point, respectively.

The boundary integral equation for velocity potential ϕ is expressed as follows, in the usual Boundary Element technique referred by Brebbia and Walker (1980),

$$\begin{aligned}\phi(P) = &-\int_{\Gamma_H} \phi \frac{\partial \phi^*}{\partial n} d\Gamma - \int_{\Gamma_B} \phi \frac{\partial \phi^*}{\partial n} d\Gamma \\ &-\int_{\Gamma_E} \left(\phi \frac{\partial \phi^*}{\partial n} - v\phi^* \right) d\Gamma \\ &-\int_{\Gamma_{SR}} \left(\bar{\phi} \frac{\partial \phi^*}{\partial n} - \frac{\partial \bar{\phi}}{\partial n} \phi^* \right) d\Gamma\end{aligned} \tag{10}$$

Substituting the fundamental solution ϕ^* by Eq. (9) into Eq. (10), the boundary integral equation is expressed as follows,

$$\begin{aligned}2i\phi = &-\frac{1}{2}\Bigg[\int_{\Gamma_{SR}} \Bigg\{ \left(H_0^{(2)}(KR) - H_0^{(2)}(KR') \right) \frac{\partial \bar{\phi}}{\partial n} \\ &+ \bar{\phi} K \left(\frac{1}{R} H_1^{(2)}(KR) - \frac{1}{R'} H_1^{(2)}(KR') \right) (x - \xi) \Bigg\} d\Gamma \\ &+ \int_{\Gamma_H} \phi K \left\{ \frac{y - \eta}{R} H_1^{(2)}(KR) - \frac{y + \eta}{R} H_1^{(2)}(KR') \right\} d\Gamma \\ &+ \int_{\Gamma_E} \left\{ \left(H_0^{(2)}(KR) - H_0^{(2)}(KR') \right) v \right. \\ &+ \left. \left\{ \phi K \left\{ \frac{y - \eta}{R} H_1^{(2)}(KR) - \frac{y + \eta}{R} H_1^{(2)}(KR') \right\} d\Gamma \right. \\ &+ \left. \int_{\Gamma_B} \phi K \left\{ \frac{y - \eta}{R} H_1^{(2)}(KR) - \frac{y + \eta}{R} H_1^{(2)}(KR') \right\} d\Gamma \right]\end{aligned} \tag{11}$$

Determining the velocity potential ϕ from Eq. (11) and the hydrodynamic pressure from Eq. (12), the total seaquake force acting on the entire floating body is given by Eq. (13),

$$p = -\rho \frac{\partial \Phi}{\partial t} = -i\rho\omega\Phi \tag{12}$$

$$F = -i\rho\omega \int_{\Gamma_B} \Phi \frac{\partial y}{\partial n} d\Gamma \tag{13}$$

where ρ is the fluid density and $\partial y / \partial n$ denotes the normal dervative of y component.

ANALYTICAL RESULTS

Calculation is carried out for a barge-type floating body. The seaquake forces are computed for harmonic inputs of varying frequency between Kr = 0.01 to 0.60, where r is the half width of the body.

The results of the seaquake forces are represented by the nondimensional values as a function of the nondimensional frequency. Here, B is the width of the barge, T is the draft, h is the water depth, L is the width of the seismic seabed and D is the distance from the origin to the imaginary boundary. The vertical displacement amplitude at the seismic seabed denotes a, since $v = i\omega a\partial y / \partial n$ in Eq. (4d).

Location of imaginary boundary

First, it is necessary to find out the reasonable location of the imaginary boundary. Figure 2 shows the nondimensional distance D/r. From this figure, the stability of the solution on seaquake forces can be determined when its distance becomes more than seven times of the half width of a body.

Therefore, the distance to be used in our calculation is the seven times value.

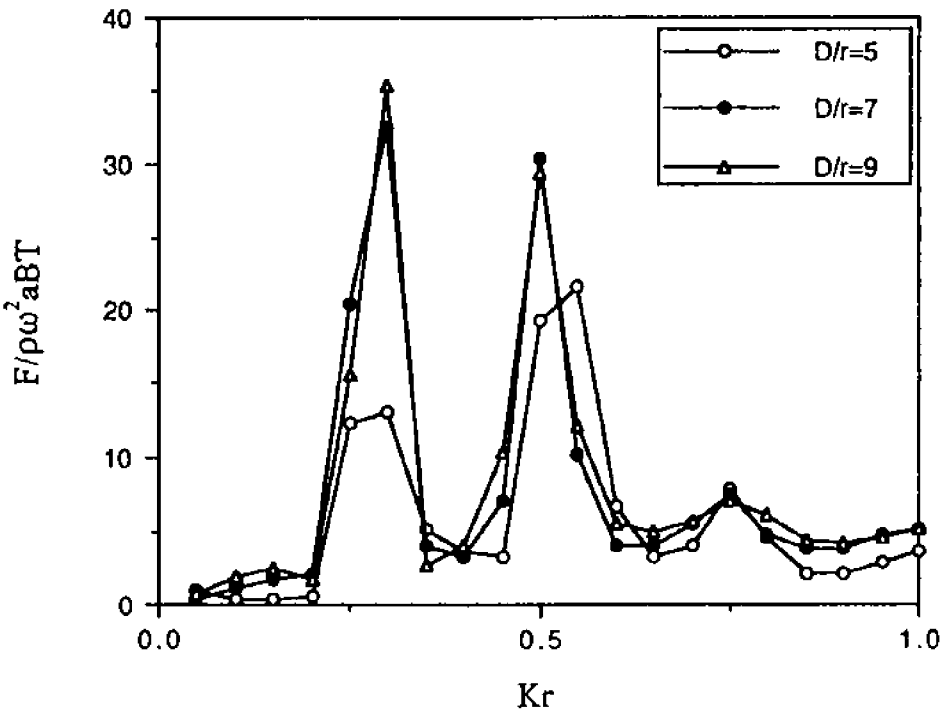

Figure 2. Seaquake forces varying locations of the imaginary boundary
B=body width, T=draft of body, h=depth, L=width of seismic seabed,
D=distance to imaginary boundary, a=vertical displacement amplitude

Effects of width of seismic seabed

Figure 3 shows the nondimensional seaquake forces with respect to the varying the width of the seismic seabed. From these figures, the frequency at resonance does not change, even if its width is shortened.

The magnitude of the seaquake force is also dependent on the width of the seismic seabed. However, these theoretical calculations require further research, including damping and diffusion in its propagation.

Hence, the width of the seismic seabed to be used in our calculations is using the value L/r = 28.

Effects of water depth

Figure 4 shows the seaquake force compared with water depth. From this figure, the magnitude of seaquake force is also dependent on frequency, and it increases substantially at resonance, because of water compression. The number of resonant frequencies for seaquake force increase according to the increase in water depth.

Calculation example of prototype

A calculation example for the prototype is preformed. The conditions of calculation are indicated: length = 28.7 m, width = 72.0 m, draft = 30.0 m, and water depth = 500.0 m.

The frequency to be use is the predominant one from the Kanai-Tajimi power spectrum as the acceleration sepectrum for the vertical vibration at seabed, as referred to by Tanjimi (1960), so that the frequency is 2.5 Hz which is equivalent to Kr = 0.38 and also indicates the acceleration of the seabed is 100 cm/sec^2.

The computed seaquake force indicates 35 MN, that is, the seaquake force becomes 30%, comparing the initial tension of the tendon if it is assumed to be the tension leg platform.

CONCLUSIONS

In order to grasp the effects of floating structures due to seaquakes, the formulation was performed by the Hybrid Boundary Element Method, and also a computation calculation was carried out.

Seaquake force is dependent on frequency, and it increases substantially at resonance because of water compression. The number of resonant frequencies for seaquake force increases according to the increase in water depth.

From the calculation example for the prototype, the seaquake force becomes 30%, compared with the initial tension of tendon on the tension leg platform.

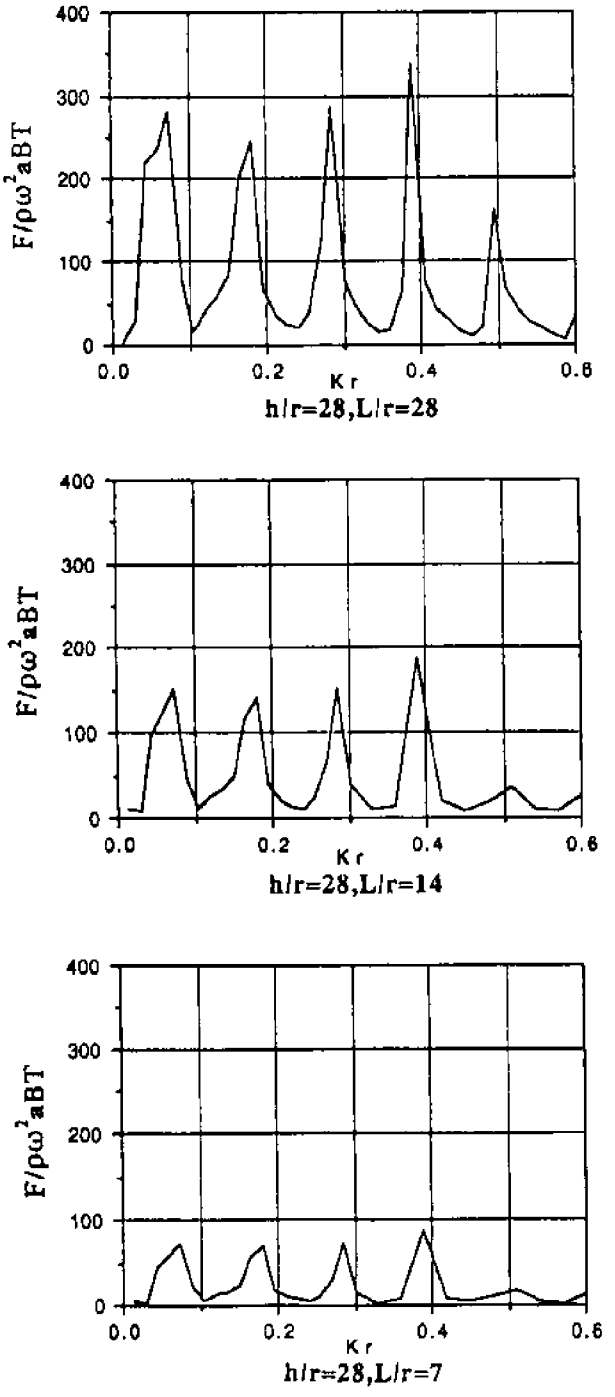

Figure 3. Seaquake forces varying width of vibration seabed
B=body width, T=draft of body, h=depth, L=width of seismic seabed,
D=distance to imaginary boundary, a=vertical displacement amplitude

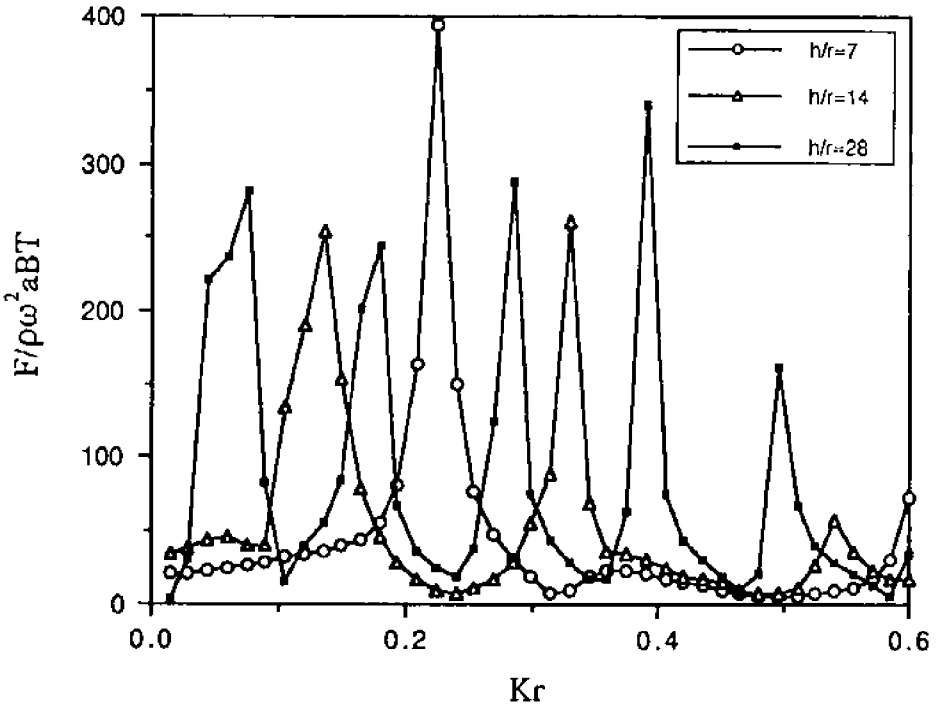

Figure 4. Seaquake forces varying water depth
B=body width, T=draft of body, h=depth, L=width of seismic seabed,
D=distance to imaginary boundary, a=vertical displacement amplitude

REFERENCES

Ambraseys, N. 1985. A damaging seaquakes. *Earthquake Engineering and Structures Dynamics*. 13:421-424.

Baba, E. 1987. A study on the effect of seaquakes on the floating body. *Jour. of Society of Naval Architects of Japan*. 162:90-98.

Baba, E. 1988. Acceleration response of a floating body to seaquake. In: Proc. 8th Ocean Engineering Symp., pp. 305-311 (in Japanese).

Brebbia, C.A., and J.J. Connor. 1976. Finite element techniques for fluid flow. Butterworth. pp. 135-137.

Brebbia, C.A., and Walker, S. 1980. Boundary element techniques in engineering. Butterworth. pp. 90-98.

Hagiwara, Y., Y. Masuko, S. Nakamura, S. Matuura, and H. Shiogiri. 1987. Seismic response property of floating-type structure for nuclear power plant (No. 2). Report of Central Research Institute of Electric Power Industry (in Japanese).

Kiyokawa, K., and Y. Inada. 1989. Mechanism of seaquake generation. In: Proc. of Coastal Engineering of Japan, Japan Society of Civil Engineers. Vol. 36, pp. 734-738 (in Japanese).

Matsuoka, K. 1988. A seismis property of floating-type structure. *Jour. of Society of Naval Architects of Japan*. **706**:214-220 (in Japanese).

Miyoshi, M. 1983. Underwater earthquakes noticed by ships. *Kokai*. **75**:103-109 (in Japanese).

Morse, P.M., and H. Feshbach. 1953. Method of Theoretical Physics, Part I. McGraw-Hill.

Okamoto, K., and W. Kato. 1989. Analysis of dynamic response of floating body due to seaquake. *Jour. of Structural and Construction Engineering*. pp. 1169-1170. Architectural Institute of Japan (in Japanese).

Tajimi, H. 1960. Statistical method of determining the maximum response of building structure during an earthquake. In: Proc. 2nd World Conference on Earthquake Engineering. Vol. 2, pp. 781-798.

Watanabe, I. 1988. Vibration problems for marine structure - prediction method for disturbance and external load as a source of vibration. Japan Intl. Marine Science and Technology Federation, pp. 111-112 (in Japanese).

A NUMERICAL ALGORITHM FOR THE FREE HARBOR OSCILLATION ANALYSIS WITH FINITE ELEMENTS

Yeon-Sun Ryu, Byung-Gul Lee, and Kyu-Dae Cho
National Fisheries University of Pusan
Pusan, Korea

ABSTRACT

This paper presents a robust numerical algorithm for the free harbor oscillation. Mathematical difficulties in the solution of governing Helmholtz equation are numerically overcome through the application of finite element technique. Eigenvalue shifting and coefficient scaling are incorporated in the subspace iteration method of eigenanalysis to treat inherent numerical singularity and ill-conditioning.

A general-purpose computer program is developed based on the algorithm and typical problems are solved. From the study, finite element method is found to be efficient and practically useful for the analysis of free harbor oscillation.

INTRODUCTION

The understanding and evaluation of long waves is of great importance to the engineers in the design and operation of harbors and in the development and maintenance of estuaries and bays. This is mainly because the long wave of the proper period can cause the resonance in a harbor or estuaries (Dean and Dalrymple, 1984; Horikawa, 1978).

For the study of long waves in two-dimensional domain, linearized continuity equation and linearized frictionless long wave equations of motion are usually considered. They can be combined and expressed as ;

$$\eta_{,tt} = g\left[(h\eta_{,x})_{,x} + (h\eta_{,y})_{,y}\right] \tag{1}$$

where $\eta=\eta(x,y,t)$ is the surface elevation, g is gravitational acceleration, $h=h(x,y)$ is water depth, and the subscript following a comma denotes the partial derivative. Under the assumption of constant water depth over the domain, Eq. (1) is written as the so-called wave equation;

$$c^2(\eta_{,xx} + \eta_{,yy}) = \eta_{,tt} \tag{2}$$

where $c = \sqrt{gh}$ is the phase velocity.

A solution of Eq. (1) or Eq. (2) with proper initial and boundary conditions consists of space-dependent functions f(x,y) and time-dependent functions. The evaluation of f(x,y), which is variously called as free oscillation mode, characteristic mode, or eigenfunction, is the major concern of this study. The results of the study can be also

used in the solution procedure of forced oscillation problems since they may be represented as a linear combination of free oscillation modes (Courant and Hilbert, 1962).

Derivation and property of governing equation, solution methods and numerical techniques with the emphasis on the finite element method, and associated numerical algorithm for the development of computer code are addressed in order. Finally, a few numerical examples are presented and the results are discussed before the general applicability of finite element technique is assured.

CONSIDERATIONS ON GOVERNING EQUATION

Since Eq. (2) is linear, the solution can be expressed as a sum of monochromatic wave functions

$$\eta(x,y,t) = \sum \alpha f(x,y) e^{iwt} \tag{3}$$

Hence the governing equation for the free harbor oscillation can be expressed as the Helmholtz equation in a harbor domain D

$$c^2(f_{,xx} + f_{,yy}) + \omega^2 f = 0 \tag{4}$$

with the boundary condition on all boundary

$$f_{,n} = 0 \tag{5}$$

where n is unit outward normal vector at boundaries. Eigenvalues ω^2 and eigenfunctions f(x,y) have the physical meaning of natural frequencies squared, and the corresponding modes respectively. Natural period of each mode is recovered as $T=2\pi/\omega$.

Although the governing Helmholtz equation has been derived under the assumption of constant water depth, it is no more constant in real harbors. Thus Eq. (4) cannot be directly solved for the free oscillation analysis in a harbor with complex bottom topography. Furthermore, it is not easy at all to analytically impose the boundary conditions of Eq. (5) when the general geometric boundary is involved. In this regard, an efficient and practically applicable scheme to evaluate free oscillation periods and modes in a real harbor should be provided.

AVAILABLE METHODS OF ANALYSIS

For the analysis of free harbor oscillation, field observations and hydraulic model experiments have been used (Ippen, 1966). But they cannot be pursued or are very expensive in case of newly-designed harbors. Therefore, analytical or numerical methods must be developed and some of them are shown to be applicable (Wilson, 1966; Ryu and Lee, 1985).

The governing Helmholtz equation, Eq. (4), is a homogeneous linear partial differential equation of eigenproblem. The boundary condition of Eq. (5) is of

homogeneous Neumann type. Thus, the first solution of rigid body mode is always expected, which is trivial. Like other kind of differential equations, it can be analytically solved only when the domain and the boundary are geometrically simple and mathematically tractable. Some of them are available and summarized by Wilson (1966). If any geometric complexity in the domain and the boundary is involved, analytical methods may not be applied or fail to get the solution. In such a case, which is very common in real-world problems, numerical methods have to be devised and applied.

Among the various numerical methods, finite difference method (FDM) and finite element method (FEM) have been widely used for such a class of problems. But the FDM, due to an over simplification or approximation of governing equation, may yield poor solutions when highly complex boundary or bottom topography is involved (Tacker, 1977). A pilot application of FEM for the free oscillation analysis of geometrically simple harbor can be found (Ralston and Wilf, 1967). However, successful application of FEM in other fields related to the characteristic analysis may be found (Zienkiewicz, 1971), where the FEM is shown to be robust. Therefore the application of FEM on the free oscillation analysis in a real harbor should be taken into consideration and a numerical algorithm as well as a general-purpose computer program for the practical use should be developed.

FINITE ELEMENT EQUATION

For the numerical solution of Eqs. (4) and (5) with FEM, the domain is idealized using proper number and size of finite elements. Then, the water depth in a subdomain or a finite element is kept constant so that Eq. (4) will be valid. Although this is an only approximation in FEM, bottom topography *in situ* can be realized through the proper mesh refinement.

To derive a finite element equation, the eigenfunction in an element is interpolated with element nodal values $f_i^{(e)}$ as

$$f(x,y) = N_i(x,y) f_i^{(e)} \tag{6}$$

where N_i is properly chosen interpolation polynomial, and the summation convention is used for the repeated subscripts herein. Then, the Galerkin's procedure may be used to get an element equation, where the interpolation functions N_i are used as weighting functions of the residual integral over the element domain $D^{(e)}$.

Superposition of element equations or element matrices $K^{(e)}$ and $M^{(e)}$ with boundary condition, Eq. (5), leads to the system finite element equation to be solved. It is a generalized algebraic eigenvalue equations for the whole domain and boundary

$$KR - \omega^2 MR = 0 \tag{7}$$

where $K = \sum K^{(e)}$ and $M = \sum M^{(e)}$.

The eigenvalue ω^2 represents the numerical solution of natural frequency squared and the corresponding eigenvector R contains nodal values of engenfunction $F_i^{(e)}$. Element matrices are expressed as

$$K_{ij}^{(e)} = c^{(e)} 2 \int_{D^{(e)}} (N_{i,x} N_{j,x} + N_{i,y} N_{j,y}) dD \tag{8}$$

$$M_{ij}^{(e)} = \int_{D^{(e)}} N_i N_j dD \tag{9}$$

where $c^{(e)} = \sqrt{gh^{(e)}}$, and $h^{(e)}$ is constant water depth in each element.

Here, several notes are addressed on the finite element equation in relation to numerical computations. Theoretically, matrix eigenproblem of Eq. (7) is solvable as matrices K and M must be positive definite or semi-definite. However, in most numerical methods, positive definiteness of K and positive semi-definiteness of M are required. The matrix K does not satisfy the positive-definite condition since it contains the rigid body mode due to the Neumann type boundary conditions of Eq. (5). Thus it is singular in nature. The singularity of matrix K usually causes the numerical difficulties in the numerical eigensolution procedure.

Another computational difficulty of numerical ill-conditioning can arise when the magnitudes of elements in K and M are of significant difference. The orders of element magnitude in K and M are of $O(h^{(e)}/D^{(e)})$ and $O(D^{(e)})$ as can be respectively seen in Eqs. (8) and (9). Thus, such a undesirable situation will happen in case the area $D^{(e)}$ of the finite element would become considerably larger than the water depth $h^{(e)}$, which is the common case in reality with very large domain in relatively shallow water. In order to overcome above-mentioned difficulties during the numerical computation, effective techniques should be devised in the computational algorithm.

SOLUTION ALGORITHM

Since the matrices in the generalized algebraic eigenvalue problem of Eq. (7) are real and symmetric, all the eigenvalues are real. The number of linearly independent eigenvectors that can be constructed is the same as the size of matrices, even if there exist multiple eigenvalues. In practice, however, the lowest few eigensolutions are of engineers' concern. Among a variety of available numerical methods for the solution of generalized algebraic eigenvalue problems the subspace iteration method is suitable for the partial eigensolution of large scale problems (Bathe, 1982; Ryu, 1984).

Prior to the application of any numerical eigensolution method, proper modifications on Eq. (7) need be made to treat the problems of numerical ill-conditioning and singularity. To alleviate numerical ill-conditioning, scaling of M is introduced in Eq. (7) as

$$M^* = 10^{-s} M \tag{10}$$

Depending on the problems at hand a scaling factor s is so chosen that the orders of magnitude in the elements of matrices K and M* are made approximately the same. Hence the numerical ill-conditioning can be avoided. For the treatment of singularity, shifting strategy is effectively applied in the computational procedure

$$K^* = K + \sigma M^* \tag{11}$$

where is a shifting parameter, which must be so chosen that K* is no longer singular matrix. Thus, a modified equation to be numerically solved and recovery procedure of original eigenvalues are respectively expressed as

$$K^* = K + \sigma M^* \tag{11}$$

$$K^* R = \lambda M^* R \tag{12}$$

where the foregoing modifications do not affect eigenvectors.

The solution procedure described above is transcribed in the following step algorithm, which is ready to be coded.

STEP 1. Input data, which includes the information of finite elements and nodal points.

STEP 2. Construct element matrices and assemble them to form system matrices K and M.

STEP 3. Choose or calculate σ and s, and modify the matrices to get K* and M*.

STEP 4. Call the subroutine SUBSPACE to solve Eq. (12).

STEP 5. Recover the eigenvalues using Eq. (13) and calculate natural periods.

STEP 6. Normalize the eigenvectors as $R_i \leftarrow R_i/\max |R_i|$.

STEP 7. Output the results.

NUMERICAL EXAMPLES

Based on the step algorithm in the previous section, a computer program FEHOA (Finite Element Harbor Oscillation Analysis) is developed using the linear triangular elements. Automatic mesh generation routine is incorporated in the program. The program has been tested for several example problems and a real harbor. Only a few typical examples are presented herein. Domain, boundary, and bottom topography of these are described in Table 1.

For the cases SC and CC, analytical solutions are available (Proudman,1953; Defant, 1960; Horikawa, 1978);

$$SC: \quad \omega^2 = c^2\pi^2(k^2/a^2 + m^2/b^2); \qquad k,m = 0,1,2... \tag{14a}$$

$$f(x,y) = \cos(k\pi x/a)\cos(k\pi y/b) \tag{14b}$$

$$CC: \quad J_1(\omega\rho/c) = 0 \tag{15a}$$

$$f(r,\theta) = J_0(\omega r/c) \tag{15b}$$

where a and b are two sides of rectangular domain in x and y direction, J_0 and J_1 are the zeroth and first order Bessel functions, r, θ are polar coordinates, and ρ the radius of

circular domain, respectively. Analytical eigenvalues for a few lowest modes are listed in Table 2 and they are to be used for the quantitative comparison with numerical results.

For the cases SV and CV, trends of the results can be investigated. For this purpose, Hidaka's result will be referred, which states that the wave amplitudes in shallower region are consistently larger than those in deeper region (Hidaka, 1932).

Table 1. Description of example problems

Case	Domain & Boundary	Water depth(bottom topography)	Remarks
SC	square	constant : h = 20 , m	$-80 \le x \le 80$, km
SV	a=b=160km	variable : h = 10-x/8000, m	$-80 \le y \le 80$, km
CC	circle	constant : h = 20 , m	$0 \le r \le 80$, km
CV	ρ = 80km	variable : h = 20(1-r/80000)^2, m	$-180^\circ \le \theta \le 180^\circ$

Table 2. Lowest eigenvalues and natural periods for example cases

	Mode	SC Analytic	SC Numerical	SV Numerical	CC Analytic	CC Numerical	CV Numerical
ω^2	1	.755E-07	.781E-07	.246E-07	.112E-06	.117E-06	.447E-07
	2	.755E-07	.781E-07	.290E-07	.112E-06	.117E-06	.447E-07
	3	.151E-06	.160E-06	.561E-07	.377E-06	.327E-06	.989E-07
	4	.302E-06	.324E-06	.664E-07	.377E-06	.327E-06	.989E-07
	5	.302E-06	.324E-06	.963E-07	.792E-06	.574E-06	.184E-06
T (sec)	1	22857.1	22485.5	40039.8	18740.0	18383.3	29724.2
	2	22857.1	22485.5	36924.3	18740.0	18383.3	29724.2
	3	16162.4	15705.5	26534.9	10236.1	10982.3	19977.5
	4	11428.6	11035.9	24374.6	10236.1	10982.3	19977.5
	5	11428.6	11033.9	20249.2	7058.3	8294.0	14665.2

RESULTS AND DISCUSSIONS

Finite Element Meshes

For both cases SC and SV, 81 nodal points are equally spaced in the square domain and boundary. Center node (node number 41) is taken as origin of rectangular coordinate axes. Table 3 contains nodal coordinates for a half domain and the rest are symmetrically located. Bottom topography data are not listed since they can be easily evaluated from the topography functions given in Table 1. The idealized square domain consists of 128 right triangular finite elements.

Table 4 contains the same kind of information for the cases CC and CV. Nodal points are located on 6 concentric circles whose radii are 2, 3, 5, 10, 20 and 40 k, respectively. On each circle, nodes are generated with equal circumferential angle space of 30°. Locations of nodes are so selected as to minimize the aspect ratio of a finite element. Hence there are 73 nodes including center of domain andboundary. Polar coordinates of these are listed in the table for a half domain. There are 132 triangular elements in the finite element model for both CC and CV.

Input Parameters

In the numerical computation, σ=0.1 and s=6 are used for all the cases. Number of modes to be required in the subspace iteration method is 10.

Numerical Results and Discussions

Numerical results for the lowest few modes are also presented in Tables 2 through 4.

As expected from the anlaytical solutions for SC and CC, planar and polar symmetry and skew-symmetry are represented in the numerical solution of each eigenmode including typical rigid body modes. For the cases SV and CV, larger amplitudes of the lowest eigenmodes consistently appear in the shallow region. They are excellent representation of Hidaka's result. Hence the algorithm and developed program are thought to have reasonable qualitative performance.

Numerical eigenvalues ω^2 in Table 2 show a good agreement with analytical ones for the cases SC and CC. Eigenvalues for the cases SV and CV are also reasonable since the natural periods T are consistently larger than those for SC and CC, respectively. Such a trend well represents the physical phenomena of free oscillation, which can be also drawn from the cross comparison of the results of all cases. Therefore the robustness of the finite element numerical algorithm has been proven, which is based on the qualitative trends and quantitative accuracy of finite element solutions.

CONCLUSION

A finite element program for the analysis of free oscillation in a harbor domain with general bottom topography and geometrically complex boundary is developed and successfully tested. Since the governing Helmholtz equation is valid only when the water depth in a domain is constant, it is transformed into a generalized algebraic eigenvalue

Table 3. Nodes and eigenvectors in a half domain (square cases SC and SV)

Node No.	Coord. x (km)	Coord. y (km)	Normalized Eigenvectors Mode 1 SC	Mode 1 SV	Mode 2 SC	Mode 2 SV	Mode 3 SC	Mode 3 SV	Mode 4 SC	Mode 4 SV	Mode 5 SC	Mode 5 SV
1	-80	80	-0.518	-1.000	-0.999	0.930	0.955	1.000	0.856	0.821	-0.439	-1.000
2	-80	60	-0.540	-0.936	-0.954	0.923	0.906	0.769	0.711	0.762	-0.526	-0.553
3	-80	40	-0.591	-0.733	-0.791	0.927	0.705	0.116	0.258	0.664	-0.711	0.431
4	-80	20	-0.665	-0.422	-0.541	0.941	0.393	-0.586	-0.221	0.493	-0.904	0.770
5	-80	0	-0.752	-0.049	-0.243	0.959	0.020	-0.935	-0.439	0.210	-0.997	0.063
10	-60	80	-0.468	-0.704	-0.994	0.551	0.906	0.497	0.826	0.189	-0.262	-0.334
11	-60	60	-0.486	-0.652	-0.938	0.548	0.840	0.354	0.640	0.174	-0.328	-0.117
12	-60	40	-0.535	-0.504	-0.772	0.552	0.647	0.012	0.173	0.164	-0.508	0.251
13	-60	20	-0.609	-0.281	-0.520	0.562	0.355	-0.331	-0.305	0.137	-0.696	0.316
14	-60	0	-0.696	-0.018	-0.222	0.575	0.010	-0.478	-0.510	0.068	-0.783	-0.003
19	-40	80	-0.310	-0.489	-0.948	0.246	0.705	0.224	0.672	-0.186	0.234	-0.067
20	-40	60	-0.325	-0.452	-0.889	0.245	0.647	0.154	0.473	-0.171	0.177	0.008
21	-40	40	-0.373	-0.348	-0.721	0.249	0.493	-0.010	-0.003	-0.119	0.001	0.133
22	-40	20	-0.446	-0.191	-0.468	0.256	0.266	-0.171	-0.481	-0.047	-0.183	0.143
23	-40	0	-0.533	-0.007	-0.169	0.265	0.000	-0.233	-0.682	0.021	-0.263	0.020
28	-20	80	-0.068	-0.342	-0.874	0.012	0.393	0.093	0.507	-0.378	0.758	0.006
29	-20	60	-0.083	-0.316	-0.814	0.012	0.356	0.060	0.305	-0.348	0.696	0.031
30	-20	40	-0.130	-0.242	-0.645	0.015	0.266	-0.015	-0.174	-0.261	0.518	0.071
31	-20	20	-0.202	-0.131	-0.391	0.021	0.138	-0.088	-0.654	-0.135	0.334	0.069
32	-20	0	-0.288	-0.000	-0.091	0.027	-0.007	-0.112	-0.854	0.006	0.257	0.024
37	0	80	0.219	-0.244	-0.786	-0.159	0.021	0.032	0.436	-0.460	1.000	0.010
38	0	60	0.205	-0.225	-0.725	-0.158	0.010	0.017	0.237	-0.424	0.923	0.018
39	0	40	0.158	-0.171	-0.555	-0.156	0.000	-0.016	-0.244	-0.322	0.737	0.030
40	0	20	0.086	-0.091	-0.300	-0.152	-0.007	-0.047	-0.725	-0.170	0.550	0.028
41	0	0	0.000	0.003	0.000	-0.146	-0.010	-0.053	-0.925	0.004	0.472	0.011
46	20	80	0.510	-0.179	-0.696	-0.279	-0.355	0.004	0.508	-0.485	0.811	-0.004
47	20	60	0.495	-0.165	-0.635	-0.278	-0.335	-0.001	0.312	-0.447	0.719	-0.002
48	20	40	0.447	-0.125	-0.464	-0.276	-0.263	-0.015	-0.171	-0.339	0.524	0.000
49	20	20	0.374	-0.065	-0.209	-0.272	-0.148	-0.027	-0.654	-0.179	0.334	-0.000
50	20	0	0.288	0.005	0.091	-0.268	-0.007	-0.026	-0.854	0.006	0.256	-0.006
55	40	80	0.758	-0.140	-0.620	-0.356	-0.677	-0.007	0.689	-0.483	0.294	-0.021
56	40	60	0.742	-0.129	-0.559	-0.355	-0.630	-0.009	0.490	-0.445	0.197	-0.020
57	40	40	0.693	-0.097	-0.387	-0.353	-0.484	-0.014	0.002	-0.337	-0.001	-0.019
58	40	20	0.619	-0.049	-0.131	-0.349	-0.263	-0.017	-0.483	-0.177	-0.190	-0.019
59	40	0	0.533	0.007	0.169	-0.346	0.000	-0.012	-0.682	0.009	-0.264	-0.021
64	60	80	0.929	-0.119	-0.571	-0.398	-0.900	-0.012	0.883	-0.476	-0.251	-0.032
65	60	60	0.910	-0.109	-0.508	-0.396	-0.828	-0.012	0.670	-0.437	-0.341	-0.031
66	60	40	0.858	-0.081	-0.335	-0.394	-0.630	-0.013	0.171	-0.330	-0.533	-0.031
67	60	20	0.783	-0.040	-0.078	-0.391	-0.336	-0.012	-0.316	-0.172	-0.717	-0.030
68	60	0	0.696	0.007	0.222	-0.387	0.010	-0.007	-0.510	0.011	-0.784	-0.030
73	80	80	1.000	-0.113	-0.559	-0.412	-0.999	-0.013	0.999	-0.475	-0.509	-0.036
74	80	60	0.971	-0.103	-0.490	-0.409	-0.900	-0.013	0.741	-0.433	-0.575	-0.035
75	80	40	0.916	-0.077	-0.315	-0.406	-0.677	-0.013	0.227	-0.326	-0.761	-0.034
76	80	20	0.840	-0.037	-0.058	-0.403	-0.355	-0.011	-0.257	-0.169	-0.939	-0.034
77	80	0	0.752	0.008	0.243	-0.399	0.020	-0.005	-0.439	0.013	-0.999	-0.033

Table 4. Nodes and eigenvectors in a half domain (circular cases CC and CV)

Node No.	Coord. r (km)	Coord. θ (°)	Normalized Eigenvectors Mode 1 CC	Mode 1 CV	Mode 2 CC	Mode 2 CV	Mode 3 CC	Mode 3 CV	Mode 4 CC	Mode 4 CV	Mode 5 CC	Mode 5 CV
1	0	0	0.000	0.000	0.000	0.000	0.000	0.000	0.000	0.000	1.000	1.000
2	2	-90	-0.023	-0.003	-0.032	-0.022	-0.002	-0.001	-0.002	0.000	0.996	0.999
3	2	-60	-0.004	0.009	-0.039	-0.020	0.000	0.000	-0.002	-0.001	0.996	0.999
4	2	-30	0.016	0.018	-0.036	-0.013	0.002	0.001	-0.001	-0.001	0.996	0.999
5	2	0	0.032	0.022	-0.023	-0.003	0.002	0.001	0.002	0.000	0.996	0.999
6	2	30	0.039	0.020	-0.004	0.009	0.000	0.000	0.002	0.001	0.996	0.999
7	2	60	0.036	0.013	0.016	0.018	-0.002	-0.001	0.001	0.001	0.996	0.999
8	2	90	0.023	0.003	0.032	0.022	-0.002	-0.001	-0.002	0.000	0.996	0.999
14	5	-90	-0.057	-0.007	-0.079	-0.056	-0.010	-0.007	-0.008	-0.001	0.982	0.994
15	5	-60	-0.010	0.022	-0.097	-0.052	0.002	-0.003	-0.013	-0.006	0.982	0.994
16	5	-30	0.040	0.045	-0.089	-0.034	0.012	0.004	-0.005	-0.005	0.982	0.994
17	5	0	0.079	0.056	-0.057	-0.007	0.010	0.007	0.008	0.001	0.982	0.994
18	5	30	0.097	0.052	-0.010	0.022	-0.002	0.003	0.013	0.006	0.982	0.994
19	5	60	0.089	0.034	0.040	0.045	-0.012	-0.004	0.005	0.005	0.982	0.994
20	5	90	0.057	0.007	0.079	0.056	-0.010	-0.007	-0.008	-0.001	0.982	0.994
26	10	-90	-0.113	-0.014	-0.158	-0.114	-0.035	-0.025	-0.030	-0.003	0.931	0.975
27	10	-60	-0.019	0.045	-0.193	-0.106	0.008	-0.010	-0.047	-0.023	0.931	0.975
28	10	-30	0.080	0.092	-0.177	-0.069	0.043	0.016	-0.017	-0.020	0.931	0.975
29	10	0	0.158	0.114	-0.113	-0.014	0.035	0.025	0.030	0.003	0.931	0.975
30	10	30	0.193	0.106	-0.019	0.045	-0.007	0.010	0.047	0.023	0.931	0.975
31	10	60	0.177	0.069	0.080	0.092	-0.043	-0.016	0.017	0.020	0.931	0.975
32	10	90	0.113	0.014	0.158	0.114	-0.035	-0.025	-0.030	-0.003	0.931	0.975
38	20	-90	-0.221	-0.029	-0.310	-0.239	-0.121	-0.094	-0.107	-0.013	0.743	0.891
39	20	-60	-0.037	0.095	-0.379	-0.221	0.028	-0.036	-0.163	-0.086	0.743	0.891
40	20	-30	0.158	0.193	-0.346	-0.144	0.149	0.058	-0.056	-0.073	0.744	0.891
41	20	0	0.310	0.239	-0.221	-0.029	0.121	0.094	0.107	0.013	0.744	0.891
42	20	30	0.379	0.221	-0.037	0.095	-0.028	0.036	0.163	0.086	0.743	0.891
43	20	60	0.346	0.144	0.158	0.193	-0.148	-0.058	0.056	0.073	0.743	0.891
44	20	90	0.221	0.029	0.310	0.239	-0.120	-0.094	-0.107	-0.013	0.744	0.891
50	40	-90	-0.403	-0.058	-0.575	-0.513	-0.364	-0.353	-0.351	-0.056	0.181	0.498
51	40	-60	-0.061	0.206	-0.699	-0.474	0.107	-0.127	-0.506	-0.325	0.182	0.498
52	40	-30	0.296	0.416	-0.636	-0.307	0.471	0.226	-0.155	-0.269	0.184	0.499
53	40	0	0.575	0.513	-0.403	-0.058	0.364	0.353	0.351	0.056	0.184	0.499
54	40	30	0.699	0.474	-0.061	0.206	-0.107	0.127	0.506	0.325	0.182	0.498
55	40	60	0.636	0.307	0.296	0.416	-0.470	-0.226	0.155	0.269	0.183	0.498
56	40	90	0.403	0.058	0.575	0.513	-0.363	-0.353	-0.351	-0.056	0.184	0.499
62	80	-90	-0.548	-0.067	-0.838	-1.000	-0.649	-1.000	-0.820	-0.317	-0.471	-0.844
63	80	-30	0.452	0.833	-0.894	-0.558	1.000	0.782	-0.180	-0.683	-0.470	-0.843
64	80	-60	-0.056	0.442	-1.000	-0.899	0.351	-0.218	-1.000	-1.000	-0.472	-0.843
65	80	0	0.838	1.000	-0.548	-0.067	0.649	1.000	0.820	0.317	-0.469	-0.843
66	80	30	1.000	0.899	-0.056	0.442	-0.350	0.218	1.000	1.000	-0.471	-0.844
67	80	60	0.894	0.558	0.452	0.833	-0.999	-0.782	0.180	0.683	-0.472	-0.843
68	80	90	0.548	0.067	0.838	1.000	-0.648	-1.000	-0.820	-0.317	-0.470	-0.843

problem using standard finite elements with approximated uniform water depth in an element. Due to the Neumann type of boundary condition, mathematically, system matrices become singular in nature. Depending on the domain scale of problems at hand, significant difference in the order of magnitude between two system matrices may appear, which would cause numerical ill-conditioning. Thus the shifting of eigenvalues and scaling of matrix elements are incorporated in the solution algorithm to overcome inherent numerical difficulties.

Typical problems are analyzed and the results are found to be quantitatively accurate and qualitatively reasonable.

From the investigation of numerical results, it is concluded that the developed numerical algorithm and finite element program are very robust and practically useful. Hence it can be effectively used for the analysis of free oscillation characteristics in real-world harbors.

ACKNOWLEDGEMENTS

This paper was supported by NON-DIRECTED RESEARCH FUND, Korea Research Foundation, 1991, and the presentation at PACON 92 is supported by Research Center for Ocean Industrial Development, National Fisheries University of Pusan.

REFERENCES

Bathe, K.J. 1982. Finite Element Procedures in Engineering Analysis. New Jersey: Prentice-Hall.

Courant, R., and D. Hilbert. 1962. Methods of Mathematical Physics, Vol.2, New York: Wiley.

Dean, R.G., and R.A. Dalrymple. 1984. Water Wave Mechanics for Engineers and Scientists. New Jersey: Prentice-Hall.

Defant, A. 1960. Physical Oceanography. Vol.1. Pergamon Press.

Hidaka, K. 1932. Problem of water oscillations in various types of basin and canals. Memmoir of Imperial Marine Observatory Kobe, part I (99-219).

Horikawa, K. 1978. Coastal Engineering, An Introduction to Engineering. Univ. of Tokyo Press.

Ippen, A.T. 1966. Estuary and Coastline Hydrodynamics. New York: McGraw-Hill.

Proudman, J. 1953. Dynamical Oceanography. New York: John Wiley & Sons.

Ralston, A., and H. S. Wilf. 1967. Mathematical Method for Digital Computers. Vol.2, New York: John Wiley & Sons.

Ryu, Y.S. 1984. A study of nonlinear structural and design sensitivity analysis methods. Ph.D. diss., The Univ. of Iowa.

Ryu, Y. S., and B.G. Lee. 1985. An application of the finite element method for the free oscillation analysis in a harbor. *Bull. of National Fisheries University of Pusan.* **25(2)**:7-12.

Tacker, W.C. 1977. Comparison of finite element and finite difference schemes. *J. of Physical Oceanography.* **8**:676-679.

Wilson, B.S. 1966. In: Encyclopedia of Oceanography, ed. R. W. Fairbridge. New York: Academic Press.

Zienkiewicz, O.C. 1971. The Finite Element Method in Engineering Science. New York: McGraw-Hill.

MANAGING MARINE RESOURCES FOR RESEARCH AND EDUCATION

Craig D. MacDonald
Department of Business, Economic Develolpment & Tourism
Honolulu, Hawaii U.S.A.

ABSTRACT

The management of marine resources is growing ever more complex as the intensities and kinds of ocean use increase and diversify. In Hawaii, ocean research and education activities have multiplied to the level that they are becoming involved in user conflicts, for example. These activities also are associated with a number of other issues that have prompted the formulation of State ocean policies to address them. This paper is a concise representation of the predominant issues and policies that bear on managing marine resources for research and education in Hawaii. As such, this paper is intended to serve as a useful context for other coastal regions with related activities and management interests.

INTRODUCTION

In most locales, management of marine resources (and activities) for research and education rarely occurs at this time. The need is emerging, but is overshadowed in most cases by conflicts involving more traditional uses of the ocean (e.g., fishing and recreation). Increasing population and related trends (economic development, waste disposal, etc.) all point to heightened use of coastal and ocean resources in the future. Increased use for other purposes ultimately will impact how ocean research and education can be conducted. Hawaii recently gained significant experience in this policy area.

Among Hawaii's economic activities, ocean research is growing rapidly in importance (MacDonald and LaBarge, 1990). Annual revenues for ocean research grew from $20 million in 1980 to $62 million in 1989 (ibid) and potentially could increase to a projected $151 million in 1996 (MacDonald, et al., 1991). Hawaii's ocean also offers extensive opportunities for marine education. For example, the University of Hawaii at Manoa offers a total of 205 marine-related courses (University of Hawaii, 1989); the State of Hawaii Department of Education involves public school students (K-12) with the ocean through formal class work and field trips; and, numerous diverse organizations (e.g., Federal, State and County government agencies, nonprofit organizations and businesses) provide a broad spectrum of informational seminars and classes on ocean-related topics.

Management issues associated with ocean research and education activities were identified in the process of developing the *Hawaii Ocean Resources Management Plan* (Hawaii Ocean and Marine Resources Council, 1991). The issues and policies presented derive largely from participation of a twenty-member focus group (led by the author) composed of knowledgeable representatives from a cross section of Hawaii's key research and education organizations. The issues were affirmed and the ensuing policy recommendations adopted by the Hawaii Ocean and Marine Resources Council after extensive State agency and statewide public review. The Council was mandated by the 1988 Hawaii State Legislature (Chapter 228, Hawaii Revised Statutes) and appointed by the Governor to define the context in which Hawaii's ocean resources should be managed and developed.

A full account of the resource base, infrastructure support, regulatory framework and recommended implementing actions associated with these issues and policies is provided in MacDonald (1991). Hawaii's circumstances are not unique; related issues in varying degree probably occur throughout the developed coastal nations of the world. For example, management measures to address marine research and education activities have been instituted in Australia (Great Barrier Reef Marine Park Authority, 1992), and the Florida Keys National Marine Sanctuary is considering strategies to address related matters in Florida (National Ocean Service, 1992).

MANAGEMENT ISSUES

User Conflicts

There is a growing incidence of user conflicts involving ocean recreation and fishing activities and research and education activities in the nearshore environments of the populated main islands. Ocean research and education need to be recognized as legitimate ocean uses on par with and deserving the same considerations afforded any other ocean use activity in Hawaii.

Research-related

The problem is particularly acute where disturbance of carefully controlled experiments and interruption of long-term studies diminishes or jeopardizes the integrity and completeness of research results. That possibility is especially likely in the case of artificial reef-related work and where extensive floating or submerged instrumentation and sampling arrays are involved. The result could be an undetected bias leading to faulty conclusions or premature termination of the project if interference were overt. A related but different kind of threat derives from the potential impacts of coastal development on critical or unique research areas that may inadvertently be degraded or destroyed.

The only legal mechanism currently enabling exclusive use of the ocean for research and education purposes is Chapter 190D, Hawaii Revised Statutes. This law provides for leasing the ocean within State waters, but is narrowly framed and so restrictive that it is of limited applicability.

Education-related

User conflicts also occur during field trips for educational purposes, most notably at popular tide pool locations. These conflicts generally involve shoreline fishermen or occur between the different field trip groups themselves. Field trips are conducted by virtually all grade levels in public and private schools, by nonprofit groups and by a variety of undergraduate and graduate programs in all of Hawaii's colleges and universities.

Conflicts involving multiple field trips at a single tide pool or reef flat site are perhaps the most troublesome kind. The educational opportunity being offered is diminished. The resulting congestion contributes to overuse of the site and to resource degradation, which further reduces the educational value of the experience. This problem is greatly aggravated by two factors: 1) the convergence of users at preferred locations at the same time because of favorable conditions caused by the tides, and 2) the small number of appropriate sites that can serve as alternatives to disperse and distribute the effort.

The matter of access is also an issue in this case because of the limited extent of protected shoreline suitable for field trip use, especially by elementary school grades. Access is restricted by homeowners at some preferred study locations and by the military at certain bases where the physical conditions for reef and tide pool study are exceptional. Little can be done to control the timing of the tides, but conflicts could be reduced among the educational groups involved by more tightly organizing the user schedules and by seeking additional access to new sites from the proper military authorities.

Need for Definition of "Marine Education"

There is growing interest among the general public for interpretation and display at popular resource sites (e.g., Hanauma Bay Beach Park and Marine Life Conservation District) and growing demand for general information on marine-related matters. In response, an array of governmental, nonprofit and volunteer organizations as well as businesses are offering a wide range of information services and products. This is a desirable trend which ultimately will lead to a more sophisticated body politic and marine constituency in Hawaii and should be encouraged. However, management problems are arising in regard to the interpretation of what constitutes "marine education." The concept of quality control needs to be introduced in relation to the educational programs offered.

For example, the Department of Parks and Recreation, City and County of Honolulu, has adopted administrative rules intended to reduce use of Hanauma Bay Beach Park to a level that is less damaging to the bay's environment. The regulations adopted also are intended to reduce the commercial use of public facilities and increase the educational value of the resource. But, some tour operators provide "educational" activities as a part of their package and seek continued commercial access on that basis. For this reason, the City and County of Honolulu is rethinking its administrative rules.

The number of accessible major and unique ocean and coastal resource sites statewide is relatively small. Almost certainly public use of them will exceed their environmental capacities, as occurred at Hanauma Bay, if limits are not set on the kinds and levels of activities that are to be permitted. As part of the process that establishes such limits, marine education will have to be clearly defined to prevent unintended uses. This precaution is especially important in the face of growing demand for "ecotourism" and the rise in the number of businesses and organizations that are catering to this market segment.

Attitudinal Behavior

The reduction in educational value visited upon popular tide pool and other coastal field trip sites derives as much from "misuse" as from "overuse." The behavior of educators intent on providing specimens for demonstration purposes may fall short of what is required to maintain the sustained viability of the marine community they so routinely sample. For example, care must be provided and survivorship should be highly considered in holding and returning live specimens to the tide pool or reef environment after the class or field trip is over.

The teaching should be to convey understanding and appreciation of the ocean system. Students of all ages should first be taught to care in order that they may protect the diversity of Hawaii's marine life. Informed attitude is the key to developing a conservation ethic and practicing responsible ocean and coastal stewardship. Educators

and all environmental interpreters are role models for students and the general public, and they need to manifest this caring attitude in their behavior.

Care and Handling of Marine Animals and Habitats

Nationally, there is mounting interest in assuring that marine animals held captive for educational and research purposes be properly and considerately cared for and maintained. This has been especially true for marine mammals, but it is expected to apply more forcefully in the future to fish and invertebrates as well. A number of professional societies are establishing standards and guidelines for their memberships to follow. These organizations include, for example, the American Association of Zoological Parks and Aquariums, American Society of Zoologists, Animal Behavior Society, Ecological Society of America and International Union for the Conservation of Nature and Natural Resources.

In any set of guidelines it would be necessary to provide for care and handling in a number of situations: (1) while in the field, (2) while in transport, (3) while in the controlled, monitored classroom environment (temporary), (4) while in zoos, aquariums, oceanariums or related facilities (permanent), and (5) in the use of prepared specimens. These guidelines should be extended to include the treatment of marine and coastal habitats. It also would be desirable that commercial operators engaged in "ecotourism" be involved in this process and abide by the guidelines as well.

The State of Hawaii Department of Education (DOE) has on hand a set of general guidelines urging that thoughtful consideration be given by teachers and students when using the various marine environments for educational purposes (DOE, 1983). The Waikiki Aquarium has adopted specific animal handling instructions for their docents and interpreters as have several other such marine resource centers in Hawaii. However, with the growing power and popularity of animal rights groups, like the 300,000-member People for the Ethical Treatment of Animals, the State needs to consider a more formal position statement supporting responsible research and education, as much to protect research and education and their contribution to the State as to protect the organisms and their habitats.

Water Safety and Liability

Water safety and liability are contentious issues of notable importance. The personal welfare of students must be provided for in balancing potential risks against the benefits of hands-on experience and field observation. Course work and visual aids are fine, but true literacy in marine-related fields requires direct exposure to foster full understanding and appreciation.

Regulations regarding planning, authorization and safety provisions for water-related field trips in natural environments are stipulated in Section 2250.1, DOE Policies and Regulations. There it is recommended that approval of a water-related field trip request submitted by a teacher be made by the district superintendent rather than the school principal, as otherwise would be the case. Risk and liability are deemed higher for such field trips and require a higher level of authorization than usual. The general safety guidelines and provisions for water-related field trips adhered to by the DOE are included in the publication *A Compendium: Coastal Field Sites in the State of Hawaii* (DOE, 1983).

In order to make wise decisions, there is a need for administrators to personally experience the same kind of field trip conditions as their students. The administrators' informed familiarity with marine educational programs, including actual field site visitation, seems crucial if the administrators are to thoroughly and properly assess matters of student safety and liability.

Ocean and Coastal Interpretive Education

As part of the overall effort to raise the level of marine literacy in Hawaii and to generate responsible stewardship, there is a need for greater public awareness of Hawaii's scenic, natural and cultural/historic ocean and coastal resources. Ocean and coastal interpretive education can help residents and tourists (including in-state travelers) better appreciate and understand what these resources have to offer in regard to their beauty, qualities and special meaning (Governor's Ocean Resources Tourism Development Task Force, 1988). This appreciation in turn instills a heightened sense of value which leads to increased care and concern that these resources be wisely managed.

There are no statewide or regional ocean and coastal interpretive plans in Hawaii, only some for specific sites. A few of Hawaii's coastal attractions have interpretive signs. Most only identify the name of the site, with little or no additional information provided. Often the signs are too brief and printed only in English. A relatively cost effective means of educating very large numbers of people, including school students, about Hawaii's ocean resources is being underutilized.

POLICY RECOMMENDATIONS

The overall policy objective is to develop a supportive State management system that encourages and promotes marine education and that fosters the growth, continued viability and effectiveness of ocean research in Hawaii. The following policies are intended to meet that objective. No priority order is implied.

A Mitigate user conflicts between research and non-compatible ocean use activities so that ocean research projects are not jeopardized.

B Reduce user conflicts between other marine-related and education groups and prevent overuse of the most preferred coastal field trip sites.

C Ensure that proper stewardship attitudes are manifested among researchers, educators and other interpreters and students.

D Prevent questionable "educational" activities from occurring in Hawaii's marine and coastal protected areas.

E Ensure that Hawaii's school students are safe around the water and derive maximum benefit from ocean-related field trips and excursions.

F Increase public awareness of Hawaii's scenic natural and cultural/historic ocean and coastal resources through interpretive education.

Appropriate actions to implement these policies are articulated in the *Hawaii Ocean Resources Management Plan* (Hawaii Ocean and Marine Resources Council, 1991). In 1992 a cabinet-level advisory body, the Coastal and Ocean Management Policy

Advisory Group (COMPAG), was appointed by the Governor of Hawaii to work with the affected State agencies in setting priorities and overseeing the implementation of these policies. Based on a survey of these agencies by the COMPAG, the recommended actions were given a high-medium priority in 63% of the responses and 68% of the responses indicated the actions were ongoing or planned.

REFERENCES

Governor's Ocean Resources Tourism Development Task Force. 1988. Enhance, preserve, restore: an interim report on the wise use of Hawaii's coastal and nearshore resources for the promotion and development of the ocean recreation and tourism industries. Honolulu: State of Hawaii Department of Business and Economic Development.

Great Barrier Reef Marine Park Authority. 1992. Basis for zoning - the Great Barrier Reef Marine Park Cairns Section and the Cairns Marine Park, 1992. Townsville,Queensland.

Hawaii Ocean and Marine Resources Council. 1991. Hawaii Ocean Resources Management Plan. Honolulu: State of Hawaii Department of Business, Economic Development and Tourism.

MacDonald, C.D. 1991. Ocean research and education. In: Hawaii Ocean Resources Management Plan Technical Supplement. pp. 6-15. Honolulu: State of Hawaii Department of Business, Economic Development and Tourism.

MacDonald, C.D., and A.L. LaBarge. 1990. Ocean R&D spending patterns in Hawaii: analysis and outlook. In: Proceedings of the Fourth Pacific Congress on Marine Science and Technology, PACON '90. pp. 65-72. Honolulu: PACON International.

MacDonald, C.D., C.F. Keown, A.L. LaBarge, and H.E. Deese. 1991. Strategic market planning for Hawaii ocean R&D: comparative rating and industry potential. In: OCEANS '91 Proceedings. pp.709-715. New York: IEEE Oceanic Engineering Society.

National Ocean Service. 1992. Draft management alternatives and component strategy descriptions II - the Florida Keys National Marine Sanctuary. Washington, D.C.: National Oceanic and Atmospheric Administration.

State of Hawaii Department of Education, Office of Instructional Services. 1983. A Compendium: Coastal Field Sites in the State of Hawaii. RS 83-4146. Honolulu.

University of Hawaii, Marine Option Program. 1989. Marine and aquatic-related courses at UH Manoa. Honolulu.

AN OVERVIEW OF OCEAN THERMAL ENERGY CONVERSION AND ITS POTENTIAL BY-PRODUCTS

Thomas H. Daniel
Natural Energy Laboratory of Hawaii Authority
Kailua-Kona, Hawaii, U.S.A.

ABSTRACT

Ocean Thermal Energy Conversion (OTEC) is a promising technology with potential to provide a significant proportion of human energy needs from a renewable source, i.e., extraction of energy from the temperature difference between solar-heated tropical surface water and the cold deep water of the ocean.

A commercial-sized OTEC plant will require pumping hundreds of cubic meters per second of warm and cold seawater through its heat exchangers. The large amount of energy required to pump these enormous volumes of water through the plant is usually considered a "parasitic loss" of the energy generation, so the discharge water can be available without further energy costs for other uses. From another perspective, commercially valuable uses of the discharge water can significantly reduce the cost of electricity produced by an OTEC system.

Potential co-products of an OTEC system include energy-related uses such as space cooling, condensation for distillation processes, industrial process cooling, and fresh water production; mariculture/aquaculture of plants and animals; and agriculture using the cold fresh water which condenses on pipes carrying the cold seawater to grow valuable temperate crops in the tropics.

INTRODUCTION TO OTEC

The Resource

The sun warms the surface of the tropical oceans, so that average year-round sea surface temperatures exceed 24°C for most of the band between the tropics of Cancer and Capricorn. The deep water in the ocean is cold everywhere, so that a typical tropical temperature profile has a warm surface layer separated from the cold deep water by a thermocline through which the temperature decreases rapidly with increasing depth (Figure 1). The annual average temperature difference between the surface and 1,000 m depth thus exceeds 20°C throughout the tropical region (Figure 2).

Useful energy can be extracted from this thermal heat sink by processes known as Ocean Thermal Energy Conversion (OTEC). Though the small available temperature difference inherently limits OTEC processes to achievable heat-to-electricity efficiencies less than 3%, the available resource (Figure 2) is large enough to provide more than 10 terawatts (10^{13} watts) of electricity continuously - without significantly affecting the ocean thermal structure. This amount of energy, about 300 Quads/yr, is approximately equal to the total energy consumption for all human activities. None of the other presently investigated terrestrial alternatives to fossil/nuclear energy can approach the size of this OTEC resource (von Arx, 1974).

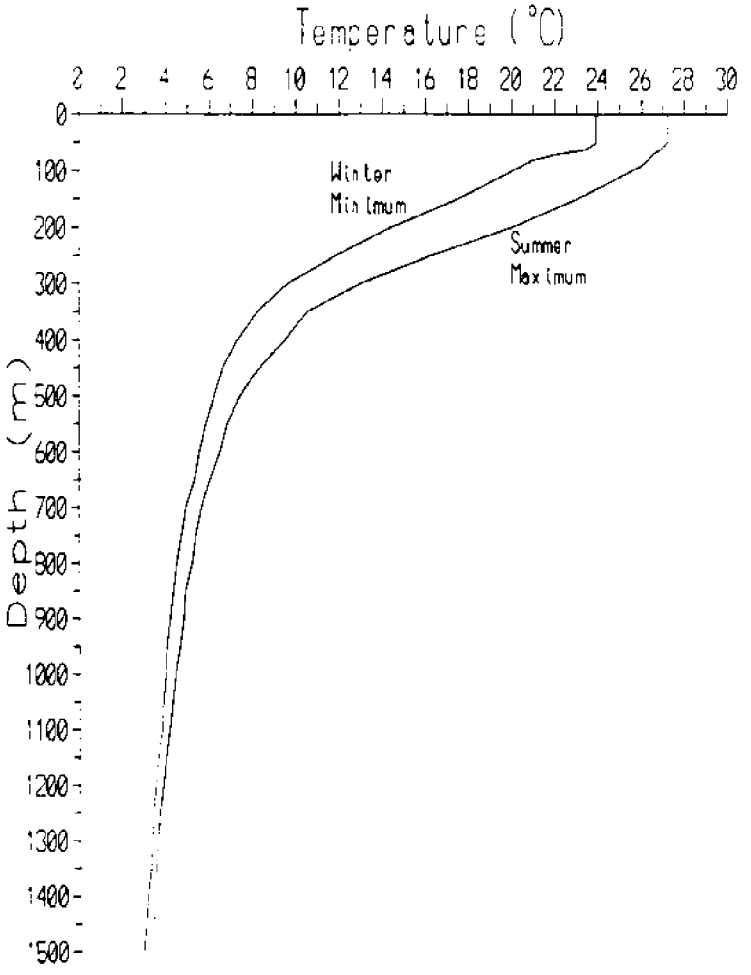

Figure 1. Typical tropical oceanic temperature profile

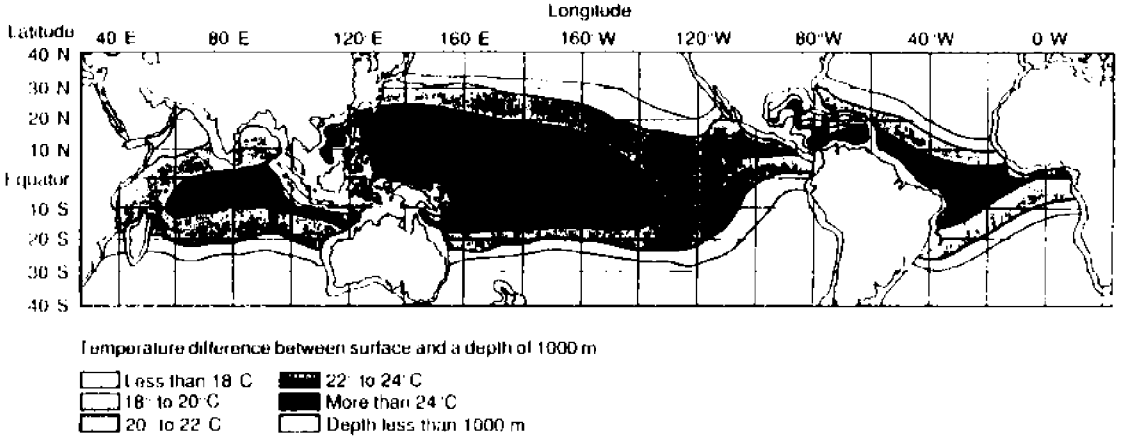

Figure 2. Global distribution of the OTEC resources

OTEC Systems

OTEC energy extraction schemes are generally classified as either closed-cycle or open-cycle (cf. Cohen, 1982; Penney and Daniel, 1989). In closed-cycle systems (Figure 3), a working fluid such as ammonia, vaporized by thermal contact with warm surface water, turns a turbine and is then condensed back to a liquid when heat is extracted through thermal contact with the cold deep water. This process requires large surface area heat exchangers to extract heat from the relatively small available temperature difference. Work at the Natural Energy Laboratory of Hawaii (NELH) over the past 12 years has demonstrated that biofouling of these heat exchangers can be controlled, that aluminum will work well as the heat exchanger material and that "roll-bonded" aluminum heat exchangers can provide a cost-effective method for construction of the large scale heat exchangers required for OTEC.

In the open-cycle process (Figure 4), the warm seawater vaporizes in a near vacuum and the water vapor itself turns the turbine before being condensed back to liquid water by thermal contact with the cold seawater. If the cold seawater does not come in direct contact with the water vapor, i.e. if a surface condenser is used, fresh water is produced as a by-product. The energy conversion is, however, more efficient if a direct contact condenser, in which the steam directly contacts the cold seawater, is used. This leads to a complex thermoeconomic tradeoff between freshwater and electricity production (Block, et al., 1984). The major problem with open-cycle systems is that, because they develop only a small pressure difference across the turbine, they require extremely large turbines to produce a relatively small amount of energy. A ten-meter diameter turbine might produce 5-6 Mw power output, and larger turbines probably can't be constructed (Penney, et al., 1984).

Both types of OTEC system require similar volume flows of seawater. A 100 Mw (net electrical output) plant, for example, will require on the order of 250 m^3/s of cold seawater from 1,000 m depth, and economic optimization leads to an even larger volume flow requirement for the easier-to-obtain warm surface seawater (Avery, 1992; Vega, 1991; Daniel, 1988). The pipeline to convey the deep cold water to the surface must be on the order of 10 meters diameter for this 100 Mw plant, and construction and installation of the cold water pipe represents the major portion of presently projected costs for OTEC plants. Current designs utilize concrete or fiberglass reinforced plastic (FRP) pipelines, which are very expensive both in fabrication and deployment. "Soft" or "inflatable" pipeline designs using flexible materials with the pumps at the bottom end hold tremendous promise for reducing both material and deployment costs of cold water pipeline, but much testing and engineering are needed to verify their feasibility and practicality.

Research at NELH

Work at the Natural Energy Laboratory of Hawaii at Keahole Point on the Big Island has led to significant breakthroughs in the design of both closed- and open-cycle OTEC systems. Experiments originally sponsored by the U.S. Department of Energy demonstrated that biofouling in the warm water heat exchangers can be completely controlled with environmentally benign low concentrations of electrolytically-generated chlorine (Larsen-Basse and Daniel, 1983; Sansone and Kearney, 1984, 1985; Berger and Berger, 1986) and that aluminum corrosion is not a problem in warm tropical seawater (Larsen-Basse, 1983). Later experiments funded by ALCAN Aluminium International tested heat exchanger modules and developed the idea of using roll-bonded aluminum heat exchangers - this latter concept leading to an 80% reduction in the projected cost of closed-cycle OTEC plants (Fitzpatrick, et al., 1989; Johnson, 1989). DOE sponsored research on open-cycle processes demonstrated that the amount of energy required to

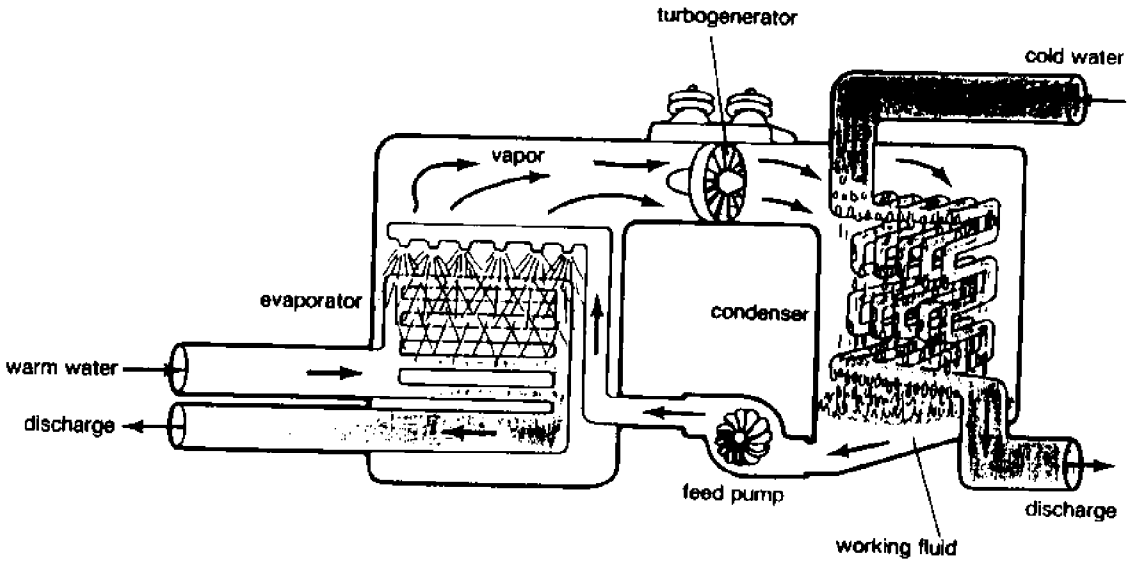

Figure 3. Closed-cycle OTEC schematic diagram

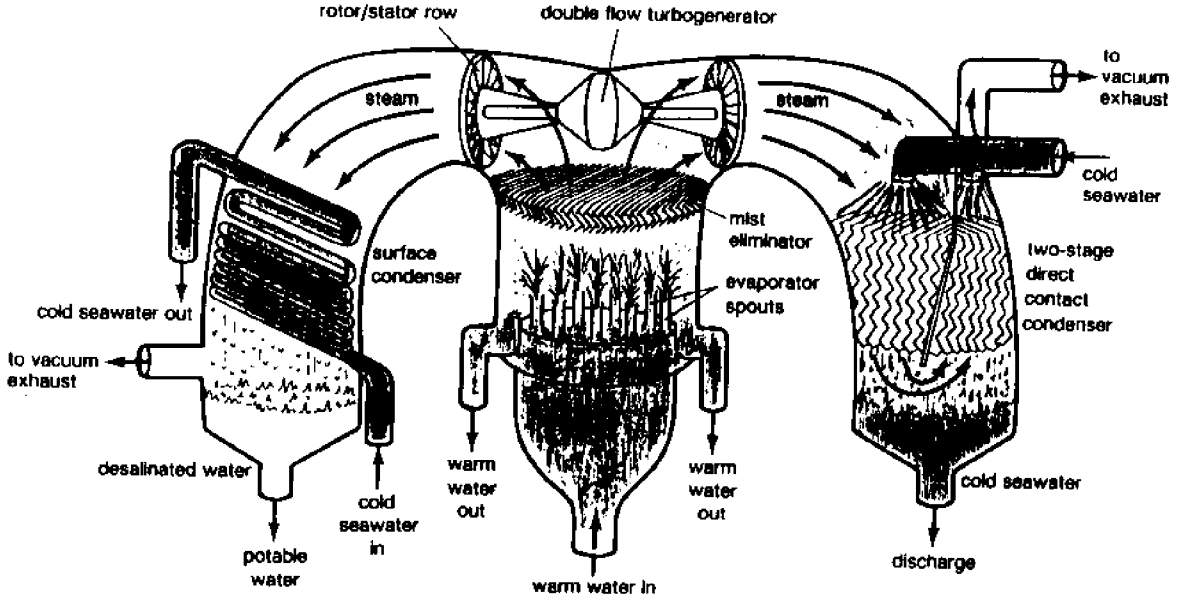

Figure 4. Open-cycle OTEC schematic diagram

remove non-condensible gases from the seawater is significantly less than the amount needed for the same job in freshwater, dramatically reducing the "parasitic losses" involved in removing these naturally occurring gases from the seawater (Krock and Zapka, 1984).

Another recent project at NELHA has demonstrated the feasibility of using directional drilling techniques developed by the oil industry to bore nearly horizontal holes from a site onshore through the coastline to a breakout through the bottom offshore. It is hoped that pilot holes drilled in this way could be reamed to much larger sizes to serve as the conduit for bringing deep seawater ashore, thus resolving the most expensive segment of typical pipeline installations. The pilot project successfully completed a 15 cm diameter, 200 m long slant drilled hole breaking out at about 10 m depth 100 m offshore (Wilkins, et al., 1992). Though initial difficulties in drilling through the uneven Hawaiian lavas made the initial hole more expensive than hoped, the project developed methods which should make drilling of future holes more economical. A test at the end of the program enlarged about 2 m of the hole to a 60 cm diameter, demonstrating the practicality of reaming the hole to a larger diameter. Further development of this technology is planned soon.

Present Status

The Pacific International Center for High Technology Research (PICHTR) is presently constructing the open-cycle "Net Power Producing Experiment," at NELH. This facility, when operational at the end of 1992, will produce a gross power of 210 kw from a generator mounted atop a 13 m (40 ft) vacuum structure. Approximately 170 kw will be required to operate the pumps and vacuum system, leaving a net power output of about 40 kw which will be fed to the local grid. This will represent the first production of net power from open-cycle OTEC.

A consortium formed by ALCAN Aluminium International, the Marconi Division of General Electric Company of Great Britain, Hawaiian Electric Industries and Makai Ocean Engineering of Waimanalo, Hawaii plans to build a 100 kw (gross) demonstration plant at NELHA in 1993. The plant will use existing seawater supplies and roll-bonded aluminum heat exchangers.

From a practical point of view, these two demonstration plants will begin to offset the large cost which NELHA now pays for electricity employed to pump the seawater which is used by a wide variety of projects at the facility.

Future Prospects

As noted above, OTEC has tremendous potential to supply the world's energy. If even a small part of this potential is realized, large volumes of deep seawater will be pumped to the surface. This deep cold water provides opportunities for development of a myriad of by-products, many of which may significantly improve the economic viability of the energy generation process.

In mid-1992, several groups around the world are considering development of OTEC plants. Sites actively being considered include Fiji, St. Croix, Guam, The Cook Islands and Mauritius. Several of these projects have been given an impetus by the apparent cost savings involved in the roll-bonded aluminum heat exchangers, but further progress awaits a demonstration of their application in the real world.

KAD Partners, an outgrowth of Aquaculture Enterprises which is growing Maine Lobster at NELHA, plans to build a 1 Mw OTEC plant to pump the water for a planned expansion of their lobster operations. The State of Hawaii will install the cold water pipeline and plans to use excess water pumped for the project to supply other tenants at NELHA. The Environmental Impact Statement for this project is now under review, and plans call for the first increment to come on line in mid-1995. This project also plans an exciting Ocean Science Center which will take advantage of the availability of large volumes of flowing warm and cold seawater to create exhibits showing habitats ranging from arctic to tropical. The developers anticipate that this Center, which will also serve as the visitor center for NELHA and will include the OTEC plant as a major attraction, will attract one million visitors a year. In addition to providing significant revenue to the project, it will serve as the focus of NELHA's public education efforts.

OTEC BY-PRODUCTS

Water Characteristics

The deep cold water required for production of OTEC energy has several features which make it valuable for a variety of other uses (Sansone, et al., 1988; Smith, et al., 1986). Figure 5 presents a schematic diagram showing some of the synergistic uses of the seawater which must be pumped for OTEC power generation.

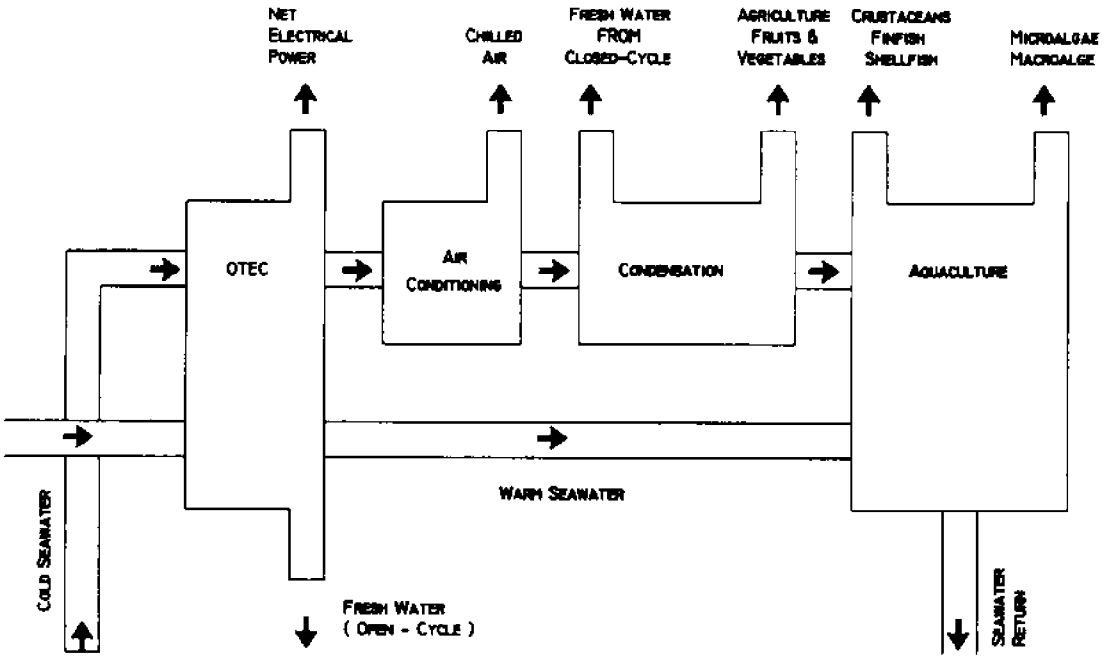

Figure 5. Schematic of a multi-product OTEC system

The deep water has three important characteristics: First, the water is **COLD**. Commercial OTEC plants will require cold water at about 4°C, coming from about

1,000 m depth at most sites. The low temperature allows the culture of coldwater species which would not normally survive in the tropics. It also provides the opportunity for cost-effective control of temperature, which is often critical for aquaculture, merely by controlled mixing of surface and deep water. A wide range of commercial applications including building air-conditioning, refrigeration and various condensation processes can also use the coldness directly. In addition, the cold fresh water which condenses from the humid tropical atmosphere on pipes or heat exchangers carrying cold seawater can be used as potable water or to irrigate temperate plants.

Second, the water is **RICH** in dissolved inorganic nutrients, providing great improvements in the growth of marine plants compared to their growth in nutrient-poor tropical surface seawater.

And third, the water is **CLEAN**. It has very few pathogens, so that delicate organisms can be grown in it without expensive sanitization, and few viable plant cells so that pure microalgal strains can be cultured without competition.

Energy Saving Uses

Several of the potential OTEC by-products are related to energy saving uses of the cold deep water temperature in the warm tropical climates where the OTEC resource exists.

The most obvious of these is building air-conditioning, or space cooling. All of the buildings at NELH and various tenant companies are cooled with deep sea water. A variety of systems are used, ranging from surplus automobile radiators with a fan to an assortment of heat exchanger implementations.

Two current projects are using the cold water as a condensing medium for distillation processes: one company is recycling freon from air conditioning systems by distilling it using a solar still for vaporization and cold seawater for condensation. Another project uses similar systems for distilling ethanol for motor fuel from sugar cane molasses.

Some proposed projects use various schemes to extract the energy contained in the temperature difference between the cold deep water and the warm surface environment for refrigeration and freezing plants. One tenant is already using the cold seawater in a dehumidifying system to dry its product.

Various schemes have been proposed for condensing potable fresh water from the humid tropical atmosphere on pipes or heat exchanger surfaces carrying the cold deep water. Rough calculations indicate that up to 5 liters of fresh water could be obtained for every 1,000 liters of cold seawater (Prakash, et al., 1989). With OTEC cold water flow rates of many cubic meters per second, thousands of cubic meters per day of potable water could be produced - enough to meet all the needs of a community being served by OTEC electricity.

Cold Agriculture

Observations of condensation on the cold water pipes initially led to research on the possibility of crop irrigation by such condensed water. It was quickly recognized that the coldness of the water which condenses on such surfaces is valuable in itself. Strawberries grown at NELH in cold condensed water have five times the sugar content of control strawberries grown under ambient conditions. Seasons can be controlled - if

the cold seawater flow is speeded up, the strawberries quickly go dormant. If it is reduced two weeks later, they send out runners and begin to produce new fruit.

Asparagus requires four winters to become tender - preliminary experiments indicate that it tastes good after only two months of temperature cycling. Alstroemeria is an alpine flower which requires high sunlight and low temperatures. The high insolation at NELH combined with watering with cool condensed water has produced very high yields of these commercially valuable blossoms. Mushroom culture also requires a wide range of temperatures at different development stages and NELH is currently entertaining proposals to grow mushrooms using the availability of warm and cold temperatures at Keahole Point.

A "Cold-Ag" workshop sponsored by the University of Hawaii SeaGrant College Program in July 1992 has brought together a range of agriculturists and plant physiologists to discuss the role of cold in plant growth. The workshop concluded that little is known about the importance of temperature variations but there appears to be tremendous potential for research and development.

Aquaculture/Mariculture

Aquaculture of many species has been attempted at NELH (Fast and Tanouye, 1988; Daniel, 1984, 1985). Animal species grown in both government and privately sponsored research have included abalone, sea urchins, salmon, steelhead trout, oysters (food and pearls), clams, prawns, hirame (Japanese flounder), and mahi mahi (dolphin fish) and opihi (Hawaiian limpets). Both macroscopic and microscopic plants are also being cultured including nori (Porphyra), ogo (gracillaria), Macrocistus, Spirulina and Dunaliella.

All of these projects have utilized the available temperature difference to provide cost-effective temperature control - most have required the cold temperatures available from the deep seawater.

CONCLUSIONS

As shown in Figure 5, there is a wide range of possible OTEC by-products. As noted in Prakash, et al. (1989), each process has different temperature constraints, so that many different ones can be performed in series as the water warms up. Optimization of the overall system should provide the best possible range of temperatures for each process.

These by-products all look economically attractive in conjunction with an OTEC plant which provides the water at no additional cost. Once OTEC plants become operational, the challenge will be to find enough uses for the extremely large volumes of water which will be available. Work done thus far has merely scratched the surface of the possible uses for the deep cold seawater.

REFERENCES

Avery, W. H. In Press. Ocean Thermal Energy Conversion. London: Oxford U. Press.

Berger, L. R., and J. A. Berger. 1986. Countermeasures to microbiofouling in simulated ocean thermal energy conversion heat exchangers with surface and deep ocean waters in Hawaii. *Appl. & Environmental Microbiology.* **51**(1186-98).

Block, D.L., M.A. Girgis, J.C. Huggins, R. McCluney, L. Rotundo, J.A. Valenuela, B.J. Hutchings, W.D. Stacy, R.G. Sam, and B.R. Patel. 1984. Thermoeconomic optimization of OC-OTEC electricity and water production plants. Florida Solar Energy Center: FSEC-CR-108-84.

Cohen, R. 1982. Energy from the ocean. *Phil. Trans. R. Soc. Lond. A.* **307**(405-37).

Daniel, T.H. 1984. OTEC and cold water aquaculture research at the Natural Energy Laboratory of Hawaii. In: Proc.: PACON 84. Honolulu: MRM2/47-52.

Daniel, T.H. 1985. Aquaculture using cold OTEC water. In: Oceans '85 Conference Record. pp. 1284-89.

Daniel, T.H. 1988. Ocean thermal energy conversion and the Natural Energy Laboratory of Hawaii. In: OTEC Aquaculture in Hawaii, eds. A.W. Fast and K.Y. Tanoue, pp. 5-48. UH Seagrant.

Fast, A.W., and K.Y. Tanoue, eds. 1988. OTEC Aquaculture in Hawaii. UNIHI-SEAGRANT-MR-89-01 Honolulu: UH Seagrant College Program.

Fitzpatrick, N.P., V. Hron, E. Hay and F.A. Johnson. 1989. Alcan's ocean thermal energy (OTEC) program. In: Proc.: 9th Miami International Congress on Energy & Environment.

Johnson, F.A. 1989. A 250 kw closed cycle land based ocean thermal energy plant. In: Proc. Intl. Conf. on Ocean Energy Recovery. Honolulu: Hawaii Natural Energy Institute.

Krock, H.-J., and M.J. Zapka. 1986. Gas evolution in open cycle OTEC. In: Proc. 5th Symp. on Offshore Mechanics & Arctic Engineerng. Tokyo. pp. 612-17.

Larsen-Basse, J. 1983. Effect of biofouling and countermeasures on heat transfer in surface and deep ocean Hawaiian waters - early results from the Seacoast Test Facility. In: Proc. ASME/JSME Thermal Engineering Joint Conf. Vol. 2, pp.285-9.

Larsen-Basse, J., and T.H. Daniel. 1983. OTEC heat transfer experiments at Keahole Point, Hawaii, 1982-1983. In: Proc. Oceans '83. San Francisco: Mar. Tech. Soc.

Larsen-Basse, J., S. Jain, J.A. Berger, and L.R. Berger. 1987. Effect of marine microbiofouling and countermeasures on corrosion of some aluminum alloys under OTEC heat exchanger conditions. In: Proc. Corrosion 87. San Francisco: NACE. Paper #346.

Mencher, F.M., R.B. Spencer, J.W. Woessner, S.A. Katase, and D.K. Barclay. 1983. Growth of nori (*Porphyra tenera*) in an experimental OTEC-aquaculture system in Hawaii. *J. World Maricul. Soc.* **14** (458-470).

Penney, T., D. Bharathan, J. Althoff, and B. Parsons. 1984. Open-cycle ocean thermal energy conversion (OTEC) research: progress summary and a design study. ASME: 84-WA/Sol-26.

Penney, T.R., and T.H. Daniel. 1988. Energy from the ocean: a resource for the future. In: Science and the Future: 1989 Yearbook. Chicago: Encyclopaedia Britannica. pp.98-111.

Prakash, A., J. Craven, N. Fitzpatrick, and E. Hay. 1989. Recent advances in ocean thermal energy conversion (OTEC) technology and OTEC-based aquaculture. In: Proc. Caribbean Conference. 5 p.

Sansone, F.J., and T.J. Kearney. 1984. Unusual chlorine kinetics of tropical seawater, and the potential environmental effects. In: Proc. PACON 84. Honolulu: MRM2/35-39.

Sansone, F.J., and T.J. Kearney. 1985. Chlorination kinetics of surface and deep tropical seawater. In: Water Chlorination: Environmental Impact and Health Effects. Vol. 5, eds. R.L. Jolley, et al.

Sansone, F.J., S.V. Smith, J.M. Price, T.W. Walsh, T.H. Daniel, and C.C. Andrews. 1988. Long-term variation in seawater composition at the base of the thermocline. *Nature*. **332**:14-717.

Smith S.V., et al. 1986. Time series measurements of nutrients in deep seawater. In: Proc. PACON 86. Honolulu.

von Arx, W.S. 1974. Energy: natural limits and abundances. *Oceanus*. **17**:2-13.

Wilkins, G.A., J. Muller, A. Lowe, and L. Findley. 1992. Directional drilling through lava at Keahole Point, Hawaii: accomplishments and projections. Presented at PACON 92 Conference. Kailua-Kona, Hawaii.

OCEAN SPACE UTILIZATION: THE BLUE REVOLUTION

Patrick K. Takahashi
University of Hawaii
Honolulu, Hawaii, U.S.A.

Joseph R. Vadus
National Oceanic and Atmospheric Administration
Washington, D.C., U.S.A.

ABSTRACT

Over fifty participants from the United States, Japan, France, South Korea and other nations from government, industry and academia participated at a workshop during PACON '92 to discuss the potential of Project Blue Revolution. Proposed was a one hectare (about 100,000 square feet) integrated ocean resource development and management floating platform for operation around the turn of the century at a cost of $500 million. The conferees argued that in consideration of the potential economic and environmental benefits to mankind, the cost of this incubator plantship can be well justified compared to current and planned mega space and military projects. The potential for international cooperation is excellent, with a proposed next step to be a jointly funded development of a strategic plan.

WORKSHOP ORGANIZATION

The special workshop on ocean space utilization for the Blue Revolution was co-chaired by Joseph Vadus of the National Oceanic and Atmospheric Administration and Patrick Takahashi of the University of Hawaii and the Pacific International Center for High Technology Research. Six presentations were made by:

- Koichiro Yoshida of the University of Tokyo on his work with designing floating structures;
- Haruo Yamamoto of Kajima Corporation reporting on the activities of the Floating Structures Association of Japan;
- Craig MacDonald of the Hawaii Department of Business, Economic Development and Tourism on the marketing of ocean resource products and research capabilities;
- Joseph Vadus of NOAA on international programs;
- George Hagerman of SEASUN Power Systems, who sent a set of viewgraphs reporting on a study he was completing for the State of Hawaii on wavepower (this report is available from the State of Hawaii Department of Business, Economic Development and Tourism); and
- Patrick Takahashi, who overviewed the Blue Revolution concept (Takahashi and Matsuura, 1991).

After the initial panel presentations, questions were posed to arrive at consensus directions. A following section summarizes these responses.

HISTORY OF PROJECT BLUE REVOLUTION

When then President Ronald Reagan proclaimed the national Exclusive Economic Zone (EEZ--the 200 nautical mile region adjacent to territorial land) in 1983, he doubled the jurisdictional area of the Nation and made Hawaii, in combined land-sea domain, the second largest State in the Union. The USA has the largest EEZ in the world, of which 85% is located in the Pacific Ocean. This EEZ space holds high promise for development in tune with nature to enhance national productivity (National Science Foundation, 1986).

Since the Proclamation, Hawaii has hosted a myriad of ocean resource conferences, workshops and gatherings, and in parallel, has become the national R&D center for ocean energy, seabed resource recovery, open ocean mariculture, next generation floating structure design and the integration of these elements into a comprehensive program (Takahashi and Yuen, 1989). The Governor of the State of Hawaii, John Waihee, in the Foreword of the Governor's 1986 Symposium on Ocean Science and Technology remarked, "These Proceedings are rich with a variety of information on the ocean. They cover the research that is necessary to know the potential the ocean represents, the technology that will allow Hawaii to employ the ocean to its advantage and the commercial application of that technology to produce economic development and jobs for our people" (State of Hawaii, 1986). U.S. Senator Daniel Inouye (D-Hawaii) has been particularly active in supporting this endeavor, as summarized in his article on "The American Blue Revolution--A Solution for the 21st Century," published in the September 1992 issue of *Sea Technology* (Inouye, 1992).

The Pacific International Center for High Technology Research has begun the process of developing a team to plan for such as project. The Hawaii State Legislature in 1992 created a Research Professorship for the Blue Revolution at the University of Hawaii to help guide the research that can provide fundamental input to the pre-commercial project.

A major international marine incubator enterprise such as Project Blue Revolution now has a greater probability of success because several active national and international ocean resource programs have been initiated. In Great Britain, their "Wealth From the Oceans" program has been managed since 1990 by the Department of Trade and Industry (DTI) in cooperation with the private sector. The Science and Technology Agency of Japan has prepared and initiated a strategic plan for ocean technology. In the United States, the National Science Foundation and National Oceanic and Atmospheric Administration brought together 35 national ocean specialists in June of 1992 to prepare a proactive report entitled "Ocean Resources 2000: Planning for Ocean Resource Development and Management" (McKinley, 1992).

SUMMARY OF VERY LARGE FLOATING STRUCTURE PROJECTS

Koichiro Yoshida and Haruo Yamamoto surveyed the examples of VLFSs in Japan. Among them include:

- Kamigoto Islands Crude-Oil Storage Base and Barge System;

- five year at-sea experiments of the semisubmersible, Poseidon, for meteorological and oceanographical data acquisition and proof of safety and reliability of design method;

- floating concept for Kansai New International Airport; and

- concept of a ring-shaped semi-submersible for creation of business space in Ise Bay.

In addition the Floating Structure Association has established task forces for feasibility studies on the following:

- floating airport;

- floating facilities for waste disposal;

- integrated floating port facilities, including techno-superliners;

- floating resort / sports facilities;

- oceanographic research base;

- multi-purpose floating cities; and

- floating highways.

The Floating Structures Association of Japan was formed in July 1990 to promote social capital development through ocean space utilization. One hundred and fourteen leading companies, including contractors, shipbuilding, financial and real estate firms are represented.

The Japanese government has for 1993 allocated $386 million for marine R&D, with the Ministry of International Trade and Industry ($107 million), Science and Technology Agency ($97 million) and Ministry of Agriculture, Forestry and Fisheries ($84 million) being the largest spenders. In comparison, it was reported that the U.S. National Oceanic and Atmospheric Administration has a budget of $1.3 billion, IFREMER (France) $190 million, Alfred Wegener Institute for Polar and Marine Research (Germany) $400 million, and the Natural Environment Research Council (United Kingdom) $220 million. (It was later mentioned in the follow-up discussion that the National Aeronautics and Space Administration has an annual budget of around $14 billion.)

Joseph Vadus reported on mega-projects announced for Japan and Korea:

- Obayashi Corporation ECOLAND project (1000 hectare marine city in harmony with nature to accommodate 45,000 people at a cost of $100 billion over 25 years);

- Tobishima Corporation Pan Japan Sea Tap Plan to build a square floating multipurpose city in the middle of the Japan Sea for international access and cooperation from Japan, China, CIS and Korea (4 KM x 4 KM breakwater structure, which would contain a floating 1 KM radius habitat for up to 100,000 people at a cost of $250 billion over a 25-year period);

- Osaka marine corridor plan for the Kansai region (a multi-stranded, multifunction cable used to provide high-speed trains for passenger and cargo transport, pipelines for oil, gas, water, air, power and communications, a 20-year plan at a cost of about $220 billion); and

- KORDI multi-purpose marine town development for Pusan (580 hectare artificial island spanning a time frame of 13 years at a cost of about $6.4 billion).

WORKSHOP RESULTS

What are the major applications (commercial foci) for Project Blue Revolution?

There was a strong sense that definitive products or services must be delivered, and that the private sector was a key component. The model served by the Floating Structures Association of Japan with more than 100 companies and five banks might be considered in developing an international team. Among the applications discussed included an integrated incubator plantship, waste management facility, energy generation platform, seabed minerals refinery, ocean ranching homeport and an observatory for ocean research. The R&D capability, however, has to be a secondary consideration to complement the commercial product or utility service.

What are some of the socio-enviro-political justifications for the project?

A key selling feature of Project Blue Revolution relates to the environmental benefits that can accrue. Early public education of the concept could be key to long term success. Among the justification points for operation on the open ocean include:

- reduction of stress in near coastal waters;

- removal of certain industries and processes away from populated regions so that any wastes can be recycled;

- good potential for total systems development in harmony with nature;

- creation of new fisheries and biomass plantations to help feed the world and provide alternative sources of cleaner energy;

- possibility of easier and more workable permitting and regulatory approvals, thus, minimizing delays; and

- the prospect for enhancement of the environment should the various proposed options for global warming remediation prove to be successful.

What are some effective examples for establishing a consortium for government, industry and academic partnership?

Japan's Government-Industry cooperative efforts, Apollo and the space shuttle are some examples which have succeeded because of these partnerships.

What is the potential for international partnership?

There was a unanimity of opinion that the potential was good. The end of the Cold War reduced military expenditures and opens to question the sensibility of major space projects. The ocean is a last frontier ideal one for economic development with a commons that needs to be protected for the world. There was a sense that cooperation can be developed if mutual benefits can be shown.

Where should be the locus of operation?

The location of the initial platform will no doubt be driven by funding. However, site selection criteria need to be established to pick a best international site, or one that is ideally mission oriented.

What is the optimal size?

Again, to a good degree the amount of dollars will determine the scope of the program and design. One concept is to start small and modularize. Another is to pick a mission and design to an operational need. From an engineering standpoint, ultimate scale-up requires a practical modular size. A 100,000 square foot (or one hectare) platform was deemed as a good design point for incubator applications.

What are some possible strategies for funding an internationally cooperative project?

Before international funding can succeed, there must be a credible feasibility and marketing plan. While a B-2 bomber might cost nearly $1 billion and the Space Experiment could cost up to $50 billion, the military-aerospace industry already exists to propose and lobby for such expenditures. In Japan there are industrial alliances such as the Floating Structures Association capable of managing such a project. On the surface, in the United States, there is no equivalent organization or Federal agency equipped to start and implement this type of enterprise. However, the recent reduction in defense needs, coupled with a call for dual applications—current civilian and long-term military—might stimulate a hybrid organization where Federal funds can be earmarked for specific economic development projects in the spirit of the transcontinental railway system, which opened up the West.

Is the use of Japan's "Aquapolis" applicable? Others?

There was a general feeling that past generation platforms, or even naval craft, were too costly from a maintenance standpoint. There are new materials, equipment and designs that can be marshalled for the 21st Century.

What should be the source of energy?

All options should be initially studied, but OTEC has particular advantages because of the nutrient-rich fluids useful for co-product development. Wave energy conversion can be added to produce energy while absorbing wave forces to ease forces on the platform.

Who should be the lead organization?

A cooperative feasibility study group should be established. The lead organization will thus depend on the specific application, location, and funding sources. A multinational consortium, or organization with international contacts might be best for this purpose.

What are some other factors requiring consideration?

Little, if any, consideration has been given to the regulatory and policy environment within which the floating platform would operate when ready for deployment. The implications of State (3-12 miles), Federal (EEZ to 200 miles) and International territorial sea conflicts need to be addressed. Regulatory considerations are also raised in regard to whether the platform would be bottom moored or surface propelled. These matters are essential to business planning and risk assessment as they entail potential "hidden" costs and uncertainty that need to be identified as soon as possible in the strategic planning process.

Future activities?

Plan for and hold a more comprehensive and structured workshop with greater industrial involvement. This meeting should also involve representatives from the environmental groups. The session co-leaders, Vadus and Takahashi, were charged with a task to organize and follow-up on these activities.

CONCLUSIONS

The overall conclusions were:

- An optimal size is about one hectare, which can be built, tested, and operated for about $500 million.
- A target date of the Year 2000 is reasonable.
- There are huge food, energy, materials and ocean space benefits, with a potential for positively affecting the environment.
- International cooperation will facilitate progress.

REFERENCES

Inouye, D.K. 1992. The American Blue Revolution: a solution for the 21st century. *Sea Technology*. September:23-26.

McKinley, K., ed. 1992. U.S. Ocean Resources 2000: planning for development and management. Report for National Science Foundation and National Oceanic and Atmospheric Administration by Hawaii Natural Energy Institute. University of Hawaii. October.

National Science Foundation. 1986. Engineering solutions for the utilization of the Exclusive Economic Zone resources. October.

State of Hawaii. 1986. Proceedings of Exploring and Applying Hawaii's Great Ocean Resources, Governor's Symposium on Ocean Science and Technology. November.

Takahashi, P.K,. and R.M. Matsuura. 1991. Blue Revolution 2000. In: Proceedings of the National Science Foundation First International Workshop on Very Large Floating Structures, pp. 1-6. Honolulu, Hawaii. April 24-26.

Takahashi, P.K., and P.C. Yuen. 1989. Ocean resource development in Hawaii, In: Proceedings of the Oceans '89 Conference, IEEE 89CH2780-5, pp. 32-37.

A STUDY ON SALT DAMAGE; PRODUCTION OF SEA-SALT PARTICLES

Kenji Hotta
Nihon University
Chiba, Japan

Soichiro Ogawa
Tokyo Electric Power Service Co. Ltd.
Tokyo, Japan

ABSTRACT

Damage resulting from sea-salt particles present in the air increases every year. The damage of these particles may extend to unexpected areas such as human health, vegetation and soil. According to the questionnaire survey done by the author, along with gradual reduction of the natural coastline by replacing with artificial coastal structure such as breakwaters, the damage resulting from salt particles is growing at even a faster pace than before.

Theoretically, it is explained that the most important factor in the generation of the sea-salt particles is air bubbles which rise to the surface of the ocean, burst, and release hundreds of tiny particles containing sea-salt nuclei into the air.

In this paper, using a high-volume air sampler to compare different types of coastal formations, an attempt was made to determine the characteristics of sea-salt particle generation.

INTRODUCTION

Damage resulting from sea-salt particles present in the air increases every year. The damage of these particles may extend to unexpected areas such as human health, vegetation, and soil.

General research into salt damage has been carried out in a variety of areas. From an engineering standpoint, studies have been done concerning subjects such as 1) the corrosion mechanism affecting buildings and other facilities or equipment, 2) the design of corrosion resistant materials, and 3) the method of diagnosis of corrosion as well as corrosion-related maintenance. From a scientific standpoint, research has been directed towards areas such as 1) the mechanisms which generate sea-salt particles that cause salt damage, and 2) the transportation of sea-salt particles by the wind.

Sea-salt damage is on the increase. Moreover, a questionnaire survey carried out by the authors of this paper has revealed that along with the gradual reduction of natural coastline by replacement with artificial coastal structure such as breakwaters and other man-made structures, the damage resulting from salt particles is growing at an even faster pace than before (Hotta and Matsumoto, 1989). The present research is, therefore, concerned with obtaining fundamental data that will help avoid such damage, and assist in drawing up proposals for projects to develop a comfortable living environment in coastal areas. Using a high-volume air sampler to compare different types of coastal formations (artificial and natural beach coastlines), an attempt was made to determine

the characteristics of sea-salt particle generation. The primary results of this research are presented.

EXPERIMENTAL METHOD

Generation and Dispersal Mechanisms of Sea-Salt Particles

Theoretically, it is explained that the most important factor in the generation of sea-salt particles is air bubbles which rise to the surface of the ocean, burst, and release hundreds of tiny particles containing sea-salt nuclei (each approximately 10^{-14} to 10^{-15} gm) into the air (Asakur and Miyazaki, 1989). As Figure 1 illustrates, once airborne, the wind easily carries these particles to land.

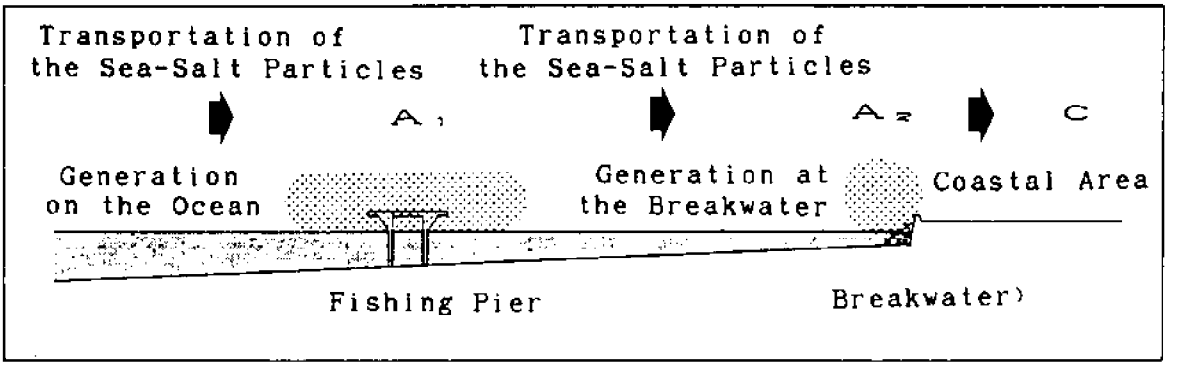

Figure 1. Transportration process of the sea-salt particles

Measurement Method

Measurements were carried out in two steps as follows:

Step 1: In order to grasp the difference between the quantity of sea-salt particles produced at the ocean surface and at the coast, measurements were carried out at both locations, and results were compared (Figure 2).

Step 2: The quantity of sea-salt particles and its relationship with wind speed and wave height factors was investigated by comparing various measurements taken at sandy beaches and behind breakwaters (Figure 3).

Measurements were carried out according to the method illustrated in Figure 3. First, a device

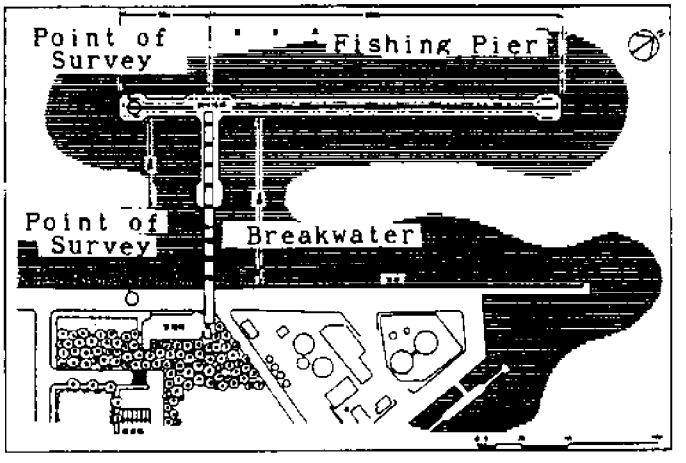

Figure 2. Location of the fishing pier

for collecting sea-salt particles (high-volume air sampler) was set up behind a wave-breaking point, in a horizontal position, facing the ocean, and within 160 degrees to the wind direction. Only when the wind blows from the ocean to the beach, sampling was carried out for a period of one hour. The air was passed through filter paper, following which the amount of chloride ions absorbed by the filter paper was measured and analyzed by an absorptiometry method (Kashimoto, 1984). The measured quantity of sea-salt particles was expressed in terms of suction volume of the air per hour (mg/m^3). Conditions pertaining to wind direction, wind speed, and wave height, prevailing at the time of the sample were also measured.

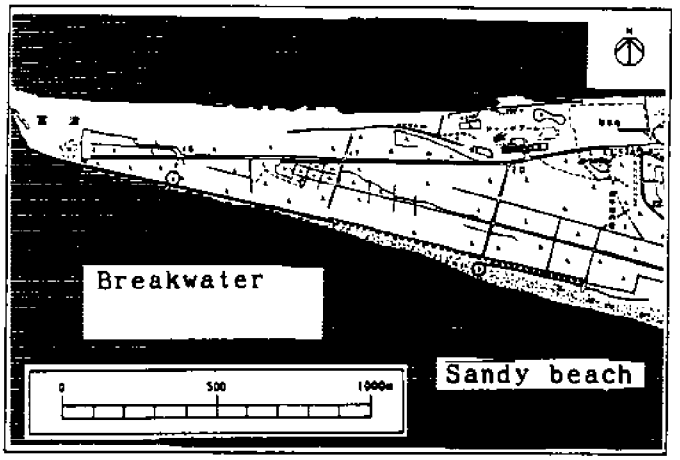

Figure 3. Location of survey point

RESULTS AND CONCLUSIONS

Step 1: Determining the quantity of sea-salt particles in the ocean air and at the coastal air

As can be seen in Table 1, measurements were reported during the measurement period when wind direction was within the set-up ranges.

November 26, December 3, 10:
Condition A - light wind, low waves (no breaking of waves at sea), hardly any waves spilling over the rock breakwater.

December 17:
Condition B - medium winds, medium waves (at sea, at measurement number 10 & 11), whitecaps occasionally visible, rough seas causing waves to spill over the rocks at breakwaters.

As shown in Figure 4, under Condition A, measurements of airborne sea-salt particles obtained both at sea and at coastal areas varied to a certain degree, but there was only a slight difference in quantity.

According to the results obtained under Condition B, while observations at sea were similar to those under Condition A, those at the coast revealed a considerable increase in particles. Coastal measurements under these conditions were approximately 4.4 to 7.1 times as great as those taken at sea.

Observations at Step 1 can, therefore, be summarized as follows:

Under conditions such as Condition A, airborne sea-salt particles are found at sea as well as at coastal areas. A certain amount of chloride is, therefore, always present in the air.

Table 1. Results of measurement

#	Date	Time	Wave Heights (cm)	Fishing pier		Coastal area	
				Amount of NaCl (mg/m^3)	Wind Speed (m/s)	Amount of Nacl (mg/m^3)	Wind Speed (m/s)
1	91/11/26	13:30-14:30	17.0	0.0331	1.25	0.0270	2.45
2	91/11/26	14:40-15:40	20.0	0.0156	0.56	0.0211	2.00
	Average			0.0244		0.0241	
3	91/12/03	10:50-11:50	10.0	0.0321	1.88	0.0221	3.38
4	91/12/03	12:00-13:00	15.2	0.0097	2.14	0.0240	1.73
5	91/12/03	15:15-16:15	16.0	0.0057	0.62	0.0076	0.65
	Average			0.0158		0.0179	
6	91/12/10	10:35-11:35	13.0	0.0386	1.84	0.0474	1.30
7	91/12/10	11:45-12:45	14.5	0.0200	2.24	0.0163	1.00
8	91/12/10	12:55-13:55	15.5	0.0146	1.68	0.0160	0.11
9	91/12/10	14:30-15:30	13.5	0.0045	1.39	0.0087	0.71
	Average			0.0194		0.0221	
10	91/12/17	10:50-11:50	67.5	0.0152	7.86	0.1097	4.82
11	91/12/17	12:00-13:00	60.5	0.0115	6.75	0.0672	3.89
12	91/12/17	13:10-14:10	49.0	0.0111	6.04	0.0486	3.91
	Average			0.0126		0.0752	
	Total			0.2117		0.4157	

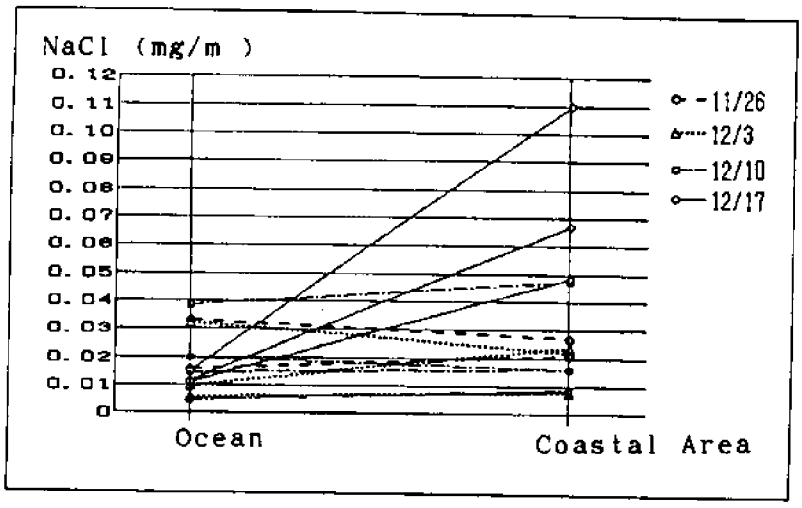

Figure 4. Amounts of sea-salt particles

However, under Condition B, there was a large difference between the results obtained at sea and at the coast. This is probably because there was little tendency for the waves to break at sea. In other words, the breaking of waves is considered to be a key factor in the generation of sea-salt particles.

At sea, wind speed and wave height have little effect and the measured quantity of sea-salt particles remains fairly uniform and small, relative to measurements taken at the coast. On the other hand, the quantity of sea-salt particles at the coast grows along with the increase in wind speed and wave height. As shown in Table 1, sea-salt particles produced at sea (A_1) and at the coastline (A_2) are dispersed in the atmosphere and driven towards coastal (C) and inland regions by the wind when we assumed that volumes reported in Table 1 are relative to "1" for the quantity measured at sea;

$$A_1 + A_2 = C$$

Condition A			
1 (low)	(very low quantity similar at the coast to that obtained at sea)	1 (low)	(1:1)
Condition B			
1 (low)	(much higher volume quantity at the coast compared to that at sea)	6 (high)	(1:6)

Step 2: Determining quantity of sea-salt particles at sandy beaches and breakwaters

There were 23 measurements reported at sandy beaches and 21 at breakwater locations during the measurement period with wind direction in the set-up ranges.

Relationship between sea-salt particles and wind and wave conditions

As shown in Figure 5, a high correlation between quantity of sea-salt particles and wave height was observed at both sandy beaches (r = 0.8420) and breakwaters (r = 0.8350). On the other hand, in regard to the relationship between sea-salt particles and wind speed, Figure 6 shows that there is a slight correlation at sand beaches (r = 0.5597) but a low correlation at breakwaters (r = 0.2299).

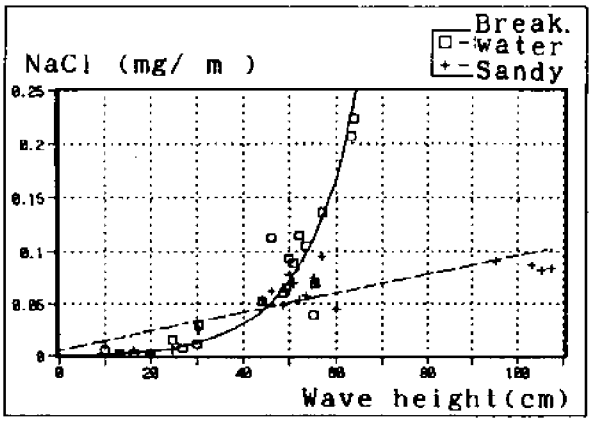

Figure 5. Relationship between wave heights and NaCl

Since observed quantities of sea-salt particles are greatly influenced by wave height (the higher the waves, the greater their breaking action), it is reasonable to conclude, as indicated in Step 1 above, that a very important factor in the generation of sea-salt particles is the breaking action of waves. However, in regard to wind speed, it is not so much the generation of sea-salt particles as the distance and the area over which they become dispersed that is directly influenced by the wind.

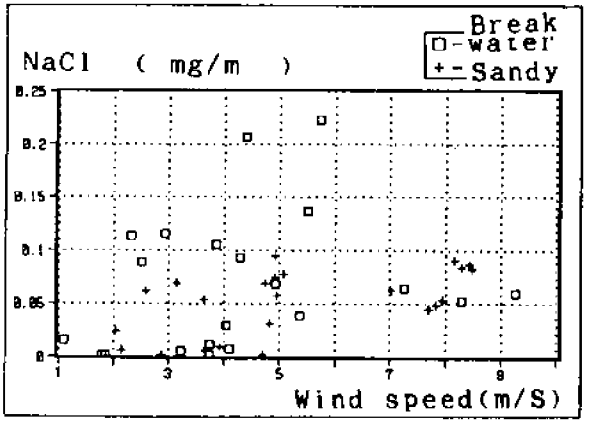

Figure 6. Relationship between wind speeds and NaCl

Model equations

Figure 5 shows model equations stating the relationship between the quantity of sea-salt particles and wave height, based upon the values obtained through experimental observations.

1) Sandy beaches: quantity of sea-salt particles (Y_1)
wave height (X_1)

$$Y_1 = 0.00561 + 0.00091X_1 \quad (1)$$

Determinant coefficient $R^2 = 0.7089$
Multiple correlation coefficient $R^2 = 0.8420$

2) Breakwaters: quantity of sea-salt particles (Y_2)
wave height (X_2)

$$Y_2 = 0.00089 \times 1.09147^{X2} \quad (2)$$

Determinant coefficient $R_2 = 0.8320$
Multiple correlation coefficient $R_2 = 0.9122$

Figure 7 shows regression lines derived from model equations for both locations.

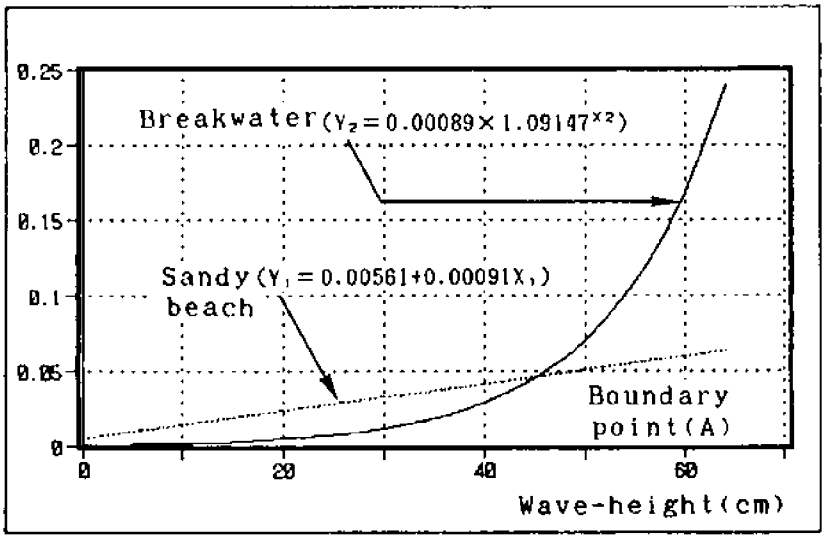

Figure 7. Regression curve by wave height and NaCl

Whereas a linearly increasing trend in the quantity of sea-salt particles measured at sandy beaches corresponds to an increase in wave height, at breakwaters, there tends to be an exponential increase in sea-salt particles.

For both locations, there are points at which trend changes in the quantity of sea-salt particles occur (A: Figure 7). When waves are smaller than at point A, the quantity of particles is larger at sandy beaches although the difference between the quantities measured at the two locations is small. Beyond point A, as wave height increases, there is a sharp rise in the quantities measured near breakwaters as compared to those measured at sandy beach, and the difference between quantities measured at the two locations also increases.

Under normal conditions, the quantity of sea-salt particles measured behind concrete blocks (cement breakwaters) is about 1.5 to 2.0 times that measured near a sandy beach. As wind speed and wave height increase, this difference in quantity grows to a factor of 5 times or possibly even more. This strongly suggests that where breakwaters are constructed, there will be an accompanying increase in salt damage.

The quantity of sea-salt particles at coastal areas varies according to whether the coastline in question consists of sandy beaches or breakwaters (different compositions of coastline) with the breakwater coastline having the large quantity. This is believed to result from the different breaking action of waves characteristic of these different types of coastline.

In this research, a method of determining the impact of sea-salt particles in terms of detecting and measuring in the coastal regions, which have not been cleared yet, is basically established.

Action to preserve beaches as well as the increased utilization of coastal areas is likely to increase in the future. Accordingly, the need for constructing breakwaters will also increase. As a result, it is likely that salt damage will be increasingly aggravated (Hotta, 1989; Ogawa, 1991).

In this respect, and for the maintenance of all types of facilities and vegetation found near coastal regions, as well as for the preservation and amenity of human activities in such residential areas, the present research has provided useful basic data.

The model equations contained herein are only useful for these particular data collection sites. Continuing these measurements by increasing the number of samples, improving the accuracy of the model equations for additional measurements, and carrying out measurements of sea-salt particles present in other areas, will provide data that is more universally useful and applicable.

REFERENCES

Asakura, S., and T. Miyazaki. 1989. A study on the density of salt content in the air. In: Architectural Institute of Japan Conference Proc. November.

Hotta, K. 1991. Oceanic Architecture and Environment. Maruzen Publishing Co. Ltd.

Hotta, K., and Y. Matsumoto. 1989. A study on the natural environment and amenity in the coastal regions. In: Architectural Institute of Japan Proc. November.

Kashimoto, N., and S. Tomisaka. 1984. Bubble. Asakura Publishing Co., Ltd.

Ogawa, S. 1991. A fundamental study on sea-salt particle in the coastal area. Ph.D. diss., Nihon University.

DERIVING PUBLIC BENEFITS FROM PRIVATE MARINA DEVELOPMENT

M. Carolyn Stewart and Valerie W. McMillan
Office of State Planning
Honolulu, Hawaii, U.S.A.

ABSTRACT

Hawaii is currently experiencing an increased interest in private marina development. All of the proposed marinas will require the use of public resources, e.g., dredging of entrance channels and breaching of the shoreline. The State of Hawaii Office of State Planning has drafted guidelines for the planning and development of private marinas. Of importance to the development of these guidelines was the "public trust doctrine," the body of law establishing that all tidelands and navigable waters are subject to a "public trust" for the benefit of the state's citizens with respect to certain rights of usage, particularly those of commerce, navigation and fishing. Based on the principles of the public trust doctrine, the draft guidelines call for the maximization of public benefits from the use of public trust resources in the development of private marinas. The Hawaii Coastal Zone Management Program has been named the lead agency for determining and negotiating the public benefits to be required of each private marina development. This responsibility entails formulating a mechanism for cooperating with the developers and incorporating various agencies' concerns, developing criteria for evaluating public benefit proposals relative to the public trust resources affected by specific projects, and selecting the type and amount of public benefits to be required of each proposed marina.

INTRODUCTION

Hawaii is currently experiencing an increased interest in marina development. Much of the demand is being generated by private developers planning major residential or resort complexes for which marinas will serve as a featured attraction. Many of the marina proposals call for the blasting of fast lands for the creation of the marina basin. However, even these marinas, developed solely on private lands, will require use of public resources, such as the dredging of entrance channels and the breaching of the shoreline. The public's right to the use and enjoyment of shoreline and ocean resources is embodied in the public trust doctrine. Marina development is a controversial issue in Hawaii and elsewhere, in part because it entails the private use of public trust resources for private gain. This paper discusses the public trust doctrine as it relates to marina development in Hawaii.

THE PUBLIC TRUST DOCTRINE

The concept of public trust is derived from Roman law, which assured all citizens access to air, running water, the sea and seashore. In other words, the public had an unalienable right to certain land and water resources, held in stewardship by the state. This concept has evolved and been refined over the ensuing 1500 years; and, its essence is embodied in a body of law known as the Public Trust Doctrine:

> The Public Trust Doctrine provides that public trust lands, waters and living resources in a State are held by the State in trust for the benefit of all

of the people, and establishes the right of the public to fully enjoy public trust lands, waters and living resources for a wide variety of public uses (Slade, 1990).

The Public Trust Doctrine applies both to publicly and privately held shorelands and submerged lands. While the private title to the lands (*jus privatum*) may be conveyed to private ownership, the public title (*jus publicum*) remains vested with the State and cannot be abdicated. "With little exception, the public's *jus publicum* rights are dominant to a private owner's *jus privatum* rights" (Kelly and Slade, 1991). Even though owners may hold legal title to the trust lands, waters and living resources as private property, they may not prevent the public from using these resources vested with *jus publicum* rights.

A number of cases have helped clarify the public trust doctrine in Hawaii.[1] In addition, the Hawaii Constitution recognizes the State's responsibilities as steward of these public trust resources. Article XI (1) states:

> For the benefit of present and future generations, the State and its political subdivisions shall conserve and protect Hawaii's natural beauty and all natural resources, including land, water, air, minerals and energy sources, and shall promote the development and utilization of these resources in a manner consistent with their conservation...All public natural resources are held in trust by the State for the benefit of the people.

Originally, the public trust lands were those subject to the ebb and flow of the tide. This definition has evolved to include the lands beneath other navigable water bodies that do not experience tidal fluxes, such as large lakes. In many states, the landward boundary of public trust lands extends to the ordinary high water mark. In Hawaii, the ordinary high water mark, or *ma ke kai*, is interpreted as the upper reaches of the wash of the waves, other than storm and tidal waves, usually evidenced by the edge of the vegetation growth, or the upper limit of debris left by the wash of the waves (Chapter 205A-1 Hawaii Revised Statutes; *In Re Ashford*, 50 Haw. 314, 315, 440 P.2d 76, 77 (1968); *In Re Sanborn*, 57 Haw. 585, 594, 562, P.2d 771, 777 (1977).

Navigation, commerce and fishing are the traditional uses of public trust lands and waters protected by the Public Trust Doctrine. Current uses that may also be protected include recreation, environmental protection and scenic beauty. The Supreme Court decision in *Phillips Petroleum v. Mississippi* (1988) extended state interest in lands beneath tidal waters to include bathing, swimming, recreation and mineral development. In Hawaii, *State v. Zimring* (58 Haw. 106, 566 P.2d 725 (1977)) also specified that both commercial and recreational uses are included in the term "navigation."

MARINAS AND THE PUBLIC TRUST DOCTRINE

Marina development is both consistent and inconsistent with the Public Trust Doctrine. Marinas may improve public access to trust resources by providing slips,

---

[1]*King v. Oahu Railway and Land Co.*, 11 Haw. 717, 725 (1899); *In Re Ashford*, 50 Haw. 314, 315, 440 P.2d 76, 77 (1968); *Hawaii v. Sotomura*, 55 Haw. 176, 182, 517 P.2d 56, 62 (1973); *In Re Sanborn*, 57 Haw. 585, 594, 562 P.2d 771, 777 (1977); *State By Kobayashi v. Zimring*, 58 Haw. 106, 121, 566 P.2d 725 (1977);and *Kaiser Aetna v. U.S.*, 444 U.S. 164 (1979).

ramps and other related boating services. However, marinas may also hinder access to public trust resources by providing only exclusive use of a shoreline or boating facility.

On the one hand, marinas may positively contribute to the public's access to trust resources by enhancing access for navigation and fishing, as well as other recreational pursuits. These public benefits are particularly important in Hawaii, where many of the resident and tourist recreational activities are focused on the use of coastal and ocean resources. In fact, "the unprecedented growth of the commercial ocean recreation sector and the number of personal boats have significantly increased the demand for additional small boat harbor facilities" (Tarnas and Stewart, 1991). In other words, demand for marina facilities far exceeds supply. As of March 31, 1992, there were approximately 2900 recreational vessels statewide on waiting lists for slips at small boat harbors. To put this number in perspective, there are only 2200 slips total available in the State. Given the high cost of marina development in Hawaii, private marina development can fill a need in the State and, at the same time, improve the use of and access to public trust resources.

On the other hand, marina development and maintenance usually have some detrimental physical and ecological impacts on the coastal lands and waters. The physical alterations associated with marina development may impact water flow, coastal and marine wildlife habitat, water quality and public shoreline access. Clearly, dredging an entrance channel and breaching the shoreline to connect a marina created from fast lands to the ocean represent irrevocable changes to public trust resources and constitute uses of these resources for private profit. The resources of submerged lands potentially impacted during dredging - coral reefs, other marine life habitats and surf breaks, for example - are public trust resources used for fishing and recreational purposes. Breaching the shoreline interrupts lateral access along the shore and the public's ability to recreate on the beach. Creation of a navigational channel may also disturb swimming and nearshore navigation along the shoreline.

Herein lies the dilemma and challenge faced by the Hawaii State government. There is a need to balance the public benefits derived from the use of public trust resources with the private use of and profit from those same resources. Therefore, when the State grants the use of public trust lands to private owners, it is obligated to assure that these lands are "used by the private owners in such a manner as not to unduly interfere with the public's several rights under the public trust doctrine and so as to promote the public interest" (State of Hawaii, 1991).

DRAFT GUIDELINES FOR PRIVATE MARINA DEVELOPMENT

The State of Hawaii, Office of State Planning (OSP) has drafted guidelines for private marina planning and development to assure protection of the public interest while fulfilling recreational boating needs. In addition to minimizing the potential environmental and socio-economic impacts of marina development, marina developers are expected to provide benefits to the public for the use of the public trust resources. Examples of public benefits that could be agreed upon between the State and a private marina developer include:[2]

[2]Adapted from Hawaii (1991).

(1) Direct cash payments;

(2) Public use at public marina rates;

(3) On-site preservation of natural resources;

(4) Off-site public boating facilities;

(5) Recreational facilities;

(6) Ocean resource use enhancement;

(7) Public access; and

(8) Public water safety and rescue programs.

Contributions such as these will ensure that the public benefits from the private use of public trust land and water resources. By negotiating a public benefits package with the marina developer, the State upholds its trustee responsibilities.

The Hawaii Coastal Zone Management (CZM) Program has been named the lead agency for determining and negotiating the public benefits to be required of each private marina development. The CZM Program is ideal for this endeavor because of its comprehensive coastal planning and policy development role, and its on-going coordination role between various government agencies. With regard to the public benefits determination process, the CZM Program responsibilities entail:

(1) formulating a mechanism for cooperating with the developers and incorporating various agencies' concerns;

(2) developing criteria for evaluating public benefit proposals relative to the public trust resources affected by specific projects; and

(3) selecting, for each proposed marina, the type and amount of public benefits to be required of each developer.

The CZM Program will submit public benefits recommendations to the Board of Land and Natural Resources. As the steward of State land and waters, the Board will review and act on public benefits reports during its deliberations on permit applications or lease requests associated with marina development.

The public benefits process has not yet been tested. However, it is expected that applications for permits to develop one or more private marinas will be filed within the next year.

CONCLUSION

The controversy surrounding private marina development sparked the concept of requiring public benefits from developers using public trust resources. However, marinas are not the only private uses of public trust resources. For example, some shore protection structures, such as groins and some revetments, are built at least partially seaward of the shoreline, in the public trust area. Others, built inland of the shoreline, can negatively affect the public trust by exacerbating erosion of the beach area.

It is possible that these uses of the public trust resources may also be subject to the public benefits requirement in the future. In addition, uses of or impacts to other public resources by private interests - such as pollution of ground water - may also warrant a similar program for compensating the public. Therefore, what has begun as a response to a particular use of the public trust may have far-reaching consequences for public resources management. However, the immediate challenge for the CZM Program is to devise a process that is fair and equitable, to both the developer and the public, for determining the public benefits to be required relative to the public trust resources affected.

REFERENCES

Hawaii, Office of the Governor, Office of State Planning. 1991. Draft state planning and evaluation guidelines for private marina development (unpublished).

Hwang, D.J. 1991. Shoreline setback regulations and the takings analysis. *University of Hawaii Law Review* **13**(1):1-56.

Kelly, J.A., and D.C. Slade. 1991. The public trust doctrine and coastal zone management: towards a model policy. In: Coastal zone '91: Proceedings of the seventh symposium on coastal and ocean management, eds. O.T. Magoon, et al., pp. 28-40. July. Long Beach, CA. New York: American Society of Civil Engineers.

Lam, V.J. 1991. Beach access: A public right? *Hawaii Bar Journal* **23**(1):65-87.

Slade, D.C., ed. 1990. Putting the public trust doctrine to work: the application of the public trust doctrine to the management of lands, waters and living resources of the coastal states. Washington, D.C: Coastal States Organization.

Tarnas, D.A., and M.C. Stewart. 1991. Harbors. In: Hawaii Ocean Resources Management Plan Technical Supplement. pp. 29-37. Honolulu: Hawaii Ocean and Marine Resources Council.

PAN JAPAN-SEA TOTAL OCEAN NETWORK PROJECT: DOUBLE-STAGE MERRY-GO-ROUND

Ko Tomino
Tobishima Corporation
Tokyo, Japan

ABSTRACT

Eastern Asia can be defined as comprising the South China Sea, East China Sea, Japan Sea, and Okhotsk Sea. The five nations along the Japan Sea--Japan, the Republic of Korea, the Democratic People's Republic of Korea, China, and Russia--possess great potential. This region has lately attracted considerable attention as a potential nucleus of development in the 21st century that will equal North America and Europe in scope.

The Pan Japan-Sea Total Ocean Network Project (TOP) is proposed as a way to link the five Japan Sea nations, which possess significant development potential, by a single marine network, and to promote broad-based exchanges with other economic blocs. To that end, a double-stage merry-go-round concept comprising macro (regional) and micro (local) merry-go-rounds is proposed. These will consist of clusters of local metropolitan facilities arrayed around the Japan Sea rim, and a new, international marine city to serve as their center, all linked by transportation networks. This paper offers a necessarily brief overview of the TOP project and its rationale (Figure 1).

INTRODUCTION

The broad purpose of the Pan Japan-Sea TOP concept is to contribute to global harmony through economic and cultural development of the entire region in cooperation among the nations bordering the Japan Sea. The primary goal of this plan is to overcome the barrier of physical distance within the region by creating a large-scale cross-border transportation network to foster the exchange of people and goods.

This can be accomplished by the creation of a marine city, called Acropolis, which will serve as a base for the entire area. Further, located around Acropolis will be a group of strategic cities, called Polis. Underneath each Polis will be a group of city facilities, called City, which will function as the base for the development of each area. Finally, a transportation network linking the entire area will be constructed.

The concept was named the Pan Japan-Sea Double-Stage Merry-Go-Round because the social infrastructure of this plan can be compared to a three-dimensional merry-go-round in terms of its schematic arrangement and function.

THE MACRO MERRY-GO-ROUND: A SUPER INFRASTRUCTURE TO MATERIALIZE INTERNATIONAL HARMONY

In this project, a gigantic circular transportation network running around the Japan Sea region will be constructed to link all areas. A group of strategic cities will be formed along the network to serve as footholds for the development of each area. Moreover, this circular network will support a broad range of international exchanges by

radially linking each strategic city with an international marine city to be constructed in the center of the Japan Sea.

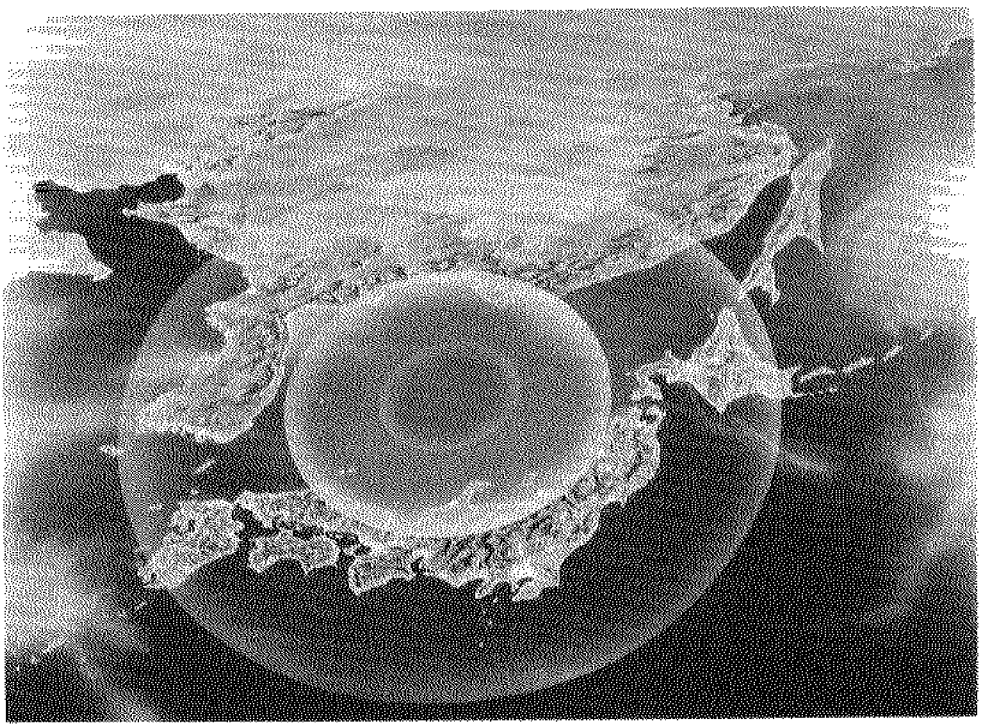

Figure 1. Pan Japan-Sea Map

The project will provide an excellent distribution network by employing state-of-the-art transportation systems, such as linear motor car and other land, sea, and air transportation facilities, e.g., by construction of international airports, ports, new canals, and so on, in each strategic city. The construction of the Mamiya-Soya-Tsushima Straits crossing road, which will provide all-weather connecting transportation, is part of the project. The trip around the Japan Sea by linear motor car will take half a day, while the trip from the marine city in the Japan Sea to each strategic city will take several hours by high speed boat or about one hour by airplane (Figure 2).

INTERNATIONAL FREE CITY: ACROPOLIS

Acropolis, the core of the Pan Japan-Sea area, is an international free city that will regulate the distribution functions for other economic blocs as well as manage the harmonious development of each of its areas. This city will be jointly administered by the five nations along the Japan Sea, and thereby promote extensive global business activity.

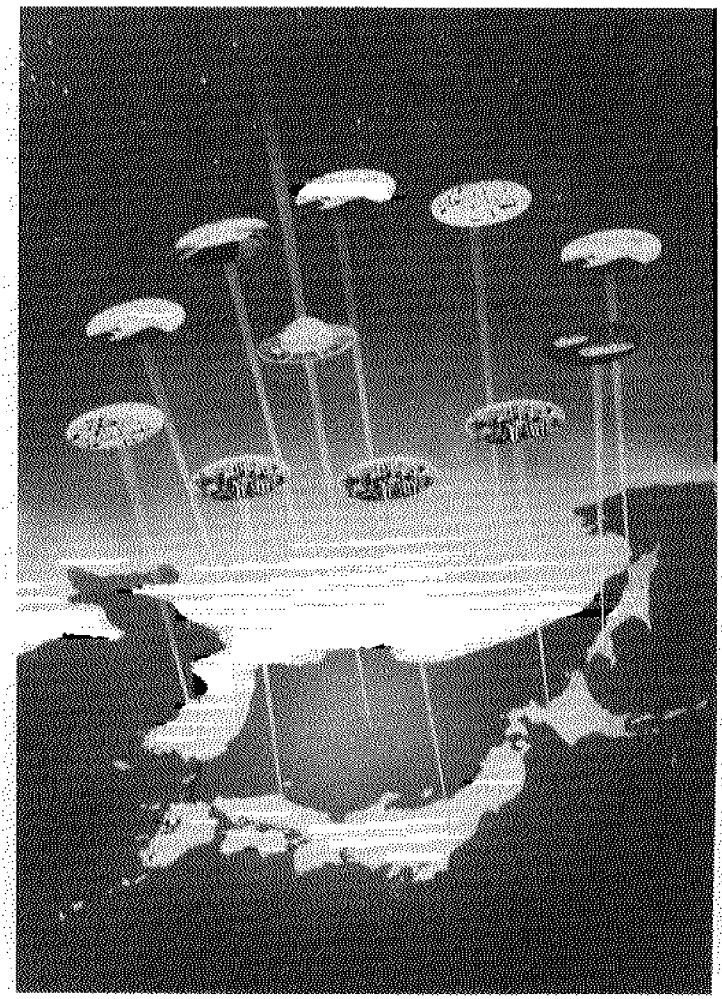

Figure 2. Macro merry-go-round

BASES FOR INTERNATIONAL EXCHANGE: POLIS

The Polis will be the bases for routine exchanges, transcending ideology and race, among nations along the Japan Sea. They will form gateways for socialist countries to participate in Western economic bloc activities.

INTEGRATED TRANSPORTATION NETWORK

The Japan Sea is a vast enclosed sea area connected to other oceans by four straits: Mamiya, Soya, Tsugaru, and Tsushima. The total length of the Japan Sea is approximately 1,000 km, and the circumference is 6,000 to 7,000 km. The integrated transportation network envisioned by this plan will efficiently link the entire area by state-of-the-art transportation systems such as linear motor cars, high-speed boats, and other systems.

THE MICRO MERRY-GO -ROUND: CREATION OF ATTRACTIVE AREAS BY STATE-OF-THE-ART ASSESSMENT TECHNOLOGY

Making the best use of their features, the base cities (Polis) will function as industrial bases for agriculture, fisheries, resources, high technologies, etc. Farther in the future, these bases will become highly advanced information cities engaged in dynamic economic activities. Arranged around these base cities there will be urban facilities (City), including recreation facilities suited to the local natural environment, tradition, and culture. Together, these facilities will form a micro merry-go-round that will contribute to the development of the area.

COMPOSITION OF THE CITIES

The cluster of urban facilities (City) essential for the formation of local infrastructures will emerge in each base city. These cities will feature business-related areas such as financial and commercial districts, and industrial and resource storage areas, as well as people-oriented areas, such as research, education, and resort areas, offering healthy and prosperous living environments.

CREATION OF POLIS AND CITIES GIVING PRIORITY TO THE NATURAL ENVIRONMENT

The Japan Sea is in effect an enclosed sea area. Should it be contaminated by the wastes generated due to development of the region, the damage would be serious. To prevent such an event from taking place, the project will apply state-of-the-art "green" technology from the outset in order to preserve the environment. Therefore, the creation of environment-and-human-friendly Polis and Cities will be pursued based on the environmental characteristics and traditions of each area.

REGIONAL TRANSPORTATION NETWORK

A transportation network extending throughout the region is planned that will connect the base cities by a circular linear high-speed rail network. The first stage of the project will be the construction of trunk lines for transporting products. This will be followed by expansion of transportation facilities into surrounding regions by upgrading or expanding the existing infrastructure, or by creation of trunk lines between cities. This development will be implemented in coordination with the overall development of each region.

INTRA-AREA DEVELOPMENT PROCESS

At the beginning of the project, five types of micro merry-go-rounds will be arranged in each base city around the Japan Sea so as to utilize each country's production element. Each micro merry-go-round will add other base city functions depending on its development level, and ultimately it will have a function equivalent to that of the Japanese Pacific Belt area. By this means it will equalize the standard of living and services throughout the entire region.

PRODUCTION ELEMENT OF EACH COUNTRY

Each country has its own production element, as follows:

- Japan: Advanced technologies and financial capital
- Russia: Abundant natural resources in its Far East region
- China: Agricultural products and labor force in three north-eastern provinces
- South Korea: Intermediate technologies and financial capital
- North Korea: Mineral products and labor force

THE JAPAN SEA ACROPOLIS: CREATING THE IDEAL INTERNATIONAL MARINE CITY WITH A BENEFICIAL ENVIRONMENT

As the nucleus of the transportation network and economic activities of the Japan Sea economic bloc, the Japan Sea Acropolis (Figure 3) will be jointly administered by every country involved. It will thereby realize the principle of international harmony across a broad field.

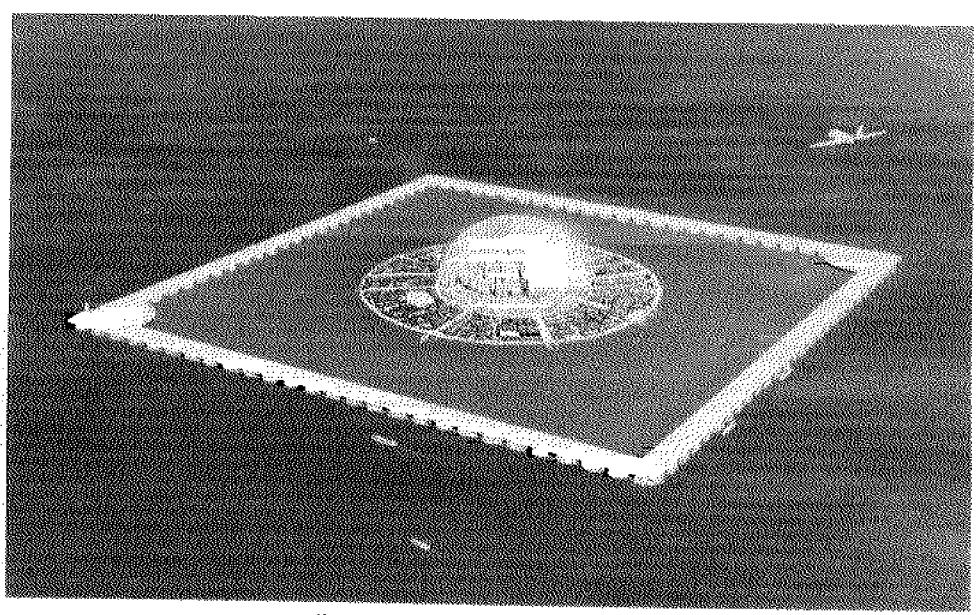

Figure 3. Overall view of Acropolis

Japan Sea area, at a depth of 280-300 m, at 135 degrees east longitude and 39.2 degrees north latitude. The construction process will be as follows: First a 4 km square breakwater will be built on the ridge. An artificial island of 3.14 million square meters will be built in the center of the breakwater.

Acropolis will accommodate several types of facilities. The upper part of the man-made island will contain a group of facilities with international functions, serving as the base for a wide variety of economic activities as well as residences. In the lower part, waste disposal facilities such as sewers will be built. This zone will also function as an ocean farm (Figure 4).

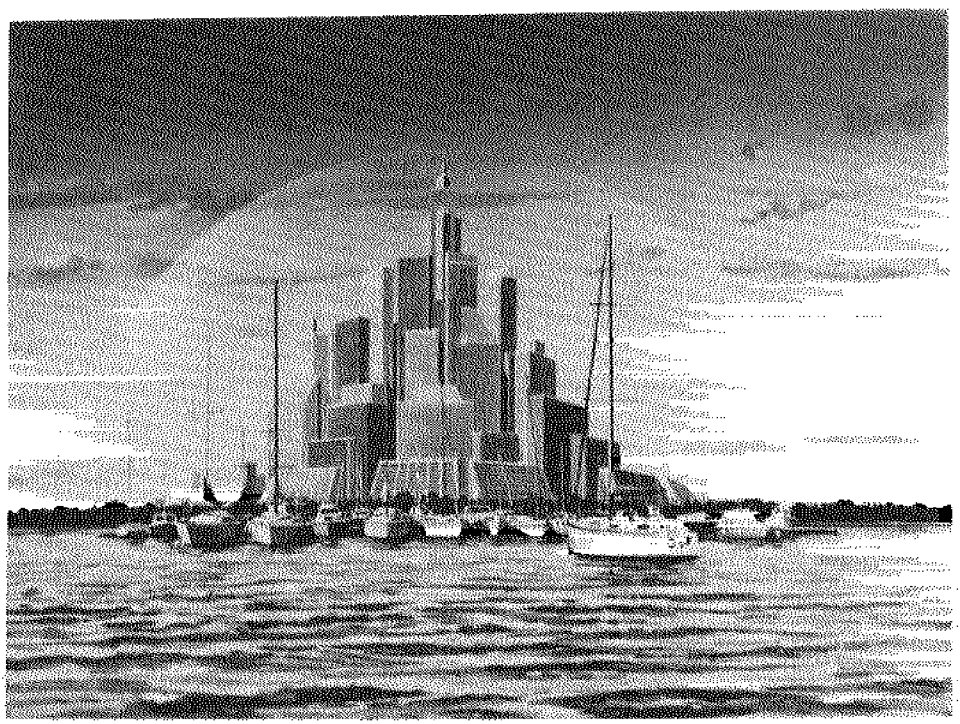

Figure 4. Marina facilities - Acropolis

Airplane runways and other transportation facilities, such as loading and unloading areas for ships, will be constructed on the upper part of the surrounding breakwaters (Figure 5). Moreover, this area will function as a storage base with several types of storage facilities. It will include a capacity for 300 million kiloliter oil tanks, equivalent to Japan's oil consumption for 16 months. Thus, equal distribution of resources among the nations will be achieved.

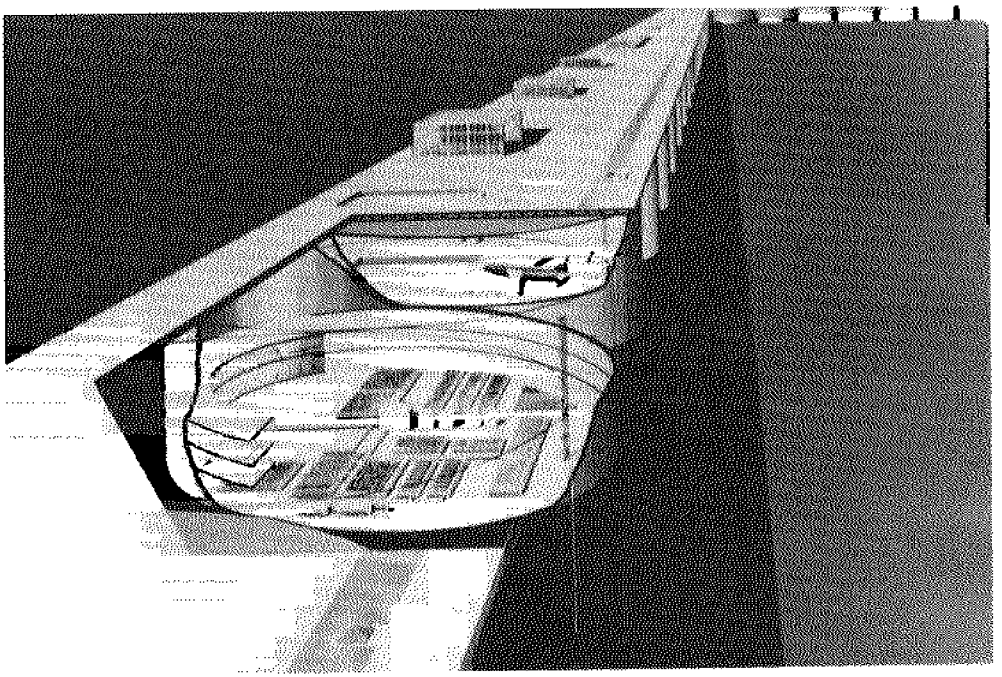

Figure 5. Drawing of multi purpose uses within breakwater

The main energy source for Acropolis will be an ocean thermal energy conversion plant. It is estimated that approximately 800,000 kw of power can feasibly be generated from June to October by installing eight 100,000 kw generators. When superconducting technology makes efficient storage systems possible in the future, ocean thermal energy conversion alone will be sufficient to meet the energy requirement of each facility in the man-made island (Figure 6). It will also be possible to supply electricity to strategic cities. Furthermore, plan also includes exploration of several other marine energy resources as well as the desalination of sea water using biotechnology. In other words, the Japan Sea Acropolis will be a product of human dreams across a variety of advanced technologies.

CONCLUSIONS

The primary goals of the Pan Japan-Sea TOP concept are to build a cosmopolitan city, Acropolis, that will function as a center for economic and cultural exchanges among nations that border on the Japan Sea, and to establish a distribution base to serve the entire region. Clearly, the TOP project can provide an extremely significant stimulus for economic and cultural development, both locally and internationally, in an environmentally sound manner. It can also serve as a major vehicle for further development in all areas.

The estimated total cost and the time required to realize this concept is 33 trillion yen over a period of 15 years. At present, we are actively promoting research and development of relevant technologies.

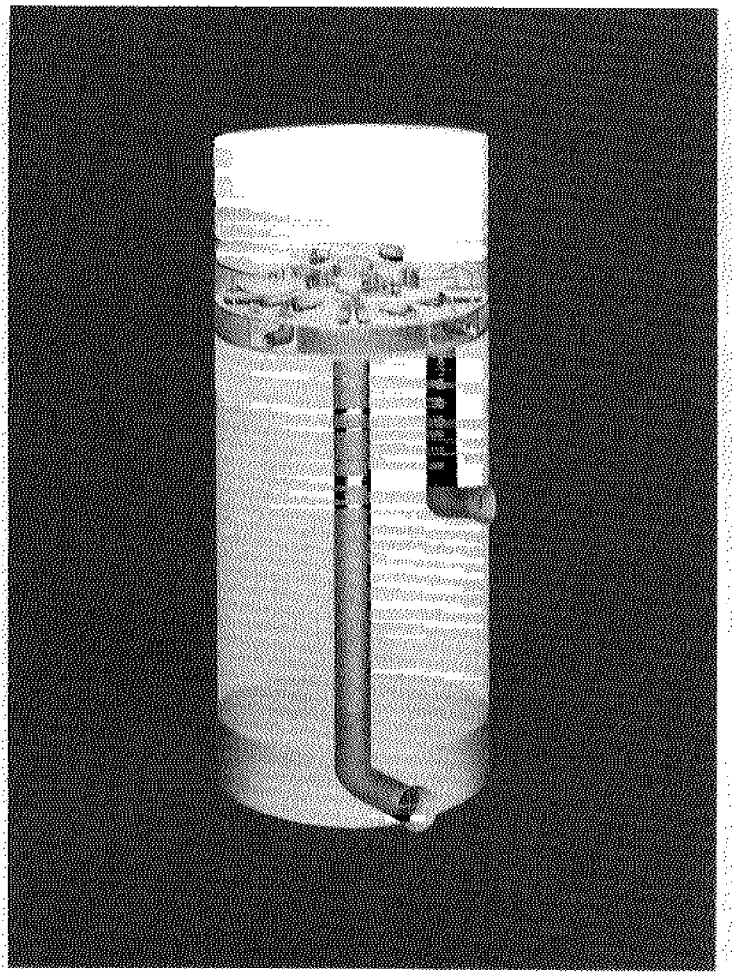

Figure 6. Ocean thermal energy power conversion and energy facilities

ACKNOWLEDGMENTS

It has been my great fortune to have received the substantial cooperation of a number of persons in the course of bringing this paper to completion. First and foremost, I would like to take this opportunity to express my sincere gratitude to Professor Takeo Kondo (Marine Architecture Engineering, Department of Science and Engineering, Nihon University), for his considerable guidance in a number of areas.

I would also like to express my thanks to Ms. Yoko Fujita (President, Fast International Co., Ltd.), who has undertaken the task of translating this paper.

REFERENCES

Kobayashi, H., S. Kurisaki, A. Matsue, and K. Tomino. Pan Japan Sea TOP plan: plans to build a multi-purpose floating island. Tobishima Corporation.

Kondo, T. 1992. Pan Japan-Sea TOP concept. Presented at Intl. Conf.: Does New Development of Energy-related Environmental Technology Play a Key Role in the Continuance of Mankind? Kyoto International Convention Center.

Ogawa, K. 1991. The opening of the North-East Asia and Sibera era. *Nihon Keizai Shimbun.*

Terai, K. 1986. The whole picture of gigantic projects. TBS Britannica.

Toma, T. 1991. The Emergence of Pan Japan Bloc: The Gigantic Market for the 21st Century. Sochisha.

Tomino, K. 1992. Pan Japan-Sea Top Concept II: International Marine City in Japan-Sea Area. Tobishima Corporation.

Uehara, H. 1982. Ocean Thermal Energy Power Conversion. Ohm Publishing.

DEVELOPMENT OF A FLOATING-TYPE BUILDING MOORED IN A COASTAL AREA

Masami Matsuura, Kunihiro Ikegami and Kazuo Masuda
Mitsubishi Heavy Industries, Ltd.
Nagasaki, Japan

ABSTRACT

Floating-type buildings will be moored for a long time in a specific site, and will be used by a number of people. At the design stage, therefore, it is important to determine the design criteria from the points of view of safety and comfort. In the present development, referring to investigations on vibration of high buildings and conducting human response tests by using a forced oscillating carriage, design criteria was decided in terms of acceleration of motion of a floating-type building.

Based on the design criteria, a floating-type building mounted on a barge was designed for a hotel barge as a case study. Particularly, a mooring system and methods of motion reduction were studied theoretically and experimentally. Theoretical calculation is based on a time-domain simulation method including the effect of nonlinear reaction forces due to the mooring system. Tank tests with a 1/30 scale model were carried out to evaluate the mooring forces and motions in waves and wind. The results were discussed from the points of view of engineering feasibility.

INTRODUCTION

In viewing the prospects for effective utilization of ocean space, several new concepts have been proposed (for example, Yoshida, et al., 1990; Terai, 1990). Most of them consist of very large systems using huge floating or fixed structures and are investigated aiming at big developments in the future. On the other hand, a simple concept with high actuality in the near future is discussed in this paper aiming at creation of new space in coastal area. Utilization of ocean space as living and working space for citizen seems promising to provide new space for coastal countries like Japan. Various floating-type buildings are anticipated to be utilized as offices, hotels, recreational facilities and so on in the near future. Ocean space utilization by using floating-type structures should be promoted further in coastal areas where these kinds of structures are most feasible. Floating-type buildings have several advantages, for instance, lower cost and shorter period of construction than ocean space utilization by reclamation because of factory-built applied to main parts of structures.

Figure 1 shows an artist's concept of a floating-type building, and it typically demonstrates the topic of the present study. This paper discusses some of the engineering feasibility studies for developing floating-type buildings. Figure 2 illustrates a floating-type oil storage system completed in 1988 at Kami-Gotoh in Japan (Ikegami, et al., 1990; Shuku, et al.,1988). The entire system consists of 5 huge storage barges. It is now in full operation and each barge is filled with crude oil. Its mooring system consists of large dolphins and rubber fenders as shown in Figure 3. The present study is based on the experience in engineering of this project. Basically, the same technology can be applied to floating-type buildings. However, there are some different areas in the development of floating-type buildings utilized by many people. At the design stage,

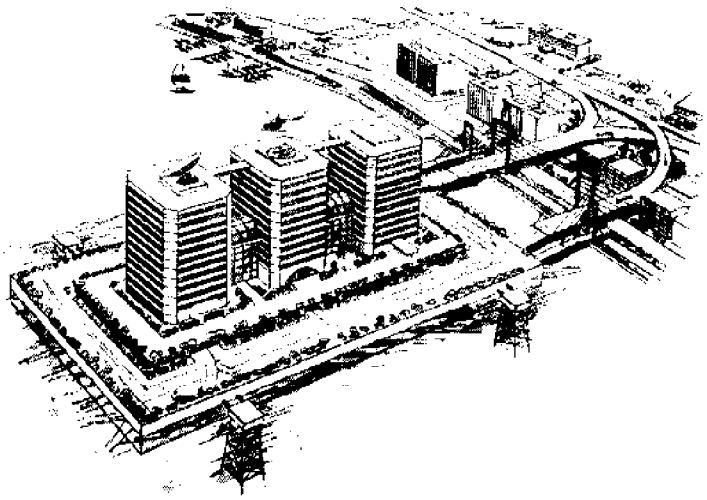

Figure 1. Artist's concept of floating-type building

Figure 2. Floating-type oil storage system at Kami-Gotoh in Japan

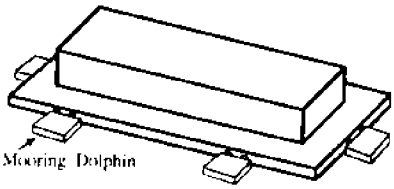

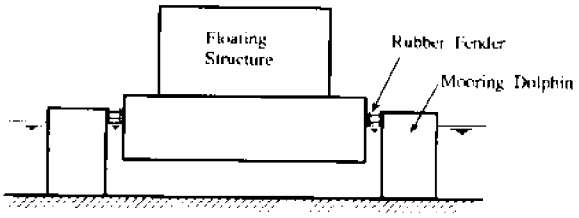

Figure 3. Mooring system with dolphin and rubber fender in shallow water

therefore, it is important to determine design criteria from the point of view not only of safety but also of comfort.

In the present paper, reference to investigations on vibration of high building on land and conducting human response tests, design criteria is discussed for comfort. For a case study, a prototype design is introduced and examined based on assumed site and design conditions. Then, this paper presents a study on a mooring system and methods of motion reduction in order to suit the prototype to the design criteria by use of theoretical calculations and model tests. Finally, evaluations of floating-type buildings based on our concept are discussed from the points of view of safety and comfort.

DESIGN CONDITIONS

Basic Design Condition

Assumed basic design conditions are shown in Table 1. An assumed floating-type building consists of a barge-type floater and an upper structures, and produces space and facilities for a maximum of 2,500 people. For the case study a site was assumed to be in a coastal area, shallow water and rather calm sea, and Nagasaki Bay was tentatively selected, as shown in Figure 4. Site selection is very important in such developments and should be made essentially from the social and economical viewpoints as well as technical ones. However, the present paper describes an outline of the study focusing on the engineering feasibility of floating-type buildings.

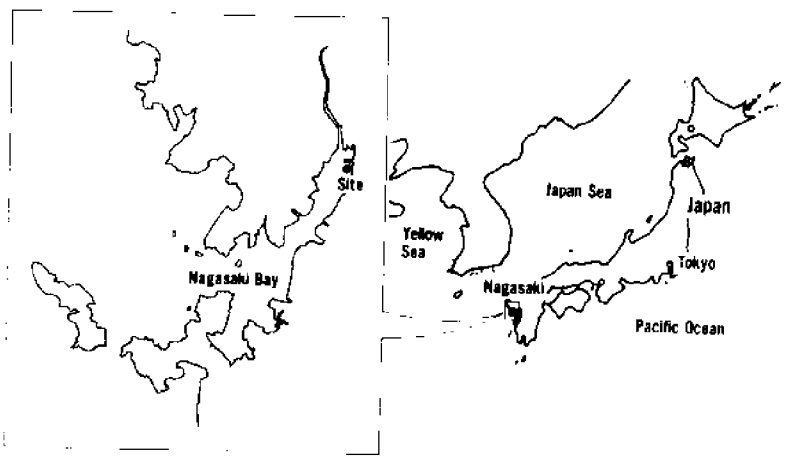

Figure 4. Tentatively selected site of the floating-type building for the present study

Environmental Conditions

The assumed site is conveniently sheltered from ocean waves. However, there are waves generated in the bay by strong winds in storm conditions. Environmental conditions were determined based on data of the Meteorological Observatory located near the site. Two types of storm conditions were determined as shown in Table 2. Storm conditions corresponding to 100- and 5-year return period are used for discussion about safety and comfort, respectively. Tidal range must be taken into consideration in designing a mooring system, and the maximum value is 5.0 m above the lowest level of a tide level including the effect of harbor oscillations. Mean water depth corresponding to the lowest sea level is 8.5 m.

Table 1. Basic design conditions.

Barge type floater

Deck Area : 10,000 m^2

Displacement : 30,000 ton

Upper structures

Floor Area : 25,000 m^2

Capacity : 2,500 persons

Facilities : Hotel, convention hall, offices, restaurants, shopping plaza, parking spaces, etc.

Site condition

- Coastal area near land
- Shallow water
- Rather calm sea

Table 2. Environmental conditions.

Environmental Condition		100 Year Storm	5 Year Storm
Wind speed (10 min. Mean)		42.5 m/s	27.5 m/s
Waves	Significant wave height	2.0 m	1.3 m
	Significant wave period	4.0 s	3.3 s

Design Criteria

Design criteria are considered from the points of view of safety and comfort. Design criteria for safety can be defined based on allowable force of the mooring system.

With respect to comfort, it is difficult to define design criteria, since comfort is related to human psychological responses and is unclear. There were several research projects about the relationship between vibration and human response introduced by Ikegami, et al. (1989). Figure 5 shows typical data of human responses based on a reference. Human responses vary according to magnitude of acceleration, but the influence of motion period is rather small on human responses. From this figure it can be seen that almost all persons notice accelerations beyond 10 gal. In environments with acceleration of 10 to 25 gal, persons are affected by the vibration but are able to work as usual.

In order to better understand human responses, tests were carried out by using forced oscillating carriage with horizontal motions as shown in Figure 6. The test results are summarized in Table 3. From the test results it can be stated that there were no problems in doing daily work in circumstances with accelerations from 10 to 25 gal.

From these investigations, it can be said that allowable accelerations are in the range of 10 to 25 gal. This guideline is also supported by data of vibration caused by a strong wind measured for existing tall buildings as shown in Figure 7. As a design criterion, acceleration of 10 gal is assumed tentatively for a 5-year storm condition. Acceleration of 10 gal is rather severe for floating-type structures; however, it was selected as a target value of the present study.

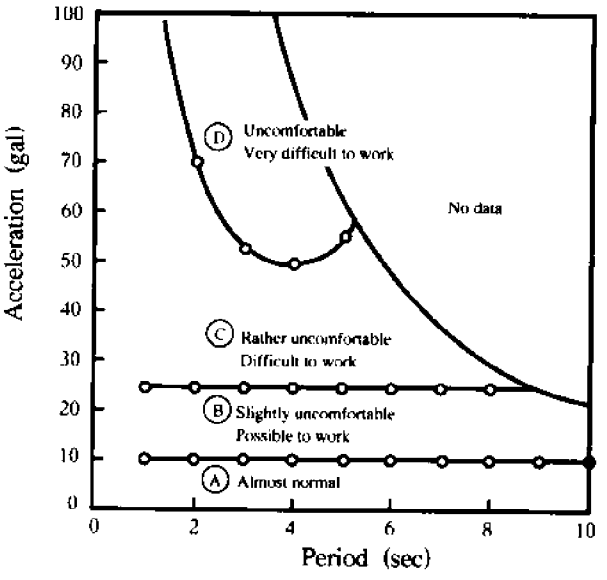

Figure 5. Relationship between acceleration and human response

Table 3. Results of human response test

Acceleration	Human Responses, etc.
3 gal	- Possible to notice slight motions occasionally
10 gal	- Possible to notice motions - No motion of water in a glass - No problem in freehand drawing
25 gal	- Furniture with casters move - No motion of water in a glass - Slight difficulty in freehand drawing
50 gal	- No problem in standing up - Slight influence on walking - Not to feel danger

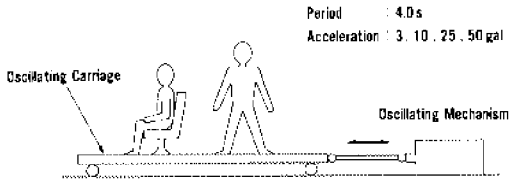

Figure 6. Human response test

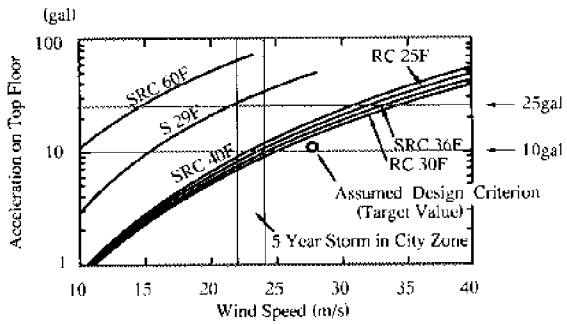

Figure 7. Vibration on tall buildings caused by a strong wind

PROTOTYPE DESIGN

Basic Design of Prototype

The principal dimensions of a prototype designed for the present study are shown in Table 4. Simplifying the problem, a barge-type floater and a square-type upper structure were adopted. For the mooring system, rubber fenders and mooring dolphins are arranged as shown in Figure 8. Figure 9 shows the cell-type rubber fender adopted in the study. As shown in Figure 8, the reaction force of rubber fender is kept almost constant after the deflection of the fender exceeds about 20 % of the original length. It is possible, therefore, to transfer the mooring force to the dolphin without generation of excessive reaction even if the fluctuating loads due to waves and wind are superimposed on the steady loads. Design allowable deflection of the cell-type fender was assumed to be 35% strain in the present study. Because this mooring system based on rubber fenders and dolphins can keep the position of a floating structure within small horizontal displacements, it is convenient to access from land to moored floating structures by a bridge. Also, it is well adapted to mooring in shallow water and can allow for large changes of sea water level.

Motion Reduction Method

In order to polish up the prototype design and improve comfort, methods of motion reduction were examined. From several candidates of motion reduction methods, three types of simple and reliable methods shown in Figure 10 were selected and further investigations were carried out theoretically or experimentally. One is the case of increasing displacement by additional ballast in order to increase total mass of a floating body. Another is a mooring system with tandem fenders used to reduce fender reaction forces. The other uses a hydraulic damper added in the mooring system in order to increase damping forces.

Table 4. Principal dimensions of prototype

Length	120 m
Breadth	96 m
Draft	2.54 m
Displacement	30,000 ton
Wind area	3,460 m^2
Number of floors	14 floors above deck 2 floors under deck

Theoretical Calculation

In order to verify feasibility of the prototype design and the effect of the motion reduction methods described above, theoretical calculations were carried out. The nonlinear computer simulation program with a time domain motion analysis method was used in the study. This computer program has been developed by Fujii, et al. (1982) and was improved for the present study in order to take into account the effect of damping forces of the mooring system. Calculations were carried out in irregular waves and fluctuating winds corresponding to a 100-year storm and a 5-year storm. Bretschneider-Mitsuyasu's spectrum and Davenport's spectrum were used for irregular waves and fluctuating wind, respectively.

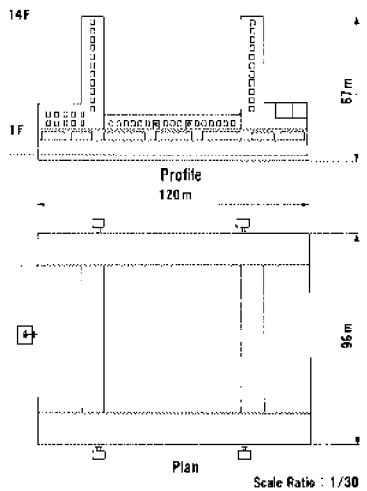

Figure 8. Modeling of floating-type building

Figure 11 shows the summary of calculation results. Maximum values of fender deflections, horizontal accelerations and roll motions are given in the figure as the results for each method of motion reduction as well as the basic case. Fender deflections are lower than design allowable value of 35 % fender deflection in all cases; therefore, it is said that safety of the mooring system is proven. As mentioned above, the assumed target value of acceleration is 10 gal for 5 year storm condition. In the case of 2.54 m draft: the basic draft condition, horizontal accelerations are beyond 10 gal. Vertical accelerations are not shown in the figure but they are negligibly small. In the case of 4.5 m draft: the case of increasing displacement by additional ballast, motions are remarkably small in comparison with the case of 2.54 m draft. The motion reduction methods using tandem fenders and hydraulic dampers appear to be effective for the reduction of horizontal accelerations. As a result, it is confirmed that safety of the prototype is basically insured. Some motion reduction method must be applied in order to improve comfort of the prototype.

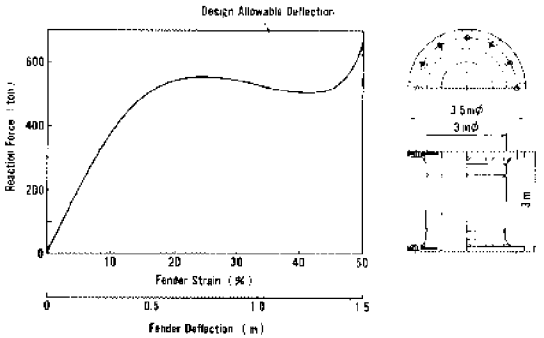

Figure 9. Cell-type rubber fender

Motion Reduction Method	Effect
Additional Ballast	to Increase Mass
Tandem Fender	to Reduce Fender Reaction Force
Hydraulic Damper	to Increase Damping Force

Figure 10. Concept of motion reduction method

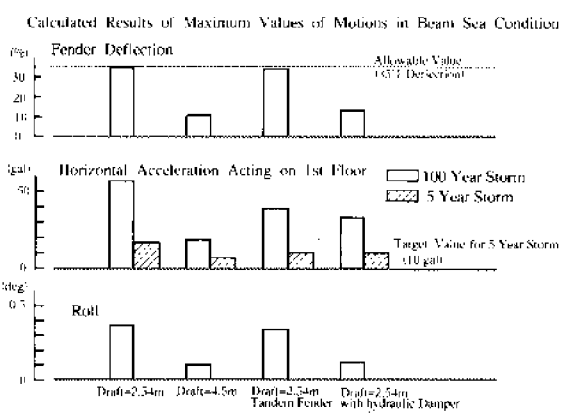

Figure 11. Calculated results for various motion reduction methods

EVALUATION WITH TANK TESTS

Test Procedure

As an extensive investigation, model tests with a 1/30 scale model were carried out to evaluate the mooring forces and motions in irregular waves and fluctuating wind as shown in Figures 12 and 13. The tests were carried out in the Shallow Water Basin of the Nagasaki Research and Development Center, Mitsubishi Heavy Industries, Ltd. Regarding the model of the mooring system, nonlinear reaction force of rubber fender versus fender deflection: constant reaction force characteristics shown in Figure 9 were simulated by use of springs and weights as shown in Figure 14. Oil dampers were used in the tests aimed at examining the effect of hydraulic dampers on the absorption of motions, and simulated damper characteristics versus deflection speed are given in Figure 14. All data in the figure were converted to full scale values. Measurements were made for motion, acceleration and mooring forces.

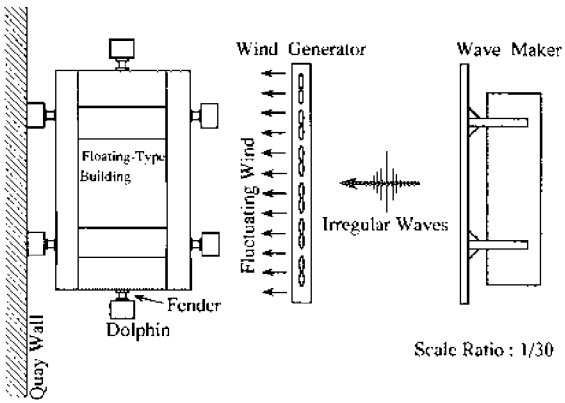

Figure 12. Arrangement of model tests

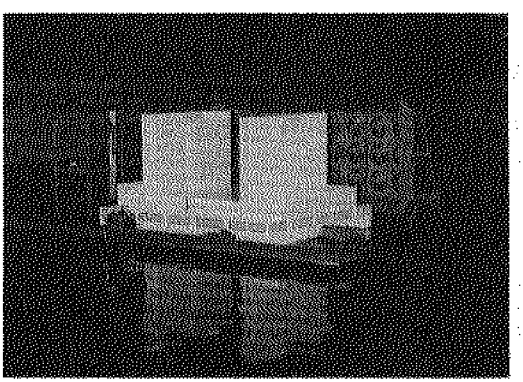

Figure 13. Outlook of model tests

Test Results

Figure 15 shows the measured maximum values of fender reaction forces versus fender deflection. In the figure the results are classified into two groups for 100-year storm conditions and 5-year storm conditions, respectively. Measured fender deflections were very small in comparison with the design allowable deflection of 35%. Therefore, it is said that safety for the mooring system of the prototype is confirmed. And, from this figure the remarkable effects of the hydraulic damper were observed on the reduction of motions and fender reaction forces. Figure 16 shows the measured results of horizontal accelerations acting on lower and upper floors. For our study, measured accelerations are beyond the assumed target value of design criterion 10 gal. In particular, accelerations on the upper floors are large due to the influence of roll motions. However, the prototype design seems to be improved as its accelerations to the same extent as existing tall buildings on land. From these results, it seems that acceleration of 10 gal is

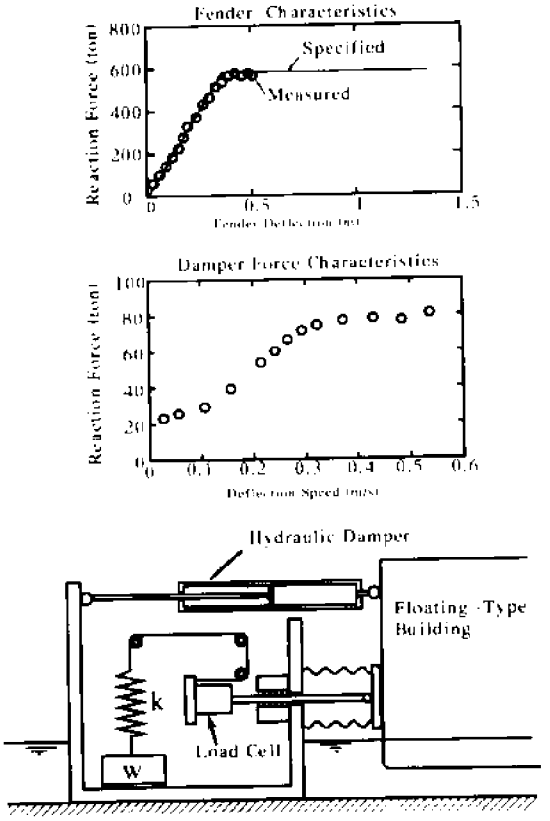

Figure 14. Models of rubber fender and hydraulic damper

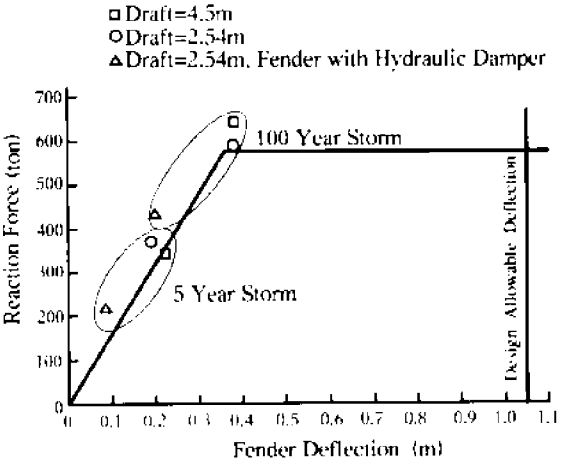

Figure 15. Measured mooring forces compared with the design allowable deflection

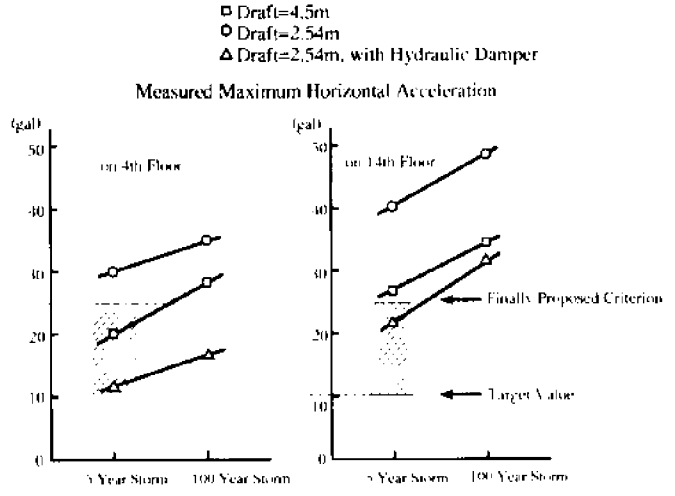

Figure 16. Measured accelerations compared with the proposed criterion

too severe for floating structures to exist in 5-year storm conditions. Twenty-five gal is proposed as the design criterion for acceleration related to comfort. Comparison of measured and theoretically calculated accelerations is shown in Figure 17 for mooring systems with and without hydraulic dampers. Calculated accelerations are slight larger than measured ones, but fairly good agreement is obtained between the calculated and the measured ones. Therefore, it is proven that theoretical calculations are useful as a design tool for these developments.

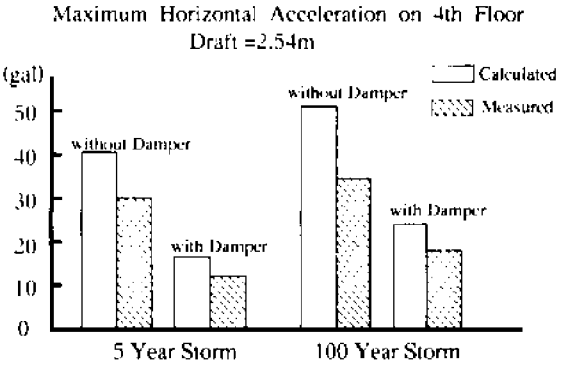

Figure 17. Comparison of measured and calculated accelerations

CONCLUDING REMARKS

In the present paper, an engineering feasibility study on development of floating-type buildings was introduced. Because floating-type buildings will be utilized by many people, it was pointed out that design criteria must be taken into consideration from the points of view not only of safety but also of comfort. Maximum allowable values for motion accelerations were proposed as design criteria on comfort for a 5-year storm condition. Referring to investigations on vibration of high buildings on land and conducting the human response tests, design criteria was discussed for comfort. As a result of the study, acceleration of 25 gal for 5-year storm condition was finally proposed as the design criterion prescribing comfort of floating-type buildings.

As a case study the prototype design and the design procedure were introduced. Based on the prototype design, further investigations were carried out on mooring systems and methods of motion reduction in order to match the prototype to the design criteria by use of theoretical calculations and model tests. Regarding safety, it was confirmed that the mooring system with rubber fenders is feasible for floating-type buildings moored in coastal areas. With respect to comfort, it was confirmed that accelerations were the same as existing tall buildings on land. Therefore, it can be said that floating-type buildings based upon the prototype design are basically feasible for development of space for human activity. In order to further improve comfort of the prototype design, examples of motion reduction methods were described. Increasing displacement and the mooring system with hydraulic dampers or tandem fenders were introduced and discussed with respect to its validity to reduce motions and improve comfort.

REFERENCES

Fujii, H., K. Ikegami, and M. Shuku. 1982. Design of mooring system of oil storage in shallow water. *Applied Ocean Research*. 4(1).

Ikegami, K., H. Tayama, and T. Tanahashi. 1990. One year field measurement of mooring system for the world's first floating type oil storage system in Kami-Gotoh, Japan. In: Proceedings of the Ninth International Conference of Offshore Mechanics and Arctic Engineering, Houston.

Ikegami, K., M. Matsuura, T. Tsukabe, and K. Masuda. 1989. Development of floating offshore building. In: Proceedings of the Ninth Ocean Engineering Symposium. The Society of Naval Architects of Japan. (in Japanese)

Shuku, M., and K. Ikegami. 1988. Oil storage and mooring system (Kamigoto Project). In: Proceedings of TECHNO-OCEAN '88 Symposium. Kobe, Japan.

Terai, K. 199). Ocean city. In: Proceedings of PACON 90. Tokyo, Japan.

Yoshida, K., N. Oka, and T. Arima. 1990. A concept for creation of business space by using huge ringlike semisubmersibles. In: Proceedings of PACON 90. Tokyo, Japan.

MODEL TESTS ON MULTI-UNIT FLOATING STRUCTURES IN WAVES

Koichiro Yoshida
University of Tokyo
Tokyo, Japan

Kentaro Kobayashi
Sumitomo Heavy Industries, Ltd.
Tokyo, Japan

Hiroko Suzuki
University of Tokyo
Tokyo, Japan

Ja-Sam Goo
National Fisheries University of Pusan
Pusan, Korea

ABSTRACT

We have carried out model tests on an offshore floating structure composed of multiple floating bodies and some foundation units. Wave exciting forces on floating bodies and dynamic responses of the structure in waves were measured. In the test of wave exciting forces, up to five semi-submersible-type floating units were modeled to a scale of 1/80, and one-, three-, and five-unit systems were fixed in regular and transient waves. In this experiment, the effects of hydrodynamic interaction among floating bodies on their wave exciting forces were investigated. In the test of dynamic responses, three or five floating units were connected to each other and linked to one or two foundation units settled in the model basin. Structural wave loadings on connections and motion responses of multi-unit systems were measured in head, beam, and oblique wave conditions. Results of these tests were compared with theoretical predictions and successful agreements were obtained both on wave exciting forces and elastic structural responses.

INTRODUCTION

Since 1987, the authors have been proposing a new concept of a large offshore floating structure like a city expanding widely in ocean space. The structure consists mainly of a number of semi-submersible-type floating units and some foundation units which settle the floating units in the sea. Several floating units are bunched and connected to each other as a functional city module, and various kinds of city modules will be linked by bridges or piers and will build up a multi-functional offshore city. This concept is proposed for ocean space utilization and was presented at PACON '90 as a "comprehensive offshore city" by Yoshida, et al. (1990). Figure 1 shows an imaginative illustration of the offshore city widely spreading within several kilometers offshore range. An appropriate size of each floating unit is estimated about 100 m^2. On its deck, various kinds of city functions can be built up. Figure 2 illustrates an example of recreation module on a semi-sub-type floating unit.

Figure 1. Imaginative illustration of an offshore city

Due to dynamic motion characteristics of semi-submersible-type floating units, this offshore floating structure can be expected to hardly respond to sea waves as compared with other types of floating structures. However, with the intention of improving the amenities of life in the offshore city, floating units are planned to be fixed to sparsely-positioned foundation units so as not to move nor drift by environmental forces such as waves, current, wind, etc. For this rather new structural system, it is important to confirm that the structural system has a sufficient strength against environmental forces and that the magnitude of motion responses is small enough. With respect to engineering feasibility, especially in waves, we have recently carried out some basic model tests of multi-unit floating structures in the experimental model basin. By using up to five floating unit models, wave exciting forces acting on each unit, wave bending moments on the connections between units and dynamic motion responses of the structures were measured.

As is widely recognized, hydrodynamic forces acting on multi-unit structures in waves are greatly influenced by hydrodynamic interactions among floating bodies. Therefore, the effect of hydrodynamic interactions between units is one of the greatest interests of our experiments. In the test of wave exciting forces, one-, three-, and five-unit systems were tested in head, beam, and oblique waves in order to obtain hydrodynamic interactions on wave exciting forces.

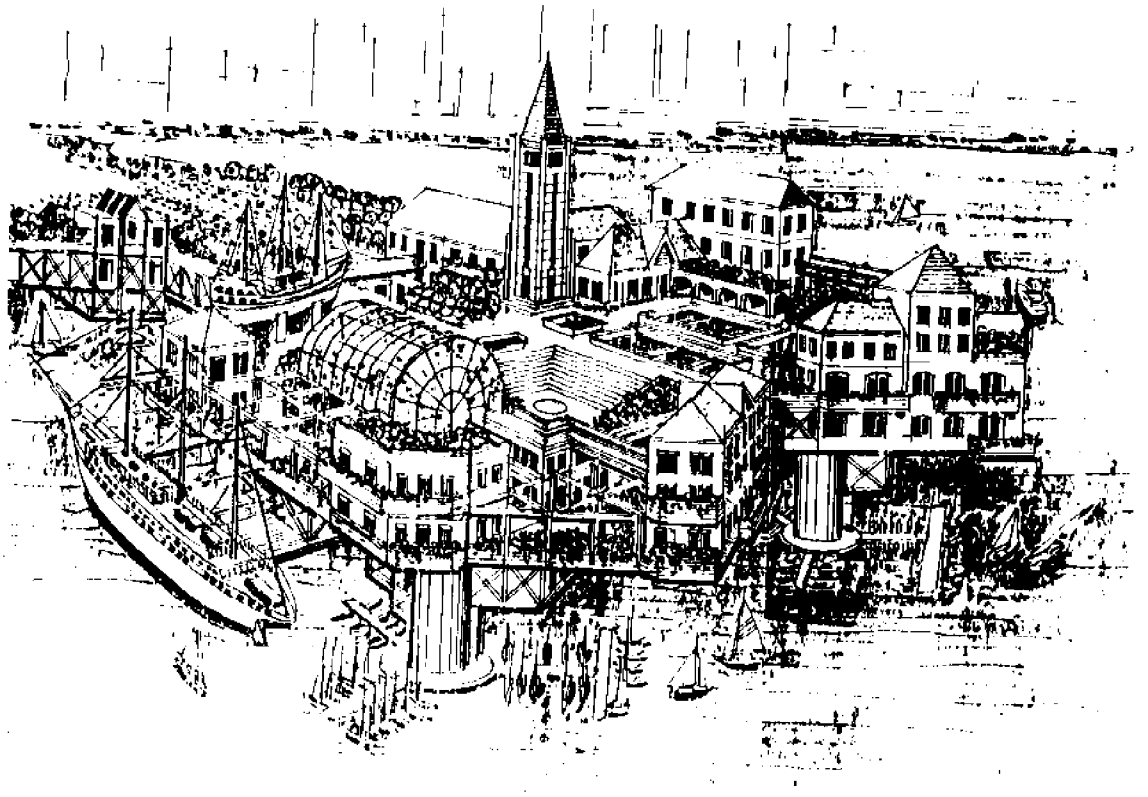

Figure 2. Imaginative illustration of a recreation module

In the test of dynamic responses, three or five floating units were connected to each other with and linked to one or two foundation units settled in the model basin. Elasticity of the model structures was simulated to that of the assumed offshore city and structural wave loadings and motion responses were measured in various wave conditions.

In the following sections, results of tests are analyzed in detail and are also compared with theoretical predictions using a recently developed calculation method by Goo, et al. (1990).

MODEL TESTS

Floating Unit Model

Figure 3 shows the floating unit model which was used for all model tests in waves. The actual size of overall length and breadth is assumed to be 100 m and 80 m, and the displacement of 1 unit is assumed to be about 39,000 tons in actual scale. The configuration and its size are similar to typical four-column, lower-hull-type semi-submersibles. It has a hexagonal upper structure deck plan, although its lower hull has a square shape. Six sides of the hexagonal deck can be used to connect to the deck of the next unit. The model was made in scale of 1/80 and made of clear acrylic plastic. In the

columns and lower hull are openings for weights in order to set-up displacements, KG, and second moment of inertia, etc., as shown in Table 1. In total, five models were made and used in the tests of wave exciting forces and dynamic responses in waves.

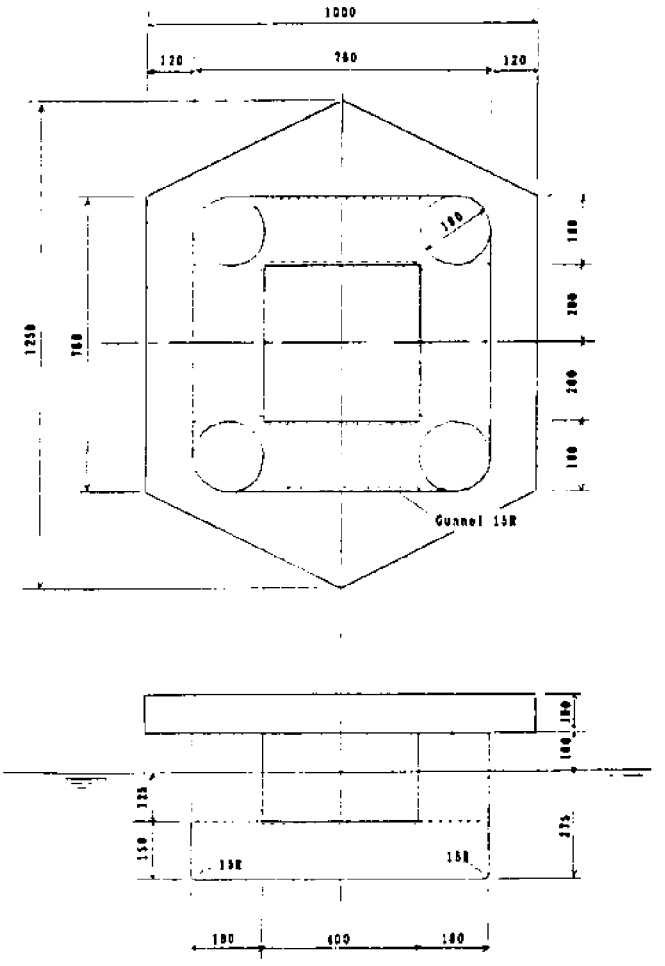

Figure 3. Principle dimensions of a floating model

Foundation Unit Model

The function of foundation units is to moor and fix the neighboring floating units on the seafloor in order to reduce dynamic motions of floating bodies in waves and minimize drift by wind or current. Therefore, the realistic foundation unit must be like a gravitational offshore platform. However, in our experiments, the foundation units were simplified to a truss structure so as not to interfere incident waves as much as possible. Two foundation units were made, and they functioned only to keep the multi-unit structural models mentioned below at right position in the model basin.

Multi-Unit Structural Models

Using several floating unit models, two types of structural models were composed for dynamic motion and structural response tests in waves. Figure 4 is an example of offshore city arrangement. There are several functional clusters (modules), and 1 cluster is composed by about 10 to 20 floating units connected to each other. The clusters are fixed in the sea by foundation units which are marked black in Figure 4. As can be seen, a wide variety of connection patterns is allowable, because of its hexagonal upper structure shape. But for the model tests, we adopted two basic and typical patterns of connection, indicated at A and B in Figure 4. We simplified A and B patterns and modeled by straight line-up of floating units as shown in Figure 5.

Model A: 5-unit system with 2 foundation units at both ends
Model B: 3-unit system with 1 foundation unit at one end

These two models were used in the test of dynamic responses in waves.

Table 1. Principal particulars of a floating unit

Items	Experimental model(1/80)	Real dimensions
Size of deck	1250 × 1000 mm	100.0 × 80.0 M
Depth of deck	100 mm	8.0 M
Depth of unit	475 mm	38.0 M
Draft	275 mm	22.0 M
Air gap	100 mm	8.0 M
Section of float	760 × 760 mm	60.8 × 60.8 M
Diameter of column	180 mm	14.4 M
Displacement	74.317 kg	39001.6 ton
KG	196 mm	15.68 M
KM	227.5mm	18.2 M
GM	31.5mm	2.52 M
Kxx, Kyy	0.404 L (L=760 mm)	0.404 L (L=60.8 M)

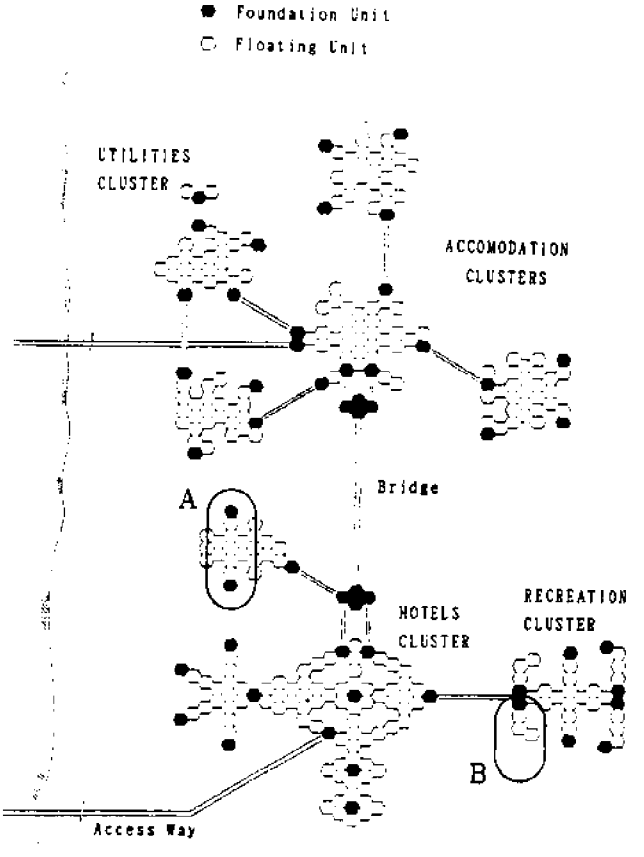

Figure 4. An example of offshore city arrangement

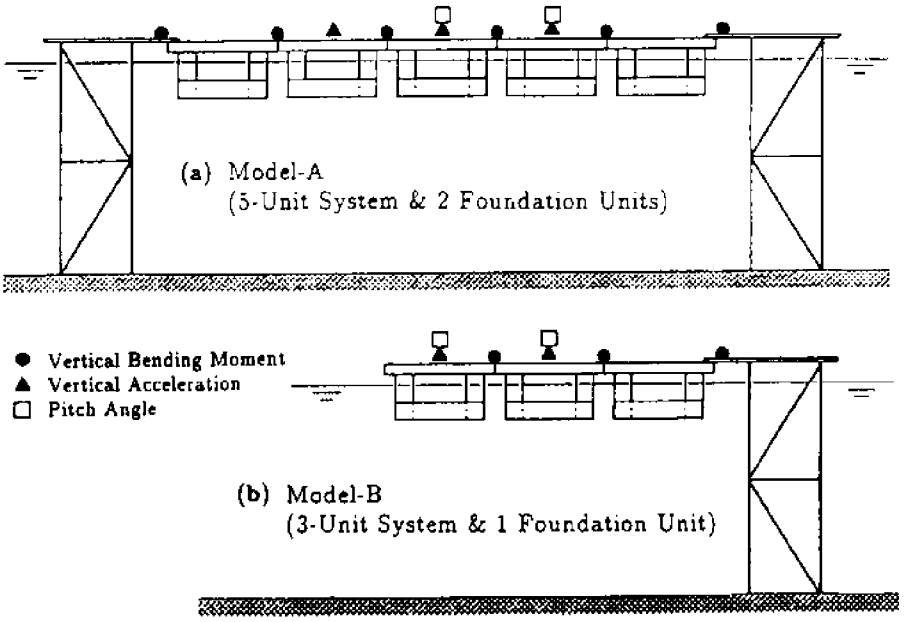

Figure 5. Multi-unit models for the test of dynamic responses in waves

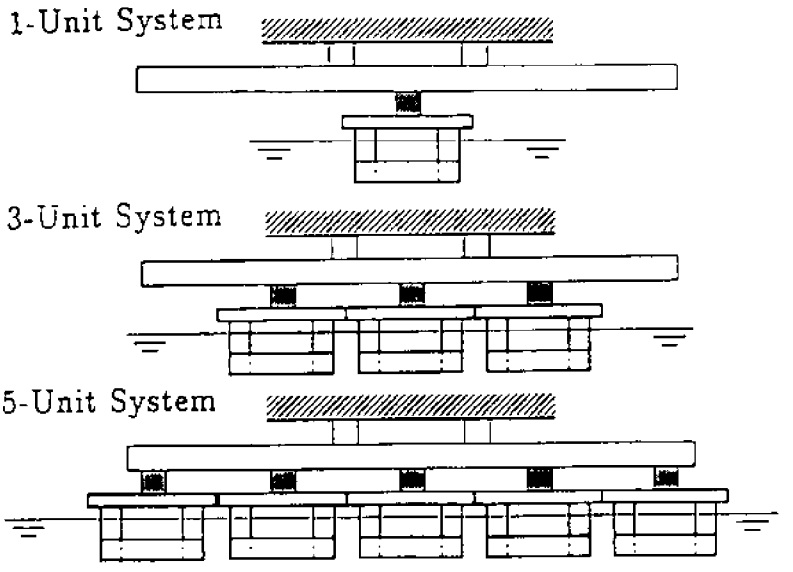

Figure 6. Models for the test of wave exciting forces

Wave Exciting Force Measurement

In order to evaluate the hydrodynamic interactions clearly, we conducted the measurement of wave exciting forces in waves. In the test, one-, three-, and five-unit systems were fixed in waves as shown in Figure 6. Wave exciting forces acting on each unit were measured separately by each load cells. (The units were not connected to each other on their decks.) Wave directions were varied as 0, 45, and 90 degrees. Wave frequency (ω) was also varied from 3 to 10 (rad/s) in regular and transient wave tests. Surge, sway, and heave exciting forces were mainly measured.

Dynamic Response Measurement

In the dynamic motion and structural response tests, two multi-unit structural models, A and B mentioned above, were used. Measurements were carried out on structural bending moments acting on connections between units, vertical acceleration and pitch angle of each unit motion in waves. Measuring points are indicated by symbols in Figure 5. Connections between units were modeled by aluminum plates and the elasticity of model structures was simulated to that of the assumed offshore city. Supposing that floating units are connected on their upper structure decks by welding, we assumed the depth of deck, the breadth of deck, and the thickness of deck plate were 8 m, 60.8 m, and 23 mm, respectively. Other structural members, such as stiffeners and girders were neglected.

THEORETICAL CALCULATION METHOD

For the comparison between experimental results and theoretical predictions, a numerical calculation method including three-dimensional hydrodynamic interaction among multiple floating bodies are adopted. This calculation method was developed by Goo, et al. (1989, 1990) combining the three-dimensional source distribution method and interaction theory proposed by Kegemoto & Yue (1986, 1987). This method can be used for predicting wave exciting forces and motions of multiple floating bodies of arbitrary shape, and also for predicting elastic structural responses of huge offshore structures supported by a number of floating bodies in waves.

The calculation program is based on a combination of the three-dimensional source distribution method, the wave interaction theory for hydrodynamic forces, and the finite element method for structural analysis of a linear elastic framed structure. Using this program, it is unnecessary to perform full diffraction or radiation computations which are usually time consuming for multiple three-dimensional floating bodies. Furthermore, dynamic structural responses of multi-unit floating structures can be calculated simultaneously.

For more details about theoretical background and calculation method of three-dimensional hydrodynamic interactions, refer to the previous paper by Goo, et al. (1990).

TEST RESULTS AND DISCUSSION

Wave Exciting Forces

Figure 7 shows the results of wave exciting forces acting on one unit. The unit is isolated, so there is no interaction between floating bodies. The abscissa is circular wave frequency (ω) in model scale, and the ordinate is heave and surge exciting forces per unit wave amplitude. Experimental results are shown by circles and theoretical calculation results by the three-dimensional source distribution method are shown by dotted lines. The agreement is very good and this assures the basic accuracy of our program on the estimation of wave exciting forces.

Figure 8 shows the wave exciting forces acting on the three-unit system in wave direction 0°. Experimental results of heave and surge exciting forces acting on each individual unit are shown by triangles. Because there are multiple bodies, hydrodynamic interaction among the units occurs, and wave exciting forces are very much influenced by it and fluctuate. In Figure 8, two kinds of calculation results are plotted by curves. One is the calculation which does not account hydrodynamic interaction (shown by dotted lines), and the other is the one which takes hydrodynamic interaction into account (shown by solid lines) based on the theory stated in the previous section.

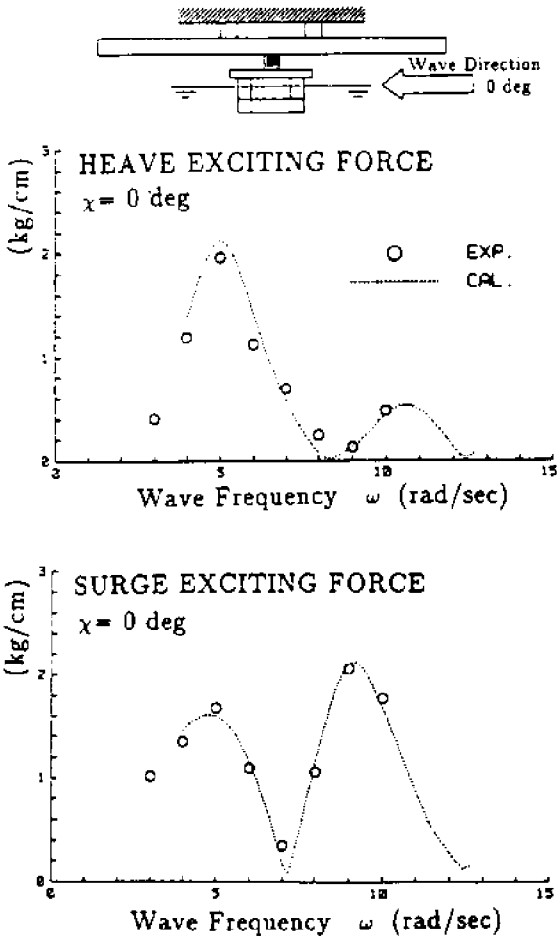

Figure 7. Wave exciting forces (one-unit, wave direction = 0°)

Looking at the graphs on the right hand side, it can be said that the calculations with interaction (solid lines) estimate experimental results very well. For the other two units, positioned in the down-stream of waves, the fluctuation is getting soft and calculation results, more or less, overestimate the experimental results. This might be caused by wave energy dissipation. As the wave direction is 0°(parallel to the line-up of multiple bodies), wave height might be decreasing along the wave propagation, due to the viscosity effect. In Figure 9, exciting forces at wave direction of 45° are shown. Because the wave incident angle is oblique, there are expected less energy dissipation. In this case, theoretical estimations agree well even for the units in down-stream of waves.

Concerning the results of five-unit system, only the case for wave direction = 0° is shown in Figure 10. As can be seen from this figure, in comparison with Figure 8, the

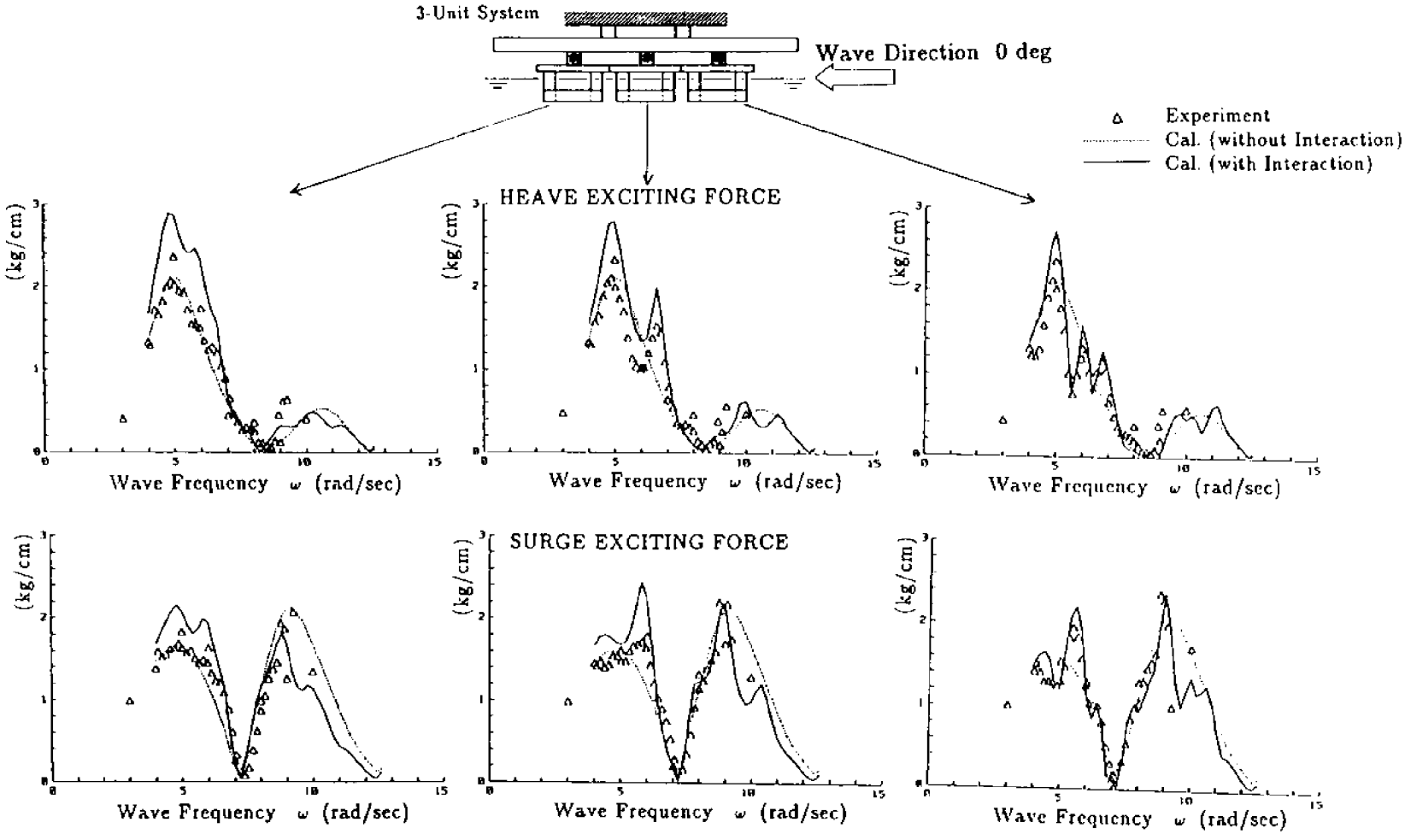

Figure 8. Wave exciting forces (three-unit system, wave direction = 0°)

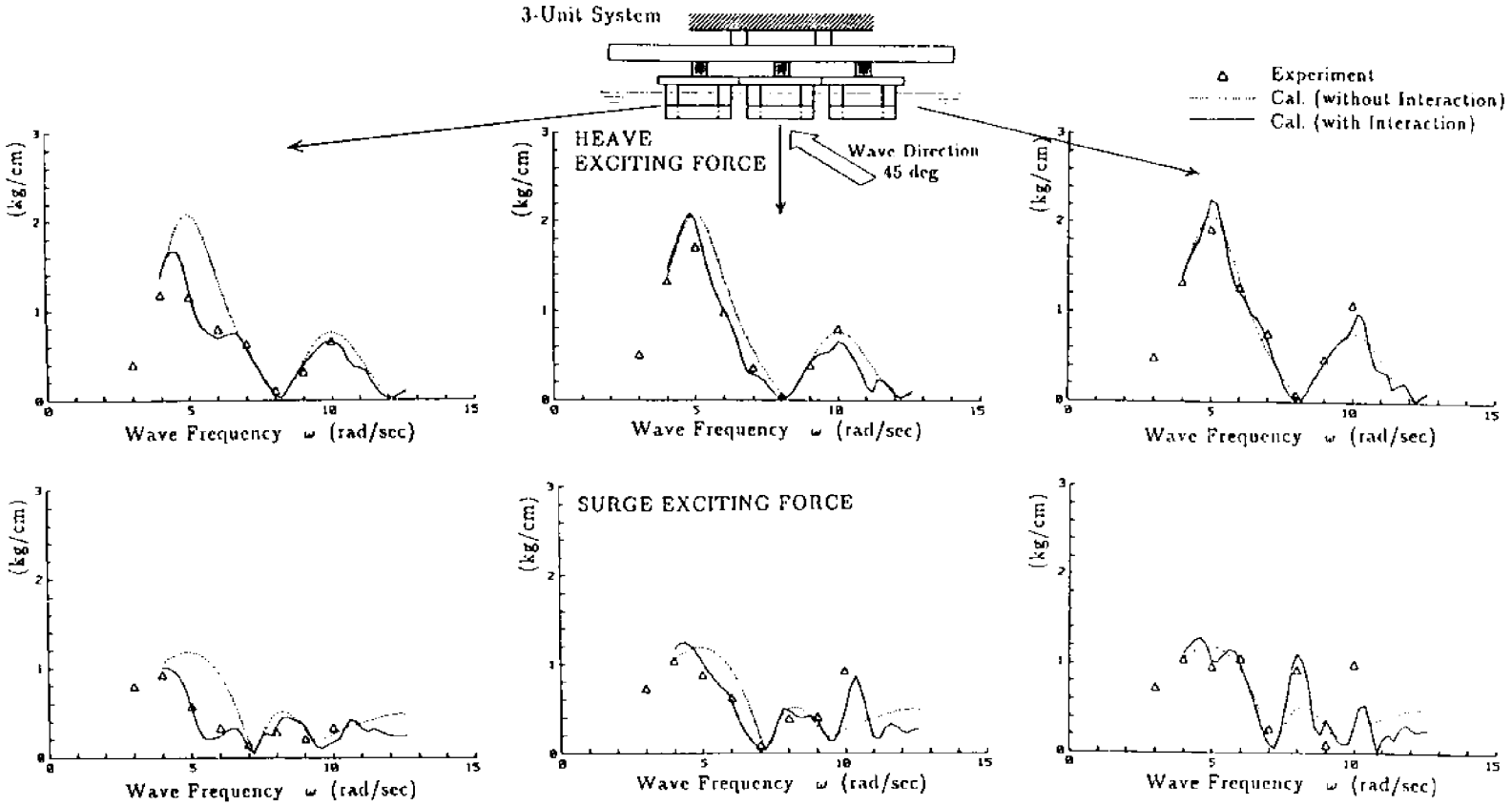

Figure 9. Wave exciting forces (three-unit system, wave direction = 45°)

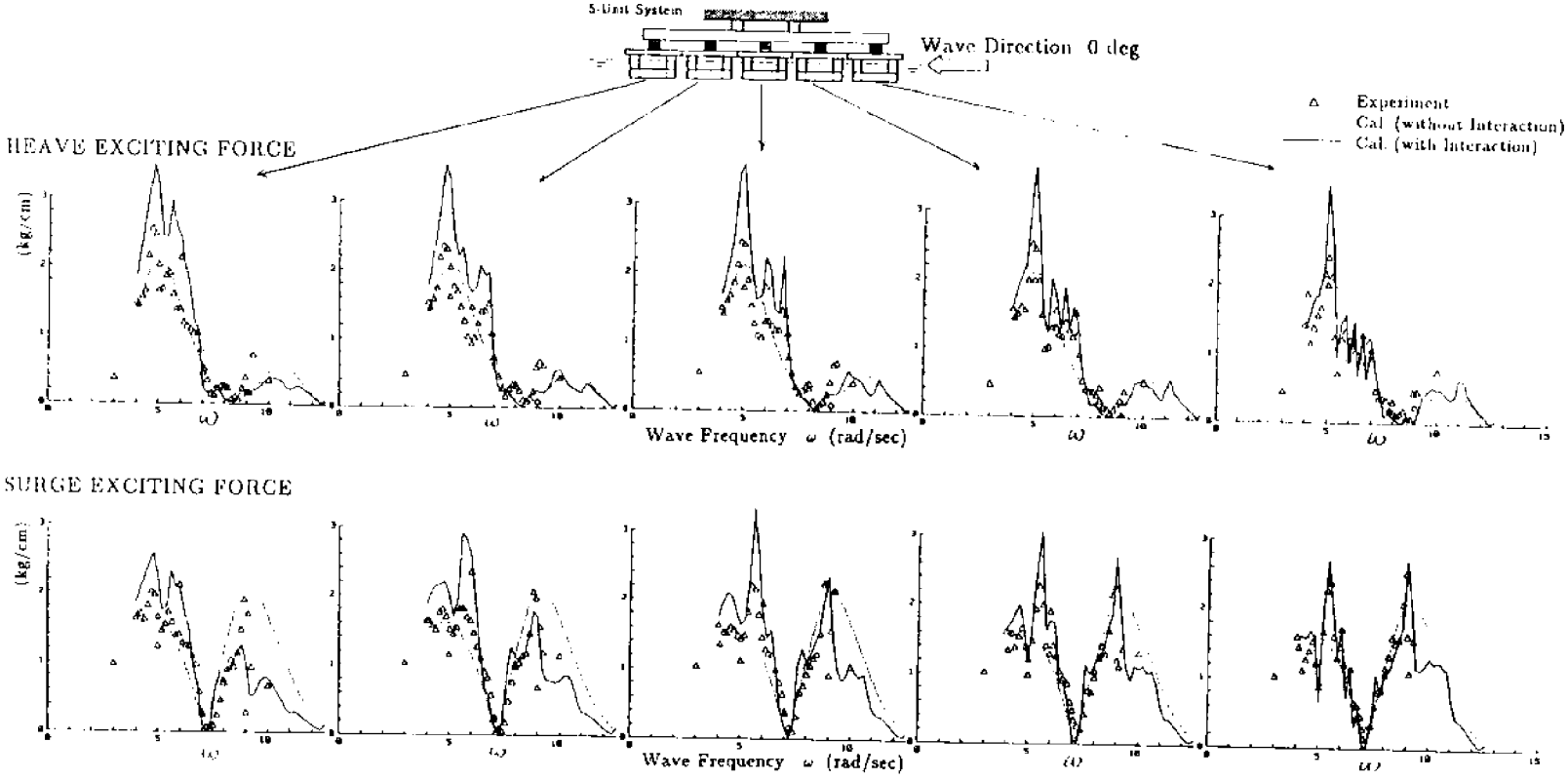

Figure 10. Wave exciting forces (five-unit system, wave direction = 0°)

more units there exist, the stronger the fluctuation is. Interaction effect is considerably strong on the experimental results and both of heave and surge forces fluctuate so much. Calculated solid lines, in spite of that, coincide pretty well with those fluctuating experimental results. As in the case of the three-unit system, calculations are generally overestimating for the following units along wave propagation. However, this is caused by the same reason mentioned above, and in oblique and beam wave conditions, estimations are successful.

Dynamic Motion and Structural Response

Figures 11 and 12 show some results of dynamic responses in waves about structural model A, which consists of five floating units and two foundation units. In Figure 11, vertical bending moments acting on each connection between units are shown for wave directions of 0°, 45°, and 90°. Although measurements were made on all connection points, only three points are shown in Figure 11 due to space limitation. Experimental results are plotted by circles and estimated structural responses are shown by dotted and solid lines. In the estimation of structural responses, the multiple floating units were modeled by a linear elastic framed structure, and the stiffness of connections was determined by static deformation tests of the model experimentally.

The solid lines indicate calculated results including interaction effects, and the dotted lines indicate neglecting ones considering only phase differences of wave exciting forces. Experimental results show considerably low bending moments in head (0°) and oblique (45°) waves. In beam sea condition (90°), however, large bending moments were observed at around natural frequency of the structure ($\omega = 4.7$ rad/s). Because the floating units line up straight, wave exciting forces in beam sea condition act on each unit simultaneously. This causes a resonance of the structural system, and it can be said that the beam sea condition is undesirable from the view point of structural responses.

Both estimated curves, including or neglecting interaction effect, generally agree well with experimental results. But around the resonance, the calculation results somewhat overestimate experimental results. The reason for this could be the estimation error of hydrodynamic and structural damping coefficients.

Figure 12 shows vertical accelerations measured on three central units. In head and oblique wave conditions (0 and 45 degrees), the acceleration responses are negligible even at center unit. In beam wave condition (90 degrees), however, due to the resonance of structural responses, vertical acceleration amplitudes are also considerable. Theoretical estimations are fairly well except at around resonance frequency. On the results of pitch motion responses of units, the similar comment can be said as above.

Figure 13 shows an example of dynamic structural responses about model B, which consists of three floating units and one foundation unit. Vertical bending moments acting on each connection are slightly higher than those of model A. Vertical acceleration and pitch angle responses are not shown in figures, but they are more significant comparing with those of model A. The theoretical predictions are also satisfactory about model B except for very low frequencies.

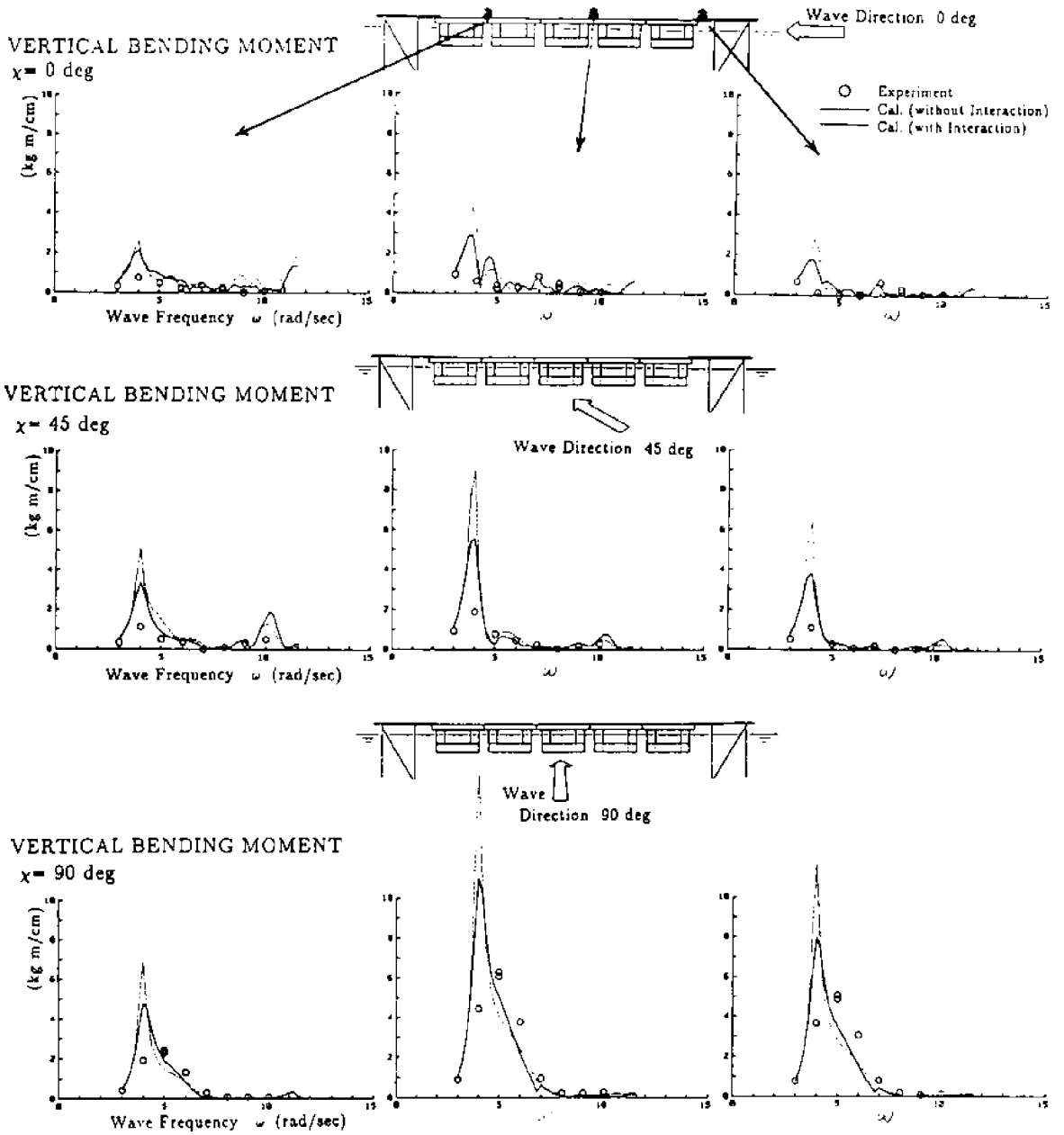

Figure 11. Dynamic responses in waves (Model A, vertical bending moment)

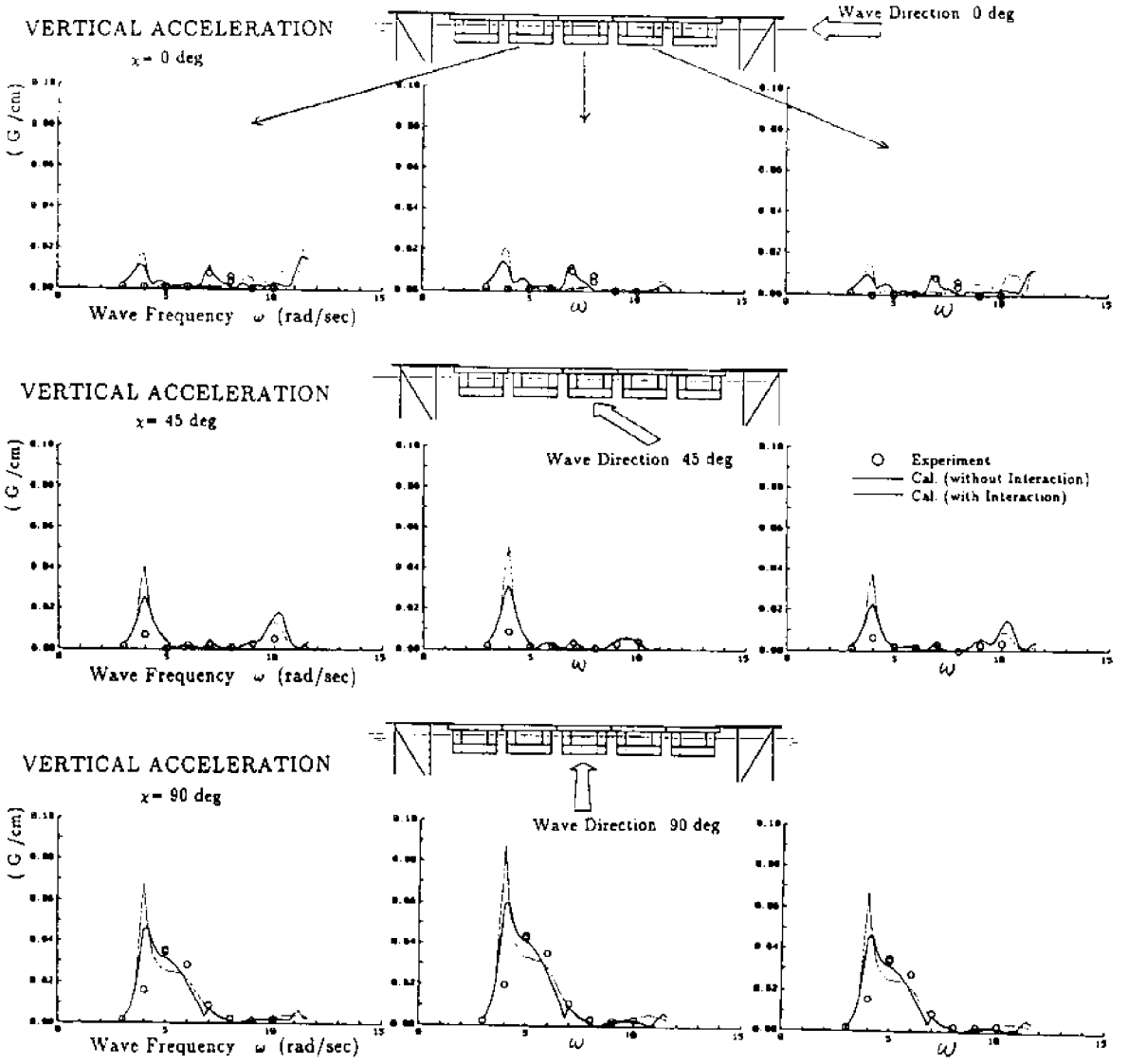

Figure 12. Dynamic responses in waves (Model A, vertical acceleration)

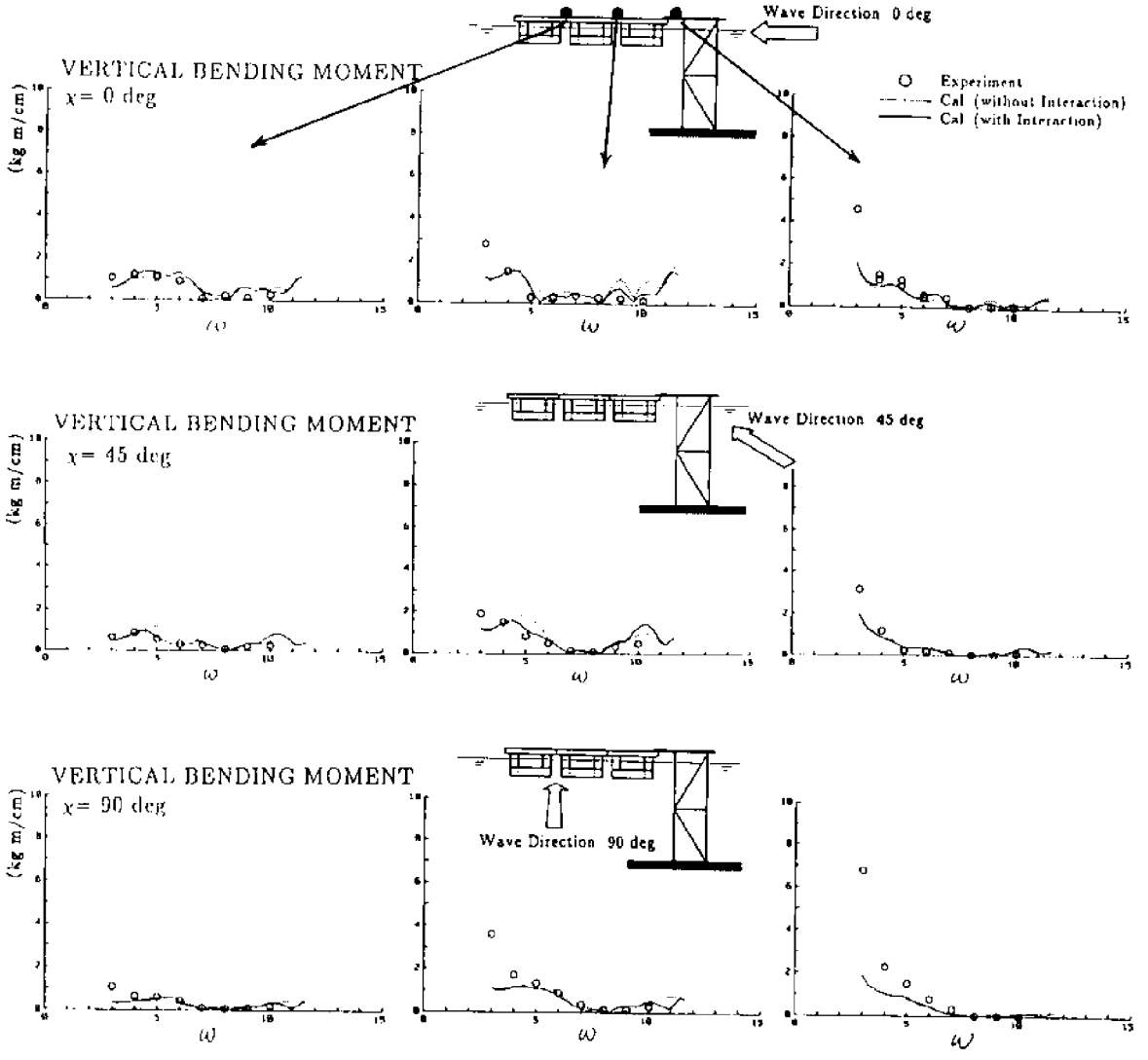

Figure 13. Dynamic responses in waves (Model B, vertical bending moment)

CONCLUSION

We have investigated the wave exciting forces and dynamic responses of offshore floating structures composed of multiple floating bodies and foundation units. As the results of experimental study and comparison with theoretical calculations, we have obtained the following conclusions:

(1) Hydrodynamic interactions significantly affect wave exciting forces acting on multiple floating bodies.

(2) The theoretical calculation method can estimate wave exciting forces accurately in linear range including the interaction effect.

(3) Wave exciting forces acting on the units downstream of waves are reduced by wave energy dissipation along wave propagation; the theoretical method slightly overestimates them.

(4) Dynamic motion and structural responses of multi-unit systems with foundation units can be estimated well using the proposed theoretical calculation method.

REFERENCES

Goo, J.S., and K. Yoshida. 1989. Hydrodynamic interaction between multiple three-dimensional bodies of arbitrary shape in waves. *Journal of the Society of Naval Architects of Japan*. **165**.

Goo, J.S., and K. Yoshida. 1990. A numerical method for huge semi-submersible responses in waves. *SNAME Transactions*. **98**.

Kegemoto, H., and D.K.P. Yue. 1986. Interactions among multiple three dimensional bodies in water waves. *Journal of Fluid Mechanics*. **166**.

Kegemoto, H., and D.K.P. Yue. 1987. Wave-induced motions of multiple floating bodies. *Journal of Society of Naval Architects of Japan*. **161**.

Yoshida, K., S. Tsuchiyama, N. Nakamura, et al. 1990. Comprehensive offshore city. In: Proc. 4th Pacific Congress on Marine Science and Technology (PACON '90).

THE EFFECT OF HUMAN TRAMPLING ON BIODIVERSITY OF ROCKY SHORES: MONITORING AND MANAGEMENT STRATEGIES

Deborah M. Brosnan
Lewis and Clark College
Portland, Oregon, U.S.A.

ABSTRACT

Rocky shore communities are coming under increasing pressure from human trampling. I carried out experiments on two rocky shores in Oregon, U.S.A., and found that trampling significantly changes community structure. Foliose algae and mussels are dislodged by trampling. Algal turf is resistant to trampling and dominates heavily trampled shores. Based on results from these experiments, I devised a monitoring and management plan for Oregon's rocky shores. This plan includes monitoring for trampling damage, using the indicator species concept; foliose algae, algal turf and mussels are proposed as indicators of trampling damage. Recovery and protection of heavily used shores can be achieved by rotating visitors within or between shores, and by setting up designated pathways. Increased education and public awareness play an important role in shore protection. On-site aquaria, volunteer groups to lead guided walks, and circulation of education information are suggested as potential ways of achieving this goal.

INTRODUCTION

Rocky shores are important recreational and educational resources. Worldwide, these areas are coming under increasing pressure, and human impact on rocky shores is becoming a major concern. Trampling and harvesting have major effects on marine intertidal organisms, and this trend is likely to increase as tourism and population growth bring more and more visitors to the shore.

To encourage and manage the use of marine resources, many nations have designated marine parks, gardens and wilderness areas. Typically, these are areas of high biodiversity where harvesting is prohibited. A designated reserve in a biologically rich area is a prime attraction to visitors. Ironically, increased use degrades the very resource the reserve was set up to protect; this degradation is primarily due to trampling (e.g., Boalche, et al., 1974; Beauchamp and Gowing, 1982; Liddle and Kay, 1987; Kay and Liddle, 1989; Liddle, 1991; Povey and Keough, 1991; Brosnan and Crumrine, 1992). The recent surge in ecotourism will only exacerbate the problem. Several agencies and organizations have recognized the extent of human impact in preserves and called for urgent scientific research on the issue (for example, Liddle, 1991; Lubchenco, et al., 1991; United States National Park Service, 1992).

In this paper I report studies on human trampling impact on rocky shores in Oregon U.S.A. I address two issues: detection of human impact, and management strategies to deal with it. I first describe experimental studies carried out on two intertidal shores. The main questions of these studies were: what effect does human trampling have on marine intertidal communities, and how can we detect this impact? Are all species equally affected, or are there just a few susceptible species? We often hear

descriptions of how a habitat or ecosystem has been destroyed since it became popular with visitors, but the exact nature of the change is unknown. We need this information to detect human impact and to manage marine resources effectively.

In the second part of this paper, I present management options for managing marine intertidal areas based on results from the above studies. Although designed for Oregon shores, it can easily be adapted for marine intertidal and subtidal habitats worldwide. The management plan includes strategies for detecting and monitoring human impact, and ways to minimize damage to marine communities.

EXPERIMENTAL STUDY OF TRAMPLING ON MARINE COMMUNITIES

I studied the effect of human trampling on marine intertidal communities by conducting experiments at two sites in Oregon: Yaquina Head, a heavily visited site, and Little Whale Cove, a pristine site.

Yaquina Head is a state designated Outstanding Natural Area located 2 kilometers north of Newport, Oregon. The shore consists of flat basaltic benches, and boasts tidepools, marine mammals, and seabird nesting areas. It is a popular attraction for tourists, and school groups, with approximately 400,000 visitors every year (Bureau of Land Management, unpublished data). Our observations showed that visitors to Yaquina Head follow specific paths across the intertidal zone. These areas are subjected to extremely heavy trampling. Observations indicated that organisms are trampled about 155 times/hour on a normal spring day when about 145 visitors per hour visit the intertidal (Brosnan and Crumrine, 1992). On a busy day, the number of visitors on the shore may exceed 1,000 per hour, and trampling rates are likely to be higher on these days (Bureau of Land Management, pers comm).

At Yaquina Head, the inter-tidal community of the mid- and upper-shore is dominated (about 70% cover) by algal turf (*Endocladia muricata* and *Gelidium* sp.). Turf species are usually uncommon on local shores, and occupy less than 10% of space at pristine sites. By contrast, foliose algae, abundant elsewhere, are rare at Yaquina Head. Similarly, mussels are uncommon and mostly confined to crevices at Yaquina Head, although they dominate many other Oregon shores.

Little Whale Cove is located 12 km north of Newport and, like Yaquina Head, has a shoreline consisting of basaltic platforms. However, access to Little Whale Cove is restricted. It is necessary to cross private property to reach the shore from land, and heavy surf prevents access by boat. Consequently, Little Whale Cove is considered a pristine shore that is not subjected to significant human traffic. The upper-shore assemblage consists mainly of foliose algae (*Iridaea cornucopiae, Pelvetiopsis limitata,* and *Fucus distichus*), and barnacles (*Semibalanus glandula* and *Chthamalus dalli*). The mid-shore region is dominated by mussels (*Mytilus californianus*) and a few gooseneck barnacles (*Pollicipes polymerus*) which together cover almost 100% of the rock surface (for a complete community description, see Brosnan and Crumrine, 1992).

Experiments

Human Exclusion at Yaquina Head

I selected an area 8 meters wide and 15 meters long of one of the heavily-trampled paths. From March to September, 1991, this area was bisected by a barricade that isolated

the northern half but allowed human traffic to continue as usual along the southern half. At the end of September, I removed the barricade and humans were allowed to re-enter the area. I collected data on community composition by monitoring percent cover of algae and sessile invertebrates (individual species were identified). Data were collected monthly between March and September, and in November and December to monitor post exclusion changes.

Experimental Trampling at Little Whale Cove

A randomized block experiment was used to test the effect of trampling on the uppershore algal-barnacle assemblage, and the midshore mussel assemblage. I set up four blocks at each tidal height, with two treatments per block (trampled and untrampled). Algal-barnacle plots measured 20x20 centimeters, and mussel plots were 20 x 30 cm. I trampled each plot 250 times on one day every month, from March 1990 to March 1991, and collected data on algal and sessile invertebrate cover in each plot. Analysis was by ANOVA on transformed data (Sokal and Rohlf, 1981) (full details are given in Brosnan and Crumrine, 1992).

RESULTS

Human Exclusion at Yaquina Head

Results from the six month exclusion phase of the experiment were dramatic (Figure 1). In the human exclusion (non-trampled) plots, algal turf declined from a relative abundance of 31% at the start of the experiment, to 4.7% in August. At the same time foliose algae increased from 62 to 94.5 percent cover, due mainly to an increase in *I cordata*.which remained uncommon in the trampled plots. In the trampled plots, foliose algae were less abundant, and algal turf increased to 38% cover. When the barricades were removed, foliose algae declined rapidly in the previously untrampled plots. By December 1991, percent cover had fallen to 28%, and did not differ significantly from the trampled area (mean canopy cover of 24%). The decline in the untrampled areas was due almost entirely to loss of foliose algae, mainly *I. cordata*. In December, both trampled and previously untrampled areas were dominated by algal turf. Mussels did not recruit to the experimental areas during this period.

Experimental Trampling at Little Whale Cove

Algal-Barnacle Assemblage

Human trampling significantly reduced cover of foliose algae (Figure 2). Foliose species declined from 80% to 35% one month after trampling started. This decline continued, and foliose species remained low for the duration of the experiment. By contrast, canopy cover remained high in the untrampled controls, and showed only small scale natural seasonal fluctuations (Figure 2).

Mussel-Beds

Trampling had major effects on the mussel bed. Initial percent cover of mussels was 98% on trampled, and on untrampled plots. After three months of trampling, 40% of the mussels were lost from trampled plots. One year after the experiment started, 50% of the mussels were lost from trampled plots. Mussels were not dislodged from untrampled plots during the experiment.

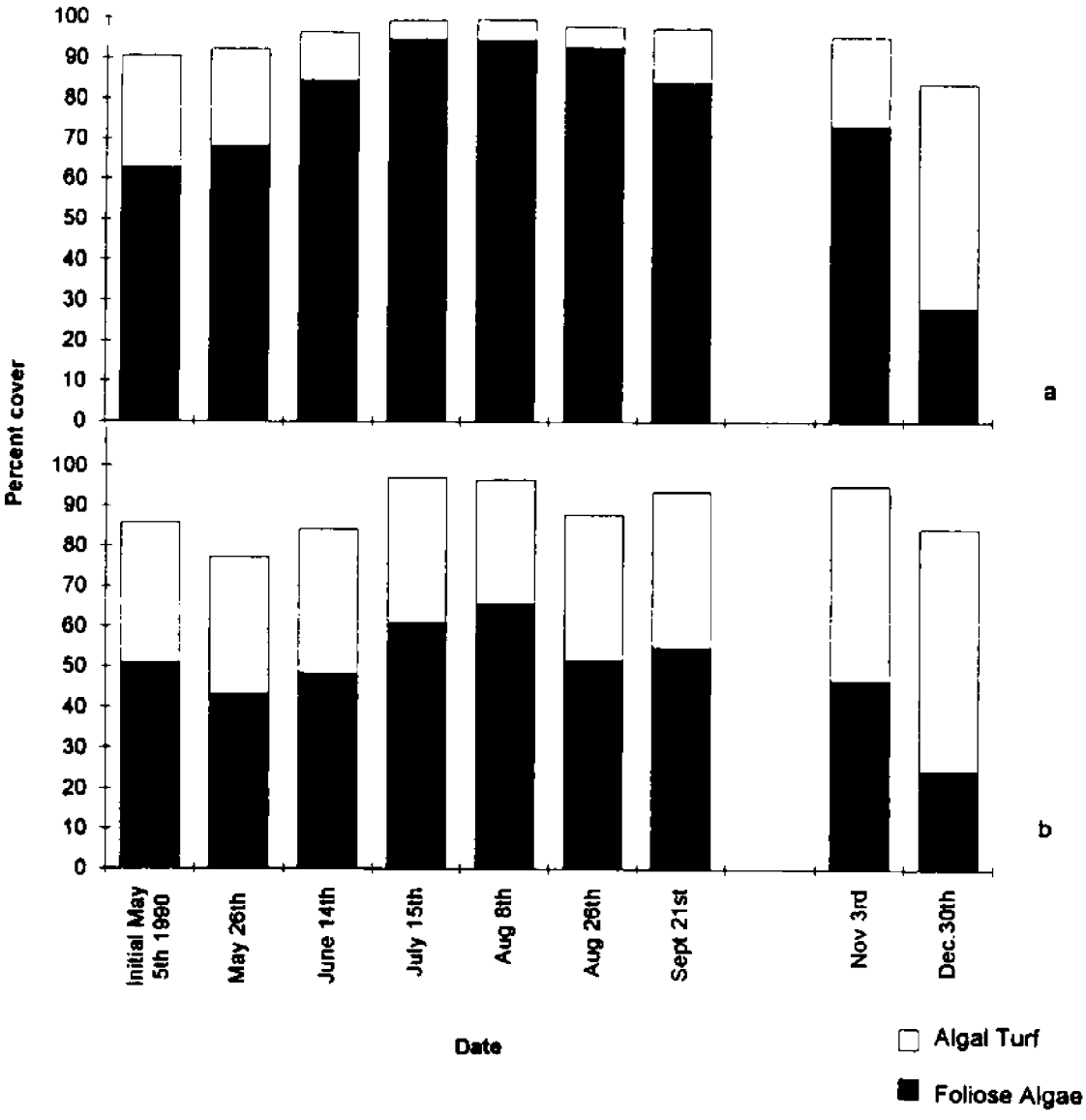

Figure 1. Relative abundance of foliose algae and algal turf at Yaquina Head. a. Exclusion area. Trampling was prevented from May to the end of September, and allowed to proceed as normal subsequently. b. Path area. Trampling continued as normal during both phases. There was no difference in algal cover between the areas at the start of the experiment. Percent cover of turf and foliose algae differed significantly between trampled and non-trampled areas from May 25th to September ($p<0.001$). By December, three months after trampling restarted, these differences had disappeared ($p>0.05$).

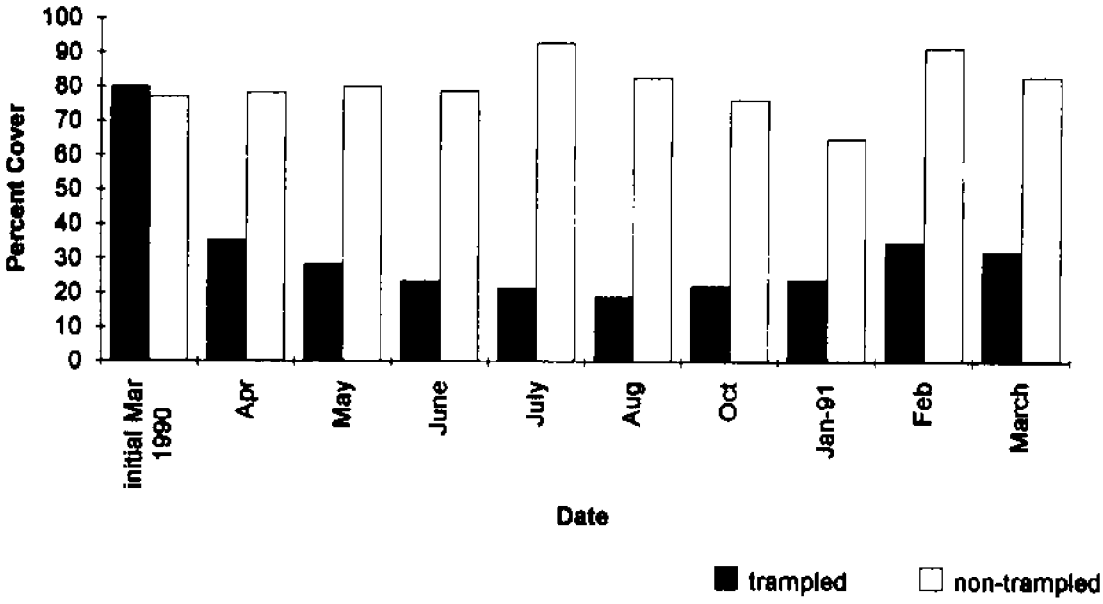

Figure 2. Effect of trampling on abundance of foliose algae at Little Whale Cove. Trampled plots were trampled 250 times per month, control plots were untrampled. Initial cover of foliose algae was the same in trampled and untrampled plots. After one month of trampling, trampled plots had significantly lower algal cover than untrampled plots ($F=95.62$ $p<0.001$), and this difference continued throughout the experiment ($p<0.01$).

Conclusions

Trampling significantly affects marine communities by dislodging organisms, or by weakening their attachment strengths so that they are removed by wave action. These effects can change the entire community profile of a shore. Rocky shores, which are normally dominated by algal-barnacle assemblages and mussel beds, become areas where low-lying algal turf predominates and mussels are uncommon.

MANAGEMENT STRATEGIES

Armed with our knowledge of the effects of trampling on marine communities, we can devise management strategies for these areas. Our goal is to minimize impact on communities, while at the same time maximizing recreational and educational use. I propose a management strategy that incorporates three techniques:

1. monitoring of human impact, including use of the indicator species concept as a monitoring tool;

2. recovery and protection of heavily used shores; and

3. educational approaches to minimize human impact.

Monitoring for Human Impact

Trampling can dramatically affect marine intertidal communities. However some species are more susceptible than others. This study showed that foliose algae and mussels are susceptible to trampling, whereas algal turf is resistant. Similar results have been found in studies on rocky shores elsewhere (for example: Boalche, et al., 1974; Beauchamp and Gowing, 1982; Povey and Keough, 1991). For example, Beauchamp and Gowing (1982) in California, found that a foliose alga, *Pelvetiopsis limitata*, was rare at a heavily trampled shore, but common in less trampled areas. In England, Boalche, et al. (1974), noted that the once dominant foliose alga *Ascophyllum nodosum* declined dramatically when visitors to the shore increased after a parking lot was constructed.

Trampling-resistant, or trampling-susceptible species may be used to evaluate human trampling impact by application of the **indicator species concept** (Brosnan and Crumrine, 1992). For example, Brosnan and Crumrine (1992) suggest that a heavily trampled shore is characterized by an absence of foliose algae (such as *Iridaea* and fucoid species), and an abundance of algal turf. Similarly, an abundance of foliose species in the upper-shore, and of mussels in the mid-shore indicates an undamaged ecosystem with little trampling The indicator species concept has wide scale applicability and has been successfully used in endangered tropical systems (Kremens, 1992; Courtney, pers. comm.). It has also been suggested as a tool for monitoring changes in communities due to global climate change (Lubchenco and Navarette, 1990).

The indicator species concept can work effectively to monitor trampling on rocky shores in Oregon. Managers can evaluate the extent of damage to the system by regular monitoring (monthly for the Oregon coast) of the abundance of foliose algae, algal turf, and mussels. Because only three groups of species are counted, the technique can be easily used by personnel with little training in species identification or ecology. I have successfully used this concept to train volunteers at two shores on the Oregon coast (Yaquina Head and Cannon Beach). Training takes less than a day. In Table 1, I outline how the concept can be used to make decisions regarding human impact and recovery plans.

The indicator species concept has the potential for wide scale application. Related species and functional groups are common to many communities around the world (Stephenson and Stephenson, 1972). Even when functional groups are not equivalent between geographic regions, the indicator species concept may still be a useful tool for detecting human impact. For example, coral reef and intertidal reef flats are subject to intense human impact (Liddle, 1991). Reef walking has similar effects to intertidal trampling. In reef-flat communities, branching corals, particularly *Acropora*, are most severely affected by reef walkers (Liddle, 1991); by comparison unbranched dense forms, e.g., *Porites*, are less susceptible.

Recovery and Protection of Marine Communities

If an intertidal community is determined to be damaged by trampling, managers may wish to protect the community from further damage and to restore it to its former condition. There are a number of possible options, including: rotation within and between shores, designated pathways, and increasing the role of education and public awareness in shore management.

Table 1. A monitoring strategy for Oregon's rocky shores using the indicator species concept. Monthly monitoring of the abundances of the three indicator groups (foliose algae, algal turf and mussels) can be used to estimate human impact on rocky shores, and to decide on management action. Ideally monitoring should be carried out on trampled areas and on non-trampled control areas close by.

Indicator Species	If abundant	If rare
Foliose Algae	no significant tampling impact. Continue normal monitoring	indicates heavy trampling. Initiate recovery strategy
Algal Tuff	this indicates heavy trampling. Initiate recovery plan	no significant trampling. Continue normal monitoring
Mussels	and found in large multi-layer beds on all flat surfaces, this indicates no significant trampling Continue normal monitoring	especially if confined to crevices and depressions in rocks, this indicates heavy trampling Initiate recovery plan

For large shores, such as Yaquina Head, it is feasible to encourage use of just part of a shoreline. This can be achieved by limiting access to other areas that are under protection. For example, at Yaquina Head, Brosnan and Crumrine (1992) suggested that the shore be divided into four main sections, and that one of the sections be closed off for a recovery period of 3 months to several years. There are several advantages to this strategy. Only a relatively small part of the shore is closed at any one time, and visitors are less likely to cross into an exclusion area if it is only a small fraction of the total shore (pers. obs.). The recovery area may also act as a source of recruits for trampled areas.

Management of each site is important; however, a larger scale, regional approach to protection of intertidal areas is preferred. For example, at least five other high biodiversity sites are located within 50 km of Yaquina Head. A regional manager can encourage use of one or two sites each year, and of alternative sites in the following years. This can be achieved by signs, and by advertising strategies that direct visitors to particular areas.

As a way of minimizing further damage to intertidal communities, pathways can be designated. These can be set up in pre-existing paths, that have already been created by trampling. Because of strong surf, it is not possible to put up boardwalks or other permanent structures in rocky intertidal areas. However small arrows, and signs providing information on species, can be set into the rock. This method has been successfully used in subtidal snorkeling trails (Rogers, Virgin Islands National Park, pers. comm.; and pers. obs.). Advantages to this approach are that signs encourage visitors to stay on pathways, provide information about the marine life, and are fairly unobtrusive. A disadvantage is that they require cleaning to remove fouling organisms.

Education and Increased Public Awareness as a Management Strategy

Ultimately, if human impact on shores is to be minimized, and shores effectively managed for human use, education and public awareness will play major roles. There are three main ways in which this can be achieved.

On-site Aquaria Touch-tanks and Display Tables

Brosnan and Crumrine (1992) successfully used this strategy at Yaquina Head, to inform visitors on ways of minimizing damage to marine intertidal life. In a survey of visitors, all found that the aquaria increased their awareness, and made them less likely to inadvertently damage marine organisms.

Enlisting Local Involvement

Local volunteer groups can play an important role in marine protection. At present, there are a number of these groups operating on rocky shores in Oregon. With little training, these groups can monitor the shore for damage, and lead guided walks on the shore for school and recreational groups.

Developing Educational Guides for Schools and Tourists

Many school groups use rocky shores in Oregon, to demonstrate marine life, biodiversity, and ecology. A few areas, particularly Yaquina Head, receive the brunt of these visitors. Often students arrive with no prior training in what to look for, or with no specific projects in mind. Pre-trip packages can be sent to schools, containing information on how to protect marine life, and projects that can be carried out during their visit. Adopting this strategy has the dual advantages of minimizing damage to marine communities and making the shore experience more worthwhile for students. A similar approach can be used with visitors, by providing brochures and information at shore access points. Brochures should include checklists and information on the biology and ecology of species present.

An ideal management strategy will integrate all these options into a single plan. For example, guided tours will reduce trampling on "recovery" parts of a shore much more effectively than will a barricade. Similarly, on-site aquaria will increase the opportunity to explain to visitors the rationale behind recovery and protection; this is much better than simply posting signs.

The management strategies discussed here were based on studies on Oregon's intertidal areas. However, they are relevant to other marine ecosystems, where human effects stress fragile communities. For example, all the options presented above are applicable to reef flat areas and subtidal coral reef sites.

ACKNOWLEDGEMENTS

Thanks to Steven Courtney for comments on this manuscript. I'm very grateful to his feet, and to Lana Crumrine's, Stacy Keizer's, and Evie Weitter's feet. Lana Crumrine helped with data collection and monitoring at both sites. Special thanks to Carl Halvorson for allowing me access to Little Whale Cove, and to Jan Auyong for inviting me to attend PACON.

REFERENCES

Boalche, G.T., N.A. Holme, N.A. Jephson, and J.M. Sidwell. 1974. A resurvey of Colemans intertidal traverse at Wembury, South Devon. *Jour. Mar. Biol. Ass. U.K.* **54**(551-553).

Beauchamp, K.A., and M.M. Gowing. 1982. A quantitative assessment of human trampling effects on a rocky intertidal community. *Marine Environmental Research.* **7**(279-293).

Brosnan, D.M,. and L.L. Crumrine. 1992. Human impact and a management plan for the shore at Yaquina Head Outstanding Natural Area. A report to the Bureau of Land Management, Salem OR

Kay, A.M., and M.J. Liddle. 1984. Tourist impact on reef corals. Report to the Great Barrier Reef Marine Park Authority, Townsville, Australia.

Kremens, C. 1992. Assessing the indicator properties of species assemblages for natural areas monitoring. *Ecological Applications.* **2** (203-217)

Liddle, M.J. 1991. Recreation ecology: Effects of trampling on plants and corals. *Trends in Ecology and Evolution.* **6** (13-16).

Liddle, M.J., and M.M. Kay. 1987. Resistance, survival and recovery of trampled corals on the Great Barrier Reef. *Biological Conservation.* **42** (1-18).

Lubchenco, J., and S. Navarette. 1990. Use of keystone species as indicators of global change (abstract) Conference on northern and southern hemisphere responses to global change. La Serena, Chile December 1990.

Lubchenco, J.L., A.M. Olson, L.B. Brubaker, S.R. Carpenter, M.M. Holland, S.P. Hubbell, S.A. Levin, J.A. McMahon, P.A. Matson, J.M. Melillo, H.A. Mooney, C.H. Peterson, H.R. Pulliam, L.A. Real, P.J. Regal, and P.G. Risser. 1991. The sustainable biosphere initative: an ecological research agenda. *Ecology.* **72** (371-412)

Povey, A and M.J. Keough. 1991. Effects of trampling on plant and animal populations on rocky shores. *Oikos.* **61** (355-368).

Sokal, R.R., and F.J. Rohlf. 1981. Biometry. W.H. Freeman and Company, USA.

Stephenson, T.A. and A. Stephenson. 1972. Life Between Tidemarks on Rocky Shores. San Francisco: W.H. Freeman.

United States National Park Service. 1992. A report on the status of U.S. National Parks. Washington D.C.

PUBLIC-PRIVATE RISK SHARING FOR SEAPORT INVESTMENT: WEST COAST COAL TERMINAL EXAMPLES

Willard Price
University of the Pacific
Stockton, California, U.S.A.

ABSTRACT

Seaports are public enterprises and, as such, are not viewed as business risk takers. In an attempt to understand public port strategic decisions this research examines the financial risk associated with capital investment. The role of private developers and their risk sharing with public ports is explored. Concepts of decision theory are introduced, followed by examples of west coast ports responding to a sudden, but false, demand for coal exports. The paper is intended to stimulate further research resulting from the coal experience. The research was originally supported by the Sea Grant Program, Hancock Institute for Marine Studies, at the University of Southern California.

INTRODUCTION

Seaports are, for the most part, public enterprises (Price, 1981). They are politically owned facilities governed by local governments, special districts and state governments in the United States. Their purposes can be debated, but most port owners view their objectives as follows:

a. Control uses of waterfront land within their jurisdiction

b. Provide opportunities for maritime cargo movements (imports and exports)

c. Develop other water related operations such as fishing, recreation, ship repair, passenger ships and marinas

d. Stimulate economic activity and jobs within their region

e. Provide financial independence by ensuring that revenues exceed costs.

Yet seaports, like other public infrastructure, are capital intensive. They require significant financial investment in facilities before operations can be conducted. Therefore, critical decisions on capital investment should be publicly deliberated before funds are committed and financial uncertainty is faced. As public agencies an important policy issue is whether seaports should be engaged in investments where risk exists for financial losses.

Public seaports are "owned" by the constituents of the particular political jurisdiction, be it a city, special district or larger government at the state or federal level. As owners, these citizens are not often aware of their ownership status and may not feel they have any ability to influence investment decisions and, especially, may not be willing to risk increased general taxation to cover port losses from bad investment decisions. Port investments do not normally require the citizen-owner to make an actual financial

commitment, except when financial performance requires that they provide a direct subsidy for seaports through general tax support for survival and success.

This research is not primarily focused on the policy question of subsidizing seaports, but rather the principal concern of the paper is

1. the financial risk occurring in facility development at these public agencies and

2. how port managers address risk in investment decisions, including sharing risk with private operators

SEAPORT INFRASTRUCTURE NEEDS AND CAPITAL INVESTMENT STRATEGIES

The infrastructure needs of seaports occur both on and off port property. Within their boundaries, ports must dredge ship channels, build seawalls and piers, acquire cranes and other loading equipment, construct terminal storage facilities, provide rail tracks and truck roadways, in addition to necessary utility systems. Outside the boundaries they must ensure adequate connections to highway systems and railroad switching yards and cargo transfer facilities. In essence, ports need to create substantial public works with inevitable congestion and environmental effects on neighboring communities, the travelling public as well as other commercial activities.

This significant infrastructure does not come cheap and the source of such large capital expenditures is not obvious or easy to acquire. Like many other public works systems ports do not, in most cases, generate sufficient excess revenue or establish asset management accounts that make new construction or renovation/repair activities directly fundable.

Ports often depend on outside investors to provide the huge capital requirements. Those investors may well be higher levels of government providing grants or loans. In the U.S., federal transportation and water resource programs have been willing to offer extensive assistance for construction of connecting systems off the port property. The federal government has been far less involved with piers and terminals at seaports, to a much lesser extent than they have been willing to support airports. The main governmental contributors have been the Army Corps of Engineers for dredging channels and the Commerce Department for capital projects generating employment. Importantly, these sources of grants have been getting scarce with federal retrenchment.

Seaport enterprises, therefore, are increasingly self-sufficient for both capital and operating expenses. Ports are unique in America, for they receive less subsidy than other public works yet they are normally content with the resulting burden to raise capital without governmental grants. In the past ports used debt more easily -- interest rates were low and debt capacity was not exceeded. More affluent ports often retained net income for specific investments and no one questioned port financing loans.

But the risk avoiding strategy for seaports has relied on the willingness of private capital to flow to the waterfront. The port industry has for some time debated whether they should be "landlord ports", leasing land to facility operators or whether they should be "operating ports", conducting pierside cargo movements with their own personnel and supervision. Each port commission must set policy on its landlord or operating status, but in the landlord model it is necessary for large private contributors to be able and willing to provide investment for facilities and infrastructure. The implications of their

private role in port investment is that the public owners will be "taken off the hook" in terms of risk that they might be required to undertake by using retained earnings or floating revenue bonds for capital needs.

As public agencies and landlord ports, these public managers can or ought to be avoiding risk for the port owner. If the port institutions demonstrated an interest in taking financial risk and expecting a meaningful return, they would be practicing a different strategy than commonly experienced the public sector. Instead it is assumed the traditional "concept of risk avoidance" is the expected behavior of public managers and the preferred strategy of port owners.

THE DEVELOPMENT DECISION PROCESS AND RISK

One valuable aspect of the decision process for seaport infrastructure development is the long deliberate process involved in these significant financial choices (Dowd and Jonson, 1991). As a result there are several stages along the way where port management is faced with a "go-no go" decision, where risk to the owners can be recognized and analyzed. At each stage development projects can be continued or abandoned as risk levels are examined and found acceptable or unacceptable.

The earlier stages require less sunk costs and involve less financial losses when projects are rejected. Naturally the most critical stage is the commitment to construction, where demand weakness can create huge financial burdens for port investors. With alternative uses and revenues considered, investors are obliged to determine the risk associated with cargo revenues and make rational decisions.

The life cycle of development decisions can be modelled as follows, focusing on the logical stages and the critical decisions along the way (Figure 1).

As decision makers proceed on the development path, potential losses mount so the quality of the analysis becomes increasingly important. Decision makers must face the uncertainty and risk present in revenue and cost projections and, as long as they avoid the large expenditure of construction, they keep the danger low. But throughout this process two features haunt the capital development process:

1. How do decision makers measure uncertainty and risk; do they have confidence in their knowledge of the probabilities associated with demand and revenues particularly?

2. Do they fully inform port leadership and constituent-owners of their knowledge of risk; do they conduct worst case scenarios in the event they lack confidence in forecasts as major capital investments are decided?

There is no doubt this view is pessimistic, seriously concerned about the downside risk of port development. Certainly some projects, maybe a high proportion of port developments, are blessed with near certain information on revenue-cost analysis and most managers do not hesitate to proceed. But it is precisely the times when ports face real uncertainty, where they do not have confidence in the likelihood of demand, that more sophisticated analysis is important. Difficult decisions in the face of uncertainty, or the lack of information, is also the most interesting aspect of the development decision process to observe and study.

Above all, this research assumes it is preferable to minimize public sector risk, to ensure public port owners do have their taxes at risk. This distinction between the public and private sectors regarding risk tolerance in the port industry is itself an important hypothesis deserving testing.

Stage	DESCRIPTION	CRITICAL DECISIONS
Planning	1. Consider new services and/or facilities and conduct preliminary market estimates of cargo movements.	
	2. Prepare an initial engineering plan and cost estimate, with a preliminary financial cash flow.	PRELIMINARY ANALYSIS
Design	3. Complete detailed engineering and environmental plans, including a comprehensive financial analysis and market forecast.	TECHNICAL ANALYSIS
	4. Obtain all environmental approvals and permits, revise plans and financial analysis as needed.	FINAL ANALYSIS
Construction	5. Conduct construction and testing of facilities & equipment, accept work from contractors/suppliers.	
Implementation	6. Implement facility operation, comparing actual performance with plan expectations.	
	7. Revise or update facilities and cargo uses to respond to changing market conditions.	REVISION ANALYSIS
Maintenance	8. Rehabilitate or reconstruct facilities as needed for optimal maintenance strategy.	MAINTENANCE ANALYSIS
	9. Shut down facility, sell off equipment or facilities and reuse land.	TERMINATION ANALYSIS

Figure 1. Model of the life cycle of development decisions

General Concepts of Risk

Risk can be conceptualized across an uncertainty-risk-certainty continuum (Overstone, 1990; Turban and Meridith, 1991). Uncertainty involves little knowledge about the likelihood of outcomes. Risk suggests historical knowledge about the frequency or probability distribution of several outcomes for a particular variable. Certainty is achieved when a single outcome is known with confidence. Since certainty is difficult to attain, a further analytical method, Bayesian Analysis, seeks expert information which can improve upon our decision under risk by providing insights on the actual outcome expected during the next period.

A hypothetical, but conceptually powerful example of risk analysis is presented. As a model for coping with uncertainty and risk, it provides a guide to seaport investment decisions and a framework for further research.

Example of a Port Decision under Uncertainty and Risk

Port Decision - Alternative Fee Methods

Cargo Outcomes	Fee/ton	Fixed Lease	Min-Max Lease
High Volume	$2000	600	1200
Mod. Volume	600	600	540
Low Volume	60	600	300

(Present value net pay off values to the port, $000)

1. With UNCERTAINTY and no additional information or cargo outcomes use these rules:

   a) Risk Avoidance - choose Maximum of Minimum payoffs of each decision. This ensures the best payoff given the worst outcome.

   [60, 600, 300] - use Fixed Lease at $600

   b) Equal Likelihood of each outcome - given no better information is available. Calculate expected payoff.

   Average payoff [887, 600, 680] - use Fee/Ton at $877

2. With RISK, prior information on historical probabilities is known say High = .25, Moderate = .20, Low - .55

   Expected [653, 600, 573] - use Fee/Ton at $653 Payoff

   NOTE: Even with fairly pessimistic probabilities, where over 50% of the time we would only receive $60,000 per year, the decision rule tells us to take a chance on the $2,000,000 payoff of the Fee/Ton alternative. Do ports get enticed with these bigger payoffs and neglect downside risk?

THE WEST COAST COAL FRENZY OF THE EARLY 1980s

Ten years ago, west coast ports went on a coal development frenzy. Responding to predictions of large increases in coal movements through west cost ports, destined for Pacific Rim nations shifting energy generation to coal, 26 ports began the process of considering new coal facility development (Figure 2). Below there was no dearth of ports seeking to capture the gold of coal revenues (Tumulty, 1982). Yet even by 1982 the massive coal movements predicted were beginning to wane, indicating that currently planned facility expansions at Long Beach, Los Angeles and Stockton were likely sufficient to serve expected demand through much of the 1980s (Price, 1982).

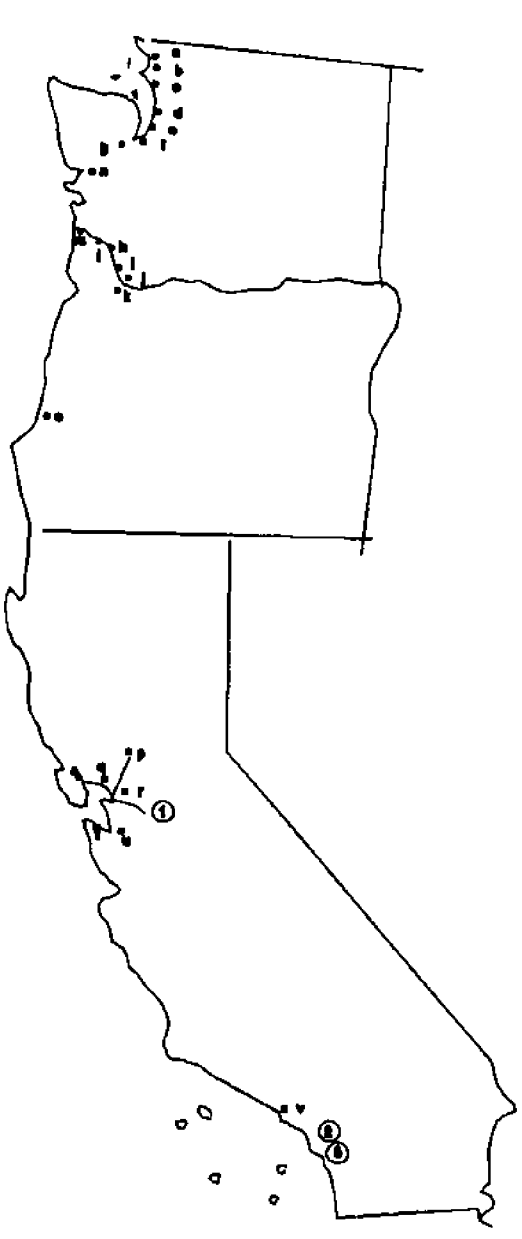

PORTS THAT EXPORT COAL

① Stockton
⑧ Los Angeles
⑨ Long Beach

PORTS PLANNING COAL TERMINALS

PUGET SOUND
a Bellingham
b Anacortes
c Tulalip
d Everett
e Tacoma
f West Tacoma
g Dupont

COLUMBIA RIVER
h Longview
i Kalama
j Vancouver
k Portalnd
l Astoria
m Warrenton

NORTHWEST COAST
n Grays Harbor
o Coos Bay

BAY/RIVERS
p Sacramento
q Benicia
r Selby
s Richmond
t San Francisco
u Redwood City

SOUTH COAST
v Port Hueneme

ALASKA
Seward

BRITISH COLUMBIA
Vancouver

PATRICK LYNCH / Los Angeles Times

Figure 2. Proposed coal terminals - West Coast Ports 1982

Therefore, as rationality would suggest, most of the ports abandoned plans for new facilities early in the development process. This occurred not only because demand was weakening but because the 26 ports were essentially in competition with each other for a market that only a few of them could serve even with the early optimistic forecasts. None the less, 3 ports did proceed further with new modern coal terminals in an attempt to serve the coal export market. Ports at Stockton, California, Portland, Oregon and Vancouver, British Columbia (BC) moved to the construction stage even with substantial uncertainty regarding the need for coal abroad. The discussion below will focus on Stockton and Portland because current retrospective information on the 10 year history was available. Further research will be needed to examine the Vancouver, BC experience (Personal interviews; Felice, 1981).

Coal developments present a valuable opportunity to understand risk taking by seaport for three reasons:

1. Modern coal facilities require extensive land and facility expenditures, relying upon large circular rail tracks, rotary or bottom car dumpers and ship loading equipment.

2. Large risk existed for public ports or private developers because of capital requirements and the weakening forecasts for coal demand seen by 1982.

3. Actual collapse of predicted coal shipments through west coast seaports experienced during the 1982 - 1992 period.

The evidence presented here is anecdotal, based on conversations with port mangers who are familiar with the histories at Stockton and Portland. The research has not attempted to obtain information from the analyses conducted by each port along the development process or to determine the methods used in decisions to deal with uncertainty or risk. Much of this type of data is held closely by public ports or considered proprietary by private developers. But some initial suppositions will be made regarding decision making and financial risk in the final section on lessons learned.

THE PORT OF STOCKTON OPERATES A MODERN COAL TERMINAL

The Port of Stockton was in the coal business before the surge of coal enthusiasm in the 1980s. It was easier and quicker for the Port to plan a modernization of its coal facility and an increase in its capacity. They constructed a large circular rail track and a continuous bottom dumping capability which was the most impressive coal facility development on the west coast in 1982. In 1992 it is quite active and known as Dock 12/13, with 37 feet of water depth.

Choosing to shift financial risk to a private operators, the Port signed a 10 year contract with Metropolitan Stevedore of Wilmington, California in 1982, where Metropolitan was given land under a lease but developed all other facilities at their own cost. They maintain the new equipment themselves and pay rent to the port as well as a fee for each ton of cargo movement. The lease also required a minimum payment to the Port, regardless of the amount of cargo.

A development time line is shown for Stockton's development and operation over the last 10 years:

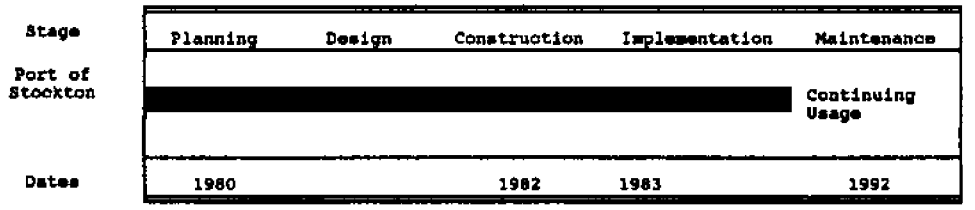

Stockton's Dock No 12/13, originally developed for the coal market, has not realized the cargo such a modern facility could serve. Instead Metropolitan and the Port have used these facilities to ship sulfur, clay, petroleum coke as well as limited coal movements to reap the maximum revenues for Metropolitan - as well as Port fees. While the Port of Stockton has not suffered financial losses under a lease arrangement which guaranteed minimum payments, the private operator has likely realized less income than forecast. But Metropolitan continues to operate the terminal and have just signed a new lease agreement with the Port. An ideal situation of public-private risk sharing is demonstrated here. The public port has minimized the danger to its financial health and the private operator has taken the risk of cargo weakness. If the low demand becomes unsustainable, the company would either renegotiate the lease (if the port were willing) or abandon the site. Of course, a renegotiated less or an under-utilized facility would shift some financial risk to the port until and unless they find other uses and revenues.

Overall, it appears both parties produced the best possible outcomes considering their respective roles. The Port was not exposed to substantial risk and has received expected revenues. The private developer has stretched the uses of the facility so as to reap moderate revenues and avoid financial disaster in the face of obvious risk undertaken.

THE PORT OF PORTLAND TERMINATES COAL FACILITY CONSTRUCTION

Portland's story is more complex and disappointing. Their coal proposal in 1981 was to develop a significant and model coal facility at the confluence of the Willamette and Columbia Rivers with 45 feet of water depth. Having good rail connections and proximity of 1000 miles to Colorado, Wyoming and Montana coal fields, Portland demonstrated the most willingness of any port to provide the capacity for large coal exports.

They selected a developer who commenced construction in 1981 under an amazing political consensus among business and environmental interests. The sagging Oregon economy no doubt influenced all parties to reach for the golden ring. But it was not clear by 1982 that the developer and terminal operator had any contracts for coal movements in hand (Price, 1982). Either because of the failure to secure coal shipment or because of a financial inadequacy by the developer (or investors), the Portland coal terminal was abandoned during construction. This action by a private developer was simply a prudent decision representing the risk of doing business. The Port could have picked up the pieces and sought another private developer without any additional cost to themselves. While the Port did contribute some infrastructure to the project, they were not directly investing in the sophisticated coal terminal facility; their risk was apparently minimal. But the Port of Portland was at risk more than it realized. When the construction project was terminated in progress, the complexity of the financial risk was unexpected and unplanned. No agreement was made between the Port and the developer on the financial responsibilities in the event construction was stopped. The development essentially was

bankrupt and unable to meet its existing obligations. In order for the Port to acquire the partially completed facility for other developers or alternative uses, Portland was saddled with massive liens of over $10 million to recover the land and partially completed facility.

Portland's development time line shows the abrupt stop to the development life cycle. No alternative development plan has been executed to date:

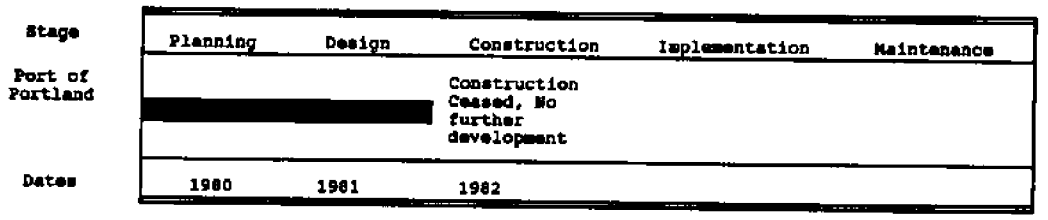

It must be concluded that Portland was placed in financial jeopardy because both the developer failed and because the Port was not protected against liability in their agreement with the developer. They took a risk at a time when the State of Oregon wanted their public agencies to stimulate economic activity Contrary to the situation in California, Portland is a state port and as such may be seen more as a risk taker. Regrettably, west coast exports of coal were, in essence, a very "risky" investment for public and private enterprises alike. If Portland had publicly debated the uncertainty, would its constituents have supported the development decision to proceed with construction? Could the Port have minimized its risk as it negotiated agreements with the developer? Would it have been possible for the Port to require performance bonds so that the Port would have been protected for the burden it actually incurred?

A complete analysis of Portland's coal terminal dilemma will require an in depth study and review of the legal arguments. For this exploration, the concluding section will speak to the lessons learned from coal development projects and will suggest an agenda for further and more extensive comparative research of port development decisions.

PORT DEVELOPMENT PROCESS AND RISKS - LESSONS LEARNED

Based on the case studies presented here certain lessons can be inferred from the coal development experience. These lessons are developed on limited evidence, but can be used to establish a research agenda for understanding port development risk.

Lessons Learned

1. Large capital plans with significant revenues and economic activity forecasted can cause public port managers to become "risk takers". They are so tempted to compete for this business that they may not adequately consider the risk of financial loss: in essence they may be willing to take the risk for the likely gain.
2. If a planned project does not have an assurance that cargoes will be moved with certainty, in effect a "binding contract", then port managers should establish a means to minimize their own risk. These can include:

    a. Maximize private sector investment, minimize port capital expenditures.

b. Provide "minimum revenue guarantees" to the port in a lease agreement, to ensure the port received returns for its financial investments.

c. Require the developers/contractor to provide adequate "surety bonds" to prevent failures and bankruptcies from obligatory liens against port property or facilities.

3. If port development decisions do not consider the probability distribution of demand and payoffs in project analysis, then they should openly present a "worst case scenario" and debate whether they should decide on "risk avoidance" before decisions are recommended. Without sufficient information about the demand risk function, then the port is financially secure only if it evaluates the worst case and accepts or rejects that outcome.

It has been argued elsewhere that ports are, for the most part, successful public enterprises

> "requiring little or no subsidy, involving the private sector to a great extent and acting entrepreneurially to the benefit of the local/regional economy...The port enterprise model provides a valuable alternative to privatization by keeping resources under public control while promoting independent business-like management." (Price, et al., 1991)

As a result, an important arena for seaport research is whether successful port managers are seriously involved with risk analysis in their capital decisions. Are successful ports "risk takers" or "risk avoiders"? They may actually become risk takers because of their success and less successful ports, on the other hand, may well be the only enterprises concerned with risk avoidance.

Of course, some ports are taking risks about which they are not fully informed. They are, in effect, blind gamblers with public port owners truly at risk.

REFERENCES

Interviews were conducted with managers at the Port of Stockton, Owen Block and Pat Huff and with Floyd Sheldon, Director, Port of Redwood City, who was deeply involved with Oregon port matters during the coal development at Portland and at Astoria where he was previously Port Director. The coal development at Roberts Bank of the Port of Vancouver was discussed with Tom Dowd at the University of Washington, but since limited data was available, a discussion of Vancouver was not included here.

Dowd, T.J., and C. Jonson. 1991. Port capital investment decision making: a process. Port Management Series. Washington Sea Grant, University of Washington.

Felice, M. 1981. Coal. Port Surroundings. April. pp. 8-11.

Oberstone, J. 1990. Management Science: Concepts, Insights and Applications. Chapter 1. West Publishing Co.

Price, W. 1982. Seaport development decisions: the response of west coast ports to the rediscovery of coal. ASPA National Conference. Honolulu, Hawaii.

Price, W. 1981. Seaports as public enterprises. In: Making Ocean Policy, ed. F.W. Hoole, et al. Westview Press.

Price, W., J. Fawcett, and K. West. 1991. Seaport management and state policy. California Policy Choices, University of Southern California, Volume 7.

Savas, E.S. 1987. Privatization: The Key Better Government. Chatham House.

Truban, E., and J.R. Meridith. 1991. Fundamentals of Management Science. 5th Edition. Irwin. Chapter 3.

Tumulty, K. 1982. Coal boom may not be as big as ports' dreams. *Los Angeles Times*. January 10.

DYNAMIC GEOMORPHOLOGY AND COASTAL ENGINEERING OF YANGPU HARBOUR, HAINAN ISLAND, CHINA

Ying Wang and Dakui Zhu
Nanjing University
Nanjing, China

ABSTRACT

Yangpu Harbour is located in the northwest of Hainan Island. It is constituted by Yangpu Bay and Xinying Bay. During 1983-1989 we carried out a series of research work for building deepwater harbour, and studied sedimentation of the embayments. This paper presents a summary of the work on the dynamic geomorphology and coastal engineering of the embayments.

COASTAL GEOMORPHOLOGY

The area of Yangpu Harbour includes three structural systems. Consequently, this location has been subject to a large number of tectonic movements since Pliocene. The major structural system trends toward the northeast. The northern part of Hainan Island borders on a large east-west trending graben feature and Yangpu Bay lies within the southern part of the associated trough feature. During Pliocene and Quaternary, 3000 m of sediment have deposited in the graben as a shallow nearshore facies called the Zhanjiang Formation. There is a substantial amount of volcanic activity associated with the tectonic movements that have occurred in this part of the island. This is evidenced by the rocks, primarily basaltic, exposed on the north side of the bay. The rocks on the south side of the bay are part of the Zhanjiang Formation and consist mostly of gravel, sand and clay in various proportion. The embayment is the topographic expression of the fault that separates the basalt from the Zhanjiang Formation sediments. The area north of the embayment has been subject to neotectonic movements since early Holocene that have continued to the present (Ding, 1964).

Yangpu Harbour consists of two embayments - Yangpu and Xinying. Xinying Bay is a tidal embayment with an area of 50 km^2. Two rivers enter in the embayment, the Dashui River from the east, and the Spring River from the southeast. Their combined drainage basin area is 1419.44 km^2 (Figure 1).

The mouth of the embayment is 550 m wide and has a cross-section area of about 5000 m^2. The mouth area is referred to as the Baimajing Strait. Fluvial sediment carried into the eastern side of the embayment by the two rivers has formed two distinct river deltas. During each tidal cycle, the fine fractions of the delta sediment is eroded and transported seaward during the ebb tide. Near the deltas, more than 90% of the residual sediment in tidal channel and lower beach environments is coarser than 0.1 mm. Muddy sediments are carried onto the tidal flats during flood where they are trapped by the mangrove vegetation. Consequently, the coastline is migrating seaward. According to historical records, the towns of Zhonghe and Xinzhou were the sites of seaport 1000 years ago, during the Tang Dynasty. Currently, however, they are landlocked. In Qing Dynasty, seaport moved to Xinying Town. But now, even a small 20-ton boat can only navigate to Xinying only during hightide time.

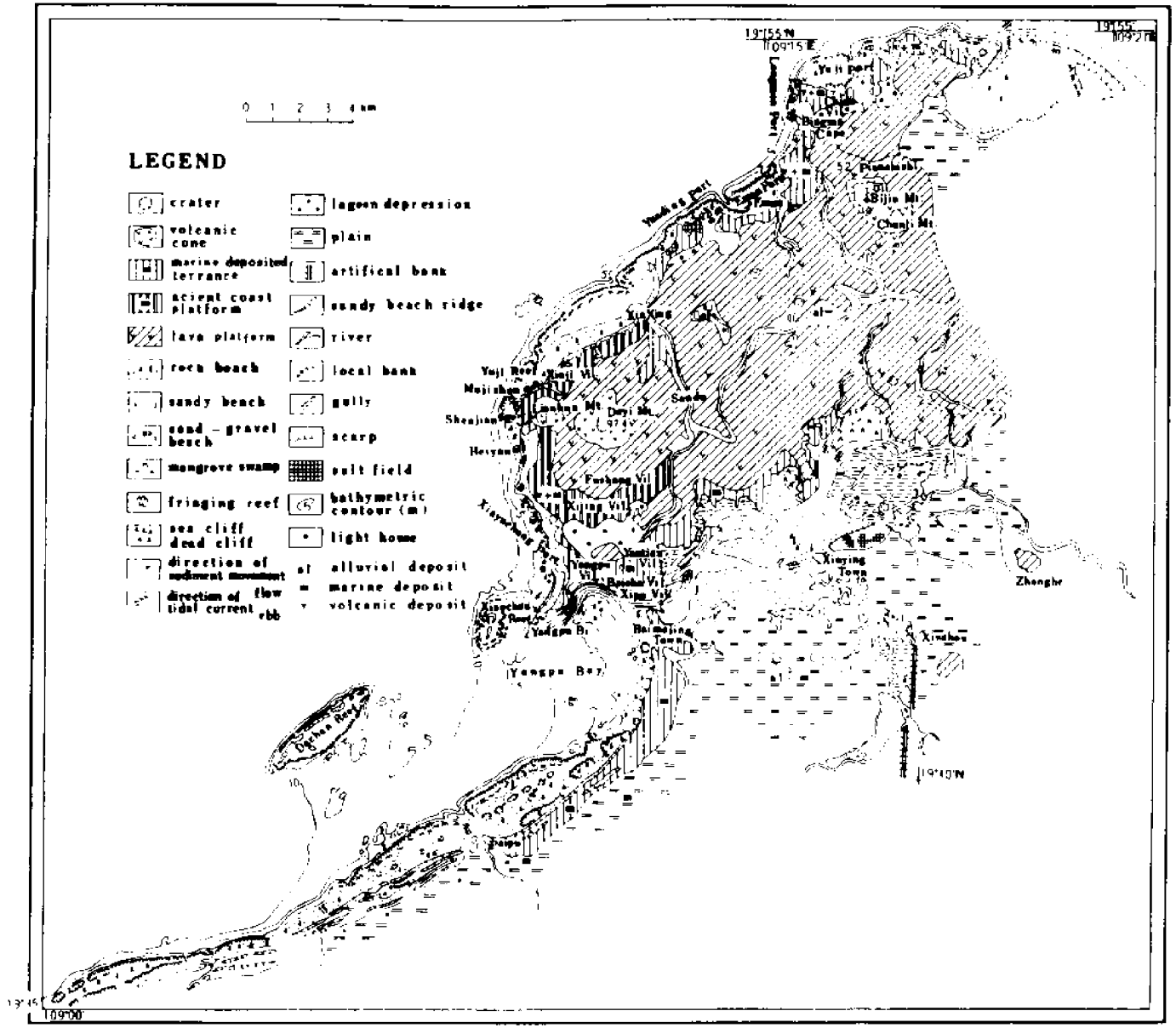

Figure 1. Coastal dynamic geomorphologic map of Yangpu Harbour

The northern part of Yangpu Bay is developed on a basalt platform. There were two periods of volcanism. The first one occurred in the late Pleistocene, dating back to 52,000 YBP. It formed a lava field which covered a sand deposit. Another eruption took place 25,000 YBP. And the latest eruption occurred in the Holocene (Wang, 1990). The lava which emitted at that time consists of olivine basalt and tholeiite basalt. It is the olivine basalt of oceanic crust, and the tholeiite of mid-ocean ridge. So it may be an interesting phenomenon if there was/is sea floor spreading in the Beibu (Tonkin) Bay (Nicholls and Ringwood, 1973; Wang, 1990).

The north shore of Yangpu Bay consists of a series of basalt cliff. In the inner part deposits muddy sediment and grows up mangrove while the outer part is presently in erosion.

On the south side of the bay, cliffs that were developed in the Zhanjiang Formation are presently eroded. The Zhanjiang Formation supplies sand and silt for the embayment.

The main tidal channel from Baimajing strait to the ebb tidal delta (block gate shoal) is 10 km long, 400-500 m wide and about 5-25 m deep. The bottom sediment of the main channel consists of three distinctive layers. The upper layer is muddy marine sediment. The middle layer is composed of sand and gravel deposited by river currents. The lower layer consisted of Zhanjiang Formation sediments (silt and clay). The main channel is an ancient river valley that was eroded along two major faults in pre-Holocene river valley. The upper and lower reaches of the channel became the sites of sediment deposition that eventually infilled those parts of the ancient river valley. However, the channel was kept open because of daily erosion of sediment by tidal currents.

The ebb tidal delta at the western end of the tidal channel is currently an area of shoals with maximum water depths of about 5 m. This shallow area is about 400 m long and 80-150 m wide. The ebb tidal delta stratum consists of three layers. The top layer is primarily marine mud (0-3 m). The middle layer is about 7 m thick and consists of sand and gravel deposited by river currents. The lower layer consists of Zhanjiang Formation sediments (indurated silt and clay). The ebb tidal delta developed in three stages. Firstly, before 8500 YBP, the channel was cut by river currents which eroded the Zhanjiang Formation and deposited a 7 m thick layer of sand and gravel. Secondly, during the Holocene sea level rise, the entire embayment was flooded. Finally, tidal currents which developed in the bay deposited marine mud resulting in a gradual shoaling of the ebb tidal delta to its present depth of about 5 m. Core ^{14}C data suggest that this water depth has been maintained over the past 2000 years with net deposition of only about 70 cm since that time.

The sand bank area forms the south side of the Yangpu Bay. The area of the bank lying about the zero contour is about 2.5 km^2. Between 1955-1980, this area has increased by about 0.7 km^2. An area of less than 2 m water depth represents about 40% of the total area of the bay. This area also shows an enlargement of about 0.7 km^2 between 1955-1980, i.e. an increase of <5%. The sand bank is developed on an erosion platform of Zhanjiang Formation. Its sediment forms a thin veneer about 0-2 m thick on the platform surface

COASTAL DYNAMICS

Wind and Wave

Wind variation shows two dominant modes. One of these blows NNE-ENE off the land. This wind is relatively strong but does not produce large waves because of the

shelter effect of land, i.e., there is a short wave fetch with respect to the outer bay. The other major component blows from the sea in a SSW-WSW direction. Because of the exposed nature of the outer harbour, this mode of wind produces the largest waves and is responsible for most sediment transport in the harbour, and of coastal erosion. It can also have a disturbing influence on ships that use the harbour as an anchorage.

The components of the tidal wave climate include wind-generated waves (78%) and sea swell (12%). The most frequent waves entering the harbour are from the southwest. Waves propagating from this direction are also among the largest that enter the harbour. The average height of SW propagating wave is 0.83 m with an average period of 4.5 second. Because the breaking depth of the 4.5 second waves is only 0.8 m, their effect on the erosion of sediment is felt primarily on the southwestern edge and top of the sand bank.

Tide

Tides in Yangpu Bay are of the irregular diurnal type. The mean tidal range is 1.81 m. During the survey of November, 1988, the measured range was 3.8 m. Observations over several tidal cycles show that the ebb portion is shorter (12 hours) than the flood portion (13 hours). This difference is reflected in ebb current velocities with tend to be higher than those observed during the flood. Mean flood velocity (Vf) is above 22 cm/s, and mean ebb velocity (Ve) is 27 cm/s (Table 1). There are differences in flood and ebb velocity depending on water depth. During flood, mean surface water velocity (Vf,s) is above 23 cm/s. Middle water velocity (Vf,m) and bottom water velocity (Vf,b) reach 24 cm/s. During the ebb, surface water currents (Ve,s) have a mean velocity of 31 cm/s. Middle water (Ve,m) and bottom water (Ve,b) flows are respectively 27 cm/s and 24 cm/s. During the ebb, tidal current velocities show a decreasing trend from east to west starting at the mouth of the inner harbour near Baimajing. At Baimajing, surface velocities during the flood reach 51 cm/s. Middle and bottom water velocities are considerably high reaching values of 88 and 84 cm/s, respectively. During the ebb, the surface water flows have a maximum velocity of 84 cm/s while middle and bottom water velocities flow at a rate of 86 and 97 cm/s, respectively.

Table 1. Maximum tidal velocity (cm/s)

Station		Surface	Middle	Bottom
Baimajing	flood	51	88	84
	ebb	84	86	97
Main Channel (Yangpu Vil.)	flood	42	67	56
	ebb	68	53	45
Ebb Tidal Delta	flood	57	49	22
	ebb	54	75	56

At the main channel (Yangpu Village), maximum surface water flow during the flood stage of the tide is 42 cm/s. Middle water and bottom water flows are 67 and 56 cm/s. During the ebb cycle, surface, middle and bottom water maximum velocities are 68, 53 and 45 cm/s. At the mouth of the outer harbour, in the ebb tidal delta, the maximum velocity of surface water during the flood stage is 57 cm/s. And middle and bottom water

velocities are 49 and 22 cm/s. And during the ebb stage, the surface water maximum flow is 54 cm/s. Middle is 54 cm/s. Bottom is comparable to surface values 56 cm/s.

All of the bottom water velocities are above the threshold value necessary for the erosion and transport of silt and fine sand particles. Maximum ebb velocities are generally higher than flood values so that the modal transport direction of sediment is from the inner to the outer bay.

Residual flow presents water velocities and directions in the absence of tidal flow. These flow are important in understanding sediment distribution patterns (Table 2). The residual flow of surface water has a large river component and tends to follow a direction parallel to the axis of the tidal channel. During the wet season there is less coherency of the residual flows between surface and bottom water (Wang and Aubrey, 1987).

Table 2. Residual flow velocities (cm/s) and direction

Station	Surface	Middle	Bottom
Baimajing	6/187	3/95	3/102
Main Channel	12/301	11/116	12/107
Ebb Tidal Delta	7/230	5/164	8/215

Suspended Particulate Matter

In general, the concentration of suspended particulate matter (SPM) in the water column of Yangpu Harbour is about 0.1 kg/m^3. Near Baimajing the integrated (surface, middle and bottom water) SPM concentration during the flood stage average 0.088 kg/m^3 (Table 3). During the ebb cycle, this value increased to 0.103 kg/m^3. At Yangpu Village, SPM during the flood is somewhat higher than at Baimajing and is similar to the ebb value. SPM measurements at the swash platform station are slightly lower than those observed at Yangpu Village and are comparable to the ebb value noted for the Baimajing station.

Table 3. Suspended particulate matter concentration (Kg/m^3)

Station	Flood	Ebb
Baimajing	0.088	0.103
Yangpu Village	0.116	0.119
Ebb Tidal Delta	0.102	0.102

SEDIMENT SOURCES

There are three major sources of sediment in the Yangpu Bay area. The most important source is material derived from the Dashui River. The drainage basin of this river is 648.3 km^2. The annual discharge of sediment from the basin into the inner bay (Xinying Bay) is about 74,000 tonnes per year. The Spring River enters the bay from the

southeast. Its drainage basin has an area of 577.8 km^2. The river's annual sediment discharge is about 67,000 tonnes per year. All of other small rivers draining into the bay have a total drainage basin area of about 81.3 km^2 and account for an annual sediment discharge of 15,000 tonnes per year. So the total discharge from all river sources is 156,000 tonnes per year. The weight equates to a sediment volume of about 62,000 m^3 per year.

The second most important sediment source is from coastal erosion. Most of the coastal erosion occurs in the Zhanjiang Formation along the southern coast of the outer harbour. Each year this source contributes 22,000 m^3 of sediment. The northern basaltic coastline is also being eroded but at a significantly slower rate than the southern coast. Its annual contribution of sediment is about 2,000 m^3 of sediment. The total contribution of sediment from coastal erosion processes is 24,000 m^3 each year.

The third source of material is from coral reefs that are established on offshore islands, at the northwestern end of the bay, and at various locations along the south coast (Figure 1). Sediments in the ebb tidal delta area contain about 33% $CaCO_3$, those along the subtidal areas of the south shore contain about 22-23% $CaCO_3$. In the inner bay, the sediments contain only about 0.6-0.9% $CaCO_3$. The distribution of $CaCO_3$ in outer bay sediments is consistent with the distribution of reefs along the coastline. It also shows that the sediment from the outer bay is not transported too far into the inner bay. The total amount of sediment from this biogenic source is estimated to be not greater than about 4,000 m^3 per year. The total amount of sediment supplied to the bay area from all sources is about 91,000 m^3 per year.

COASTAL ENGINEERING

Yangpu Harbour is a natural harbour. The main channel is 10-23 m deep and 500-800 m wide. The huge water and large currents are major factors for keeping channel open. The Northern, Eastern and Southern parts of the harbour are 10m-deep marine terraces that stop the wind wave from north, northeast, east and south. The frequency of strong winds is a little, >6 wind (force) scale only 0.42%. Wave heights $H_1/10 < 0.5$ m are 99%, $H_1/10 \leq 0.8$ m are 99.88%, but those $H_1/10 \geq 1$ m are only 0.06%. The frequency of wave height ≥ 1.2 m is zero. So, Yangpu Harbour is a good harbour. The harbour area, geologically, is a platform of basalt and the Zhanjiang Formation. The geologic base is quite good. And an abundant rocks material, broad land area. But now, the problem is only a blocked gate shoal and shallow waters, requiring dredging for a navigation channel.

Yangpu Harbour is a tidal inlet, in which Xinying Bay is a tidal water trap: the main channel is the tidal water pass; the block gate shoal is the ebb tidal delta. Core data and regional geomorphological analysis show: the main channel and block gate shoal were originally a fossil river valley 8,500 YBP. The valley's elevation is minus 25-30 m. The top surface of the river deposits has a minus 20 m elevation. The ancient river's gradient was 0.07%. The ancient Dashui River and Spring River joined the ancient river valley in the area of today's Xinying Bay, which finally entered the open sea at the -20 m contour through the main channel and block gate shoal. With the post-glacial sea level rise, the coastal plain was drowned as Yangpu Harbour and ancient river valley were filled with marine sediment while the ancient river valley was kept as today's deep water channel because of the tidal flushing and scoring of tidal prism. But, the section of the block gate shoal disappeared due to siltation.

Dating data (according to ^{14}C) from the block gate shoal show: the average sedimentation rate was 0.16 cm/a during the last 8500 years. And during the last 3000 years the rate was 0.10 cm/a, which is consistent with the world wide sea level change processes and now (according to ^{210}Pb inventory analysis) is 0.52-1.06 cm/a. Hence, the natural formation process of the block gate shoal is shown.

We have worked out the erosion and siltation budget for the last decades of the area by comparing the six 1947-1983 navigation maps and the bathymetric maps. In this work, we transferred the different depth bases of various maps into a same theoretical depth base, and then calculated the volumes of the block gate shoal, the main channel at different periods. We find the block gate shoal with an erosion rate 2-10 cm/a during 1947-1974, a siltation rate 7.2-4.5 cm/a during 1974-1983; and the main channel with an erosion rate of 1.2-5 cm/a during 1947-1974, a siltation rate of 5 cm/a during 1974-1983. In general, however, the block gate shoal and main channel were both subjected to slight erosion during last fifty years. The total erosion volume of the block gate shoal is one million cubic meters and that of the main channel is 0.7 million cubic meters.

Therefore, for the past 8000 years, the sedimentation rates of the area have been very small and the submarine reliefs are nearly stable although sometimes there was slight erosion or siltation, which does not interfere with constructing a harbour and digging a navigation channel in the area.

Tides in Yangpu are irregular diurnal type. The mean tidal range is 2 m and tidal prism is 200 million cubic. Tidal cycles show that the ebb current velocities are above the threshold value necessary for the eroding and transporting silt and fine sand particles (Figure 2).

According to dynamic geomorphology analysis, the paper verified the advantageous conditions for construction of Yangpu Harbour, suggested the optimum direction as 45°-225° of navigation channel passing through the block gate shoal (ebb tidal delta), and predicted that the siltation rate following digging the channel will be about 0.5 m/y.

REFERENCES

Ding, G. 1964. On some problems about the Quaternary geology of Hainan Island. Quaternary Geology of China. pp. 207-233. Beijing: Science Press. (in Chinese)

Nicholls, L.A,. and A.E. Ringwood. 1973. Effects of water on olivine stability in tholeiites and production of silioasatureted magmas in the island-arc environment. *Jour. of Geol.* **81**:285-300.

Wang, Y. 1990. The volcanic coast in the area of northwest Hainan Island. *Acta Geographica Sinica* **45**:321-330. (in Chinese with English abstract)

Wang, Y., and D.G. Aubrey. 1987. The characteristics of the China coastline. *Continental Shelf Research.* 7:329-349.

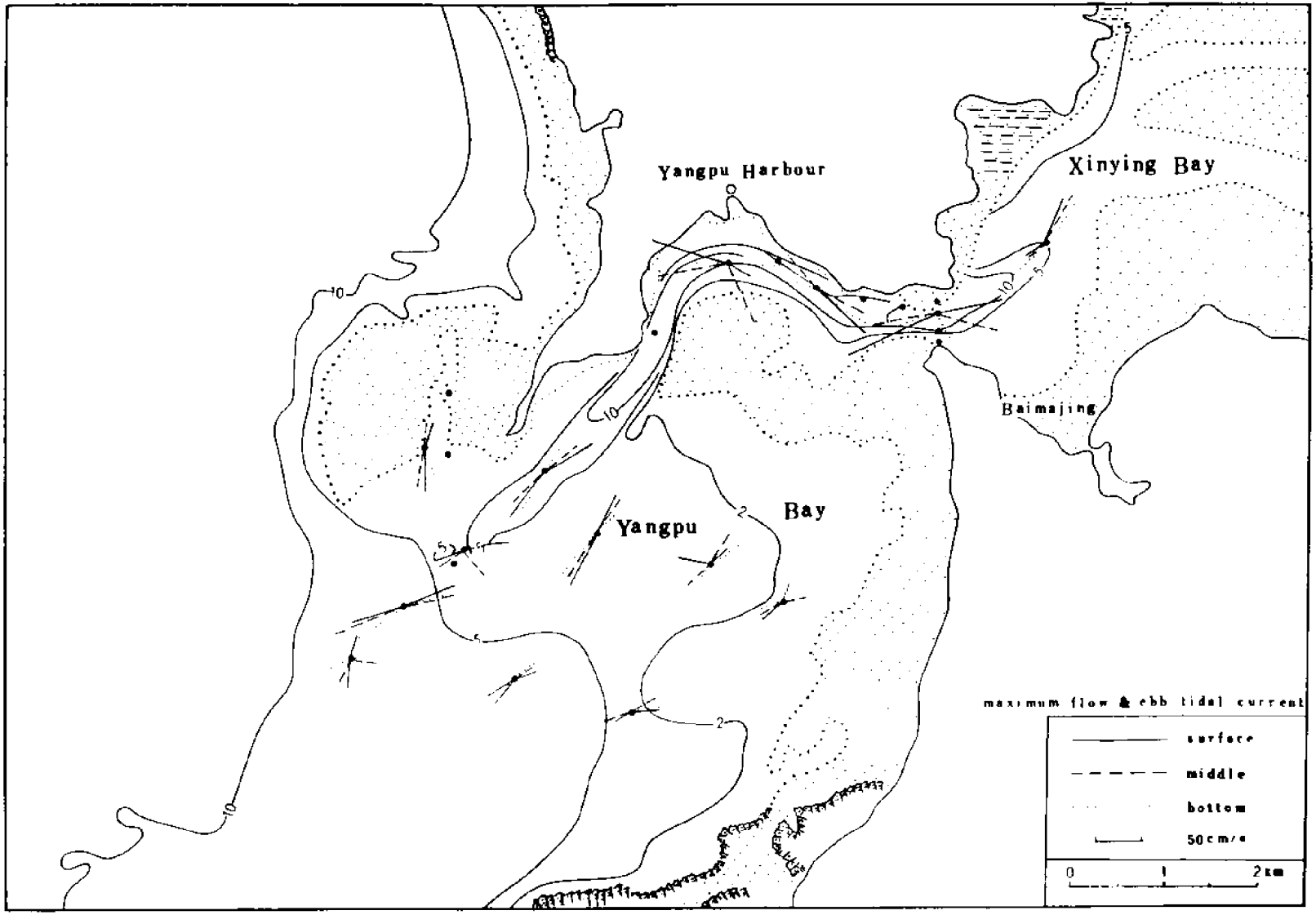

Figure 2. Tidal current in Yangpu Harbour

SYSTEMS CONCEPT FOR AN OFFSHORE MARICULTURE FACILITY

Ron Bregman and Patrick Takahashi
University of Hawaii
Honolulu, Hawaii, U.S.A.

ABSTRACT

As the world's population rapidly increases and changes its dietary habits, tremendous demands will be placed on mariculture (aquaculture in the marine environment) to produce large quantities of fishes, crustaceans, mollusks, and seaweeds. Meanwhile, floating platform technology now provides the capability of working on and below the surface of the ocean many miles from the nearest coastline. Horizontal positioning of the platform, with respect to geographical location and orientation, can be achieved utilizing the renewable energy sources available. Proposed applications for large floating structures include international airports, military bases, ocean mining, industrial facilities, waste treatment plants, ocean energy conversion, weather stations, recreation centers, and offshore mariculture.

The use of floating platforms for offshore mariculture appears to have many advantages over conventional mariculture techniques. Mariculture will become more and more restricted in coastal areas due to increasing population densities, land usage, oxygen depletion, waste disposal, and agricultural-industrial-domestic runoff. Offshore mariculture offers advantages due to the large mixing and dilution ratios of the containment area to adjacent water masses, which increases productivity and the associated economic benefits. Another potential advantage involves the ability to use deep ocean water, which is nutrient-rich and pathogen-free, to further improve productivity and systems design.

INTRODUCTION

Mariculture is a term used to designate aquaculture within the marine environment. Since the marine environment includes bays and estuaries, as well as the world's oceans, offshore mariculture is used to distinguish culturing activity in unprotected marine waters, regardless of its distance to the nearest coastline. Offshore mariculture is a relatively new concept. Although much of the fundamental technology that it requires is already well advanced, new applications will be needed in the future.

Some advantages from locating a mariculture facility in the offshore environment include (P2M, 1991):

1. A virtually unlimited supply of water available at different temperatures.

2. Avoidance of coastal-zone use conflicts.

3. Increased survival, growth rates, stocking densities, and product quality.

4. Facility mobility and the ability to change location seasonally.

In addition, an offshore mariculture facility can be developed in conjunction with artificial upwelling of nutrient-rich water, electrical power production, deep seabed mining, and other ocean resources utilizing a large floating platform for a base of operations (Takahashi and Yuen, 1991). This concept is illustrated in Figure 1.

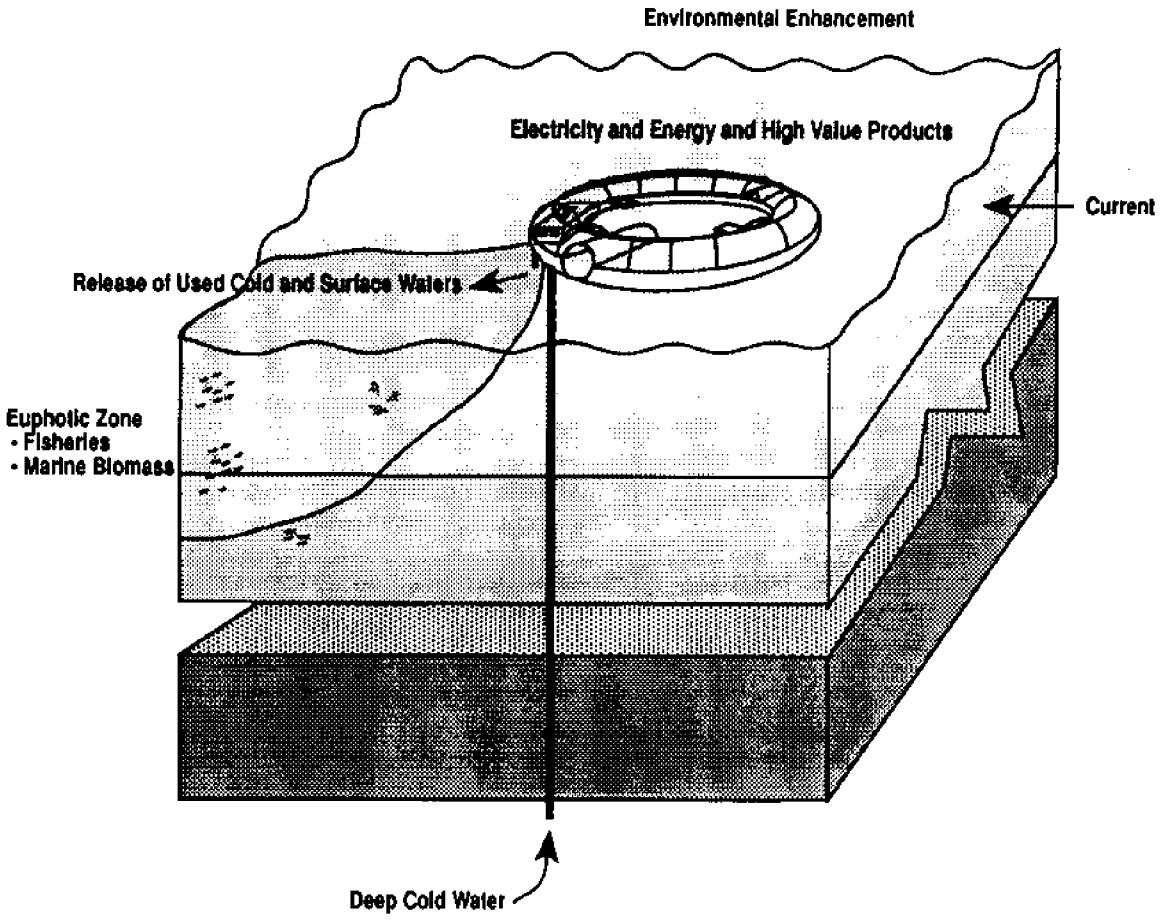

Figure 1. Systems concept for an ocean resources platform

Although the benefits mentioned above are important to consider, the offshore environment remains a more uncertain legal and political environment to operate in than the coastal zone. Moving away from the overlapping jurisdictions of local, state and federal governments is an appealing prospect; however, constraints of a more international nature will be encountered.While an enormous amount of time and money is required to satisfy the numerous regulations concerning the use of near-shore waters, at least they are discernable. The requirements to be satisfied in offshore waters are yet to be determined, as well as the extent to which a mariculture facility operating offshore could be legally protected (Hanson, 1974).

OFFSHORE PLATFORMS

The base of operations for an offshore mariculture facility should be designed according to the type of species to be cultivated, containment methods, harvesting and processing needs, geographic location, and other appropriate factors (Ribakoff, 1974). Options can be broadly categorized into coral atolls, bottom-supported structures, and floating platforms.

Coral atolls occur naturally in many parts of the Pacific Basin and would require a minimum amount of modification and capital investment due to their natural morphology. Pacific Basin atolls can be grouped into six major chains: the Marshalls, Gilberts, Carolines, Marianas, Line Islands, and the Hawaiian Archipelago. Any development of mariculture in these areas should give serious consideration to the following characteristics of atolls:

1. Enclosed basins or lagoons of various depths and diameters occur naturally in many cases

2. Because of a volcanic foundation, atolls are usually in close proximity to deep water where phytoplankton nutrients are abundant.

3. Atolls are highly stable and survivable, and require little regular maintenance.

4. Many atolls lie within inhabited island areas where some type of economic development is desired.

The majority of bottom-supported structures have been constructed by the offshore oil and gas industry. The basic design of these platforms consists of a flat deck, a supporting framework, and pilings or legs which are embedded or anchored in the sea floor. Since the platform is moored and rigid, it is considered to be highly stable and no motions other than vibrations resulting from wave impact are usually discernible on deck. The major disadvantage, with respect to offshore mariculture applications, is that this type of structure is generally limited to water depths of approximately 100 meters (300 feet).

Floating platforms, including conventional ships and barges, as well as semisubmersible platforms, appear to be the most promising concept for offshore mariculture development. The chief advantages of semisubmersibles are a high level of motion stability and high survivability in extreme environmental conditions. The major disadvantage results from the fact that water-plane area is minimal giving relatively little buoyancy force per unit of submersion. Overturning moments and added loads must be compensated for by ballast adjustments, in contrast to the spontaneous compensation occurring in ships and barges (Ribakoff, 1974).

Another concept, which is especially applicable for large floating structures in turbulent seas is indirect displacement. Indirect displacement with pneumatic stabilization has the following advantages over conventional direct displacement vessels (Innis, 1991):

1. Simpler on-shore construction of smaller modules.

2. Greatly reduced forces at module junctions.

3. Reduced draft and mass.

4. Greater ability to absorb impact loads.

5. Greater ability to utilize the energy causing destabilization.

The principle behind indirect displacement is that the vessel is supported on a compressible bubble of air rather than incompressible water. The bubble acts as a shock absorber to mitigate pitch and heave motions due to changes in the surface conditions of the ocean.

CONTAINMENT SYSTEMS

Potential species for offshore mariculture can be broadly categorized into the following groups:

1 Fish

2. Crustaceans

3. Mollusks

4. Seaweeds

5. Marine mammals and reptiles

The type of containment system to be designed is highly dependent upon the species chosen to be cultured.

Containment systems for fish involve either physical enclosures or aggregation devices (passive containment). Submersible cages appear to be the only type of physical containment having any potential for the offshore environment. Since water movement produced by waves is largely a surface phenomenon and the water particles rotate in circular orbital motions, a submerged cage is less susceptible to damage from waves than conventional cages. In deep water, the wave motion at a depth of one-half the wave length is considered to be negligible.

Optimal cage volume is believed to be approximately 4000 square meters (40,000 square feet); however, analysis based on the biological behavior of the particular fish species to be cultured should be conducted on an individual basis. The cage should also be designed so that it is possible to operate it safely from the surface even under unfavorable weather conditions, which are common in the offshore environment. The final design of a submersible cage system, including the number, size, shape, materials, mooring, and ballasting of cages will also depend on other systems to be used in conjunction with the containment system.

It is anticipated that, in the future, cage-culture will become obsolete. The combination of economics and severe weather conditions will lead to methods of passive containment. Passive containment is defined as a system that keeps fish in the vicinity of a desired area without the use of walls or cages. With any passive containment system there exists the possibility of losses due to emigration; however, systems can be established which require little maintenance and will attract and hold natural fishery resources (Brock, 1991).

Passive containment systems capitalize on the behavior of fish and include attraction to light, sound, and shelter. Pneumatic barriers (bubble fences) appear to have potential for offshore mariculture applications. Assuming an enclosure several hundred meters in diameter could be deployed at a depth of 600 meters (2000 feet), the advantages of such a system would be numerous. The system would be survivable in any weather, no biofouling would occur, bubbles would automatically oxygenate the enclosed water column, surface waters would remain calm within the enclosure since the bubbles act as wave absorbers, and a degree of artificial upwelling could occur by entraining deep water with the rising bubbles. Furthermore, if hydrogen production systems could be integrated with offshore mariculture, the bubble fence concept would be an attractive use for the waste oxygen that this process produces (Hanson, 1974).

ARTIFICIAL UPWELLING

The offshore environment is believed to have tremendous potential for mariculture. Since the majority of oceanic surface waters are practically nutrient deserts, the most promising concept for offshore mariculture is artificial upwelling. More than 40% of the world's fisheries catch comes from 0.1% of the ocean's total surface area, where natural upwelling occurs. Artificially upwelled fisheries may actually create a new maritime industry, as deep ocean water at depths from 200 meters (700 feet) begins to increase in nutrient-rich and pathogen-free characteristics.

It has been demonstrated that fish can be conditioned to congregate at a feeding site. With offshore mariculture, artificial upwelling of deep ocean water offers the opportunity to capitalize on this behavior. Deep ocean water, at a depth of 600 meters or 2000 feet (nominally) contains two orders of magnitude more nitrates (NO_3, NO_2) and a magnitude more phosphates (PO_4), compared to surface waters (Table 1). As the majority of the nitrogen and phosphorous contained in deep ocean water is derived from the decay of previous biological production from the upper layers of the world's oceans, deep ocean water represents an ideal source of nutrients for photosynthesis and mariculture production (McKinley and Takahashi, 1991).

Table 1. Comparison of surface and deep (600 meters/2000 feet) seawater

Parameter	Surface Water	Deep Ocean Water
Temperature (°C)	26	8.9
Nitrogen (NO_3 plus NO_2)	0.2	39.0
Nitrogen (NH_4)	0.4	0.2
Phosphorous (PO_4)	0.2	3.0

Maintaining relatively dense, artificially upwelled water at or near the surface is a significant engineering challenge. The three ways to achieve surface retention are through physical containment or by lowering its density through dilution or solar heating. Creative engineering design, which makes efficient use of the natural energy fluxes available, is essential to establishing the feasibility of any artificial upwelling system. In addition, an offshore mariculture system could utilize nutrient concentrations or temperature differential barriers as a means of passive containment to retain stock.

RENEWABLE ENERGY SOURCES

The oceans are the world's largest solar energy collector and storage system. Incident solar radiation is stored either directly or indirectly in various forms within the global ocean system. Specifically, solar energy is stored directly in the form of thermal heat, and indirectly as wind, waves, and currents created by the temperature differences between the oceans and the surrounding atmosphere.

Types of direct solar energy systems include passive solar heating, active water and space heating, photovoltaics, and thermal electrical systems. While solar energy conversion techniques appear to have low conversion efficiencies (5 to 20%), this is offset by the fact that the energy resource is free and infinitely renewable. The important technical benefits of an ocean-based, solar energy conversion system would be the proximity to an excellent thermal sink and source of working mass, mobility of rotation and translation, space available for large solar collector areas, and logistical ease in initial construction and maintenance.

Another major source of renewable energy is the wind. Wind energy has considerable application potential in the offshore environment. This is due to the fact that wind patterns are more consistent over and near large bodies of water. In addition, many offshore areas have consistently high average wind speeds. A preliminary concept, integrating solar and wind power to produce electricity for an offshore floating platform is illustrated in Figure 2.

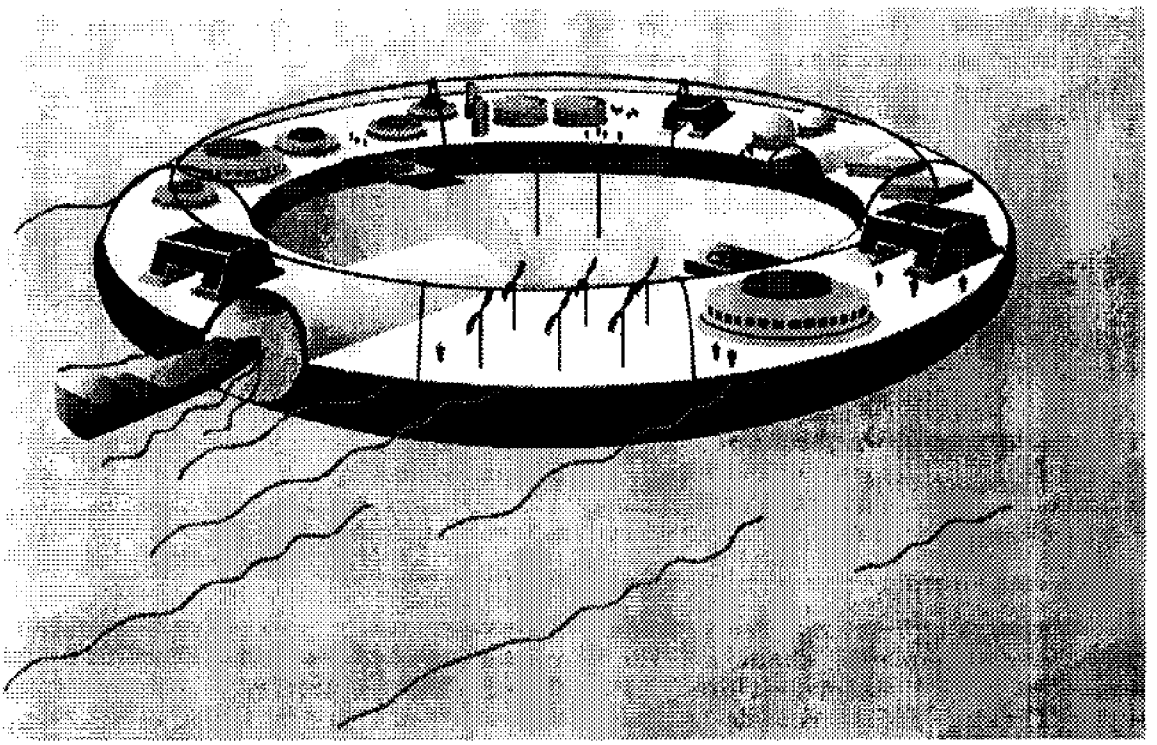

Figure 2. Preliminary concept integrating solar and wind power

The two basic types of wind machines are mechanical and electrical. Recent interest has focused on electricity production. In general, the larger the wind machine, the more power it can extract from the wind; however, there are limiting factors which must be considered in designing these machines. These include blade balance and vibrations, effect of wind gusts, gravitational and gyroscopic forces, and the blocking effect of the tower itself. Costs rise geometrically with size, and blade diameters in excess of 100 meters (300 feet) can develop excessive amounts of stress. Under high wind conditions, there is also potential for excessive stress to be placed on the blades. Protective measures must be designed to automatically shut the systems down by folding the blades or tilting the tower back under these conditions (Pryde, 1983).

The most potentially valuable source of renewable energy associated with the ocean is ocean thermal energy conversion, commonly known as OTEC. This is because the waste effluent from OTEC systems can be utilized as the nutrient source for mariculture systems. The basic concept of OTEC is to extract energy from the temperature difference between surface and deep ocean water (at approximately 1000 meters or 3000 feet). Solar energy absorbed and stored as heat in the upper layer of the ocean and cold water transported from the polar regions provide the source of this temperature differential. In equatorial areas, the temperature differential is sufficient (20 degrees centigrade) for OTEC operations year-round.

The open-cycle OTEC system uses seawater as the working fluid and has the advantage of producing desalinated fresh water as a by-product. In addition, refrigeration and mariculture systems could be designed based on the availability of cold, nutrient-rich water which would be available for use at no extra cost. The major components still undergoing development for OTEC systems are open-cycle turbines and flexible cold water pipes using bottom-mounted pumps. While there have been numerous development projects over the past decade, none have reached commercial fruition to date. Utilization of small-scale OTEC in conjunction with offshore mariculture systems may prove to be essential to the continuing development of such technology.

CONCLUSION

Current technology has reached a level in which the construction of an offshore mariculture facility based on a large floating platform appears to be technically feasible; however, since any project of this magnitude also needs to be justified economically and socially, other factors besides the state of the existing technology must also be considered. In the case of offshore mariculture, large floating platforms, containment systems, artificial upwelling concepts and renewable energy systems need to be designed, integrated, and analyzed for overall costs and benefits to society as a whole. While the cost of producing food from agriculture and fisheries are expected to continue to rise exponentially due to decreasing land, fossil-fuels, and natural fish stocks, mariculture costs should continue to decline with technological improvements and become increasingly competitive with time.

ACKNOWLEDGMENT

The authors would like to acknowledge the assistance of Dr. Cengiz Ertekin in the development of this paper.

REFERENCES

Brock, R.E. 1991. Passive containment systems: biological aspects. In: Workshop on Engineering Research Needs for Off-Shore Mariculture Systems, pp. 337-354. Honolulu, Hawaii. September 26-28.

Hanson, J.A. 1974. Open Sea Mariculture - Perspectives, Problems, and Prospects. Oceanic Foundation. Hawaii: Dowden, Hutchinson & Ross, Inc.

Innis, D.A. 1991. Pneumatically stabilized floating platforms. In: First International Workshop on Very Large Floating Structures, pp. 107-115. Honolulu, Hawaii. April 24-26.

McKinley, K.R., and P.K. Takahashi. 1991. Deep ocean water, artificial upwelling, and open ocean mariculture: a promise for the future. In: Oceans '91 Proceedings, vol. 1, pp. 195-199. Honolulu, Hawaii. October 1-3.

Pisciculture Marine de Monaco S.A.M. (P2M). 1991. First fully integrated offshore fishfarm. In: Workshop on Engineering Research Needs for Off-Shore Mariculture Systems. Honolulu, Hawaii. September 26-28.

Pryde, P.R. 1983. Nonconventional Energy Resources. Environmental Science and Technology Series: John Wiley & Sons, Inc. and V.H. Winston & Sons.

Ribakoff, S.B., G.N. Rothwell, and J.A. Hanson. 1974. Platforms and housing for open sea mariculture. In: Open Sea Mariculture - Perspectives, Problems, and Prospects. Oceanic Foundation, Hawaii.

Takahashi, P.K., and P.C. Yuen. 1991. Hawaii: The Center for Pacific Ocean Resources Technology (CPORT). In: Oceans '91 Proceedings, vol. 1, pp. 189-193. Honolulu, Hawaii. October 1-3.

SYSTEMS FOR CONTROL OF ENVIRONMENTAL CONDITIONS IN REGIONAL MARINE ECOSYSTEM - A FUNDAMENTAL STUDY

Masaaki Sakuta, Yoshihiro Suenaga, Norimasa Takagi,* Akio Kuroyanagi, Hiroshi Kondo, and Takayuki Kurata

Nihon University
Chiba, Japan

*National Research Institute of Fisheries Engineering
Yamaguchi, Japan

ABSTRACT

This study is being executed as a part of the consolidated research carried out by Nihon University. The study is being developed basically by two main research groups: the first group working on the development of a structure comprising marine control systems and on the investigation of geographical conditions, and the second group researching the repercussion effects caused by these marine control systems as well as various peripheral techniques.

INTRODUCTION

In Japan, where about one-third of fishery is imported from various foreign countries, techniques for increasing and nurturing fishery resources are required, in order to enhance productivity in the seas controlled by Japan. This need results from an increase in demand and coastal fishery restrictions in these foreign countries. Furthermore, the development of optimal utilization of ocean space has also become necessary. Through marine observation, the authors have decided to evaluate changes in both the physical and biological environments by installing a structure at Futaoi Island, Shimonoseki City, Yamaguchi prefecture.

The overall aims of this project included:

1) Development of recreation space, which efficiently uses coastal areas,

2) Increased efficiency of fishing along coastal areas, and

3) Establishment of a marine area control system and evaluation of the effect of creating ocean space.

OUTLINE CONDITIONS FOR TEST AREA

Outline of Area

Futaoi Island is situated at Hibiki-Nada, 12 km offshore to the northwest of Shimonoseki City (Figures 1 and 2). Futaoi Island occupies a small area of 2.32 km^2, and has 41 households and a population of 164.

The coast line has a total length of 13.31 km, and is gently curved towards the south. The main industry is fishing. Its climate is comparatively warm as a result of the Tsushima Warm Current and its annual average air temperature is 16.1°C. Its rainfall is 1.715 mm.

TEST OUTLINE

Results of Preliminary Test on Marine Area

Tests at Futaoi Island bay showed that the seabed topography inside the bay has a comparatively gentle slope to about 10 m depth, but past this area, the slope drops away sharply to create many undulations. The seabed geology indicated substantial gravel and reefs from the shore to about 15 m depth. Further out, large-grain sand, medium-size sand, and fine-grain sand were widely distributed (Regional Fishery Plan for Futaoi Island, 1985; Hydrographic Dept. of Maritime Safety Agency, 1985).

Inside the bay, a tidal current was flowing, forming a large vortex. The water temperature at the 15 m depth layer had a maximum of 25.0°C at low tide, and a minimum of 24.38°C at high tide. The salt content was a maximum of 33.5%, and a minimum of 32.5%. Both above values were measured at high tide.

Sunken Structure

The Ocean Conditions Control Structure used in the present study and installed in the marine area was the Rock Reef Type-12, whose shape is shown in Figure 3. At positions 1.5 m away from both ends of concrete frame measuring 10.4 m in width, 6.6 m in length and 3.85 m in height, two pieces of natural stone 70 to 80 cm long were placed,and at their center (3.6 m), natural stones with diameters of 20 to

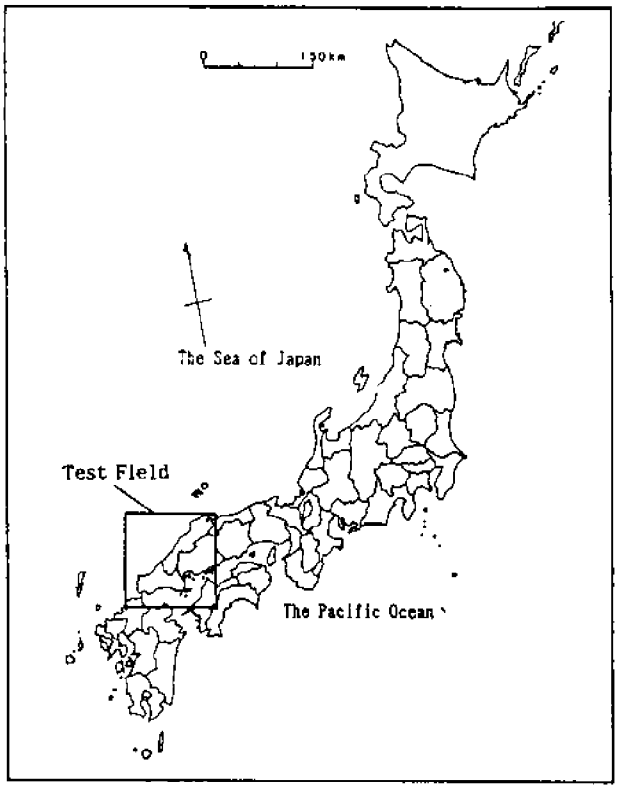

Figure 1. Location of the test field

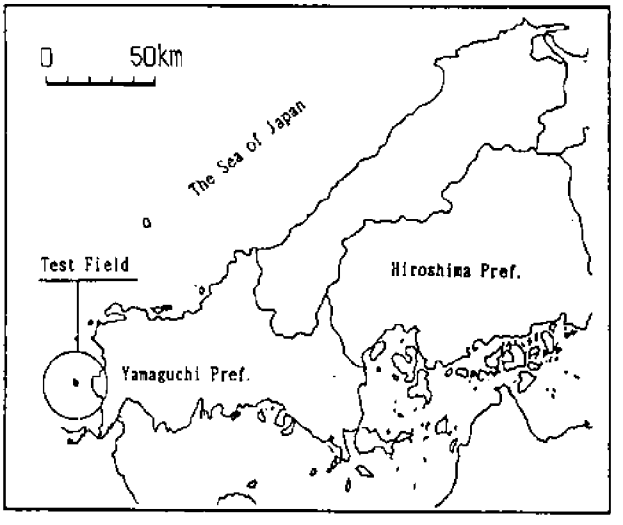

Figure 2. Test field

40 cm were piled up. This structure has two functions. The first is the function of an artificial reef allowing fry and young fish to shoal and reside there. The second is the function of a spawning ground where fry and young fish can shoal, grow and spawn.

In addition, natural stones have the power to activate living things, and through their use, a living environment is created which is conducive to habitation by living organisms (Ocean Fisheries Experimental Station of Yamaguchi Pref., 1988; Sakuta, et al., 1987).

The structure was installed on October 23, 1989, in a marine location 100 m offshore at depth of 12 m as shown in Figure 4. The structure was installed at a right angle to the predominant flow in the bay, and visual observation of the aggregation of living organisms was made by diving surveys (Sugawara, et al., 1989).

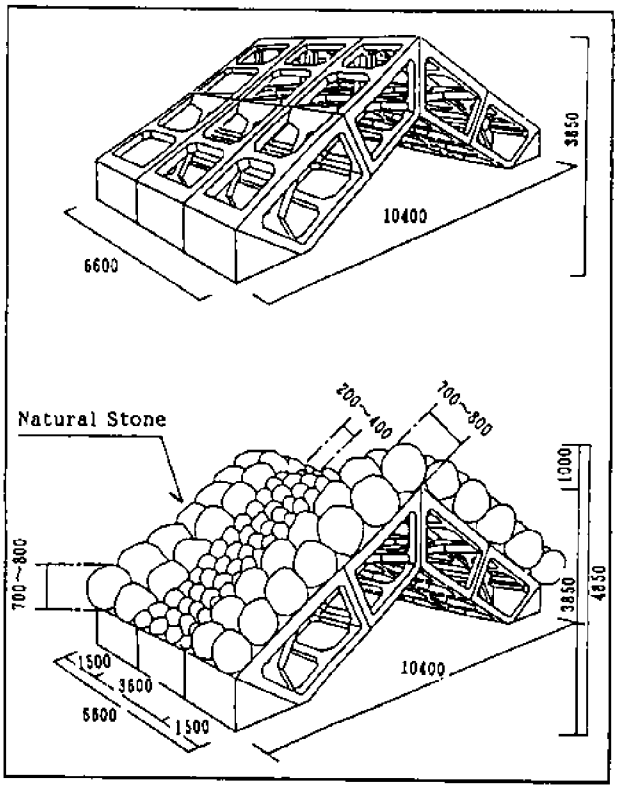

Figure 3. Ocean conditions control structure (Rock Reef Type-12)

DIVING SURVEY RESULTS

After the structure was sunk, visual diving surveys were carried out five times in order to evaluate biological aggregation conditions in the period February to December, 1990. The investigation method used was camera and video photography. For the quantitative evaluation of living organisms, the area separation method was used.

Installation Conditions

The installation conditions of the structure were maintained in a satisfactory state without excavation due to bottom-layer flow and sinking of the structure by its own weight. Furthermore, no damage to the natural stones due to currents was observed, and the required quantity of natural stones was piled up.

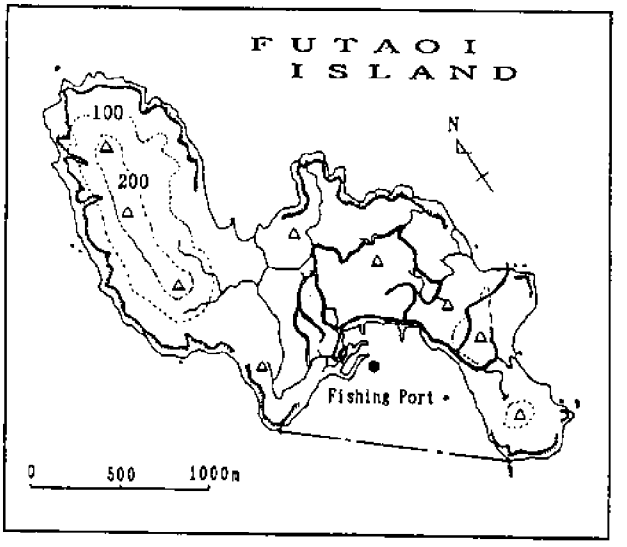

Figure 4. Location of the structure

The west side of the artificial reef is mainly formed by the boulder zone. The east side features many natural reefs, and is severely undulated. The highest location is 7.0 m.

Aggregation Conditions of Living Organisms

Viewed from the results of the diving survey carried out during the period from February to December, 1990, the fish distribution expanded as the days elapsed, and the body length of fish and the apparent quantity also increased.

In particular, the aggregation of *Trachrus japonicus, Apogon semilin eatus* and *Chromis rotatus notatus* was conspicuous, and these three kinds of fish were found in shoals in the area surrounding the artificial reef. Useful fish such as *Parapristipoma trilineatum, Pagrus major, Girella punctata, Epinephelus awoara,* etc., have now been confirmed to be present. Since there is no significant current on the west side of the artificial reef, and the topography is quite uniform, many kinds of fish are to be found such as *Girella punctata,Chromis rotatus notatus, Suezichthys gracillis,* etc., because the vicinity of the artificial reef was favorably affected by the Structure. On the east side, which is greatly affected by the natural reefs found there, many kinds of fish such as *Suezichthys gracillis, Thamnaconus modeatus, Stephanolepis cirrhifer, Oplegnathus fasciatus,* and *Trachurus japonicus* were gathered around the artificial reef and natural reefs.

Furthermore, regarding shore-grown organisms, the number of *Turbo cornutus* with a shell height of 70 mm or more and of *Haliotis discus* with a shell height of 90 mm or more, both found on and inside the artificial reef, were 0.07 pcs/m^2 and 0.29 pcs/m^2, respectively.

However, in December 1990, there were found to be 0.29 pcs/m^2 each of *Turbo cormitus* and *Haliotis discus,* thus indicating that the number of living *Haliotis discus* is tending to increase.

Biological Four Compartments Model

This study examines an predict method which first evaluated the changes in wave patterns, currents and other aspects of the physical marine environment, then attempts to clarify the impact these changes will have on biological production. If a regional environmental impact system relies totally on-side observations, there are limitations in scale.

Thus development of a predict method which incorporates a quantitative analysis-based 'structural model' of the coastal zone region is desirable (Administration Inspection Bureau, 1985).

We attempt here to construct a biological model and to consider the characteristics of the model (Kishi, et al., 1981).

This model is based largely upon Kishi's producer, PO_4-P as a limiting nutrient, zooplankton as a predator of chlorophyll-a and detritus as particles produced the mortality of plankton and by egestion. The dissolved detritus is not considered as a first step because its variation with time is very slow.

Phytoplankton: P

$$dP/dt = V_1(T,N) \cdot V_2(I(t)) \cdot P - \beta \cdot P - \alpha \cdot P - P/(P+D)g(P,D) \cdot Z \quad (1)$$

Zooplankton: Z

$$dZ/dT = g(P,D) \cdot Z - \gamma \cdot g(P,D) \cdot Z - \delta \cdot Z - \varepsilon \cdot Z \quad (2)$$

Detritus: D

$$dD/dt = \beta \cdot P + \alpha \cdot P + \delta \cdot Z - \phi \cdot D \quad (3)$$

Nutrient: N

$$dN/dt = -V_1(T,N) \cdot V_2(I(t)) \cdot P + \beta \cdot P + \phi \cdot D + \varepsilon \cdot Z \quad (4)$$

where the formation of Eqs. (1) to (4) are indicated in Table 1.

Discussions about Stability and Uniqueness

If the systems of biomass represented by Eqs. (1) to (4) have solutions, biomass will in time oscillate diurnally. The integrated value of each biomass during one day will not vary.

We replace such mean values of P, Z, D and N during one day with P', Z', D', and N', respectively, and P'+Z'+D'+N' = constant, and call such values the "steady state solutions." The steady state solutions will satisfy the following equations

$$\{V_1(T,N') \cdot V_2(I(t))dt - \beta - \alpha\} \cdot P' - g(P',D') \cdot Z = 0 \quad (5)$$

$$\{(1-\gamma) \cdot g(P',D') - \delta - \varepsilon\} \cdot Z' = 0 \quad (6)$$

$$\phi \cdot D' - \{V_1(T,N') \cdot V_2(I(t)) - \beta\} \cdot P' + \varepsilon \cdot Z' = 0 \quad (7)$$

$$P'+Z'+D'+N' = M = \text{const.} \quad (8)$$

we may conclude from Eqs. (5) to (8) that:

(i) The system is stable for any parameter values.

(ii) If P'+Z'+D'+N' is constant, then P', Z', D' and N' will be independent of the initial values and will take the fixed values.

(iii) If we can decide the value of P', Z', D' and N' based upon observations, the values of any there parameters can be decided (e.g., we solve Eqs. (1) to (4) numerically for two different initial values under the values of parameters shown in 4-3). Figure 5-a shows the time-dependent values of P, Z, D and N for the initial values; P=3.0, Z=7.54, D=0.374, N=0.05; these values are selected to be near values observed in large tank test in 1988. Figure 5-b shows the time-dependent values of P, Z, D and N for the initial values; P=0.374, Z=0.05, D=3.0, N=7.54.

Table 1. Formation of biological terms in the four compartments model

Growth of phytoplankton	$V_1(T,N) \cdot V_2(I(t)) \cdot P$ $V_1(T,N) = V_m \cdot N/(Ks + N)$ $V_2(I(t)) = a \cdot I \cdot \exp(1 - a \cdot I)$ $I = I(t)$ $= I_{opt} \cdot \sin^3(\pi/12)t \cdot \exp(-kd)$ (day time) $= 0$ (night time)
Extracellular release	$\beta \cdot P$
Grazing	$g(P,D) \cdot Z$ $g(P,D) = R_{max}(1 - \exp(-\lambda \cdot P + \lambda \cdot P^*))$ (if $P > P^*$) $g(P,D) = 0$ (if $P < P^*$)
Natural death of P	$\alpha \cdot P$
Egestion of Z	$\gamma \cdot g(P,D) \cdot Z$
Natural death of Z	$\delta \cdot Z$
Bacterial decomposition of D	$\phi \cdot D$
Urine of Z	$\epsilon \cdot Z$

where V_m : maximal photosynthetic rate
Ks : half saturation constant
I_{opt} : maxiaml light intensity on sea surface
a : constant in light-photosynthetic curve
k : light extinction coefficient
d : water depth
β : extracellular release rate
R_{max} : maximal grazing rate
λ : constant in grazing curve
P^* : threshold of P in grazing
α : natural death rate of P
γ : excretion rate of Z
δ : natural death rate of Z
ϕ : bacterial decomposition rate of detritus
ϵ : urine by Z

These two time-dependent features of four biomass systems show that, for the same parameter, the solutions of this system approach to the same points for different initial values.

This fact shows that the solutions of this system are stable.

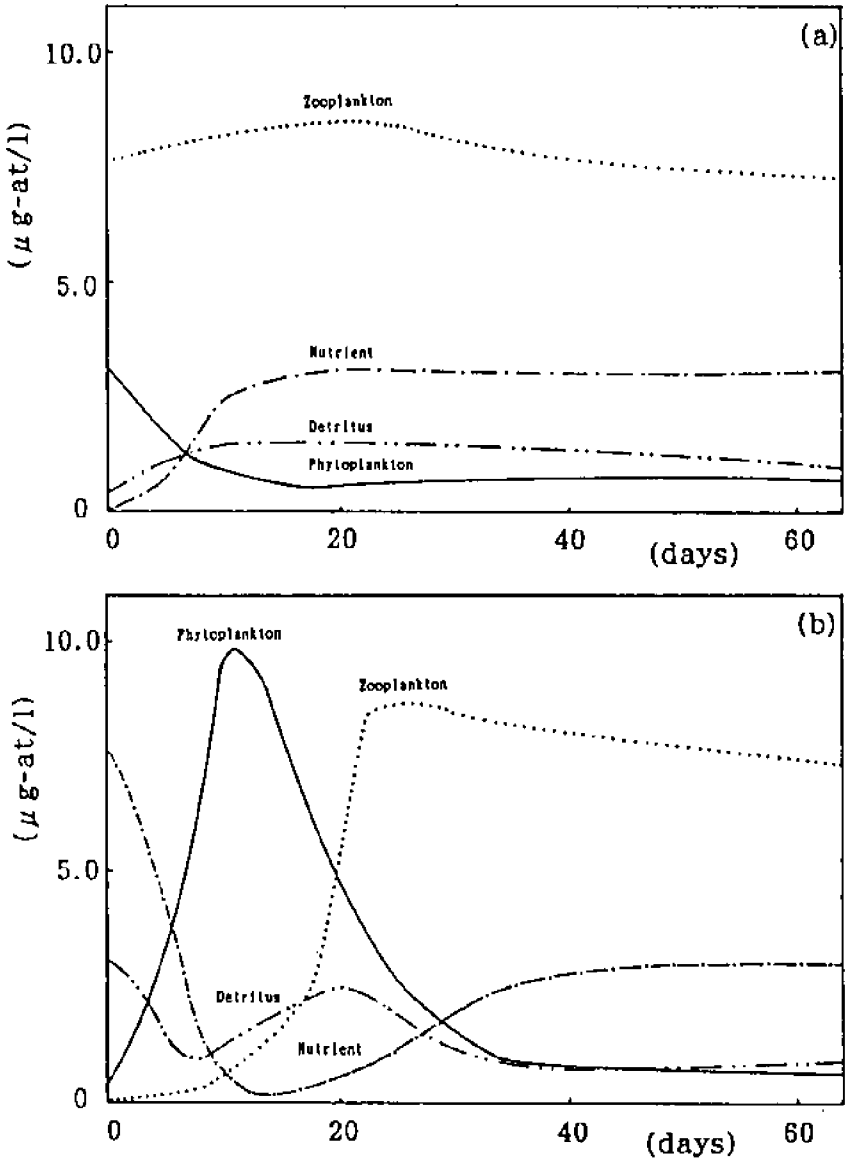

Figure 5. Time-dependent features of P, Z, D, and N (integrated with t in Eqs. (1) to (4)). Initial values are different in (a) and (b), but in the time solutions they reach the same values.

FUTURE ACTION TO BE TAKEN

As diving investigation on the structure was repeated, it has been confirmed that fish and shellfish are aggregating to the structure to the same degree as on the natural reef on the east side, which has already become good fishing ground.

From this, it is expected that if, in the future, this structure is provided with a feeding environment and the biological effects improve, the function of the structure as a breeding ground and the awareness and feeling towards the "Fisheries Controlled for Resource Management" by fishermen at Futaoi Island will be enhanced, with a positive attitude being developed.

Regarding the future schedule, the authors will undertake investigation and examination into the following:

1) Continuous investigation into changes in awareness of fishermen by the formation of a fishing ground.

2) Continuous investigation into the biological effects due to installation of the structure.

3) Continuous measurement of growth rate of seaweed presently introduced on the structure, and investigation into activity characteristics of infant abalone by stocking abalone seeds.

4) Examination of selectivity of stones as living areas for seaweed and abalone.

5) Examination of the relation between the light quantity and the growth quantity, and the feeding environment formation method.

6) Examination of the possibility of realizing marine stock farming through fishing ground formation by dumping natural stones into the marine area.

7) Examination of the environmental predict method of the regional marine taking into consideration biological productivity.

REFERENCES

Administration Inspection Bureau, General Affairs Agency, ed. 1985. Present condition and problems of fishing promotion. Printing Office, Ministry of Finance.

Hydrographic Dept. of Maritime Safety Agency. 1985. Basic maps and investigation report for coastal sea areas. March.

Kishi, M.J., K. Nakata, and K. Ishikawa. 1981. Sensitivity analysis of a coastal marine ecosystem. *J. Oceanographical Soc. of Japan*. **37**:120-134.

Ocean Fisheries Experimental Station of Yamaguchi Pref. 1988. Operation report for fiscal 1987. March.

Regional Fishery Plan for Futaoi Island, Shimonoseki City, Yamaguchi Prefecture. 1985. March.

Sakuta, M., N. Takagi, and Y. Suenaga. 1987. Investigation of biological aggregation conditions on multipurpose artificial reef. In: Proc. of Symp. of the Arch. Inst. of Japan. October.

Sugawara, R., Y. Takagi, A. Kuroyanagi, and M. Sakuta. 1989. Fundamental research concerning effective utilization of coastal areas.

REDUCING THE RISK OF PEARL OYSTER DISEASES IN POLYNESIAN LAGOONS

Neil Anthony Sims
Black Pearls, Inc.
Kona, Hawaii, U.S.A.

ABSTRACT

Pearl oyster diseases have become endemic in most major pearl culture areas. Poor oyster health and farm mortalities have profound impacts on the profitability of individual farms, result in increased pressure on already depleted natural stocks, and cause instabilities in the pearl market. This paper discusses management approaches to disease prevention in new pearl culture areas in the Pacific Islands.

The etiology of pearl oyster diseases is often poorly understood, and the available literature is meager. Commensal organisms, parasites, pathogens and secondary infections are difficult to distinguish in bivalves, and the taxa associated with pearl oyster diseases in different culture areas are diverse. It is therefore inappropriate to base farm size limits on estimates of the original stock abundance, phytoplankton production and oyster filtration rates, or lagoon water turnover, particularly where no disease has yet been identified. Histories of disease patterns, farming practices and farmed stock numbers in different lagoons could provide useful guidelines, but such information is carefully protected.

Management must be based on the understanding that there is a continuum of increasing disease risk with increasing farm numbers and densities. The industry itself must determine its own acceptable limits on the number of farms in any enclosed body of water, the number of oysters on farms, spacing and cleaning regimens, and restrictions on stock transfers. The short-term rewards of higher production must be balanced against the increased risk of disease. No ecologically determined limit can provide any assurances.

INTRODUCTION

The culturing of pearls is often described as "more art than science." Indeed, outside of a solid body of Japanese and Indian work on the Akoya oyster (*Pinctada fucata*), there has been little publicly-funded research into the techniques of growing pearl oysters and culturing pearls. Pearl farmers perhaps prefer to cultivate the mystique of the trade, but this condemns much research to overly-protective proprietary concerns.

In the last few decades, however, independent pearl culture has become established throughout S.E. Asia, Australia and the atolls of the Pacific (Table 1). Particularly in the small island countries of Polynesia and Micronesia, pearl culture developments have the potential for dramatic improvements to rural economies, previously reliant on copra, pearl shell and fisheries resources, and the vagaries of these commodity markets. Pearl culture brings lucrative returns, and wider socio-economic benefits: reversing rural-urban drift and revitalising atoll economies by providing stable employment and demand for support industries. The best example is in French Polynesia, where 2,300 people are directly employed in an industry worth US$41 million

Table 1. Pearl culture areas throughout the world

AREA	SPECIES CULTURED	EXPORTS[1]
JAPAN	*P. f. martensii*	Domestic production 1988 : $476 million[2]
OKINAWA	*P. margaritifera* *Pteria penguin* *P. maxima*	One farm only. Hatchery-bred. Hatchery-bred.
FRENCH POLYNESIA	*P. margaritifera*	$41 million in 1989
N.W. AUSTRALIA	*P. maxima*	$71 million in 1989
W. AUSTRALIA (Shark Bay)	*P. albina albina*	Four farms.
N.E. AUSTRALIA (Gt Barrier Rf)	*P. margaritifera* *P. radiata*	Several farms. Experimental.
CHINA	*P. f. martensii*	$8 million in 1988
TAIWAN	*P. f. martensii*	$2 million in 1988
KOREA	*P. f. martensii*	$0.3 million in 1988
INDONESIA	*P. maxima*	$12 million in 1989
PHILIPPINES	*P. maxima*	$4 million in 1989
MALAYSIA	*P. maxima*	$1 million in 1988
THAILAND	*P. maxima*	$1 million in 1988
BURMA	*P. maxima*	$0.6 million in 1989
INDIA	*P. fucata*	$3 million in 1989
COOK ISLANDS	*P. margaritifera*	Manihiki. Others developing.
PALAU	*P. maxima?*	One farm.
FIJI	*P. margaritifera*	One farm only.
MEXICO (Pacific coast)	*P. margaritifera*	Experimental. Now defunct?
SUDAN	*P. margaritifera*	Fluctuates. For shell only.

NOTES : (1) U.S. dollar exports to Japan. Source : Pearl Oyster Information Bulletin #2, p. 8.

(2) May include re-exports and processed products. Source : Gervis and Sims, in press.

in exports per annum (1989 data, Table 1; Coeroli, 1991). Black pearl culture has also become rapidly established in the Cook Islands, where the first harvest occurred only in 1989, yet the current value is around NZ$6 million (US$4 million).

Other Pacific Island governments and development agencies are keen to emulate these successes in French Polynesia and the Cook Islands. Pilot programs have recently begun in the Marshall Islands, Federated States of Micronesia, Tonga, the Solomon Islands, Kiribati, and Tuvalu, assessing pearl oyster resources, and intiating spat-collection and grow-out trials. While wild pearl oyster stocks are often scarce, research advances with pearl oyster hatchery technology offer scope for expansion of pearl culture to lagoons with depleted stocks, or none at all.

This bright prospectus is somewhat dimmed by the Damoclean Sword of pearl oyster diseases. These have, at some time or another, decimated pearl farm stocks in almost every established pearl culture area in the world (Table 2). Mass mortalities among pearl farms usually have unknown etiology, but invariably result in poor quality pearls, directly reducing farm profitability, and damaging the market price and the industry's reputation. Greater pressures are placed on wild stocks to replenish the farm losses, and oyster transfers from one region to another become increasingly risky. Mortalities can also spread to wild pearl oysters and other bivalves (*P. maculata*, *Tridacna maxima*, *Arca ventricosa*, and *Spondylus varius* (Coeroli, 1983; M. Coeroli, pers. comm.), decimating the pool of natural broodstocks and subsistence resources.

The threat of pearl oyster diseases makes pearl culture less attractive to private investors, governments and aid agencies, adding an air of uncertainty to what is otherwise a stable, lucrative development option. The highly protective nature of the industry means that technology and capital assistance programs are essential for fostering locally-owned and operated farms, with their broader-based benefits. However, governments and international aid donors are wary of the economic dislocation and political costs of association with boom-and-bust development. Prevention and control of pearl oyster diseases will remove these uncertainties, providing for the long-term growth of pearl culture across the Pacific, and ensuring the economic viability of otherwise-impoverished atolls.

REVIEW

Pearl Oyster Diseases: Causes

Earliest records of pearl oyster disease were from wild *P. fucata* stocks in Ceylon, where around 10% were infected with an unidentified "yellow disease" (Herdman, 1903). Most pearl culture industries have at some time suffered from persistent, heavy mortalities among farmed stocks. Disease and pollution problems have plagued the Japanese industry since 1962 (Hollyer, 1984), with "very high mortalities" and "low quality pearls" (George, 1978, p 41). North-Western Australia, and French Polynesia also suffer farm mortalities, with low retention rates and poor quality pearls.

Pollution and over-production are usually blamed first. Poor quality Japanese pearls are sometimes attributed to the continual farming of the same area. The depletion of nutrients or essential trace metals from the water or substrate has been suggested (Matsui, 1958), but not proven. Pearl farm management in Japan therefore moves spat, juveniles and seeded oysters between several different locations (Matsuda, 1979).

Table 2. Reports of "pearl oyster disease"

AREA	SPECIES	YEAR	NOTES
JAPAN	*martensii*	1962-present	Undescribed disease and pollution problems (Hollyer, 1984; George, 1978)
			Nutrient or trace metal depletion (Matsui, 1958)
FRENCH POLYNESIA	*margaritifera*	1984-present	Mortalities up to 82% in some lagoons (Cabral, 1989)
			Due to detrital build-up on farms, and over-crowding? (Reed, 1985; Low, 1986)
			Vibrio isolated, not proven pathogenic (Parc, 1980, in Coerloi, 1983)
			Protozoan parasite in intestinal tract (unconfirmed reports)
			Slow growth indicates psysiological weakening? (Lachhar-Cheffort and Intes, 1989)
			Abnormal lysosomes due to stresses (Grizel, 1986, in Cabral, 1989)
			Due to cyclone-induced changes? (Anon., 1987)
			Due to increase in water temperatures? (Anon, 1987; Porter, 1991)
			Spread to wild *P. margaritifera, P. maculata, Tridacna maxima,* etc. (Coeroli, pers. comm.)
AUSTRALIA	*maxima*	1960's-present	Due to oil spills? (Yamashita, 1986)
			"Protistan parasites" in digestive gland (Wolf and Sprague, 1978) actually lysosomes (Pass and Perkins, 1985)
			Virus-like particles in digestive gland cells (Pass, et al., 1988)
			Bacteria: *V. harveyi,* others - primary or secondary pathogen? (Dybdahl and Pass, 1985; Pass, et al., 1987)
SUDAN	*margaritifera*	1910-20's	Detrital build-up on farms, overcrowding (Crossland, 1957).
		1980's	Sperhical bodies in the digestive gland epithelia (Nasr, 1982)
SRI LANKA	*fucata.*	1900's	Unidentified "yellow disease" (Herdman, 1903)
MEXICO (Pacific coast)	*margaritifera*	1960-70's	No details

Build-up of detritus under farms (Crossland, 1957; Reed, 1985; Lowe, 1986) has also been associated with epidemics. Crossland (1957, p 124) reported heavy mortalities of cultured *P. margaritifera* in the Red Sea due to overcrowding, causing "poisoning from excreta or lack of oxygen". Oil spills were blamed for the extensive mortalities on Australian pearl farms from the late 1960's onwards (Yamashita, 1986; Kearney, 1976, in Uwate, et al., 1984), only because no likely pathogen or parasite was identifiable (Wolf and Sprague, 1978). Hynd (unpubl., in Potter, 1983) surmised that physiological stresses are contributing factors, but rarely causes of diseases.

Disease problems are often associated with bacteria or protistans, but these could be either pathogens, commensals or saprophytes. Bacteria build-ups in recirculating tanks on transfer vessels, and on oyster holding grounds were associated with diseases in Western Australia (Dybdahl and Pass, 1985; Pass, et al., 1987). Three bacteria isolated from moribund or dead *P. maxima* (*Vibrio harveyi*, *V. alginolyticus* and *Pseudomonas putrefaciens*) were shown to be pathogenic by experimental inoculations, but their actual role in the mortalities remains unclear (Dybdahl and Pass, 1985).

Anomalous structures in histological preparations are difficult to isolate and culture, and symptoms are usually non-specific. The symptoms among infected *P. margaritifera* in the Red Sea were similar to other epidemics, with shrinking of the mantle and cessation of feeding (Nasr, 1982). Spherical bodies in the digestive gland epithelia were suggested as the causative agent. However, the "extensive host tissue damage" from "protistan parasites" in the digestive gland of *P. maxima* (Wolf and Sprague, 1978, p 263) was considered by Pass and Perkins (1985) to be necrotic autolysis, and a symptom, rather than a cause, of the mortalities. The common protistan parasite, *Perkinsus spp*, has been found in *P. margaritifera* and *P. sugillata* on the Great Barrier Reef, but these were from wild stock samples, with no symptoms (Goggin and Lester, 1987).

Atrophy of digestive gland cells may be due to reduced food intake in diseased pearl oysters, as recently dead or dying pearl oysters undergo autolysis (ibid). Pass, et al., (1988) described inclusion bodies containing smaller virus-like particles in the enlarged nuclei of digestive gland cells of both normal and diseased *P. maxima*. The structures were considered lesionous, but it was not possible "to assign any pathological significance to them" (ibid, p 166).

In French Polynesia, mortality rates from seeding to harvest have reached as high as 82% in some lagoons (Cabral, 1989). The problem has proven transferrable between lagoons (Reed, 1985), suggesting some infectious agent. *Vibrio alginolyticus* and *Beneckea vulnifica*, were isolated from *P. margaritifera* from Rikitea lagoon, French Polynesia, but no proof of pathogenicity was found (Parc, 1980, in Coerloi, 1983). There are also unconfirmed reports of a protozoan parasite found in the intestinal tract of diseased oysters.

Gradual physiological weakening of pearl oysters is inferred from evidence of decreased growth during the time of heaviest mortalities in French Polynesia (Lachhar-Cheffort and Intes, 1989). Again, it was not clear, however, whether this was a cause or a symptom. Grizel (1986, in Cabral, 1989) reported abnormal lysosomal activity due to physiological stresses. Others suggest that the rash of cyclones in French Polynesia during 1983 (Anon., 1987) or a slight increase in water temperatures (ibid; Porter, 1991) may be associated with the mortalities. However, Cabral (1989, p. 217) asserts that "no satisfactory explanation has been found," and the best response is "management of cultured areas" and "improvement of cultivation techniques" (ibid, p. 223).

Losses on farms in French Polynesia have been improved by better handling and farming practices, but once the disease becomes endemic, it is difficult to eradicate. Excessive mortalities still occur on farms in French Polynesia, and over the last few years have spread to wild stocks of *P. margaritifera*, and other bivalves (e.g. the pipi pearl oyster, *P. maculata*, the small giant clam, *Tridacna maxima*, and *Spondyllus* sp: M. Coeroli, pers. comm.).

The pathology of most pearl oyster diseases is still little understood. Nevertheless, the geographical range of disease outbreaks and the taxonomic diversity of suspected pathogens underscores the problem for management of pearl culture lagoons - you never know what will hit you. How then, can you even begin to prevent its outbreak?

Disease Controls

A prima facie association of "poor farming practices" with disease outbreaks is based on the assumption that stressed or weakened pearl oysters are more susceptible to infection. Overcrowding on a farm, growing oysters close to the bottom or where circulation is poor, inadequate cleaning of oysters or dumping of tailings from cleaning or pearl slurry back into farm waters are all now widely recognised as increasing the risk of an outbreak of disease, or increasing the resulting mortalities if a disease is already endemic. Management can therefore minimise the chances of disease outbreak or transmission from area to area by regulating farming practices and pearl oyster transfers.

Farming regulations which could be, or are already applied include :

(i) confining farming (or large farms) to areas of adequate circulation or flushing;
(ii) rotation of intensively farmed areas, to allow them to lie "fallow" for a period;
(iii) restricting the discharge of chemical pollutants into farming waters;
(iv) farming on long-lines or rafts suspended well above the substrate;
(v) ensuring adequate spacing of oysters on farm platforms or lines;
(vi) ensuring regular cleaning of oysters to minimise stresses from fouling;
(vii) restricting the build-up of organic material beneath seeding houses or cleaning platforms; and
(viii) limiting the total number of oysters held on a farm or within a lagoon.

This last measure has proven the most problematic. The means of determining the quota level is critical to the entire management debate. Several methods have been used to estimate allowable quotas in Manihiki lagoon, Cook Islands, on the basis of simple ecological models. These are examined below.

Modelling Pathogen Outbreaks

Prevention and control of an aquaculture disease is largely based on the ecological characteristics of the parasite or pathogen. The causative organism is first identified, and its abundance correlated with various environmental factors or with different farming techniques. However, even monitoring of bacteria levels has proven difficult enough in the marine environment, without attempting to predict future levels or responses to ecosystem changes (Farley, 1988; Rodrick, et al., 1988; Venkateswaran, et al., 1989).

The models of pathogen prevention proposed for the Cook Islands have been based on estimates of primary productivity, lagoon and ocean water exchange rates, and original wild stock abundance (Table 3). The quota is therefore based on prediction of the critical load point imposed on the lagoon ecosystem by pearl farming. The underlying assumption is that at some certain point, the oysters become stressed and susceptible to disease. There has been little consideration of the relative loadings of different farming methods and different ecological capacities, and no real consideration of the actual cause of the disease outbreaks. If the etiology is unknown it is clearly premature to extrapolate from a few knowns to set a quota. You cannot prevent the unpredictable.

Intes (unpubl.) and Intes, et al., (1990) suggest that lagoon phytoplankton are depleted by farmed *P. margaritifera* in French Polynesia, causing feeding stresses and subsequent mortalities. The concentration of farm stocks in the upper 10 m of Takapoto lagoon increases demands on primary production within this stratum by an estimated 1000% (ibid). However, *P. margaritifera* naturally occurs in greatest abundance in this shallowest stratum, and the increasing pearl oyster abundance with depth in most lagoons is only due to fishing pressure (Sims, 1990 b). Original abundances of pearl oysters in the shallowest strata could therefore have been much higher than current levels of cultured pearl oysters.

Galenon and Coeroli (1991) extrapolate from the pumping rate of termperate-water edible oysters and an estimate of the turnover rate of Manihiki lagoon water. It is presumed that lagoon water can be pumped through a pearl oyster only once before phytoplankton depletion, metabolic wastes or bacterial levels become unsafe. If based on primary production limits, this implies 100% filtration efficiency and no phytoplankton regeneration within the lagoon. If metabolic wastes are the problem, the lagoon's capacity to support nutrient loading needs to be assessed. If bacterial or other pathogen levels are critical limits, the specific microbes need to be identified and monitored.

However, even models of biomass production for edible oyster and mussel culture are still only tentatively proposed (Héral, et al., 1984; Dame, 1990; Carver and Mallet, 1990; Fréchette, 1991; Héral, 1991; Grant, 1992). In these temperate environments, where total primary production and conversion ratios are available, and the food chains are relatively simple, it is still considered "premature to use ... models for predicting the ... trophic capacities of ecosystems" (Héral, 1991, p. 61). In tropical lagoon ecosystems, primary production and energetic pathways are both highly complex and poorly described.

Reports from French Polynesia also suggest that disease problems are greatest in the more enclosed lagoons. Less turnover of lagoon water in enclosed lagoons should allow greater nutrient build-up and greater primary production. It would therefore appear that primary production is not the principal limiting factor.

Similarly, Goldman and Goldman's (1991) use of a wild stock to farmed stock ratio of 2:1 has no ecological basis. Extrapolating from this theory, if the wild stock is fished to extinction it follows that all farming should then be halted. If the wild stock proliferates, however, there are supposedly then no real limits to the number of oysters which could be farmed.

The reliance on stock estimates in this model is also unrealistic. Due to the patchy distribution of pearl oysters, the confidence limits around stock estimates are inherently wide, with 95% confidence limits sometimes three or more times the mean densities (Sims, 1990b).

Table 3. Models of sustainable pearl oyster numbers in Polynesian lagoons

AUTHORS	YEAR	MODEL
Intes, et al., and Intes (unpublished)	1989	Estimated rate of phytoplankton filtration by oysters, and primary production extrapolated from New Caledonia. Concentration of oysters in upper 10 m of water column considered overloading (by 1000‰). **... but** primary production will increase with greater nutrient loading by farmed oysters. Also, oysters are naturally at greatest densities in upper 10 m, but fished out there.
Goldman and Goldman	1991	Estimated wild stocks, and applied 2:1 ratio of wild to farmed shell. **... but** stock assessment methods are inherently inaccurate. This model also implies that if wild stock regenerates, then farming can continue to expand.
Galenon and Coeroli	1991	Estimated lagoon water turnover time (8 years) and pearl oyster filtration rate. **... but** filtration estimates based on edible oysters in temperate waters, assumed oysters only filter water once, and no regeneration of phytoplankton. Also did not distinguish between nutritional, metabolic and pathogenic stresses.

DISCUSSION

Preventative management of pearl oyster diseases is not feasible without improving the knowledge of the causative organisms: their identity, and their epidemiology. The current paucity of knowledge is due to two main factors :

(i) bivalve pathology is still a developing science, with disease-causing organisms identified with difficulty among even the most-studied oysters and mussels; and

(ii) pearl farmers are very reluctant to share information about mortality rates on their farms, wanting to prevent any stigma of disease associated with their pearls.

The first problem could be partly addressed by an increased commitment from research organisations and development agencies. Increased funding for research into pearl oyster pathology would be clearly cost-effective, given the opportunity-cost for under-farming a lagoon. The revenues lost are in direct proportion to how much any management model underestimates the sustainable farm quota. In French Polynesia, for example, if the quota underestimates the sustainable level in all lagoons by a factor of two times the present production, "lost" revenues are in the order of US$82 million per year.

The most important advances in pearl oyster pathology, however, require a recognition of the mutual benefits to be gained from greater sharing of information on diseases. There is a particularly strong incentive for French Polynesian farmers and government agencies to assist other Pacific atoll pearl producers in minimising disease problems. International jewellery trade authorities recently bestowed the official trade name "Tahitian black pearl" on all *P. margaritifera* pearls (Coeroli, 1991). This means that poor quality black pearls produced from diseased areas in other Pacific islands will reflect badly on the French Polynesian product. With the small, lucrative market niche for black pearls, instabilities due to uncertain quality will be to the detriment of all.

Cabral (1989) and Lachhar-Cheffort and Intes (1989) offer some data on mortalities on co-op farms, and among wild stocks. However, a more detailed account is needed of mortalities on all farms in all French Polynesian lagoons. Such an account should specifically include, for each lagoon:

(i) the lagoon size, depth, water turnover rate, and other ecological characteristics,

(ii) estimates of the numbers of farmed pearl oysters, methods of farming employed, and wild stock levels for each year,

(iii) description or data of the epidemiology of the disease, where and when the first outbreaks occurred, what percentage losses were sustained, and when the mortalities began to abate.

Only with this information would it be possible to begin to guess at the numbers and densities at which farmed oysters can be supported in another lagoon before becoming vulnerable to unknown or undescribed pathogens. Management of pearl culture in other developing areas would then have a real basis by which to begin to estimate allowable farm quotas.

There is also a need for management in developing pearl culture areas to reassess their goals. Management efforts in the Cook Islands to date have emphasised an extremely conservative approach, with the goal of ensuring that no pearl oyster diseases

become established (Sims, 1990a, 1991; Goldman and Goldman, 1991; Galenon and Coeroli, 1991). This is an unrealistic expectation.

There is a continuum of increasing disease risk with increasing farm numbers and densities. The only guaranteed assurance of no pearl oyster diseases is if there is no pearl farming. Management must explicitly recognise that there is always a probability of disease outbreaks, and this must be impressed upon the local enforcement authorities and the farmers. Although most pearl farmers in Manihiki recognise the value of setting a quota for farmed oysters in their lagoon, the corollary of individual farm quotas is not well supported (Sims, 1990a). Farmers must decide for themselves the level of risk with which they wish to live.

CONCLUSIONS

The issue of pearl oyster disease prevention is of critical importance to the economic development of many Pacific atolls. There is a need for further research, but there is a greater need for closer co-operation between all pearl producers. With the potential value of this industry to the Pacific atolls, the ultimate returns to all are unquestionable.

ACKNOWLEDGEMENTS

Dr. Dale Sarver, Moshe Rappaport and Kate Sims provided useful comments on this manuscript.

REFERENCES

Anonymous. 1987. Etat des connaissances sur les mortalities anormales de nacres. E.V.A.A.M. Tahiti, French Polynesia.

Cabral, P. 1989. Some aspects of the abnormal mortalities of the pearl oysters, *Pinctada margaritifera* L. in the Tuamotu Archipelago (French Polynesia). Advances in Tropical Aquaculture: Tahiti. Feb 20-March 4. AQUACOP. IFREMER. *Actes de Colloque.* **9**:217-226.

Carver, C.E.A., and A.L. Mallet. 1990. Estimating the carrying capacity of a coastal inlet for mussel culture. *Aquaculture.* **88**:39-53.

Coeroli, M. 1983. *Pinctada margaritifera*. In: Milieu lagonaire. Etat des connaissances., Peche Document No. 7, pp. 1-20. E.V.A.A.M., Service de la Mer. Polynesie Francaise.

Coeroli, M. 1991. Pearl production and marketing in French Polynesia. S.P.C. Pearl Oyster Information Bulletin. **#3**: pp. 2-3.

Crossland, C. 1957. The cultivation of the mother-of-pearl oyster in the Red Sea. *Aust. J. Mar. Freshw. Res.* **8**:3-49.

Dame, R.F. 1990. Ecosystem dynamics and bivalve culture. Abstracts, 1990 Annual Meeting, National Shellfisheries Association. Williamsburg, Virginia.

Fréchette, M.M. 1991. Carrying capacity and density dépendence (Workshop Report). ICES Mar. Sci. Symp. **192**:78.

Dybdahl, R., and D.A. Pass. 1985. An investigation of mortality of the pearl oyster, *Pinctada maxima*, in Western Australia. Fisheries Department of Western Australia Report No. 71. Fisheries Department. Perth.

Farley, C.A. 1988. A computerized coding system for organs, tissues, lesions and parasites of bivalve molluscs and its application in pollution monitoring with *Mytilus edulis*. *Marine Environmental Research*. **24**:243-249.

Galenon, P., and M. Coeroli. 1991. Mission report: investigation on pearl farming in Manihiki (Cook Islands) 5-12 June. EVAAM, Ministere de la Mer. Tahiti, French Polynesia.

George, C.D. 1978. The Pearl. A report to the Government of Papua New Guinea. The Food and Agriculture Organisation of the United Nations, and the Asian Development Bank. Samarai, Milne Bay Province, Papua New Guinea.

Goggin, C.L., and R.J.G. Lester. 1987. Occurrence of *Perkinsus* species (Protozoa, Apicomplexa) in bivalves from the Great Barrier Reef. *Dis. Aquat. Org*, **3**:113-117.

Goldman, B. and E. Goldman. 1991. Pearl culture industry ecological considerations. Report to the Minister of Marine resources following a visit to Manihiki Lagoon in January. (Unpublished Report).

Grant, J. 1991. Modelling carrying capacity: simplifying a complex situation. *Out of the Shell*. **2(2)**:4-5.

Héral, M. 1991. Approches de la capacite trophique des ecosystemes conchylicoles: synthese bibliographique. *ICES Mar. Sci. Symp*, **192**:48-62.

Héral, M., J.-M. Deslous-Paoli, D. Razet, and J. Prou. 1984. Essai de mise en evidence *in situ* de parametres biotiques et abiotiques de l'eau et de l'interface eau-sediment interventant dans la produciton de l'huitre. *Crassostrea gigas*. *Oceanis*. **10 (4)**:465-475.

Herdman, W.A. 1903. Report to the Government of Ceylon on the pearl oyster fisheries of the Gulf of Manaar. Part I. The Royal Society, London.

Hollyer, J. 1984. Pearls - jewels of the sea. *Infofish Marketing Digest*. **5**:32-34.

Intes, A. (unpubl.). 1988. Pearl farming responsible for its own death? Presentation to VIth Int. Coral Reef Cong. Townsville. August.

Intes, A., C. Charpy-Roubaud, L. Charpy, L. Lemasson, and E. Morize. 1990. Les lagons d'atolls en Polynesie Francaise: Bilan des travaux du program "ATOLL" (1981-1987). III. L'atoll de Takapoto. Papeete. ORSTOM. pp. 111-123

Lachhar-Cheffort, N., and A. Intes. 1989. Les caracteristiques biologiques du stock naturel d'huitres perlieres, (*Pinctada margaritifera*. L. 1758) dans l'atoll de Takapoto. Ministere de la Rechereche Scientifique, Rapport Final des Journels de la Recherche, pp. 55-63.

Lowe, J. 1986. Report on visit to Ahe (French Polynesia) in December, 1986.

Matsuda, Y. 1979. Factors limiting the development of aquaculture: A Japanese experience. Woods Hole Oceanographic Institute - 79-47.

Matsui, Y. 1958. Aspects of the environment of pearl-culture grounds and the problems of hybridization in the genus *Pinctada*. In: Perspectives in Marine Biology, ed. A.A. Buzzati-Traverso. U. Calif. Press, Berkeley and L.A. pp. 519-531.

Nasr, D.H. 1982. Observations on the mortality of the pearl oyster, *Pinctada margaritifera*, in Dongonab Bay, Red Sea. *Aquaculture*. **28**:271-281.

Pass, D.A., and F.P. Perkins. 1985. Protistan parasites or residual bodies in *Pinctada maxima*. *J. Invertebr. Pathol.* **46**(**2**):200-201.

Pass, D.A., F.P. Perkins, and R. Dybdahl. 1988. Viruslike particles in the digestive gland of the pearl oyster *Pinctada maxima*. *J. Invertebr. Pathol.* **51** (**2**):166-167.

Pass, D.A., R. Dybdahl, and M.M. Mannion. 1987. Investigations into the causes of mortality of the pearl oyster, *Pinctada maxima* (Jameson), in Western Australia. *Aquaculture*. **65**:149-169.

Porter, B. 1991. The black pearl connection. *Connoisseur*. April 1991:120 - 126,157.

Potter, M. 1984. Mollusc culture in Queensland. In: The Potential of Aquaculture in Queensland, eds. B.R. Pollockm and R.H. Quinn, pp. 47-55. Conf. Workshop Ser. Dep. Primary Ind. Fish. Res. Branch, Dep. Primary Ind., Brisbane, Qld, Australia.

Reed, W. 1985. Brief report on prospects for pearl farm at Ahe: Ste Perle du Pacifique Sud. ms.

Rodrick, G.E., K.R. Schneider, and F.J. Sierra. 1988. Abstracts. 1988 Annual Meeting, National Shellfisheries Associatio., New Orleans, Louisiana. p. 200.

Sims, N.A. 1990a. Discussing and drafting a National Pearl Oyster Fisheries Management Plan. Report to the Cook Islands Government and U.S.A.I.D. (U.S.A.I.D.: Suva.)

Sims, N.A. 1990b. The black-lip pearl oyster, *P. margaritifera*, in the Cook Islands. M.S. thesis. University of New South Wales.

Sims, N.A. 1991. A study on the cultured black pearl industry of the Cook Islands. A report to the Australian International Development Assistance Bureau, and the government of the Cook Islands. November.

Tenore, K.R., CJ. orral, N. Gonzalez, and N. Lopez-Jamar. 1985. Effects of intense mussel culture on food chain patterns and production in coastal Galacia, N.W. Spain. In: Proc. Siuec (1982: Nov. 21 - 27: Rio Grande, RS, Brazil) Vol. I, p. 321-328.

Uwate, K.R., P. Kunatuba, B. Raobati, and C. Tenakanai. 1984. A review of aquaculture activities in the Pacific Islands region. Pacific Islands Development Programme, East-West Center. Honolulu.

Venkateswaran, K., H. Nakano, T. Okabe, K. Takayama, O. Matsuda, and H. Hashimoto. 1989. Occurrence and distribution of *Vibrio* spp., *Listonella* spp., and *Clostridium botulinim* in the Seto Inland Sea of Japan. *Applied and Environmental Microbiology*. March:559-567.

Wolf, P.H., and V. Sprague. 1978. An unidentified protistan parasite of the pearl oyster *Pinctada maxima* in tropical Australia. *J. Invertebr. Pathol.* 31 (2):262-263.

Yamashita, S. 1986. The Torres Strait pearling industry. In: Torres Strait Fisheries Seminar, eds. A.K. Haines, G.C. Williams, and C. Coatespp. 118-119. Port Moresby, February, 1985, Australian Government Publishing Service, Canberra.

DESIGN OF A TURNING CLB AND PLANNING FOR A SMALL SCALE MINING TEST

Yoshio Masuda
Japan Resources Association
Yokusuka, Japan

Michael J. Cruickshank
University of Hawaii
Honolulu, Hawaii, U.S.A

James A. Abernathy
Capital Improvement Projects Administration
Majuro, Republic of the Marshall Islands

ABSTRACT

Recently the Government of the Republic of the Marshall Islands (RMI) applied to the Government of Japan for technical cooperation assistance to test the feasibility of cobalt crust mining using the Continuous Line Bucket (CLB) system. In preparation, components of the CLB system were designed and tested to scale including those for the ball roller parallel drive, bucket guidance and dumping, and controlling the bucket path during turning of the mining vessel. Using these test results a small scale CLB of 40 t/d capacity has been designed to test the feasibility of the Turning CLB system for crust mining on a commercial scale. It is suggested that if the Turning CLB system is suitable for mining deep seabed minerals such as crusts and nodules it will also be suitable for mining shallow water deposits such as placers and sands.

VARIATIONS IN MINING METHODS TESTED

The three principal methods originally proposed and tested for deep seabed mining of manganese nodules were a two or three phase hydraulic lift with a passive or active miner, an autonomous mining vehicle to shuttle between the seabed and the surface platform, and a continuous line bucket (CLB) system operating with a continuous loop of drag buckets attached to a flexible line. The hydraulic system has been most widely tested and is highly rated for production operations based on large economies of scale; the shuttle system is highly sophisticated but has not been sufficiently developed to test in an operating mode; the CLB system employs the least sophisticated technology and because of its simplicity, adaptability, and low cost has been proposed for the mining of high-cobalt crust at moderate production rates in the Republic of the Marshall Islands.

The CLB system consists essentially of a long endless rope loop suspended from a surface vessel to the seabed and to which are attached standard drag dredging buckets at regular intervals. Each bucket moves across the seabed at a rate, and for a period of time, determined by a combination of the rope speed, the rope slack on the bottom, and the speed and direction of the vessel from which the rotating loop is suspended. The buckets full of seabed material are continuously raised to the surface, emptied on board the vessel and returned to the seabed on the downward passage of the rope. Production rate is determined by the rope speed and the spacing of the buckets on the line.

This system has been successfully tested at sea in four different configurations:

Original CLB: The original system separated the upward line from the downward line by the ship's length, suspending them from the bow and stern of the vessel, which was then caused to move sideways by thrusters or by drifting broadside to the prevailing current. Tests were carried out off Tahiti in 1970 from the 2,500 ton Chiyoda-Maru No. 2, and off Hawaii in 1972 from the 16,000 ton Kyokoyou-Maru No. 2.

Two Ship CLB: In this case the separation of the ropes was adjusted by suspending the loop between two ships. Tests were carried out during the period 1974-76 by the French Center for Exploration of the Ocean (CNEXO).

Hydro-Dynamic CLB: Separator plates or specially configured buckets were used to separate the ropes using natural hydro-dynamic forces. Small scale tests were carried out in 1975 from the vessel Tokai University No. 2 in the Ogasawara area of Japan.

Turning CLB: By steering the mining vessel on a circular course, trailing the empty buckets over the stern and bringing up the loaded buckets amidships from inside the arc, good separation of the lines can be achieved. This method was tested in 1987 in model scale at a depth of 50 m (Figure 1) using a coastal fishing boat.

Of the four methods tested the Turning CLB is believed to be superior because of the simplicity of achieving a wide and safe separation of the two lines and the better control possible with the single, forward moving vessel.

The arc or the circular path taken by the vessel will be constrained by the nature of the deposit in which mining is taking place but it appears that seamount crust deposits may be well suited to the use of this approach.

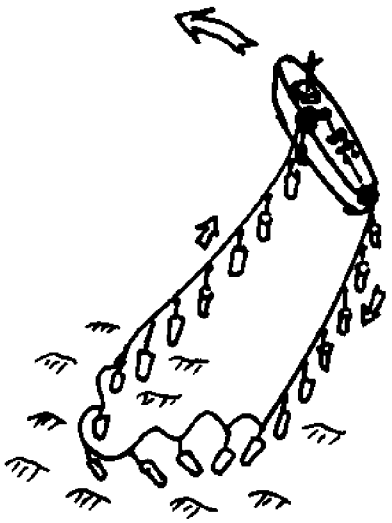

Figure 1. Principle of turning CLB

IMPROVEMENT OF THE CLB MINING SYSTEM

The design of the traction mechanism for the CLB is a critical factor in the efficiency of the system and has been varied in each of the tests.

The mechanism used in the 1972 Hawaii test at 5000 m depth (Figure 2) used 13 traction wheels, an 85 mm rope and buckets suspended from two bails at the front and rear of each bucket. The buckets and their suspension bails were able to dump on the first vertical drop and pass through the traction wheels without removal and re-attachment. Unfortunately the large size of the mechanism prevented its use on a smaller vessel and a more compact design was adapted for subsequent tests using multiple parallel wheels (Figure 3). The drive was powered by a 33 kw, 3 speed motor and factory tests confirmed available traction forces of 4 tons at 0.2 m/s, and 2 tons at 0.4-0.8 m/s. There was, however, no way to pass the buckets through the mechanism and they would have to be

individually removed and re-attached to the line during the test. A "magic hand" crane was designed to remove the loaded buckets, dump them, and return them to the line beyond the traction mechanism. The awkwardness of this activity led to further improvements in design.

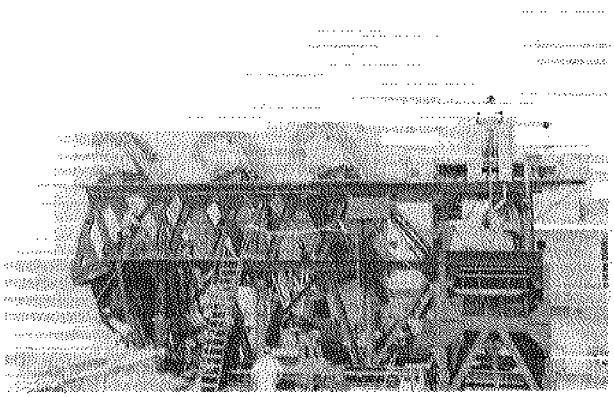

Figure 2. Front traction machine on Kyokuyou-Maru-No. 2

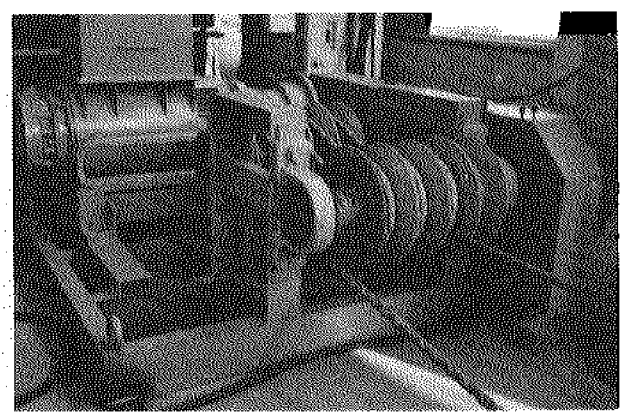

Figure 3. Multi wheels traction machine

New Ball Roller Traction Machine

Bail rollers were developed by Kouyou Co. in Japan for hauling large and bulky commercial fishing nets. They were used in the 1972 Hawaii CLB test for rope handling, and during the 1973 and 1975 tests on board the Tokai University vessel they were used to hoist the CLB rope with the buckets attached. Since the results in each case were

acceptable, plans were made to use the ball roller parallel drive system to replace the multi-wheel traction drive.

A cross section of a 5 ton, 60 cm ball roller for commercial CLB mining is shown in Figure 4. It consists of a pair of rubber balls inflated with high pressure air. The rope is passed between the balls and held in place by the air pressure which also supplies the holding force for the traction line. Operation is very smooth and the bucket suspension ropes can pass through the ball rollers easily. Figure 5 illustrates a factory test of parallel ball rollers driving a rope line with small buckets attached. In the full scale system eight ball rollers will be installed and driven by independent hydraulic motors in each parallel drive.

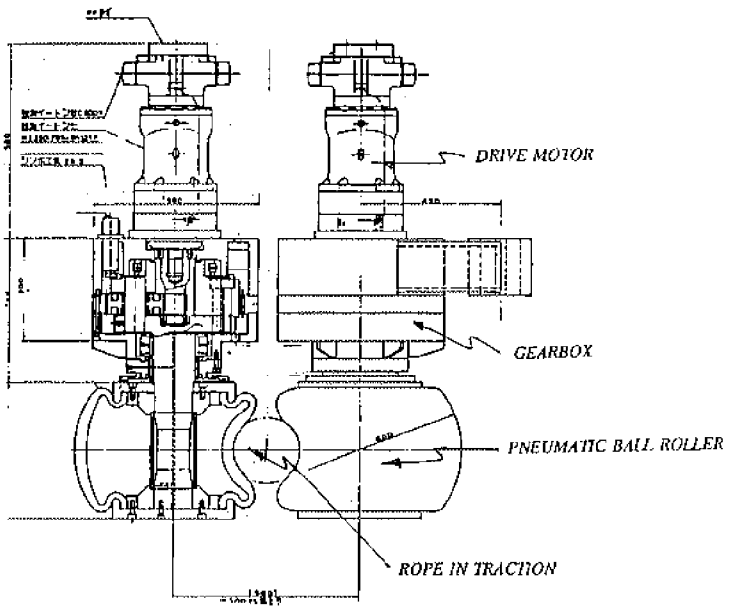

Figure 4. Cross section of 5 ton, 60 cm ball roller

Bucket Dumping Device

Throughout many CLB tests several different kinds of dumping mechanisms have been tested. The best method involved the suspension of the bucket upside down, by its two bails. To do this the full bucket line is guided onto the deck by the first guide wheel which directs the rope to a horizontal position without twisting. The suspended buckets are then guided to a sharp vertical drop which dumps the load into a chute and the empty buckets continue through the traction mechanism (Figure 6).

In the stern, another ball roller traction device pulls the rope, and the buckets slide on a curved guide plate to the side of the stern guide wheel which delivers them back down into the sea.

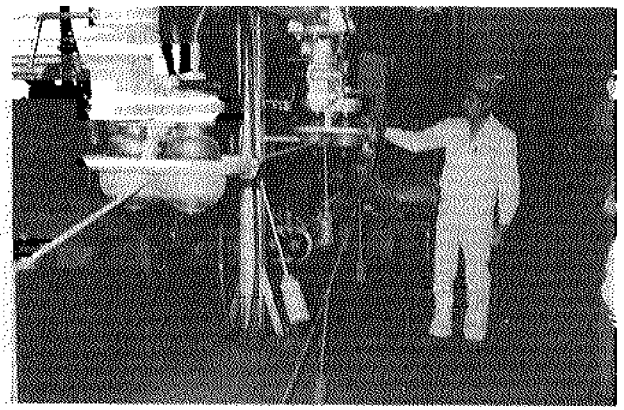

Figure 5. Ball roller traction test

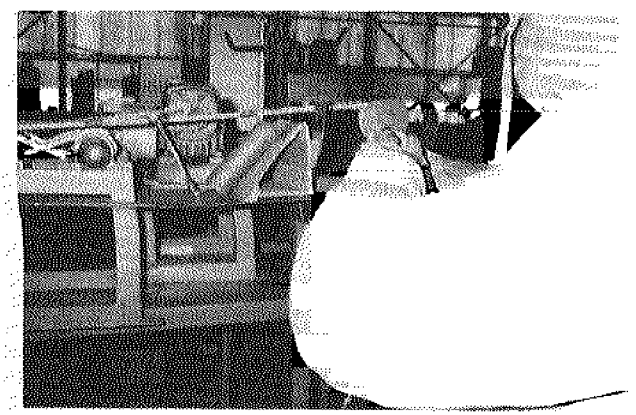

Figure 6. Bucket dumping model test view

After dredging on the seafloor, the rope with filled buckets is pulled up again to the vessel and the first guide wheel to repeat the process. The design has been well tested and is considered to be reliable.

BUCKET AND ROPE

The only underwater parts of the CLB system are the buckets and rope. This is a simple, but important part of the mining system.

Bucket Test

Tokai University conducted 24 single line bucket dredging tests on Minami-Torishima using two kinds of buckets. There were no empty buckets from these tests, and an average 100 kg/bucket of crust was dredged without bucket loss. Both bucket types which dredged cobbles, nodules and pavement during the tests would be suitable for the CLB.

Line

Polypropylene braided or plaited line was used for the CLB tests because of its buoyancy in the water. It is weak in creep characteristics, however, and polyester or nylon rope may be more adaptable and last longer.

RESOURCES OF PACIFIC ISLAND SEAMOUNTS

Significant deposits of high-cobalt metalliferous oxides containing potential ore grades of cobalt, nickel, copper, manganese and platinum group minerals have been identified on seamounts between the depth of 800 and 2400 m in the Exclusive Economic Zones (EEZ) of many of the Pacific islands including the 5th Takuyou seamounts in the Japanese EEZ, Palmyra in the U.S. EEZ, and Labibjet, Sylvania, and Jebro seamounts in the Republic of the Marshall Islands (RMI). The latter deposits are reported to have the highest commercial potential for any Pacific Island nation.

The cobalt content of these deposits is generally higher in value than that reported for deep seabed manganese nodules which are of similar composition but are found at depths generally between 5000 and 6000 m. The amount of deposit characterization conducted to date by numerous countries including the United States, Japan, Germany, France, South Korea and others is sufficient to indicate that the high-cobalt encrustation presents a significant minerals potential, given an appropriate technology for recovery.

More important, however, is some new information concerning the physical nature of these deposits which affects the potential for their mining using the CLB system. A recent survey of the very large 5th Takuyou seamounts, which are for the most part flat topped, resulted in a series of dredge hauls recovering an average of 100 kg per bucket of cobbles, nodules, and broken pavement in a relatively short tow (Figure 7; author communication). This distribution of easily dredgeable oxide material mixed with nodules has been observed also in each of the flat topped seamounts referred to previously and may alter the concepts of dredgeability normally applied to the better known hard pavement type crusts most commonly described in the literature.

ECONOMIC ESTIMATES OF CRUST MINING AND PROCESSING IN RMI

Candidate seamounts with crust deposits in the EEZ of the Marshall Islands are shown in the map presented as Figure 8. Three of these, Labibjet (1), Sylvania (3), and Jebro (5), have been selected as prime candidates for economic evaluation. Labibjet Seamount is narrow but has a rich distribution of cobble type crust; Sylvania Seamount, located near Bikini atoll is very large and has an extensive distribution of 10-15 cm thick crust; and Jebro Seamount, located near to Majuro the capital of RMI, is well located for testing.

Figure 7. Gathered cobble type crust

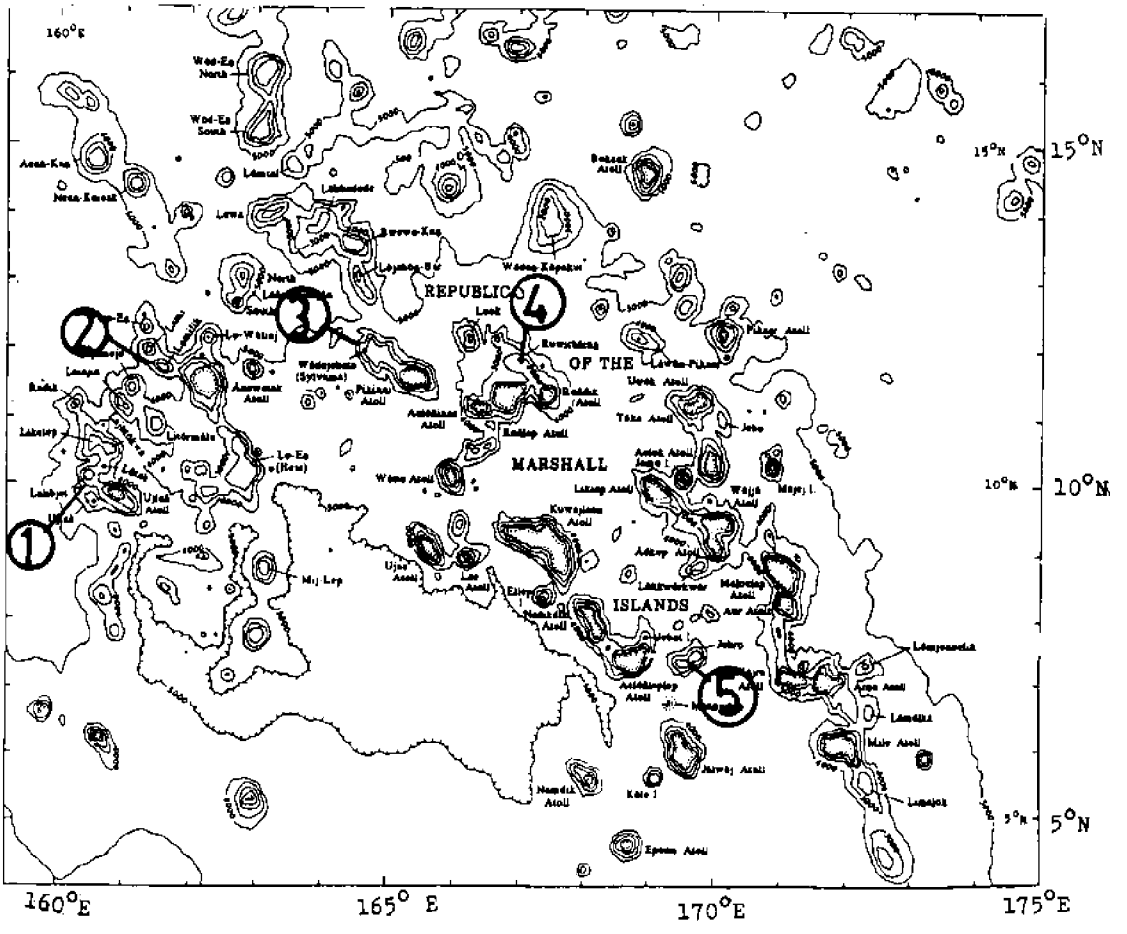

Figure 8. Crust deposits and islands in Marshall Islands

Tentative Crust Mining Proposal

It is proposed to plan for a 400 ton/day mining operation out of Majuro in the RMI. A 15,000 ton vessel conversion will be fitted with a ball roller traction system using 3,000 m of 90 mm diameter rope with 1.5 m^3 buckets attached every 50 m. A traction rate of 0.8 m/s will require 400 kw and the buckets will be discharged automatically on board the vessel. A monthly production cycle of 20 days over 11 months each year will result in an annual production of around 88,000 tons.

Tentative Estimated Costs

The following numbers are based on data from a U.S. Environmental Impact Statement for cobalt crust in the EEZ of the Hawaiian and Johnston Islands (USDOI, 1990) and are scaled down, for illustration, to a 400 ton/day CLB operation. At a cost of 15,600 Yen/t ($120) the annual operating costs are estimated to be about Yen 1.4 billion ($10.8 million). Capital needs for the mining system are estimated to be in the region of Yen 1.5 billion ($11.5 million) and for the processing system Yen 8.5 billion ($65.5 million), for a grand total of Yen 10 billion ($77 million).

Income from sales, based on Table 1, are estimated to be Yen 9,540 million ($74 million).

Table 1. Income from saleable commodities

Commodity	Production (t/y) (Recovery @ 80%)	Price (Yen/kg)		Income ($Yx10^6$)	
cobalt	582	5,000	($18/lb)	2,830	
nickel	297	1,300	($4.75/lb)	380	
MnO_2*	24,800	250	($0.90/lb)	6,320	
Total				9,540	($74x$10^6$)

* Use of battery grade MnO_2 is proposed for this fraction, based on existing, verified markets in Japan.

With mining costs of approximately Yen 1.4 billion ($10.8 million) and processing costs of approximately Yen 4.5 billion ($34.6 million), total costs would amount to Yen 5.9 billion ($45.4 million). This would give a gross annual profit before taxes of Yen 3.6 billion ($27.7 million) and, on the same basis, an annual return on investment of over 30%.

Small Scale Test of the CLB

In order to verify the feasibility of the CLB system in the mining scenario proposed it is necessary to operate the system in a scaled test on the RMI deposits. This can be done at 1/10 scale to produce 40 t/d by the simple conversion of an ocean going vessel at small cost. Sea trials for hydraulic systems under these conditions are inevitably much costlier

due to the scaling effects. About 1000 tons of crust material dredged during the proposed tests would be used to develop an appropriate system for processing, thus reducing the investment risks for development of the full scale production system.

OTHER USES OF CLB TECHNOLOGY

The CLB system has been tested for manganese nodule and crust mining in water depths as great as 5,000 m. The adaptation of the system to mine placer deposits, or industrial materials such as phosphorites, sands, or gravels in coastal water depths of a few tens of meters should be quite straightforward. The mechanical improvement gained by use of the ball roller makes for a simple and reliable system of mechanical dredging in the oceans with few environmental effects. This system could well be applied to beach sand replenishment in Hawaii and other island communities where coastal protection and enhancement has become of significant economic importance.

REFERENCES

Japan Resources Association. 1992. Crust deposit research reports, I, II, III and IV: Internal documents prepared by the JRA Crust Study Committee.

Masuda, Y., M.J. Cruickshank, and J.L. Mero. 1971. Continuous bucket line dredging at 12,000 feet. In: 1971 Offshore Technology Conference Proceedings. Houston, TX.

Masuda, Y., M.J. Cruickshank, J.A. Abernathy, and R. Winston, 1991. Feasibility study of crust mining in the Republic of the Marshall Islands. In: Oceans '91 Proceedings. Honolulu, Hawaii. October 1-3.

Masuda, Y., and M.J. Cruickshank, 1991. Mechanical design developments for a CLB mining system. In: Oceans '91 Proceedings. Honolulu, Hawaii. October 1-3.

Hein, J.R., J-K Kang, et al. 1992. Cooperative research by USGS and KORDI on marine mineral deposits in the Marshall Islands: unpublished cruise report, US Geological Survey. Menlo Park, CA.

Tokai University. 1990. Cobalt-rich manganese crust: A pictorial publication by Tokai University, Cobalt RMC Investigation Group, Japan.

USDOI, 1990. Proposed marine mineral lease sale: Exclusive Economic Zone adjacent to Hawaii and Johnston Island. U.S. Department of the Interior, Minerals Management Service and State of Hawaii, Department of Business and Economic Development, EIS/EA MMS 90-0029, v. 1 & 2. August.

BENEFICIAL USES OF FERROMANGANESE MARINE MINERAL TAILINGS

John C. Wiltshire
University of Hawaii
Honolulu, Hawaii, U.S.A.

ABSTRACT

Both ferromanganese crusts and nodules present potential processors with enormous volumes of tailings of dubious environmental character: most processing scenarios fail to utilize the uneconomic manganese itself, leaving a total waste volume on the order of 96% of the incoming ore. We envision at least one scenario which could result in both the removal of tailings from a processing plant and an increase in the supply of useful building materials at little or no cost to either the processing or construction industries -- transforming a tenacious waste into a novel resource. Ongoing experiments have demonstrated considerable potential for turning acid leach tailings into dark composite facing stone, fancy black tile, novelty ceramics and concrete aggregate. It has been shown that concrete made with up to 25% tailings can have compressive strengths above 4,000 psi. Tailings melted with a small amount of flux can be made into very hard attractive ceramic tiles. Tailings can also be cold-cast or sprayed with a resin binder into an infinite variety of shapes and coatings.

INTRODUCTION

It is likely, given the interest of the Japanese, Korean, and Indian governments as well as private sector groups, that within the next twenty years there will be a marine mining operation for manganese nodules or crusts (Markussen, 1990). Such an industry could be a major economic boon to a developing Pacific island economy. This has been well recognized by the State of Hawaii which has strongly supported ferromanganese research through its marine mining program for many years. However, a serious environmental problem remains unsolved and largely unconsidered. Ferromanganese crust and nodule processing presents potential processors with enormous volumes of tailings of dubious environmental character (U.S. Department of the Interior, 1990). Most acid leach processing scenarios fail to utilize the uneconomic manganese itself, leaving a total waste volume on the order of 96% of the incoming ore. Each current disposal proposal seems flawed: (1) backhauling to the initial mine site is costly and might run afoul of EPA or UN marine dumping regulations (NOAA, 1981), (2) subsea disposal near a coastal processing site means almost inevitable community opposition (NOAA, 1981), (3) tailings ponds use large amounts of land and may run the risk of allowing heavy metals to leach into aquifers over time (Department of the Interior, 1990), (4) agricultural soil amendment for improving barren lava or coral rubble appears to require prohibitive amounts of supplementary phosphate (El Swaify and Chromec, 1985), and (5) the slag resulting from energy intensive pyrometallurgical processing may have potential as road ballast but would more likely be relegated unsightly tailings ponds (NOAA, 1981). In any case, few processors would opt for smelting in all but those locales where energy is very cheap (Johnson, 1990). This unfortunately rules out a smelting operation in almost any Pacific island environment.

We envision at least one other scenario which could result in both the removal of tailings from an acid leach processing plant and an increase in the supply of useful

building materials at little or no cost to either the processing or construction industries -- transforming a tenacious waste into a building product. Ongoing experiments have demonstrated considerable potential for turning acid leach tailings into dark composite facing stone, fancy black tile, specialty ceramics, or concrete aggregate (Wiltshire, 1991).

PROCESSING AND NATURE OF TAILINGS

The U.S. Bureau of Mines (Department of the Interior, 1990) has shown that, while their extracted value metals vary widely, tailings from crusts and nodules are essentially identical. Accordingly, results obtained from either product should prove valid regardless of which industry ultimately unfolds. Unfortunately the original industrial tailings from manganese nodule processing days are gone. Therefore in our initial experiments we had to manufacture tailings by experimenting with various leach processes. We discovered that by greatly increasing leach times, a low pressure sulfuric-acid leach system can, in fact, duplicate the yields of an industrial high pressure leach (Wiltshire, 1991). It was this three-metal sulfuric acid leach system which we used to produce tailings on a bench scale processing operation. The leach technique is fully described by Haynes, et al. (1985). All the products were geochemically analyzed for comparison with the initial ore. Approximate yields of the process were 85% Cu and Ni and 80% Co. This is a three-metal (Cu, Ni, Co) recovery scheme which does not recover manganese. The leaching operation seeks to disrupt the manganese oxide crystal structure, reducing Mn^{+4} to Mn^{+2} via the reaction $MnO_2 + H_2SO_4 \rightarrow MnSO_4 + H_2O + 1/2\ O_2$. This disruption allows the lattice-bound Cu, Co, and Ni to be solubilized as their sulfate salts. As the sulfuric acid is depleted, Mn^{+2} is reoxidized to Mn^{+4} and remains in the tailings as MnO_2. The acid depletion also allows iron to precipitate as $Fe(OH)_3$.

CRITERION FOR THE ESTABLISHMENT OF USEFUL BUILDING PRODUCTS

The construction industry is very conservative in the acceptance of new products. In order to be accepted new products must be fully tested. In addition, these products must: 1) meet or exceed the properties of current products or 2) nearly equal the properties of current products but at a much lower cost. The key advantage to ferromanganese tailings in this regard is cost. These tailings are a waste material that would cost a processing operation an estimated $9 million a year to dispose using tailings ponds (Loudat, et al., 1992). This means that tailings would be available at no cost to the potential operation wishing to make building products out of them. Possibly, such a secondary user of the tailings would receive a small fee for their removal. In the event that the building products created used a high percentage of tailings with respect to other constituents, the overall materials cost of the building products would be low compared to the competing products.

The second important criterion is unusual properties of the tailings. We assume that these would be largely due to the manganese content. In particular, manganese is noted for its scavenging ability of other elements. This is what allowed the manganese nodules to form in the first place. This ability may be expected to increase product strength. Woolsey, et al. (1992) have proposed a very innovative scheme using this property to supply coal burning electric power utilities with ground nodules as stack cleaners. Manganese nodules have a very large surface area/volume ratio. Much of this is still retained in the tailings. This may lead to an ability to act as a desiccator, perhaps in turning a slow drying product into a rapidly drying product. This has a particular application for quick drying concrete. Manganese and iron being relatively heavy

elements will also likely give any product a greater density than it would have had otherwise. It is these unique properties as well as cost that make ferromanganese tailings an interesting material for the building products industry.

AGGREGATES IN CONCRETE

The American Concrete Institute (1990) has done a considerable amount of work on admixtures to concrete. This includes the successful incorporation of superplasticizers to increase concrete durability and blast furnace slag to increase strength and weight. Specialty concretes for the marine environment have been given a lot of study. Another area of major ongoing research is the texturing of concrete pavements particularly to provide tough skid-resistant roadways. This is done both by sculpturing the concrete with grooves and also by adding gritty material to the concrete. Although mineral tailings other than blast furnace slag were not used directly in this work, the approaches and testing methods are applicable.

Our concrete work began by testing varying mixtures of Portland cement, coarse sand and tailings. Mixtures were made with 0-60% tailings in the concrete. Two sets of experiments were conducted. The first involved tailings which were not fully neutralized after processing (see Figure 1). These tailings had been washed and had a pH of approximately 4. They were made into standard eight inch long, four inch diameter, concrete testing cores and tested for compressive strength by a commercial concrete testing company after curing for 33 days. The sample containing no tailings had a strength of 3460 psi effectively the same as the standard value given for concrete of 3500 psi. The other samples decreased considerably in strength with increasing amount of tailings. To determine whether the decrease in strength was solely due to the tailings content, the experiment was repeated with tailings which had been fully neutralized. The results were very different. Compressive strengths above 4000 psi were achieved in concrete containing 20-25% tailings. The strength decreased fairly rapidly to 1000 psi for concrete containing 50% tailings. Although 1000 psi concrete could not be used in buildings, it would still be applicable for driveways and many other paving applications. Several non-standard size samples exhibited very high compressive strengths (in the range of 5000-6000 psi) although they contained over 40% tailings. These results are considered suspect and are being rerun.

In addition to increased strength the tailings appear to give the concrete several other interesting properties. The fine grained nature of the tailings appears to make the concrete more moldable and bubble-free. This was demonstrated in two ways. First, a moldability test was performed using a 12" by 4" latex rubber mold of an ornamental Japanese carp. The mold was made with considerable attention to fine detail. This fine detail was picked up in a casting by the concrete containing 30% finely ground tailings but not by the standard concrete. Further, the ferromanganese concrete gave a much smoother bubble-free surface. The surface textures were compared in another test by examining cut surfaces of the ferromanganese tailings concrete and a standard precast concrete brick. The ferromanganese surface had bubble pits over less than 2% of its surface. These pits ranged in size from pinholes to 2 mm in diameter averaging about 500 microns. By contrast, the precast brick had pits covering over 20% of its surface ranging to 8 mm in diameter and averaging about 2 mm in diameter. The difference was very marked. The precast brick had a rough surface the ferromanganese a very smooth surface. In addition, the tailings give the ferromanganese concrete a considerably greater density than regular concrete in that iron and manganese are being substituted for the less dense silica and aluminum of sand and the ferromanganese concrete has less than one-tenth the bubbles found in regular concrete.

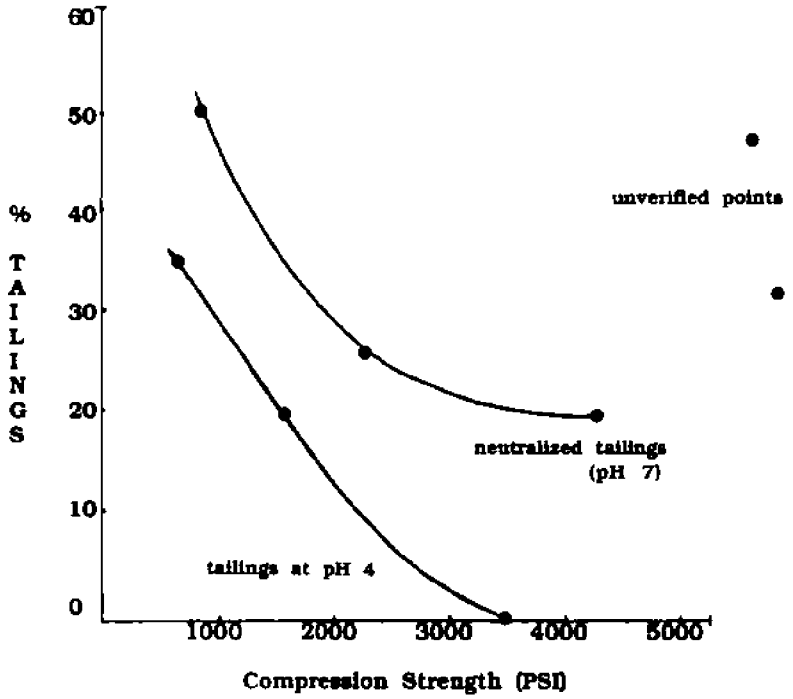

Figure 1. Compression strength of concrete made with manganese nodule tailings

Greater density and bubble reduction are two particularly important properties for concrete to be used in the marine environment or in freeze-thaw situations. In the marine environment wave action compresses air into the pores and pits of the concrete which over time breaks the concrete down. The same action results from water freezing and expanding in these pores. The lower number of pores subjected to this action the longer the concrete will endure. There is evidence to indicate that ferromanganese surfaces repel the growth of organisms (Department of the Interior, 1990). If this can be confirmed, it may be that ferromanganese concrete would not be covered as quickly with algae or encrusting organisms which would offer advantages for outfall pipes as well as many other marine and terrestrial structures.

Clearly there are considerable avenues for further research on the properties of ferromanganese tailings concrete. Initial indications of increased compressive strength, superior moldability, higher density and lower porosity give reason to believe that particularly for specialty concretes the addition of the ferromanganese waste is imparting very economically desirable characteristics. Further research will involve more rigorous testing of these properties by a commercial concrete testing laboratory.

CERAMIC APPLICATIONS

The second major direction of our research is geared toward the production of ceramics. This involved the melting of the tailings in a high temperature kiln alone and in combination with a variety of fluxes. The first step was to determine a melting temperature for the tailings. As might be expected the tailings do not melt at a unique

temperature but in fact melt over a range. The melting range is centered on 1280°C. This was determined using Orton ceramic cones, a standard practice in the ceramics industry. The accuracy of this method is ±20°C. The melting temperature was lowered slightly by the addition of fluxes. The tailings were introduced into the kiln as a powder at room temperature. In order to contain the melted tailings high temperature clay vessels were fabricated. After considerable experimentation, a rectangular design three inches by five inches with two inch high walls was decided on. It was made of thin walled, cone 10, high fire, raku clay. These clay holders were dried at 80°C for 24 hours before being fired to 1300°C. After cooling the powdered tailings were poured into the holders for a second firing. The kiln temperature was slowly ramped up at a rate of approximately 5°C/min. The melting temperature was held for at least one hour. Cooling rate was not monitored but took 6-8 hours to return to a temperature at which the clay holders could be removed.

The tailings alone melted to give a rough gray metallic surface. The material could be cut with a standard rock saw to give tiles of different sizes (the clay edges of the holders being cut off). The tiles did not have a uniform surface and the interior contained a large number of bubbles in the melt. The tiles suffered considerable brittleness and would break if dropped on a hard surface.

To alleviate the lack of uniformity of the melt, fluxing agents were added to the tailings. Experiments were performed using three fluxes: boric acid, borax, and lithium tetraborate. The resulting melt was a ferromanganese borosilicate glass containing 50-95% tailings. The glass melted to a perfectly smooth surface and vitreous lustre. The glass was extremely hard exhibiting a hardness of 7 on the Mohs scale. This extreme hardness makes the material of great value to the building industry because of resistance to wear. It can still be easily cut using a rock saw. The three different fluxes gave slightly different colorations. The best flux was the lithium tetraborate. In small amounts it gave the ferromanganese glass a pearly jet black finish and a dense bubble-free glass. Unfortunately, the lithium tetraborate was also the most expensive flux. Boric acid is a much cheaper flux. It gave a brown bubble-free glass but was required in higher quantities (20-40%) to achieve these results. Borax is the cheapest flux. It gave a patterned glass of somewhat less lustre. Experiments were also conducted using 0-40% basaltic sand to raise silica and aluminum contents. In general, the basaltic sand did help to produce a better glass in small amounts but the larger quantities gave little additional improvement. The resulting glasses are much denser than a normal silica glass. The chemical scavenging properties of manganese and the dense bubble-free glass may make an excellent material to encapsulate nuclear or toxic waste. The only negative properties of the glass which we encountered were brittleness leading to shattering along conchoidal fractures after impact.

We now need to take our ceramic research one step further. We have proven the concept that useful glasses can be made from manganese tailings. We have manufactured a hitherto unknown class of ceramic glasses - ferromanganese borosilicates. We have shown that these ceramic glasses have unusual and useful properties. Indeed, the glass chemistry may lead us to speculate that a series of useful electrical properties may exist which, as yet, we have not tested. We now need to optimize the products that can be made, specifically building tile. We are quantifying the solid solution melts to maximize useful properties and appearance. Once sufficient tiles of an optimized design are made, they will be sent to an independent ceramics lab for testing. This will allow an industrial evaluator to better categorize the market for the tailings products and estimate their value.

COLD CASTING AND COLD SPRAYING APPLICATIONS

Approximately a dozen building tile designs have been fabricated using a cold casting technique. This technique involves mixing of acid free tailings material with a binding agent (typically 70% tailings and 30% binder) and casting in a mold. Molds are either latex rubber or glass depending on the nature of the object to be cast. The use of rubber molds permits easy mold making of any available object or surface for duplication. Glass molds give a superior product in that the surfaces are extremely smooth and no final polishing is required. The glass molds are limited to predesigned patterns. In general, the most successful glass molds have been made by cutting glass construction blocks in half and using the textured interior surfaces as the molds. Casting is done by pouring the liquid material (tailings plus binder) into the molds once the molds are precisely leveled on a flat surface. The molds are coated lightly with a commercial mold release to facilitate release. On hardening, which takes several hours at room temperature, the product undergoes 1-2% shrinkage which also facilitates an easy release from the mold.

The properties of the resulting cold cast tiles are largely dependent on the nature of the binding agent used. Typically, a standard grade casting resin was used for the binder. This is identical to that used in most fiberglass applications. For higher grade exterior tiles epoxy resin and marine grade epoxy resin were also used. Naturally, the strength of the tile significantly increased with the use of high-grade epoxy binder. The standard casting resin tiles failed an acid test involving submergence in concentrated acid. The tile broke down as the binder dissolved. The idea of this test is to simulate the long term effects of the exposure to acid rain. Another test found the tiles less porous to water than standard ceramic tile. A four month exposure test to intense sun and rain was conducted by covering a slanted roof top with various tile designs and comparing those with controls left indoors. At the end of the test period the exposed tiles showed some color fading as well as pitting in the size range of 0.5-1 mm covering 2-3% of the tile surface. The pitting is presumed to be an indication of tile breakdown under UV radiation. The controls left indoors showed no change. The results of these experiments indicate a stability problem for the cold cast tiles under external use if low grade casting resin is used. Work with higher grade epoxy resin will repeat the work to date.

The cold cast mix is very applicable to a range of decorative products. Its ease of moldability makes it extremely versatile in terms of the nature of the finished product. A range of art objects including small statues, turtle and fish castings, Hawaiian petroglyphs, name plates and letters have been cast. The tailings material casts very well and further takes on a lustrous sheen when polished. The shiny, lustrous, black finish of the products has, in fact, created a demand for the tailings in the University of Hawaii art department as a coating.

If the tailings are ground finely enough (fine silt to clay range) they can be sprayed with a resin from a commercial paint gun. This creates a rust prevention product which has a hard black surface. A number of biological studies have indicated that the manganese significantly resists the growth of organisms. This may mean that manganese spray coated products would be less likely to develop mildew or other bacteriological growth. It may also be a beneficial coating for corrosion resistance and reduction of organism encrustation in the marine environment. Tests are being designed to quantify these properties during in situ ocean tests.

CONCLUSIONS

In the Ukrainian Republic waste manganese fines from terrestrial mining operations have been so successfully utilized for building materials that a commercial manufacturing plant was dedicated in 1990 (Yuri Bruyakin, Moscow Mining Institute, personal communication). Osaki, et al. (1987) have had success producing light weight aggregates from marine ferromanganese tailings. We are excited at the prospect of transmuting an environmental burden into an economic asset, ameliorating one of the few major constraints to deep-sea marine mining. The production of marine-related sculpture from this most archetypal marine product must await the touch of the artist's hand, but preliminary results confirm the efficacy of producing high margin products such as ceramic tile and facing stone, along with more humble low margin assets such as concrete and brick. The predominantly dark color of these products is generally considered attractive, but offers a high heat absorbance that may have utility in solar heating products. In many scenarios these products could be introduced to remote communities that would have had to import them; in other scenarios they will have to compete favorably with long established materials that offer substantial resistance to market penetration. Even in the latter case, processors may have considerable success co-opting traditional markets by offering voluminous raw materials at highly competitive prices. This observation is key, because of an overriding concern here must be assurance of almost 100% utilization on a real time basis. Anything less would result in a backlog of tailings which require disposal by the less satisfactory means cited above.

Accordingly, our immediate challenge is establishing as many applications as soon as possible, well in advance of actual commercial mining. Each must be evaluated for physical strength, aesthetic appeal and commercial viability. With a diverse suite of options arrayed before him, a ferromanganese processor can proceed with some confidence in the inevitable disappearance of his primary waste. Whether this will result from utilization of the entire product suite or one single gluttonous market remains the great unknown. Major consumers may be industries with applications completely different from those examined here. Unexplored horizons include drilling mud and the possibility that the metal scavenging nature of ferromanganese metals may be ideal for fixing radioactive wastes in marine manganese ceramics. Either application could consume the entire output of tailings. The supreme irony would be a future wherein tailings are actually in demand, responsive to market forces and actually contributing to the income of the primary processor!

ACKNOWLEDGEMENTS

This research has been supported by the U.S. Department of the Interior's Mineral Institute Program administered by the Bureau of Mines through through the Generic Mineal Technology Center for Marine Minerals under grant number G1185128-1504. This work was also supported by the State of Hawaii Department of Business, Economic Development & Tourism and is contribution 103 of the Ocean Resources Branch.

REFERENCES

American Concrete Institute. 1990. Manual of Concrete Practice. Detroit.

Aplin, C.L., and G.O. Argall. 1973. Tailings disposal today. In: Proc. First Intl. Tailings Symp., p. 861.October 31 - November 3. Tucson, Arizona. San Francisco: Miller Freeman Publications.

El Swaify, S., and W. Chromec. 1985. The agricultural potential of manganese nodule waste material. In: Marine Mining: A New Beginning, ed. P. Humphrey, p. 319. Honolulu: State of Hawaii, Dept. of Planning and Economic Development, Honolulu.

Haynes, B., and S. Law. 1982. Predicted characteristics of waste materials from the processing of manganese nodules. BU Mines IC 8904, p.10.

Haynes, B., et al. 1985. Characterization of waste materials from manganese nodule processing. In: Marine Mining: A New Beginning, ed. P. Humphrey, p. 319. Honolulu: State of Hawaii, Dept. of Planning and Economic Development, Honolulu.

Johnson, C.J. 1990. Future technical and economic dimensions of deep-sea mining. *Materials and Society*. 14:209-233.

Loudat, T.A. 1990. An economic analysis of manganese crust mining. In: Pacific Congress on Marine Science and Technology Abstracts. Honolulu: PACON Intl.

Markussen, J.M. 1990. Commercial exploitation of polymetallic nodules: when, why, who and how. *Materials and Society*. 14:397-413.

National Oceanic and Atmospheric Administration (NOAA). 1981. Deep seabed mining: final programmatic environmental impact statement. Washington, D.C.: U.S. Department of Commerce, p. 295.

National Oceanic and Atmospheric Administration (NOAA). 1991. Deep Seabed Mining: Report to Congress. Washington, D.C.: U.S. Department of Commerce, p. 14.

Osaki, K., Y. Hamada, and M. Ichijo. 1987. Basic study for production of light weight aggregate from leaching residue of manganese nodules, *Journal of the Mining and Metallurgical Institute of Japan*. **103(1197)**:778-793.

U.S. Dept. of the Interior, Minerals Management Service. 1990. Final EIS: Proposed Marine Mineral Lease Sale in the Exclusive Economic Zone Adjacent to Hawaii and Johnston Island. Honolulu: State of Hawaii, Department of Business, Economic Development & Tourism.

Wiltshire, J. 1991. Application of ferromanganese marine mineral tailings in concrete and ceramics. In: Proc. 22nd Underwater Mining Institute. September 29 - October 2. Honolulu: Marine Minerals Technology Center.

Wiltshire, J. 1992. Beneficial uses of ferromanganese marine mineral tailings.In: Pacific Congress on Marine Science and Technology Abstracts. Honolulu: PACON Intl.

Woolsey, J.R. 1992. Compliance possibilities and industrial opportunities for coal-burning utilities using offshore mineral commodities for flue gas desulfurization. In: Marine Minerals Technology Center Continental Shelf Division Technical Progress Report, pp. 17-22. Oxford: University of Mississippi.

THE ECONOMICS OF MINING MANGANESE CRUST WITH RECOVERY OF PLATINUM AND PHOSPHORUS

Thomas A. Loudat and John C. Wiltshire
University of Hawaii
Honolulu, Hawaii, U.S.A.

INTRODUCTION

This study provides a new economic assessment of manganese crust mining wherein the full resource potential is evaluated. This means that the economic analysis is based on projected recoverable tonnages of platinum and phosphorite substrate as well as cobalt, nickel, copper, and ferromanganese. The additional costs to process Pt and phosphoritic substrate are also included. The analysis allows the determination of characteristics of a profitable mine site under specific mining, processing, and target metal price assumptions.

OBJECTIVES

The following research objectives are undertaken in this study:

1. Assess the resource potential of cobalt-rich manganese crusts occurring within the Hawaiian and Johnston Islands EEZ's.

2. Prepare a base case scenario under a well defined condition set within the U.S., defining all requisite systems for a one million dry ton crust per year first generation mining operation. The six crust products are: cobalt, nickel, copper, manganese, platinum, and phosphate rock.

3. Perform an economic analysis of the mining venture.
   a. Estimate the capital and operating costs of these systems in 1990 U.S. dollars.
   b. Estimate the dollar value per ton of crust mined.
   c. Perform a financial analysis of an ocean mining venture allowing the evaluation of alternative financial performance parameters.
   d. Estimate system sensitivities to different variable levels.

Achieving these objectives allows the determination of the factor set required for an ocean mining venture to be economically successful. This essentially implies the specification of a potential mine site. Achieving these objectives also allows the determination of the contribution of platinum and phosphorous recovery to the venture's profitability.

METHODOLOGY

The resource assessment estimates the crust potential of the Hawaiian Archipelago and Johnston Island. The descriptive statistics used for the resource assessment are from the crust data base compiled by Manheim and Lane-Bostwick

(1989), Arvidson, et al. (1991) and Wiltshire (1990). The statistical data used for the resource assessment also provides the parameters required to delineate profitable mine sites within the resource area.

The basic methodology used to estimate costs is described in secondary sources (EIS, 1990; Magnuson, et al., 1985; Arthur D. Little, Inc., 1984; Bureau of the Mines, 1987; and Hillman, 1983). These sources also provide an initial conceptual design for an ocean mining venture. This design is appropriately altered to reflect specific characteristics of a venture designed to mine and process manganese crusts and recover Pt and P. Estimates of costs and activity timing are obtained from secondary sources (e.g., Magnuson, et al., 1985; Arthur D. Little, Inc., 1984; Bureau of the Mines, 1987; and Hillman, 1983), or estimated by analogy or extrapolation from cost estimates published in the literature. The base case cost per ton ore mined estimate will be for the mining scenario developed in the EIS (1990). Variations on this scenario for a sensitivity analysis will include changes in ore price, quality, percentage of substrate entrained with the ore, and metal recovery.

The price per to of crust mined at point of processing can be determined as follows:

$$V_c = \Sigma\Sigma\, E_i P_i$$

where:

V_c = the dollar value per ton of ocean crust mined
E_i = recovery efficiency of product (i)
P_i = the per unit price for product (i)
i = 1.6

Price per pound for the respective minerals will equal a historical average price per unit for the base obtained from U.S. Bureau of the Mines historical price series. Statistics derived from the historical price data are used for selection of prices for sensitivity analyses.

Economic viability measures include: pay back periods, capital recovery rates, and internal rate of return of the before and after-tax profit streams from a hypothetical manganese crust mining and processing venture. A sensitivity analysis is performed by altering base case variable levels which also allows specification of a mine site.

RESOURCE ASSESSMENT

Table 1 summarizes study variables, their respective descriptive statistics, and sources for the resource potential estimation and recovery potential. Combining the resource area variable values of Table 1 with the estimated resource area, allows the estimation of the in-place resource potential of the mining area. Table 2 shows the estimated amount of crust and the respective estimates of total mineral potential for the mean values of all resource area values. To give the values some perspective, the 1990 U.S. consumption of these metals is also presented.

Table 2 shows that crusts have a substantial potential as a cobalt resource, as well as being a significant resource of Mn, Ni, and Pt. Phosphoritic substrates underlying crusts also have significant resource potential as a supply of phosphate rock for the fertilizer industry, if found and subsequently recovered with crusts of high enough grade to be mined. Using 1990 U.S. consumption levels and crust metal amounts shown in

Table 2, the Hawaiian and Johnston Island EEZ area crust resource contains 419, 181, 11, 48, and 95 years supply of Co, Mn, Ni, Pt, and P in the form of phosphate rock respectively. The Cu resource is insignificant.

Table 1. Resource area variables and values

Variables	Sample Size	Variable Range Min	Max	Mean	Std. Dev.	Source
Mean Crust Thickness (cm)		0.10	15.00	2.50	1.78	(1,3,6)
Crust Specific Gravity						(1)
Wet				1.95		(1)
Dry				1.34		(1)
Crust Grade						
Mn	773	15.10%	38.79%	25.02%	4.14%	(2)
Fe	802	5.98%	22.95%	16.89%	2.93%	(2)
Co	805	0.29%	3.02%	0.87%	0.37%	(2)
Ni	773	0.12%	1.54%	0.46%	0.17%	(2)
Cu	603	0.01%	0.55%	0.08%	0.05%	(2)
Pt (ppm)	8	0.1639	2.00	0.484	0.3934	(2,5,)
P (in phosphate rock)		0.03%	1.88%	0.51%	0.25%	(2)
Crust Coverage			100%	40.00%	16.67%	(1)
Substrate						
Phosphorite		0.06%	29.61%	16.00%	10.83%	(4)
Depth (m)	819	598	6890	2012	721	(2)

Sources:

(1) EIS (1990)

(2) Manheim and Lane-Bostwick (1989)

(3) Derived from Manheim and Lane-Bostwick (1989) Appendix A, Area A-2

(4) Arvidson, et al. (1991)

(5) Wiltshire (1990)

(6) Ritchey (1988)

Note: Values are in percent moisture free material, except for Pt. It is reported in ppm.

Table 2. In-placing mining area resource potential

Crust Weight per Unit Area

Crust Weight (mt) per Unit Area (km sq)		13,400
Percent Crust Cover	40.00%	
Crust Weight (kg) per Unit Area (m sq)	33.50	
Crust Weight (g) per Unit Area (cm sq)	3.35	
Average Crustal Thickness (cm)	2.50	
Dry Weight Density (g/cm cubed)	1.34	

In-Place Crust Resource

Crust (mt)		360,620,800
Seabed Area (km sq)	26,912	
Crust Weight (mt) per Unit Area (km sq)	13,400	

Resource Area Mineral Potential

Metal	Concentration (%)	Amount (mt)	1990 U.S. Consump. (mt)
Mn	25.02%	90,227,324	497,142
Fe	16.89%	60,908,853	
Co	0.87%	3,137,401	7,472
Ni	0.46%	1,658,856	148,403
Cu	0.08%	288,497	2,150,000
Pt (ppm)	0.4840	175	3.61
P	0.51%	1,839,166	19,188

INTEGRATED MANGANESE CRUST MINING/PROCESSING SYSTEM

The integrated manganese crust mining/processing system is hypothetical since no commercial system exists. It is presumed for this study that technical investigations lead to the conclusion that profitable mine sites do exist and that a decision is made to recover and process the crusts by a corporate rather than government entity. The assumed annual system throughput is approximately 1.4 million dry tons of manganese crust and substrate delivered to shore.

The crust mining/processing venture developed for the base case scenario allows the recovery of Pt as the metal and P in the form of high concentrate phosphate rock. The respective systems required to recover and ultimately sell all recovered metals parallel others described in the literature, with appropriate changes to allow recovery of Pt and P. A brief process system description follows.

The beneficiation method is wet high intensity magnetic separation (WHIMS) which allows the recovery of high concentrate phosphate. WHIMS concentrates the phosphate rock portion of the crust/substrate complex in the non-magnetic fraction. The target metals concentrate in the magnetic fraction. Beneficiation of the no-magnetic WHIMS fraction to concentrate the phosphate rock follows standard methods and practices of the U.S. phosphate industry.

The Pt is recovered during hydrometallurgical processing of Co, Ni, and Cu. Since the Pt occurs in two distinct forms, a hydrogenetic Pt chloride complex (up to 0.5ppm) and as elemental Pt in a NI/Fe alloy in cosmogenic spherules (more than 0.5 ppm), two recovery pathways are required. The hydrogenetic Pt chloride dissolves in the target metal solution and is recovered as sponge Pt. The Pt in the Ni/Fe alloy remains in the target metal solution sludge. It is beneficiated using Pt beneficiation methods described in the literature to concentrate the Pt (see Bennets, et al., 1987; and Gomes, et al., 1979 and 1980). This latter pathway is only relevant if the Pt concentration exceeds 0.5 ppm. Metal recoveries from the processing system are 87.50%, 86.40%, 77.30%, 87.90%, 52.89%, 90.00% for Co, Ni, Cu, Mn, P (as P_2O_5) and Pt, respectively.

Capital and operating cost summaries are presented in Table 3. A detailed discussion of the system and respective sector cost estimates can be found in Loudat, et al. (1993).

Table 3. Cost summary (millions of 1990 dollars)

	Capital Costs		**Operating Costs**	
Sector	**Amount**	**% Distrib.**	**Amount**	**% Distrib.**
Prospecting & Exploration			$7.2	3.30%
Mining	$259.7	28.21%	$52.2	23.96%
Ore Marine Transport	$131.8	14.32%	$18.6	8.54%
Ore Marine Terminal	$41.8	4.54%	$7.0	3.21%
Onshore Transport	$17.4	1.89%	$3.4	1.55%
Processing	$458.7	49.83%	$125.5	57.62%
Waste Disposal	$9.4	1.02%	$1.6	0.75%
Mining Support	$1.8	0.20%	$1.1	0.51%
Research & Development			$1.3	0.585
Total	**$920.6**	100.00%	**$217.7**	100.00%
Estimated Annual Dry Tons Crust/Substrate Processed			1.33	
Cost per Ton			**$164.0**	

Integrated crust mining system capital costs would be 920.6 million 1990 dollars with a $164 dollar per ton operating cost. The processing and mining sectors account for the majority of both capital and operating costs, compromising approximately 50% and 25% respectively of each of these costs. Various possible means exist to reduce costs. These include: in situ beneficiation, in situ beneficiation and processing, and on site

sulfuric acid production. New alternative processing methods also have the potential to significantly reduce both capital and operating costs. Operating cost reductions have the greatest potential to increase the venture IRR versus capital and pre-production cost reductions.

FINANCIAL ANALYSIS

The financial analysis was conducted using a spreadsheet model similar to that presented in Magnuson, et al. (1985). The model allows the calculation of the pay-back period (in years), capital recovery factors, and internal rate of return on investment.

The per ton crust/substrate values are derived from the metal recoveries per ton ore/substrate and the metal prices. Table 4 below shows the relevant data and the value per ton of the ore/substrate for the base case scenario.

Table 4. Ore value per ton

Metal Product	Metal Recoveries	Recovery per Ton Ore Processed	Annual Metal Weight Recovered	Base Case Metal Price	Annual Revenue (mil.$)	% of Total Revenues
Cathode Co (lbs)	87.50%	0.61%	17,904,031	$14.93	$267.33	86.14%
Cathode Ni (lbs)	86.40%	0.32%	9,347,492	$3.68	$34.43	11.09%
Cathode Cu (lbs)	77.30%	0.05%	1,454,431	$1.30	$1.90	0.61%
Mn (metric ton)	90.00%	18.09%	240,225	$2.20	$0.53	0.17%
P (30% P205 material) (mt)	52.89%	2.87%	38,123	$28.23	$1.08	0.35%
Sponge Pt (troy oz)	90.00%	0.000035%	14,941	$339.38	$5.07	1.63%
Sludge Pt (150ppm) (troy oz)	0.00%	0.000000%	0	$321.88	$0.00	0.00%
Totals					**$310.33**	
Dry Tons of Crust/Substrate Processed per Year					1,327,923	
Ore Value per Ton Crust/Substrate Processed					**$233.69**	

NOTE: Sponge and sludge Pt are approximately 75% of quoted Pt prices. Sludge Pt prices are further reduced by $17.50 per ounce for the cost of its treatment to recover Pt values. (Personal Communications with Allen Relkin of Constrade Mineral & Metals, Inc.)

Clearly, the largest revenue producer is cobalt comprising almost 90% of total annual revenues under the base case scenario. Pt is the third largest revenue producer exceeding Cu, Mn, and phosphate rock. The Pt percentage of ore value per ton increases to over 6% for 2 ppm crust Pt. When a phosphoritic substrate is encountered, its percentage of ore value per ton increase 2.5 time relative to the base case. If the phosphorite occurs as the major mineralogical phase in the substrate, the phosphate's percentage of total ore value increases 6 times relative to the base case.

FINANCIAL ANALYSIS BASIC ASSUMPTION SET

To obtain a meaningful financial analysis, a number of conservative assumptions have been made. These are as follows:

1. The crust mining venture is a corporate subsidiary of a parent mining company organized specifically for undertaking the proposed mining venture. The parent company can shield other net income from taxes using pre-production losses from the ocean mining venture. The venture is a technical and management success.

2. Capital and operating costs of any non-standard regulatory regime, if incurred, do not significantly alter estimated returns.

3. Because of the high degree of uncertainty predicting inflation over a 20 year horizon, average annual cost and price inflation over the 20 year life of the venture are assumed to be equal. Thus, no inflationary adjustments are made and all analysis financial variables (e.g., IRR) are expressed in real terms.

4. The pre-production tax rate is 40.8%, the maximum federal plus state corporate income tax rate. The tax rate incurred (post-tax credits) on the venture once production commences equals the average for U.S. mining sector companies with assets greater than $250,000,000 in 1988 increased by 20% to account for State corporate income taxes. The tax rate on net income equals 22.77% (see IRS, 1991). This rate implicitly incorporates (average) depletion allowances such a venture would obtain.

5. The parent company successfully obtains financing. Financing is 25% from parent equity capital and 75% debt financed. The annual real (i.e., reduced by inflation) interest expense is 5%. The debt is amortized over the 20 year life of the operation.

6. Cost of sales equals 2.5% of gross revenues. This includes tolling charges, commissions, and discounts.

7. Pre-production capital costs and equity contributed by the parent company are expensed the year they occur.

8. All equipment functions for the expected 20-year life of the project. Maintenance and repair annual operating costs provide for any necessary replacements.

9. Straight-line depreciation is used to depreciate all fixed plant and equipment capital. This does not include pre-production capital expenditures or capital expenditures expensed.

10. Working capital is contributed by the parent company the year production commences. Average working capital balances remain constant over the life of the venture and earn an average annual 3% real rate of return.

11. Working capital and land costs are recaptured the last year of the operation.

12. Plant and equipment salvage value equals cleanup costs. Thus, there is a $0 net plant and equipment salvage value.

ANALYSIS RESULTS

The economic analysis performed indicates that the assumed venture leads to significant savings to the mining venture parent company. This results from tax structure and expensing assumptions made. The tax savings significantly improve the economic performance of the venture such that post-tax internal rates of return (IRR) exceed pre-tax IRR's. Platinum and phosphorus both contribute to venture profitability. Pt increases the venture IRR when its crust concentration is in the 1.5 ppm range. This means that a cosmogenic fraction must be present for Pt to make positive contributions to venture profitability. Phosphorous recovery increases venture profitability at assumed base case grades, recoveries, and prices. Assuming a phosphoritic substrate occurs as the major mineralogical phase in the substrate, its recovery increases the venture IRR by almost 10%. Phosphorous recovery also dampens the negative impact on venture profitability if the base case substrate dilution rate (i.e., 25%) is not achieved. Pt and P price changes do not have significant impacts on venture profitability given their relatively small proportions of venture gross revenues.

The most important factor contributing to the success (i.e., increasing the IRR) of the manganese crust mining venture is cobalt price. Cobalt prices in the $20 per pound range, all else constant, provide a venture internal rate of return (i.e., IRR) of approximately 25%. Given their volatility however, such a Co price regime should not be relied upon for the success of the venture, in spite of current Co prices considerably above $20 per pound. Changes in Co grade also have a significant impact on the venture IRR and consequently its success. A cobalt crust grade of 1.25%, all else constant, leads to an IRR in excess of 25%.

Increasing Co recovery by 1% leads to an almost 3% increase in venture IRR. Preliminary investigations suggest that froth flotation may prove a more profitable beneficiation method than wet high intensity magnetic separation (WHIMS) assumed for this study, even though this means no P recovery. That is, the positive marginal contribution to venture profitability from recovering P, may be less than the cost of lower Co recoveries using WHIMS.

The most significant downside risks to the success of an ocean mining venture from this analysis are low cobalt prices and high substrate dilution rates. At slightly less than $13 per pound Co, the venture IRR equals 0. Cobalt prices represent the economic variable least controllable by the mining venture. The substrate dilution rate represents the major technical uncertainty in mining manganese crusts. A substrate dilution rate of only 5% above the base case value of 25%, reduces venture profitability by almost 50%. This suggests that if technical aspects of actual crust mining experience are significantly outside of ranges indicated in the EIS (1990), the venture would not likely be profitable.

CONCLUSION

A 1.25% crust grade of cobalt can serve as a minimum grade necessary for identifying crust mine sites and thus adding to U.S. cobalt reserves. Assuming Co grade is normally distributed, such a grade should occur approximately 15% of the time in the resource are. If this is the case, potential mine site(s) could support approximately 27 years of profitable crust mining at this grade cobalt, all else constant.

Table 5 presents the financial results of mining a crust cobalt grade of 1.25%. Since Mn and Ni grades are highly correlated with Co grade, their grades are

correspondingly increased as well (Mn = 30.19%, Ni = 0.866%). The post-tax internal rate of return is 30.59%, a noteworthy return even with the inherent risks of mining manganese crusts. Assuming a 1.75 Pt crust grade, the Table 6 IRR increases to 32.02%. Further assuming a major phase phosphoritic substrate this IRR increases to 32.37%.

Table 5. Mine site assumption set results

ASSESSMENT VARIABLES	**VALUE**	
Capital Expenditures		
Fixed Capital Investment	$819.2	
Pre-Production + Parent Fixed Capital	$600.5	
Tax Savings	($262.8)	
Net Parent Capital Funding	$337.7	
Pay Back Periods (in years)	**PRE-TAX**	**POST-TAX**
On Fixed Capital	4.45	5.75
On Net Parent Capital Funding	1.83	2.37
Real Rates of Return	**PRE-TAX**	**POST-TAX**
Return on Fixed Capital	22.50%	17.41%
Return on Net Parent Capital Funding	54.57%	42.22%
Internal Rate of Return	21.43%	**30.59%**

This assessment begs issues of crust thickness, contiguity, and microtopography which could impact the feasibility of ming a mine site as defined herein. Nonetheless, these issues do not diminish the conclusion of this paper that under a reasonable crust mining/processing scenario, cost and price structure, and well within observed crust grades, a crust mining venture has the potential to be successful.

ACKNOWLEDGEMENTS

This work was partially funded by the University of Hawaii Sea Grant College Program (SOEST), under Institutional Grant No. NA89AA-D-SG063 (project R/OM-13) from NOAA Office of Sea Grant, Department of Commerce. This is Sea Grant publication UNIHI-SEAGRANT-CP-93-14. This work was also supported by the U.S. Department of the Interior Minerals Management Service and the State of Hawaii Department of Business, Economic Development and Tourism. This is Ocean Resources Branch Contribution number 102.

REFERENCES

Arvidson, R.S., J.C. Wiltshire, and H.-W. Yeh. 1991. An assessment of substrate phosphorite resources in the Hawaii EEZ. Final Report on Contract No. 14-0001-30387 Continental Margins Program.

Bennets, J., E. Morrice, and M.M. Wong. 1981. Preparation of platinum-palladium floatation concentrate from stillwater complex ore. Bureau of Mines Report of Investigations. RI 8500.

Bureau of Mines. 1987. Bureau of Mines cost estimating system handbook. Bureau of the Mines Information Circular/1987. IC 9143.

EIS (Environmental Impact Statement). 1990. Proposed Marine Mineral Lease Sale in the Hawaiian and Johnston Island Exclusive Economic Zones. U.S. Department of the Interior, Mineral Management Service and the Department of Business and Economic Development, EIS/EA; MMS 80-0029. August.

Gomes, J.M., G.M. Martinez, and M.M. Wong. 1979. Recovery of byproduct heavy minerals from sand and gravel, placer gold, and industrial mineral operations. Bureau of Mines Report of Investigations. RI 8366.

Gomes, J.M., G.M. Martinez, and M.M. Wong. 1980. Recovery of byproduct heavy minerals from sand and gravel operations in Central and Southern California. Bureau of Mines Report of Investigations. RI 8471.

Hillman, C.T. 1983. Manganese nodule resources of three area in the Northwest Pacific Ocean. In: The Proposed Mining-Beneficiation Systems and Costs. Bureau of Mines Information Circular 8933.

Internal Revenue Service (IRS). 1991. Statistics of Income Bulletin. **11(2)**.

Little, ArthurD., Inc. 1984. Technical and cost analyses of manganese nodule processing techniques and their significant variation. Contract No. NA 83-SAC-00637. Reference 8909. September.

Loudat, T.A., J.C. Wiltshire, J.P. Allen, and W.C. Hirt. 1993. The economics of mining ocean crust with recovery of platinum and phosphorous. Department of Business and Economic Development State Report, State of Hawaii. Honolulu, Hawaii.

Manheim, F.T., and C. Lane-Bostwick. 1989. Chemical composition of ferromanganese crusts in the world ocean: a review and comprehensive database. USGS. Open File Report 89-020.

Magnuson, A.H., J. Flipse, F.C. Brown, and B.V. Andrews. 1985. Economic analysis of deep seabed mining systems: effects of production rate, inflation, and depletion using a revised financial model. TAMU-SG-85-203. May.

Ritchey, J.L. 1988. Cobalt rich manganese crust in the U.S. Exclusive Economic Zone: a potential source of strategic metals. *Mineral and Materials*. Oct.-Nov.:13-23.

Wiltshire, J.C. 1990. Platinum accumulation in cobalt-rich ferromanganese crusts. In: Proceedings of the Pacific Congress on Marine Technology. Tokyo:Nihon University.

THE POTENTIAL ROLE OF PASSIVE SONAR IN FISHERIES RESOURCE EVALUATION

William E. Evans and Jeffrey C. Norris
Texas A&M University
Galveston, Texas, U.S.A.

ABSTRACT

When sonar detection of marine organisms is mentioned most every one visualizes one of a vast array of fish finding active sonars. This is because passive systems have been essentially limited to military use. Submarines like to run deep and silent; therefore, sensitive listening systems are essential. In the process of developing and improving passive sonars, i.e. listening sonars rather than pinging, for the Navy's surface and sub-surface fleet, a vast variety of biological noise generators have been documented. Many fishes and most crustaceans are either direct or incidental noise makers. Many fishes actively produce sounds which are associated with courtship and territoriality. Some fishes and most crustaceans generate mechanical sound by movement, feeding and other activities. In many cases, sound generating fishes (e.g. croakers, drums, sea robins) can be identified to genus and in some cases species. Large schools of pelagic fishes, especially the tunas, make mechanical noise associated with swimming and feeding.

Over the past two decades passive sonar instrumentation and analytical techniques have become very sophisticated. In 1980, a special towed linear array passive sonar system was developed. A modified version of this array is being evaluated in the North Western Gulf of Mexico to survey demersal fishes and penaeid shrimp. Distribution as determined by acoustic contacts will be compared with the distribution and density of several target species determined using conventional bottom trawling.

INTRODUCTION

Assessing the abundance and distribution of marine animals populations, e.g. mammals, fish, and crustaceans, is fundamental to responsible management of ocean resources. Existing assessment techniques use a combination of fishery catch records, visual censuses, experimental net hauls, and active acoustics surveys (SONAR) (Johannesson and Mitson, 1983). Investigations in fisheries biology and the fishing industry encourage research and development of new assessment techniques that can detect, locate, and estimate the abundance of commercially valuable marine organisms.

Many marine animals produce sounds, either by active vocalizations or incidentally while swimming or feeding, e.g. scombrids, scaenids, scorpaenids, most penaeid and sergestid shrimps, and marine mammals. As many as sixteen species of fish and marine invertebrates found in the Gulf of Mexico are known sound makers (Fish and Mowbray, 1970). Examples of biological sources of sustained ambient noise as discussed by Myrberg 1978 are presented in Figure 1. Using acoustic monitoring to detect and locate sound-producing organisms has been suggested, but problems associated with monitoring mobile species has limited studies to evaluating stationary resources. Takemura (1972), in a paper describing the distribution of biological underwater noise in the coastal waters of Japan, demonstrates an excellent relationship between the

distribution of "frying noise" usually associated with snapping shrimp and valuable fisheries resources.

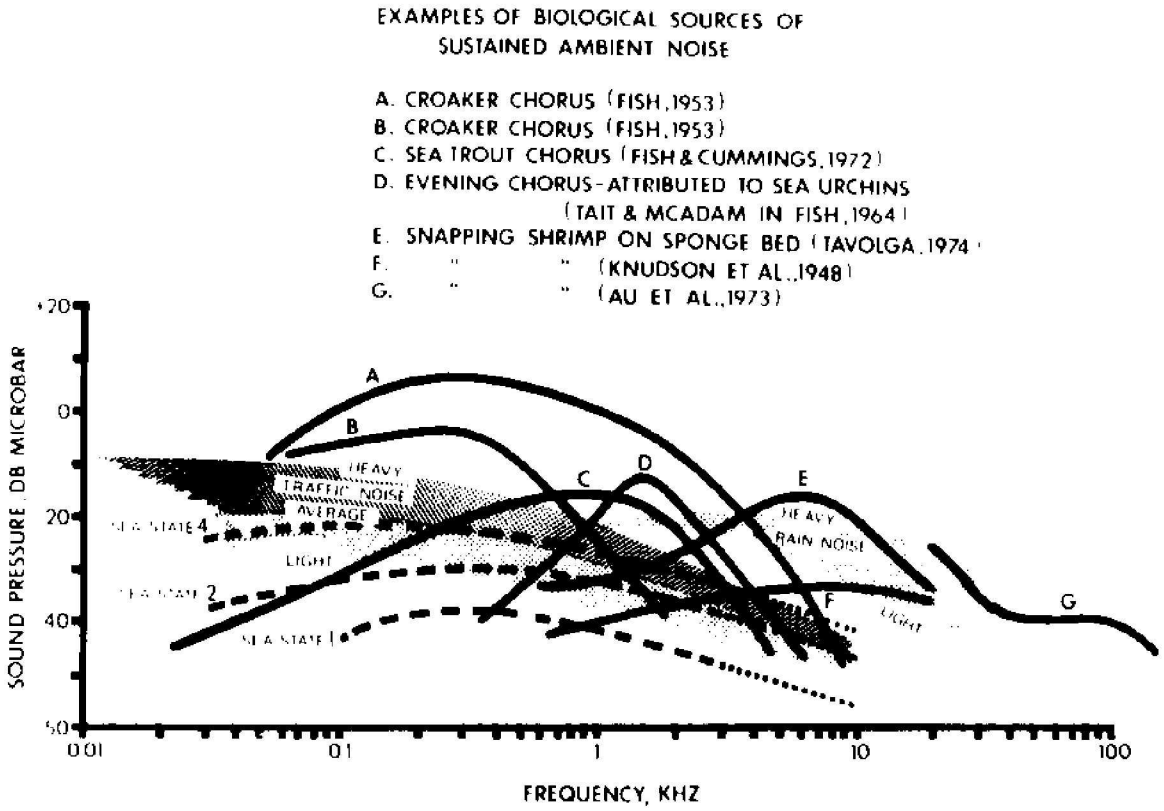

Figure 1. Acoustic spectra of several examples of biological sources of sustained ambient noise

In the late 1960's and early 1970's, the U.S. Navy started to address a similar problem in anti-submarine warfare: acoustically tracking mobile underwater targets (submarines) to determine their abundance and distribution as a function of time. The Navy benefitted from technological transfer by testing the effectiveness of hydroacoustic streamers (towed linear arrays of hydrophones) that had been first used for seismic exploration by the oil and gas industry as the receiving system of a new passive sonar system. The transfer worked. Towed acoustic array technology, coupled with the rapidly improving computer data analysis capability produced a sensitive, mobile, range detecting and tracking passive sonar. Now, after a decade and a half of Navy experience, the stage was set to transfer this capability to the detecting, locating, and assessing of biological targets, many of which constitute a major source of noise for the Naval anti-submarine warfare applications.

In 1980, a towed linear acoustic array, specially tuned to optimize the reception of biological signals, was designed for Sea World Incorporated by George Anderson with the assistance of the authors. With the support of Sea World Inc., U.S. Tuna Research Foundation, National Marine Fisheries Service, and the Office of Naval Research this

new array was initially tested at sea by scientists from the Hubbs Sea World Research Institute in San Diego, California. The initial tests were more successful than anticipated and demonstrated that a properly designed system:

- can detect and classify various species of marine mammals, in many cases well beyond visual detection range
- had the potential for detecting various species of commercial fish stocks, such as drum, croakers, and other phonating species
- demonstrated that non-vocalizing species, such as large schooling fishes such as tunas produce sounds associated with swimming, feeding, and other activities which involve opening and closing the mouth.

The linear acoustic array used in the initial tests had several distinct advantages over other systems we had used in the past. Hydrophone groups could be spatially arranged for optimal reception of specific frequency bands to optimize detection of certain species. Array depth could also be adjusted for optimum sound reception as a function of target depth and prevalent oceanographic conditions. The directional sensitivity of the array could be used to minimize ship self-noise. The array could be modified electronically to form narrow reception beams which facilitate the tracking of specific targets. In addition, the array proved to be easily transported and adaptable for use on a variety of boats and ships and easy to repair at sea.

These initial trials demonstrated that passive-acoustic analysis techniques coupled with acoustic array technology had significant potential for advances in bio-acoustic research and, possibly, in the future as a tool to improve the evaluation of fisheries resources. The refinement of these techniques is the direction for our future research.

OBJECTIVES

The goal of our continued research is to evaluate the effectiveness of various array configurations as non-disruptive methods of detecting, locating, and estimating the abundance and distribution of marine animals. The distance and direction to the animals relative to the ship could be determined by 1) knowing the directional characteristics of the array, 2) the acoustic source level of the various biological targets and 3) then, developing a computer program which then estimates the distance to these targets. Identity of the marine animals can be determined using a statistical program for isolating components of the acoustic signature similar to the techniques suggested by Fristrup and Watkins (1992).

At the present there are no clear methods for determining abundance on any more than a qualitative basis. Rate of calling and call density can provide some estimate of abundance. In the cases where individuals, groups; or stocks can be identified by the nature of their calls, e.g. sperm whales (Watkins, 1977), humpback whales (Payne and Grunee, 1983), killer whales (Ford and Fisher, 1982), and bottlenose dolphins (Caldwell, et al, 1990) numbers can be determined with greater accuracy. Data on individual identification of fishes are generally not available. In the case where certain species call individually during certain seasons of the year (croakers, toad fish), individual differences in call structure may exist and would allow for more precision in estimating abundance.

Our current research using passive sonar technology, focused on the Gulf of Mexico, includes a visual and acoustic survey of cetaceans from the Texas-Mexico border eastward to the Alabama-Florida border off shore from the 100 meter isobath to the 2000 meter isobath (Figure 2). This program (GulfCet) is sponsored by Minerals Management Service. A companion program (LATEX) which is a comprehensive oceanographic/ hydrographic study of the Louisiana-Texas continental shelf is also funded by Minerals Management Service.

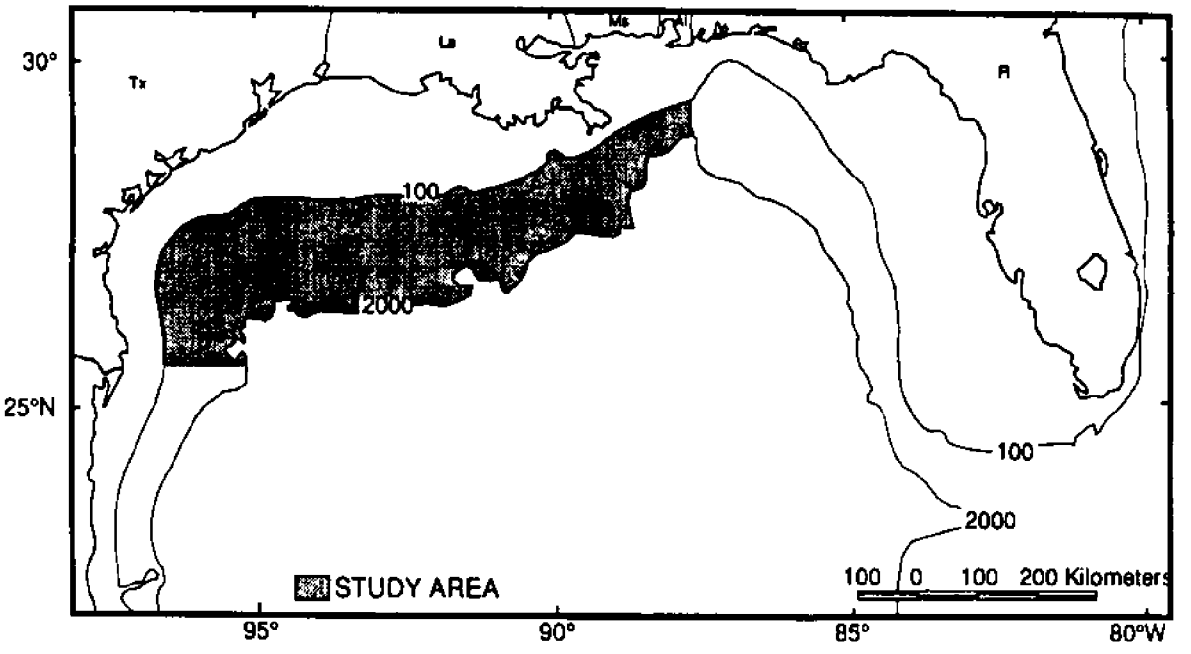

Figure 2. Map of the census area, from the Texas-Mexico border eastward to the Alabama-Florida border, off shore from the 100 meter isobath to the 2000-meter isobath

Although the main emphasis of the GulfCet program is endangered marine mammals, we are also pulling the array through areas of high densities of several species of demersal fishes and penaeid shrimp. In 1983 the Minerals Management Service published an atlas of the demersal fishes and shrimp of the soft bottoms of the continental shelf from the Rio Grande River to the Mississippi Delta. Excerpts of species lists and maps of the study area are presented in the Northwestern Gulf Shelf Bio-Atlas, Open File Report 82-04, U.S. Department of the Interior/Minerals Management Service 1983.

The towed acoustic array we are using is a modification of the original array constructed for and tested by the Hubbs Sea World Research Institute, San Diego, California. Most of the high frequency hydrophones have been replaced, and both temperature and depth modules have been installed at both the head and tail ends of the array. The array covers a frequency band from 5 Hz to 25 kHz. In order to target a broad range of species, there are three "tuned" sections or modules: a low frequency module containing eight groups of hydrophones centered at 30 Hz; single groups centered at 480 Hz, and 3.5 kHz; and two modules (front and aft) with hydrophones groups centered at 5, 10, and 15 kHz (Figure 3). The sound reception field of the array is perpendicular to the

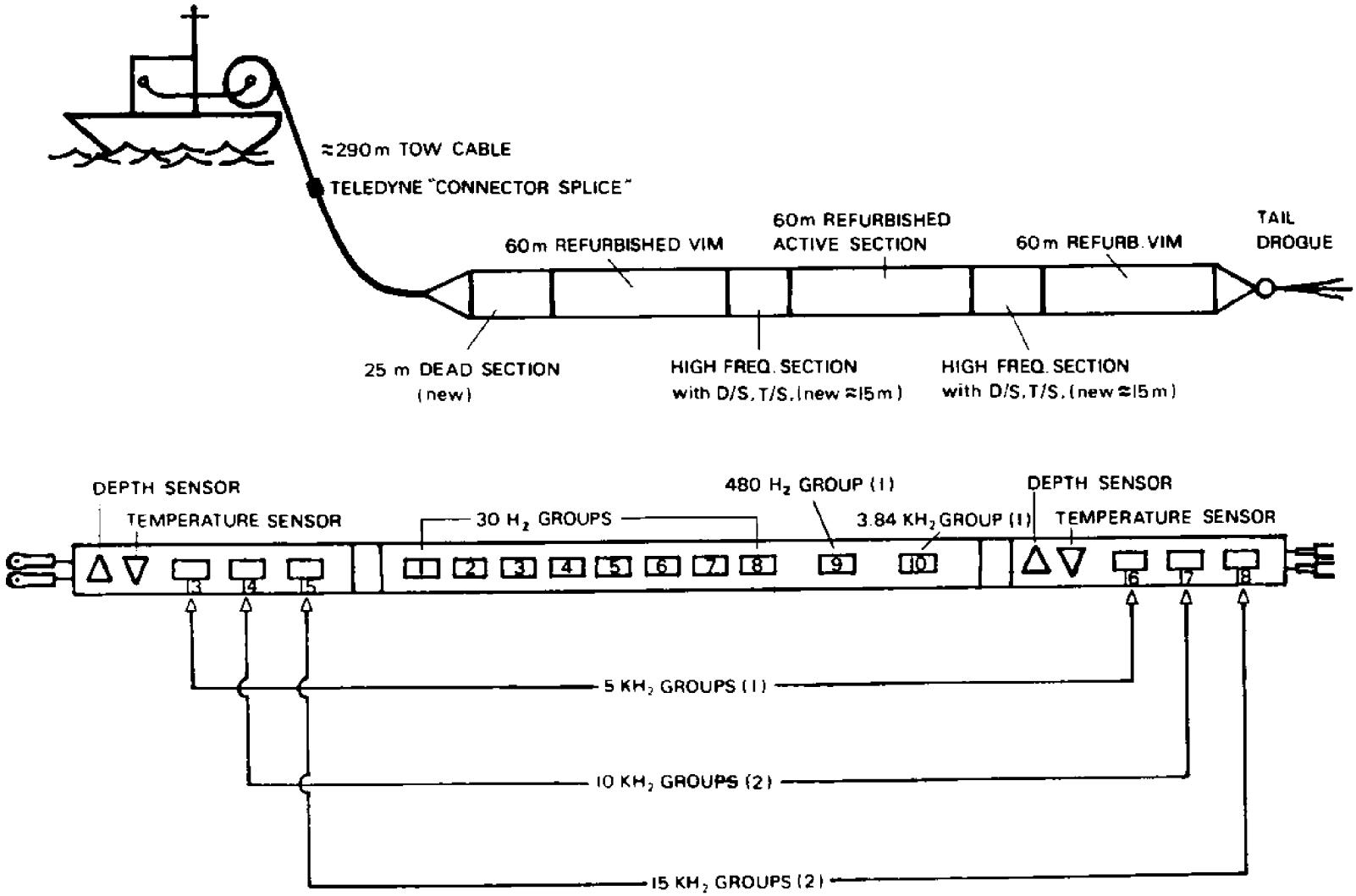

Figure 3. Diagram of the linear acoustic array, illustrating its various components including the placement of depth and temperature sensors, and the various hydrophone groups and their respective frequency ranges

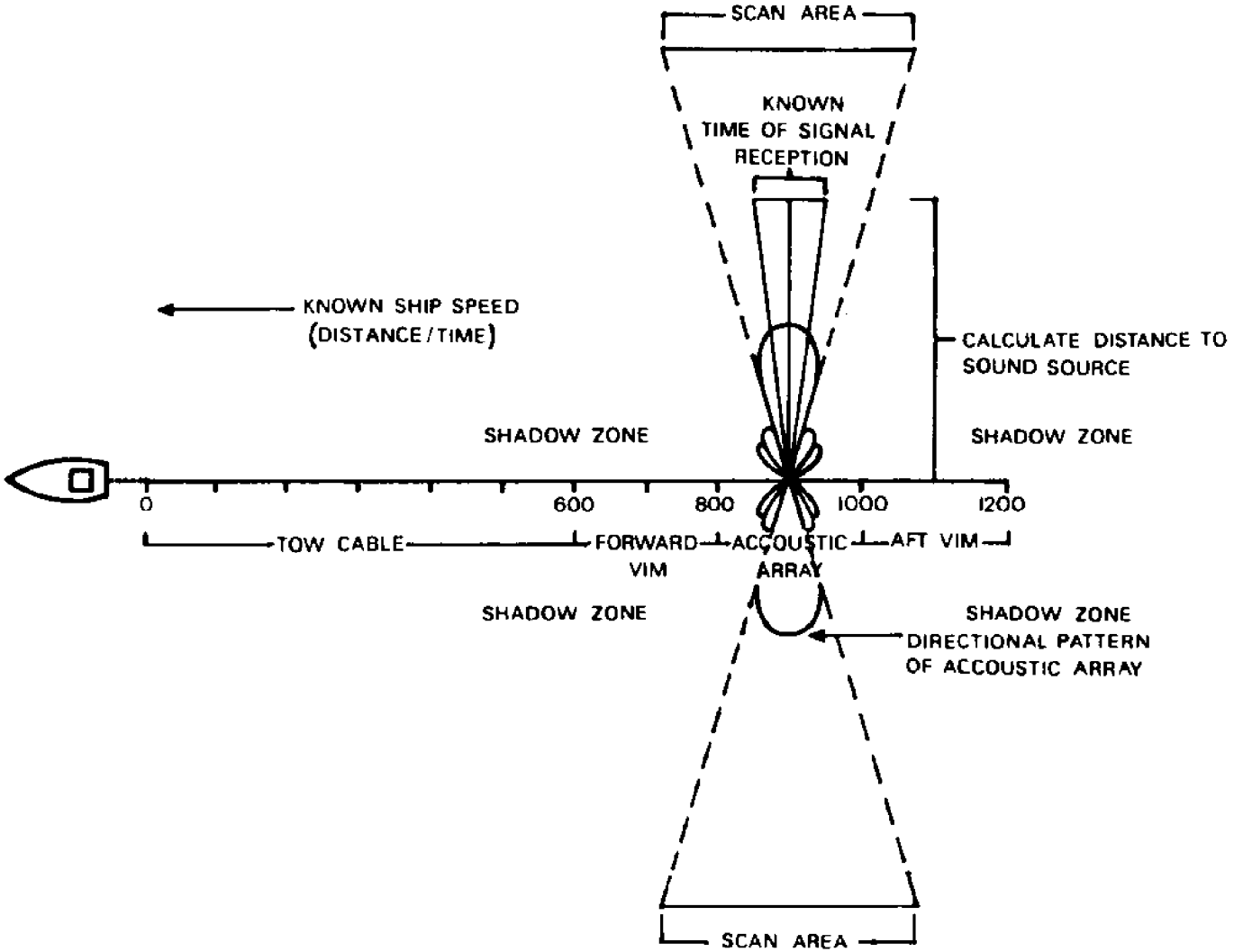

Figure 4. A sound reception field of array

direction of the tow, thus reducing self-noise from the towing vessel (Figure 4). Incoming signals are processed in real time using an on board acoustic/signal processing system. A real time frequency vs time display is monitored all the time the array is in the water. All incoming signals are recorded on an eight channel Racal Store V FM tape recorder. The frequency response of the system is limited by the hydrophones and our choice of tape speed. The analysis system and the recorder are effective from 0-100 kHz. The signal processing system currently in use utilizes a 386 CPU and the SIGNAL System Software which provides for the real time sonagraph, FFT analyses, cross correlation, signal filtering, and weighting. An illustration of the system as installed on the R/V LONG HORN is presented in Figure 5.

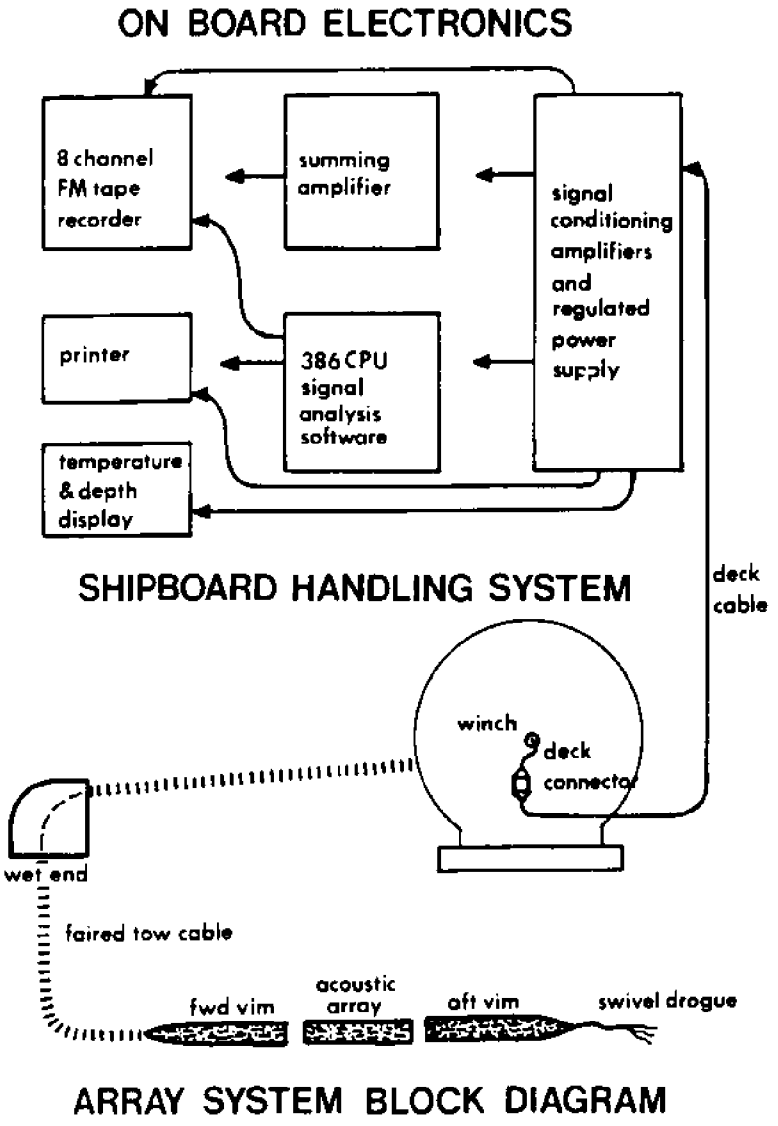

Figure 5. A diagram of the system as installed on the R/V LONG HORN

We started the first GulfCet cruise on April 15, 1992. Fourteen north-south transects starting at the Mexican-Texas border were completed between April 15 and May 1, 1992. The University of Texas Oceanographic Research Vessel LONG HORN was used for the survey. In addition to the around the clock acoustic survey, a visual survey using two 25 X 150 binoculars was conducted from dawn to dusk. Two observers and a data recorder using 10X binoculars reported sightings of marine mammals, birds, sea birds, marine turtles, fish schools, ships, boats, and unusual ocean conditions. A complete suite of oceanographic samples, including XBT stations and CTD down to 1000 meters were systematically collected along the 14 north-south transects (Figure 6).

During the cruise there were 16 sightings of seven cetacean species. There were a total of 47 acoustic contacts with marine mammals, nine of these were in association with the visual contacts. The additional acoustic contacts were at night and during sea states or weather conditions when visual observations were not possible. For example, sperm whale (*Physeter macrocephalus*) were heard on five different occasions, though seen only once. There were also several suspected fish contacts, and two recordings of shrimp. Several observers have suspected that there was noise associated with the daily migration of the deep scattering layer. Results from this initial cruise have verified this suspicion.

Passive sonar technology, such as the towed array being used in the GulfCet program, has the potential of being a useful supplement to other techniques being used to evaluate fisheries resources. Large areas can be mapped rapidly since the survey technique is continuous and not limited by the availability of light or fair weather. Temperature, depth, light transmission, and salinity sensors can be installed to provide continuous corollary environmental data.

The successful development of a passive acoustic detection technology will benefit commercial, environmental, and scientific interests and, hopefully, will help in the development of effective management programs and policies by improving the accuracy of our resource population estimates.

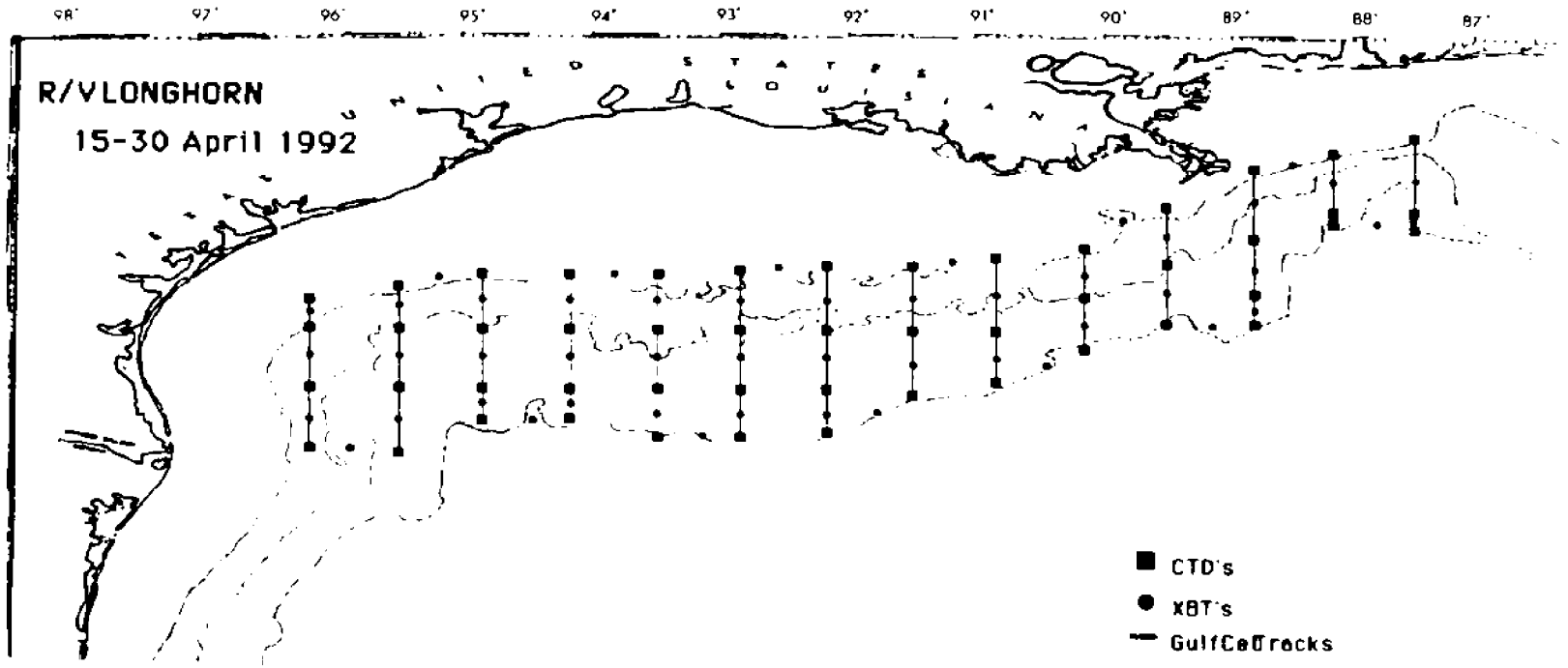

Figure 6. Map of the locations of oceanographic samples, including XBT and CTD stations

REFERENCES

Caldwell, M.C., D.K. Caldwell, and P.L. Tyack. 1990. The Bottlenose Dolphin: Recent Progress in Research. San Diego: Academic Press.

Fish, M.P., and W.H. Mowbray. 1970. Sounds of Western North Atlantic Fishes. Baltimore: John Hopkins Press.

Ford, J.K.B., and H.D. Fisher. 1982. Killer whale (*Orcinus orca*) dialects as an indication of stocks in British Columbia. Report International Whaling Commission. **32**:671-679.

Fristrup, K.M., and W.A. Watkins. 1992. Characteristics acoustic features of marine animal sounds. Technical Report, Woods Hole Oceanographic Institution.

Johannesson, K.A., and R.B. Mitson. 1983. Fisheries acoustics, a practical manual for aquatic biomass estimation. FAO Fisheries Technical Paper 240.

Myrberg, A.A. Jr. 1978. Ocean noise and the behavior of marine animals: relationships and duplications. In: Effects of Noise on Wildlife, eds. J.L. Fletcher and R.G. Busnel, pp. 169-208. New York: Academic Press.

Payne, R., and L.N. Grunee. 1983. Humpback whale (*Megaptera novaeangliae*) songs as an indicator of "stocks." In: Communication and Behaviour of Whales, ed. R. Payne, pp. 333-358. Boulder: Westview Press.

Takemura, A. 1972. Distribution of biological underwater noise at the coastal waters of Japan. *Bulletin of Japan Society of Scientific Fisheries.*

Watkins, W.A. 1977. Acoustic behavior of sperm whales. *Oceanus*. **20(2)**:50-58.

NEW DIRECTIONS IN GENE TRANSFER BIOTECHNOLOGY OF FISH

William L. Muhlach, Christopher C. Kohler, and Cynthia C. Young
Southern Illinois University
Carbondale, Illinois, USA

ABSTRACT

Numerous laboratories have reported varying degrees of success from initial attempts at producing transgenic fish. These early efforts have produced results typically characterized by low levels of transgenicity and transgene expression, as well as high levels of mosaicism. Much research is needed before this technology becomes a routine and cost effective method for the development of new genetic fish stocks. New techniques and strategies that we are using to alleviate such problems and to increase the efficiency of gene transfer technology for fish include the following: 1) utilization of zygote and/or sperm electroporation methodology, in place of microinjection, to more efficiently introduce transgene DNA into the fish embryo; 2) co-introduction of purified fish nuclear proteins with the transgene DNA to help ensure its incorporation into the cell's nucleus; 3) development of an "integration cassette" DNA construct to target the integration site to increase the frequency of chromosomal integration, reduce the incidence of deleterious insertional effects, as well as increase the chance for transgene expression; and 4) utilization of a sensitive assay for transgenicity that does not require killing the larval fish. Once developed and tested, these experimental protocols should be readily adaptable to a wide variety of aquatic organisms. Although there are certainly environmental and ethical concerns regarding transgenic work, we think that the establishment of precise experimental protocols, with predictable results, will greatly reduce the potential for long term problems and allow this powerful technology to have a significant and beneficial impact on aquatic science.

INTRODUCTION

Gene transfer biotechnology originally served as a valuable technique for basic molecular and cellular biology investigations. The power of this technology is evidenced by how quickly it moved from basic research into more applied areas such as biomedical, industrial and agricultural biotechnology applications. The introduction of foreign genes into developing embryos is now possible for a variety of animal and plant species (for review see Pursel, et al., 1989). This technology has already resulted in the development of improved plant and animal genetic stocks, the mass production of biological compounds (e.g., insulin), and is likely to become a valuable medical tool when applied to somatic cell gene therapy for humans suffering from genetic disorders. The U.S. Food and Drug Administration has recently released guidelines to pave the way for genetically engineered food products to reach the marketplace. Most importantly, these established guidelines are no stricter than those for any other food products.

Delivery of transgene DNA (foreign DNA) via standard microinjection into the one-celled fish zygote is a labor intensive, highly technical process. Moreover, the process is tenuous for fish because the transgene DNA cannot be directly delivered into the male pronucleus, as is done for mammalian species, but rather must simply be injected into the active cytoplasm of the newly fertilized egg. Furthermore, for many species of fish, the egg's chorion provides a formidable barrier to microinjection attempts. Once the

DNA has been injected, the investigator must then rely on chance that the transgene DNA actually gets incorporated into the newly forming nucleus so that it has an opportunity to integrate into the host genome. If integration is successful, additional problems can arise. For example, the integrated transgene might be located in a region of chromatin that will not allow it to be expressed, or, in the process of integrating, the transgene might destroy vital genetic information that will have deleterious effects on the viability of the embryo.

Several laboratories have reported varying degrees of success in their initial attempts at producing transgenic fish (Chourrout, et al., 1986; Dunham, et al., 1987; Chen, et al., 1989; Guyomard, et al., 1989; Rokkones, et al., 1989; Schneider, et al., 1989; Zhang, et al., 1990; Phillips, et al., 1992; Hew and Gong, 1992; Gross, et al., 1992). There is, however, much research to be done before this technology becomes routine and cost effective. Early efforts, including our own (Phillips, et al., 1992; Paleudis et al., 1992) have produced variable results that have typically been characterized by low levels of transgenicity and transgene expression, as well as a high incidence of mosaicism. Our research program fills an important niche in the application of gene transfer biotechnology to aquatic systems because it endeavors to integrate basic laboratory and applied fisheries components. In order to enhance our productivity and to make this technology routine and cost effective, we are moving away from early standard protocols and are applying new techniques and strategies.

ELECTROPORATION: HIGHER TRANSGENE DELIVERY RATE

We have been able to successfully microinject both tilapia (Phillips, et al., 1992) and salmon eggs in previous experiments. However, as an alternative to microinjecting individual fish embryos, we are now employing electroporation as a means of simultaneously introducing transgene DNA into large numbers of fish embryos (preferably at the one-cell zygote stage). Electroporation, in which a brief electrical pulse makes the membrane of a cell temporarily permeable to macromolecules, is a relatively new technique for producing transgenic animals (see Figure 1). It is expected that this methodology will greatly increase the efficiency of transgene DNA introduction into the fish embryos and gametes. Buono and Linser (1991) and Liu et al. (submitted) have reported the production of transgenic zebrafish and medaka, respectively, through the use of electroporation. We have successfully worked out the electroporation parameters that allow the introduction of marker molecules into early stage tilapia embryos. Similarly, we are planning the electroporation of sperm as an alternative means of producing transgenic fish. Gagne, et al. (1991) used electroporation of bovine spermatozoa to carry transgene DNA into bovine oocytes. The spermatozoa were not transgenic, per se, but were used as vectors to carry the DNA into the oocytes at the time of fertilization and egg activation. Fish sperm is a particularly promising model since we are able to extend sperm viability with extender solutions (Scott and Baynes, 1980).

NUCLEAR PROTEINS: ENHANCED ACCESS OF TRANSGENE DNA TO ZYGOTE NUCLEUS

The incorporation of a foreign gene into the fish genome is critically dependent upon the ability of that DNA to enter the cell's nucleus. This is typically accomplished in mammalian studies by microinjection of the DNA directly into a pronucleus shortly after fertilization. Because the physical characteristics of most fish eggs prevent direct delivery of DNA into the nuclear elements, an alternative method has been devised. A critical step in the formation of an embryonic cell nucleus after fertilization is the

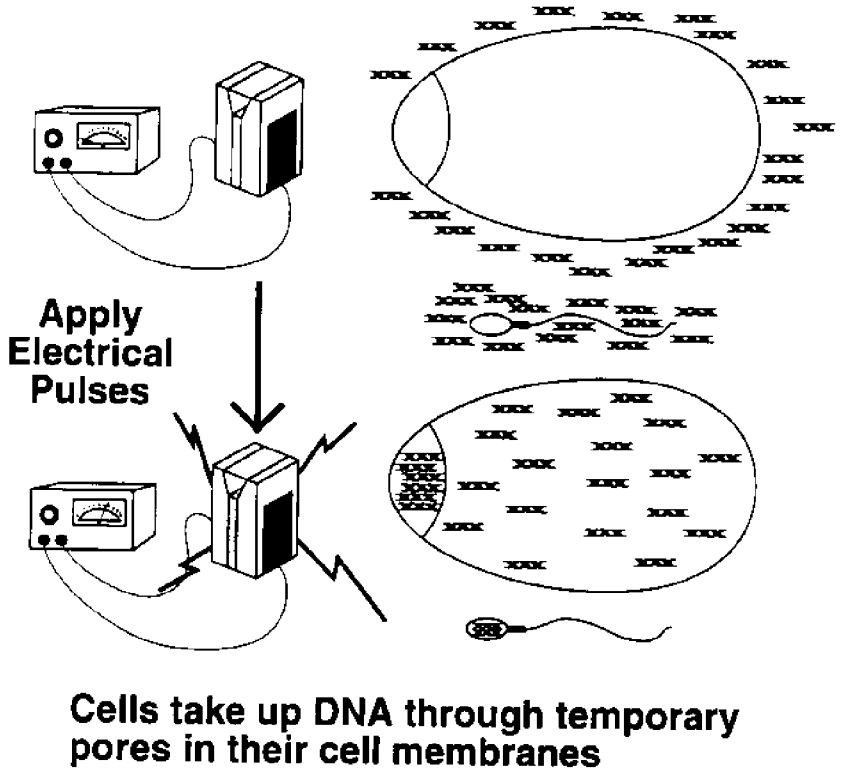

Figure 1. Gene transfer into fish by electroporation. One-cell zygotes and spermatozoa are treated with electrical pulses that cause the cell's membrane to become temporarily permeable to macromolecules such as DNA. Electroporation is quickly replacing microinjection technology as the method of choice for the simultaneous introduction of transgene DNA into a large number of fish embryos.

reassembly of the nuclear membrane. Nuclear membrane formation is an ordered process with discrete intermediate steps. One of these steps is the initial assembly of nuclear membrane around each of the chromosomal elements. The chromosomes are made up of chromatin material which mainly consists of a combination of DNA and DNA-binding nuclear proteins. The association between DNA and nuclear proteins causes the chromatin to condense. The newly forming nuclear membrane components begin to assemble around the DNA only after the chromatin is fully condensed. The nuclear membrane forms around each chromosome resulting in numerous small nuclei which subsequently fuse to form a single large nucleus containing all chromosomal elements (Alberts, et al., 1989; Newport and Forbes, 1987). It is believed that nuclear proteins play an important role in the reassembly of the cell's nucleus. Recently, Kaneda et al. (1989) reported a greater than 95% efficiency in the rapid transportation of the DNA into the nuclei of cultured cells via vesicle complexes when nuclear proteins were included. Furthermore, when plasmid DNA and nuclear proteins were co-introduced into rat liver cells, the plasmid DNA was carried into the cell nuclei and expressed at a rate 5 times greater than DNA co-introduced with non-nuclear proteins. High mobility group (HMG) nuclear proteins were used in these studies because they are known to be involved in the formation of nucleosomes, a basic element of chromatin structure. In addition, HMG proteins recognize and bind both single and double stranded DNA (Goodwin, et al., 1978; Elton, et al., 1987) and serve to protect the DNA from DNase enzymatic digestion (Hentzen and Bekhor, 1985). Using a modified method of Nicolas and Goodwin (1982), we have successfully purified fish HMG nuclear proteins (see Figure 2)

for electroporation into one-cell embryos with the transgene DNA. Co-introduction of these nuclear proteins should help to ensure that the transgene DNA is protected from degradation and increase the chance that it becomes incorporated into the nucleus (see Figure 3).

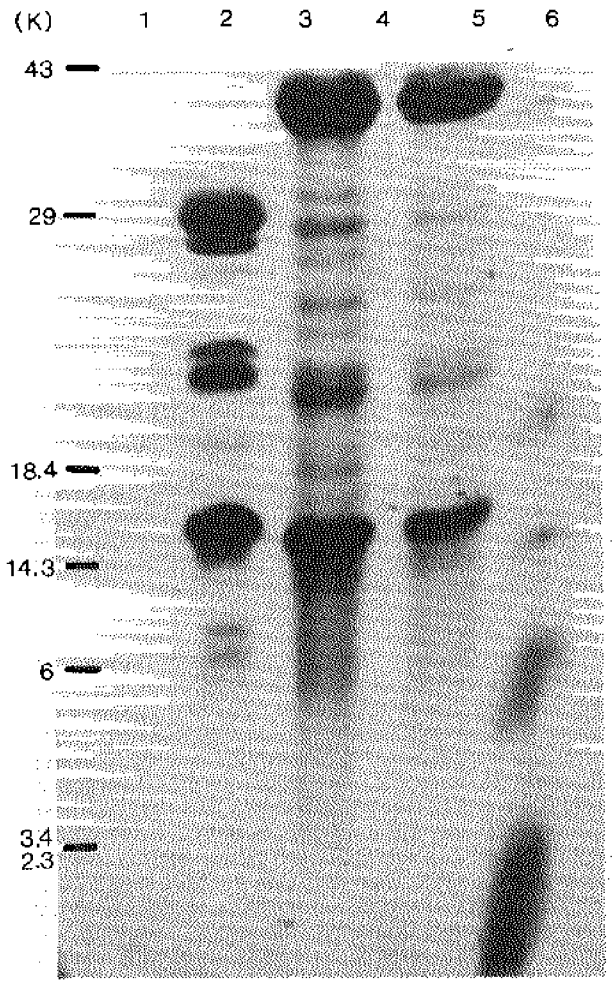

Figure 2. Purification of fish nuclear proteins. Shown here is a coomassie blue stained acrylamide gel containing high molecular weight (HMG) nuclear proteins purified from salmon (lane #3) and tilapia (lanes #4 and #5). Molecular size markers are shown in lanes #1 and #6 (lane #2 is empty). These nuclear proteins are co-introduced with foreign DNA to protect the DNA from enzymatic degradation and to help ensure that the DNA becomes incorporated into the nucleus (see Figure 3).

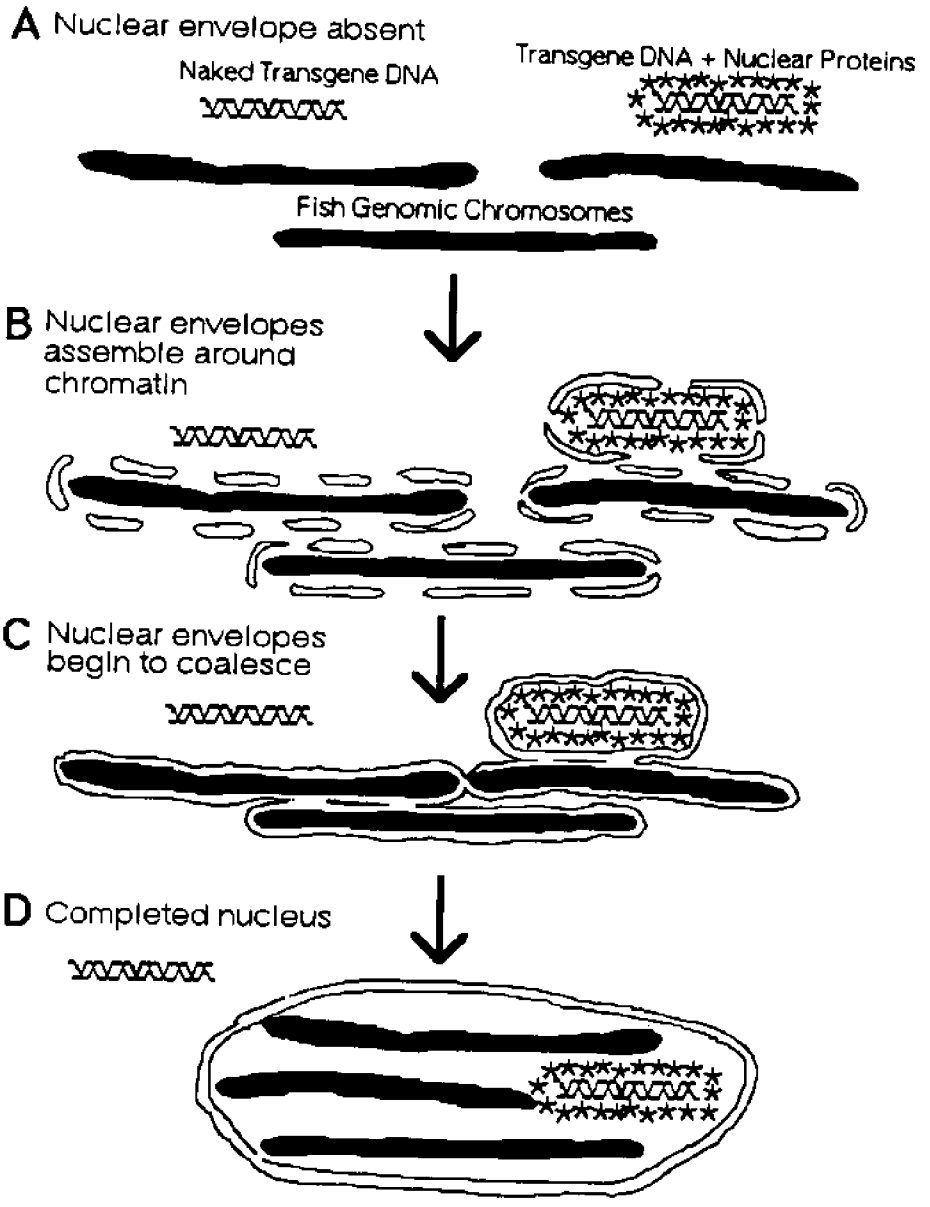

Figure 3. Illustration of the proposed action of nuclear proteins in delivering transgene DNA elements into the nucleus. Chromatin, a combination of DNA and nuclear proteins, serves as a critical factor in the reassembly of the chromosomal elements into the cell's nucleus. By ensuring that the introduced DNA has access to the nucleus, nuclear proteins can potentially enhance the chances for the stable integration of transgene DNA into the fish genome during the early embryonic period.

INTEGRATION CASSETTE TECHNOLOGY: STRATEGY TO ENSURE OPTIMAL TRANSGENE INTEGRATION INTO HOST GENOME

While the timing of the introduction of transgene DNA into the embryo and its accessibility to the host nucleus are both important considerations, the actual integration process is critical for the successful production of a transgenic fish. An undesirable integration site could be lethal if the transgene inactivates important genetic information in the host's chromosomes. Similarly, the transgene might not be functional if it becomes incorporated into a heterochromatin region of the genome that prevents it from being actively expressed. We are in the process of designing a transgene DNA construct to target the chromosomal integration site in order to: 1) increase the frequency of successful chromosomal integration of the transgene, 2) reduce the incidence of deleterious insertional effects, as well as to 3) increase the chance for transgene expression. In doing so, we are taking advantage of a biological phenomenon known as "homologous recombination" that serves as the foundation for genetic recombination during normal meiosis and the integration of retroviral elements into host chromosomes. In order to accomplish this, specific DNA flanking sequences that are homologous to DNA in the fish genome will be included at each end of the transgene DNA construct. These sequences are designed to increase the frequency of integration and to ensure that integration is at a non-lethal, expressible site within the host fish genome. For this purpose, the nucleolar region of the fish genome, containing the multiple-copy ribosomal RNA (rRNA) genes, has been selected as the integration target site. DNA sequence information is readily available for rRNA genes and these genes have proven to be highly evolutionarily conserved. We have targeted the rRNA genes because there are hundreds of genomic copies of the rRNA genes to serve as targets, and insertion (disruption) into one or more of these target genes would presumably have no effect on normal cellular processes. Since cells constantly produce ribosomes for, the rRNA genes are constitutively expressed. Therefore, an integrated transgene would be located in a chromatin region (chromosomal context) that would optimize its chance for expression. For these reasons, we consider our transgene DNA constructs to be "integration cassettes." Furthermore, due to the evolutionary conservation of the rRNA genes in vertebrates, the identification of a successful integration cassette flanking sequence for tilapia would represent a DNA construct that could be directly applied to gene transfer efforts in other fish species.

POLYMERASE CHAIN REACTION: SENSITIVE ASSAY FOR TRANSGENICITY

The sensitivity of the Polymerase Chain Reaction (PCR) protocol to amplify specific sequences of DNA permits the analysis of the genome of fish from small samples of tissue, blood, or gametes, while allowing the fish to remain alive. This is an important consideration when attempting to obtain viable brood stock for genetic studies. Additionally, this sensitivity allows for earlier screening of live animals which will provide faster, and more reliable, feedback regarding the effectiveness of transgene methodology. However, in order to use PCR techniques to detect a particular genetic element, the researcher must know the nucleotide sequence of that genetic element in order to make the necessary DNA primers. In the present application, detailed knowledge of the "integration cassette" construct makes PCR primer sequence identification relatively straight forward. After the initial PCR screening for transgenicity, transgene integration is verified for positive samples via standard Southern blot analysis (see Paleudis, et al., 1992). The digoxigenin non-radioactive chemiluminescent detection system is used in order to avoid the disadvantages associated with the use of radioactive DNA probes, namely safety risks, requirements for special laboratories and training of personnel, hazardous waste disposal expenses and protocols, instability of probes, and higher costs (Holtke, et al., 1992).

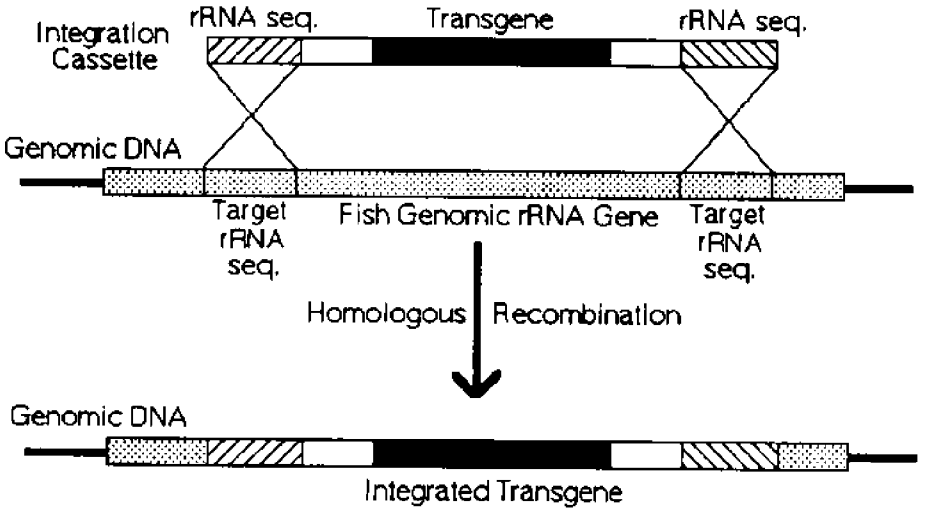

Figure 4. Integration cassette technology. Our current work with fish embryos employs a homologous recombination strategy in an attempt to increase the success rate for the production of transgenic fish while minimizing potential problems associated with random DNA integration. The transgene DNA is inserted into a DNA construct that contains flanking DNA sequences that are homologous to regions of the multiple-copy ribosomal RNA genes of the fish genome.

SUMMARY

Once developed and tested, the experimental protocols presented here should be readily adaptable to a wide variety of aquatic organisms and scientific applications. Along with the advent of gene transfer biotechnology comes significant ethical and moral considerations (Kohler, et al., 1992). However, with the use of sound scientific methodology under the guidance of established Recombinant DNA guidelines, gene transfer technology is certain to provide many more benefits than problems. In practice, gene transfer technology is not unlike the selective breeding techniques initiated thousands of years ago by our agricultural-minded ancestors, the major difference being the accelerated pace possible with modern science. Basic research done now will lay a strong foundation for very important uses of biotechnology in response to unforeseen problems and situations that mankind will face in the future.

ACKNOWLEDGMENTS

This work was supported in part by the Illinois-Indiana Sea Grant Program (grant: Gene Transfer Technology for Aquaculture, IL-NOAA-University of Illinois-86-124). The findings and opinions expressed herein are those of the authors and not necessarily those of Sea Grant.

REFERENCES

Alberts, B., Bray, D., Lewis, J., Raff, M., Roberts, K., and Watson, J.D. 1989. *Molecular Biology of the Cell*, Second Edition. Garland Publishing Inc., New York. Chapter 13. Cell growth and Division. pp. 727-790.

Buono, R.J., and Linser, P.J. 1991. Transgenic zebrafish by electroporation. *US/EG Bulletin* 1354.

Chen, T.T., C.M. Lin, Z. Zhu, L.I. Gonzalez-Villasenor, R A. Dunham, and D.A. Powers. 1989. Gene transfer, expression and inheritance of rainbow trout and human growth hormone genes in carp and loach. In: UCLA Symposium on Cell and Molecular Biology.

Chourrout, D., R. Guyomard, and L. Houdebine. 1986. High efficiency gene transfer in rainbow trout (*Salmo gairdneri* Rich.) by microinjection into egg cytoplasm. *Aquaculture*. **51**:143-150.

Dunham, R.A., and J. Eash. 1987. Transfer of the metallothionein-human growth hormone fusion gene into channel catfish. *Trans. Am. Fisheries Soc.* **116**:87-91.

Elton, T.S., M.S. Nissen, and R. Reeves. 1987. Specific A-T DNA sequence binding of RP-HPLC purified HMG-I. *Biochem. Biophys. Res. Commun.* **143**:260-265.

Gagne, M.B., F. Pothier, and M.-A. Sirard. 1991. Electroporation of bovine spermatozoa to carry foreign DNA in oocytes. *Molecular Reprod. and Dev.* **29**:6-15.

Goodwin, G.H., J.M. Walker, and E.W. Johns. 1978. The high mobility group (HMG) nonhistone chromosomal proteins. In: *The Cell Nucleus*, Vol. VI. Academic Press, Inc., New York. pp. 181-219.

Gross, M., J. Schneider, N. Moav, B. Moav, C. Alvarez, S. Myster, Z. Lin, E. Hallerman, P. Hackett, K. Guise, A. Faras, and A. Kapuscinski. 1992. Molecular analysis and growth evaluation of northern pike (*Esox lucius)* microinjected with growth hormone genes. *Aquaculture*. **103**:253-273.

Guyomard, R., D. Chourrout, C. Leroux, L Houdebine, and F. Pourrain. 1989. Integration and germ line transmission of foreign genes microinjected into fertilized trout eggs. *Biochimie*. **71**:857-863.

Hentzen, P.C., and I. Bekhor. 1985. Characterization of the 2 M NaCl-resistant chromatin fraction from chicken erythroid cells. n: *Progress in Nonhistone Protein Research*, Vol. 1 (Bekhor, I., ed.). CRC Press, Inc., Boca Raton, FL. 75-101.

Hew, C., and Z. Gong.1991.Transgenic fish: a new technology for fish biology and aquaculture. *Biology International*. **24**:2-10.

Holtke, H.J., Sanger, G., Kessler, C., and Schmitz, G. 1992. Sensitive chemiluminescent detection of digoxigenin-labeled nucleic acids: a fast and simple protocol and its applications. *BioTechniques*. **12**:104-113.

Kaneda, Yasufumi, Kunimitsu Iwai, and Tsuyoshi Uchida. 1989. Increased expression of DNA co-introduced with nuclear Protein in adult rat liver. *Science*. **243**:375-378.

Kohler, C.C., W.L. Muhlach, P.C. Phillips, and G.A. Paleudis. 1992. Environmental and ethical concerns associated with transgenic fishes. *J. World Aquaculture Society.* **22**:97.

Lu, J.-K., C.L. Chrisman, O.M. Andrisani, J.E. Dixon, and T.T. Chen. 1992. Integration, expression and germ-line transmission of foreign growth hormone genes in medaka, *Oryzias latipes. Marine Molecular Biology and Biology.* Submitted.

Marx, J. 1989. Many gene changes found in cancer. *Science.* **246**:1386-1388.

Newport, J.W., and D.J. Forbes. 1987. The nucleus: structure, function, and dynamics. *Annu. Rev. Cell Biol..* **56**:535-565.

Nicolas, R.H. and G.H. Goodwin. 1982. Isolation and analysis. In: *The HMG Chromosomal Proteins.* (Johns, E.W., ed.) Academic Press, London. pp. 41-68.

Paleudis, G.A., C.C. Kohler, W.L. Muhlach. 1992. Application of high hybridization stringency technology to the analysis of putative transgenic fish and their progeny. *J. World Aquaculture Society.* **22**:114-121.

Phillips, P.C., C.C. Kohler, and W.L. Muhlach. 1992. Procedural protocol, survival to hatching, survival to hatching and plasmid DNA fate after microinjection into tilapia zygotes. *J. World Aquaculture Society.* **22**:98-113.

Pursel, V.G., C.A. Pinkert, K.F. Miller, D.J. Bolt, R.G. Campbell, R.D. Palmiter, R.L. Brinster, and R.E. Hammer. 1989. Genetic engineering of livestock. *Science.* **244**:1281-1288.

Rokkones, E., P. Alestrom, H. Skjervold, and K.M. Gautvik. 1989. Microinjection and expression of a mouse metallothionein human growth hormone fusion gene in fertilized salmonid eggs. *J. Comp. Physiol. B.* **158**:751-758.

Schneider, J.F., E.M. Hallerman, S.J. Yoon, L. He, S.H. Myster, M. Gross, Z. Liu, Z. Zhu, P.B. Hackett, K/S. Guise, A.R. Kapuscinski, and A.J. Faras. 1989. Microinjection and successful transfer of the bovine growth hormone gene into the northern pike, *Esox lucius. J. of Cellular Biochemistry* UCLA Symposia on Mol. & Cell. Biology: Abstracts. 18th Annual Meeting: 173.

Scott, W.B., and J.H. Baynes. 1980. A review of the biology and handling and storage of salmonid spermatozoa. *J. Fish. Biol.* **17**:707-739.

Zhang, P., M. Hayat, C. Joyce, L.I. Gonzalez-Villasenor, C.M. Lin, R.A. Dunham, T.T. Chen, and D.A. Powers. 1990. Gene Transfer, expression and Inheritance of pRSV-rainbow trout-GH cDNA in the common carp, *Cyprinus carpio* (Linnaeus). *Mol. Reprod. & Dev.* **25**:3-13.

A NATIONAL MARINE SANCTUARY FOR HAWAI'I'S KOHALA

William J. Thomas
University of Hawai'i at Manoa
Honolulu, Hawai'i, U.S.A.

Steven G. Olson
National Coastal Research Institute
Portland, Oregon, U.S.A.

ABSTRACT

Title III of the Marine Protection, Research and Sanctuaries Act of 1972, 16 U.S.C. § 1431 *et seq.*, (the "Act") authorizes the Secretary of Commerce to designate discrete areas of the marine environment as national marine sanctuaries to protect their special conservational, recreational, ecological, historical, research, educational, or aesthetic qualities. The Act is administered by the National Oceanic and Atmospheric Administration (NOAA).

In December 1977, NOAA received a nomination for a humpback whale national marine sanctuary in the waters off Maui, Hawai'i. In January 1984, NOAA released a Draft Environmental Impact Statement/Draft Management Plan. Based on the comments received, subsequent review and consideration of the site was suspended.

In October 1990, Congress directed NOAA to determine the feasibility of establishing a humpback whale national marine sanctuary in Hawaiian waters. After significant public, State, and Federal consultation, NOAA published and transmitted its study to Congress in December 1991. In November 1992, the Hawaiian Islands Humpback Whale National Marine Sanctuary was designated.

Four critical factors will determine the success of the Nation's newest national marine sanctuary: 1) a clear understanding of the benefits and limits of sanctuary designation; 2) an understanding and appreciation of Hawaiian culture; 3) cooperation from marine and coastal user groups; and 4) coordination between NOAA and the State.

INTRODUCTION

The Hawaiian story of creation, the ***Kumulipo***, tells us of Earth's creation. Out of the realm of darkness, light, air, land, and water were created. The creatures that live on the land and in the water were formed and life on earth began. Among the largest creatures created were the *kohola*, or whales, whose guardian on land was the *ili-ahi*, or sandalwood tree. The ***Kumulipo*** tells us "...a procession of *kohola* are passing by, the *opule* are swimming in schools for a long distance, and the ocean is thick with them." (Beckwith, 1951; Johnson, 1981). Reflecting upon this magnificent tale, it is ironic to note that the *kohola* and its guardian, the *ili-ahi*, are both endangered species.

The ***Kumulipo*** indicates that the early Hawaiians were very aware of their environment, which they valued as a treasure for all; a treasure to be preserved for future generations. Preservation was a way of life. In westernized terms, the Hawaiians

practiced conservation and wise management of their resources because their lives and the lives of future generations; the survival of the Hawaiian race; depended on it.

Presently, we are witnessing a renewed interest in protecting one of the largest creatures referred to in the ***Kumulipo*** - the humpback whale.

HISTORICAL EFFORTS TO PROTECT THE HUMPBACK WHALE

Efforts to expand protection for the humpback whale beyond that offered by the Marine Mammal Protection Act and the Endangered Species Act date back to the late 1970s. During that period, numerous workshops and symposia dealing specifically with issues such as harassment, behavioral indicators of stress, and activities which might constitute harassment, were held. The results of this process included a set of formal recommendations by the U.S. Marine Mammal Commission, the issuance of a "Notice of Interpretation" on *Humpback Whale Harassment in the Hawaiian Islands Area* (44 FR 113, 1979) by the National Marine Fisheries Service (NMFS), and the formal submission of a proposal to the National Oceanic and Atmospheric Administration (NOAA) in 1977 for a humpback whale sanctuary in Hawaiian waters (NOAA, 1983).

The Marine Mammal Commission recommended a wide range of management alternatives to ensure the protection of the whales, including increased Federal enforcement presence during the whale season (Figure 1). The NMFS notice identified principal calving areas in Maui County waters, defined "taking" by means of harassment under the Marine Mammal Protection and Endangered Species Acts, and the identification of specific human activities which constituted harassment and, consequently, were subject to regulation (Figure 2). This notice currently serves as the principal means for protecting the humpback whale and managing its habitat in Hawai'i. The proposal for marine sanctuary status, submitted by a private researcher, recommended three boundary alternatives, all within the waters of Maui County but excluding the area referred to as Penguin Bank off the northwest coast of Moloka'i (Figure 3). The purpose of the proposed sanctuary was to *"preserve, protect, and manage essential, specialized habitat of the Hawaiian humpback whales, and to conserve genetic resources of the Hawaiian humpback breeding stock. In addition, the proposal is submitted to allow scientific research and education in support of humpback whale stock management, and to provide an ecological baseline to compare and predict the effects of man's activities on other humpback whale calving/breeding areas."*

Although the 1977 proposal was not successful, interest in protecting humpback whale populations and their habitats has continued. In October 1990, the 101st Congress directed NOAA to study the feasibility of designating a national marine sanctuary in the waters adjacent to Kaho'olawe Island (Public Law 101-515), giving special consideration to the effects of such a sanctuary on the population of *kohola*, or humpback whales, that inhabit the island's waters. In response to this directive, NOAA conducted a series of meetings in Hawai'i to solicit comments from Federal, state and local agencies and the public. The results were transmitted to Congress, published and distributed in December 1991 (NOAA, 1991).

In its report, NOAA concluded that the waters surrounding Kaho'olawe merit further consideration as a sanctuary because of their biological, cultural, and historic significance. In addition, NOAA suggested that other sites within the Hawaiian Archipelago may be investigated for consideration as a component of a possible multi-site national marine sanctuary. However, the feasibility of establishing a national marine sanctuary in Hawaiian waters appears to depend on four critical factors:

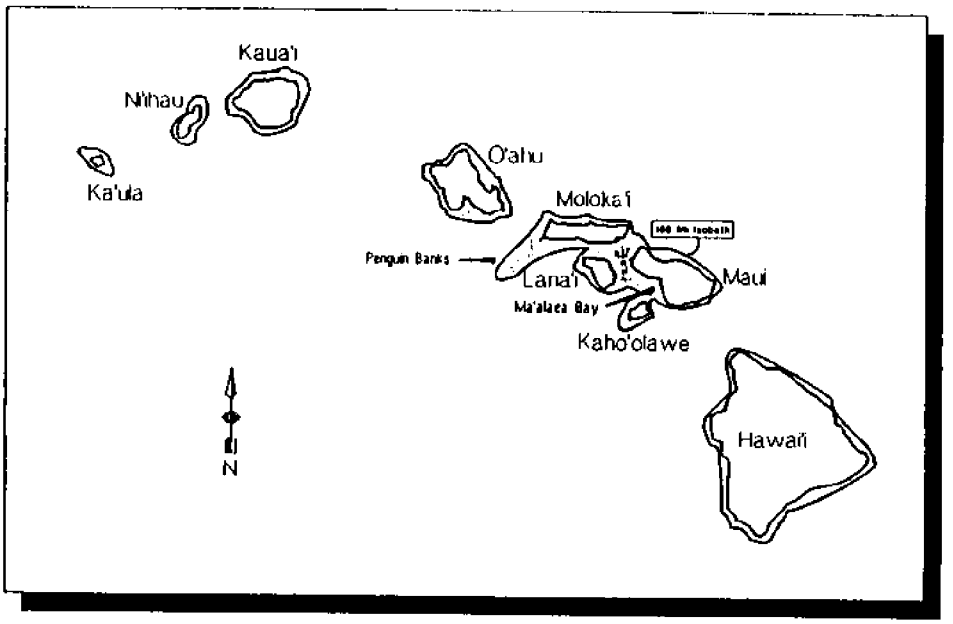

Figure 1. 1979 Marine Mammal Commission workshop recommendation

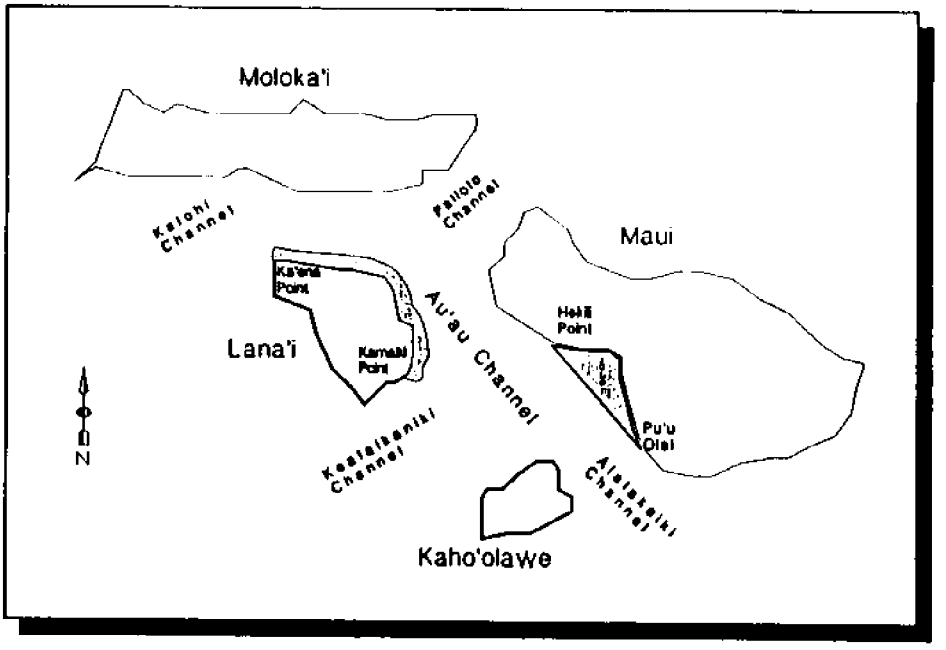

Figure 2. NMFS "Cow/Calf Zone"

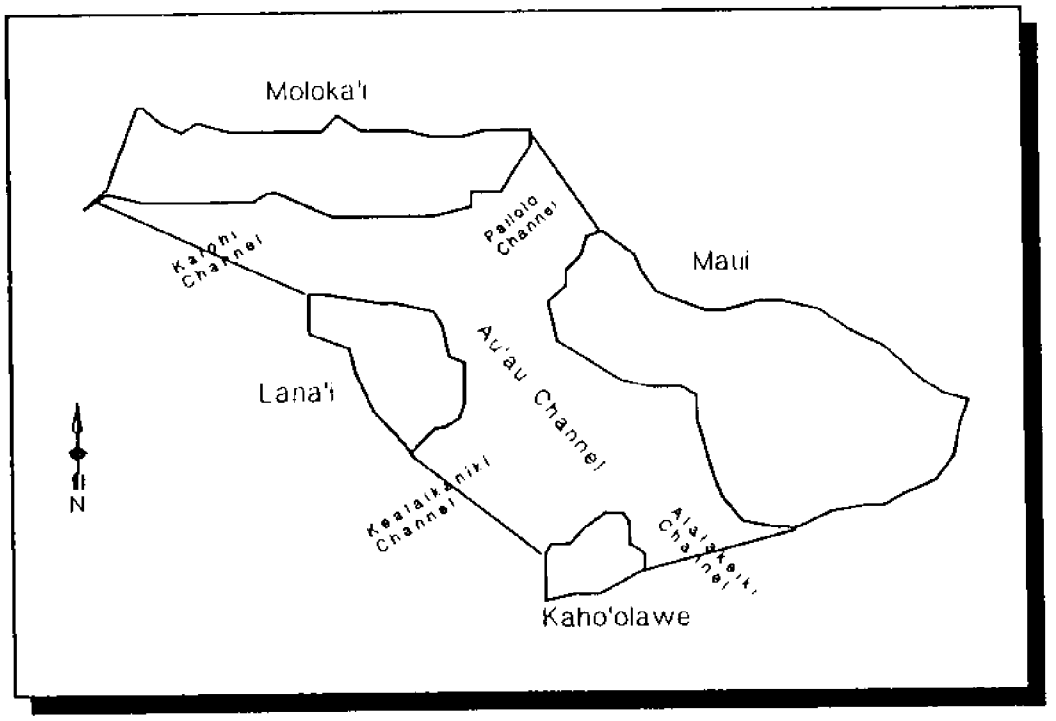

Figure 3. 1983 National Marine Sanctuary Program proposed boundaries

1) A clear description of the benefits and limits of the National Marine Sanctuary Program with respect to conservation and management of marine resources in Hawai'i;

2) An understanding and appreciation of Hawaiian culture and traditions and the incorporation of native Hawaiian interests in sanctuary planning and management;

3) Cooperation, from marine and coastal user groups, including recreational and commercial fishermen, other recreational users (such as divers, whale watchers, thrillcraft operators), coastal development interests, and environmental organizations; and

4) Coordination between NOAA and the appropriate State agencies.

THE NATIONAL MARINE SANCTUARY PROGRAM: WHAT CAN IT DO FOR HAWAI'I?

Congress passed the Marine Protection, Research and Sanctuaries Act (MPRSA) in 1972 to preserve nationally significant ocean resources. Under the MPRSA, the Secretary of Commerce may designate ocean and coastal waters, and areas of the Great Lakes, as National Marine Sanctuaries. Aside from protecting natural resources, such as fish, mammals, seabirds, and coral reefs, historic and cultural resources, such as

shipwrecks and the marine portions of ahupua'as (traditional Hawaiian land divisions that usually extend from the uplands to the sea), could also be considered for inclusion. The MPRSA provides the only opportunity under U.S. law to designate and manage discrete, offshore areas on an ecosystem basis. Other laws allow the management of individual resources, such as marine mammals and fish.

The MPRSA is administered by the Sanctuaries and Reserves Division of the Office of Ocean and Coastal Resource Management, National Ocean Service, NOAA, Department of Commerce. The major goals of the NMSP are to provide enhanced resource protection through comprehensive and coordinated management and conservation; to support, promote and coordinate scientific research on, and monitoring of, specific marine resources; to enhance public awareness, understanding, appreciation and wise use of the marine environment; and to facilitate multiple uses, to the extent that they are compatible, with the primary objective of resource protection (NOAA, 1991).

In general, Federal, State and county resource management statutes have been unable to keep pace with the increasing urbanization of Hawai'i and the pressures that are brought to bear on its resources. Recognizing this as a statewide problem, the Hawai'i legislature created the Hawai'i Ocean Resources Management Program (Act 235, HRS Chapter 228) to develop a comprehensive, coordinated, and integrated ocean policy. The Hawai'i Ocean and Marine Resources Council, formed in response to Act 235, has developed the Hawai'i Ocean Resources Plan. The Plan identified a number of issues regarding the need for coordinated, comprehensive management of Hawai'i's ocean resources (Hawaii Ocean and Marine Resources Council, 1991), including the establishment of marine conservation areas. Like the other national marine sanctuaries (Figure 4), the MPRSA can help the state of Hawai'i manage its ocean resources through a comprehensive, coordinated management regime.

Based on its experience in developing sanctuary management plans for a diversity of ecosystems and government entities, the NMSP has the capability of helping the state to tailor a resource management plan, consistent with Act 235, that will address a marine resource of State, national, and international significance: the humpback whale and a significant part of its habitat. The lessons learned from this planning process will undoubtedly provide valuable insight to the State in further addressing its other ocean resource management issues.

KAHO'OLAWE, THE KOHALA, AND HAWAIIAN CULTURE

To many Hawaiians, Kaho'olawe is the symbol of the revitalization of native Hawaiian culture. Part of this resurgence involves the traditional practices of subsistence fishing, canoe navigation, and the honoring of Hawaiian ocean and agricultural deities. *Aloha* aina, the belief that the land is the religion and the culture, and *ke ola kai*, the life of the ocean, are central to understanding the importance of Kaho'olawe to Hawaiians. In addition, its status as a *wahi pana* (sacred place) and *pu'uhonua* (place of refuge or sanctuary), makes it very significant to Hawai'i's culture.

In Hawaiian culture, the oral tradition of *mele*, or songs, chants and genealogical recitations that recorded significant historical events, do not refer specifically to the humpback whale, but to a generic whale called the *kohola*. As one of the most depleted species on earth, the *kohola's* scattered populations inhabiting the world's oceans today represent a small fraction of their former numbers and stand as reminders of man's recent history which has seen the humpbacks and other whale species extensively exploited by coastal and high seas whalers.

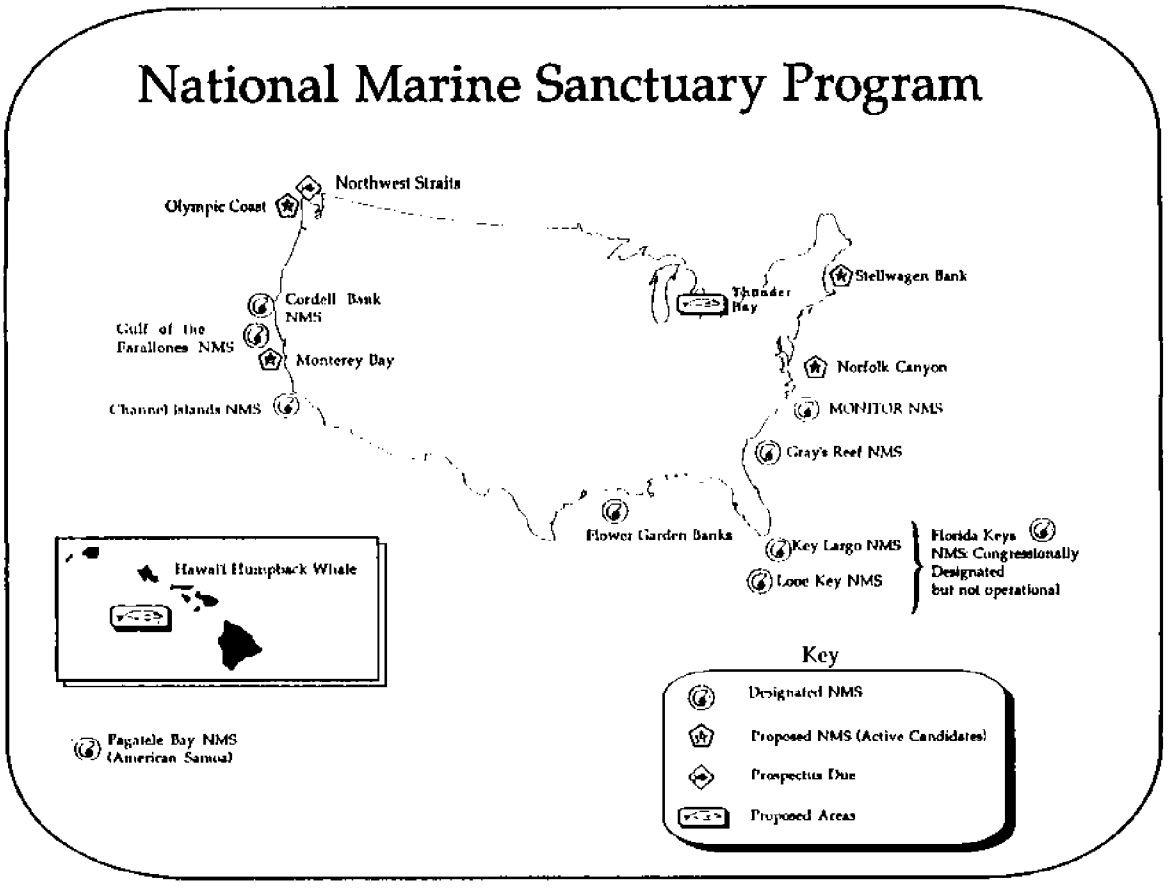

Figure 4. Status of national marine sanctuaries

Similar to the *kohola,* many feel Hawai'i has been overexploited, depleting the islands of its people, its culture, and its ocean resources. Aluli and McGregor (1991) quote a Hawaiian *kupuna* (grandparent or ancestor) to describe the importance of the ocean to Hawaiians: *Mai ke kai ke ola, mai ke kai mai ka make ... From the ocean comes life, from the ocean comes death.* As the primary source of life, Hawaiians believed depletion of the ocean's resources would lead to the end of the Hawaiian people and life itself.

Thus, like Kaho'olawe, the *kohola* is symbolic of the status of the Hawaiian culture in the twentieth century - that of an endangered culture. Creating a *pu'uhonua* for the *kohola* in Hawaiian waters will, to many, be a symbolic recognition of the importance of Hawai'i, its culture, and its resources, on a national and international scale.

SANCTUARY DESIGNATION AND THE USERS

Each winter, the shallow, warm waters surrounding the Hawaiian Islands provide an ideal place for humpback whales to breed and tend their young. These "large-winged" mammals begin entering Hawaiian waters as early as November, where

they remain until late spring when they depart for their summer feeding grounds off the south coast of Alaska (Baker and Herman, 1981). These seasonal visitors to Hawai'i represent the largest and most widely known of the three breeding populations remaining in the North Pacific (Herman, 1979).

Although sighted over deeper waters throughout the major islands, the shallow waters found within the 100-fathom (183 meter) isobath appear to be the preferred habitat and, consequently, play host to the greatest number of wintering humpbacks (Glockner-Ferrari and Ferrari, 1985). These waters have also been traditionally shared by residents and tourists, who engage in a wide range of commercial and recreational activities such as boating, fishing, thrillcraft, and diving.

Some of these activities, particularly those directly resulting from heightened enthusiasm for research and the profitability of whale watching charters, might contribute to the harassment of the species if not regulated. Such cause and effect relationships, however, are not entirely substantiated by scientific research. If such correlations are established in the future, State and Federal authorities already possess the means to amend their regulations appropriately. What human activities affect the behavior and/or biological fitness of the seasonal whale population in Hawai'i are still issues of sufficient importance to warrant further evaluation.

In most currently designated national marine sanctuaries, the effects of the designation on the user groups have been positive. For instance, the philosophy of multi-use has had a major impact on the planning and management of all marine sanctuaries, as it has allowed the input of user groups throughout the planning process. Many user groups have been active in helping develop management plans, directing research and developing successful interpretive programs. Because of the multi-use philosophy and the opportunity for local input in the planning process, fishing, diving, boating, and a number of recreational and commercial activities are allowed in most areas.

THE STATE AND NOAA: A PARTNERSHIP OF NECESSITY

The failure of the 1977 proposal was due in large part to the lack of a strong State-NOAA partnership. Although the proposal had its merits, its detractors and supporters, NOAA was left to do a lot of the day-to-day work from Washington, D.C. This made timely response to important issues impossible. The State, on the other hand, was left in an unenviable position of addressing NOAA policy questions the public had. As a result, an accurate picture of what sanctuary designation means, what it would do for the State, and its effect on the various users was not well-articulated.

In order to provide for timely response to issues of local concern, NOAA has placed a liaison in Hawai'i to work directly with the Office of State Planning. Like its counterparts in the other "study areas," the liaison is crucial to maintaining a clear line of communication between NOAA, the State and other affected public and private organizations and individuals. More importantly, it allows NOAA and the State to quickly respond to issues of national, international and local concern. If designation is to be successful, NOAA and the State must maintain this important line of communication.

THE HAWAIIAN ISLANDS HUMPBACK WHALE NATIONAL MARINE SANCTUARY

On November 4, 1992, President Bush signed Public Law 102-587 establishing the Hawaiian Islands Humpback Whale National Marine Sanctuary to "*support, promote, and coordinate scientific research on, and monitoring of, that portion of the marine environment essential to the survival of the humpback whale....*" Subtitle C of the MPRSA, also known as the Hawaiian Islands National Marine Sanctuary Act, designates areas of the marine environment "*seaward of the upper reaches of the wash of the waves on shore....*" and includes the 100-fathom isobath "*adjoining the islands of Lanai, Maui, and Molokai, including Penguin Bank, but excluding the area within 3 nautical miles of the upper reaches of the waves on the shore of Kahoolawe Island....*" In addition, "*the deep-water area of the Pailolo Channel from Cape Halawa, Moloka'i to Nakalele Point, Maui and southward....*" and the "*one hundred meter isobath adjoining the Kilauea National Wildlife Refuge on the island of Kauai....*" was included. This bill also leaves open the possibility of boundary modifications to include the waters surrounding Kaho'olawe and other areas and resources **after** sanctuary designation. Presently, NOAA and the State are in the process of developing a management plan for the sanctuary.

The eventual success of the Nation's newest national marine sanctuary is yet to be determined. Public comment, public participation, and a clear understanding of the needs the *kohola*, the State and NOAA will remain the major points that must be considered in striving to develop the most effective management plan for the sanctuary.

SUMMARY

Both Congress and the public have renewed their interest in providing protection to Hawai'i's humpback whale population beyond that afforded by the Marine Mammal Protection Act and the Endangered Species Act. The designation of the Hawaiian Islands Humpback Whale National Marine Sanctuary indicates Congress' commitment to protecting a significant endangered species. Many in Hawai'i see the protection of the *kohola* and its habitat as vital and symbolic to the national and international recognition of the importance of recovering and maintaining the Hawaiian culture.

The *kohola*, Hawai'i's native born giant, and the Hawaiian culture are endangered. As part of a cultural reawakening, people are asking: What is the significance of the nation's newest *pu'uhonua* to Hawai'i and the nation? How will Hawai'i's culture and its marine resources benefit from sanctuary designation? How can the people of Hawai'i, as *konohiki* (overseer) of their island environment, contribute to the long-term survival of the *kohola*? The answers to these and many other questions depend on the ability of NOAA,the State, and the people of Hawai'i to cooperatively manage a nationally and internationally significant marine resource.

REFERENCES

Aluli, N.E., and D.P. McGregor. 1991. Hawaiian Customs, Uses and Practices Relating to the Ocean Surrounding Kaho'olawe. October 8, 1991.

Baker, C.S., and L. Herman. 1981. Migration and local movement of humpback whales (*Megaptera novaeangliae*) through Hawaiian waters. *Can. J. Zool.* 59:460-469.

Beckwith, M.W., ed. 1951. The Kumulipo: A Hawaiian Creation Chant. Chicago: University of Chicago Press.

Glockner-Ferrari, D., and M. Ferrari. 1985. Individual identification, behavior, reproduction, and distribution of humpback whales (*Megaptera novaeangliae*) in Hawaii. Marine Mammal Commission Contract # MMC-83/06.

Hawai'i Ocean and Marine Resources Council. 1991. Hawai'i Ocean Resources Management Plan. Department of Business, Economic Development and Tourism. State of Hawai'i. January 1991.

Hawai'i Ocean and Marine Resources Council. 1991. Hawai'i Ocean Resources Management Plan. Technical Supplement. Department of Business, Economic Development and Tourism. State of Hawai'i. January 1991.

Herman, L. 1979. Humpback whales in Hawaiian waters: A study in historical ecology. *Pacific Science*. 33(1):1-15.

Johnson, R.K., ed. 1981. Kumulipo: The Hawaiian Hymn of Creation, Volume 1. Honolulu: Topgallant Publishing Company, Ltd.

U.S. Department of Commerce, National Oceanic and Atmospheric Administration. 1983. Draft Management Plan and Environmental Impact Statement for the Proposed Humpback Whale National Marine Sanctuary.

U.S. Department of Commerce, National Oceanic and Atmospheric Administration. 1991. Kahoolawe Island National Marine Sanctuary Feasibility Study.

CORAL REEF ISLANDS IN A PERIOD OF GLOBAL SEA LEVEL RISE

David Hopley
James Cook University of North Queensland
Townsville, Queensland, Australia

ABSTRACT

Unnecessary concern has been raised amongst low-lying island nations regarding the possible consequences of a greenhouse-induced sea level rise over the next century. A process approach to the problem suggests that far from disappearing, many coral islands will increase in size at least during the first 100 years of sea level change. Similarly, the application of more realistic groundwater models, to predict the future of potable freshwater resources on reef islands, suggests that the resource may actually increase in some areas during the period of sea level rise. Greater problems may result from the lack of mature soils, though plant growth may be aided by CO_2 enrichment, especially as many reef island crops belong to the C_3 group. Marine resources may also be replenished by greater circulation in lagoons, although the possibilities of some eutrophication must also be taken into account. It is suggested that the present pressures on reef islands due to population increases, and already occurring natural phenomena are more important for the planning process than the potential sea level rise of the next 100 years. Maintenance of healthy reef systems will be important in allowing these positive responses to global change.

INTRODUCTION

Concerns about global changes produced by the greenhouse effect during the 1980's quickly focused attention on the effects of sea level rise on particularly vulnerable coastal areas. Statements were made, by those who knew very little about coral reef processes, which suggested that some island nations may disappear altogether, e.g., "It is estimated that a 60 cm rise around the Maldives in the Indian Ocean would cover these coral islands and displace 177,000 people." (Falk and Brownlow, 1989)

The popular press were quick to take up this doomsday theme. For example, the *Pacific Islands Monthly* had as a feature article a special report entitled, "The Greenhouse Effect -Where Have All The Islands Gone." The report argued that "atoll states are the most helpless of all nations in face of the Greenhouse Effect" and concluded with the forecast "some of the most recently populated islands in the world may be depopulated ... and some of its most recently formed islands may disappear forever." (Roy and Connell (1989) and McLean (1989))

Not surprisingly there was an immediate political response. For example,

> If the Greenhouse Effect raises sea levels by 1 metre, it will virtually do away with Kiribati... if what the scientists say now is going to be true, in 50 or 60 years my country will not be there.
>
> –President I. Tabai
> Kiribati, Sept. 1988

> The environmental change caused by industrial progress in the developed world may slowly drown this unique paradise in its entirety.
>
> —President M. Gayoom
> Maldive Islands, 1988

Subsequently, consultants were employed to assess what measures would be required to save these nations. For example, the Delft Hydraulics Laboratory estimated that 34.3% of the national economy of the Maldives would be required to give adequate protection and 18.8% for Kiribati, 14.4% for Tuvalu, and 11.1% for Tokelau (UNEP, 1990).

Unfortunately, many of these reports did not examine the processes involved in the formation and maintenance of coral islands, two types of which with completely different origins are recognised.

1. Coral cays, usually formed on the leeside of reefs and dominated by sand-size sediments. These can be found on all types of reef, including fringing reefs.

2. Motus, shingle based islands found on the windward margins of reefs and most particularly around the outer margins of many atolls.

A process approach to an assessment of the hazards suggests that existence of reef islands will not be the problem within the next century, but that other environmental effects of global change will need consideration and planning. Paradoxically, some of the effects may be beneficial.

WAVE ACTION ON REEFS - THE FORMATION OF CORAL CAYS

In 1988, Hopley and Kinsey suggested that a rise in sea level in the period of 50-100 years would result in an increase of sediment supply to coral reef cays. They suggested that at the present time there was an overabundance of sediments on reef flats of the Great Barrier Reef (but also elsewhere in the world) which have been at sea level for a period of more than 5,000 years. The major problem is one of transporting the sediment to the cay, a process which can take place only at high tide when there is sufficient wave power passing across the reef flat. They further suggested that a small rise in sea level would see greater productivity of reef flat areas increasing from a present yield of about 0.5 kg m^{-2} yr^{-1} to as much as 4 kg m^{-2} yr^{-1}, and. therefore. the potential to supply even more sediment towards the nodal point of wave refraction. (See also Kinsey and Hopley (1991) for quantitative estimates.)

Little work has been carried out on the processes of sediment transport on reef tops, particularly in association with coral cays, but what little there is support this contention (Hopley (1981, 1982), Flood (1986), and Gourlay (1990)). Studies have shown that even under tradewind conditions of up to 25 knots, at low tide waves across reef flats of the Great Barrier Reef may be insufficient to move sediment. Sediment movement is therefore restricted to less than 50% of the time when water levels are sufficiently deep over the reef flat to allow waves of significant size, and therefore transportational ability, to pass over the reef. This is particularly prominent in areas of significant tidal range, such as the Great Barrier Reef, but is also a factor on mid-oceanic reefs where tidal range is negligible. Many of these reefs have developed reef flats at sea levels higher than present (Hopley, 1987; Nunn, 1991). As upward reef growth will almost certainly lag behind a rise in sea level it is considered that a rise of up to 0.5 m may unlock reef flat sediments for longer periods and allow them to be moved towards the coral cay. The end result is thus an increase in the size of the sand store which, under normal weather conditions has the potential for further island construction.

Most published observations on both sediment movement on reefs and of wave action support this conclusion. For example, Hopley (1982) has indicated that time of maximum sediment movement on reefs of the Great Barrier Reef varies according to tide height, wave height and location on the reef flat. Under normal winter conditions of southeastly winds of approximately 20 knots, the period of maximum turbidity on reef flats close to coral cays occurred when tidal levels were either flooding to, or ebbing from, a high water position with waves breaking close to the cay. As maximum sediment movement takes place just seaward of the wave breakpoint (King, 1972), the point of breaking of the transmitted wave on the reef flat becomes a critical factor in determining sediment mobility. Under the 20 knot southeastly conditions experienced on the Great Barrier Reef, with deep water wave heights of about 2 m, high water waves break directly on the cay beach, but at lower tidal levels the point of breaking is more distant from the cay. Maximum sediment movement thus occurs in a zone on the reef flat that oscillates about the cay according to the tide height and the height of the reformed waves crossing the reef flat. The question arises as to whether or not the net direction of sediment movement is towards the island and if it can result in an increase in beach height.

As waves move into shallow water, towards their break point, there is an increase in discrepancy between the forward orbital motion under wave crests and the slower return flow beneath troughs. The forward movement is short in duration, but high in velocity and may lead to the selective movement of coarser sediments in the direction of wave propagation, i.e., towards the cay, while finer materials that may also be moved by the slower return currents will readily move almost an equal distant in both directions. For movement of sediment of any particular size, the forward orbital velocity must exceed the required entrainment velocity. Bottom velocity has been shown to be a function of wave height and water depth (Inman and Nassu, 1956) and thus on a reef flat will vary at different stages of the tide, hence producing the noted periodicity in sediment movement.

A higher sea level will thus produce water depths which will cause greater movement of sediment towards a coral cay. Buildup of the cay itself will depend on the nature of the waves which break on the cay beach. The height of the constructed beachberm is dependent upon wave runup. Numerous studies (CERC, 1984) show that runup height varies with the wave height, wave steepness, beach slope, shape of the beach profile and roughness and permeability of the beach material.

Although most beach models and empirical formulae suggest that given adequate sediment supply (not a problem on reefs), a higher water level will produce a higher beach, there have been few applications to coral islands. However, Gourlay and Hacker (1991) working on Raine Island on the northern Great Barrier Reef found that the relative wave runup height varied in a consistent manner with the ratio of the breaker height to water depth over the reef flat, consistent with the fact that the wave heights are limited by shallow water breaking conditions over the reef flat. Gourlay and Hacker indicate that the height of the beachberm is determined by the runup height of the dominant wave action. This could be expected to occur at the highest spring tides. A beachberm elevation of 4 m could be built by small flat waves of 0.5 m height breaking directly onto the beach at the tide level as low as 2.3 m. They also showed that similar heights could be attained by the maximum breaking waves of 1.6 m, at an extreme tide level of 3 m.

Although further work is required, these data suggest that a small rise in sea level without any responding buildup of reef flat level, would result in the attainment of greater berm heights under most weather conditions, i.e., a build up of the island by an amount which could exceed the amount of increase in water level. For example, in the case of Raine Island quoted above, Gourlay and Hacker (1991) suggest that with a 0.6 m

rise in sea level, the larger 1.6 m waves would increase berm height by a further 0.8 m and 0.5 m waves would increase berm height by 1.2 m, i.e., to 4.8 m and 5.2 m respectively.

Additional to a rise in sea level, increasing incidence and intensity of tropical cyclones, hurricanes and typhoons is also quoted as a major threat to the existence of tropical coral cays. Whilst such storms can already cause catastrophic damage to reef islands, there is ample evidence to suggest that the majority of higher elevations on cays (as well as on motus, see below) are the result of emplacement during these high energy events. For example, on the Great Barrier Reef highest elevations of between 3-4 m above mean high water springs of many reef islands is not produced by any wind blown sand but largely by wave deposited materials. In the past, these high sand ridges have been attributed to higher sea levels. However, strong arguments have been put forward for emplacement during high energy events. Even the highest reef islands may be overtopped by exceptional storm waves causing major ecological disturbance and occasionally loss of life. It is unlikely that the small increase in sea level now forecast for the next 100 years will greatly increase the risk. The outer edge of coral reefs will still form a protective barrier from storm surges, the increased severity of which will be due only to changes in the inverted barometer effect (see below). This will produce only a few centimetres of extra sea level height. Whether of not this is critical for the reef islands and their human populations depends to a large extent on local conditions.

ATOLL MOTUS

Cyclonic action is even more important in the construction of atoll motus and other shingle dominated islands. The coarse detrital materials of atoll motus cannot be moved by normal wind generated waves of local origin. Major tropical storms are required for their emplacement and although atoll motus are found in low latitudes where tropical cyclones do not generate, such locations can still experience large swells generated by storms at higher latitudes. Whilst knowledge of normal wave action on reefs is limited, not surprisingly data for high energy extreme events is totally absent. Nonetheless, observations made subsequent to such events and the application of empirical methods confirm these conclusions.

The most spectacular example of island construction by a tropical cyclone was the new rampart formed on Funafuti by hurricane Bebe in 1972 (Maragos, et al., 1973; Baines, et al., 1975; Baines and McLean, 1976). On the southeastern side of this atoll, a ridge 19 km long, 30-40 m wide and up to 4 m high was formed during this single storm from material dredged up from up to 20 m depth on the reef front. On more sheltered areas discontinuous low rubble tracts formed. Under normal weather conditions since 1972, the Funafuti ridge has altered its original convex profile to a concave one, migrated 10-20 m shoreward and significantly reduced in height. In some areas, it now remains only as a rubble zone and in its migration has left large coral heads as residual reef blocks. Nonetheless, the longterm result has been a building of Funafuti motus.

Further evidence on the response of reef islands come from the Holocene record. For example, Bayliss-Smith (1988) has suggested that storms during the mid Holocene in the Solomons were more frequent and intense than at present and that at that time islands increased in size. It is also notable that in the Caribbean, where, for isostatic reasons the Holocene sea level record is one of continuous rise up to the present and therefore continuous upward growth and evolution of reef flats (Hopley, 1982), on reef complexes such as the Belize barrier reef, coral cays are more frequent than on many Indo-Pacific reefs, possibly because of the lower level of the reef flats and more continuous sediment movement over them.

A greater risk of inundation from storm surges, associated with cyclone activity on mainland and high island coastlines, is not likely to increase dramatically on open-ocean reef islands where amplification of the surge, by shoaling and funnelling effects does not take place. In the open ocean surges are essentially limited to the inverted barometer effect (1 cm for every hPa of pressure reduction) and to wave setup on the margins of the reef. An example is given by Hopley (1972) in a report on Cyclone Emily which crossed over the southern Bunker and Capricorn islands of the Great Barrier Reef in 1972. Falling from a central pressure of 945 hPa, it passed over Heron Island with a central pressure of 985 hPa, and over the adjacent mainland at 992 hPa. Nonetheless, the surge of almost 2 m on the mainalnd south of Gladstone was significantly higher than the figure of <0.8 m at Heron Island.

The general conclusion is that the application of temperate coastal erosion theories, such as that proposed by Bruun (1988) are not applicable to coral islands and their application previously suggesting erosion rates of 1-2 m per year as a result of greenhouse-induced causes (Roy and Connell, 1989) is misleading. Those who have worked on reef processes generally agree that in the short term of 50-100 years reef islands may in fact increase in size, e.g.,

> Thus it is possible that with rising sea level the broad sediment laden reef flats of Kiribati will see substantial re-working of the surficial sediment which could result in the formation of new islands and expansion, through the accretion of existing islands, at least until the existing sediments surplus is exhausted.
>
> A new phase of island building is therefore envisaged. This will be aided by the presence of the existing islands and the natural beachrock and conglomerate `seawalls' and `groynes' which will serve to trap and stabilise mobilised sediment (McLean, 1989).

and

> At least over the next 50-100 plus years coral islands seem relatively secure even if, (or especially if) reef platforms become progressively inundated. Increased tropical cyclonic activity, combined with maximum growth rates and new coral habitats will ensure sediment supply and increased water depths will increase sediment transport efficiency (Parnell, 1989).

Existing beachrock, conglomerate and other cemented island deposits such as phosphatic cay sandstone will certainly retard even changes in locations of islands. Moreover, there is sufficient evidence (in the form of very recent artefacts contained within beachrock) to suggest that the cementation processes are so rapid that they will be effectively contemporaneous with the addition of new material to reef islands. Raised tidal levels will result in higher levels of cementation, superimposed over the top of existing beachrocks. Availability of land, is therefore, not the problem for the low lying island nations over the next century as has previously been suggested.

OTHER POTENTIAL CHANGES TO CORAL REEF ISLANDS

Ground Water Resources

Concerns have been expressed for the ground water resources upon which both island peoples and vegetation depend. In general, such concerns have resulted from the

application of the now outmoded Ghyben-Herzberg model (Miller and Mackenzie, 1988). This assumes homogenous materials and that the outflow, or loss of freshwater, occurs at island margins in, or below, the intertidal zone producing a predominantly horizontal flow. Although some of the fresh water remains above sea level, the majority of it (40 units of depth for every unit of head) will reside below sea level. This model produces a great depletion in the potential for ground water resources if island size is reduced. Freshwater lenses may not occur on islands that are less than 300 m wide. However, the recently discussed layered aquifer model (Wheatcraft and Buddemeier, 1981; Herman, Buddemeier and Wheatcraft, 1986; Oberdorfer and Buddemeier, 1988; and Buddemeier and Oberdorfer, 1990) has much greater applicability to real world situations though it does suggest that the overall freshwater resource may be less than in the Ghyben-Herzberg model. The model presumes two basic geological layers possessing distinct porosities: a surficial layer, of Holocene age, of low permeability overlying deposits of high permeability, of Pleistocene age, separated by a solution unconformity at relatively shallow depths of 7-25 m. Primary mechanism for loss of freshwater is not outflow at island margins, but loss to degradation by downward mixing into the saline water in the Pleistocene deposit below. This creates a broad transition zone of brackish water.

However, this model is far less sensitive to island size and a threshold island width figure of 120 m, has been suggested for retention of the freshwater resource. Moreover, if the island size remains constant, Oberdorfer and Buddemeier (1990) have suggested that rising sea level has a counter intuitive effect on total freshwater resource for islands possessing a layered aquifer. An increase in sea level makes available more of the low permeability aquifer for retention of freshwater, increasing the total freshwater resource. However, as Parnell (1989) has noted "under current recharge conditions, the potable freshwater resource is reduced by a small amount. It is possible that recharge rates will decrease with higher temperatures and higher evapotranspiration, but if recharge increases (which is possible given increased rainfall and perhaps better land use practices) the model shows a significant increase in both potable and total freshwater resources."

Thus, a rise in sea level may not be disastrous for island ground water resources. Indeed, if accompanied by an increase in island size as seems likely and increases in rainfall as is predicted for some areas of low latitudes, ground water resources may actually increase.

Soils and Plant Growth

By definition, reef island soils are young. For example, Fosberg (1954) identified three soil series on atolls with increasing maturity:

- Shioya soil series found on the youngest sediments, deficient in almost every element essential for plant growth,
- Arno soil series with a more developed 'A' horizon and some bonding by organic matter, and
- Jemo soil series found under mature island forests and in which much organic matter is incorporated.

It is these latter soils which provide the basis for most agriculture on many reef islands. Unfortunately, even though islands may increase in size during the next 100 years, the soils on the new land area will be of the younger immature type. The major concern is that changes to the shape and orientation of islands which may result from

changes in wind directions, may lead to the erosion of at least part of the older core areas of the islands on which the agricultural soils are found.

Most concern however, has been for rising saltwater ground tables and salt contamination of low lying vegetation (e.g., Hughes and McGregor, 1990). As indicated above, this may not necessarily be so and the future for sustainable agriculture and maintenance of mature vegetation on reef islands may not be as grim as has been forecast in the past. Indeed, there may be a significant increase in the productivity of many tropical crop species found on reef islands. Crops with a C_3 photosynthetic pathway have higher magnitude physiological responses to CO_2 enrichment and with a doubling of CO_2 concentration in the atmosphere may have crop yields increasing by as much as 33%. Amongst the C_3 crops are casava, sweet potato, taro, yam, banana, papaya and coconuts (Jacobs, 1990). There have also been suggestions that CO_2 enrichment will lead to a reduction in stomatal conductance and transpiration and an increase in water use efficiency by plants. If this takes place, then even in areas where a reduction in total rainfall is predicted, there may be some offsetting for agriculture.

Marine Resources

Rejuvenation of coral growth as suggested by Hopley and Kinsey (1988) and Kinsey and Hopley (1991) should also bring about the replenishment of many of the natural marine resources, upon which island nations depend. On relatively open atolls, a slight rise in sea level may do much to increase lagoon circulation with beneficial effects. However, on atolls where few hoa (lagoon exits) exist, increasing sedimentation through building up of shingle ridges may completely close off lagoons. Such a situation occurred at Taiaro Atoll in the Tuomotus as described by Salvat, et al. (1977). Although partial closure of the lagoon took place as the result of a slight uplift, complete isolation occurred during the 19th century as the result of blocking of the remaining exit by a boulder rampart, deposited during high seas. Corals were initially killed by the uplift, but subsequently hypersaline conditions (about 43 ppt) have developed and only *Porites lobata* survives, compared to about 14 species prior to the lagoon being closed. Other fauna have been similarly restricted.

Deterioration in lagoon and near-reef water quality may also occur if nutrients are released into the marine environment during the period of global change (e.g., Hallock and Schlager, 1986). A release of nutrients can result from rising water tables producing a greater leaching of island soils which can also be aggravated if water table fluctuations reach into septic tanks and rubbish tips. Remobilisation of naturally occurring phosphate deposits, produced through the accumulation of guano, may also take place as water tables rise through island soils. A full assessment of these changes to nutrient status, and whether or not eutrophication will occur, needs further investigation.

CONCLUSION

There is no doubt that reef island environments are precarious and extremely vulnerable to environmental change. However, kneejerk reactions as have occurred as recently as two years ago, with so-called scientific assessments suggesting reactions as drastic as mass resettlement for particular island nations are excessive (Roy and Connell, 1989). There will be some local land losses and changes to the ecology of the islands, but there may well be as many gains from global change as there are losses. McLean's (1989) survey of Kiribati is an example of a true scientific approach towards assessment of the future risk. Although further work is required, particularly on the

sedimentation processes occurring on coral reefs, and also on ground water hydrology, McLean's summary for Kiribati is probably pertinent to many other reef island situations.

> On the face of it the low atolls and islands of Kiribati appear particularly vulnerable to any future rise in sea level, and while this is to a large extent true, several factors suggest that the most probable outcomes will not be as substantial nor as devastating as initially envisaged ... And yet, in addition to or regardless of any Greenhouse induced changes the population is likely to have to cope with large natural variations in physical phenomena such as fluctuations in water level, freshwater lens volume, rainfall incidence and drought for example, which will have a profound effect on land and livelihood in the future ... It should also be stressed that there is no obvious immediate danger from Greenhouse induced causes; these will take decades to have any major impact on any but the most vulnerable locations (Buddemeier and Oberdorfer, 1989). But this does not mean that the government should not capitalise on the international support for Greenhouse related environmental matters because there is a very real need to address the questions of long term planning and preparation.

As predictions for sea level rise become more conservative, e.g., no more than 25 cm by the middle of the next century, concerns about the island nations may diminish. However, as McLean has shown, the environmental problems existing on many reef islands already necessitate careful planning and management. Only by maintaining (or in some instances restoring) reef systems to a healthy state will they be able to respond to global change in the positive directions suggested in this paper. Such a policy, requiring economic, demographic and sociological as well as scientific input, is necessary even if global changes to environment were minimal. Concentration on island carrying capacities, sustainable use of resources, maintenance of water quality and widening of island nations' economies by, for example, strategic planning for the beneficial use of the 200 nm EEZ will be far more productive than design of breakwaters, rockwalls and groynes and plans for mass migration. However, it is important to remember that the costs may not be all that different and that the interest raised in the island nations at the present time should be redirected towards the planning issues raised above. In the long term (>100 yrs) if no reversal to global change trends can be achieved, then some of the more sensational forecasts may well occur, but at that stage the implications for other parts of the world, including coastlines of the most developed nations, would also be severe.

REFERENCES

Baines, G.B.K., P.J. Beverage, and J.E. Maragos. 1974. Storms and island building at Funafuti Atoll, Ellice Islands. In: Proceedings 2nd International Coral Reef Symposium, Vol. 2, pp. 485-496.

Baines, G.B.K., and R.F. McLean. 1976. Reef surveys of 1972 hurricane rampart on Funafuti Atoll. *Search.* 7 :36-37.

Bayliss-Smith, T.P. 1988. The role of hurricanes in the development of reef islands, Ontong Java Atoll, Solomon Islands. *Geographical Journal.* 154,377-391.

Bruun, P. 1988. The Brunn Rule of erosion by sea level rise: a discussion on large scale on two and three dimensional usage. *Journal of Coastal Research*. 4:626-648.

Buddemeier, R.W., and J.A. Oberdorfer 1990. Climate change and island ground water resources. In: Implications of Expected Climate Changes in the South Pacific Region: A Overview, eds. J.C. Pernetta and P.J. Hughes. UNEP Regional Seas Reports and Studies No. 128, pp. 56-67.

CERC. US Army Corps of Engineers, Coastal Engineering Research Centre, Vicksburg. 1984. Shore Protection Manual. Vol. 1 & 2.

Falk, J., and A. Brownlow, A. 1989. *The Greenhouse Challenge - What's To Be Done?* Penguin Books, (841).

Flood, P.G. 1986. Sensitivity of coral cays to climatic variations, southern Great Barrier Reef. *Coral Reefs* 5 (13-18).

Fosberg, F.R. 1954. Soils of the northern Marshall Atolls with special reference to the Jemo series. *Soil Science* 78 (99-107).

Gourlay, M.R. 1990. Wave setup and currents on reefs - cay formation and stability. In *Proceedings Engineering in Coral Reef Regions Conference* (163-178).

Gourlay, M.R. and Hacker, J.L.F. 1991. Raine Island coastal processes and sedimentology. Report Ch40/91, p. 68. Department of Civil Engineering, University of Queensland.

Hallock, P., and W. Schlager. 1986. Nutrient excess and the demise of coral reefs and carbonate platforms. *Palaios*. 1:389-398.

Herman, M.E., R.W. Buddemeier, and S.W. Wheatcraft. 1986. A layered aquifer model of atoll island hydrology: validation of a computer simulation. *Journal of Hydrology*. 303-322.

Hopley, D. 1972. The storm surges associated with cyclones Althea and Emily. In: Cyclone Althea, Part II - Storm Surges and Coastal Effects, ed. D.H. Trollope, 4.1-4.29.

Hopley, D. 1981. Sediment movement around a coral cay, Great Barrier Reef, Australia. *Pacific Geology*. 15:17-36.

Hopley, D. 1982. Geomorphology of the Great Barrier Reef: Quaternary Development of Coral Reefs. New York: John Wiley Interscience.

Hopley, D. 1987. Holocene sea level changes in Australasia and the southern Pacific. In: Sea Surface Studies a Global View, ed. R.J.N. Devoy, pp. 375-408. London: Croom Helm.

Hopley, D., and D.W. Kinsey. 1988. The effects of rapid short term sea level rise on the Great Barrier Reef. In: Greenhouse Planning for Climate Change, ed. G.I. Pearman, pp. 189-201. EJ Brill Leiden.

Hughes, P.J., and G. McGregor, eds. 1990. Global Warming-Related Effects on Agriculture and Human Health and Comfort in the South Pacific. Niarobi: SPREP and UNEP.

Inman, D.L. and N. Nasu. 1956, 1979. Orbital velocity associated with wave action near the breaker zone. *B.E.B. Technical Memorandum*.

Jacobs, B.C. 1990. CO_2 climate change and crop physiology in the South Pacific. In: Global Warming-Related Effects on Agriculture and Human Health and Comfort in the South Pacific, eds. P.J. Hughes and G. McGregor, pp. 1-23.

King, C.A.M. 1972. Beaches and Coasts. 2nd Edition. London: Arnold.

Kinsey, D.W. D. and D. Hopley. 1991. The significance of coral reefs as global carbon sinks - response to greenhouse. *Palaeogeography, Palaeoclimatology, Palaeoecology (Global and Planetary Change Section).* **89**:363-377.

McLean, R.F. 1989. Kiribati and sea level rise. Department of Geography and Oceanography, University of New South Wales, Australian Defence Force Academy, Canberra. Report to Commonwealth Secretariat, Expert Group on Climatic Change and Sea Level Rise.

Maragos, J.E., G.B.K. Baines, and P.J. Beverage. 1973. Tropical cyclone creates a new land formation on Funafuti Atoll. *Science.* **181**:1161-1164.

Miller, D.L.R., and F.T. Mackenzie. 1988. Implications of climate change and associated sea level rise for atolls. In: Proceedings 6th International Coral Reef Symposium, Vol. 3, pp. 519-522.

Nunn, P.D. 1991. Human and non-human impacts on Pacific island environments. Occasional Paper of East West Environment and Policy Institute, Vol. 13. Hawaii.

Oberdorfer, J.A., and R.W. Buddemeier. 1986. Coral reef hydrology: field studies of water movement within a barrier reef. *Coral Reefs.* **5**:7-12.

Parnell, K.E. 1989. Reefs in the greenhouse: a review. Paper presented to the 15th Conference of the New Zealand Geographical Society.

Roy, P., and J. Connell. 1989. 'Greenhouse:' the impact of sea level rise on low coral islands in the South Pacific. Research Institute for Asia and the Pacific. Occasional Paper No. 6. University of Sydney.

Salvat, B., G. Richard, G. Poli, J.P. Chevalier, and R. Bagnis. 1977. Geomorphology and biology of Taiaro Atoll, Tuamotus Archepelligo. In: Proc. 3rd International Coral Symp., Vol. 2, pp. 289-295.

UNEP, 1990. Intergovernmental Panel on Climate Change. Policymakers summary of 'A Potential Impact of Climate Change.'

Wheatcraft, S.W., and R.W. Buddemeier. 1981. Atoll island hydrology. *Ground Water.* **19**:311-320.

AUSTRALIAN INITIATIVES IN SEA LEVEL AND CLIMATE MONITORING

G.W. Lennon
Flinders University of South Australia
Adelaide, South Australia

ABSTRACT

This paper outlines a major Australian initiative to monitor rising sea level trends on behalf of the Forum Island Countries of the South Pacific. The specifications demanded by the GREENHOUSE mechanism lead to high resolution instrumentation with a focus upon datum control. Since sea level measurements are essentially relative to survey marks on land, a supporting program of geodetic survey is required in this tectonically active region.

INTRODUCTION

Long term monitoring of marine variables has always been seen to be a worthy pursuit yet rarely practised. The hazards of climate change have brought greater emphasis upon such activities, partly due to promotion by the Intergovernmental Oceanographic Commission through a series of large scale international programs such as GLOSS (Global Sea Level Observing System), TOGA (Tropical Ocean/Global Atmosphere), WOCE (World Ocean Circulation Experiment), etc. and more recently by GOOS (Global Ocean Observing System) and GCOS (Global Climate Observing System). Major commitments by Australia to establish regional high-resolution monitoring arrays for sea level and associated meteorological variables fall neatly into this plan.

A twelve-station array around the Australian coastline is almost complete and preparatory work is well-advanced for an eleven station array established on behalf of the Forum island countries of the South Pacific (Figure 1). The latter initiative is sponsored by the Australian International Development Assistance Bureau (AIDAB) which has also begun a feasibility/design study for the Maldives in the Indian Ocean. Other work on long term sea level signals continues in the ASEAN region, the Southern Ocean and more recently in Antarctica.

INSTRUMENTATION

Given that the general consensus of scientific opinion is that the historic sea level trends are of a magnitude 1.5 +/- 0.5 mm per year, a program with aspiration to identify future trends should have a resolution somewhat smaller, and possibly sub-millimetre in scale.

It was considered, based upon experience with traditional float-operated tide gauges, that these would be inadequate in this respect (Lennon and Mitchell, 1992).

For example, analysis of the historic sea level trend, based upon the Australian network, covers a wide range of results including some of negative sign, despite the fact that the Australian mainland has the reputation of conforming to a relatively stable crustal block. However, if one can assume such stability, and so consider each gauge

result as an independent attempt to measure the regional trend, one may be justified in proceeding, through averaging, to estimate the regional value. Such a luxury is denied to the Pacific because of the widespread tectonic motion over a range of spatial scales. Consequently averaging processes would have no place here so that the requirement is to search for even higher accuracy with a desirability to strive for absolute sea level.

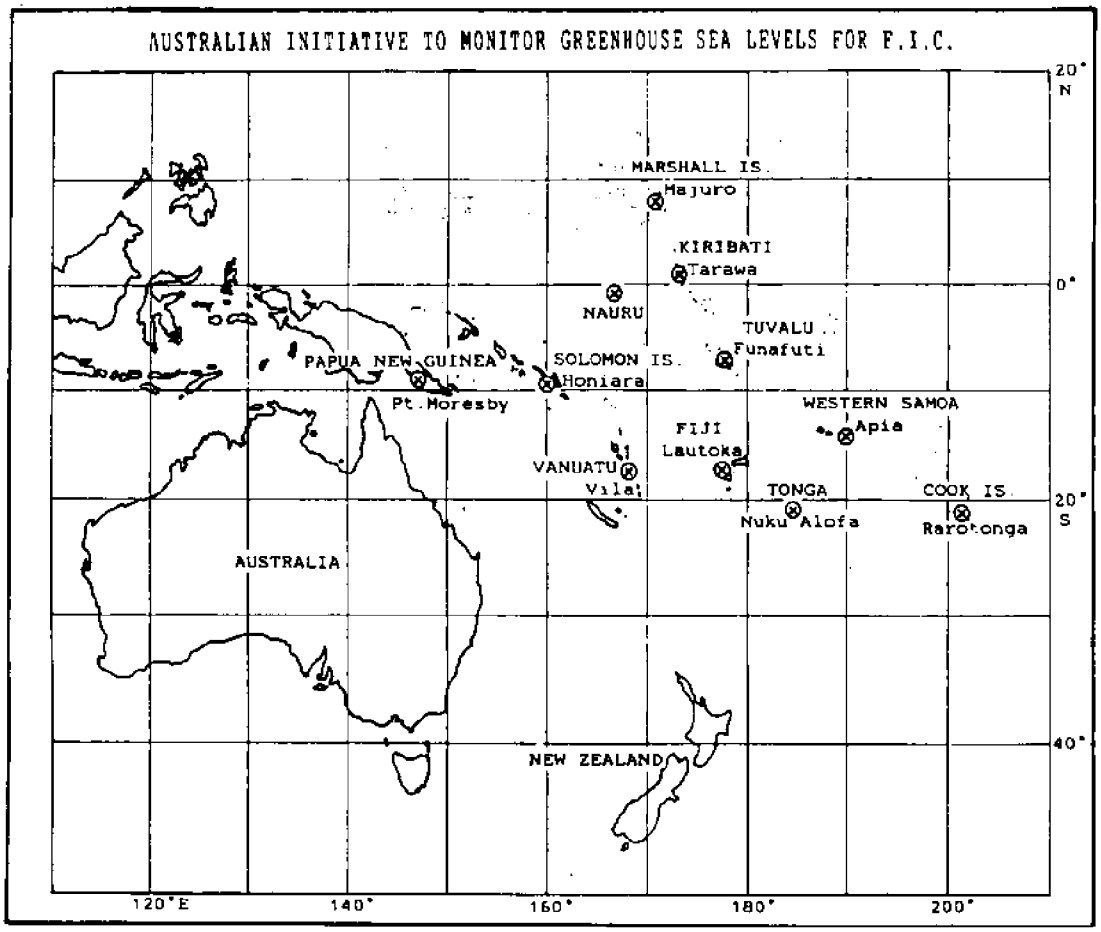

Figure 1. The array of SEAFRAME stations planned for the Pacific region

The selection process for suitable instrumentation focussed upon the acoustic Aquatrak sensor and the sophisticated 9000 series station controller and logger produced by Sutron Ltd. An important factor in this choice is the ability of this sensor to maintain a stable datum which, furthermore, is conveniently accessible to survey and geodetic procedures. A novel self-calibrating system for the time of flight of each acoustic pulse is a further attraction. The choice then is almost identical to that adopted by the National Oceanic and Atmospheric Administration (NOAA) of the U.S.A. This choice has been reinforced by experience. For example, if one takes a long time series of sea level from a float-operated gauge, one is accustomed to viewing systematic signals, such as the tides, emerging from a continuum of background noise which is suspected to be due to inferior instrumental performance and human interaction. The latter is now confirmed since a

power spectrum of a time series from the new stations shows a noise level considerably less than that for a float-operated gauge, and consequently much clearer identification of the periodic and quasi-periodic signals is possible even in the all-important low-frequency band (Lennon, Woodland, and Suskin, 1992).

The name now coined for the Australian stations is SEAFRAME (Sea Level Fine Resolution Acoustic Measuring Equipment). Figure 2 shows the main elements of a typical station, which also incorporates supplementary sea level monitoring by a submerged pressure sensor, together with the relevant meteorological parameters:

Barometric Pressure
Wind Speed and Direction
Air and Water Temperature

The primary water level is sensed at a one second sampling interval but logged at six-minute intervals as the mean of 180 samples. The supplementary sensors are logged at hourly intervals.

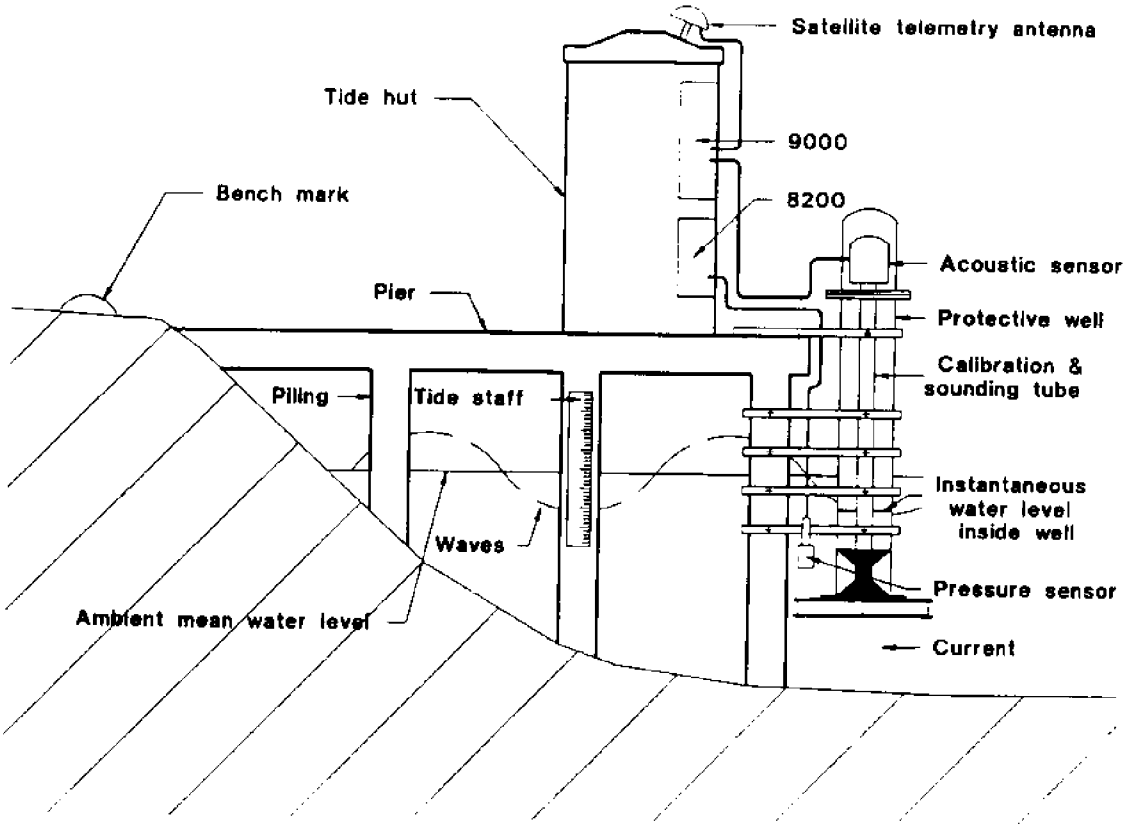

Figure 2. A SEAFRAME station

Figure 3 gives a power spectrum comparison of simultaneous data from a SEAFRAME installation and from a traditional float-operated gauge at the same site. This diagram shows the lower noise level in the low frequency band as mentioned above, and also in the high frequency band as experienced in the SEAFRAME record.

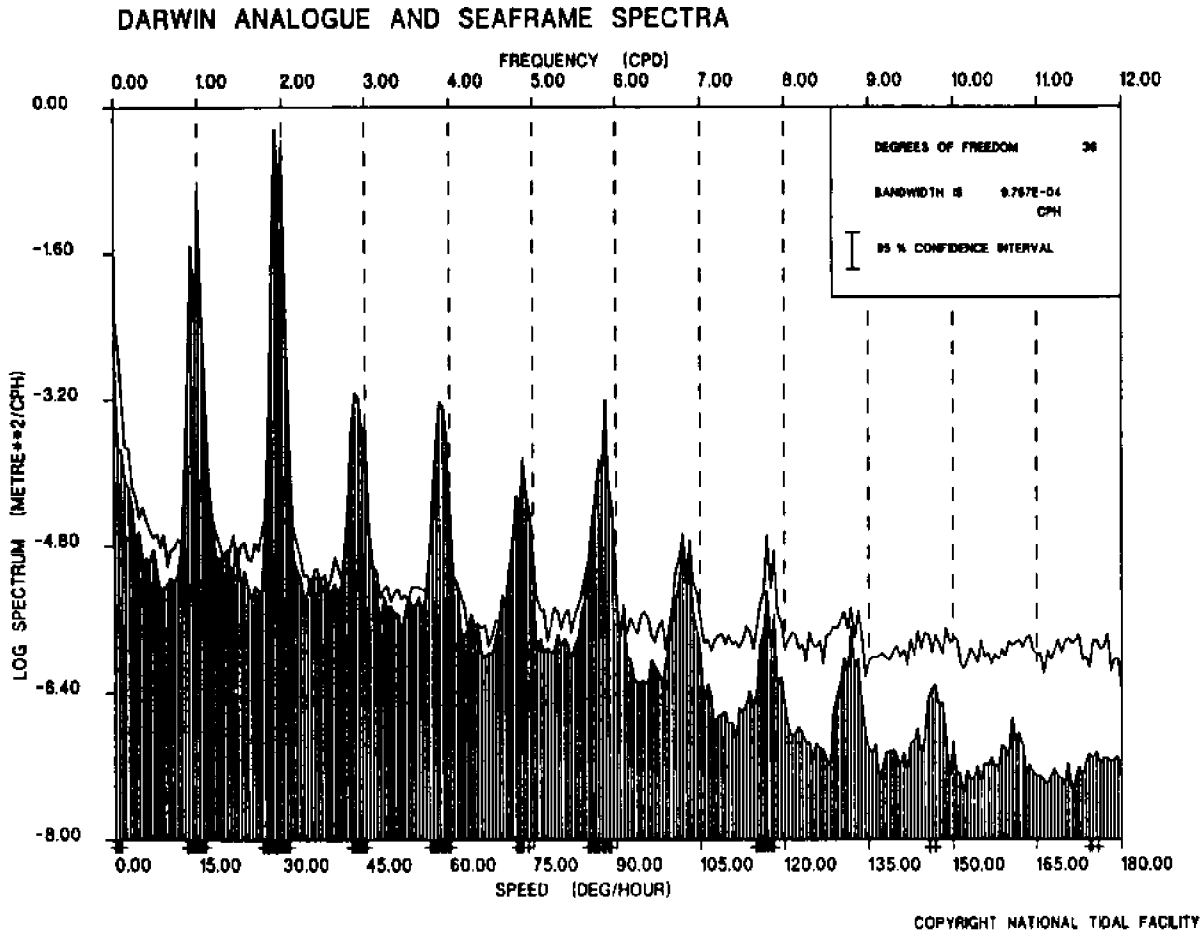

Figure 3. A comparison by power spectrum of simultaneous data from a float-operated gauge and a SEAFRAME system at Darwin. The blank plot is a spectrum of the float gauge data. The shaded plot is the equivalent from the SEAFRAME data.

The traditional gauges were always known to have unfortunate nonlinear characteristics but it can now be confirmed that, in the past, a significant contribution to the higher frequency signals has not represented true shallow-water tides but rather imperfections in an instrument based upon stilling well design.

PROJECT PHILOSOPHY

The Pacific project will gain much from its more crustally-stable Australian neighbour, but it is still necessary to consider in depth the basic argument upon which the interpretation of trends will be based.

Certain facts are clear:

- Because of its geophysical environment, the Australian case is less complex and it is possible to claim that if the true GREENHOUSE trend is identifiable anywhere, then it will be identified in Australia (Mitchell, 1992).

- For the Pacific, the project aims to establish a reference station in each of eleven countries. These stations will support a variety of products and will provide groundtruth for future satellite altimetry missions. However, in terms of GREENHOUSE trends, the initial information which they will give, but only after twenty or more years of observation, will be a simple point value, identifying the relative movement of land and sea at the site.

- Whatever the outcome, it is necessary to give due care to survey and geodetic procedures, not only to the sea level measurements referred to fixed marks on land, but also, perhaps by the Global Positioning System (GPS) and other altimetric means, to determine the relative motion of the land across each national region (Jacksa, Gilliland, and Tan, 1992). Note here that local sea level trends are the result both of oceanographic and of land level trends. Plans for the survey/geodesy program are currently under discussion (Warhurst, 1992).

- Although GPS techniques are developing rapidly at this stage, it is still uncertain as to whether vertical determination can yet be achieved, over the 1,000 Kms or so which separate some adjacent stations in the array , with a sub-centimetre accuracy necessary to maintain a role in 'GREENHOUSE' studies. There is however a prospect that field and computational procedures will soon make this possible. Meanwhile the aim is to establish a reference network on national scales.

- Attention must also be given to tidal motions of the local earth's crust in response to marine tidal loading, and other similar perturbations to survey procedures (Baker, 1992).

- The GREENHOUSE mechanism may prove to be dominated by the addition of mass to the ocean in the form of melt water, or alternatively by steric adjustment resulting from thermal change, but more likely by a combination of the two. One carries the implication of warping the regional crust, while steric effects do not suffer the same implication. Again climate change may prove to be associated with lateral shifts in the thermal zones of the ocean with a consequent shift in surface topography. Given time, it is possible that these features may be identified, thus allowing an assessment of the component parts of the sea level signal, and in particular the separation of the tectonic trends at the reference stations from the true oceanic trend.

There remain many obstacles to be surmounted and in fact, in many aspects, the program is operating at the threshold of what is physically possible so that what appears to be a routine monitoring task assumes the characteristics of a multi-faceted research program.

INFORMATION AND TRAINING

The program in the Pacific contains provision for information and training and already has a Climate Change Information Officer, in position with SPREP. The intention is to develop structures to identify and fill the needs for information about both long and short term features of climate change for a range of beneficiaries from the general public to representatives of government.

REFERENCES

Baker, T.F. 1992. Perturbations of survey procedures in the coastal zone. In: Proc. of the Second Australasian Hydrographic Symp., Special Publication 2. The Hydrographic Society.

Jaksa, D.S., J.R. Gilliland, and C.K.F. Tan. 1992. A GPS survey for the height control of tide gauges in Southern Australia. In: Proc. of the Second Australasian Hydrographic Symp., Special Publication 27. The Hydrographic Society.

Lennon, G.W., and W.M. Mitchell. 1992. The stilling well - a help or a hindrance? In: Proc. of the Joint IAPSO-IOC Workshop on Sea Level Measurements and Quality Control. October. Paris.Intergovernmental Oceanographic Commission.

Lennon, G.W., M.J. Woodland, and A.A. Suskin. 1992. Acoustic sea level measurements in Australia. In: Proc. of the Joint IAPSO-IOC Workshop on Sea Level Measurements and Quality Control. October. Paris.Intergovernmental Oceanographic Commission.

Mitchell, W.M. 1992. Sea level and climate changes. In: Proc. of the Second Australasian Hydrographic Symp., Special Publication 27. The Hydrographic Society.

Warhurst, D.F. 1992. Determination of the geodetic component of signals recorded at the Australian baseline array of super tide gauges for the measurement of absolute mean sea level. In: Proc. of the Second Australasian Hydrographic Symp., Special Publication 27. The Hydrographic Society.

SEA LEVEL RISE VULNERABILITY CASE STUDY MAJURO ATOLL, REPUBLIC OF THE MARSHALL ISLANDS

Scott P. Sullivan and Eiji Nakazaki
Sea Engineering, Inc.
Waimanalo, Hawaii, U.S.A.

ABSTRACT

A possible future concern for coastal land areas is the impact of accelerated sea level rise (ASLR) as a result of global environmental changes. Study and planning for ASLR is being accomplished by the World Meteorological Organization and the United Nations Environment Programme, and Majuro Atoll was selected as a Pacific Islands case study site. This paper presents a brief summary of the oceanographic and coastal engineering considerations applicable to the evaluation of ASLR and its potential impact on a low-lying atoll island. The investigations include determination of scenario wave and sea level conditions, analysis of wave runup and inundation of the atoll land area and other coastal impacts, and assessment of possible response strategies and shore protection measures.

INTRODUCTION

Increasing awareness is evident in general news reports and scientific journals regarding the growing concern about possible global environmental changes, such as global warming, and the potential impact on human populations. Scientists report of possible accelerated sea level rise (ASLR) as a result of global warming, and, although there is still considerable debate and uncertainty about the magnitude of possible ASLR, or even if it will occur at all, many nations are taking the possible threat very seriously and are investigating the potential impacts of ASLR and how to deal with them.

The World Meteorological Organization and the United Nations Environment Programme jointly formed the Intergovernmental Panel on Climate Change and its Coastal Zone Management Subgroup (IPCC-CZMS), to assess the vulnerability of coastal areas and response strategies for adaptation to sea level rise (IPCC, 1990; 1991). The overall study effort is being coordinated by the Ministry of Transport and Public Works of the Netherlands and the U.S. Department of Commerce, National Oceanic and Atmospheric Administration (NOAA). The IPCC-CZMS has recommended that coastal countries (1) assess their vulnerability to ASLR and other potential impacts of global climate change, and assess the assets at risk; (2) start the planning process for appropriate response strategies; and (3) develop comprehensive coastal management programs to reduce their vulnerability to ASLR.

Majuro Atoll was selected as a case study site to develop a methodology for assessing the physical, social, economic and environmental vulnerability to sea level rise, and to evaluate possible response strategies. Majuro is a typical atoll, composed of a ring shaped reef system enclosing a salt-water lagoon. The atoll is elongate in shape, 25 miles from east to west, and 6 miles from north to south. There are 64 islets located on the encircling reef, which vary in width from about 0.1 miles to 0.5 miles. The total dry land area is about 4 square miles, and the average land elevation is less than 8 feet above mean sea level. The lagoon has a surface area of about 125 square miles, with an average depth of about 150 feet.

The study was accomplished as a joint effort between NOAA, the Republic of the Marshall Islands Environmental Protection Authority (RMIEPA), the South Pacific Regional Environment Programme (SPREP) and Sea Engineering, Inc. (SEI). The case study involved the following general steps:

1 - delineation of the vulnerability zones;

2 - inventory of study area characteristics;

3 - determination of future development factors;

4 - assessment of physical changes and natural responses; and

5 - formulation of response strategies and assessment of their costs and impacts.

SEI was tasked with determining the physical vulnerability of the study area to ASLR, assessing the condition and characteristics of the shoreline, and formulation of shore protection alternatives. This paper briefly summarizes the methodology and results of the coastal engineering investigations, and how these results may impact Majuro Atolls future.

METHODOLOGY

Storm wave runup on the shoreline and coastal inundation limits, and shore protection design parameters, were determined for the study area using existing available climatic, oceanographic and topographic data for Majuro Atoll, supplemented by a site visit to field check the condition and characteristics of the shoreline. Numerical modeling techniques were used for the analysis, based on models previously developed by SEI for hurricane vulnerability analysis in Hawaii. Parameters determined included wave heights, water levels, and runup elevations/inundation limits for three scenario wave events and three sea level scenarios, as follows:

Scenario Wave Events:	annual, 50-year return period and model typhoon conditions,
Scenario Sea Levels:	ASLR0 - existing sea level ASLR1 - 0.3 m (1 ft.) rise ASLR2 - 1.0 m (3.3 ft.) rise

General methods for shore protection, erosion control and shoreline flood protection were evaluated for applicability to the study area. Primary study areas on Majuro were the commercial and population center at the east end of the atoll (commonly known as Dalap-Uliga-Darrit or just D-U-D), and the important ground water and agriculture area located at Laura at the west end of the atoll. Of the approximately 20,000 people living on Majuro, about 15,000 of them live in the D-U-D area.

Accelerated Sea Level Rise (ASLR)

A number of studies have shown that the earth has warmed by about 0.53°C (1°F) during the last century, and the earth's average surface temperature has been predicted to possibly warm by at least 1.5°C to 4.5°C in the next century (Edgerton, 1991). The atmospheric warming could cause a melting of glacier ice and the thermal expansion of

ocean water, and ultimately a global sea level rise. Analysis of the past 100 years of tide gauge records around the world shows that the global sea level has been rising at a rate of 1 to 2 millimeters annually (Edgerton, 1991). Several sources have estimated future rises in sea level due to atmospheric warming. The U.S. Environmental Protection Agency has estimated that the sea level would rise 0.5 to 2 meters globally by the year 2100. A 1987 National Research Council report estimated a global rise in sea level of 0.5 to 1.5 meters by 2100. For this case study project, the IPCC-CZMS mandated that the assessment of the vulnerability of coastal areas and evaluation of strategies for adaption to sea level rise consider ASLR of 0.3 m (1 foot) and 1.0 m (3.3 feet) by the year 2100.

Storm Waves

Estimated annual and 50-year return interval deepwater wave heights for Majuro were determined based on a statistical analysis of wind and wave data contained in the Summary of Synoptic Meteorological Observations - Area 8 (U.S. Weather Service Command) and the Local Climatological Data (NOAA) for Majuro. A scenario typhoon event was determined based on a review of historical tropical cyclones in the vicinity of the Marshall Islands, defined by a central pressure of 964 mbs and maximum sustained winds of 75 knots, a radius of maximum wind of 15 nm, and a forward speed of 12 knots. Design significant wave heights (H, feet) and periods (T, seconds) applicable to the ocean side of the atoll were as follows:

Annual		50-Year		Typhoon	
H	**T**	**H**	**T**	**H**	**T**
13	13	19	13	27	11

Stillwater Level Rise

An important step in determining storm wave runup and inundation limits is to determine the stillwater level rise along the shore. The rise in stillwater level along the shoreline during extreme wind and wave events is generally a function of three components: (1) the astronomical tide, (2) storm surge due to reduced atmospheric pressure and wind stress setup, and (3) wave setup due to momentum flux changes in a train of waves of changing amplitude. These components are considered together with the ASLR scenarios to obtain the total design stillwater levels, summarized as follows for the ocean side of the atoll in feet above MSL:

		Annual	**50-Year**	**Typhoon**
Astronomical Tide		2.6 feet	2.6 feet	2.6 feet
Pressure Drop Setup		0.3	0.4	1.7
Wind Stress Setup		0.0	0.0	0.0
Wave Setup -	ASLR1	1.8	3.0	4.0
	ASLR2	1.6	2.7	3.7
Total -	ASLR1	5.7 feet	7.0 feet	9.3 feet
	ASLR2	7.8 feet	9.0 feet	11.3 feet

Wave Runup

The vertical height to which waves will run up on a shoreline slope determines the elevation over which inland flooding by waves will occur. Experimental wave runup relationships which determine significant wave runup heights for random waves on

gentle and impermeable slopes, corrected for slope roughness and composite slopes, have been found to give reasonable runup values. The total vertical height to which water will reach along the shore is determined by adding the wave runup to the total stillwater level rise.

RESULTS

Flooding and Inundation

Calculated results of the stillwater levels and wave runup elevations and resultant backshore flooding are as follows for the D-U-D and Laura areas (EL = total elevation to which water will rise, D = distance inland the runup will extend from the MSL shoreline, and (FL) or FL = partial flooding or complete flooding, respectively, due to extensive inundation distance or the stillwater level exceeds the beach crest):

	Annual	50-Year	Typhoon
ASLR0			
D-U-D area	EL 7' D 80'	(FL)	FL
Laura	EL 6' D 60'	EL 8' D 90	FL
ASLR1			
D-U-D area	EL 8' D 90'	FL	FL
Laura	EL 8' D 80'	EL 9.5' D 130'	FL
ASLR2			
D-U-D area	FL	FL	FL
Laura	(FL)	FL	FL

As can be seen, the significant wave runup nearly reaches the shoreline crest even during an annual wave event with no ASLR. With even the lower ASLR1 all of the D-U-D area would be flooded by any wave occurrence greater than an annual event. With ASLR2 the study areas would be flooded annually. An idea of the flooding frequency can be estimated by plotting the predicted runup elevations for the annual and 50-year events on semi-log paper. Flooding being defined by the wave runup exceeding a typical "critical" beach crest elevation. Ocean-side flooding frequency estimates are as follows:

		Critical Flooding Frequency (times/years)		
	Beach Crest El.	**ASLR0**	**ASLR1**	**ASLR2**
D-U-D area	7.5 feet	1/30	1/5	>10/1
Laura	11.0 feet	<1/100	<1/100	1/1

Shoreline Erosion

More than 70% of the world's sandy coastline has experienced net erosion over the past few decades, and the remaining 20% to 30% have remained stable or shown no measurable changes. The erosion is partly due to a sea level rise of about 1 to 2 mm per year, and a sea level rise of 1 meter during the forthcoming century would be a major

factor causing recession of sandy shorelines. Bruun (1962) devised a rule governing shoreline erosion, which states that a beach that has attained equilibrium with coastal processes will respond to a rise in sea level by losing sand from the upper part of the beach profile and gaining it in the nearshore area until a new equilibrium is established. Thus, the coastline will retreat (1) as the direct result of the sea level rise, and (2) as a result of the beach erosion. Using generalized shoreline profiles and conditions the shoreline retreat due to ASLR and the dry land area which would be lost can be estimated.

	Shoreline Retreat (feet)		Dry Land Lost (acres)	
	ASLR1	**ASLR2**	**ASLR1**	**ASLR2**
D-U-D area	20 - 80	70 - 260	50	160
Laura	20 - 130	70 - 420	45	140

Existing dry land in the D-U-D area is about 510 acres and in Laura about 740 acres, so as much as 10% to 30% of the D-U-D area and 6% to 19% of the Laura area could be lost with ASLR of 1 foot and 3.3 feet, respectively.

Water Resources

The present water system that supplies the heavily populated D-U-D area relies upon airstrip catchment of rain water and ground water from Laura. A promising ground water area is found in the Laura area, reported potable fresh ground water storage ranged from 450 to 550 million gallons during 1984 and 1985, with an estimated sustainable yield of 400,000 gallons per day. ASLR may affect the loss of ground water resources in two ways. One is the increased frequency of flooding due to storm waves and high water levels. Storm flood damage is not necessarily permanent, but it may make the ground water resource unusable at a critical time. The second threat is from island area loss, either by frequent inundation of low-lying areas or by erosional loss of shoreline. Using the results of the erosion and land loss estimated by this study, and procedures for estimating the resultant reduction of the ground water lens developed by Miller and Mackenzie (1988), the loss of lens area in Laura is estimated to be:

	Lens Area (feet^2)	**Percent Loss**
ASLR0	150,000	0
ASLR1	135,000	10%
ASLR2	105,000	30%

RESPONSE STRATEGIES

Potential response options to ASLR as identified by the IPCC include protection, accommodation and retreat. For an atoll environment the accommodation options are limited, with the most viable being to raise existing structures on pilings and plan new structures with raised first levels to accommodate occasional flooding and help to minimize property damage during storms. It would be desirable to raise the general ground elevation of the atoll above the possible future still water level, however the only source of fill material would be to dredge material from the lagoon at considerable cost and potential environmental impact. Retreat to naturally occurring higher ground is not possible on low, uniform elevation atolls. In extreme conditions, and in the absence of creating higher ground which is habitable under extreme conditions, the only retreat option may be to abandon the atoll.

Atoll islets are primarily composed of unconsolidated coralline material and their shorelines require stabilization and protection against erosion by wave action which would increase with ASLR. Shore protection can also be used to prevent flooding of the backshore area by storm waves. Rock revetment can be constructed by quarrying the hard, consolidated fringing reef limestone for armor and underlayer stone. In lieu of reef flat material, revetment can be constructed using manmade concrete armor units. Coral aggregate and sand for use in the concrete mix can be obtained directly from the lagoon or old reef flat quarry sites.

In order to prevent flooding by storm waves, the revetment crest elevation should be designed to prevent significant wave overtopping despite the water level rise and severity of wave attack. In some cases, however, it is not feasible and/or economically justifiable to construct a non-overtopping structure. For example, ASLR2, when combined with the 50-year and typhoon wave conditions, results in a water level exceeding most of the land elevation of Majuro. This high water level, coupled with storm waves, makes shore protection impractical for the worst case ASLR2 scenario considering any waves greater than the annual wave event.

An illustration of the required crest elevation and approximate cost for rock revetment shore protection around the 58,000 linear feet encompassing the D-U-D area for ASLR1 and the three scenario wave events is as follows:

	ASLR1 + Wave Event		
	Annual	**50-Year**	**Typhoon**
Crest El. (Ft. MSL)	9	10	14
Cost (Million US$)	35.0	46.0	105.0

REFERENCES

Brunn, P. 1962. Sea-level rise as a cause of shore erosion. *J. Waterways and Harbors Division*. **88**. American Society of Civil Engineers.

Edgerton L.T. 1991. *The Rising Tide*. Island Press.

IPCC (Intergovernmental Panel on Climate Change), Coastal Zone Management Subgroup. 1990. The Seven Steps to the Assessment of the Vulnerability of Coastal Areas to Sea Level Rise.

IPCC (Intergovernmental Panel on Climate Change), Coastal Zone Management Subgroup. 1991. Strategies for Adaption to Sea Level Rise.

Miller, D.L.R., and F.T. Mackenzie. 1988. Implications of climate change and associated sea-level rise for atolls. In: Proc. 6th Intl. Coral Reef Symp., Vol. 3, Australia.

Index of Authors